Ground penetrating radar techniques for the determination of subsurface moisture variability

Charlton, Matthew

Ground Penetrating Radar Techniques for the Determination of Subsurface Moisture Variability

By

Matthew Charlton

A thesis submitted to the University of London for the degree of Doctor of Philosophy

Department of Geography

King's College London

March 2002

ABSTRACT

This thesis describes the development of Ground Penetrating Radar (GPR) processing techniques for spatially distributed estimation of subsurface moisture. Subsurface moisture is a very difficult variable to measure on a consistent and spatially comprehensive basis (Engman and Chauhan, 1995). Traditional measurement techniques are limited because they are time consuming, invasive and destructive. Subsurface profiling with GPR is non-invasive and rapid. However, existing GPR based methods for moisture estimation are not based on radar profiling but on signal velocity analyses taken from common mid-point (CMP) soundings. These are inappropriate for investigations of subsurface moisture variability at either large scales or high resolution because they are time consuming and spatially imprecise. The aim of the thesis was to develop moisture measurement techniques applicable in radar profiling mode.

Using a series of controlled laboratory experiments the relationship between a number of properties of the GPR signal derived in reflection profiling mode (RPM) and Volumetric Moisture Content (VMC) is investigated. Significant relationships were found for trace amplitude, amplitude spectra, and amplitude envelope with VMC for a variety of earth materials and situations. The form of these relationships is strongly dependent on the subsurface profile of soil moisture which is controlled by the hydraulic properties of each material. The techniques developed are applied in the field to the detection of moisture bodies associated with urban water leaks (in collaboration with Thames Water Utilities Ltd.) and to a plot-scale investigation of temporally varying moisture patterns on a hillslope in one of the Plynlimon catchments in Wales. Although site-specific calibration of the GPR for VMC is still required, this research shows that much can be understood in terms of subsurface moisture variation using GPR in reflection profiling mode.

Quantitative correspondence between the GPR and invasive measurements of moisture is limited by differences in sampled area and depth of investigation. GPR specific errors are introduced by the coupling of the radar with the ground surface, and the impact of (non-water controlled) profile (dielectric) variability on the GPR signal return. Improvement in GPR determination of moisture can be facilitated through further investigations designed to (a) identify the effect of moisture distribution on GPR-VMC, (b) overcome uncertainty in the subsurface volume sampled using GPR, (c) test alternative antenna configurations, and (d) test the technique over a greater range of subsurface environments.

ACKNOWLEDGEMENTS

I would like to thank all those who have contributed towards the completion of this thesis. In particular my supervisor, Dr. Mark Mulligan, who has helped in all aspects of this work, and Inês Lopes da Fonseca, for her patience, support, and for her comments on this thesis.

I am very grateful to all those who helped in the shifting sands of the laboratory and the field. Thanks, especially, to Andrew Howe for all his help with the GPR, Inês Lopes da Fonseca, Thomas Charlton, and Sarah Appleby. I would also like to thank Russ Luigolio and Nina Ninofski for their inspiration and comments. Thanks also to my colleagues at King's College London, John Wainwright, Satish Kundaiker, Elias Symeonakis, Katerina Michaelides, Mauricio Rincón-Romero, Benito Meza Diaz, Sotirios Koukoulas, for their help, ideas and discussions. Finally, without the support of all of my family, none of this would have been possible.

Much of the work carried out for this research was done in collaboration with Thames Water Utilities Ltd. I would very much like to thank Lawrence Scudder, for his ideas and comments, Dr. Jeff Whiter, and the rest of Thames Water GPR Team for collecting and sharing their field data.

Funding for this research was provided by the Natural Environment Research Council and Thames Water Utilities Ltd. (NERC CASE studentship GT19/97/9/EO). Additional funding for field work and conferences provided by King's College London Humanities Small Grant, Mr. and Mrs. B. Charlton, and Mr. and Mrs. H. Charlton

TABLE OF CONTENTS

LIST OF FIGURES

CHAPTER THREE

CHAPTER FOUR

CHAPTER FIVE

CHAPTER SIX

CHAPTER SEVEN

CHAPTER EIGHT

CHAPTER NINE

LIST OF TABLES

CHAPTER SEVEN

CHAPTER EIGHT

CHAPTER NINE

CHAPTER ONE: INTRODUCTION AND RESEARCH AIMS

1.1 INTRODUCTION

Soil moisture is an environmental variable that integrates many land surface hydrological processes and is the interface between the solid earth surface and the atmosphere (Engman and Chauhan, 1995). Representation and prediction of the spatial variability of soil moisture are needed to understand better and predict a range of processes over a range of scales from small catchments to whole continents (Western *et al.*, 1999). To enhance understanding of water movement in soil there is a need for small-scale, non-destructive measurement techniques to obtain direct, high-resolution measurements of soil water content (Nissen *et al.*, 1998). Soil moisture is a very difficult variable to measure on a consistent and spatially comprehensive basis (Engman and Chauhan, 1995). Furthermore, there have been too few data on soil moisture distribution to be certain of the true patterns that exist in nature (Western *et al.*, 1999) and, more importantly, the controls on these patterns. The existing techniques available to assess the complexity of moisture controlled hydrological processes and parameters are inadequate, even for small field studies (Beven, 1997). One method that has the potential to overcome the limitations of existing techniques is ground penetrating radar (GPR). However, in contrast to detecting water tables and determining stratigraphy, not much is known about the possibility of using GPR for the observation of soil moisture content in the unsaturated zone, in spite of the fact that it has long been recognised that the propagation velocity of radar waves is largely determined by soil water content (van Overmeeren *et al.*, 1997).

1.2 RESEARCH AIMS

The primary aim of this research is to develop techniques for using GPR as a means to derive spatially distributed values of subsurface Volumetric Moisture Content (VMC) directly (using reflection profiling mode), accurately and efficiently. This involves the following general objectives:

1. The objective and quantitative observation of GPR signal response to different materials at different moisture contents in order to evaluate the material and moisture dependence of GPR return properties.

2. The subsequent development and validation of simple empirical models to estimate VMC using derivable GPR signal parameters.
3. The identification of potential limitations to the range of application and accuracy of the estimations and the development of processes and techniques to reduce their effect.
4. The application of the GPR-VMC estimation technique to the mapping of subsurface moisture distributions with a view to identifying the patterns of sub-pavement moisture associated with urban mains water leaks, and to map the spatial distribution of hillslope soil moisture, its controls and implications for hillslope hydrological processes.

To achieve these objectives it is important first to outline the existing knowledge concerning the nature of subsurface moisture and to discuss GPR itself. Following these reviews, the potential routes to VMC estimation using GPR can be assessed and a methodology, based on a combination of controlled laboratory and field investigations, presented to enable the research aims to be satisfied.

CHAPTER TWO: SUBSURFACE MOISTURE

2.1 THE IMPORTANCE OF SOIL MOISTURE

Soil moisture is a critical variable that controls the non-linear behaviour of land-atmospheric interactions, and the effect is most pronounced when soil moisture heterogeneity is such that part of the domain is under soil-vegetation control and part is under atmospheric control (Wood, 1995). Soil moisture is therefore very important for many, and varied, environmental processes including atmospheric, plant, geomorphological and hydrological processes. In fact, because it integrates atmospheric, surface and subsurface processes, soil moisture is an important parameter in most models of earth surface processes.

Knowledge of the surface layer moisture can be used to estimate moisture fluxes at the soil surface (Schmugge and Jackson, 1997). The supply of water is of considerable importance to terrestrial plants because it determines for how long they can grow in the absence of additional inputs (Gregory, 1994). Water availability is often a primary limitation to biomass production (Radin, 1993) and it therefore has serious implications for agricultural production and land use. Knowledge of variations in soil moisture is essential for the interpretation of phenology, water use, productivity and seedling establishment, all of which can influence plant distribution patterns (Young and Nobel, 1986),

Conditions of soil moisture also influence geomorphological processes such as soil erosion, gullying and mass movement, as well as the transport of chemical constituents over and in the soil (Van Der Beken and Herrmann, 1985). Erosion of the upper, normally fertile, soil layer is dependent on its soil moisture (Weimann *et al.*, 1998). Soil behaviour and strength vary with moisture content (Whalley, 1990) and this occurs through the interaction of the soil properties with the water.

Of particular importance to this research is the impact of soil moisture on hillslope hydrology. The ability of the soil to absorb and retain moisture is crucial to the hydrology of an area (Ward and Robinson, 1990) and consequently runoff and infiltration depend on the soil moisture content (Weimann *et al.*, 1998). However, it is not simply the impact on surface runoff that means soil moisture is a significant variable. Subsurface storm

response is particularly dependent on the status of moisture in the soil because rates of subsurface flow increase considerably with increased water content. Without information on soil moisture variability, prediction and interpretation in catchment hydrology is problematic (Fitzjohn *et al.*, 1998) and many hydrological response modelling efforts fail because they do not consider subsurface moisture behaviour sufficiently well, along with many other important reasons as well.

The ability to observe soil moisture frequently over large regions could significantly improve our ability to predict runoff at a variety of scales (Jackson *et al.*, 1996) and to model water transfer processes at the basin scale in particular (Benallegue *et al.*, 1994). Moisture content has to be known as an initial condition (John, 1992) for accurate prediction. Because soil moisture determines storage capacity and rates of moisture movement, not knowing the initial moisture content will result in mis-representation of infiltration and flow processes. In fact, prediction is currently limited by not knowing enough about the role of soil moisture in generating or modifying hydrological response. Due to the importance of soil moisture in environmental systems it is vital to estimate or predict it accurately in terms of both content and distribution.

2.2 THE NATURE AND CONTROLS OF SOIL MOISTURE

The water status in soils is defined by (1) the amount of water in the soil, or soil water content (θ) and (2) the force by which water is held in the soil matrix, soil energy content or soil water potential (ψ), and these soil water attributes are related to each other through a function known as the soil water characteristic (Or and Wraith, 2000). Soil moisture is determined by the various factors which regulate the entry of water through the soil surface and the removal of water from the soil; these factors are themselves influenced by virtually all the factors and processes operating in the hydrological cycle, including soil moisture (Calder, 1997). Soil moisture is the balance between water influx and water outflow from a volume of soil. To understand soil moisture and its variability, it is necessary to understand the processes that provide, or remove, water and this can be represented by a moisture balance equation (Hoogmoed *et al.*, 1991):

$$dS = P + G + R_{on} - E_t - D - R_{off} + Irr \qquad (2.1)$$

where dS is the change in soil moisture, P is precipitation, G is groundwater inflow, R_{on} is runon or surface inflow, E_t is evapotranspiration, D is drainage, R_{off} is runoff, and Irr is irrigation (all in mm). Where there is no upward movement $G = 0$ (Hoogmoed *et al.*, 1991). Precipitation is the main input while evapotranspiration often provides the second largest quantity in the water balance (Dyck, 1985). The volumetric moisture content (VMC: θ_v ($m^3\ m^{-3}$)) determines the rate of fluxes into and out of the profile and therefore infiltration, drainage, and evapotranspiration are all dependent on the soil moisture (van Wesemael *et al.*, 1995).

When the rainfall intensity exceeds the infiltration capacity, the remaining water will runoff over the surface as infiltration-excess overland flow (Summerfield, 1991). Alternatively, where the soil is saturated, any further rainfall, even at low intensities, is able to generate overland flow (Kirkby, 1978). Saturation can be defined as the point at which all air in the soil has been displaced by water (Hook and Livingstone, 1995). The generation of runoff is dependent on the storage capacity of the soil in relation to its infiltration capacity and ability to retain water. Consequently, soil material properties are very important. Runoff response will be affected by the degree of saturation of the soil. This is dependent on porosity and manifests itself as fractional moisture content. In partially saturated soils with constant porosity, water content may be interpreted as an indicator of saturation while in fully saturated soils, variations in water content can be interpreted as variations in porosity (Greaves *et al.*, 1996).

Where moisture levels are low, water storage will tend to increase at the infiltration capacity. Any rain that exceeds this capacity will not contribute to the soil moisture balance at that point. Infiltration (f) depends on the hydraulic conductivity and available soil storage and can be simply represented by the modified Green and Ampt equation, amongst many others:

$$f = A + (B / t) \qquad (2.2)$$

where:

A = hydraulic conductivity (mm hr^{-1})

B = sorptivity (mm) (Selby, 1993)

t = time.

The hydraulic conductivity is important because it determines not only the rate at which water enters or leaves the soil, but also how the water is redistributed. The hydraulic conductivity increases with increasing VMC (Marshall *et al.*, 1996). The storage of water in the soil is influenced by the physical properties of the soil. Increased bulk density decreases water content at a given potential because porespace is reduced (Mulligan, 1996) while texture also has an influence. For example, saturated sandy soils have a lower water holding capacity than finer-textured soils (Jackson *et al.*, 1995).

Although, in the computation of the soil water balance, drainage is often assumed to be negligible (Beven and O'Connell, 1985), drainage from the base of the profile occurs at the hydraulic conductivity of the soil, K (Mulligan, 1996), again controlled primarily by moisture content at the basal flux boundary:

$$DRt = K_{sat} + (\theta / \theta_{sat})^{2b+3} \qquad (2.3)$$

where:

DRt = instantaneous drainage rate (mm hr^{-1})

K_{sat} = saturated hydraulic conductivity (mm hr^{-1})

θ = soil moisture (m^3 (water) / m^3 (pore space))

θ_{sat} = saturated moisture content (=1)

b = decay constant of soil moisture characteristic.

Field capacity (θ_f) has been defined as the amount of water remaining in the soil after downward movement under gravity has ceased (Ward and Robinson, 1990). The water in soils and aggregates can be classified as: (1) adsorption water, also called hygroscopic water; (2) viscous water, or capillary water; and (3) free water (Saarenketo, 1998). Each of these types of water influence the soil hydrology, and the electrical response of the soil, in different ways. Details of the electrical properties of soil water will be considered in more detail in Chapter Three.

Adsorption is an interfacial phenomenon resulting from the differential forces of attraction or repulsion occurring among molecules or ions of different phases at their exposed contact surfaces (Hillel, 1980). A hygroscopic water layer consists of an extremely well arranged monomolecular layer around negatively charged mineral surfaces and additional tightly and loosely bound adsorption water layers (Saarenketo,

1998). The adsorption of water upon solid surfaces is generally of an electrostatic nature with the polar water molecules attaching to the charged faces of the solids (Hillel, 1980). Adsorptive forces are more important in clay soils than sandy soils and as moisture content is decreased (Ward and Robinson, 1990).

The moisture in soil which is not bound around mineral grains as hygroscopic water, but does not respond to gravity, is usually called capillary water (Saarenketo, 1998). The upward movement of moisture by capillarity is conditioned partly by the size and arrangement of soil particles (Ward and Robinson, 1990). Matric suction is due to the physical affinity of water to the soil-particle surfaces and capillary pores (Hillel, 1980).

Water molecules more than a few molecular lengths away from the macro-molecule constitute the main bulk of the solution and this water is therefore called 'bulk' or 'free' water (Grant *et al.*, 1978). Free water, also called gravitational water, is attracted to the soil solids so loosely that it may respond to the pull of gravity and move downwards in the soil (Saarenketo, 1998).

The apportionment of the total water volume fraction (m_v) between free and bound water is governed by the specific surface area A_s ($m^2\ g^{-1}$) of the soil particles because the bound water is defined as absorbed cations that are tightly held by negatively charged particle surfaces composed predominantly of clay (Dobson *et al.*, 1985). It is the clay fraction, and more specifically the mineralogy of the clay particles, that determines the A_s of the soil mixture, and hence the portion of m_v in the form of bound water (Peplinski *et al.*, 1995).

2.3 PATTERNS AND MOVEMENT OF SUBSURFACE MOISTURE

After entering the soil, water is redistributed by movement through the subsurface. This redistribution is an important control on the nature of the spatial variability of soil moisture. The wetting of an unsaturated soil is a complex process involving matrix infiltration in soils of variable conductivity, preferential flow in pathways of complex geometry and connectivity, and perhaps some areas of saturated soil, surface runoff production and run-on (Beven, 1997). The drier the soil the greater the initial rate of entry of water into the soil because the gradient of the matric potential is then higher (Marshall

et al., 1996). The lengthening zone of wet soil behind the advancing wetting front, in which the water content is essentially constant, is called the transmission zone (Marshall *et al.*, 1996). Generally, flow is caused by gradients of both matric and gravitational potential and a gradient in matric potential implies a change of water content from place to place (Marshall *et al.*, 1996).

Three-dimensional unsaturated Darcian soil water flow in a nondeformable homogeneous porous medium is assumed to be described by the partial differential equation:

$$\frac{\partial}{\partial x}\left(K_x \frac{\partial \phi}{\partial x}\right)+\frac{\partial}{\partial y}\left(K_y \frac{\partial \phi}{\partial y}\right)+\frac{\partial}{\partial z}\left(K_z \frac{\partial \phi}{\partial z}\right)=\frac{\partial \theta_v}{\partial t} \qquad (2.4)$$

where K_x, K_y, and K_z are anisotropic hydraulic conductivity values in the x, y, and z directions, respectively, ϕ is the total hydraulic energy head ($\phi = \psi + z$), ψ is the soil water pressure head, and θ_v is the volumetric water content (Hromadka *et al.*, 1981). A Darcian approach assumes that the pressure at a particular point in the flow domain is equilibrated over some "representative elementary volume" (REV) and that the movement of water takes place in response to a pressure gradient at that scale (Beven, 1997). Vertical flow which possesses no significant component in the horizontal is a common feature of unsaturated soils in the field (Marshall *et al.*, 1996) and so the expression in the vertical dimension is all that is required. At the local scale, within the soil matrix, this assumption may be acceptable but, in a heterogeneous unsaturated porous matrix, the application of this concept at the grid scale may be dubious because of the highly non-linear dependence of the flow velocity on the local moisture and pressure gradient (Beven, 1997).

In the conduction of water through the soil, the whole of the pore space is only involved when the soil is saturated (Marshall *et al.*, 1996). At saturation, the most conductive soils are those in which large and continuous pores constitute most of the overall pore volume (Hillel, 1980) and hence saturated sandy soils conduct water more rapidly than clay soils because the resistance to water movement through the large saturated pore space of sandy soils is much less than the resistance to flow in the smaller and less connected pore space of clay soils. As the soil dries, the pathway for water movement is progressively restricted to smaller pores, and resistance to water movement increases (Rutter, 1969). This is because with flow confined to the smaller pores and also to less pore space, conductivity

decreases (Marshall *et al.*, 1996). On drying, large pored soils exhibit a significant decrease in conductivity, while for small pored soils this change is less dramatic because many of the pores retain and conduct water even at appreciable suction (Hillel, 1980). The empty pores must be circumvented so that, with drying, tortuosity increases (Hillel, 1980). This would increase travel times for moisture movement. Obviously, the degree of connectivity, and hence, reduction in subsurface travel times depends on the degree of saturation. This varies both spatially and temporally. There is evidence that, even in humid temperate areas subsurface responses depend upon the connectivity of saturated zones on the hillslopes (Beven, 1997).

As well as flow through the matrix, moisture can move through larger routes commonly termed macropores. The presence of inhomogeneities in the soil may be an important factor in the generation of subsurface stormflow (Beven, 1981). Such pathways for rapid water flow in soils may result from the structural arrangement of peds and from biological activity (Heuvelman and McInnes, 1997), and from discontinuities between the soil matrix and rock fragments. At the local scale, the macropores can transport the bulk of the flow with a minimal contribution from the soil matrix (Blöschl and Sivapalan, 1995). Although macropores make up a relatively small fraction of a soil's total porosity, they can have a disproportionate effect on the soil's infiltration properties because water flow in macropores is frequently much more rapid than Darcian flow through soil micropores, allowing infiltrating water to bypass the soil matrix and reach specific depths ahead of water moving via soil micropores (Buttle and House, 1997). In fact, flux of water in macropores has been reported to be one to four orders of magnitude greater than flow in the soil matrix (Timlin *et al.*, 1994). In the Plynlimon catchments, Wales, the hydrological significance of rapid pipe drainage may be reduced because pipes rarely discharge directly into the surface channels of the catchment; however, the pipe networks do constitute a major source of saturation (Newson and Harrison, 1978). At the hillslope scale, preferential flow may occur through high conductivity layers and pipes (Blöschl and Sivapalan, 1995). Preferential flow can induce marked vertical and lateral changes in soil water content, total potential and unsaturated hydraulic conductivity (Buttle and House, 1997).

2.4 SPATIAL AND TEMPORAL VARIABILITY OF SOIL MOISTURE

Hydrological prediction at the micro- (local) and meso- (basin) scales is intimately dependent on the ability to characterise the spatial variability of soil water content (Moore *et al.*, 1993). Natural catchments exhibit a high degree of heterogeneity and variability in both space and time (Blöschl and Sivapalan, 1995) and at a range of scales (Western *et al.*, 1998; Western *et al.*, 1999). This variability can be extreme over distances of 1-100 m (Moore *et al.*, 1993). A non-linear response from a catchment as regards runoff may, to a large extent, be explained from the point of view of spatial variability in catchment characteristics (Berndtsson and Larson, 1987). Patterns of soil moisture are complex because soil moisture integrates variability in rainfall and vegetation with the hydrological response of the catchment – in particular, variability in soils and topography (Wood, 1995). Because soil moisture is a function of the soil's physical and hydraulic properties and controlled by variables such as texture, vegetation and topography, the spatial pattern of soil moisture will reflect the spatial distribution of these controlling variables (Fitzjohn *et al.*, 1998).

In mountainous or hilly terrain soil, water distribution is controlled by vertical and horizontal water divergence and convergence, infiltration, drainage, and evapotranspiration (Moore *et al.*, 1993). Because of the difficulties associated with direct measurement or estimation of the variability of soil properties, many researchers have used only topographic attributes to characterise soil water distribution (Moore *et al.*, 1993). Variations in wetness are explicable in terms of local topography and the hydraulic properties of the soil profile (Moore *et al.*, 1988). One possibility is to determine a wetness index, such as ln(a/tanB) (Jones, 1986), based on topography. Speight (1980) shows how concave slope profiles and concave contours imply zones of high water potential. Therefore, by identifying regions of concavity it is possible to determine zones of soil water accumulation, such as hollows (Burt and Butcher, 1985). Conversely, convexities can be regarded as areas of dispersal and low soil moisture. Soil piping is sensitive to soil profile characteristics and can develop routes that are at variance with the surface topography (Jones, 1997) so that topography will give misleading estimations of moisture distribution in areas where macropores are prevalent, such as in the Plynlimon catchments, Wales. This is true for subsurface (soil) heterogeneity in general, not just for macropores.

The strong dependence of θ_v on elevation and the relationship between elevation and texture (sand, silt, clay content) are probably the source of some of the covariance between θ_v and texture (Kachanoski *et al.*, 1988). Studies conducted in association with Washita'92 (a large scale study of remote sensing and hydrology conducted on the Little Washita watershed in southwest Oklahoma in 1992) demonstrated that spatial patterns of moisture were clearly associated with soil textures and temporal patterns with drainage and evaporative processes (Jackson *et al.*, 1995, Jackson *et al.*, 1996). Another important, but rarely investigated, textural influence on soil moisture distribution is stone content. The effect of rock fragment and stone content on subsurface moisture is complex. Based on the fact that for the surface, stone cover is essentially impermeable (Dunkerley, 1995), it can be viewed that stones in the subsurface represent zones of relative dryness. The presence of rock fragments in the subsurface effectively reduces the surface area for the flux of water vertically through the profile; reducing the vertical flux of water and reducing drainage from the base of the profile (van Wesemael *et al.*, 2000). Rock fragment content also decreases the total pore volume of the soil profile such that, in a stony soil, a unit of infiltrated water will produce a greater change in VMC than in a less stony soil (van Wesemael *et al.*, 2000). Conversely, small rock fragments (1.7-2.7 cm) are responsible for maintaining low fine earth bulk density and high macroporosity in topsoils (van Wesemael *et al.*, 1995).

The distribution of moisture before a rainfall event will determine the response of the catchment to that rainfall whilst antecedent soil moisture content varies considerably in space and time (Robinson and Sivapalan, 1995). This is effected through the connectivity of flow paths both on the surface and in the subsurface. If a catchment is relatively dry there will probably be limited connectivity of subsurface patches of moisture and this connectivity may increase as a soil wets up during the event and also as soil wets and dries seasonally. Temporal variations may manifest themselves as an increase in the saturated volume during periods of wetter weather (Ward and Robinson, 1990).

The degree of moisture connectivity will directly affect hillslope hydrology and the soil moisture is therefore a principal control on all of the soil hydrological processes in a catchment. With less spatial variability, connectivity may increase and water will be able to move more quickly from one part of the hillslope to another. However, the spatial variability of soil water fluxes increases travel time variance, resulting in an increased probability of short travel times (Heuvelman and McInnes, 1997). The degree of

connectivity will not only depend on the distribution of moisture but also on the actual VMC. As discussed, increased VMC increases matrix moisture connectivity. However, overall subsurface storm response or flow will not increase in speed or magnitude until regions of high VMC are substantially connected. The speed of response will therefore depend on the antecedent moisture condition or, in modelling terms, the initial moisture content. For hydrological response to occur more rapidly VMC must act to increase saturation, so as to increase the potential for movement between pore space, and it must act to increase connectivity, which will determine overall response and is dependent on the degree of saturation of connected pore space. Alternatively response may be rapid even if there is limited moisture connectivity, through the impact of preferential flow paths; in particular, pipe flow and saturated wedges. For macropore flow to become operative certain thresholds in precipitation intensity and antecedent moisture need to be met (Blöschl and Sivapalan, 1995). Traditional estimates of travel times, based on water flow through the total pore space (matrix flow), may be grossly overestimated or underestimated if water moves through select flowpaths (Heuvelman and McInnes, 1997) depending upon the connectivity and density of these flowpaths.

2.5 MEASUREMENT OF SOIL MOISTURE: TECHNIQUES AND LIMITATIONS

Measurements of soil water are either made by measuring the soil water content or the soil water potential, which can then be related to the content. The following discussion will focus on the most common of a broad range of techniques for measuring soil moisture content. The techniques available for the measurement of soil moisture can be classified as point methods or regional / -areal methods; the difference being the area from which the estimate of soil moisture is determined. These can be subdivided into direct and indirect methods. Direct methods provide a direct estimation of moisture content, whilst indirect methods use empirical relationships between moisture and a measurable variable to determine moisture content. Indirect methods can be invasive or non-invasive depending on the degree to which the soil is disturbed by the measurement. Often this disturbance may only be at the initial stage of setting up the monitoring equipment while techniques such as remote sensing do not disturb the soil at all. The basic advantages and disadvantages and approximations of accuracy are shown in Table 2.1.

2.5.1 Direct methods

2.5.1.1 Gravimetric method

The simplest, and most common method for determining soil water content is to use the direct gravimetric method in which the mass m_w of water lost upon drying a sample in an oven at 105°C to a constant mass is found (Marshall *et al.*, 1996). The fractional content of water in the soil can be expressed in terms of either mass ($kg\,kg^{-1}$) or volume ($m^3\,m^{-3}$) ratios:

$$\theta_m = m_w / m_s \tag{2.5}$$

$$\theta_v = V_w / V_t = V_w / (V_s + V_w + V_a) \tag{2.6}$$

where θ_m, the mass (gravimetric) wetness, is the dimensionless ratio of water mass m_w to dry soil mass m_s, whereas θ_v, the volume wetness, is the ratio of water volume V_w to total (bulk) soil volume V_t, comprising the sum of the volumes of solids (V_s), water (V_w), and air (V_a) (Hillel, 1980). The water content as a volume fraction can be obtained from θ_m using:

$$\theta_v = \theta_m \rho_b / \rho_w \tag{2.7}$$

where ρ_b is the dry bulk density of the soil ($Mg\,m^{-3}$) and ρ_w is the density of water which, for most purposes, can be taken to be $1\,Mg\,m^{-3}$ (Marshall *et al.*, 1996) where 1 Mg = 1000 kg). The conversion is relatively simple for non-swelling soils in which bulk density, and hence bulk specific gravity, are constant regardless of wetness, but it can be difficult in the case of swelling soils because the bulk density must be known as a function of mass wetness (Hillel, 1980). Other disadvantages of the gravimetric approach include its destructive and invasive nature, the requirement for laboratory work, time intensive sampling and the fact that it measures over a very small volume. Furthermore, a large number of samples covering a number of depths may be required because water can be distributed unevenly in the field (Marshall *et al.*, 1996) although this is a disadvantage for most methods.

Due to the limitations and likely error associated with the gravimetric method, many workers prefer indirect methods which permit making frequent or continuous measurements at the same points, and, once the equipment is installed and calibrated, with much less time, labour, and soil disturbance (Hillel, 1980).

2.5.2 Indirect methods

2.5.2.1 Electric resistance methods

An example of a resistance technique is the use of gypsum blocks. As the soil around a gypsum block wets up, the block also wets up. The water then acts as a connector between two separate pieces of wire contained within the block. There is an associated change in the electrical resistance between the two wires and this can be directly related to the water content. The gypsum blocks can easily be calibrated for laboratory use and, because they are small and inexpensive, can be used at a high sampling density so that a relatively large area and depth can be sampled using them. However, like most of the methods discussed here, the use of Gypsum Blocks requires disturbing the soil to a large extent and they are impractical for covering large areas. Gypsum blocks also degrade over time in the soil and therefore do not offer the potential for long-term observation of soil moisture.

2.5.2.2 Capacitance methods

A capacitance probe enables soil water content to be measured in access tubes in the unsaturated zone and uses a frequency of 150MHz to measure the electrical capacitance (C) of a soil, which is a function of the dielectric constant (ε):

$$C = g\varepsilon \tag{2.8}$$

where g is a geometric factor dependent on the geometry of the electrodes of the sensor (van Overmeeren *et al.*, 1997). Among the advantages of this method, especially in comparison with the more widely used neutron probe, are speed of measurement, low cost, portability, high resolution, absence of any random counting error and lack of

radiation hazard (van Overmeeren *et al.*, 1997). However, the technique still requires site specific calibration and the construction of access tubes rendering the technique of little use for non-invasive surveys or where the ground is too hard.

2.5.2.3 Time domain reflectometry (TDR)

TDR is now widely accepted for measuring volumetric soil water content (Perdok *et al.*, 1996), because of its apparently insignificant susceptibility to properties other than moisture, such as salinity and temperature (Malicki *et al.*, 1996). The TDR measurement technique is based on the estimation of the time needed for an electromagnetic pulse to travel along metal rods (waveguides) inserted into the soil which depends upon the apparent dielectric constant of the 3-phase soil system (Timlin and Pachepsky, 1996). When an electromagnetic wave is transmitted along a transmission line of known length, velocity is determined by the time taken to travel the known distance (Topp *et al.*, 1982). The velocity of the pulse propagation is inversely proportional to the square root of its dielectric constant (Roth *et al.*, 1992). A calibration relationship between travel time and VMC is needed to use TDR for measurement of VMC (Timlin and Pachepsky, 1996). The most commonly used is that developed by Topp *et al.*, (1980). This is an empirical relationship between the relative dielectric constant (see Section 3.4), ε_r, and volumetric soil water content θ_v :

$$\theta_v = -5.3\times10^{-2} + 2.92\times10^{-2}\varepsilon_r - 5.5\times10^{-4}\varepsilon_r^2 + 4.3\times10^{-6}\varepsilon_r^3 \qquad (2.9)$$

and was found to be nearly independent of soil texture, soil bulk density, temperature and soil salinity. The relationship was determined with a standard error of estimate of about 1.3% for all soils (Paltineanu and Starr, 1997).

Because TDR has a high spatial resolution (i.e. a low sample volume), the presence of macropores, rocks, root channels and large aggregates may influence field TDR measurements (Timlin and Pachepsky, 1996). Cumbersome sampling limits applicability to transient conditions (Persson, 1997) and the method by which the travel time is obtained from the wavetrace can be a source of error for TDR measurements (Timlin and Pachepsky, 1996). In heterogeneous soils there may be a need for site-specific calibration because the models are sensitive to soil structure (Persson, 1997). Malicki *et al.* (1996)

conclude that the soil matrix influences dielectric (TDR) determination of moisture, although measurement error can be reduced by accounting for a single matrix parameter such as bulk density or porosity. TDR has been used only with limited success for measuring small spatial scale variations in θ due to limitations in equipment, such as the length of the probes (Nissen *et al.*, 1998).

Because of the limitations associated with TDR, Perdok *et al.* (1996) developed and tested a frequency domain (FD) sensor, which measures the complex impedance of the soil, producing dielectric constant results within ±1 of the TDR method for the same soils. Because the FD sensor operates at a relatively low frequency (20MHz in contrast to ~200MHz for TDR) it yields larger relative dielectric constant values and depends differently on bulk density (Perdok *et al.*, 1996). The sample measurement volume using the FD sensor is less than 100 cm^3 (Perdok *et al.*, 1996).

2.5.2.4 ThetaProbe

ThetaProbe measures VMC by the well established method of responding to changes in the apparent dielectric constant which are converted into a d.c. (direct current) voltage and is similar in principle to the FD sensor, although it uses a higher signal frequency (100 MHz) and samples a smaller soil volume (30 cm^3) (Delta-T Devices Ltd., 1998). The device measures the impedance of a sensing probe wire array, which depends upon the dielectric constant, and the principles of the method are discussed in detail in Gaskin and Miller (1996) and Miller and Gaskin (2000). In the range 0 to 1 Volt (corresponding to a soil moisture range 0 to ~ 0.55 by volume), the relationship between voltage and dielectric constant can be fitted using a 3rd order polynomial (Delta-T Devices Ltd., 1998):

$$\sqrt{\varepsilon} = 1.07 + 6.4V - 6.4V^2 + 4.7V^3 \qquad (R^2 = 0.998) \qquad (2.10)$$

or

$$\sqrt{\varepsilon} = 1.1 + 4.44V \qquad (R^2 = 0.99) \qquad (2.11)$$

This can be converted to VMC using the equation from Topp *et al.* (1980) or through a soil specific calibration. Although not yet widely used, accuracy is considered to be ±

$0.02\,m^3\,m^{-3}$ for calibration to a specific soil type (Delta-T Devices Ltd., 1998). Accuracy is known to depend on variations in soil density and composition, stones close to rods, roots, earth worm holes (or other macropores), subsoil drainage, and small scale variation in evapotranspiration losses. All of these directly affect soil moisture and it is important to take the degree of variability of these various parameters into consideration when deciding on the number of probes to use at any particular location (Delta-T Devices, 1998). Examples of the application of the *ThetaProbe* are given in Miller and Gaskin (2000) and Miller *et al.* (1997).

2.5.2.5 Neutron moderation method

The neutron moderation method is popular and is based on the ability of hydrogen to slow down fast neutrons (Marshall *et al.*, 1996).These fast neutrons are emitted from a source and near this source is a detector of slow neutrons. The probe is suspended on a cable that transmits neutron-induced pulses to an amplifier, discriminator and counting device, and it is the relation between the counting rate and the water content that is of interest (Marshall *et al.*, 1996). Near the soil surface the probe should be sufficiently deep at the first location to ensure that the volume measured is effectively infinite for the process of slowing down and diffusion of neutrons to be fully developed in the soil itself, and that none escapes through the soil surface to the air before they are absorbed in the soil (Marshall *et al.*, 1996). This limits applicability to surface moisture measurements. High labour costs and radioactive risk hazards and regulations, along with the neutron probe's individual and discrete data collection, make the neutron moderation method unsuitable for real-time soil water dynamics across large areas (Paltineanu and Starr, 1997). Furthermore, the need for site calibration make this technique less than ideal (Topp *et al.*, 1980). The gamma ray method is based on the attenuation of emitted gamma rays, which depends on the wet bulk density of the soil. This gives better depth resolution than the neutron moderation method and is more useful near the surface, but is not widely used in the field because of the difficulties in discrimination under field conditions (Marshall *et al.*, 1996).

Method	Advantages	Disadvantages	Accuracy / Precision
Gravimetric	• Direct measure of moisture	• Destructive and invasive • Time consuming when a large number of samples are required.	• Coefficient of variation of about 10% (Marshall *et al.*, 1996)
Gypsum blocks	• Can sample at a high density	• Destructive and invasive • Time consuming • Point measurement	• Unknown
Capacitance probe	• Cheap • Relatively fast	• Invasive • Point measurement	• Unknown
TDR	• Simple and relatively reliable calibration between VMC and dielectric constant • Permits frequent or continuous measurement at the same points.	• Invasive • Time consuming • Can be affected by soil structure • Limited success for small scale variations in VMC • Point measurement	• Standard calibration has a standard error of estimate of about 1.3% for all soils (Paltineanu and Starr, 1997)
ThetaProbe	• Potential for rapid surface moisture survey • Permits frequent or continuous measurement at the same points.	• Invasive • Point measurement	• $\pm 0.02\ m^3\ m^{-3}$ for calibration to a specific soil type
Neutron moderation method	• Permits frequent or continuous measurement at the same points.	• Invasive • Time consuming • Can't be used near surface • Radiation Hazard • Random error in counting • High labour costs • Point measurement	• Can be as good as 2 mm standard deviation in a total water content of 450 mm (Marshall *et al.*, 1996)
Microwave remote sensing	• Non-invasive • Better for larger area analyses • Potential for large volume of data. • Direct relations between VMC and parameters.	• Only measures surface moisture • Depth of moisture estimation tends to be unknown • Can be sensitive to roughness and vegetation. • Integrates soil moisture over large areas and is therefore of little use for small scale variations.	• Unknown

Table 2.1: Brief summary of advantages, disadvantages and accuracy of some current soil moisture measurement techniques (references are found in the text).

2.5.3 Remote sensing of soil moisture

Remote sensing may be taken to mean the observation of, or gathering information about, a target by a device separated from it by some distance (Cracknell and Hayes, 1991).

Although there are many varied forms of remote sensing, microwave techniques have been most commonly applied to soil moisture sensing applications. It is possible that microwave remote sensing could lead to a better knowledge of watershed soil surface moisture (i.e. average values and time-space variations), in order to progress with flow forecasting (Benallegue *et al.*, 1994). The theoretical basis for measuring soil moisture using microwave techniques is based on the large contrast between the dielectric properties of liquid water and of dry soil (Engman and Chauhan, 1995). The moisture content of a soil is a major determinant of the soil's spectral response (Foody, 1991). There are two modes of microwave remote sensing: active and passive.

Active methods or radars send and receive a microwave pulse and the power of the received signal is compared to that which was sent to determine the back scattering coefficient which is then related to the characteristics of the target (Jackson *et al.*, 1996). For the active microwave approach over a bare soil, the measured radar backscatter, σ_s , is related directly to soil moisture and is written in functional form as

$$\sigma_s = f(R, a, \theta_v) \tag{2.12}$$

where R is a surface roughness term, a is a soil moisture sensitivity term, and θ_v is the volumetric soil moisture (Engman and Chauhan, 1995).

For passive microwave remote sensing of soil moisture from a bare surface, a radiometer measures the intensity of emission from the soil surface (Engman and Chauhan, 1995). This emission is proportional to the microwave brightness temperature T_B (the product of the surface temperature and the surface emissivity):

$$T_B = t(H)\times[rT_{sky} + (1\text{-}rT_{soil})] + T_{atm} \tag{2.13}$$

where t(H) is the atmospheric transmissivity for a radiometer at height H above the soil, r is the smooth surface reflectivity, T_{soil} is the thermometric temperature of the soil, T_{atm} is the average thermometric temperature of the atmosphere, and T_{sky} is the contribution from the reflected sky brightness (Engman and Chauhan, 1995).

According to Jackson *et al.* (1996) there are no satellite systems in operation that are truly capable of reliable soil moisture measurement. Providing surface soil moisture on an

operational global basis from a satellite platform involves solving one of the critical problems in long wavelength passive microwave radiometry: the problem of ground resolution (Jackson *et al.*, 1995). The relationship between emissivity and soil moisture depends on the dielectric contrast across the air-soil interface and this results in some uncertainty as to exactly how thick the soil layer is for determining the dielectric constant (Engman and Chauhan, 1995). The longer the wavelength the thicker is the layer of soil which actually contributes to the emission (Paloscia *et al.*, 1993) although generally remote sensing techniques, at best, detect only surface conditions; usually the top 5 to 10 cm (Topp *et al.*, 1980).

Experimental results have shown that the effect of roughness is to increase the emissivity and reduce the sensitivity to soil moisture content (Paloscia *et al.*, 1993). This may not be a serious limitation for passive sensors but is a major factor for radar (Engman and Chauhan, 1995). Vegetation attenuates the microwave emission from the soil; it also adds to the total radiative flux with its own emission and the effect of vegetation is greatly dependent on the instrument incidence angle, frequency, and polarisation (Engman and Chauhan, 1995). Furthermore, theoretical scattering models are limited (Chen *et al.*, 1995) and as yet there is need to develop algorithms to extract VMC directly from the microwave measurement (Engman and Chauhan, 1995).

In addition to limitations associated with investigations of the vertical resolution of soil moisture fields, remote sensing techniques are also limited to investigations of large scale variability. For example, the sensors integrate the microwave signal over an area of the land surface which means that the measurement process smoothes out small-scale soil moisture variations (Western *et al.*, 1998). Soil moisture differences caused by geomorphological features, for example, can cause systematic measurement differences that are not measured by the remotely sensed data but do influence the measured field averages (van Oevelen, 1998). Such problems limit the use of remote sensing techniques in the study of the nature of spatial variability of soil moisture for hydrological purposes.

2.6 VARIABILITY AND SCALE

The observability problem alluded to earlier is particularly acute for subsurface flow processes where most measurement techniques can give only a very local indication of

the hydrological response (Beven, 1997). A notable feature of the subsurface environment is its heterogeneity (McLaughlin *et al.*, 1993). The accurate determination of soil moisture over large areas is a difficult problem using conventional in-situ approaches because of the small scale variability of soil moisture (Schmugge and Jackson, 1997). The large spatial and temporal variability that soil moisture exhibits in the natural environment is precisely the characteristic that makes it difficult to measure and use in earth science applications (Engman and Chauhan, 1995). What is needed are high-resolution observations of soil moisture patterns based on a large number of point samples allowing reliable examination of whether spatial organisation of soil moisture is present in the landscape (Western *et al.*, 1999). Another important feature of the subsurface environment is its inaccessibility (McLaughlin *et al.*, 1993). Evidently, there is a need for techniques that can overcome these limitations.

Briefly, two considerations need to be made when selecting a measurement technique. First, the techniques rarely measure at the same scale as the process of interest. Whilst most of the techniques take point measurements, much of the variability in soil moisture may take place at larger scales due to the scale of variability in controlling factors, some small scale variability may be missed because the necessary sampling resolution can rarely be achieved. Furthermore, not enough is known about the nature of spatial variability in moisture at any scale. Surface modelling of spatially continuous field variables involves interpolation from the irregular spaced samples to a grid of points (Bonham-Carter, 1994); this is one way of integrating up to the scale of interest, but requires detailed information on the scales and nature of variability. Furthermore, for such geostatistical methods to be effective a large (over 100 samples) and representative sample is required (McBratney and Webster, 1986); a goal that is often not achievable given the time constraints of most current measurement techniques.

2.7 POTENTIAL OF GPR IN HYDROLOGY AND WATER RESOURCES

Because of the high spatial variability of soil moisture, existing intrusive ground based methods such as the neutron probe and TDR which provide point measurements, are unsuitable for mapping large areas (Chanzy *et al.*, 1996) because they yield insufficient data given the limited sampling (Davidson and Watson, 1995). One potential solution is ground penetrating radar. GPR is a proximal Remote Sensing tool, similar in principle to

TDR and *ThetaProbe*, used to investigate the subsurface from the surface. GPR profiles are non-destructive and can penetrate beyond the surface layer. Due to the rapid data acquisition, large areas can be covered in a short space of time and GPR can therefore be used to measure at a variety of scales, potentially bridging the gap between scales of observation. GPR profiles can be taken in both ground- and airborne-modes, which further increases this potential.

GPR has seen successful application in many areas of hydrological research including mapping depth to bedrock and other subsurface structural phenomena (e.g. Collins *et al.*, 1989), studies of soil microvariability (e.g. Collins and Doolittle, 1987), water table delineation (e.g. van Overmeeren, 1993) and, more rarely, studies of water content estimation (e.g. Chanzy *et al.*, 1996; van Overmeeren *et al.*, 1997). Its application to high-resolution mapping of subsurface moisture distributions has been limited by the fact that in reflection profiling mode no reliable parameter can be derived that has any real physical or dielectric meaning, and common mid-point (CMP) surveys, which can be used to determine the dielectric constant, are time consuming and inaccurate for detailed assessments.

Mapping of subsurface moisture patterns can be used to understand the controls on the distribution and the movement of subsurface moisture. Clearly, the technique offers the potential for many applications, which require knowledge of these distributions. Two examples are focused upon in the current research: mains water leak detection and spatio-temporal dynamics of soil moisture for hillslope hydrology investigations.

2.7.1 Mains water leak detection

According to OFWAT current leakage in England and Wales amounts to around 29% and the trend is rising (OFWAT, 1995). This figure could be larger in the centres of industrial cities due to the age of the mains (Wilkinson and Brassington, 1991). Rapidly escalating water and energy costs indicate a need to recover water through successful leak detection programs (Prasfika, 1994). Whilst numerous methods are available for detecting leaking sections of mains distribution networks using acoustic techniques and node metering, these methods only define the location of the leak within a single arm of the distribution network (Mulligan and Charlton, 1999). The use of GPR proposed here is as a means of

focusing on the actual location of a leak where metered losses and acoustic techniques suggest that one is present. By focusing on the location of a leak using non-invasive techniques, the expense and disruption of large scale excavation is avoided.

GPR has often seen application to the mapping of utility lines and buried tanks and pipes (e.g. Caldecott *et al.* (1988), Annan *et al.* (1984), Zeng and McMechan (1997)), and application to soil moisture estimation, as discussed above. Research into the application of GPR to the detection of mains water leaks has been limited, although the technique has been successfully applied to oil leaks (King, 2000) and to the location of DNAPL (dense non-aqueous phase liquids) plumes (Annan *et al.*, 1991). In 1996 King's College London and Thames Water Utilities Ltd. teamed up to assess the potential of GPR for the efficient detection of mains water leaks.

Mains water leakage is a specific situation involving changes in subsurface moisture. Because urban surfaces are relatively impermeable, the urban subsurface tends to be dry and so the presence of a large body of water will generally indicate a leak from mains water or waste water facilities. In the region around a leak the subsurface moisture can be expected to rise significantly above that of the background moisture under a pavement or road. Furthermore, depending on the host material and the rate of leakage, such leaks will form large water bodies with a relatively distinct wet-dry boundary. This property should make them ideal for detection using GPR.

GPR is most commonly applied through operator experience of the visual appearance of subsurface features on radargrams. This is subjective, prone to error and requires very high sampling densities. The approach adopted here is to combine this kind of approach with much more functional analysis of the characteristics of the radar returns and their relationship to the sub-pavement water content of the substrate. A better understanding of water distribution in simple and complex media, through GPR assessment of moisture distributions, should provide an increased understanding of how subsurface water distribution patterns under pavements or roads might indicate the presence of a leak. The objective is therefore to locate the water bodies associated with the presence of a mains water leak, not to detect the leak itself. These methods are more likely to provide a robust, repeatable and automatable solution for the location of mains water leaks.

2.7.2 Spatio-temporal evolution of hillslope soil moisture patterns

An important aspect of hydrological research is understanding the changes of soil moisture that take place either spatially or temporally, as has been discussed. GPR can be used to derive estimates of soil moisture and the patterns of moisture that develop as the soil profile wets and dries. By relating the derived VMC estimations to other characteristics, such as stone content and porosity, for example, it is possible to understand the controls on this distribution. The implications of these patterns for surface (overland flow) and subsurface (throughflow) flow can then be addressed. For example, moisture patterns, and their variation, may affect the relative amounts of each type of flow at the plot-scale, or even larger-scales (hillslope / catchment). This can be investigated using GPR. Because the GPR is a non-invasive, or non-destructive, measurement method it is possible to monitor changes in soil moisture and infer lateral hydrological fluxes without directly interfering with those fluxes.

CHAPTER THREE: PRINCIPLES OF GROUND PENETRATING RADAR

The work of Hülsenbeck in 1926 appears to be the first use of pulsed electromagnetic techniques to determine the structure of buried features (Daniels *et al.*, 1988). These techniques have been developed extensively since then. Over this period GPR has been used for a variety of investigations. These include detection of layers of discontinuous dielectric constant such as textural interfaces (Kung and Lu, 1993; Boll *et al.*, 1993); mapping of utility lines and buried tanks and pipes (Caldecott *et al.*, 1988; Annan *et al.*, 1984; Zeng and McMechan, 1997); investigation of internal erosion in embankment dams (Carlsten *et al.*, 1995); and various soil-based applications, such as mapping of soil and rock stratigraphy (Davis and Annan, 1989), mapping depth to bedrock (Collins *et al.*, 1989), and the study of soil microvariability (Collins and Doolittle, 1987) and soil thickness (Shih and Doolittle, 1984); as well as a host of uses in archaeology (Conyers and Goodman, 1997) and in other areas. The use of GPR for soil moisture estimation has been rather limited (e.g. Weiler *et al.* (1998), van Overmeeren *et al.* (1997)).

3.1 PRINCIPLES OF OPERATION

GPR measurements are based on the transmission and reflection of an electromagnetic wave in the studied medium (Chanzy *et al.*, 1996). The radar system causes the transmitter antenna (Tx) to generate a wavetrain of radiowaves which propagates away in a broad beam (Reynolds, 1997). Variation in the electrical properties of the subsurface cause part of the transmitted signal to be reflected and this reflected signal is detected by the receiver (Davis and Annan, 1989). Part of the signal is reflected wherever it encounters a change in electrical properties (Davis and Annan, 1986). Several waves may reach the receiver antenna (Figure 3.1): a direct air-wave, a ground-wave, reflected and refracted waves, critically refracted waves, and overhead reflections (Du and Rummel, 1994). The ground-wave is that propagating directly from the transmitter to the receiver through the ground (Du and Rummel, 1994), the air-wave is that which travels directly between the transmitter and receiver antennas, the reflected waves represent energy returned directly at a boundary while refracted waves occur when a change in electrical property is encountered and the wave travels along the interface and consequently arrives later than its corresponding reflected wave. Ibáñez-Garduño *et al.* (2000) interpret the first two continuous, intense, reflections visible on a radargram as the direct air-wave and

direct ground-wave respectively, which combined are known as the direct arrivals and constitute the near-field. These aspects of GPR response have a tendency to obscure genuine subsurface reflectors; a feature known as transmitter blanking (Annan, 1997).

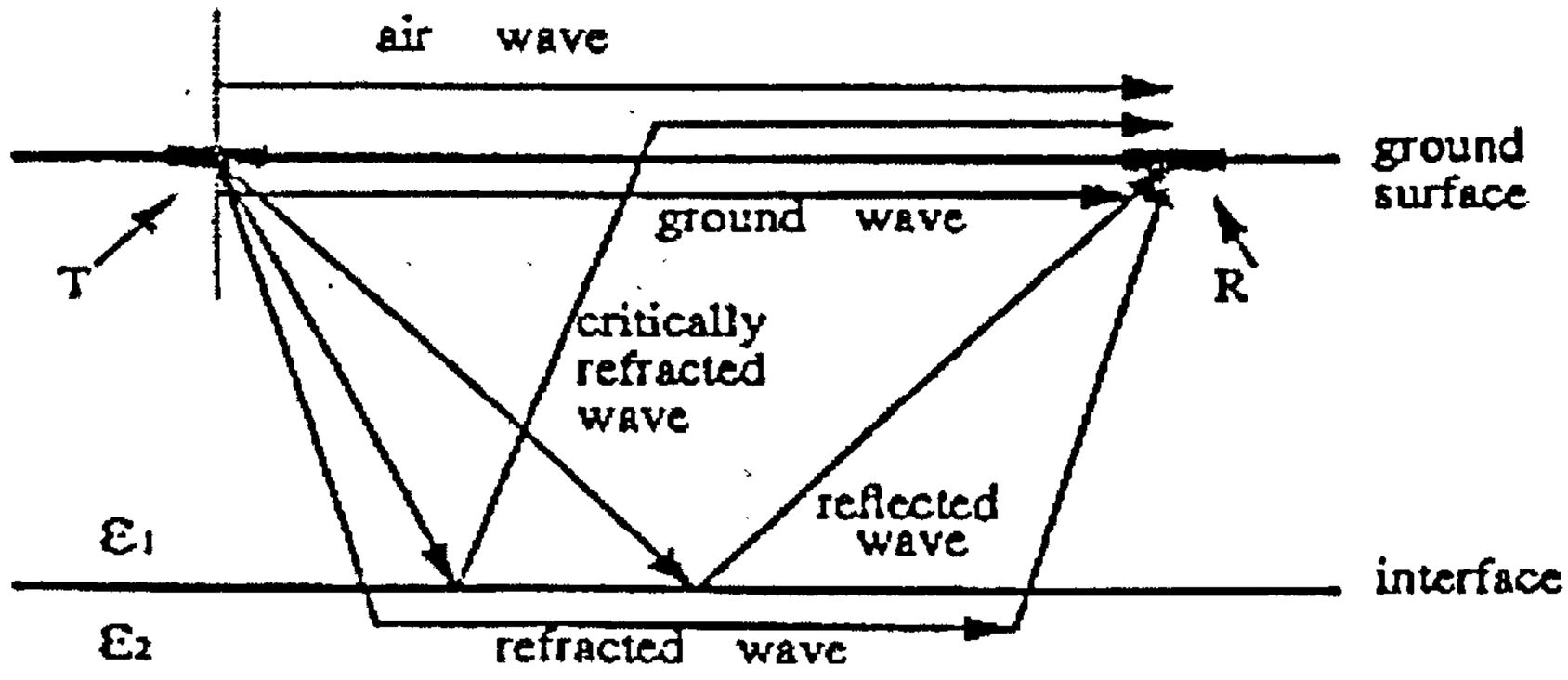

Figure 3.1: Waves reaching the receiver antenna (from Du and Rummel, 1994).

3.2 MODES OF DATA ACQUISITION

GPR is normally used in reflection profiling mode (Figure 3.2) which produces a section showing the travel time to the reflectors versus horizontal position (Davis and Annan, 1989). In this mode the radar antennae are moved over the ground surface simultaneously (Reynolds, 1997) and data can be recorded continuously (as rapidly as possible) or in stepped mode at precise locations. The depth to the reflectors is determined from the two-way travel time (TWTT) coupled with the signal propagation velocity in the ground, which must be obtained from independent velocity soundings (Davis and Annan, 1989). The wide angle reflection and refraction (WARR) sounding mode is the electromagnetic equivalent of seismic refraction and gives an independent estimate of the radar signal velocity versus depth in the ground (Davis and Annan, 1989). The transmitter is kept at a fixed location and receiver is towed away at increasing offsets (Reynolds, 1997). An alternative and preferable deployment for the same analysis is the common mid-point sounding (CMP) (Figure 3.3) where both the transmitter and receiver are moved apart (Reynolds, 1997). CMP is preferred because for WARR even slight dips in reflectors have a disturbing influence on velocity estimations and WARR acquisitions can thus lead to Root Mean Square (RMS) velocities that are systematically lower than the CMP

acquisitions (Tillard and Dubois, 1995). Derivation of velocity using CMP analyses is vital to the determination of VMC using radar as discussed in Chapter Four.

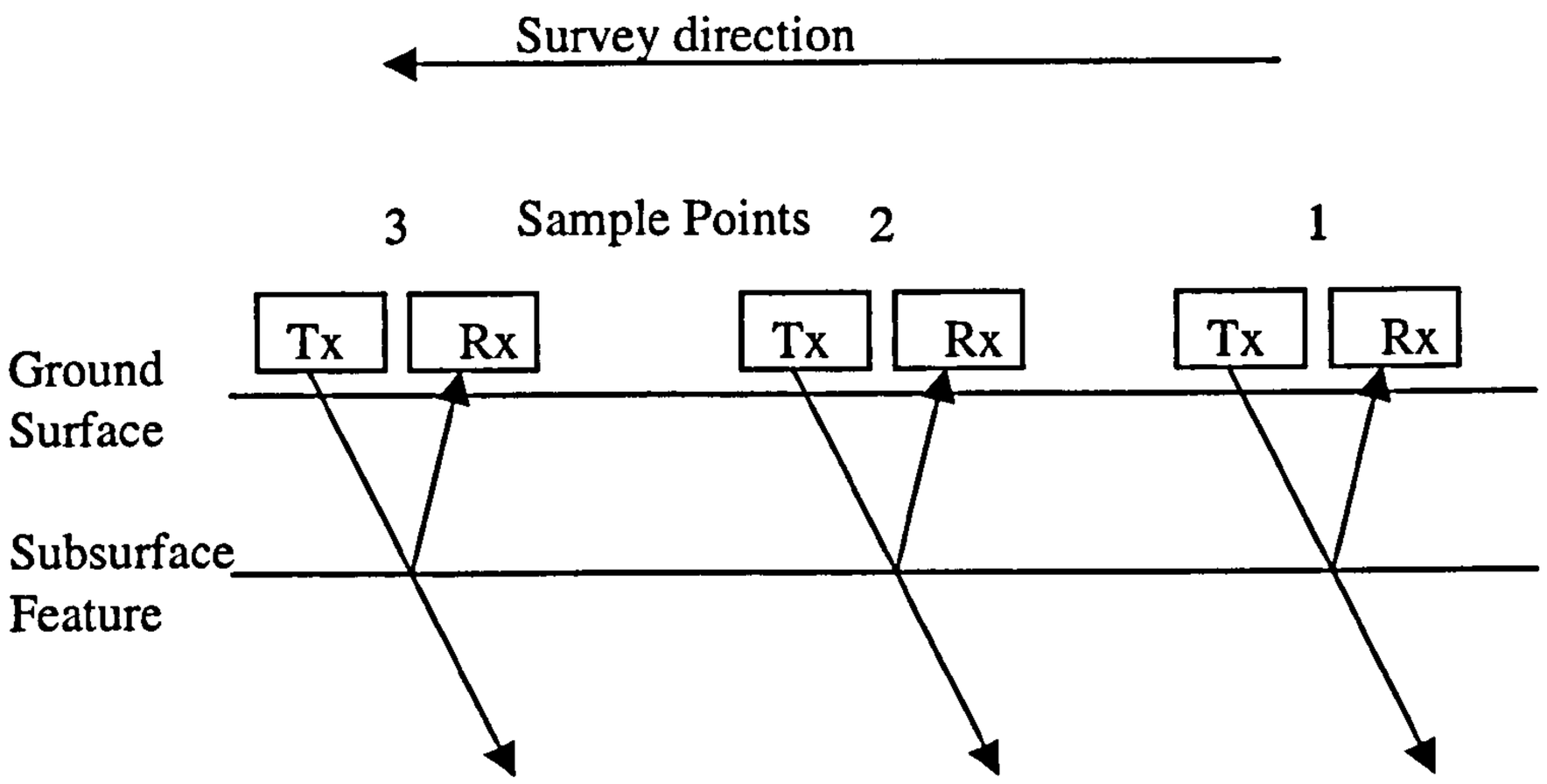

Figure 3.2: Schematic of reflection profiling mode.

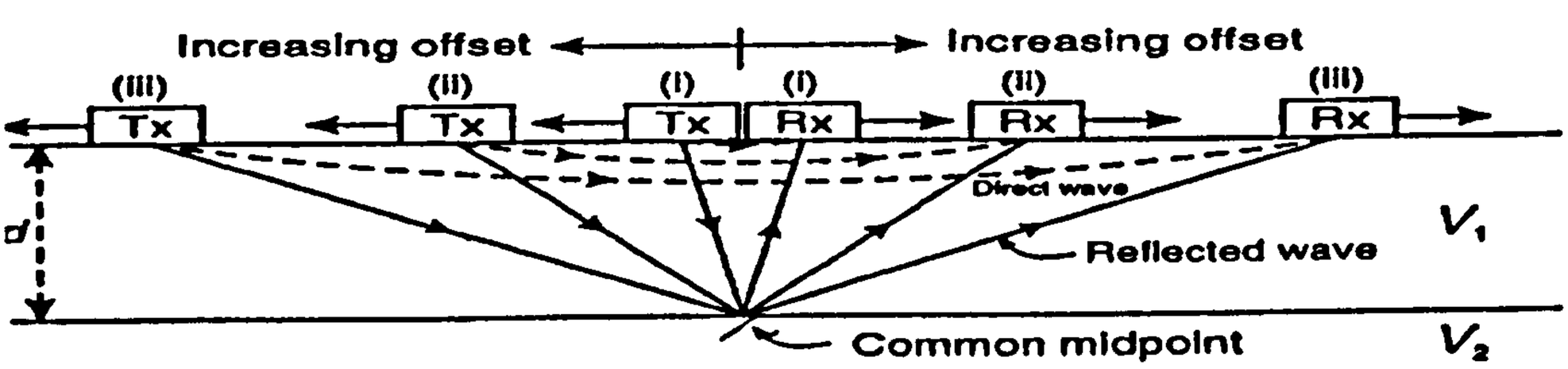

Figure 3.3: Common mid-point profiling (from Reynolds, 1997).

In transillumination mode (Figure 3.4) the transmitter and receiver are placed on opposite sides of the medium under investigation (Reynolds, 1997). This limits its applicability for most field situations where only the surface is accessible. In a zero offset gather (ZOG), measurements are taken at varying depths using the two antennas with no vertical offset and by picking the direct arrivals (Gilson *et al.*, 1996). A ZOG can be used as a stratigraphic logging technique to give profiles of electromagnetic wave velocity, relative dielectric constant and water content (Gilson *et al.*, 1996). Alternatively, in multiple offset gathers (MOG) one antenna is kept at a fixed depth while the second is moved incrementally (Gilson *et al.*, 1996). Transillumination mode is useful in borehole sounding or where the internal structure of an object needs to be known (e.g. for checking

for faults in walls or bridges). It can also be used to determine velocity through a material or structure and hence VMC.

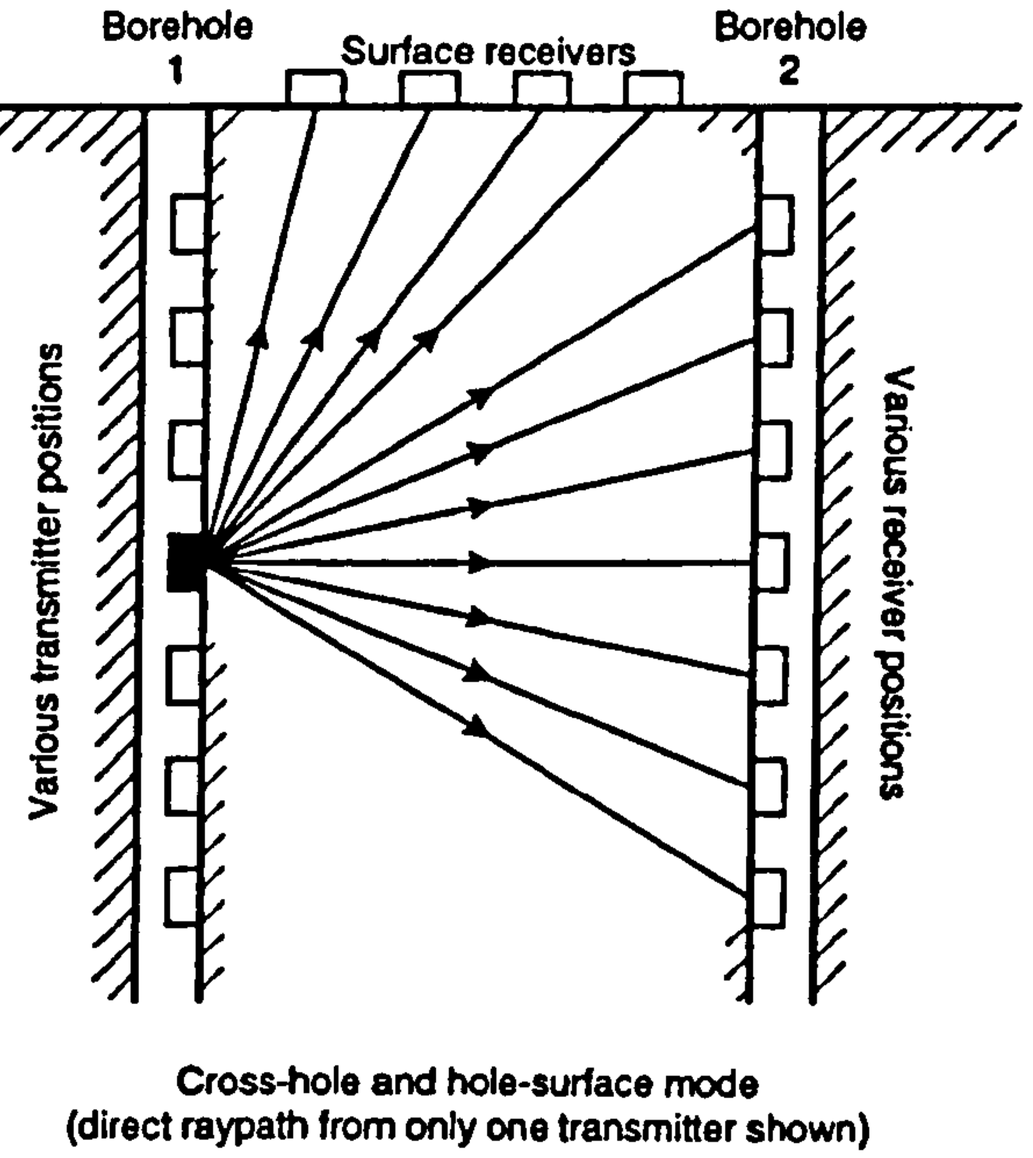

Figure 3.4: Transillumination mode (from Reynolds, 1997).

3.3 PROPAGATION OF RADIOWAVES

3.3.1 Theory

Ground radar radiation is electromagnetic radiation and its propagation is described by Maxwell's equations (Reynolds, 1997). These are treated in detail by Carcione (1996) and Greaves *et al.* (1996) within the context of GPR studies and the reader is referred to these sources for more detailed information.

Velocity and attenuation are the factors that describe the propagation of high-frequency radio waves in the ground (Davis and Annan, 1989). The speed of radiowaves (V_m) in any medium is dependent upon the speed of light in free space (c = 0.3 m/ns), the relative dielectric constant (ε_r) and the relative magnetic permeability (μ_r = 1 for non-magnetic materials) and is given by (Reynolds, 1997):

$$V_m = c / \{ (\varepsilon_r \mu_r / 2) [(1 + P^2) + 1] \}^{1/2} \qquad (3.1)$$

where P is the loss factor, such that $P = \sigma / \omega\varepsilon$, and σ is the conductivity, $\omega = 2\pi f$ where f is the frequency, ε is the permittivity $= \varepsilon_r\varepsilon_0$ and ε_0 is the permittivity of free space (8.854×10^{-12} F/m).

Radar signal velocity in low-loss geological materials ($P \approx 0$) which are amenable to radar sounding is related to the real part of the dielectric constant by (Davis and Annan, 1989):

$$V_m = c / \varepsilon_r^{1/2} \quad (3.2)$$

The success of the GPR method relies on the ability of the ground to allow the transmission of radiowaves and it is the contrast in relative dielectric constant between adjacent layers that gives rise to reflection of incident electromagnetic radiation (Reynolds, 1997). The greater the difference between the relative dielectric constant of materials in the subsurface, the larger the amplitude of reflection generated; this can be quantified using the amplitude reflection coefficient (R) (Conyers and Goodman, 1997):

$$R = (\varepsilon_1^{1/2} - \varepsilon_2^{1/2}) / (\varepsilon_1^{1/2} + \varepsilon_2^{1/2}) \quad (3.3)$$

where ε_1 and ε_2 are the relative dielectric constants in layers 1 and 2 respectively. This equation assumes no other signal losses (Reynolds, 1997). The power reflected is R^2 and this decreases as the thickness of a layer or object decreases depending on the layer thickness and signal wavelength in the medium (Davis and Annan, 1989). The roughness of the interface between two materials also affects the reflected signal power (Davis and Annan, 1989).

3.3.2 Energy loss and attenuation

As radiowaves travel through the ground there are a number of ways in which the signal energy is reduced. These are depicted schematically in Figure 3.5. The most obvious of these has already been discussed: reflection at a dielectric interface. This reduces the signal energy available for deeper reflection events. Energy is also lost as heat and by the geometrical spreading of the transmitted energy. The radar signal is transmitted in a beam with a cone angle of 90° and as the signals travel away from the transmitter, they spread

out causing a reduction in energy per unit area at a rate of $1/r^2$, where r is the distance travelled (Reynolds, 1997). This geometrical spreading has important consequences for the subsequent interpretation of the returned data because it means the response is from an average area rather than a point measurement. This footprint issue is discussed later. Scattering by inhomogeneities also plays a role (Doolittle and Collins, 1995). Mie scattering, which causes clutter noise on the radar section, occurs if there are objects with dimensions of the same order as the wavelength of the radar signal (Reynolds, 1997). Scattering of electromagnetic waves is also dependent upon the geometrical shape of the pore volume that contains the water (Shen *et al.*, 1985). Scattering from thin layers or point-type objects like boulders decrease the radar signal amplitude and these losses are often included in the attenuation term (Davis and Annan, 1989).

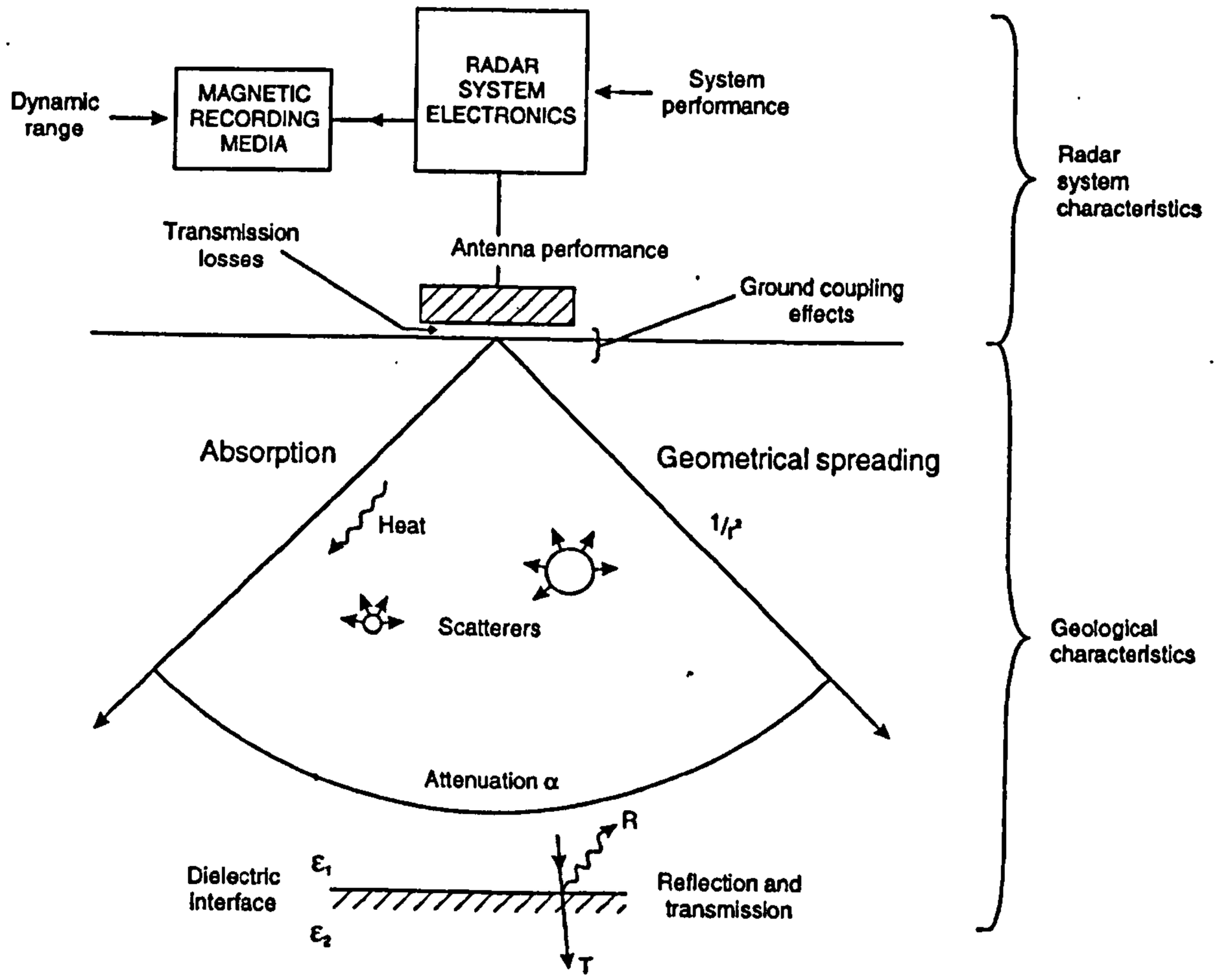

Figure 3.5: Processes that lead to reduction in signal strength (from Reynolds, 1997).

Signal attenuation at the desired antenna operating frequency is a major consideration when assessing the appropriateness of using GPR (Doolittle and Collins, 1995). The

attenuation factor (α) is dependent upon the electric (σ), magnetic (μ) and dielectric (ε) properties of the media through which the signal is propagating as well as the frequency of the signal itself (Reynolds, 1997):

$$\alpha = \omega\left\{\left(\frac{\mu\varepsilon}{2}\right)\left[\left(1+\frac{\sigma^2}{\omega^2\varepsilon^2}\right)^{1/2}-1\right]\right\}^{1/2} \qquad (3.4)$$

where $\omega = 2\pi f$ where f is the frequency (Hz), μ is the magnetic permeability ($4\pi\times10^{-7}$ H/m), σ is the bulk conductivity at the given frequency (S/m), and ε is the dielectric permittivity where $\varepsilon = \varepsilon_r \times 8.85\times10^{-12}$ F/m and ε_r is the bulk relative dielectric constant. The formula is valid for non-magnetic materials only.

In a low-loss medium, attenuation is most usefully expressed (Davis and Annan, 1989) by

$$\alpha = (1.69\times10^3 \cdot \sigma) / \varepsilon_r^{1/2} \text{ in dB/m} \qquad (3.5)$$

where $\sigma = \sigma$d.c. + $\omega\varepsilon''\varepsilon_0$ combines both d.c. conductivity and dielectric losses.

Radars operate at frequencies where the capacitive properties dominate the conductive properties and thus attenuation remains essentially constant at different conductivities (Davis and Annan, 1989). Soil water is an important factor affecting the attenuation properties of a soil. The attenuation of signals in soils and building materials increases with increased frequency and is largely dependent on water content (Olver and Cuthbert, 1988) and so can be used as an estimator of soil moisture. Other factors influencing signal attenuation include the concentration of dissolved salts in the soil solution and the amount or type of clay present. Furthermore, interactions between these two components are also important. Ions absorbed on clay particles undergo exchange reactions with ions in the soil solution and contribute to the electrical conductivity of the soil (Doolittle and Collins, 1995). The role of attenuation is significant both for GPR use and subsequent interpretation. The degree of attenuation present in a material determines the achievable depth of penetration. Furthermore, if attenuation is high then the reflected signal will be too weak to be detected by the receiver (Olver and Cuthbert, 1988) and consequently a given interface may never be detected.

3.3.3 Range, penetration and resolution

As well as attenuation, other characteristics of the system affect the achievable depth of penetration. These characteristics are all interrelated and force a GPR operator to strike a balance between penetration depth and vertical resolution. To ensure a suitable depth of penetration, system performance, Q, should be as large as possible (Davis and Annan, 1989). It is defined as:

$$Q = \frac{\xi_T \xi_R G_T G_R g \sigma_c e^{-4\alpha L}}{64\pi^3 f^2 L^4} \tag{3.6}$$

where Q is system performance or ratio of the transmitter signal amplitude to the minimum receiver sensitivity, ξ_T is transmitter antenna efficiency, ξ_R is receiver antenna efficiency, G_T is transmitter antenna gain, G_R is receiver antenna gain., L is distance to target, α is attenuation of medium, f is frequency, g is backscatter gain of target, and σ_c is target scattering cross-sectional area. Penetration depth in homogeneous media is mainly determined by wavelength λ (m):

$$\lambda = c/(f\sqrt{\varepsilon_r}) \tag{3.7}$$

and as a result, penetration depth of the ground-wave decreases with increased antenna frequency and increased soil moisture (Du and Rummel, 1994) through its effect on the dielectric constant. Whereas the depth of penetration of the radar in rocks and dry soils is usually some tens of metres, it is considerably less if the soil is wet, especially in the case of wet clayey soils, which generally have a high conductivity (Wensink, 1993). One means of enhancing the depth of penetration is to use a lower frequency antenna because attenuation decreases with falling frequency (Wensink, 1993). It is easier to put more power into the transmitted pulse at lower frequencies, which increases Q and thus the range (Davis and Annan, 1989). However, because of the accompanying increase in wavelength, the resolving power is reduced (Wensink, 1993). Where high resolution is preferred it can be increased by increasing the bandwidth; this requires that the centre frequency of the radar be increased (Davis and Annan, 1989).

Vertical resolution is the ability of the signal to distinguish two signals that are close to each other in time (Davis and Annan, 1989) and is a function of frequency (Reynolds, 1997). The maximum theoretical resolution (z) can be taken as ¼ of the pulse wavelength of incident radiation (Reynolds, 1997):

$$z = v/(4f) \tag{3.8}$$

The pulse envelope encloses the oscillatory radar pulse and if the travel time to two individual targets is similar, the pulses (and the envelopes) overlap (Annan, 1997). It is generally accepted that the two events can be distinguished as opposed to having one large event if the targets are separated in time by a time difference of half the envelope width (Annan, 1997).

Horizontal resolution is inversely proportional to the square root of the attenuation and consequently it is better over a high loss material than over a low loss material (Reynolds, 1997). Spatial resolution is also affected by the conical beam width of the downgoing radiowaves (Reynolds, 1997). Radiation fore and aft from the antenna is usually greater than to the sides, making the illumination pattern on a horizontal subsurface plane approximately elliptical in shape meaning that the footprint is always looking not only directly below the antenna but also in front, behind and to the sides as it travels across the ground (Conyers and Goodman, 1997). Consequently, the radar response is from an area beneath the radar, not a discrete point and this increases with depth below the radar (Figure 3.6). Horizontal resolution is better over a high loss medium because increased dielectric constant and conductivity decrease the spreading of the signal (Annan, 1997, Conyers and Goodman, 1997):

$$A = (\lambda/4) + (D/(\varepsilon^{1/2}-1)) \tag{3.9}$$

where A is the long dimension radius of footprint, D is depth (z), and is λ wavelength (so that increasing frequency decreases footprint dimensions by decreasing wavelength). All units are metres. The narrower the beam width, the greater will be the spatial resolution (Reynolds, 1997). The elliptical footprint can be converted to an approximate measurement area using equation 3.10 and volume using Equation 3.11:

$$Area = \pi \times A \times (A/2) \tag{3.10}$$

$$Volume = Area \times (D/3) \tag{3.11}$$

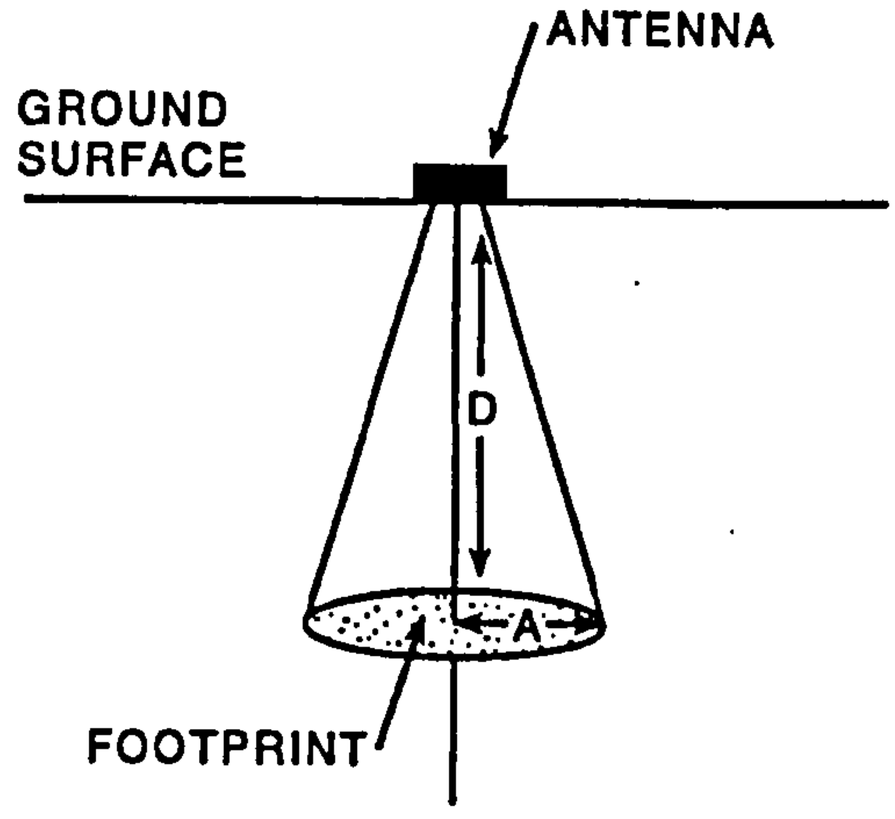

Figure 3.6: Schematic of GPR footprint (from Conyers and Goodman (1997)). D is depth (m) and A is long dimension distance (m).

3.4 DIELECTRIC PROPERTIES OF EARTH MATERIALS

As already mentioned, reflections are generated with each change in electrical properties, or more particularly with changes in the dielectric constant. For example, reflections from subsurface sediment boundaries are caused by contrasts in the dielectric properties of different sediment types or grain sizes (Jol and Smith, 1992). For most geologic materials, ε_r lies in the range 3-30 and consequently the range of radiowave velocities is large (Reynolds, 1997). Table 3.1 summarises a selection of dielectric constant values for a variety of geological materials. Notably the dielectric constants for most geologic materials tend to range between 2 and 8 unless wet. Consequently, variations in the electrical properties of soil are usually associated with changes in volumetric moisture content (Davis and Annan, 1989). Therefore, it should be possible to use the GPR to derive estimates of soil water content.

Material	Dielectric Constant	Signal Velocity (m ns^{-1})
Air	1	0.30
Fresh Water	80	0.033
Sea Water	80	0.01
Dry Sand	3-6	0.12-0.17
Wet Sand	25-30	0.055-0.060
Wet Silt	10	0.095
Dry Clay Soil	3	0.173
Wet Clay	8-15	0.86-0.110
Average 'soil'	16	0.075

Table 3.1: Dielectric constant and signal propagation velocity for geological materials (adapted from Reynolds, 1997).

3.4.1 Dielectric behaviour

The most important parameters affecting the dielectric response of geologic materials are generally thought to be porosity, clay content, water saturation and measurement frequency although there is little agreement as to the specific form of the dielectric property-hydrogeologic property relationships due to scatter in experimental data (Knoll and Knight, 1994). The dielectric value is a measure of the ability of a material to store a charge for a given applied field strength, while dielectric loss is a measure of the proportion of the charge transferred in conduction and stored in polarisation (Saarenketo, 1998). The application of an electric field causes all the positive charges to move along the direction of the field and all the negative charges to move in the opposite direction, so that the material now contains a large number of dipoles, which are defined as pairs of equal, but opposite point-charges which are arbitrarily close (Nussbaum, 1966). A dielectric in which this charge displacement has taken place is said to be polarised, and its molecules are said to possess induced dipole moments, which produce their own field adding to that of the external charges (Lorrain and Corson, 1979). There are three basic polarisation processes (Lorrain and Corson, 1979): (i) induced or electronic polarisation, in which the centre of the negative charge in a molecule is displaced, relative to the centre of positive charge, when an external field is applied; (ii) orientational polarisation, in which molecules with a permanent dipole moment tend to be aligned by an external field, the magnitude of the susceptibility being inversely proportional to the temperature; and (iii) ionic polarisation which occurs in ionic crystals.

The dielectric behaviour of a material is described in terms of its complex permittivity (ε^*) and complex conductivity (σ^*), which are interrelated (Reynolds, 1997):

$$\varepsilon^* = \varepsilon' + i\varepsilon'' \text{ (for a non-conductive material)} \quad (3.12)$$

$$\varepsilon^* = \varepsilon' + i(\varepsilon'' + \sigma_s / \omega\varepsilon_0) \text{ (for a material with conductivity)} \quad (3.13)$$

$$\sigma^* = \sigma' + i\sigma'' = j\omega\varepsilon_0\varepsilon^* \quad (3.14)$$

where ε' denotes the real part of the dielectric value, ε'' denotes the imaginary part and ω is a frequency term (Saarenketo, 1998). ε' is a measure of the amount of polarisation in a material (Knight and Nur, 1987). The ratio of ε^* to ε_0 is known as the complex relative dielectric permittivity of the medium (Shen *et al.*, 1985). The imaginary part of the dielectric value represents energy loss and both the ionic conductivity and relaxation effects contribute to these losses (Sabburg *et al.*, 1997).

Overall the apparent dielectric constant at a given water content is a function of many factors including: (i) frequency, temperature and salinity; (ii) volumetric moisture content; (iii) the ratio of bound water to volumetric moisture (θ_{bw}/θ_v), which is related to the soil surface area per unit volume; (iv) the bulk density; (v) the shape of the soil particles; and (vi) the shape of the water inclusions (Paltineanu and Starr, 1997).

At a given water content, ε_{er} (effective relative dielectric constant) increases with decreased frequency, the increase becoming more pronounced below ~25 MHz (Wensink, 1993). At radar frequencies, various dielectric dispersion processes occur and, in moist soils, the most important are ionic conductivity and bound-water relaxation (Carcione, 1996). At lower frequencies, ionic conductivity effects will predominate causing the dielectric loss factor to vary inversely with frequency (Sabburg *et al.*, 1997). At frequencies below ~10^{13} Hz, there is also a contribution from atomic polarisation (Knight and Nur, 1987). At higher frequencies polarisation losses become dominant (Sabburg *et al.*, 1997).

At frequencies $\geq$ 1000 MHz the values of ε_{er} are insensitive to salinity, mineralogy and other soil properties but with decreasing frequency ε_{er} is seen to depend on salinity (represented by conductivity) to an increasing degree (Wensink, 1993). Furthermore, most studies using GPR are conducted at frequencies less than 1000 MHz and consequently these effects can be expected to be relatively significant. Salt content often

increases with clay fraction and, therefore, clay soils would be expected to possess higher ionic conductivity producing greater signal loss at lower frequencies (Sabburg *et al.*, 1997).

Although Roth *et al.* (1992) claim that relationships of VMC vs DC for mineral soils do not vary substantially between soils of different texture or structure, work by Sabburg *et al.* (1997) suggests that the real part of the soil dielectric constant is roughly proportional to sand content and inversely proportional to clay content. Dielectric constants of organic soil samples and materials measured at a variety of moisture levels were lower when compared with mineral soils (Roth *et al.*, 1992). Dry rocks have negligible dielectric loss and the real part of the relative dielectric permittivities of these rocks is practically frequency-independent in the 800-1200 MHz frequency range (Shen *et al.*, 1985). Dielectric constant increases with compaction if samples are dry, and decreases with compaction if fully saturated (Knoll and Knight, 1994).

3.4.2 Dielectric properties of water in soils

The variation of soil dielectric properties is determined principally by moisture content and the proportion of water that is held in bound states (Sabburg *et al.*, 1997). Changing pore fluid from air to water results in an enhancement in measured dielectric constant of the bulk material (Knoll and Knight, 1994). This is due to the fact that the dielectric constant of water is substantially higher (Table 3.1) than that of most other geological materials and it is also highly attenuating. At frequencies higher than ~25 MHz, ε_{er} increases with water content and σ_e is a function of water content, increasing with water content irrespective of wet density (Wensink, 1993).

The arrangement of electrons in the water molecule gives it electrical asymmetry such that although the molecule has no net charge, it is an electrical dipole with each hydrogen atom having a partial positive charge and the oxygen atom a partial negative charge (Hillel, 1980). Consequently, water has a dipole moment, which is a measure of the tendency of a polar molecule to orient itself in an electrical or magnetic field (Hillel, 1980). The strong intermolecular forces in liquid water are caused by the electrical polarity of the water molecule (Hillel, 1980). The large dielectric constant of water in an

electrostatic field is attributable to the orientation of the dipole moments (Lorrain and Corson, 1979).

The dielectric constant of water in soils depends on the degree of bonding of the water molecules around the soil particles (Saarenketo, 1998). Free water may be expected to have similar dielectric properties to those of pure water, but the relaxation time of bound water must be longer than that of pure water because of the stronger forces linking the bound water molecules to their environment, and to that extent bound water may be considered as 'ice-like' (Grant *et al.*, 1978). Consequently, the dielectric constant of bound water is much less than that of free water, and hence the effects of the latter will dominate (Sabburg *et al.*, 1997). At frequencies higher than ~25 MHz, ε_{er} increases with VMC, indicating that ε_{er} is mainly determined by the relaxation of the free pore water (Wensink, 1993) while the dependence of ε' and ε'' on soil textural composition is a consequence of the role played by bound water (Peplinski *et al.*, 1995).

The electrical properties of water within soil are not the same as for the same water after extracting it from the soil because the viscosity and ion content of water in soil are not the same (Saarenketo, 1998). When soil minerals are exposed to water, exchangeable ions go into solution, forming an ionic halo around the particles and contributing to electrical conduction (Saarenketo, 1998). The presence of salts in the soil water directly influences the dielectric behaviour of soils, especially at frequencies <30 MHz (Paltineanu and Starr, 1997) but ε' is not as sensitive to the salinity of the formation water as is the d.c. conductivity (Shen *et al.*, 1985).

3.5 SUMMARY

In this chapter the basic principles of GPR operation and the fundamental applicable physics have been outlined. With regards to the estimation of soil moisture using direct methods a number of useful signal characteristics can be identified, which may be useful in VMC determination. The principal effect is the generation of reflection events because of changes in dielectric constant associated with changing moisture conditions. Of equal importance are the effects of water on signal attenuation. A measurement of signal attenuation may offer a robust means of VMC estimation. To enhance this potential for near surface moisture distributions, a higher antenna frequency can be used because

higher frequencies are more susceptible to signal loss. However, many other aspects of the subsurface environment and the GPR system used for the survey affect the GPR response. In the following chapter the potential methods of deriving moisture content using different aspects of the GPR response are reviewed, with a view to establishing those that may be most useful for the direct assessment of VMC.

CHAPTER FOUR: GPR AND SOIL MOISTURE DETERMINATION

4.1 INTRODUCTION

GPR has the potential for rapid soil moisture assessment and the idea of determining moisture with GPR was first proposed by Ulriksen (1982, cited in Du and Rummel, (1994)). However, very little research has centred on using GPR as an *in situ* water detector (Weiler *et al.*, 1998) even though the dielectric constant is dramatically affected by water. Furthermore, although recent research has focused on developing more direct, potentially more robust and less time consuming radar techniques such as using the actual trace amplitude data, the majority of soil moisture surveys using GPR utilise CMP velocity analyses as the means by which moisture can be derived. To provide a quantitative interpretation of a trace, some signal characteristics must be chosen that will be related to soil moisture (Chanzy *et al.*, 1996). This section aims to outline those characteristics that have been, and can be, used to estimate soil moisture using GPR. This requires an understanding of the characteristics of a GPR signal and an understanding of potential GPR response to moisture.

4.2 CONCEPTUALISING GPR RESPONSE

4.2.1 The PulseEKKO 1000A GPR system

For this study a PulseEKKO 1000A GPR system (Sensors and Software Inc., Figure 4.1) has been used because, for laboratory research, its bistatic (separate transmitter and receiver) antenna system enables all modes of data acquisition and using two antennas separated by a small distance significantly improves the signal-to-noise ratio (Davis and Annan, 1989). Two antenna frequencies have been used, 900 and 450 MHz, because they are most appropriate for near surface studies requiring a reasonable level of vertical resolution, such as near surface soil moisture monitoring. Antenna frequencies of 225 and 1200 MHz are also available.

Figure 4.1: The Sensors and Software Inc. PulseEKKO 1000A GPR system. Shows (from left to right) 450 MHz antennae, console unit, and 900 MHz antennae connected to transmitter, receiver, cables and adjustable handle.

4.2.2 General characteristics of GPR response

A radar return is a time-varying signal (an electrical voltage which varies with time (Connor, 1982) that comprises a series of reflected versions ('events') of the transmitted pulse ('wavelet') whose characteristics, more or less complex, are dependent on specific aspects of the system. For interpretation it is important to know the form of the transmitted pulse (Reynolds, 1997). The PulseEKKO 1000A system transmits a signal whose characteristics can largely be controlled by the user. This signal can be triggered continuously in time, with a time delay, or triggered by the operator. The transmitter produces a minimum duration, high voltage pulse (Davis and Annan, 1989) and the antenna is then designed to radiate this signal with fidelity so that the pulse that is entering the ground is a reasonable facsimile of the electronically generated pulse (Annan, 1997). The transmitted pulse of the PulseEKKO GPR systems reduces to a wavelet in time that has three half cycles with relative amplitudes of [1, -2, 1] or [-1, 2, -1] depending on polarity which is defined based on the sign of the voltage of the first half cycle (Sensors & Software Inc. 2001). Although the GPR is supposed to return replicas of the transmitted pulse when part of the signal is reflected (Annan, 1992), the received waveform will be an attenuated version of the transmitted waveform that acquires a random phase (and perhaps a random amplitude) on reflection (Van Trees, 1968). In general, the electronics and antenna form an interactive pair which, combined with ground conditions, govern the shape and frequency of the radiated pulse (Annan, 1997).

Each time the signal is transmitted and received the amplitude data are recorded as a single radar trace (see Figure 4.2). Received continuous analogue signals are sampled in time based on a selected sampling interval and plotted as amplitude against two-way travel time (TWTT) in graph mode or as a series of traces at position x (or trace number) against TWTT. Returned radar signals (A-scans (see Figure 4.2)) at each point where the GPR is placed are used to form a 2-D electromagnetic transect (the B-scan images) (Boryssenko *et al.*, 2000). This display is analogous to a seismic section (Reynolds, 1997) with a sequence of reflection amplitude observations recorded and plotted over successive increments of time; namely, a time series (Burt and Barber, 1996). Amplitudes are measured in microvolts (uV) and can be digitised and recorded as 16-bit integers (-32768 to 32767) known as digital numbers (DN) (Chanzy *et al.*, 1996). It is also possible to output individual traces with the actual microvolt values.

The time window (TW) is defined as the amount of time, measured in nanoseconds (ns), that the receiving antenna will listen to and record the reflected radar-wave energy (Conyers and Goodman, 1997). Too short a time window could mean that the desired target or depth is not reached, while too long a time window will increase survey time but will ensure that a target can be detected. The sampling interval is dependent on the frequency of the antennas used with higher frequencies requiring finer time sampling (Sensors and Software Inc., 1996). Recommended sampling intervals for each frequency are shown in Table 4.1. With a finer sampling interval, vertical resolution is improved but survey time is increased. In noisy environments, one way of increasing data quality is to collect more than one trace at each survey position, average them and save the averaged trace (Sensors and Software Inc., 1996). This is 'stacking' and it increases the signal-to-noise ratio because noise, which is usually a random addition to the trace, tends to zero when averaged (Sensors and Software Inc., 1996). Increasing the number of stacks used may improve data quality but also increases survey time.

Centre Frequency (MHz)	Recommended Sampling Interval (ps)
225	400
450	200
900	100

Table 4.1: Recommended sampling intervals for antennae frequencies of 225, 450, and 900 MHz.

For this research the focus is on functional methods (methods which derive some aspect of the GPR signal that is a function of the VMC). Compared to visual methods, the actual requirement for detailed spatial and vertical sampling is less stringent for these methods although higher resolutions will result in improved data quality. For both visual and functional approaches, improvement of the signal-to-noise ratio, through increased stack size, is beneficial and vertical resolution, using an appropriate sampling interval, should be sufficient to ensure all parts of the received signal are sampled accurately. Overall, the data requirements for visual techniques are much higher. However, horizontal resolution for both visual and functional techniques should be determined by the likely variation in the subsurface variable of interest.

4.2.3 Measurement and analysis domains

A summary of the five basic visualisations of GPR (or Geophysical data) are shown in Figure 4.2. A signal may be represented in the time domain as a plot of instantaneous amplitude against time or in the frequency domain as a plot of its spectral component amplitudes versus frequency (Connor, 1982). Although closely related, the frequency of a system cannot be measured at a particular instant in time because frequency is a property of the system dependent on its actual evolution through time (Wishart, 1996). Therefore, data collected in the time domain have to be transformed into the frequency domain. This is achieved using a Fourier Transform. Using the Inverse Fourier Transform it is also possible to convert from the frequency domain back to the time domain. By decomposing a time series into time-frequency space, one is able to determine both the dominant modes of variability and how those modes vary in time (Torrence and Compo, 1998). As an alternative to the time and frequency domain representations, a third approach, collectively known as time-frequency methods, enables study of the behaviour of signals in both the time and frequency domains (Oonincx, 1997). It involves the transformation of the time domain data into the frequency domain to derive complex signal attributes and then transforms them back for visualisation in the time domain.

The GPR uses measurements in the time domain to measure variations through depth in the spatial domain (SD). The time scale can be converted to a spatial scale by multiplying one-way travel time by signal velocity. If velocity were constant through space, the time domain would be a perfect surrogate for the spatial domain. The potential vertical

variation of VMC requires explicit consideration of the spatial domain. Care must be taken to delineate carefully the time domain in terms of the spatial domain because changes in the nature of that space (e.g. a soil horizon, water content variability) affect dielectric constant and therefore signal velocity, and an equal increment of time may not represent an equal increment of space.

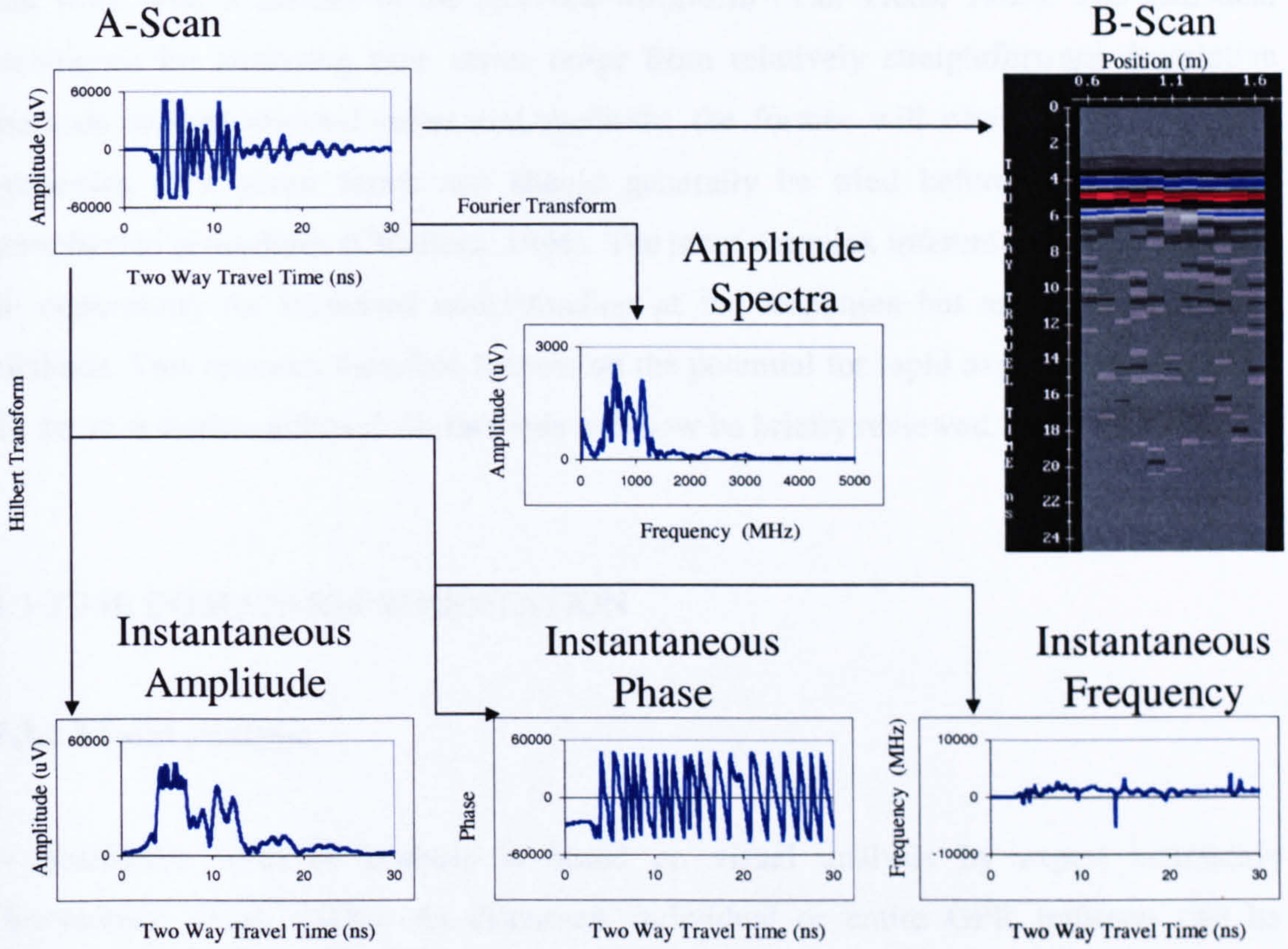

Figure 4.2: Schematic of GPR measurement and analysis domains. Time domain traces (A-scan) can be arranged by sample position (B-scan) and processed into frequency domain (amplitude spectra (Fourier Transform)), and time-frequency representations (instantaneous amplitude, phase and frequency (Hilbert Transform)).

4.2.4 Derivable signal characteristics

The three basic measurement and analysis domains (time, frequency, time-frequency) provide the five basic methods of signal response visualisation that are used in GPR and Geophysics (trace amplitude, amplitude spectra, instantaneous amplitude, instantaneous phase, and instantaneous frequency), whilst the fourth domain (spatial domain) places the signal response into the context of subsurface space. For discrimination, classification, or

detection, effective features must be extracted (Chen, 1986) and it is the main aim of this research to identify those that are most useful in analyses of VMC. Features with good physical meaning or representing some physical characteristics are intuitively appealing, but they may not be effective unless they can be properly quantified (Chen, 1986). Classical and modern time series methods not only provide valuable information directly, but also provide variables for feature extraction (Shiavi and Bourne, 1986). The problem of analysing a time series signal is greatly simplified if we can find a sufficient statistic and work with it instead of the received waveform (Van Trees, 1968). The statistical techniques for analysing time series range from relatively straightforward descriptive methods to sophisticated inferential methods; the former will often clarify the main properties of a given series and should generally be tried before attempting more complicated procedures (Chatfield, 1996). The more complex inferential methods present an opportunity for increased understanding of the responses but are time consuming methods. This research therefore focuses on the potential for rapid assessment offered by the basic statistics, although all methods will now be briefly reviewed.

4.3 TIME DOMAIN REPRESENTATION

4.3.1 Visual analysis

A qualitative level of analysis is based on visual analysis by expert estimation (Boryssenko *et al.*, 2000). As discussed, individual or entire GPR transects can be presented for visual analysis. The former tend to be more useful for understanding the characteristics of signal response. The latter allow visualisation of the subsurface, and are therefore useful for structural assessment and contextualizing the individual trace responses. Numerous display parameters are available for enhancing subsurface detection of targets using GPR. Various features can be identified visually that can help subsequent signal velocity analysis and other quantitative analysis. Visual analysis is not appropriate other than to determine regions of interest and confirm responses that are related to specific peak behaviours.

In the time domain, signal duration corresponds to the time window and is therefore set before data is acquired. It therefore provides no useful means of characterising GPR response. Conversely, identification of specific signal events allows characterisation in

terms of magnitude, polarity and duration. The shape of the interfered wave varies with the water content because a variable dielectric constant brings about changes in reflectivity and time lag shifts in the reflections (Inagaki, 2000). The time to a given reflector provides a great deal of information on the signal / subsurface properties before that reflector. This is especially useful if the depth of the reflector is known because signal velocity can be determined. Owing to the importance of velocity determination in GPR studies, in particular in VMC estimation, this will be discussed in detail in the next section.

The length of time required for a sinusoidal function to complete one cycle is termed its period (Burt and Barber, 1996). The pulse period for a complete cycle is inversely proportional to the antenna frequency (Reynolds, 1997) and because the transmitted pulse consists of three half cycles the wavelet duration is 1.5 times the period as shown in Table 4.2.

Antenna Frequency (MHz)	One-cycle Period	Pulse Duration
225	4.444	6.667
450	2.222	3.333
900	1.111	1.667

Table 4.2: Relationship between antenna frequency and one-cycle period and pulse duration.

To increase the chance of detecting a target, gain can be applied while data is acquired. Applying the correct gain is important for object detection using visual methods but has no impact on the actual raw amplitude values. The PulseEKKO 1000A system allows application of the following types of gain (Sensors and Software Inc., 1996):

- Constant Gain. Using this gain type, all amplitudes are multiplied by a constant factor.
- Spreading and Exponential Compensation (SEC) gain. This gain type gradually ramps up the gain factor down the trace to compensate for attenuation losses with depth.
- User Defined.
- Automatic Gain Control (AGC). This method applies a gain that is inversely proportional to the signal strength.

4.3.2 Velocity analysis: the traditional approach

4.3.2.1 Signal velocity determination using CMP / WARR methods

There are a number of methods for deriving electromagnetic wave velocity using GPR. Du and Rummel (1994) derived velocity using WARR analyses (see Section 3.2). From all of the waves that may reach the antenna, the ground-wave can be best used for velocity determination, because its propagation path and the transmitter-receiver spacing are known (Du and Rummel, 1994). Alternatively, both Greaves *et al.* (1996) and van Overmeeren *et al.* (1997) use the CMP technique. The antenna configuration for CMP analysis was shown in Figure 3.4 and involves separating the transmitting and receiving antennas by a given increment from a common centre point. This increases the two-way travel time between the antennas and, if velocity is unchanging for a given reflection, the reflection should slope away at an even rate. The slope of this reflection depends on the velocity of the material through which the signal propagates. According to van Overmeeren *et al.* (1997), the following velocities can be inferred from CMP measurements: velocity of direct waves through the ground ('ground-wave'); velocity of reflected waves; and in special circumstances, velocities of refracted waves.

There are a number of different ways of determining the wave velocity using data collected from CMPs. Van Overmeeren *et al.* (1997) use the slope of the reflections from the CMP profile (Figure 4.3). The slope of the alignments of the first arrivals gives the velocity of the wave that travels directly from transmitter to receiver through the air and should be $0.3\,m\,ns^{-1}$. The second alignment stems from the wave that travels directly from transmitter to receiver through the upper part of the ground and this velocity is dependent on the dielectric constant of the soil, and hence on the soil composition and soil water content. Hyperbolas in the CMP measurements are reflections from interfaces between layers with different dielectric constants, *i.e.* different propagation velocities. The curvature of a reflection hyperbola depends on the propagation velocity of the radar waves; hence a velocity analysis of a CMP measurement will yield the average velocity to the depth of the reflector.

Greaves *et al.* (1996) use a much more complex means of deriving velocity estimations. Because the data in their survey were all collected with the CMP geometry, normal-moveout (NMO) velocity analysis can be applied at any or all of the CMPs to define the

subsurface velocity. There are a variety of schemes used in NMO velocity analysis but the one selected was the semblance amplitude approach where the data in the CMPs are normal-moveout corrected and stacked using a range of trial velocities. The amplitudes versus time over the whole range are then contoured and displayed as a velocity spectrum. To interpret the NMO velocity field derived from the multioffset data, it is necessary to calculate interval velocities and to find the relationship of radar propagation velocity to other geo-electric properties. Interval velocity was calculated using the Dix formula:

$$V_N^2 = \frac{t_n v_N^2 - t_{N-1} v_{N-1}^2}{t_N - t_{N-1}} \qquad (4.1).$$

where V_N is the interval velocity ($m\,s^{-1}$); v_N is the RMS velocity up to the bottom of layer N ($m\,s^{-1}$); v_{N-1} is the RMS velocity up to the bottom of layer $N-1$ ($m\,s^{-1}$); t_N is the vertical two-way travel time up to the bottom of layer N (s); and t_{N-1} is the vertical two-way travel time up to the bottom of layer $N-1$ (s) (Tillard and Dubois, 1995).

This technique for wave velocity determination was also used by Tillard and Dubois (1995) and Fisher *et al.* (1992) where RMS velocity as a function of time was estimated by performing NMO corrections for a range of velocity values and contouring the corresponding distribution of stacked amplitudes. However, because of the strong instability of interval velocity calculation caused by uncertainties in the reflection time and RMS velocity assessment, velocity analysis using Dix's formula is limited (Tillard and Dubois, 1995). Applying NMO corrections using the estimated stacking velocity functions simultaneously flattens all the reflections only if they all have the same dip; a dip-moveout (DMO) correction removes the dip-dependence of stacking velocities (Fisher *et al.*, 1992). In the case of an inclined reflector, if there is no dip correction, the hyperbola slope overestimates the propagation velocity (Tillard and Dubois, 1995).

The advantages of determining velocity using the CMP method are that it requires no prior knowledge of the subsurface, is not intrusive, uses the radar data acquisition only, and can determine a velocity profile anywhere within the survey although acquiring the data is a slow process (Greaves *et al.*, 1996). Use of the underground-wave velocity applied to the rest of the profile may be generally realistic in a homogeneous environment but it provides only a rough estimate for multilayer terrains having variable porosity or variations in water saturation (Tillard and Dubois, 1995). Furthermore, using the CMP

method, the velocity of the medium below the lowest reflector cannot be determined (Reppert *et al.*, 2000). Sometimes, a situation is encountered when a low-velocity layer is located above a high-velocity layer, where no reflections can be obtained below the high-velocity layer, and consequently, the high-velocity layer cannot be obtained using traditional techniques (Reppert *et al.*, 2000).

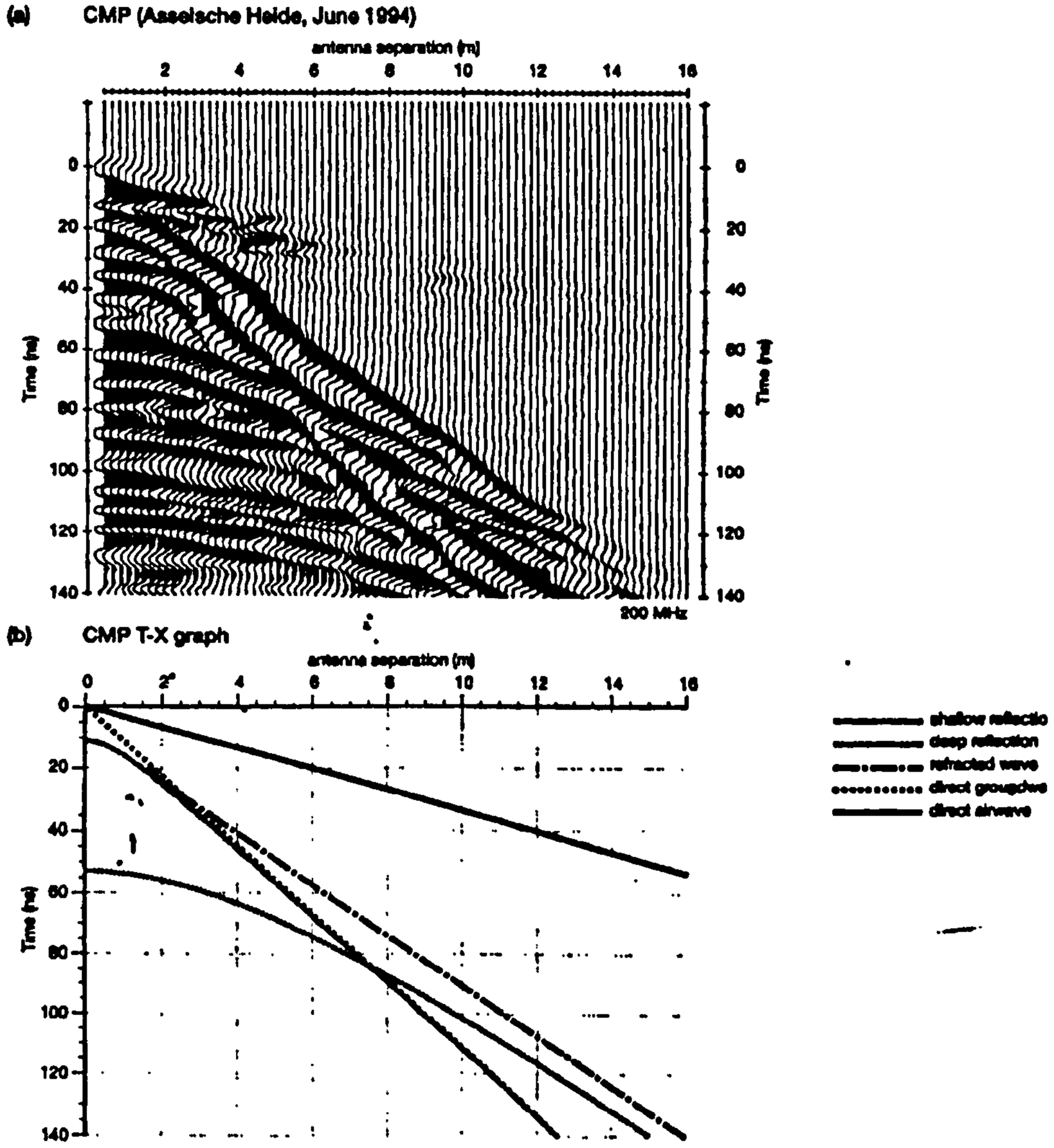

Figure 4.3: Example of CMP analysis (from van Overmeeren *et al.* (1997); (a) CMP measurement; (b) time-distance graph).

4.3.2.2 Velocity derived from borehole / transillumination measurements

Redman *et al.* (2000) employed borehole radar to measure soil water content during an infiltration experiment. Borehole GPR used in the transillumination mode is capable of directly determining the electromagnetic wave velocity and attenuation (Redman *et al.*,

2000) although this technique is not practical for most field applications, as discussed in Section 3.2.

4.3.2.3 Velocity derived from depth correlation techniques

A third means of deriving the velocity of radar waves is to correlate travel times in radar sections with interfaces of known depth. Van Overmeeren *et al.* (1997) used this approach and compared the GPR estimations of VMC against capacitance probe data from access tubes. The advantage of this method is that the travel time values read from radar sections are much more precise than the velocity determination from CMP analysis (van Overmeeren *et al.*, 1997). Furthermore, it is much more rapid in terms of data acquisition. From a radargram the two-way travel time (TWTT) from G_0 to the reflector of known depth (d) can be determined. The velocity (v) of the signal can then be determined:

$$v = d / (TWTT / 2) \quad (4.2)$$

Use of the ground-wave may limit the accuracy of depth-correlation techniques or CMP analyses because the depth of penetration may not be known because its propagation depends on the unknown dielectric constant.

4.3.2.4 Calculation of dielectric constant

Once the velocity has been determined the dielectric constant can be estimated using the following equation:

$$\varepsilon_r = (V_a/V_m)^2 \quad (4.3)$$

where

ε_r is relative dielectric constant.

V_a is velocity of wave through air (0.3 m/ns).

V_m is velocity of signal through material (m/ns).

4.3.2.5 VMC derivation

Both Du and Rummel (1994) and Greaves *et al.* (1996) use the Topp *et al.* (1980) equation to calculate VMC from the dielectric constant. Although the equation is said to operate independently of texture, bulk density, temperature and salinity effects, the radar response for deriving the dielectric constant does depend on such properties although to a lesser extent with increased VMC. Therefore, the estimated value may be more inaccurate for GPR. This problem is exacerbated by the fact that the method of determining velocity from a CMP is crude and the fact that GPR does not take a precise point measurement like TDR and *ThetaProbe* but its velocity estimates are averaged over a greater volume. When using TDR, Perdok *et al.* (1996) state that the calibration curve is not as unambiguous as the Topp curve suggests. This is supported by Roth *et al.* (1992). Thus, if it is limited for use with TDR, it is going to be limited for use with GPR and further illustrates the need to develop other means of using GPR as a means of soil moisture acquisition.

4.3.2.6 Dielectric mixing models

Many other mixing models are available to relate soil water content and dielectric constant. The relationship between water content and dielectric constant has been discussed in several articles, and dielectric mixture models have been constructed to describe the mathematical relations of soil particles, water and air (Saarenketo, 1998). To model or invert dielectric data successfully, the interrelationships of all of the above parameters must be considered (Knoll and Knight, 1994). Electromagnetically, a soil medium is, in general, a four-component dielectric mixture consisting of air, bulk soil, bound water, and free water (Hallikainen *et al.*, 1985). Four factors combine to determine the dielectric constant of a composite material (Knoll and Knight, 1994):

- Individual dielectric constants of components,
- Volume fractions of the components,
- Geometries of the components and
- Electrochemical interactions between the components.

Results clearly show that dielectric properties depend upon the volume fractions, geometries and surface properties of the individual components and that much of the scatter in DP-HGP crossplots is due to systematic variation in interrelated hydro-geological (HGP) and dielectric parameters (DP) (Knoll and Knight, 1994). Because the dielectric constant is a volume property, the volumetric fraction of each component is involved (Jackson *et al.*, 1996). Electromagnetically, the volumetric measure of water content is preferred because the dielectric constant of the soil-water mixture is a function of the water volume fraction in the mixture (Hallikainen *et al.*, 1985).

The simplest mixing model is that presented by Topp *et al.* (1980), which requires only the dielectric constant as an input. Greaves *et al.* (1996) present two mixing formulae, which require that the saturation and porosity of a sample are determined from the dielectric constant. Assuming a three-phase mixture of grains, water, and air results in the following semi-empirical complex refractive index method (CRIM) type mixing formula:

$$\sqrt{K_e} = \phi S_w \sqrt{K_w} + (1-\phi)\sqrt{K_g} + \phi(1-S_w)\sqrt{K_a} \qquad (4.4)$$

Alternatively, the Hannai-Bruggeman formula, that expresses the complex dielectric response of the sample in terms of the complex dielectric response of the mineral grains and the pore fluids that make up the sample:

$$K_e = K_w \phi^m \left(\frac{1-\frac{K_g}{K_w}}{1-\frac{K_g}{K_e}} \right)^m \qquad (4.5)$$

In these equations K_e, K_w, K_g, K_a are the dielectric constants of the sample, water, mineral grains and air respectively, ϕ is porosity, S_w is sample saturation and m is a constant relating to grain cementation. In practice it is impossible to derive both the sample porosity and water saturation from just the dielectric constant of the sample (Greaves *et al.*, 1996). The Brugman-Hanai-Sen model, used by van Overmeeren *et al.* (1997), extends the relation between soil water content and dielectric constant to include the propagation velocity of radar waves in unsaturated sands and the degree of water saturation. This model shows the non-linear behaviour of propagation velocity decreasing

as VMC increases and the more linear increase of dielectric constant with increased VMC. The advantage of this is the ease with which it is possible to estimate VMC from the propagation velocity although it is limited to unsaturated sands.

Dobson *et al.* (1985) present a more complex theoretical four-component mixing model. However, they state that not all of the input quantities are readily available for specific soils and some of these parameters are not constant over time for a given soil so that, for certain applications, simple empirical models with input parameters that can be easily determined are more convenient. It is for this reason that the Topp *et al.* (1980) equation is still the most commonly used means of extracting VMC from soil dielectric data.

4.3.3 Amplitude methods

The approach to deriving VMC using GPR outlined above has a number of limitations, not least a reliance on empirical relations, accuracy of velocity determination and the length of additional time needed to collect the data. If an event can be identified in a radargram, the time to that event will provide information on the subsurface conditions above that event but will tell us nothing else about that event. Furthermore, the techniques generally focus on a means of deriving dielectric constant and its conversion to VMC using mixing models of variable complexity and which usually require some *a priori* information on the subsurface. An analysis of velocity addresses the issue of event timing in relation to depth but ignores the characteristics of the reflections themselves.

Each event has a variable magnitude. This is expressed by means of the amplitude which refers to half the total height of the wave, whilst the total height is frequently termed the 'double amplitude' (Manley, 1945) and is equivalent to the range. GPR response is a combination of such events in sequence and the magnitude of the event is dependent on the nature of the dielectric contrast and sources of signal loss. Thus by assessing the amplitude characteristics of the signal response it should be possible to derive information on subsurface moisture. Real radar signals are also narrowband in the sense that the spectrum is concentrated within some small band about the median frequency (theoretically the transmitter frequency) and may be written in the form (Rihaczek, 1996):

$$s(t) = a(t)\cos[2\pi f_0 t + \phi(t)] \qquad (4.6)$$

Here, the function *s(t)* describes the waveform in the time domain and the function *a(t)* describes how the oscillation amplitude varies from one cycle to the next, f_0 is the fundamental frequency, t is time and ϕ is the phase angle (Rihaczek, 1997). The amplitude will provide information that is directly related to the radar response to subsurface changes. Section 3.3.1 discussed how the theoretical amplitude can be quantified using the reflection coefficient. However, this requires *a priori* knowledge of subsurface dielectrics and signal propagation velocities. An approach that can derive this amplitude data directly is required. A recent attempt was made to use this potential by Tarussov *et al.* (1994) and Chanzy *et al.* (1996).

4.3.3.1 Ground-wave amplitude

The aim of Tarussov *et al.*'s (1994) work, which was extended by Chanzy *et al.* (1996), was a quantitative assessment of soil water content, based on GPR amplitude measurements. They used a Pulse EKKO IV GPR system with 200 MHz antennas in both airborne and ground modes. Here the first cycle free of interference with the air-wave is utilised. This, they claim, corresponds to the beginning of the signal and the maximum ringing amplitude from this interval (25-45 ns on Figure 4.4) was chosen to characterise the ground-wave amplitude by calculating the difference between the maximum (positive) and minimum (negative) values. This corresponds to the range for a defined signal cycle and forms the basis of their analysis. Ground-wave amplitude values were inversely proportional to the water content over a range of VMC from about 0.10 to about 0.40, with a correlation coefficient of 0.92 (Figure 4.5).

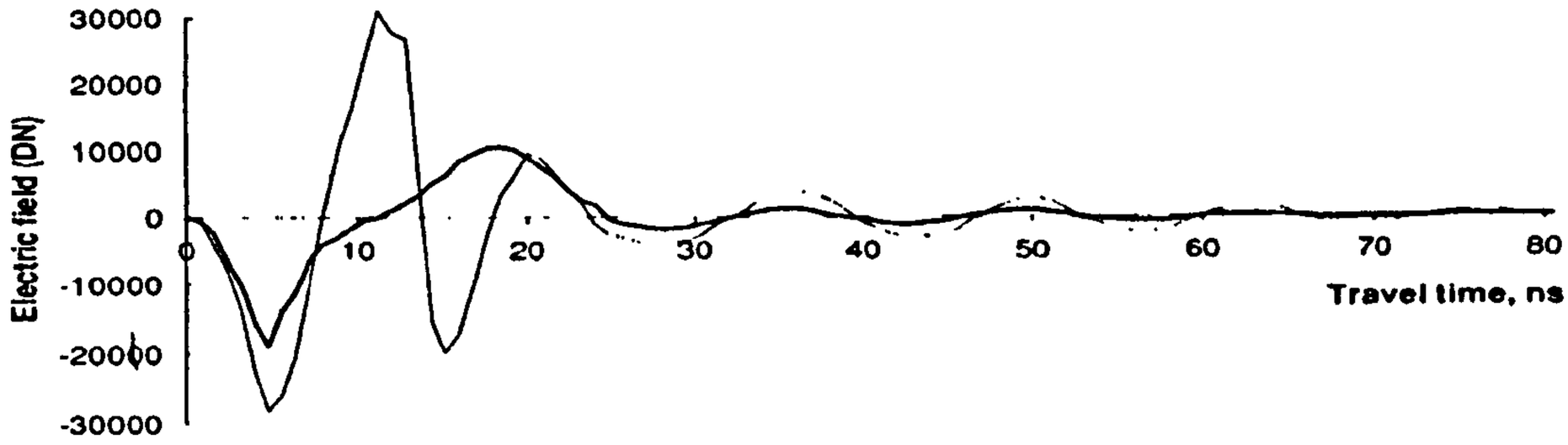

Figure 4.4: GPR traces from Chanzy *et al.* (1996). Bold line is wet soil, fine line is dry soil.

There are a number of potential problems with the amplitude approach of Chanzy *et al.* (1996). Avoiding the zones of interference between air- and ground-waves makes sense but in so doing a lot of ground-wave information may be lost depending on how wet the soil is. At 200 MHz on dry sand (most conducive to propagation) the TWTT of the ground-wave can be expected to be approximately 7ns based on antenna separation of 0.5m (for Pulse EKKO 1000A 225 MHz) and a propagation velocity of 0.15 m ns^{-1} using the following equation:

$$TWTT = (d/v) * 2 = 6.67 \quad (4.7)$$

Using a fast value for wet sand (0.06) the arrival of the ground-wave can be expected at about 17 ns. By reference to Figure 4.5 it is evident that the method outlined above misses the ground-wave and in fact provides a measure of amplitude and soil moisture at depth in the subsurface. Chanzy *et al.* (1996) measure the amplitude in the harmonic ringing section of the ground-wave. Harmonic ringing is explained by the coupling between the antennas and the ground due to the electrical conductivity of the ground (Chanzy *et al.*, 1996) and manifests itself as a relatively consistent waveform in terms of magnitude and wavelength. Whilst using the harmonic ringing section of the trace may be reliable in simple environments, additional reflections in complex sub-surfaces may completely obscure these small magnitude cycles.

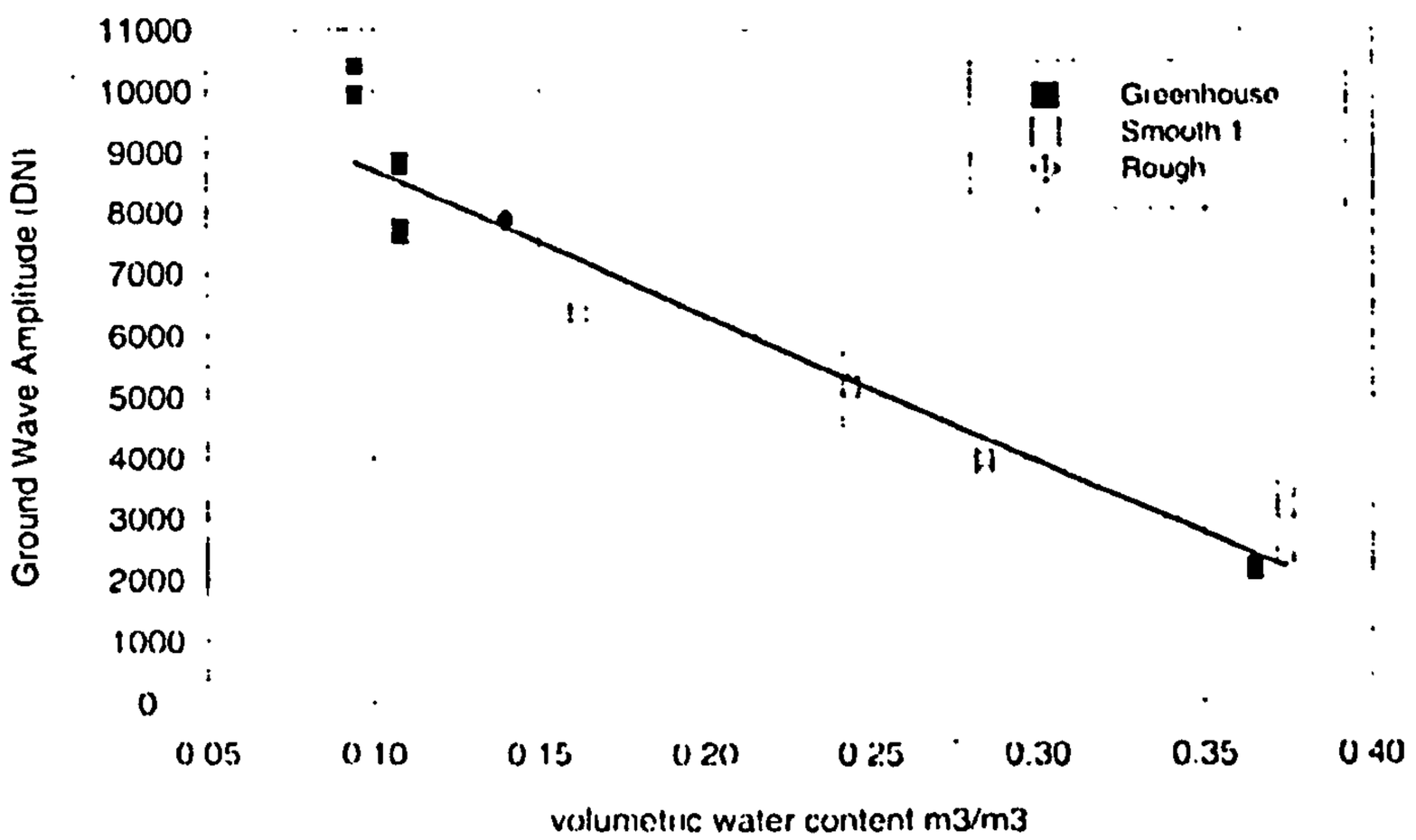

Figure 4.5: Amplitude-VMC results from Chanzy *et al.* (1996).

4.3.4 Attenuation

Section 3.3.2 discussed the basic attenuation processes. Attenuation accounts for changes in various system characteristics (such as the GPR system, material properties and water content) as well as the spreading of the electromagnetic wave as it propagates from the transmitting antenna (Ziemer *et al.*, 1998). A spherical wave spreading into the ground will decrease inversely with the distance of the waveform into the ground and will decrease exponentially depending on the conductivity losses in the material (Annan, 1997). The latter of these two options will depend on both the material properties and the water content. Whilst attenuation primarily affects the magnitude of any potential reflections, and may even prevent the occurrence of some, it also affects other waveform characteristics (such as frequency and duration, sharpness of waveform) due to the related signal dispersion processes. Dispersion manifests itself as a change in pulse shape with delay time and occurs when the velocity or attenuation vary with frequency (Annan, 1996). It is proposed here that by measuring changes in signal characteristics a method can be derived which would function as an effective measurement of the signal attenuation.

4.3.5 Basic statistics for signal characterization

In time series analysis any variable changing through time can be characterised using basic descriptive statistics. Rather than attempting to assess true physical parameters such as the dielectric constant or the attenuation coefficient, these methods are based on empirical modelling of the time-varying behaviour of an observed series and attempting to discover statistical regularities consistent with whatever physical processes happen to be operating (Burt and Barber, 1996). This means that the selected statistic representing the GPR response can be related to the changing VMC conditions in the subsurface using simple functions. Whilst this may ignore the physical basis of the response, it should enable accurate and efficient estimation of VMC and its distribution, and should enhance understanding of the effects of the moisture on the signal. More complex statistical approaches can also be employed, such as the autocorrelation coefficients, which measure the correlation between observations at different distances apart and provide an important guide to the properties of a time series (Chatfield, 1996). These complex statistical

methods also offer potential for assessing the response of the GPR signal to changes in the subsurface environment.

4.3.6 Signal modelling

The parameter estimations associated with the autocorrelation technique offers the potential to model aspects of the signal response. It is also possible to model signal response *a priori* and test the fit of such models to the actual data. The underlying concept is to develop several signal models, which correspond to different activities or situations and then decide which model best describes the ongoing signal epoch; it is a signal classification technique (Shiavi and Bourne, 1986). Signal modelling approaches to time series analysis are well reviewed by Shiavi and Bourne (1986), Burt and Barber (1996), Chatfield (1996) and Ziemer *et al.* (1998) and range from simple smoothing and differencing to more complex autoregressive modelling. This approach is very useful for understanding the physics of the radar response to specific moisture conditions but is potentially very time consuming and is oriented more towards theoretical investigations than practical implementation. Thus such complex modelling approaches are not considered any further in the current research.

4.4 FREQUENCY DOMAIN REPRESENTATION

4.4.1 Fourier analysis

A signal consists of an infinite set of waves whose frequencies are harmonically related (Connor, 1982). This can be analysed by Fourier techniques to separate various frequency components with the total range of these frequencies representing the frequency spectrum of the signal (Connor, 1982). The Fourier analysis converts information about the variation of amplitude with time (time domain information) into information about the variation of amplitude with frequency (frequency domain information) (Wishart, 1996). Therefore, as an alternative to representing the waveform as a plot of voltage versus time, it could be represented by two plots: one of amplitude versus frequency and the other of phase versus frequency; plots known as amplitude and phase spectra (Ifeachor and Jervis, 1993).

4.4.2 Amplitude spectra analysis

The observed shapes of the resulting amplitude spectra and the changes in them are often helpful in the understanding and interpretation of the waveforms (Ifeachor and Jervis, 1993). From these spectra, visual analysis and statistical approaches can be used to characterise the amplitude response and the frequency characteristics of that amplitude response. The highest peak represents the central frequency, which is determined by the transmission frequency used. The amplitude value corresponds to the statistical maximum value for the spectra while the actual frequency value may reveal something about the change in system response. Frequency response always occurs as a spread about the centre frequency. This spread is measured as the bandwidth. This is likely to change if anything generates a change in frequency behaviour. The Nyquist Frequency is the maximum obtainable measurement frequency and is used for designing sampling. It is of limited use in this research other than to define a maximum limit for frequency response.

The work of Chanzy *et al.* (1996) demonstrated a water influence at 65-75 MHz frequency using 200 MHz antennas suggesting, that VMC may have a specific response in the frequency domain. Thus by identifying each peak in the spectra they can be classified in terms of its magnitude and frequency. However, because GPR response is likely to be very complex the changes in amplitude spectra can be characterised in the same way as for time domain traces by simple descriptive statistics.

Frequency data are most often used in GPR applications to provide filters for excluding noise and unwanted reflections in the GPR image. Such filters change the raw trace and are therefore of little use where trace analysis is quantitative and not visual. However, such filters can be used to our advantage in two ways. First, they can be used to smooth a response and remove unwanted reflections leaving the major responses of the system; one of which should be the water response if it forms a discrete body of water. Secondly, a filter can be designed to remove all frequencies incrementally and attempt to identify a specific frequency response associated with moisture in terms of both frequency and magnitude. The filtering process is very time consuming, requiring automation and a well-designed, conceptually rigorous filter.

4.5 TIME-FREQUENCY DOMAIN REPRESENTATION

Fourier series and transforms cannot easily localise information in the time domain (Braun and Feldman, 1997). Because the time domain in GPR data is representative of depth, this fundamentally limits frequency domain techniques to exploring the characteristics of response, rather than spatially locating that response. When analysing transient signals, such as might be generated by variability in GPR response, it is often not sufficient to have only a time or frequency representation (Oonincx, 1997). The more physically meaningful time-frequency spectra allow the internal structure of a time history to be examined in a way that the individual time and frequency domains do not (Hammond and White, 1996). The advantages are that the time-frequency decompositions permit projections of the time history onto a space that allows separation of components of the signal so as to facilitate enhancement, detection (of events), filtering, classification (of phenomena) and re-synthesis (Hammond and White, 1996).

The single-value extraction of an envelope and other instantaneous functions of a signal are based on the Hilbert integral transform (Feldman, 1997). A properly digitised waveform is processed via the Hilbert transform to obtain the analytic signal given by (Chen, 1986):

$$a(t) = x(t) + jx'(t) \tag{4.8}$$

where $x'(t)$ is the Hilbert transform of trace $x(t)$ and j is a constant. Normally only the real part ($x(t)$) of a complex-valued signal is plotted, but the imaginary (or quadrature) (equivalent to $x'(t)$) component can be used to reveal some useful information about the signal (Sensors and Software, 1996).

Barnes (1998) outlines the steps involved in the estimation of the instantaneous amplitude and instantaneous phase. If the phase (see equation 4.6) is rotated, the maximum value that the trace assumes during the phase rotation is the envelope (instantaneous amplitude), and the phase rotation that gives rise to the maximum value is the instantaneous phase reversed in sign. Only two rotations are needed if they differ by $\pi/2$ radians. The real trace is taken as the first rotation and a $-\pi/2$ radians phase rotation (the Hilbert transformation) is taken as the second producing an imaginary trace. The instantaneous amplitude and

phase can then be calculated from the real and imaginary traces. There are a number of effective features that must be used together (Chen, 1986) and these can be derived using the PulseEKKO 4.2 Software. The mathematical expressions given here are taken from Sensors and Software (1996).

The raw trace amplitude $x(t)$ has already been discussed in detail. Instantaneous amplitude is given by:

$$e(t) = \sqrt{x^2(t) + x'^2(t)} \tag{4.9}$$

The instantaneous amplitude outlines the envelope of the trace and is independent of phase so that it may have its maximum at points other than the peaks and troughs of the real trace, especially where an event is the composite of several reflections (Sensors and Software, 1996). The envelope amplitude is associated with the reflection strength of the signal so that a large value of envelope amplitude usually indicates major changes in the subsurface layers (Chen, 1986) and is an interpretational tool that describes waveform shape (Sensors and Software, 1996). Compared to the raw trace amplitude, the instantaneous amplitude provides only positive values. Equation 4.9 shows that if the Hilbert transform is excluded then the instantaneous amplitude is the equivalent of the absolute trace value. The addition of the imaginary part means that the instantaneous amplitude only approximates the absolute real trace and thus may have different statistical properties.

The instantaneous phase is measured between $-\pi$ and $+\pi$ and is given by:

$$\phi(t) = \tan^{-1}\left[\frac{x'(t)}{x(t)}\right] \tag{4.10}$$

Instantaneous phase is used to emphasise the continuity of events (Sensors and Software, 1996). If there is a discontinuity in the layer structure, it will be detected from the instantaneous phase even when the signal strength is not high (Chen, 1986). Because phase is independent of the trace envelope, it can often make weak coherent events more prominent, and this is even the case for events that interfere with one another (Sensors

and Software, 1996). The phase angle (ø) is a signal parameter that changes the oscillation period with time (Rihaczek, 1996). Two waves having the same period have a constant phase-difference, which is the difference between the two phase-angles; if the phase-difference is π radians the waves are said to be anti-phased and if the phase-difference is zero, they are said to be in-phase (Manley, 1945). The result is that a reflection may occur at a different time or over a longer period of time and may occur as a negative peak (trough) rather than a positive peak. As such it can be generated by changes in subsurface dielectric properties.

The dominant frequency, derived from the phase, can be used to detect rapid changes in layers (Chen, 1986). It is used as a correlation tool and the frequency character will change as the lithology changes, the thickness changes or at interfaces such as the water table (Sensors and Software, 1996). Instantaneous frequency is a derivative of instantaneous phase and is given by:

$$w(t) = \left[\frac{1}{2\pi}\right]\frac{d\phi(t)}{dt} \tag{4.11}$$

Like the time and frequency domain representations, the complex attributes can be used for both visual and statistical signal characterisation.

4.6 POTENTIAL GPR RESPONSE TO CHANGING MOISTURE CONDITIONS

An underlying assumption in this research is that because water creates dielectric contrasts in the subsurface environment, and produces attenuation of the GPR signal, the *distribution* as well as the magnitude of wetness may also influence the radar response. The distribution of moisture may generate reflections in GPR data. The strength of these reflections may be dependent on the magnitude of the dielectric contrast and signal attenuation. The distribution of moisture will depend on the nature of the host material, and the material properties, which will also have a direct impact on the GPR signal, and the resulting water bodies can be broadly categorised into five classes: discrete, wetting front, water table, perched water table, and diffuse. Each of these will vary through both space and time as the inputs and outputs of the subsurface system change. As Section 2.4 indicated, spatial variability in the subsurface properties which generate these moisture

distributions can also be highly variable. Thus, the potential moisture patterns to which the GPR signal responds can be very complex. This will affect the measurement of VMC using GPR.

As a discrete water body is traversed, a distinct change will occur in the GPR response at the clearly defined dry-wet boundary. This can be compared to a more gradual change associated with diffuse water bodies, in which dry-wet boundaries are less distinguishable. At its extreme, a diffuse water body will be more or less continuous across the entire area of interest. Lateral variations in moisture content should be relatively easy to assess with GPR. However, very complex distributions result from both lateral and vertical moisture variation. Water infiltrating from the surface may form a more or less distinct wetting front depending upon the material characteristics of the subsurface. This would produce high dielectric contrasts with the drier material below and therefore strong reflection events. The water content above the wetting front will determine the degree of signal attenuation and, therefore, actual the reflection strength.

Conversely, where there is a water table a strong reflection will be generated in the GPR data at the dry-wet interface. If the water table is shallow then the magnitude of the reflection will depend almost entirely on the dielectric contrast between the dry zone above the saturated zone below. Water rising up through the profile from the water table (e.g. capillary rise) may produce a less discrete interface. In this case the reflection generated will be weaker than if the material above the water table were dry. The strength of the reflection will also depend upon the depth to the water table, which may increase spreading and scattering losses weakening the signal response. The reflection strength will also depend upon the nature of the material above the water table, especially its VMC, which may increase signal attenuation. Water that moves down through a material profile may become inhibited at an interface between a material with higher hydraulic conductivity than the material below it. Water becomes trapped and may begin to spread laterally or rise towards the surface again. In addition, water will continue to move down through the profile through the other material, producing a more diffusive wetting front below the perched water table. Therefore, multiple reflections may be generated. Clearly, the complexity of the subsurface patterns of moisture will have a direct impact on the GPR response and the measurement of VMC using GPR.

4.7 SUMMARY

This chapter has outlined a number of the existing techniques for estimating soil moisture. For the estimation of high resolution subsurface moisture patterns these techniques tend to be inappropriate because they are time consuming (e.g. CMPs), cannot be applied in most field applications (e.g. borehole / transillumination), or rely on continuous subsurface reflectors of already known depth (e.g. depth correlation methods). The more recently developed amplitude methods have a less precise physical or electrical definition. In order to derive, accurately and efficiently, VMC distributions over large areas, reflection profiling mode must be used. Whilst it has been shown that reflection coefficients or attenuation potentially provide physically meaningful data, their relationship to VMC in the absence of a priori data is unclear and often indeterminable. To overcome this problem, and to provide the most rapid but accurate estimate of VMC possible, the potential use of statistical signal characteristics was discussed. These offer the potential to produce simple empirical models to estimate the VMC from a GPR derived parameter, and provide an opportunity for increasing the understanding of GPR response to changing moisture conditions as outlined in the previous section. In order to develop, test and apply such relationships fully, an experimental methodology is required that incorporates the development of increasingly complex subsurface environments under controlled conditions. The methodology of the research is discussed in the following chapter.

CHAPTER FIVE: METHODOLOGY

5.1 INTRODUCTION

In the previous Chapters, the nature of subsurface moisture (Chapter Two) was discussed and the GPR technique outlined (Chapter Three). The potential for integrating these two areas of interest (hydrology and GPR) with the aim of satisfying the primary aim of this research, the development and application of models that estimate VMC and its distribution, was addressed in Chapter Four. This Chapter discusses the methodology developed to satisfy the primary objective and the other research aims; the general structure of the analysis is depicted schematically in Figure 5.1. The research is characterised by four stages, which are addressed in separate chapters of this thesis:

1. Assessment of material properties and GPR response in the absence of moisture and in a spatial context with the specific aims of:

- Establishing whether or not material property- and GPR-variation are related.
- Assessing the sensitivity of GPR response to other sources of subsurface variability (structure and anomalies).
- Identifying the potential limitations of the GPR method within the context of subsurface moisture determination.
- Discussing the implications of these features for subsequent experimental design and data interpretation.

2. Characterisation of GPR response to changing subsurface VMC and material conditions. This principally involves:

- An assessment of a range of different methods of signal characterisation using reflection profiling mode GPR data.
- From this, understand the GPR response (both the effect of moisture on the GPR signal and the manifestation of this effect in the derived signal characteristic) and the development of models for VMC estimation using the selected GPR parameters.
- Validate the models by application to other GPR data acquired using the same experimental configuration. Through this validation, an assessment of the accuracy, precision and repeatability of the developed technique allows a

discussion of error and reliability in soil moisture distribution, and the implications of this for further analyses.

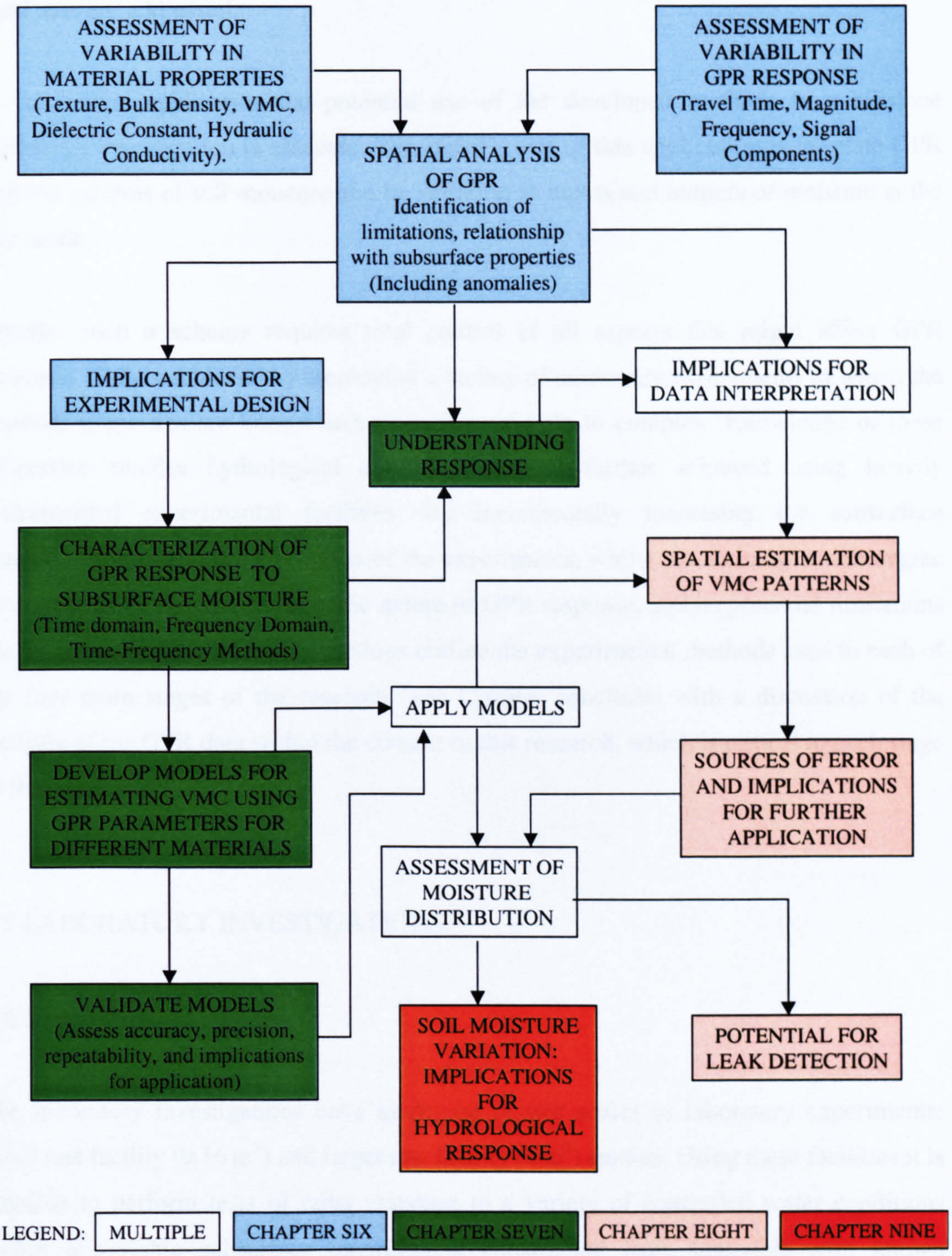

Figure 5.1: General outline of the research methodology and its relation to the structure of the remainder of the thesis.

3. Application of the models to the spatial estimation of VMC patterns with a view to investigating moisture variation and the patterns of moisture that may occur as a consequence of a water leak. Through a further discussion of the sources of error encountered in a more complex experimental situation, the implications for application to field data are addressed.

4. As a final application the potential use of the developed methods in a hillslope hydrology investigation is assessed. The specific aim of this application is to relate GPR derived patterns of soil moisture and its variation to inputs and outputs of moisture at the plot-scale.

Clearly, such a scheme requires total control of all aspects that might affect GPR response. This is achieved by employing a variety of laboratory experiments in which the material properties are known and range from simple to complex. Knowledge of these properties enables hydrological control, which is further achieved using heavily instrumented experimental facilities. By incrementally increasing the subsurface complexity throughout the progress of the experiments, whilst maintaining a high degree of experimental control, the specific nature of GPR response, and its potential limitations can be assessed. The following sections outline the experimental methods used in each of the four main stages of the research. The Chapter concludes with a discussion of the analysis of the GPR data within the context of this research, which is critical to each stage of the analysis.

5.2 LABORATORY INVESTIGATIONS

5.2.1 Introduction

The laboratory investigations have made use of two scales of laboratory experiments: small test facility ($0.16\,m^3$) and larger test facility ($8\,m^3$) studies. Using these facilities it is possible to perform tests of radar response to a variety of controlled water conditions within a variable subsurface environment constructed from materials with known properties. The ability to control and change the system characteristics enables the research to begin in simple materials and then to allow development of functional relationships and methods by decomposing the inherent complexity of radar response into

its component parts. Increasing system complexity in a stepwise manner allows one to isolate the causes of particular aspects of the radar response. In addition to developing the functional relationships, these facilities allow initial investigations into the estimation of soil moisture distributions in the subsurface using GPR

5.2.2 Large scale dry experiments

A series of large-scale dry experiments were performed prior to any attempt at using the GPR in wet conditions. This work aims to characterise the nature of subsurface reflections beneath different configurations of layered material. In particular these experiments seek to determine variability in GPR response in the absence of moisture and relate this to variation in the subsurface in terms of the spatial variability of material properties and the impact of the presence of objects that may produce anomalous GPR responses. This is necessary to provide a background to the wet experiments. The dry experiments concentrate on the simplest situation possible with the objective of adding complexity incrementally so that all aspects of the radar return can be understood with confidence. Particular attention is paid to repeatability and error in GPR characterisation of simple to complex environments and the implications this may have for the design of experiments for deriving GPR-VMC relationships. This involves the following:

- the study of the variability of propagation parameters and spatial characterisation in the absence of moisture,
- the study of radar response to multiple layers of material with different dielectric properties, in particular the multi-boundary response of GPR in materials from gravel through to fine sand,
- the analysis of boundary locations in multi-frequency mode,
- testing the ability of the GPR to detect dielectric anomalies,
- the quantification of noise and boundary effects in the box, testing radar collection parameters, and determining the impact of radar coupling on boundary detection.

To facilitate this analysis of the variability in GPR response in the absence of moisture, a controlled subsurface environment has to be constructed, consisting of layers of contrasting material properties and a dielectric anomaly (a *ThetaProbe*). The constructed subsurface environment must be of sufficient surface area and depth to investigate fully

the impacts of subsurface variation on the GPR response. This requires the development of a specialist facility, which is now discussed in detail within the further context of assessing spatial patterns of moisture, for which the facility will also be used (see Section 5.2.5).

5.2.2.1 Large test facility (LTF)

Many of the widely accepted principles of subsurface hydrology and soil science are based on laboratory experiments conducted in small columns packed with relatively uniform material; as such it is difficult to extend laboratory results to the field (McLaughlin *et al.*, 1993). The purpose of the large test facility is to enable the construction of controlled subsurface environments of known properties and to facilitate the production of water bodies of controlled size, geometry, rate and wetting fronts for investigation with GPR. This kind of controlled and controllable facility is essential to underpinning research in the functional characterisation of radar response to subsurface properties and processes. Proper experimental characterisation of GPR response can only be carried out under controlled conditions where subsurface complexity can be added incrementally and the radar response examined in detail. Due to the sensitivity of radar response to external features, the test facility needs to be large enough to provide a zone of study that is unaffected by external reflections and provides sufficient space for spatial radar profiling. The increased size (2 m × 2 m × 2 m) of the facility also allows more detailed characterisations to be achieved. In the translation of laboratory experimentation to field conditions it is critical that reflection profiling and CMP modes are supported in the laboratory. By increasing the size of the facility, CMP analyses will be possible and will provide more powerful analysis because the antennas can be separated over greater distances allowing increased separation of individual reflections.

This facility (Figure 5.2) is the first indoor facility of its kind in the UK. Though much smaller facilities exist for work in trans-illumination mode, this is the first indoor facility of sufficient size for work in reflection profiling mode and common mid-point (CMP) mode. Using reflection profiling mode GPR in a laboratory commands very large overheads because the facility must be of sufficient size to provide a reasonably sized transect with the GPR footprint inside the subsurface material. Outdoor test sites such as the EIGG (Environmental and Industrial Geophysics Group of the British Geological

Society) outdoor test site in Leicestershire provide some control on subsurface conditions using buried reflectors in a uniform substrate. However, such facilities do not provide the capacity to control and manipulate the physical properties of the subsurface substrate itself (density, texture, porosity, stone content, and layering) as well as its moisture conditions.

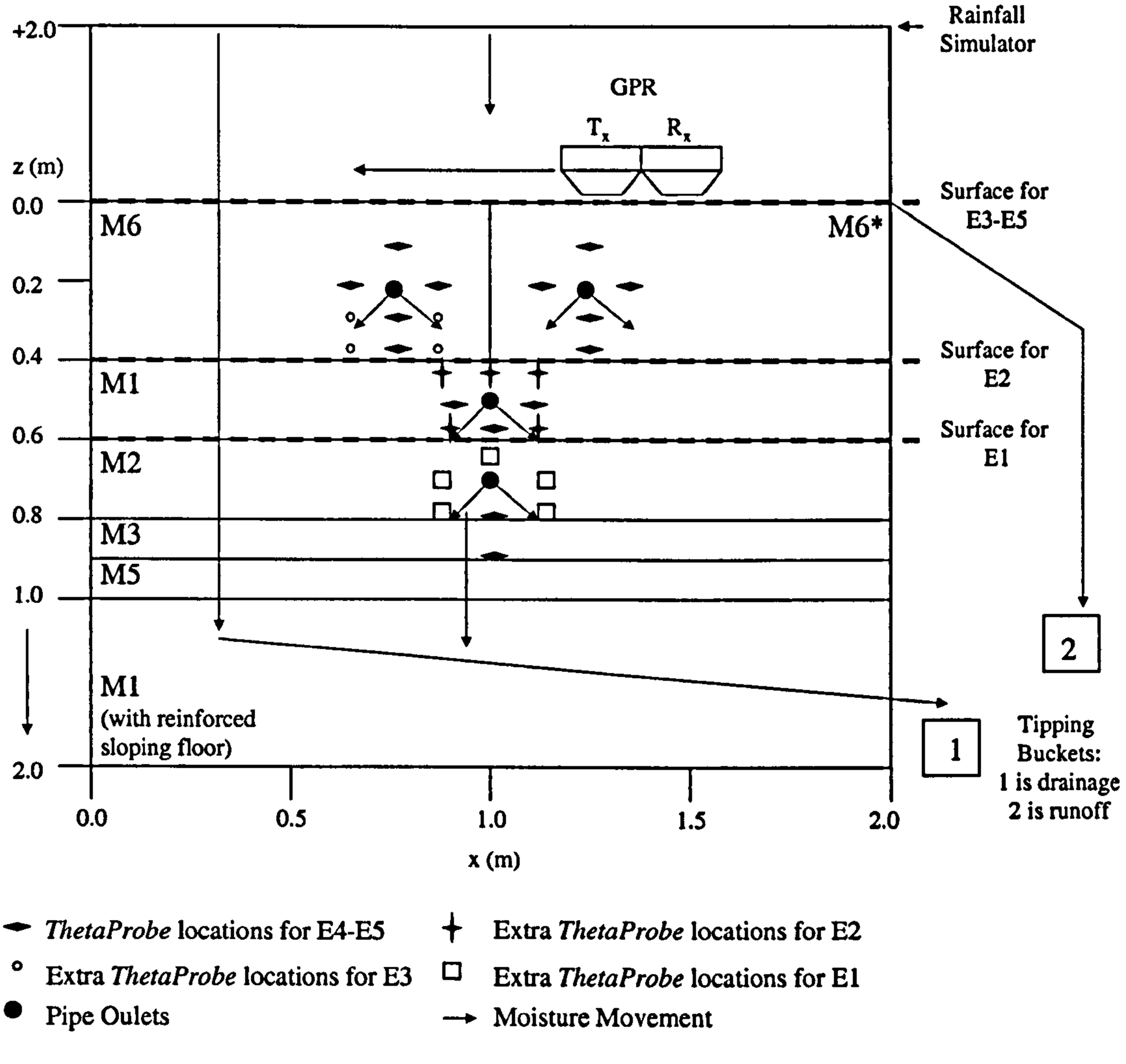

Figure 5.2: Schematic of the large test facility. Shows material configuration for LTF WET Experiments (Section 5.2.5) including the incrementing surface between experiments. Section y = 0.0-1.0 m drawn to scale. M6* consists of M6 with rock fragments. Also shows the approximate *ThetaProbe* locations for each experimental run. Locations for E4-E5 were the final configuration; probes were moved to the extra locations shown between E1 and E2, E2 and E3, and E3 and E4. Schematic also indicates four outlet pipes, rainfall simulator, tipping buckets for drainage and runoff, and GPR transect direction.

Similarly, these outdoor test pits also do not provide the capacity for intensive monitoring and measurement of subsurface moisture conditions. Outdoor test sites are normally used to compare geophysical instruments' detection of subsurface features using visual techniques. The research carried out here focuses on the functional rather than visual characterisation of radar response and this requires much more control upon the radar environment in material and hydrological terms. An indoor facility for the development of specification sub-surfaces, with controlled and heavily monitored hydrological conditions in a low noise environment, is much more appropriate.

Details of the construction can be found in Mulligan and Charlton (1999) and the following discussion is adapted from that source. The facility was constructed over 9 months from March 1998-January 1999 and had to be constructed, as much as possible from non-metal materials to minimise the potential for spurious reflections. Given that $8m^3$ of geological materials amount to around 10 tonnes when dry and nearer 15 tonnes when saturated, the box itself must have a very high compressive strength.

The whole facility (Figure 5.3) is constructed in a basement laboratory with reinforced floor and built from 1" marine ply reinforced with 8 2x3" wooden supporting braces attached at the corners with 4" steel bolts. Support is also provided by four six-tonne breaking strain polyester webbing load braces. These provide sufficient support for a full load of sediment and water. The marine ply is treated and covered in roof sealant for waterproofing. There is a gravel supported sloping floor with butyl rubber retainer for drainage into a tipping bucket (0.2 mm resolution, Environmental Measurements Ltd, UK). The top half of one side can be removed to facilitate infill and removal of sediment from the lower half of the facility. The use of a 1 tonne capacity Key Industrial palette box stacker which lifts palette boxes to a height of 1.5-2 m allows sediment transfer into and out of the upper half of the facility.

One side of the box is kept clear for sediment infill and removal. All instrument wires and dehumidification tubing enter the box from the opposite side leaving two free sides for characterisation of the subsurface by trans-illumination, if required. To facilitate the development of various types of subsurface on an $8\,m^3$ basis, large amounts of sediment must be kept in storage. This is achieved using stacked 1 tonne capacity palette boxes, which can be wheeled to and from the facility with a palette box stacker. A total of 25 tonnes of sediment are kept in the laboratory (Figure 5.4).

The transfer of 10 tonnes of sediment is a time consuming and laborious task. Experiments are therefore designed to minimise the movement of sediment to and from the facility by building up complexity in a stepwise manner and by making most changes to the near surface sediment layers. Sediments are built up a layer at a time and are separated to prevent mixing of different materials using high-hydraulic conductivity geo-textiles. All sediments are dielectrically (using *ThetaProbes*) and texturally characterised (Laboratory Particle Size Analysis). The depth of each layer is measured with a metric tape. For future research using the facility, the presence of stones and other materials in different layers can be rapidly characterised by image processing of plan-view digital camera imagery. This has not been carried out here because materials were homogeneous with the exception of the M6 material with rock fragments.

Figure 5.3: Image of large test facility. Shows LTF with front open for material filling. Dehumidifier piping and rainfall simulator also shown.

Internal pipes capable of controlled leakage are also an integral part of the facility. The pipes used are not intended to replicate mains water utilities because the purpose of this study is not to detect pipes themselves but to develop techniques for the examination of the water bodies associated with leaks from these pipes. As such the purpose of the leaking pipes in the facility is simply to provide water leaks into the substrate at

controllable and known rates and depths whilst not interfering with the radar observation of the leak bodies. The pipes were constructed of nylon reinforced 1 cm diameter hose. Four leak hoses enter the box at four different depths but, owing to their flexibility, can be placed anywhere in the subsurface material. The leaks lines are connected to a single source of water, monitored by an RS infra-red turbine flow meter (Titan Enterprises, UK) connected to the MICROLINK data acquisition and control system (BIODATA Ltd., UK) which forms the backbone of the data control and collection system. Leak flow rates are displayed in real time on a Dell Pentium 333 MHz computer using MICROLINK Windmill or HP VEE software. Flow is controlled manually using a high sensitivity flow controller with output rates fixed according to the flow meter output on a local monitor.

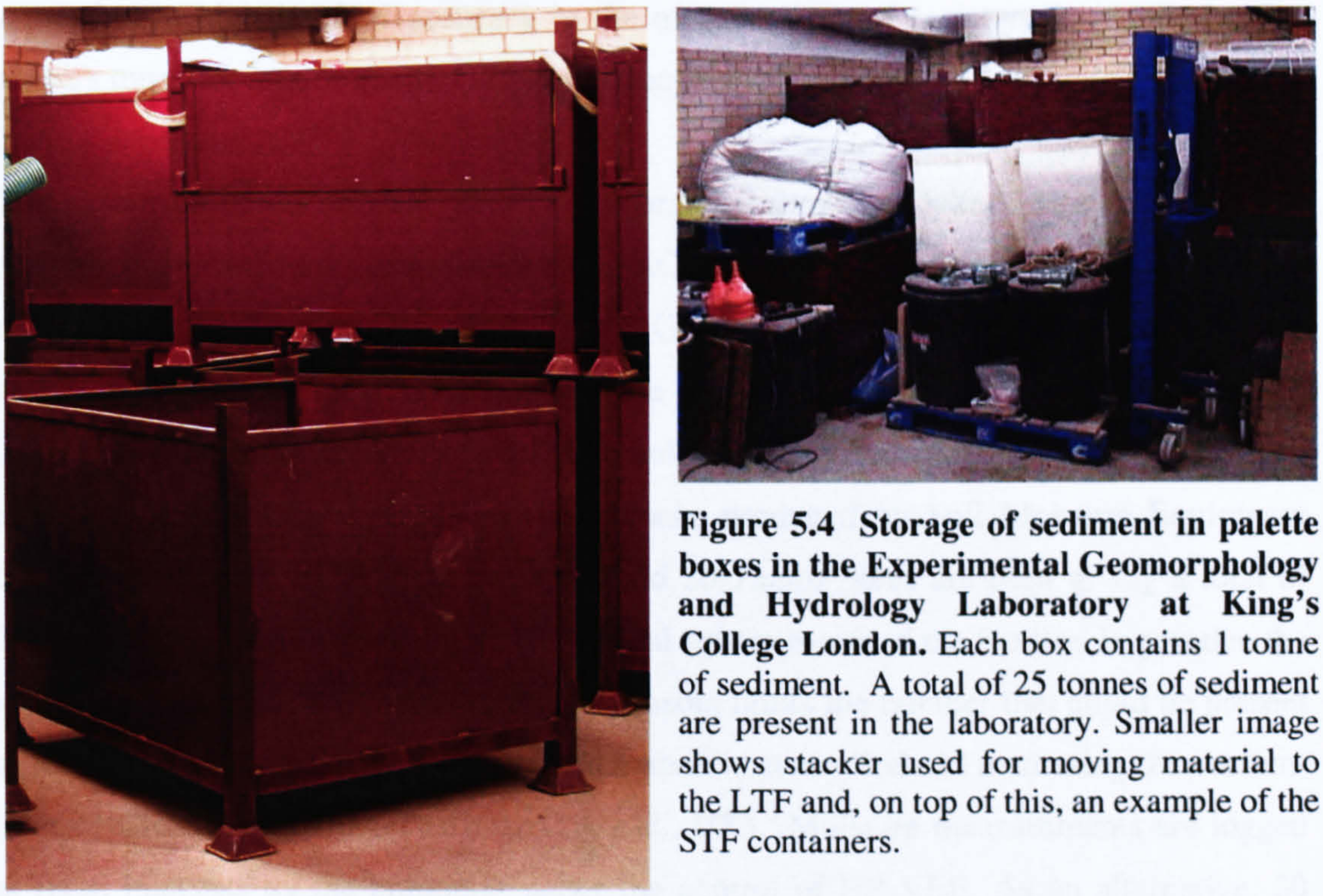

Figure 5.4 Storage of sediment in palette boxes in the Experimental Geomorphology and Hydrology Laboratory at King's College London. Each box contains 1 tonne of sediment. A total of 25 tonnes of sediment are present in the laboratory. Smaller image shows stacker used for moving material to the LTF and, on top of this, an example of the STF containers.

The distribution of surface and subsurface soil moisture is also influenced by the water arriving at the ground surface. Rainfall simulation is controlled to provide test storms to enable the investigation of water movement down from the surface and leak detection in the presence of such infiltrating water (rather than in a dry subsurface), and the spatial distribution of soil moisture following controlled rainfall events. These two methods of application potentially have different impacts on the radar response to soil water principally as a result of changes to system geometry. Rainfall simulation is achieved

using a sprinkler system suspended from the wooden frame, which has been bolted to the top of the box. Rainfall rates are tap-controlled in the same way as the water leaks are. Excess spray is trapped by a plastic shroud and guided into a series of gutters through to a further Environmental Measurements tipping bucket gauge. The rate of rainfall can be calculated in real time as the flow-meter input minus the tipping bucket output from the gutters.

One of the most critical aspects of a successful laboratory radar test facility is a high - density moisture monitoring system. In order to characterise in detail the location and form of water leaks using in-situ measurements, an extensive measurement grid is necessary. The moisture measurement system developed for this project requires a large number of inexpensive sensors, which are small in size and low in metal content. At the same time a high level of accuracy in the measurement of moisture is required. The sensors must not interfere with GPR radio frequencies.

The system is based on two types of sensor: *ThetaProbes* (Delta-T Devices, UK) and resistance measurements of moisture using AC excitation of gypsum blocks. *ThetaProbes* use the same physical principle as TDR and GPR and thus provide a directly comparable and accurate measurement. Because they are of high cost, only 20 *ThetaProbes* are used in the moisture measurement system. The bulk of the spatial measurement is performed using the much less expensive gypsum blocks produced by Soil Moisture Equipment Corp., USA. In total 238 gypsum blocks and 20 *ThetaProbes* are used giving a total of 258 moisture measurements within the central square metre of the facility. In practice the amount of electrical wire required for the sensors limits the number that could be present in the facility. The moisture measurement system is controlled and read using the custom-built MICROLINK modules (BIODATA Ltd., UK). Moisture measurements are logged at fixed intervals by the computer under the control of HP VEE. As an alternative, 20 *ThetaProbes* and the tipping bucket gauges were connected to a DataTaker 600 Data-logger. This was necessary to enable experimentation whilst additional circuit boards designed for the gypsum blocks were being added to the MICROLINK.

In order to allow repeated leak experiments from a dry basis, a drying or dehumidification system also had to be installed. Whilst dehumidification is common and relatively straightforward for low-density materials, dehumidification of a solid $8m^3$ mass of sediment proved much more of a challenge. The system developed comprises a CAD500

desiccant dehumidifier with a drying capacity of 16 litres per hour (CALOREX Ltd., UK) coupled with a high-pressure direct drive fan system (SECOMAK Ltd UK). The design criterion for the system was to allow drying of the 8 m^3 mass from saturation to below 10% humidity within 14 days. Realistically no system available will provide better drying capacity than this. Drying of the material *in situ* is achieved with 200 metres of perforated polyester coil reinforced plastic 2" ducting covering two sides and the base of the facility at 15 cm intervals coupled with two 6" vents to the top of the facility. The dehumidification is employed between experiments to dry the sediment for repeat experimentation. Drying can be observed in real time using the moisture measurement system. The tubing of the dehumidification system can be seen in Figures 5.4 and 5.5.

The facility is surrounded by a wooden gantry to allow access to the sediment surface for CMP and reflection profiling mode data collection using the PulseEKKO 1000A ground penetrating radar (Sensors and Software Ltd., Canada). Data is collected on a regular grid (Figure 5.5) covering the central square metre of the box to avoid the edge effects that are experienced outside of this zone. Whilst these edge effects can be filtered using time domain processing they add extra complexity to the radar return and to the processing so avoiding these effects is very useful.

Figure 5.5: Data collection grid for the PulseEKKO 1000A GPR system inside LTF.

5.2.2.2 LTF DRY experimental data

For these experiments material was layered using the configuration outlined in Table 5.1. These materials are summarised in Table 5.2 and represent a range of particle sizes, potentially different hydraulic conductivities (and therefore moisture distributions), and potentially different effects on the GPR signal through attenuation. These materials therefore allow construction of varied subsurface environments and have a potentially varied effect on moisture distribution and GPR response. Table 5.2 provides a brief description of the experimental properties. Details of the properties of each material can be found in Section 6.2. The properties of each of these materials were derived using the methods outlined in Section 5.2.3, upon excavation of each layer after the LTF DRY GPR data had been collected.

Material	Upper Limit (m below surface)	Lower Limit (m below surface)	Layer Thickness (m)
M1	0.00	0.20	0.20
M2	0.20	0.48	0.28
M3	0.48	0.60	0.12
M4	0.60	0.88	0.28
M5	0.88	1.02	0.14
M1	1.02	1.60	0.58

Table 5.1: Details of material configuration for dry experiments.

Material	Particle Size Description	Potential Hydraulic Conductivity	Potential Signal Attenuation
M1	Gravel	High	Low
M2	Coarse Sand	High	Low
M3	Mixed Sand	Moderate	Low
M4	Fine Sand	Moderate	Low
M5	Finer Sand	Low	Low
M6	Silt / Clay	Low	High

Table 5.2: Brief characteristics of each experimental material.

The GPR data collected for these experiments included two grids (one at 0.1 m horizontal resolution and one at 0.2 m resolution) for each of the two GPR antenna frequencies considered in this research: 450 MHz for increased penetration depth and 900 MHz for increased subsurface resolution and greater control of the measurement volume. Due to their differing wavelengths and configurations, these can be expected to respond in different ways to subsurface variation. GPR data were collected using a variety of time

windows and sampling intervals for initial exploratory purposes. For the grid data a time window of 50 ns and a sampling interval of 10 ps were used to ensure complete recording of the returned GPR signal. An additional set of 900 MHz (due to its higher resolution) experiments were conducted using suspended mode GPR data in order to identify signal characteristics and assess the potential offered by this technique for moisture estimation. GPR traces were collected at suspension heights of 0 m, 0.4 m and 0.95 m using a wooden frame attached to the LTF, and at three separate locations (x = 0.5, 1.0 and 1.5 m) using the same data acquisition parameters as for the dry grids.

5.2.3 Material properties

Six materials (M1-M6) were used in the laboratory experiments representing a range of particle sizes and complexities. Because both water behaviour and radar response are dependent on various interrelated material properties, these need to be known in order to interpret the results of the wet experiments. Table 5.3 summarises the material properties measured, where the samples were collected, and the number of samples. For materials M1-M5, 30 samples were collected across a 1 m^2 grid in each layer as the material was excavated after the LTF DRY experiments in preparation for the wet experiments. Texture and bulk density were determined in this way. M6 was not used in the dry experiments so 30 samples were collected from the surface layer in the LTF WET experiments prior to experimentation. Hydraulic conductivity and *ThetaProbe* calibration was performed on material sampled from storage. In association with the *ThetaProbe* calibrations, gravimetric moisture content and bulk density samples were also determined for each material. Furthermore, *ThetaProbes* were used to derive estimates of dielectric constant and signal propagation velocity from 100 samples taken by inserting the probe into the surface of each layer across the 0.1 m resolution dry grids on excavation of the materials. Each of the methods for obtaining these data are now outlined. The methods are equally applicable to the lab and field investigations. These properties can be related to variability in GPR response.

5.2.3.1 Particle size analysis

Particle Size Analysis was performed using the dry sieving technique for M2-M5 and using the wet sieving technique with sedigraph analysis for M6 and the field samples. For details of the wet and dry sieving techniques see McManus (1988) and Whalley (1990). For M1, which consisted solely of gravel, the long dimension of 30 stones was measured.

Material Property	Sample Source	Number of Samples for Each Material
Texture	Dry Grid Excavation*	30
Bulk Density LTF	Dry Grid Excavation*	30
ThetaProbe Calibration	Storage	10
Bulk Density STF	Storage	10
Gravimetric Moisture Content	Storage	10
Porosity	STF at Saturation	Variable (see Chapter Six)
Dielectric Constant	Dry Grid Excavation*	100
Hydraulic Conductivity	Storage	5

Table 5.3: Number of samples for each material property assessed in the research. Sample source indicates whether the sample was derived from a particular material configuration or otherwise. All samples were random. *For M6, samples were collected using the LTF WET configuration prior to experimentation.

5.2.3.2 Dry bulk density

Variations in bulk density between experiments and materials may affect both the distributions of moisture and the measurements of the moisture (e.g. by altering *ThetaProbe* calibrations or having a direct impact on the GPR profile). Dry Bulk density measurements were collected using a dry bulk density ring (height = 3 cm; diameter = 4 cm). Dry bulk density was also determined at the time of the *ThetaProbe* calibrations by filling a 500 ml beaker with each material. Because there is no potential material compression with depth using the latter method, it may be expected to provide more consistent data than using the samples from the dry experiments. Bulk density is defined as the weight of a volume of dried soil divided by the original volume (Dingman, 1994):

$$\rho_b = m_s / V_t \qquad (5.1)$$

where m_s is mass of dry soil (g) and V_t is total volume (cm^3).

5.2.3.3 ThetaProbe calibration

The theory behind *ThetaProbe* estimates of VMC is outlined in Chapter Two. Voltage data read from the *ThetaProbe* can be converted to dielectric constant and VMC data using a general or soil-specific calibration equation, or using the Topp *et al.* (1980) relationship; all of which can be fitted by a linear relationship or a third order polynomial (Delta T Devices, 1998). The Topp *et al.* (1980) route to VMC estimation is analogous to the approach used with CMP data for GPR and first calculates $\sqrt{\varepsilon}$ using equation 2.10 or 2.11, then uses equation 2.9 to calculate VMC from ε $(= (\sqrt{\varepsilon})^2)$. The standard *ThetaProbe* calibration uses the simple linear relationship between the complex refractive index (equivalent to $\sqrt{\varepsilon}$) and VMC, θ, of the form (Delta T Devices, 1998):

$$\sqrt{\varepsilon} = a_0 + a_1 \cdot \theta \tag{5.2}$$

The parameters a_0 and a_1 have recommended values of 1.6 and 8.4 respectively for mineral soils and 1.3 and 7.7 respectively for organic soils. These values are entered into the following equations to determine VMC (Delta T Devices, 1998):

$$\theta = \frac{[1.1 + 4.44V] - a_0}{a_1} \quad \text{(Linear standard calibration)} \tag{5.3}$$

$$\theta = \frac{[1.07 + 6.4V - 6.4V^2 + 4.7V^3] - a_0}{a_1} \quad \text{(Polynomial standard calibration)} \tag{5.4}$$

ThetaProbe measures the dielectric constant (ε) of the soil. The relationship between the measured dielectric constant of a soil and its water content (θ) depends on the particular composition of the soil thus necessitating soil-specific calibration to minimise the errors associated with converting *ThetaProbe* output (V) to soil water content (Delta T Devices, 1998). The following protocol was used (Delta T Devices, 1998). A sample of damp soil was collected, disturbing it as little as possible so that it is at the same density as *in situ*. The *ThetaProbe* was inserted to measure the probe output, V_w. Equation 2.10 was used to calculate $\sqrt{\varepsilon_w}$. The damp sample is then weighed, (W_w), and its volume (L) measured.

The sample is then oven-dried and the probe output in the dry soil, V_0 is measured. The dry sample is weighed (W_0) and equation 2.10 was used to calculate $\sqrt{\varepsilon_0}$. This equals a_0 and will usually have a value between 1.0 and 2.0. The volumetric water content θ_w of the original sample can then be calculated:

$$\theta_w = \frac{(W_w - W_0)}{L} \tag{5.5}$$

Then:

$$a_1 = \frac{\sqrt{\varepsilon_w} - \sqrt{\varepsilon_0}}{\theta_w} \tag{5.6}$$

and will usually have a value between 7.6 and 8.6. The water content determined from a calibrated *ThetaProbe* can then be calculated using either equation 5.3 or equation 5.4. To perform material-specific calibrations ten 250 ml samples were collected for each material, to which different volumes of water were added. Using these ten samples mean values of a_0 and a_1 were calculated using the above procedure to produce calibrated equations for each material. The results are reviewed in Section 6.2.

5.2.3.4 Gravimetric moisture content

Gravimetric moisture content was determined to calibrate and separately to validate *ThetaProbe* VMC estimates. Validation of *ThetaProbe* VMC estimates involves independently checking the experimental VMC estimations, and independently testing the calibration equations. Gravimetric moisture content was determined using the procedure outlined in Section 2.5.1.1. For independently testing the VMC calibration equations, 10 samples were collected for each material, wetted, weighed, *ThetaProbe* voltage measured, oven dried for 24 hrs at 105°C, and then re-weighed. *ThetaProbe* VMC was estimated using the specific calibration equation for each material and then plotted against VMC calculated from Gravimetric Moisture Content.

5.2.3.5 Porosity

Porosity was determined from all saturated *ThetaProbe* VMC measurements for each material during the STF experiments. This means that the estimate was derived under identical conditions (not subject to compression with depth) for each material but is dependent upon the accuracy of the calibrated *ThetaProbe* estimations. It also assumes that the recorded value corresponds to total saturation.

5.2.3.6 Hydraulic conductivity

Hydraulic conductivity is a hydraulic parameter that may indirectly influence radar response because it is an important control on water infiltration, redistribution and the VMC of a system. With knowledge of the hydraulic conductivity of the laboratory materials it is possible to design experiments which allow sufficient time for water redistribution before radar data is collected, thus minimising one potential source of uncertainty in the results because three dimensional characterisation of water dispersion in a complex medium is difficult even with an extensive network of moisture sensors. Where redistribution times are too long for feasible separations between radar profiles, or where material differences result in complex patterns of moisture distribution, knowledge of the hydraulic conductivity allows the nature of the water distribution to be accounted for when interpreting VMC and radar results.

Five samples of each laboratory material were collected from material in storage and placed in a 500 ml beaker. Hydraulic conductivity was measured using the mini-disk infiltrometer technique (Decagon Devices, 1998) in which the starting volume of a full infiltrometer was recorded. At zero seconds the infiltrometer was brought into contact with the material surface and volume was then recorded at 10 s time intervals as the water infiltrated. The volume is converted to depth of water infiltrated by subtracting the starting volume reading and dividing by the area of the disk on the infiltrometer, 7.92 cm^2. To derive the hydraulic conductivity the method outlined in Appendix One was used.

5.2.4 Developing the VMC-GPR relationships using the STF

For deriving relationships between moist soils and dielectric constant it is possible to simplify the problem by considering only pure sand, or pure clay, mixed with air and water (Hasted, 1973). The approach adopted here is to test and characterise the GPR response after each successive water addition to a given material using the GPR in reflection profiling mode and to relate the quantitative measurements of the signal to independent estimates of VMC. These experiments represent the main investigations of the research and aim to develop models that estimate VMC using derivable GPR signal characteristics and to understand and explain GPR response to changing moisture and material conditions. This requires an experimental design that enables an average VMC to be determined in a relatively small volume of material (to minimise potential spatial variations), with minimal disturbance of the GPR signal, and where independent estimates of VMC (for model development and testing), can be acquired without disturbing the experimental configuration during each experiment.

5.2.4.1 Small test facility

A small test facility (STF) (Figure 5.6) was constructed. The STF consists of a plastic container 0.45 m wide, 0.60 m long, and 0.60 m deep, surrounded by gravel (M1, see Table 5.2) and placed in the centre of the LTF. The STF was designed to allow water into the substrate at its surface as evenly distributed infiltration and to drain out through a tap into a tipping bucket to measure drainage. Drainage was assisted by a waterproof concrete base, which sloped towards the outlet and reduced the depth of material to 0.58 m. Moisture measurements were made using seven *ThetaProbes* (Delta-T Devices Ltd.), at the depths indicated on Figure 5.6, and connected to a DataTaker 600 data-logger, logging every two minutes. Although, *ThetaProbe* measures moisture from a considerably smaller volume of material (about 30 cm^3 (Delta-T Devices, 1998)) than the GPR (unknown and variable), taking the average estimated VMC of the seven calibrated *ThetaProbes* and comparing this with a GPR estimate derived from a constant material depth (0.58 m), these differences should be reduced. The observed moisture measurements will be used for developing relationships with derivable GPR signal characteristics and for providing validation data to VMC estimations made using the GPR.

5.2.4.2 Experimental details

Table 5.4 summarises the experiments performed using the STF. Six experimental runs were performed using six separate materials (M1-M6) placed inside the STF. Water was added in five litre increments from dry to saturation every 25 minutes, although for M6 saturation was never achieved and its low hydraulic conductivity meant that water took much longer to infiltrate and redistribute which required longer separation times. To minimise the effects of moisture distribution, radar profiles were taken 20 minutes after each successive increment of added water, allowing the water to infiltrate fully into the facility. All radar data were collected using a bistatic Sensors and Software PulseEKKO 1000A GPR system, a time window of 30 ns (to ensure the whole facility was imaged when saturated), a sampling interval of 50 ps (to ensure complete sampling of returned waveforms), with 32 stacks (32 traces averaged to produce one during profiling to reduce noise) and an antenna frequency of 900 MHz (to achieve maximum vertical resolution and reduce the impact of GPR footprint area). 20 traces were collected and then averaged to provide a single trace for each water addition and each material, from which a GPR parameter can be calculated. Details of how the GPR data were analysed are discussed in Section 5.4.

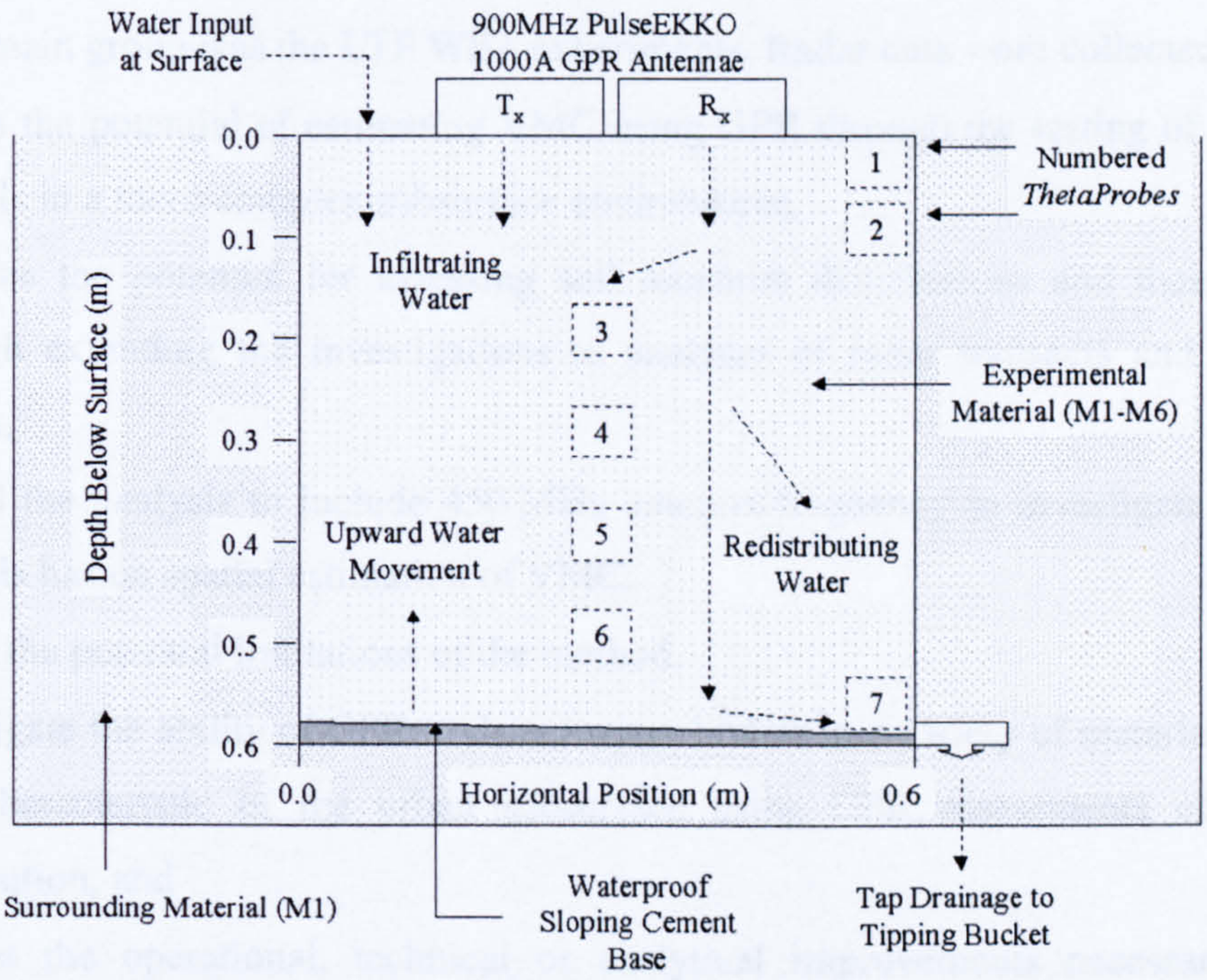

Figure 5.6: Schematic of experimental configuration using the small test facility.

After completion of the wetting runs for each material, the drainage tap was opened and water allowed to drain until no more water would drain. Drainage times lasted between 1-15 hours depending on the hydraulic conductivity of the material. For these drying runs the GPR was left recording traces every 30 seconds. These data were used to test the relationships developed using the wetting runs.

Experiment Group	Materials Used	Water Increments (l)	Maximum Volume of Water Added (l)	Aim
Wetting	M1	5	56.05	Developing VMC relationships.
	M2	5	49.15	
	M3	5	39.35	
	M4	5	50.40	
	M5	5	52.10	
	M6	5	38.80	
Drainage	M1-M6	N/A	N/A	Testing VMC relationships

Table 5.4: Details of experiments performed using STF.

5.2.5 Spatial variation of subsurface moisture

The next main group was the LTF WET experiments. Radar data were collected to:

- assess the potential of estimating VMC using GPR through the testing of developed models in a more complex subsurface environment,
- examine the potential for assessing soil moisture distributions and their variation through extending the investigations to analyses of radar transects and to greater depths,
- extend the analysis to include 450 MHz antenna frequency to investigate the effect that this has on spatial estimation of VMC,
- assess the potential limitations of the method,
- investigate the ability of GPR to detect water bodies in a variety of materials more or less characteristic of the urban subsurface using GPR assessments of moisture distribution, and
- suggest the operational, technical or analytical improvements necessary for the routine detection of soil moisture using GPR

To achieve these aims a series of experiments were conducted using the LTF in which subsurface pipes were used to leak different volumes of water into different materials at different depths. Details of how the materials were layered are shown in Table 5.5 and are illustrated in Figure 5.2. The material profile was constructed incrementally between experiments to provide a variety of subsurface environments. For E1 the top layer consisted of M2, for E2 the top layer was M1, and for the remaining experiments M6 was used as the top layer, although between x = 0.5-1.0 m, the rock fragments had been removed to produce a moderately more homogeneous clay layer. The details in Table 5.5 represent the material configuration for the complete profile. For E5 a layer of bricks was added to provide the equivalent of a pavement in an urban subsurface. Details of the experimental hydrology and the GPR transects are summarised in Table 5.6.

Material	Upper Limit (m below surface)	Lower Limit (m below surface)	Pipe Position (x,y,z) (m)
M6	0	0.4	0.75, 1.0, 0.2
M6*	0	0.4	1.25, 1.0, 0.2
M1	0.4	0.6	1.0, 1.0, 0.5
M2	0.6	0.8	1.0, 1.0, 0.7
M3	0.8	0.9	N/A
M5	0.9	1.0	N/A

Table 5.5: Details of material layering and pipe locations for the final material configuration. Pipe locations are metres below surface when full. *This side of the profile contained M6 with rock fragments.

Experiment	Primary Material[1]	Water Volume Added (l)	Rate of Leak ($l\,hr^{-1}$)	Nature of Leak	Length of GPR transect (m)[2]
E1	M2	55	60	Diffuse	1.0 (1.0)
E2	M1	60	261.72	Diffuse	1.0 (1.0)
E3	M6	85.26	211.68	Concentrated	0.5 (0.75)
E4	M6[3]	157.66	253.94	Concentrated	0.5 (1.25)
E5	M2[4]	124.66	211.68	Diffuse	1.0 (1.0)

Table 5.6: Experiment details: materials and water volumes. Notes: [1]The primary material represents the material into which the water was added. [2]Value in brackets represents the x-coordinate at the centre of the transect. [3]M6 with rock fragments. [4]Pavement added at surface of profile adds 0.05 m to profile depth.

The experiments for the assessment of moisture distribution were designed with consideration for a variety of potential subsurface water leak conditions that may arise

and that may affect the detection of the moisture patterns associated with a leak. The experiments can be summarised within the context of leak detection (Table 5.7):

E1	M2 layer leak. To see if a water leak can be identified in a sand layer with high hydraulic conductivity. To assess the potential effect of rapid vertical redistribution and the impact of a hydraulic interface (the M3-M2 boundary) on moisture distribution. Assessment of leak characteristics in two different materials and whether it is still possible to see the material interface under leak conditions.
E2	M1 layer leak with mix to lower leak. To see if a water leak can be identified in a gravel material and to assess to what extent it is easier to identify a leak in a gravel rather than a sand material. It also offers the opportunity to establish whether or not the previous leak appears under another leak and the extent to which the radar response has been affected by dispersion / movement over time.
E3	M6 layer leak. To see the extent to which leak detection is possible in a simple clay material and for comparison with other materials.
E4	M6 layer leak with rock fragments. To see the extent to which leak detection is possible in a typical urban subsurface material where large rock fragments result in a complex subsurface hydrology and may produce complex GPR signal returns.
E5	M2 layer leak with pavement. To see how the situation changes when a pavement is added. To see to what extent a leak at depth can be identified through pavement, clay material and antecedent moisture.

Table 5.7: The moisture distribution experiments.

All experiments were carried out using reflection profiling mode. All profiles were taken at 0.01 m spatial resolution across 0.5 or 1 m transects perpendicular to the leaking pipe. A transect was taken both before and after water was added at 450 and 900 MHz antenna frequencies. The sampling interval used was 10 ps with a time window of 50 ns to ensure both maximum detail and inclusion of the entire box image even when water was added. *ThetaProbes*, surrounding each pipe, were sampled every minute so as to validate the GPR estimations. These also provide data on water content and dielectric constant changes for each run. Figure 5.2 summarizes the changing *ThetaProbe* locations for each experiment.

5.3 FIELD INVESTIGATIONS

Field investigations were performed to apply and validate the analytical techniques developed by mapping moisture distributions in two different situations: the detection of mains water leaks, and an analysis of the nature and dynamics of soil moisture spatial

variability. Emphasis was placed on the spatial patterns that develop as the soil wets and dries and the impact of this pattern generation on flow connectivity at the hillslope scale. This will be used to demonstrate the utility of the GPR as a tool in investigations of spatial variability. Two distinct methodologies are involved. First, comparing the structure of the subsurface variability between the measured subsurface parameters and the recorded GPR returns. Secondly, applying and validating the analytical techniques developed earlier in the research.

5.3.1 Mains water leak detection

The urban subsurface environment is much more complex than any of the environments generated in the laboratory. Mains water leaks are likely to be of larger magnitude in terms of rate and areal extent than can be generated in the laboratory. Thus field explorations of leak sites were necessary to complement the laboratory analyses. A Thames Water Leak Detection team utilised GPR in an attempt to detect mains water leaks using Visual Analysis. The current research sought to develop GPR as a direct, accurate and efficient technique for objective leak detection. Because our interest in GPR is for measuring spatially distributed subsurface variables, the approach adopted in this research is to locate mains water leaks through measurement of their associated VMC distributions, utilising the methodologies described rather than from visual analyses.

The Thames Water Utilities GPR team visited a number of known leak sites identified using standard techniques. Surveys at 19 sites were provided by the Thames Water team. Of these, two known leaks were selected based on complete survey information concerning location, main size, and full survey details (Table 5.8). An important feature of these leaks is the different size of the main. Because the size of the main can be expected to affect the rate and size of the leak, the potential use of the developed GPR techniques for different types of leak can be assessed. At each leak site a series of GPR surveys were performed over the leak site prior to excavation and repair. On excavation the GPR surveys were visually validated where possible. No other calibration and validation data were available. This is not a problem because the aim is to identify a leak based upon estimations of the relative moisture distributions in the subsurface; this does not require the absolute VMC values. All surveys used in this research included one grid over the leak zone and transects along the pipe itself stretching 5 m either side of the

centre of the suspected leak. Each grid, centred over the leak, consisted of 13 profiles at 0.02 m resolution separated by 0.20 m. For each leak site radar data were acquired using an antenna frequency of 450 MHz, a time window of 40 ns, a sampling interval of 0.2 ns, and four stacks.

Leak Name	Leak Latitude	Leak Longitude	Main Size (m)	Road or Footpath
2 Adam's Square, Eltham	51°27'33.952" N	00°07'44.422" E	0.1	Path
Cromwell Road, South Kensington	51°29'42.176" N	00°10'58.328" W	0.75	Road

Table 5.8: Details of Thames Water field investigations.

5.3.2 Small-scale soil moisture variability, Plynlimon, Wales

To assess the potential use of GPR to map soil moisture distributions with a view to understanding the relationship between spatio-temporal moisture dynamics (changing patterns of moisture connectivity with time) and hillslope / catchment hydrological response, a field campaign was conducted between July and October 1999. In addition to the collection of GPR data at the plot-scale to estimate patterns of VMC, independent VMC data are required to either calibrate or validate the GPR estimations, and information on the subsurface soil characteristics is required in order to interpret GPR response and determine likely subsurface variability and its effect on moisture distributions. To relate the GPR derived patterns of moisture variation to its effect on hillslope response, knowledge of moisture inputs (rainfall) and outputs (overland flow, throughflow, evaporation and drainage) is required. To facilitate this data collection and analysis, the fieldwork methodology outlined below was used.

5.3.2.1 The field site

The field site chosen for this research is located on a hillslope in the Cyff, a sub-catchment of the Wye Catchment, Plynlimon, Wales. It forms part of the Centre for Ecology and Hydrology research catchments and consequently there are a lot of support data available. This includes a network of weather stations, rain gauges and channel

flumes. Furthermore, recent work using GPR for depth to bedrock studies has been performed at this site (see Howe, 2000). Consequently, an instrumented plot already exists and the site provides useful information on soil moisture.

5.3.2.2 Experimental plot design

The original field plot is documented in Howe (2000), is south facing and is about 454 m above sea level. Above this existing plot, a 2 by 2 m plot (Figure 5.7) was constructed. Although this plot is small, and can therefore be expected to present limited moisture variation, the emphasis of the research at this stage is on an assessment of potential offered by GPR, and not a comprehensive assessment of hydrological response. Thus the plot was designed to provide controlled conditions, as much as possible, by measuring inputs and outputs over a limited hillslope area. The sides and upper section of the plot were closed off to external flow using a trench (up to 0.6 m deep (see Figures 5.8a and 5.8b)) lined with plastic. This results in the only moisture input to the plot being from rainfall, which is measured using a tipping bucket raingauge (0.2 mm resolution, Environmental Measurements Ltd, UK) connected to a DataTaker 600 data-logger. The plot was selected to minimise the influence of topographic and vegetation variation on the distribution of soil moisture because surface roughness affects the coupling of the GPR system to the ground (see Chapter Eight). A series of 14 *ThetaProbes* were laid at two depths (0.1 and 0.3 m) below the surface in seven pits (see Figure 5.8c) at the locations shown in Table 5.9. The network of subsurface *ThetaProbes* provide information on horizontal and vertical variability in soil moisture, on the temporal changes of soil moisture, and also enable the calibration and validation of GPR estimates of VMC. No measurement of drainage was made because the depth to bedrock is shallow, with a maximum of about 0.7 m, and the presence of unconsolidated shale at approximately 0.3 m beneath the soil surface. Detailed information on overland flow and throughflow is available from a 2 m trench which runs across the bottom of the plot with a gutter that flows into tipping buckets gauges at the surface and at 0.3 m depth respectively. All instruments were connected to a DataTaker 600 data-logger with *ThetaProbe* measurements logged every 10 minutes and gauges logged on an event basis.

5.3.2.3 Experimental data

During construction of the experimental plot a trench (Figure 5.8) was dug upslope and to the sides from which soil horizon thickness data were measured using a metric tape measure every 0.5 m laterally along the trench to supplement soil auger validations of soil GPR depth estimations. To avoid disturbance to the site during the campaign, at the end of the field campaign (April 2000), soil samples for texture, bulk density, porosity and depth were collected using soil auger methods and by digging pits. 49 samples for bulk density, texture and porosity were collected from the seven *ThetaProbe* pits using bulk density rings while excavating the *ThetaProbes*. In each pit samples were collected at 0.05, 0.1, 0.2, and 0.3 m beneath the surface on the upslope side of the pit and at 0.05, 0.1 and 0.2 m beneath the surface on the left hand side of the pit facing upslope. 25 soil auger samples were taken at 0.4 m spacing to determine soil depth, soil horizon thickness, and provide additional textural information. Eight samples were collected by Howe (2000) to calibrate the *ThetaProbes*. Excavation of the *ThetaProbes* prevented the use of the soil around the *ThetaProbes* themselves due to excessive disturbance. A 0.1 m resolution topographic survey (Figure 5.9) was conducted so that information on the likely influence of the form of the land on moisture could be determined.

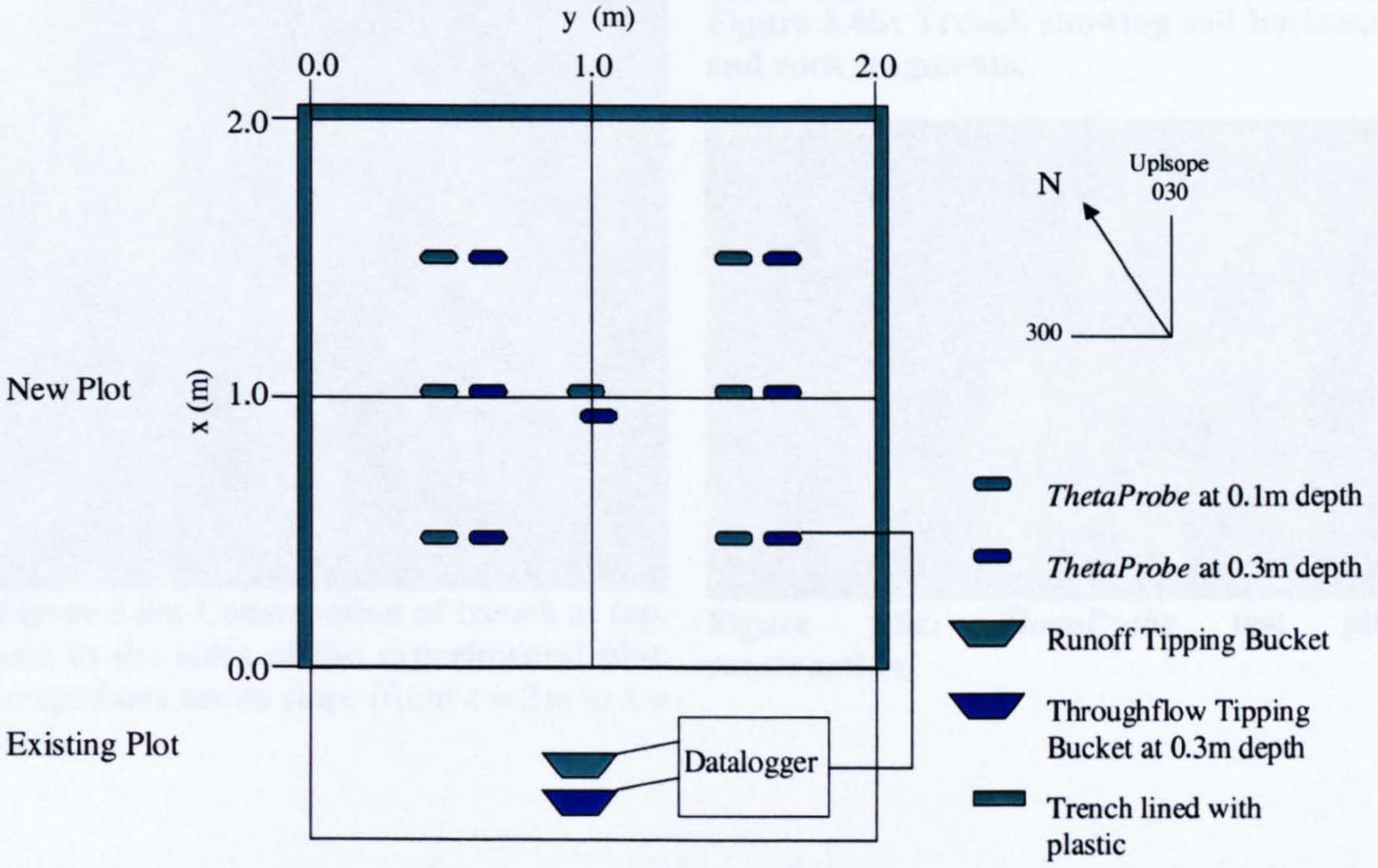

Figure 5.7: Details of experimental plot instrument layout, Plynlimon.

Test Pit Number	*ThetaProbe Number*	x (m)	y (m)	z (m) (below surface)
1	1	1.45	0.5	0.1
1	2	1.55	0.5	0.3
5	3	0.45	0.5	0.1
5	4	0.55	0.5	0.3
2	5	1.45	1.0	0.1
2	7	1.55	1.0	0.3
3	11	1.45	1.5	0.1
3	12	1.55	1.5	0.3
4	13	0.95	1.0	0.1
4	14	1.05	1.0	0.3
6	15	0.45	1.0	0.1
6	16	0.55	1.0	0.3
7	17	0.45	1.5	0.1
7	18	0.55	1.5	0.3

Table 5.9: *ThetaProbe* locations in the experimental plot.

Figure 5.8a: Construction of trench at top, and to the sides of the experimental plot. Image faces across slope (from x = 2 m to x = 0 m).

Figure 5.8b: Trench showing soil horizons and rock fragments.

Figure 5.8c: *ThetaProbe* test pit construction.

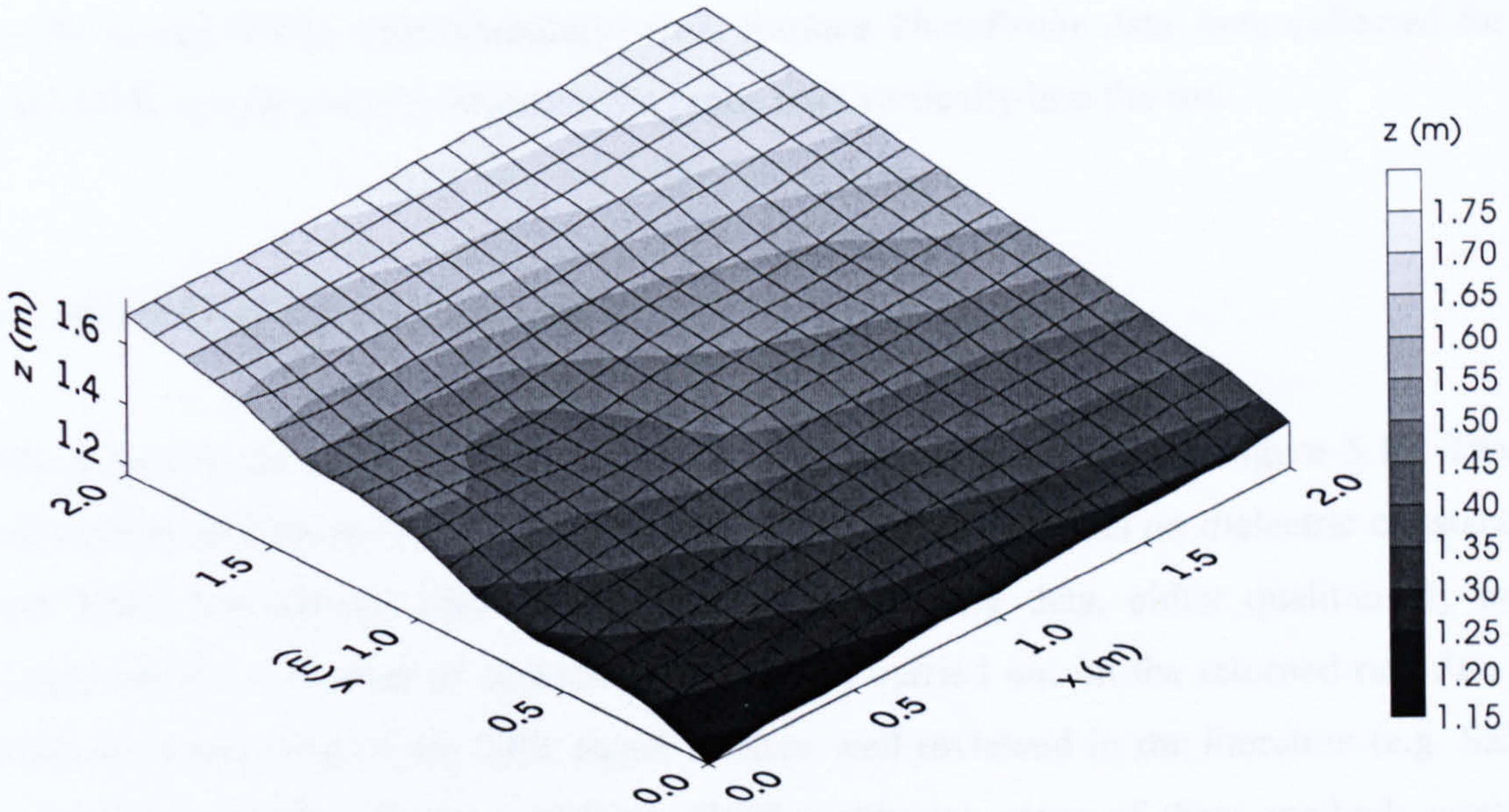

Figure 5.9: Topography of experimental plot.

5.3.2.4 GPR survey data

Because this research aims to study the spatially varying patterns of soil moisture that emerge as the soil wets and dries through time, surveys were repeated from July to October 1999 so that conditions are initially dry, become dryer and then become much wetter. Details of each set of surveys are summarised in Table 5.10.

Campaign	Date	Profile Day	Grid Data Collected		
			900 MHz	450 MHz	*ThetaProbe*
1	8th July	1	Yes	No	Yes
1	9th July	2	No	Yes	Yes
2	15th July	8	Yes	Yes	Yes
3	14th August	38	Yes	Yes	Yes
4	21st August	45	Yes	Yes	Yes
5	25th September	80	Yes	Yes	Yes
6	30th October	114	Yes	No	Yes

Table 5.10: Details of the GPR data acquired during the field campaign.

On each of six survey campaigns radar data were collected at a spatial resolution of 0.1 m within the plot at 900 and 450 MHz antenna frequencies perpendicular to the upslope direction along the survey lines shown in Figure 5.8. Radar data were acquired using a time window of 60 ns to ensure sufficient penetration depth and a sampling interval of 50

ps for compatibility with laboratory work. Surface *ThetaProbe* data were collected for each GPR sample point by inserting the probe rods vertically into the soil.

5.4 ANALYSIS OF RADAR DATA

The stages involved in the analysis of all GPR data are depicted in Figure 5.10. The acquisition of both the GPR data and independent subsurface data on dielectric constant and VMC has already been discussed. Before analysing data, either qualitatively or quantitatively, a number of operations are usually carried out on the returned raw data. Such pre-processing of the GPR signal is often well reviewed in the literature (e.g. Sai and Ligthart (2000), Young and Deng (1995)) although some of these methods work robustly only for specific scenarios and therefore do not work properly with other scenarios (Sai and Ligthart, 2000). Signal processing procedures are necessary to compensate or minimise undesirable effects and enhance the radar images of subsurface regions (Boryssenko *et al.*, 2000). Each processing stage will alter the raw data to some extent (unless it is only applied for visual analysis) and, therefore, processing of the radar data was kept to a minimum in order to preserve the original amplitude values and therefore the potential impact of the subsurface moisture on the signal. Thus the analysis of the GPR data comprised six stages:

1. Processing of the original time domain data to produce the raw data for each of the other four basic visualisations, using batch processing (to reduce processing time) of the data in the PulseEKKO 4.2 GPR software. The data can also be displayed using the software to enhance understanding of the potential GPR response and test the application of a variety of filters and gains to increase the detection of subsurface features, where appropriate.
2. Export of individual traces from PulseEKKO 4.2 software using the LST_PTS sub-routine and batch processing to Microsoft Excel where a series of macros were written to decrease processing time involved in the re-arrangement of traces.
3. Using the arranged traces in Microsoft Excel, individual traces are displayed to determine the analysis start time, which corresponds to the approximate surface of the ground, G_0. The analysis start time is approximated as timezero (defined as the direct air arrival and represents the first energy of arrival (Olhoeft, 2000)) minus the air-wave travel time (AWTT: 0.567 ns at 900 MHz and 0.833 ns at 450 MHz for the PulseEKKO 1000A GPR system), because this first wave is not really timezero

because it takes a small amount of time for the pulse to travel from the transmitting to the receiving antenna (Conyers and Goodman, 1997). Timezero may change during a survey if the operating temperature of the equipment varies greatly (Young *et al.*, 1985) and is a function of the system timing, cable lengths and antenna position (Olhoeft, 2000). Consequently, all GPR pre-processing begins with realigning the first break. This can be done in numerous ways all of which depend on the identification of the first break. In seismic analyses operators pick first-break events using a combination of amplitude, phase, trace-to-trace continuity and wavelet character (McCormack *et al.*, 1993). Traces are then aligned at G_0 for display in SURFER.

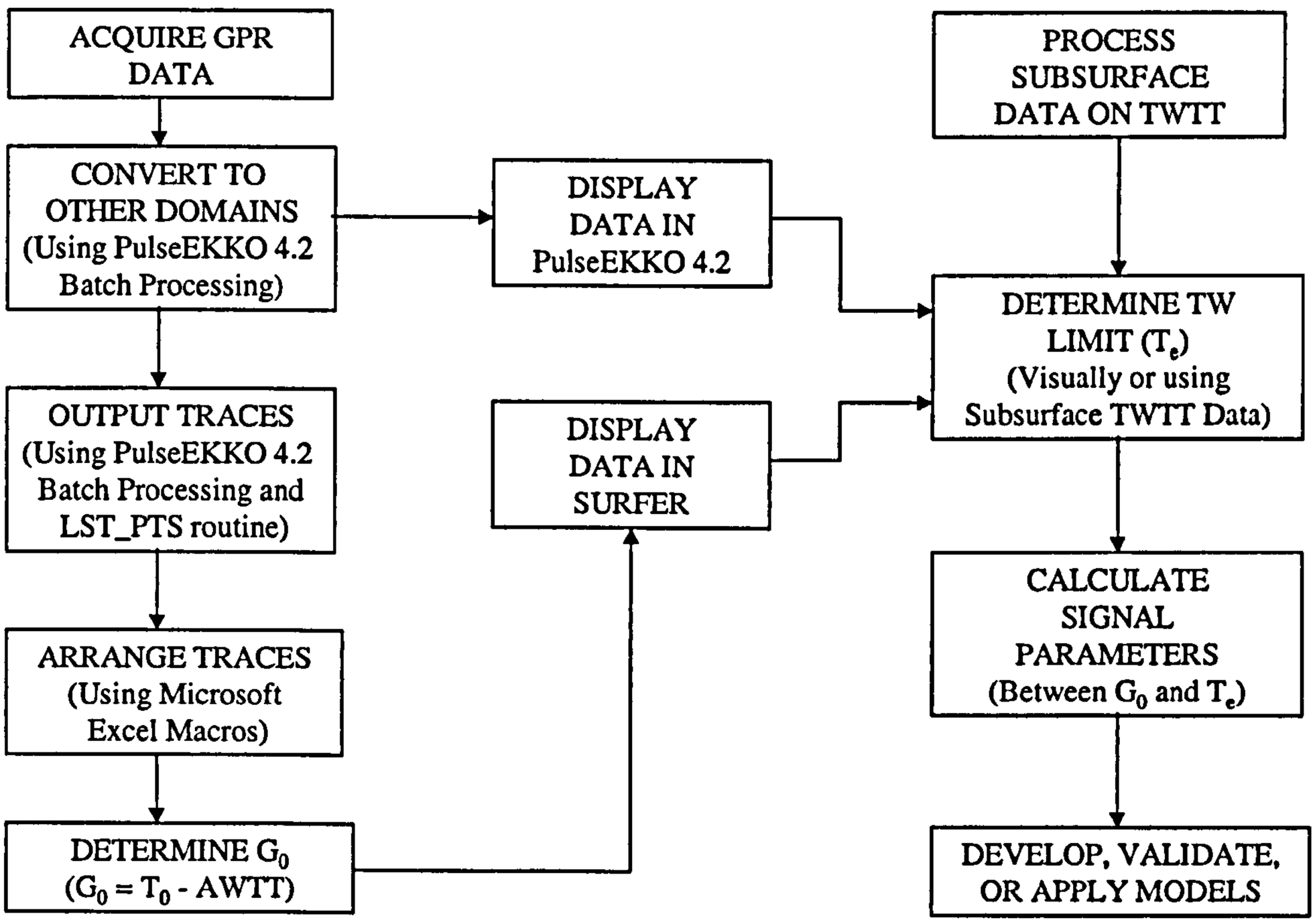

Figure 5.10: Schematic representation of GPR data analysis (for details see text).

4. Using either visual analysis, or data available on subsurface dielectric values, the analysis end time can be calculated (T_e). The analysis end time corresponds to the base reflection of the STF, the base of the material profile in the LTF, or some other definable limit in the case of field data. Using visual analysis, T_e can be determined for the analysis of velocity using depth correlation methods (because it gives a value

for TWTT) or in the absence of other subsurface data. Where subsurface dielectric data are available, T_e can be calculated by adding theoretical TWTTs (derived using equations 3.2 and 4.7) to G_0. For the STF experiments, TWTTs were calculated from the dielectric constant distribution based on the seven *ThetaProbes* and assuming a vertically incident plane wave as in simple synthetic radargram analyses. This assumption is affected by the finite separation of the radar antennae, which increases the travel distance, and therefore TWTT, by a small amount, which decreases with increasing depth to reflector. For the LTF experiments, the *ThetaProbe* distributions discussed earlier were used. Calculation of reflection coefficients then enable the end time to be determined objectively as the zero-crossing prior to a peak of sign indicated by the reflection coefficient that is closest in time to the theoretical travel times. Because changing VMC affects TWTTs, the analysis end time was adjusted to accommodate this variation based on subsequent *ThetaProbe* TWTT estimations.

5. The selected statistic, chosen to characterise signal response, is then calculated for all data between the start and end times. By dynamically adjusting the T_e for each experimental run, it is possible to control for measurement depth ensuring that the estimate of VMC is derived from a controlled depth in the subsurface (0.58 m in the case of the STF experiments). Because the dielectric constant increases as a function of increasing VMC, the TWTT of the signal propagating through a constant depth will increase. Thus, to maintain a constant measurement depth, the analysis time window (G_0 to T_e) should expand to accommodate these changes. This constrains the data analysis to a constant volume but variable time but is only possible where full data are available on subsurface dielectric behaviour (such as in the STF and LTF experiments). By focusing on the trace data between G_0 and T_e, it is also possible to eliminate unnecessary GPR data at the start and end of a trace, which occurs because it is the nature of radar data acquisition that there is a zone of amplitude data prior to the first break and because radar data must be collected with a time window sufficient to identify the target of interest. Consequently, there is often a lot of data acquired that is not relevant to the analysis. This data will produce bias in the amplitude data characterisation, which will potentially obscure any statistic that may be related to a subsurface property.
6. For the development of a model to estimate VMC using a GPR signal characteristic (Chapter Seven), a relationship is fitted by plotting the observed *ThetaProbe* VMC against the value of each statistic for each material. This model can then be applied to

estimate the spatial distributions of VMC (Chapters Eight and Nine), and the model estimates validated (Chapters Seven to Nine).

5.5 SUMMARY

A detailed methodology has been presented, which sets out to meet the objectives outlined in Section 1.2 through a combination of controlled laboratory conditions to develop and test models to estimate VMC using a GPR signal characteristic, and understand the nature of GPR response under conditions of changing moisture, and apply and the validate the models in the context of estimating a variety of laboratory and field moisture patterns. Characterising and understanding the nature of GPR response and its variability in the absence of moisture is a critical first step; this is the focus of the next Chapter.

CHAPTER SIX: GPR RESPONSE IN DRY SUBSURFACE ENVIRONMENTS

6.1 INTRODUCTION

The first stage in this analysis is to characterise the variability in GPR response and to relate this to variability in subsurface properties in the absence of moisture. Spatial variability of the subsurface is likely to be the greatest problem associated with GPR detection of a water body of any kind (see Chapter Five). This spatial variability may manifest itself as a change in subsurface material properties (texture, bulk density, VMC, porosity, and hydraulic conductivity), subsurface structure (distribution of materials, layering, water tables), and the presence of anomalies (objects which may be the target of the GPR survey, or may be unexpected, increasing signal complexity and scattering GPR energy, and which may therefore obscure the desired information).

Variability in GPR response arises from the interaction of the propagating GPR signal with the variability in the subsurface environment. Variations in these subsurface components will affect the distribution of dielectric constant and this in turn will influence the signal propagation through the subsurface. GPR parameters such as attenuation, magnitude and timing will also be affected. Material properties will also have an indirect impact on GPR by affecting movement and distribution of air/water through available pore space. Consequently, the more complex the subsurface environment the more complex should be the expected GPR response. Variability in GPR response using all five of the basic visualisations (trace amplitude, amplitude spectra, instantaneous amplitude, phase and frequency) can be expected and can be categorised by variation in:

- Signal Propagation Velocity (SPV) / Two-Way Travel Time (TWTT) / Reflector Depth (D). These are all related as discussed in Chapters Three and Four. Spatial variability in propagation velocity may make even continuous reflectors less continuous. Signal propagation velocity needs to be accurately estimated before any attempt is made to interpret radar images from the test facility, especially in terms of converting TWTT to depth.
- Magnitudes of Signal Events. The nature of the subsurface dielectric contrasts will affect the strength of reflection events. Attenuation by subsurface materials will act to reduce response magnitudes. The direct interaction of the GPR signal with the subsurface can be expected to produce variability in the direct waves (air and ground) and thus affect the identification of signal events. To characterise the variability of

event magnitudes a number of approaches to signal characterisation were discussed in Chapter Four.

- Frequency. Any component of the subsurface that effects a change on the time domain characteristics of response can equally be categorised by its frequency domain response.

Knowledge of the character of GPR response to the different types of subsurface variation is important in order to understand how representative of this variation GPR response is, and to assess whether or not the variability in GPR response is solely a function of subsurface variability in material properties or subsurface structural features, and to what extent the GPR is more sensitive to certain types of variability. It is feasible that GPR response will accurately represent subsurface moisture variability in homogeneous environments. However, the introduction of anomalies or other variability (such as inherent GPR signal characteristics) may reduce the success of this representation. To address these issues, the variation in material properties is first established as a background to all laboratory work and within the context of the LTF DRY experiments. Then the following situations are investigated:

- Variability in GPR boundary depth estimation (SPV / TWTT / D).
- Variability in character and identification of signal features.
- Horizontal and vertical variability in time domain statistical signal characteristics.
- Impact of subsurface anomalies.

In addition to explaining GPR response, the impacts of antenna frequency and station spacing on subsurface variation estimation are assessed, and the implications for experimental design, GPR use, and soil moisture estimation are discussed. Knowledge of the potential background response allows it to be controlled (especially measurement depth) or accounted for in subsequent moisture analyses and should enable the specific impact of moisture on GPR response to be investigated in detail. Such an analysis can only be achieved if the characteristics of the subsurface environment are known in detail; hence, the requirement for large-scale, controlled laboratory experimentation. It is expected that this work will enable the extension of the GPR to a situation in which subsurface moisture is largely responsible for changes in GPR data.

6.2 PROPAGATION THROUGH EXPERIMENTAL MATERIALS

6.2.1 Introduction

The measurement of particle size, bulk density, VMC, porosity, hydraulic conductivity, and dielectric constant were outlined in Section 5.2.3 for each of the six experimental materials, M1-M6. Presented below are the results of these analyses and an attempt to characterise the variability in these material properties with a view to understanding variation in GPR signal response.

6.2.2 Particle size distribution

Figure 6.1 shows the percentage gravel, sand, silt and clay components for each of the six experimental materials. With the exception of M6 the materials consist largely of one component. M1 is a gravel material with 100% over 2 mm. M2-M5 are dominantly sands with either gravel (M2 and M3) or silt (M4 and M5) in addition to the sand component. Figure 6.2 shows the difference between the fine-earth fractions (0-2 mm) for M2-M6. The cumulative particle size frequency distribution shows that M2 is a coarse sand with 98% greater than 1 mm and is a very well-sorted material. M4 and M5 are both fine-grained sands in which 100% of the particles are smaller than 1 mm. The major difference is that for M4 only 53% is less than 0.25 mm whilst for M5 97% is. M3 is a mixed sand which represents an intermediate between the coarse and fine sands. Whereas the M2, M4 and M5 sands tend to be grouped in one or two textural classes, M3 is more complex with a dominance between 0.25-0.5 mm and then 0.5-1 mm but with 15% greater than 1mm. M6 is the most complex material with a large clay component and large fine sand component. The median diameters (D_{50}) for the materials are shown in Table 6.1 and were derived by reading them from Figure 6.2. For M1, D_{50} was derived by measuring a sample of 30 stones. These values serve as a useful quantitative means of relating texture to other material characteristics, which might influence GPR response and moisture behaviour (in particular, porosity and hydraulic conductivity).

The Coefficient of Variation (CV) for each material is low except for the complex materials. In all cases the D_{50} CV corresponds to the textural class with the highest percentage fraction for each material, except for M6. For M6, the D_{50} class is 0.02-0.063

mm but the greatest percentage is below 0.02 mm (44.15%). Using this class reduces the CV for M6 to 0.130 and shows that variability in classes with low percentage contributions can be high.

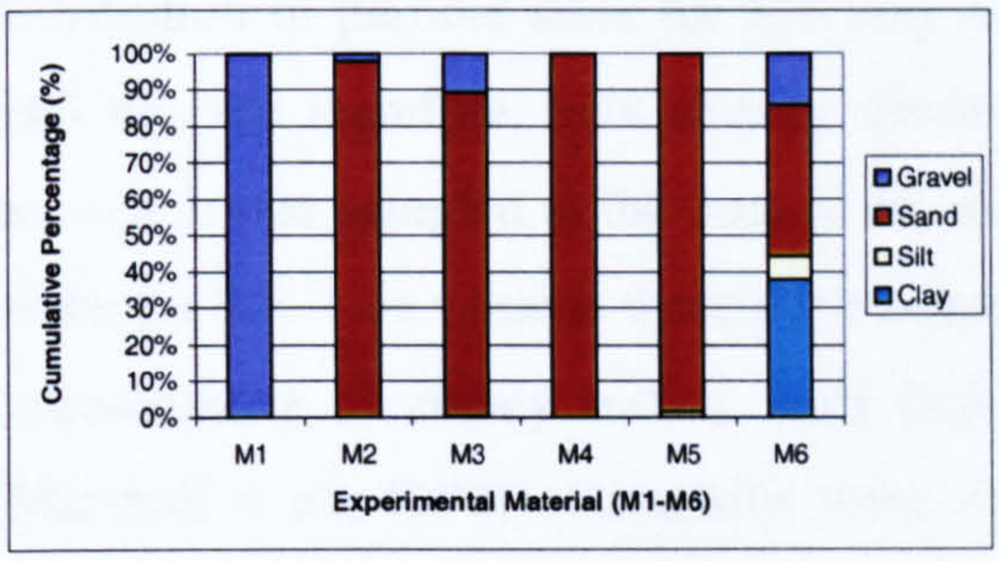

Figure 6.1: Particle size distribution for each experimental material: gravel, sand, silt and clay percentage fractions.

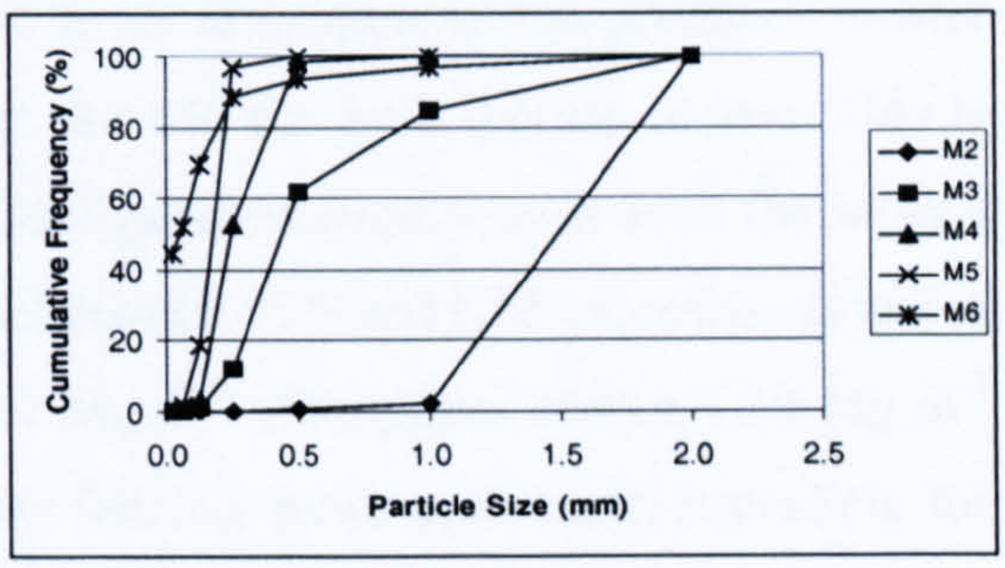

Figure 6.2: Cumulative frequency graph of particle size distribution for each experimental material.

Material	Median Particle Diameter (D_{50}) (mm)	Coefficient of Variation for D_{50} Textural Class
M1	11.750	0.231
M2	1.490	0.006
M3	0.440	0.070
M4	0.240	0.021
M5	0.175	0.045
M6	0.055	0.957 / 0.130

Table 6.1: Median particle diameter (D_{50}) (mm) for each of the six experimental materials.

6.2.3 Bulk density

Bulk density may affect VMC (by changing porosity), dielectric constant and therefore signal propagation velocity (by affecting the character of the propagation path), and *ThetaProbe* estimates of VMC (Delta T Devices, 1998). Bulk density data for both the LTF (derived from 36 samples taken across a 1 m^2 grid at 0.2 m resolution on excavation of each layer) and the STF (derived during the *ThetaProbe* calibrations which are discussed later) are shown in Table 6.2. These data demonstrate a higher mean bulk density and more variation for the LTF data.

Values of bulk density using the STF represent materials with no compaction (the materials were placed into a 500 ml beaker) and therefore have much lower values than

the LTF data in which materials were variably compacted depending upon their depth in the dry profile. M1 has a high value for LTF and a low value for STF due to the problems of sampling this material using the STF method. The LTF results for M2-M4 are consistent with values for sands (1.6 Mg m^{-3} (Dingman, 1994)), although due to compaction they are slightly higher. Like M3, it might be expected that the complex distribution of particle sizes for M6 may result in an arrangement that produces greater packing, and therefore, bulk density. However, for M6 the bulk density is low. This is because it was sampled at the start of the wet-configuration experiments from the surface of the profile. This value is therefore consistent between STF and LTF experiments and is representative of clayey surface soils (e.g. 1.1 Mg m^{-3} (Dingman, 1994); 1.12 Mg m^{-3} (Marshall *et al.*, 1996)). Generally, these results indicate more open particle packing for the STF data compared to the LTF data, which may produce different hydrological and GPR responses.

Material	Bulk Density (Mg m^{-3}) for LTF			Bulk Density (Mg m^{-3}) for STF		
	Mean	Standard Deviation	Coefficient of Variation	Mean	Standard Deviation	Coefficient of Variation
M1	1.7624	0.1397	0.0793	1.0849	0.0266	0.0246
M2	1.8184	0.0478	0.0263	1.1785	0.0403	0.0342
M3	1.8707	0.0908	0.0486	1.1777	0.0286	0.0243
M4	1.6814	0.0304	0.0181	1.1114	0.0413	0.0371
M5	N/A	N/A	N/A	1.2492	0.0363	0.0291
M6	1.145	0.089	0.0777	1.0891	N/A	N/A

Table 6.2: Bulk density for the experimental materials.

6.2.4 *ThetaProbe* calibrations: VMC and porosity

6.2.4.1 ThetaProbe calibrations

Although the LTF DRY experiments have no added moisture it is necessary to know initial moisture and other dielectric properties to confirm dryness and to establish theoretical GPR response, respectively. In this research, these data are derived using *ThetaProbes*. Material specific *ThetaProbe* calibrations will reduce *ThetaProbe* estimation error compared with the generalised calibration. These calibration equations can then be applied to the moisture data later in the research. The polynomial soil-specific calibration was used for all *ThetaProbe* derived VMCs throughout this research. The calibration parameters derived using the method outlined in Chapter Five are shown in

Table 6.3 along with the estimated average VMC at saturation (derived from the STF wetting experiments). Whilst there is little variability in a_0, as indicated by the values of the coefficient of variation (CV) in Table 6.3, variability in a_1 decreases with D_{50}. Thus with reduced D_{50} there is greater chance of a more accurate *ThetaProbe* estimation. The poor contact between the metal rods of the *ThetaProbe* and the gravel material may have resulted in some inaccuracy. It was only possible to place the *ThetaProbe* in one M6 sample to obtain a value for V_0 once oven-dried because all of the other samples became baked solid and desiccated. Therefore, the M6 calibration must be used with caution. As an alternative the standard calibration could be used but this is likely to overestimate the VMC values as shown by comparing the standard VMC results in Table 6.3 which uses the same *ThetaProbe* voltage reading as for M6.

Material Calibration	a_0			a_1			θ (Porosity) ($m^3 m^{-3}$)
	Mean	Standard Deviation	CV	Mean	Standard Deviation	CV	
Standard	1.60	N/A	N/A	8.40	N/A	N/A	0.413
Topp *et al.*	N/A	N/A	N/A	N/A	N/A	N/A	0.407
M1	1.49	0.0127	0.0085	9.90	3.7110	0.3748	0.470
M2	1.60	0.0082	0.0051	8.43	2.6613	0.3157	0.405
M3	1.72	0.0068	0.0040	9.73	1.3579	0.1396	0.281
M4	1.61	0.0080	0.0050	9.36	0.5323	0.0569	0.350
M5	1.59	0.0085	0.0053	9.54	0.8155	0.0855	0.389
M6	1.59	N/A	N/A	10.32	N/A	N/A	0.337

Table 6.3: Calibration parameters for estimating VMC from *ThetaProbe* for each material using polynomial relationships.

6.2.4.2 Testing ThetaProbe VMC estimations against gravimetric estimations

Calibrated *ThetaProbe* estimates were tested against gravimetric estimates to assess the potential error in the VMC estimation that will be related to the GPR signal. For each material 10 samples were collected, water was added, *ThetaProbe* voltage readings were taken, weighed, dried, reweighed, gravimetric moisture content calculated using equation 2.5, bulk density calculated, and water content as a volume fraction calculated using equation 2.6. In addition, the results using the standard *ThetaProbe* calibration and the

Topp *et al*. (1980) route to VMC estimation using *ThetaProbe* were investigated using the same data.

The results of plotting the observed VMC against the *ThetaProbe* estimations using the three approaches to *ThetaProbe* calibration are shown in Figures 6.3 to 6.5 along with their corresponding standardised residual plots for each test. These figures demonstrate that whilst significant error can occur using the material specific calibrations, as confirmed by the standard residuals and tending to over-predict at higher VMC values, absolute maximum prediction error, summarised in Table 6.4, is smallest for the calibrated equations and largest for the generalised and Topp calibrations, which produce similar results. M2 is an exception in which the Topp method has the lowest maximum error. It is important to note that error is greatest for M1 and M2 and reduces with D_{50} for the other materials. The standardised residuals indicate that the form of the calibration relationship is in error such that estimation error increases after 0.2 $m^3 m^{-3}$ for all methods, but M1 and M2 are the most seriously affected.

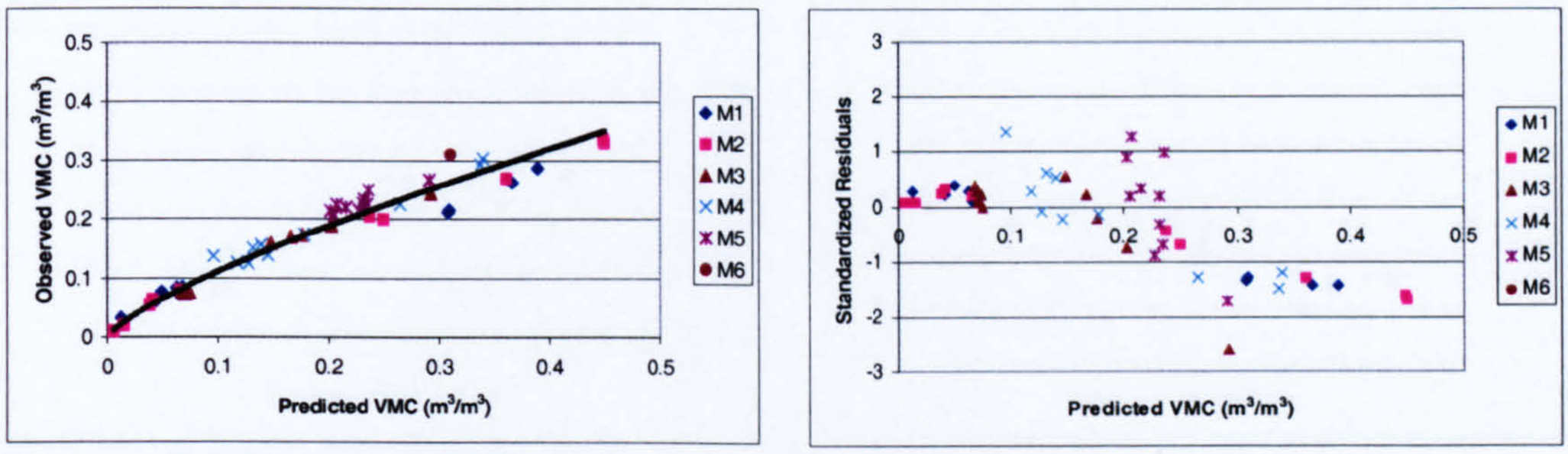

Figure 6.3: Observed VMC (derived gravimetrically) against predicted VMC (using calibrated *ThetaProbe* equations) for each experimental material and plot of standardized residuals against predicted VMC. Black line represents power function fitted to all data.

Error in *ThetaProbe* estimations is introduced as *ThetaProbe* errors (repeatability between probes), calibration errors (errors in the values of a_0 and a_1), and sampling errors (soil variability and insertion errors), which in total amount to ±0.05 $m^3 m^{-3}$ for a soil-specific calibration and ±0.06 $m^3 m^{-3}$ for a generalised calibration (Delta-T Devices, 1998). With the exception of the two coarse materials (M1 and M2), measured RMS error (Table 6.5) is below that expected for calibrated *ThetaProbes* but generally higher than expected using the other methods. Calibrated M1 and M2 estimates exceed even the

estimated error using the other methods. This indicates the importance of calibration and that for coarser-grained materials, *ThetaProbe* is an inaccurate means of measuring VMC or dielectric constant (as demonstrated by the poor performance of the Topp *et al.* calibration). Error may therefore be introduced into the estimations of TWTT for later experiments and the development of VMC-GPR relationships.

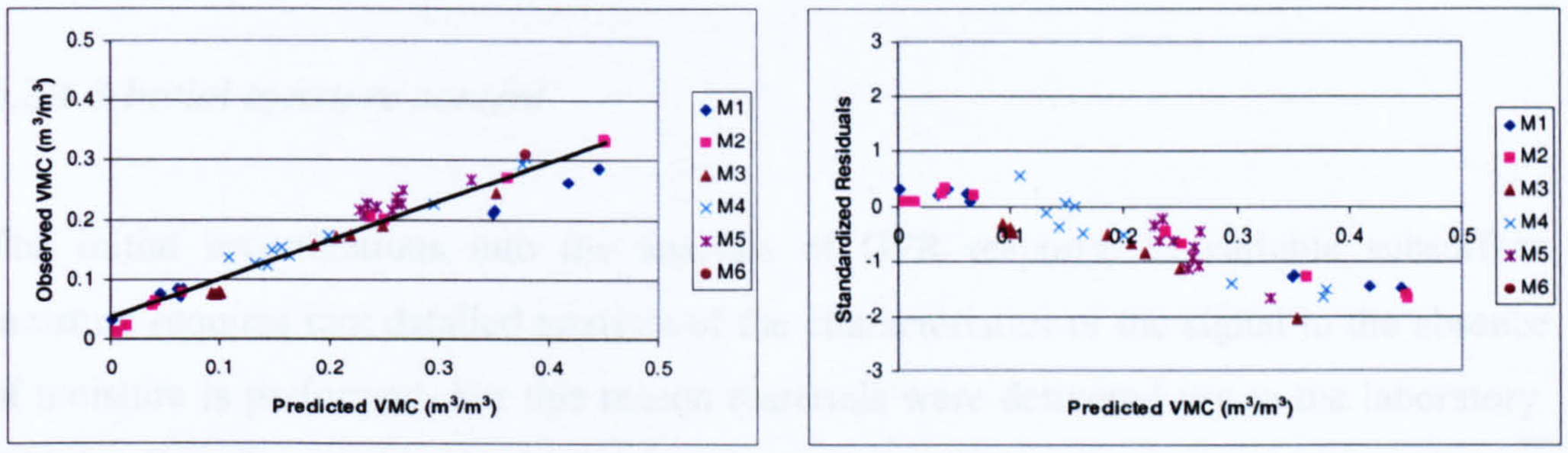

Figure 6.4: Observed VMC (derived gravimetrically) against predicted VMC (using generalised calibration method) for each experimental material and plot of standardized residuals against predicted VMC. Black line represents linear function fitted to all data.

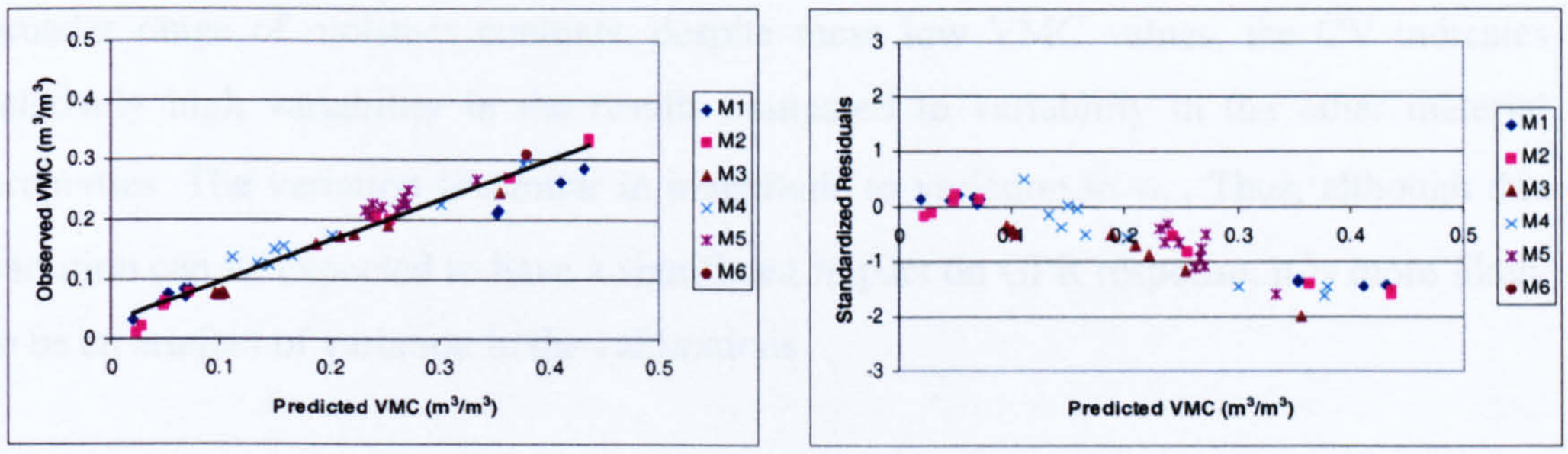

Figure 6.5: Observed VMC (derived gravimetrically) against predicted VMC (using Topp *et al.* Calibration equations) for each experimental material and plot of standardized residuals against predicted VMC. Black line represents linear function fitted to all data.

Material	Maximum Absolute Deviation of Predicted from Observed VMC ($m^3 m^{-3}$) using three alternative *ThetaProbe* Calibrations		
	Material Specific Calibration	Generalised Calibration	Topp *et al.* Calibration
M1	0.1039	0.1592	0.1492
M2	0.1198	0.1214	0.1068
M3	0.0488	0.1093	0.1119
M4	0.0446	0.0843	0.0843
M5	0.0242	0.0625	0.0668
M6	0.0002	0.0698	0.0695

Table 6.4 Maximum absolute deviation using three alternative *ThetaProbe* calibration methods

Material	RMSE Predicted from Observed VMC ($m^3 m^{-3}$) using three alternative *ThetaProbe* Calibrations		
	Material Specific Calibration	Generalised Calibration	Topp *et al.* Calibration
M1	0.0646	0.0953	0.0918
M2	0.0632	0.0641	0.0594
M3	0.0269	0.0453	0.0463
M4	0.0125	0.0332	0.0374
M5	0.0168	0.0473	0.0498
M6	0.0002	0.0698	0.0694

Table 6.5 RMS error using three alternative *ThetaProbe* calibration methods

6.2.4.3 Initial moisture content

The initial investigations into the analysis of GPR response to variable subsurface moisture requires that detailed analysis of the characteristics of the signal in the absence of moisture is performed. For this reason materials were delivered dry to the laboratory. Initial soil moisture was checked using the calibrated *ThetaProbe* equations and show (Table 6.6) that at the beginning of the dry and wet experiments materials had a maximum of 3.3% VMC. Results for M2 and M4 were affected because they were too dry for the calibration equations. This indicates the need to calibrate *ThetaProbes* over a broader range of moisture contents, despite these low VMC values, the CV indicates relatively high variability in the results compared to variability in the other material properties. The variation is similar in magnitude to variation in a_1. Thus, although this variation can be expected to have a significant impact on GPR response, it is more likely to be an artefact of variation in the calibrations.

Material	Initial Moisture for Dry and Wet Experiments ($m^3 m^{-3}$)		
	Mean	Standard Deviation	Coefficient of Variation
M1	0.0184	0.0050	0.2694
M2	-0.0064	0.0006	-0.0933
M3	0.0068	0.0012	0.1705
M4	-0.0031	0.0006	-0.1791
M5	0.0044	0.0009	0.2046
M6	0.0327	0.0058	0.1778

Table 6.6: Initial moisture content for dry and wet experiments.

6.2.4.4 Porosity

The porosity estimates shown in Table 6.3 were derived from the maximum VMC recorded for each STF wetting experiment using calibrated *ThetaProbes* and are included on Table 6.7. These estimates are subject to potential differences between *ThetaProbes*. Table 6.7 shows the average VMC for the final water addition for each material for the entire STF volume. These data tend to be lower than the maximum data and may indicate *ThetaProbe* error, compaction differences, or a more realistic porosity estimation if all pore space is assumed to be filled with water. This latter effect was not observed for M6 in which total saturation was never achieved. For M6 the maximum recorded VMC is probably more accurate than the average. Also included on Table 6.6 is the mean porosity calculated for each material from all saturated *ThetaProbe* readings throughout the course of the STF wetting experiments, along with their standard deviations and CVs.

These data indicate that VMC at saturation (porosity) generally decreases with D_{50}, although there is little difference for M4 and M5. M3 has the lowest porosity, which is a result of the mix of particle sizes. The porosity of M6 may be lower than the measured value because *ThetaProbe* cannot be inserted in the stones and rock fragments of the material. Such objects can be expected to reduce the effective volume available as pore-space. Variation in porosity estimations is generally low but varies with each material. All CVs are below 0.05 with the exception of M5. Such variation will potentially have a significant effect on GPR response by affecting the total volume of moisture that can enter a material and by promoting differences in the spatial distribution of moisture content. Furthermore, variation in initial VMC and texture appear greater than variation in porosity, though VMC and porosity will have a greater impact on dielectric constants and therefore GPR response.

Material	Final STF Experiment	All Saturated STF Data			Max Recorded VMC ($m^3 m^{-3}$)
	Mean *ThetaProbe* Estimated Porosity ($m^3 m^{-3}$)	Mean ($m^3 m^{-3}$)	Standard Deviation ($m^3 m^{-3}$)	CV	
M1	0.4358	0.4416	0.0170	0.0385	0.4696
M2	0.3844	0.3835	0.0068	0.0177	0.3966
M3	0.2707	0.2652	0.0122	0.0458	0.2804
M4	0.3331	0.3358	0.0115	0.0344	0.3507
M5	0.3303	0.3328	0.0243	0.0732	0.3862
M6	0.2456	0.3196	0.0136	0.0424	0.3384

Table 6.7: *ThetaProbe* derived porosity: average for STF, standard deviation, CV, and maximum recorded.

6.2.5 Hydraulic conductivity

Using the method outlined in Chapter Six and Appendix One, hydraulic conductivity (K) was determined for each of the experimental materials. Figure 6.6 shows an example data set and the fitted polynomial line for materials M1-M3 and Figure 6.7 shows the same for M4-M6. Table 6.8 shows the calculated hydraulic conductivity based on estimations of A2 from Decagon (1998). M1 produces a very low K estimate although laboratory observations demonstrated very rapid moisture movement through the large inter-particle spaces. This underestimation is a result of very poor contact between the mini-disk infiltrometer and the stony material surface. The remaining five materials demonstrate a decline in K with a decrease in D_{50} (i.e. from M2-M6), although K is slightly higher for the mixed sand, M3.

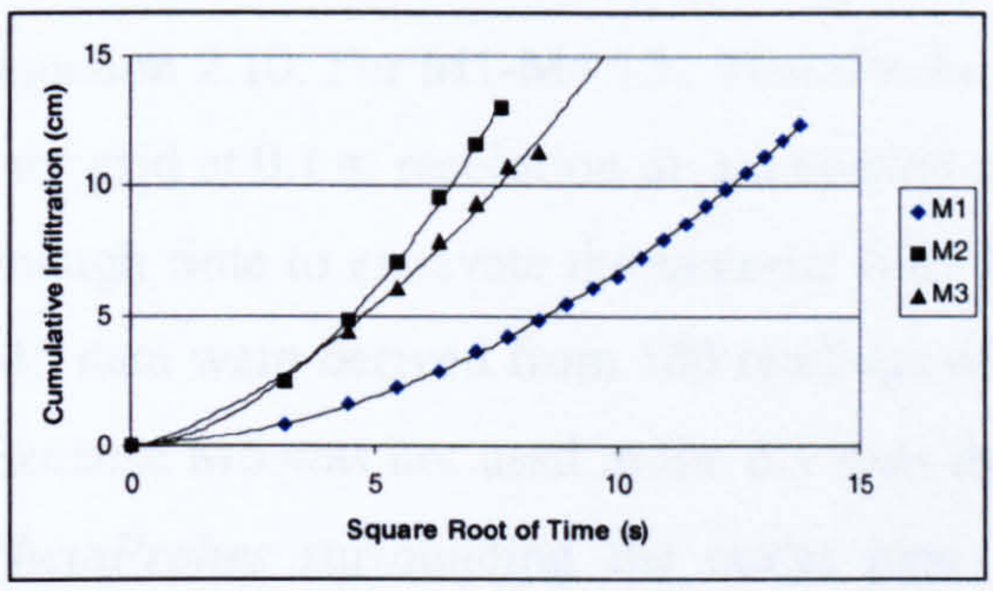

Figure 6.6: Example cumulative infiltration curves for M1-M3 and their associated 2nd order polynomial for parameter estimation.

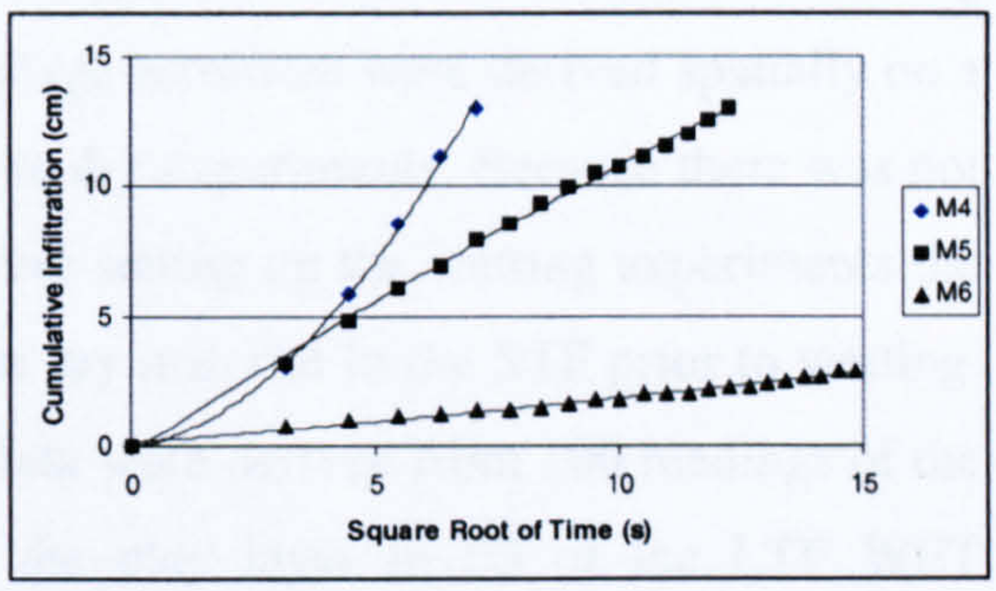

Figure 6.7: Example cumulative infiltration curves for M4-M6 and their associated 2nd order polynomial for parameter estimation.

Hydraulic conductivity has important implications for the distribution of moisture but will have no impact on dry GPR response because there is no water. Low K values will produce moisture that moves slowly down through the material profile. Low K values may also increase lateral movement and may encourage moisture concentration. High K will result in water that moves rapidly down through the profile. If impeded by a layer with lower K, lateral spreading and water table rise will be induced. Increased K variability within materials will result in complex moisture distributions. For GPR analysis, profiles equally spaced in time, and subject to the same volumes of added water, may respond (with variable reflection patterns) to different moisture distributions for different materials. For those materials in which there is a large amount of variability in

the value of K (especially M4 and M5), this can be expected to complicate the GPR response in spatial applications.

Material	Mean Hydraulic Conductivity ($mm\,hr^{-1}$)	Standard Deviation ($mm\,hr^{-1}$)	Coefficient of Variation
M1	295.33	190.49	0.64
M2	920.22	258.11	0.28
M3	984.94	465.21	0.47
M4	738.71	599.01	0.81
M5	488.89	581.40	1.19
M6	31.24	19.01	0.61

Table 6.8: Calculated hydraulic conductivity ($mm\,hr^{-1}$) for each laboratory material.

6.2.6 Dielectric constant and signal propagation velocity

From the *ThetaProbe* calibration procedure dielectric constant is calculated using equation 2.10. For M1-M4 121 *ThetaProbe* voltage estimates were derived spatially on a $1m^2$ grid at 0.1 m resolution on excavation of the dry experiments. Because there was not enough time to excavate the material fully before setting up the wetting experiments the M5 data were derived from 100 readings of the dry material in the STF prior to wetting. Because M6 was not used in the dry runs the data were derived from 100 readings of the *ThetaProbes* surrounding the outlet pipe in the clay layer in E3 of the LTF WET experiments.

Material	Dielectric Constant			Signal Propagation Velocity ($m\,ns^{-1}$)		
	Mean	Standard Deviation	Coefficient of Variation	Mean	Standard Deviation	Coefficient of Variation
M1	2.7977	0.1646	0.0588	0.1796	0.0052	0.0291
M2	2.3890	0.0157	0.0066	0.1941	0.0006	0.0031
M3	3.1896	0.0401	0.0126	0.1680	0.0011	0.0063
M4	2.4996	0.0164	0.0066	0.1898	0.0006	0.0033
M5	2.6621	0.0277	0.0104	0.1839	0.0010	0.0052
M6	3.7201	0.2293	0.0616	0.1558	0.0050	0.0318

Table 6.9: Dielectric constant and signal propagation velocity for M1-M6.

Compared with the generalised data in Table 3.1, the measured dielectric constants are generally lower than expected for dry sands (3-6). This may be because the materials were so dry when measured (materials were factory-dry and therefore have no residual

moisture), or may be a consequence of their being well-sorted materials. Certainly, the two poorly-sorted, complex materials (M3 and M6) have values which match more closely the data in Table 3.1. No significant relationships exist between the derived dielectric constant and the other material properties; although porosity produces the strongest result. For the fine-earth materials (M2-M6) there is a weak, insignificant relationship suggesting a decrease in dielectric constant as particle size (D_{50}) increases. This may occur because an increased volume of material contributes a higher dielectric constant. This indicates that with decreased porosity (and increased bulk density), dielectric constant increases. This is a function of the higher dielectric constant of material than air, and the absence of water, and is confirmed by equation 4.4.

The consequence of these dielectric values is that all materials can be expected to have high signal propagation velocities (SPVs), although these will be lower for M3 and M6. Table 6.9 confirms this, presenting SPV calculated from the dielectric constant using equation 3.2. Variability in dielectric constant and SPV is very low with the exception of M1 and M6, which is due to problems with the insertion of the probes in these materials. The variability in M6 might indicate more variability than previously suggested in the VMC data derived from *ThetaProbe* estimations.

6.2.7 Summary

The materials used in this research demonstrate little variability in their material properties within each material. However, the properties contrast between each material with each having different textural, hydraulic and dielectric properties. In terms of GPR response the most significant of these properties in the absence of water is the dielectric constant. Hydraulic conductivity is not important. Dielectric constant varies between materials in a way that appears weakly consistent with particle size and porosity but, like all properties, varies little within individual materials. Upon addition of water the dielectric contributions of both material and air will decline, and in combination with higher porosity may produce higher final dielectric values due to increased volumetric water content. This indicates that GPR is most likely to derive a volumetric measurement of moisture content.

It is unknown to what extent small variations within the materials will affect GPR response. It is likely that the limited potential horizontal variation in material properties, which has been assessed completely for the first four material layers (M1-M4), will produce limited horizontal variation in GPR response. Conversely, the variability between materials has been shown to affect vertical GPR response. Dielectric contrasts caused by different material properties will generate reflections at each material interface. Although these have been shown to be theoretically very weak, it is these variations that are most likely to dominate GPR response in the absence of moisture. It is the purpose of the next sections to assess to what extent this is true and to establish the utility of GPR in spatial variability studies.

6.3 VARIABILITY IN GPR RESPONSE

6.3.1 Introduction

For the GPR method to work, the relationship between variability in the subsurface and variability in the GPR response needs to be investigated. It has been established that there is limited within-material variability and that the principal source of GPR response will be in the differences between the dielectric properties of the different material layers. These are small and are likely to produce weak reflection events. GPR response will be reasonably uniform in the horizontal plane at different depths beneath the surface and this variability should be representative of the actual variability in the subsurface. A series of dry experiments were therefore conducted: (1) to establish the degree of variability in GPR response in the absence of moisture and in homogeneous layered materials (2) to relate the variability in GPR response to dielectric variability in subsurface materials, and (3) to discuss the implications of the GPR response for subsequent GPR interpretation. Using the dry experimental configuration the potential variability in GPR response was investigated using GPR data collected at 0.1 and 0.2 m horizontal spacing and at both antenna frequencies. These data are now analysed to investigate vertical variability (through boundary depth analysis) and horizontal variation in GPR response.

6.3.2 Boundary depth estimation

Many GPR applications are oriented to the detection of layers of discontinuous dielectric constant (Kung and Lu, 1993) and the detection of textural interfaces (Boll *et al.*, 1993). The presence, depth, and lateral extent of soil diagnostic horizons are used to classify soils and these horizons often have abrupt boundaries which contrast with overlying horizons in physical and chemical properties and typically produce strong reflections and recognisable GPR imagery (Doolittle and Collins, 1995). GPR has been used for layer thickness estimations such as the estimation of soil thickness above bedrock (e.g. Howe, 2000) and for ice thickness (e.g. Arcone 1982). Due to the non-unique character of GPR data it is not always possible to discern whether fluctuations in TWTTs to such horizons are due to depth changes or changes in dielectric properties above the interface. Using controlled laboratory conditions, involving dry layered materials, it is possible to investigate the effects of material variation and anomalies on TWTT variability. The detection of material boundaries is important within the context of this work because both the visual and velocity techniques of analysis require the robust and reliable identification of subsurface boundaries and their depths. For the quantitative assessment of GPR signal characteristics it is important to test the accuracy of GPR depth estimations to define correctly the vertical estimation space for GPR data, to isolate layer-specific responses, and determine variability and its causes in the vertical domain.

6.3.2.1 Visual interpretation

Figure 6.8 shows a 900 MHz grid at 0.1 m resolution. The profiles are arranged side by side (with lines separating the transects) rather than as a grid for clearer visualisation of the details. No processing other than a 6-point down the trace average was applied to the image, which was taken straight from the PulseEKKO 4.2 software display. It is clear from this image that the horizontal interfaces produce very weak reflections; some of which are almost undetectable. However, the presence of a diffraction hyperbola (indicating a subsurface anomaly) is clearly present in the first eight of the eleven profiles in the grid. The maximum intensity of the hyperbolic reflection occurs in profile six across the centre of the grid. To increase the detection of the boundaries, an AGC gain (Gain maximum = 40 DN; Window Width = 2.0 pulses) was applied (Figure 6.9). This obscures the hyperbolas by increasing surrounding noise, but allows the presence of

nearly continuous reflectors to be identified. Interpretation is aided by plotting all profiles as one transect.

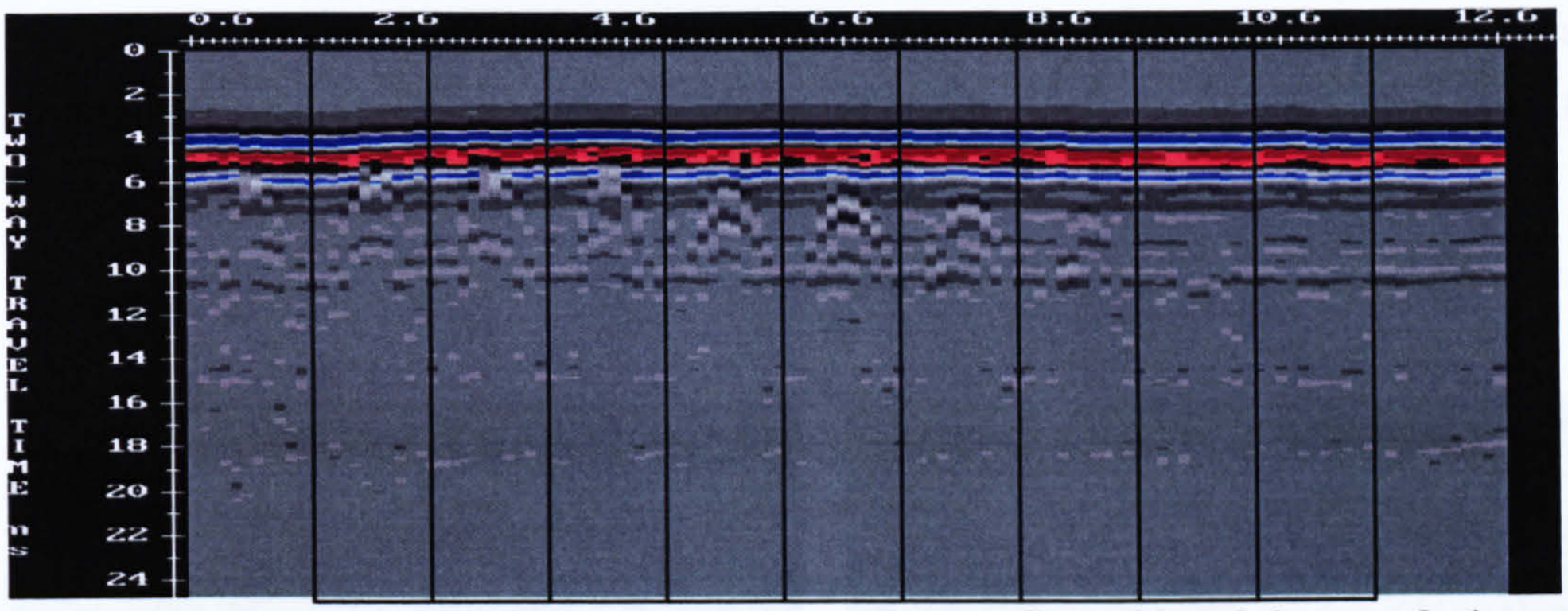

Figure 6.8: Sequence of GPR transects across dry profile grid at 0.1 m resolution using 900 MHz. 6-point down-the-trace filter applied. Top axis shows relative horizontal position; vertical axis shows TWTT (ns). Lines show approximate start of each transect.

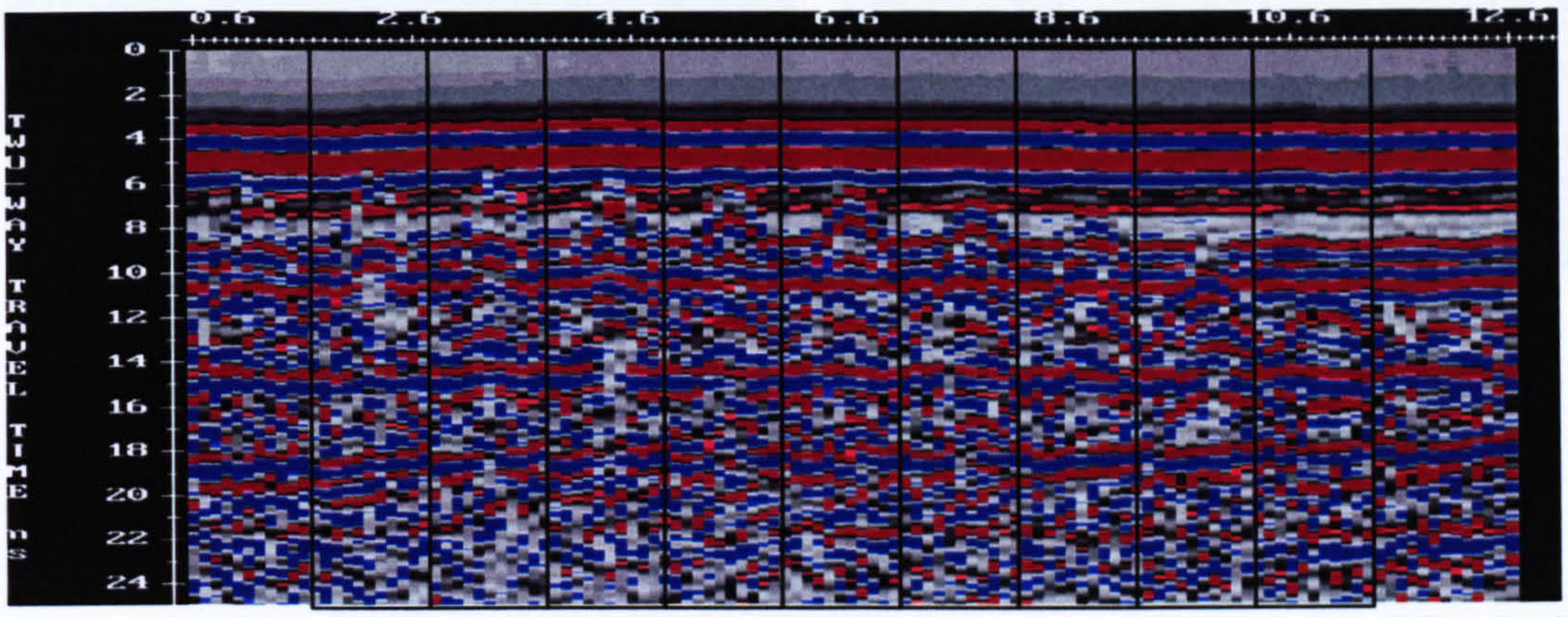

Figure 6.9: Same sequence as for Figure 6.9 but with the addition of an AGC gain (gain maximum = 40 DN; window width = 2.0 pulses) to increase detection of horizontal reflectors.

At a coarser station spacing (0.2 m) the horizontal reflectors are less clearly discerned and there is no clear visualisation of the hyperbolas (Figure 6.10). This can be expected to influence the accuracy of the depth estimations because the identification of a feature, which can potentially change TWTTs and magnitudes is not possible. At 450 MHz and 0.2 m resolution (Figure 6.11) the reflections are even less clear, although they are still identifiable. There is no evidence of the diffraction events, although the signal appears disturbed. The broader reflections (due to the longer wavelength of the lower antenna frequency and demonstrated clearly by comparing the average traces for 450 and 900

MHz data at 0.2 m resolution in Figure 6.12) will increase uncertainty in depth estimation (through reducing resolution of closely spaced events and increasing TWTT ambiguity) and reduce the success of anomaly detection. At 0.1 m resolution the 450 MHz data still does not identify the hyperbolae and disturbance in layer estimations is evident. It is clear from all of these images that there is variability in the characteristics of the layer reflections indicating subsurface variability in the horizontal and vertical planes. It is necessary to identify the causes of these variations.

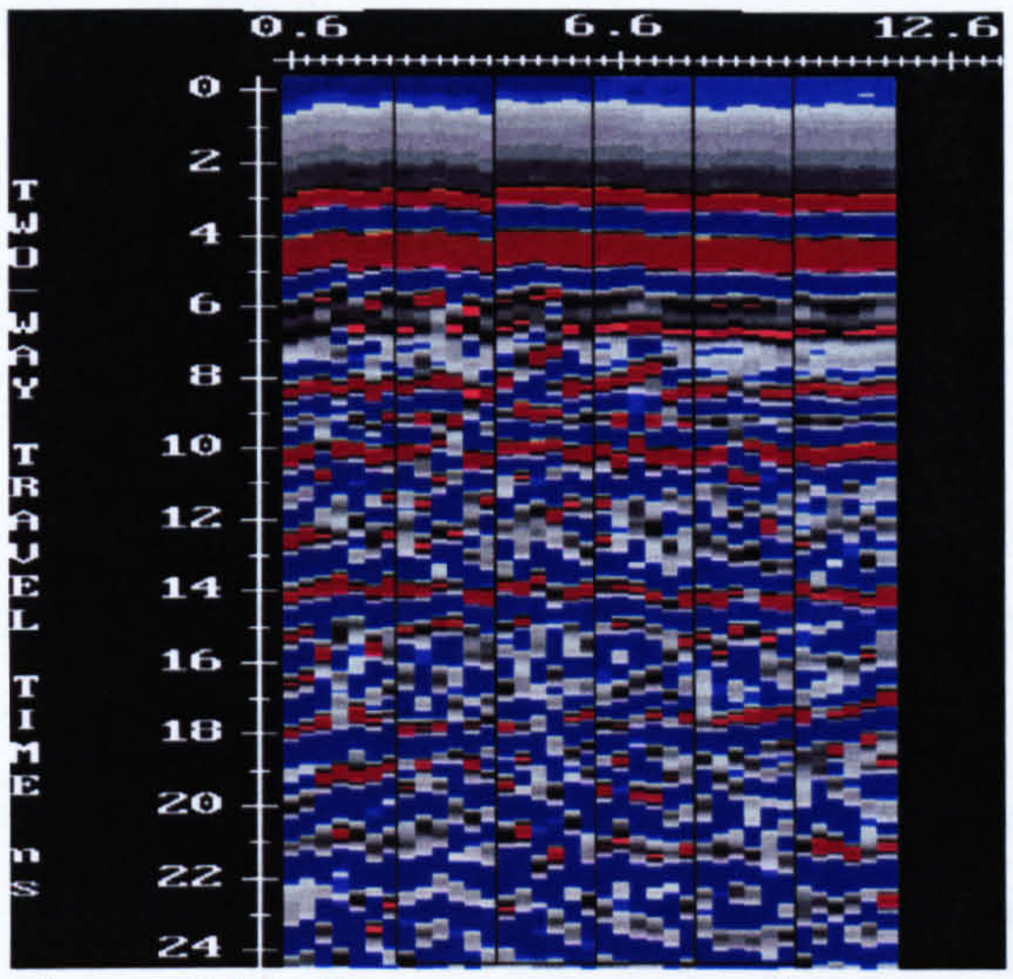

Figure 6.10: Same sequence as for Figure 6.9 but at 0.2 m horizontal resolution.

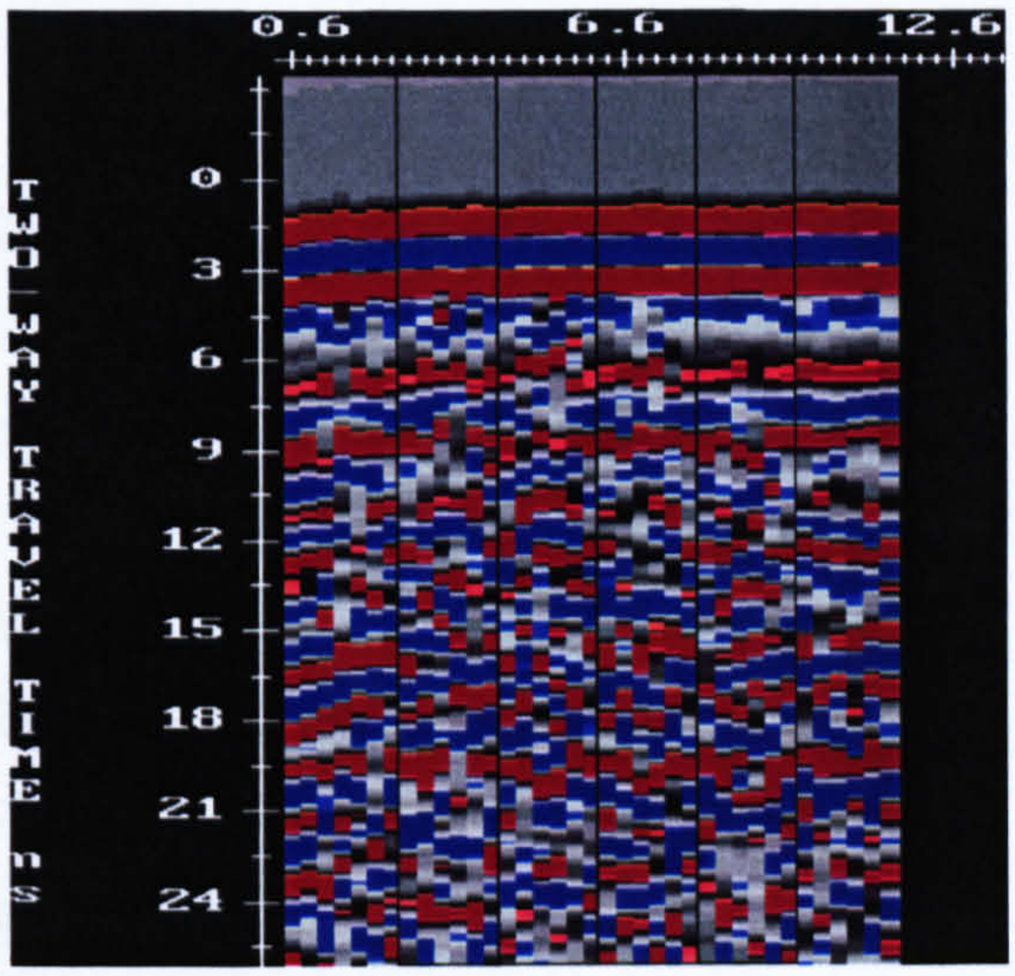

Figure 6.11: Same as for Figure 6.10 but using 450 MHz antenna frequency.

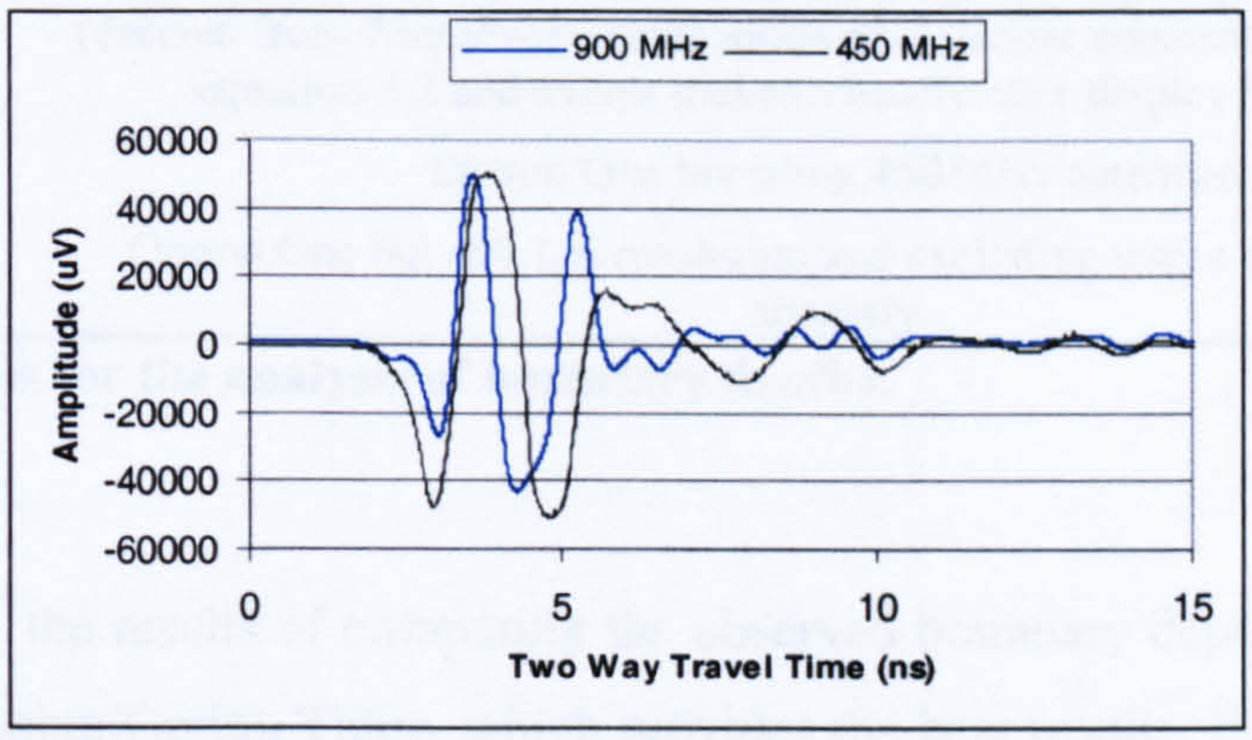

Figure 6.12: Average time domain traces for the 0.2 m horizontal resolution grids using the dry configuration at 900 and 450 MHz antenna frequencies. Traces aligned at first break.

6.3.2.2 Depth estimations

To estimate the accuracy and variability of depth estimations, three options were used as summarised in Table 6.10. These options compare 900 MHz estimations at 0.2m horizontal resolution (Figure 6.10), 450 MHz estimations at 0.2 m horizontal resolution (Figure 6.11), and 900 MHz estimations at 0.1 m horizontal resolution (Figure 9.8 and 9.9) and exclude the disturbed traces associated with the anomaly. The time domain data were converted to depth using:

$$d = (TWTT/2) \times v \qquad (6.1)$$

where d is depth (m), TWTT is two-way travel time (ns), and v is velocity ($m\,ns^{-1}$). Use of the underground wave velocity applied to the rest of the profile may be realistic in a homogeneous environment but it provides only a rough estimate for multilayer terrains having variable porosity or variations in water saturation (Tillard and Dubois, 1995). This can be expected to over- or underestimate the depths of homogeneous materials depending on their actual SPVs. Because all dielectric constant data are known, the depth scale can be calculated by applying a layer-specific conversion based on *ThetaProbe* estimates of dielectric constant and velocity using equation 3.2.

Method of Analysis	Details
Option One	Time converted to depth based on an layer-specific signal propagation velocity (derived from *ThetaProbe* estimations of dielectric constant), converted using equation 3.2 and events picked visually after display in SURFER.
Option Two	Option One but using 450 MHz antennae.
Option Three	Option One but at 0.1 m resolution and excluding traces disturbed by the anomaly.

Table 6.10: Options for the analysis of boundary depths.

Figure 6.13 shows the results of comparing the observed boundary depths with the GPR estimated depths using Option Three, which provides the best results. Figure 6.14 shows the standard residuals for each Option. Figure 6.15 shows the change in CV with depth for each Option. The results of these analyses can be summarised:

- Mean depth estimation for all methods is generally within 0.02 m of the expected value. M1 / M2 boundary is an exception in which error can be up to 0.08 m. This is due to the direct arrivals. There is a large discrepancy for the 0.2 m boundary which

indicates inaccurate depth estimation near the surface. The depth error is approximately 0.08 m except for Option Three, which is 0.11 m.

- Mean becomes more accurate with depth. There is increasing convergence between the observed and mean estimated depths with increasing depth beneath the surface. However, the range of estimation tends to increase with depth. This indicates reduced depth estimation accuracy with depth; especially below 0.6 m. Consequently, variation tends to increase with depth. Fluctuation in variation at 0.4 m depth.
- Residuals are generally small; all being significantly below 1.96 (roughly 95% of the observations should fall in the range [-1.96, +1.96] (Burt and Barber, 1996)). This demonstrates reasonably accurate estimation for all methods.
- Using lower frequency increases near-surface error (e.g. the error for the boundary at 0.2 m depth is now 0.11 m), producing high residuals. All means are estimated more poorly. Variation with depth is reduced and is more consistent between depths. The increased error in depth derivation for 450 MHz compared to 900 MHz antennas means that the 900 MHz antennas are more appropriate for controlling measurement volume and therefore for determining VMC in the near subsurface. For 450 MHz, there is increased interference near the surface as a consequence of the broader wavelets. The error as a result of the larger direct arrival means boundary detection is only possible with any certainty below 0.3-0.4 m depth.
- The narrower reflections for 900 MHz allow more detail to be picked out. However, due to the poor spatial resolution of this grid (0.2 m) spatial aliasing occurs and the greater vertical detail simply acts to obscure the coherent layer responses. Excluding the disturbed traces reduces variation, but doesn't much improve the 0.2 m boundary (still affected by the direct arrivals). Estimates at 0.48 and 0.6 m depth are improved, but at 0.88 and 1.02 m, depth estimates are still affected by disturbance due to hyperbola which spreads with depth.
- The anomaly could not be identified at 0.2 m resolution, so that the events selected may actually correspond to this disturbance rather than to a layer boundary. Excluding the disturbed data from the analysis reduces the number of samples used ($n = 20$), but improves depth estimations resulting in greater certainty in the picked depth for each layer.

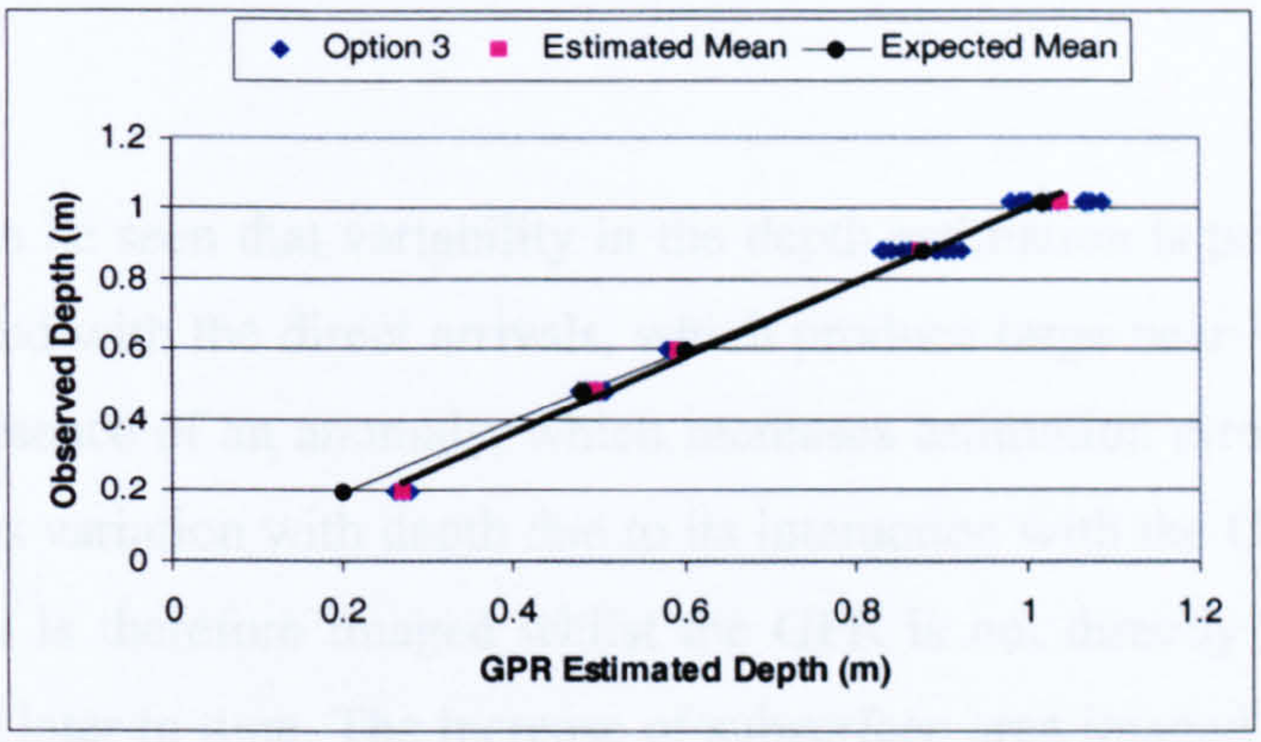

Figure 6.13: Comparison of observed (expected) depth with GPR estimated depth using option three (see Table 6.10). Also shows mean estimated depth. Lines indicate increasing accuracy in mean depth estimation with depth.

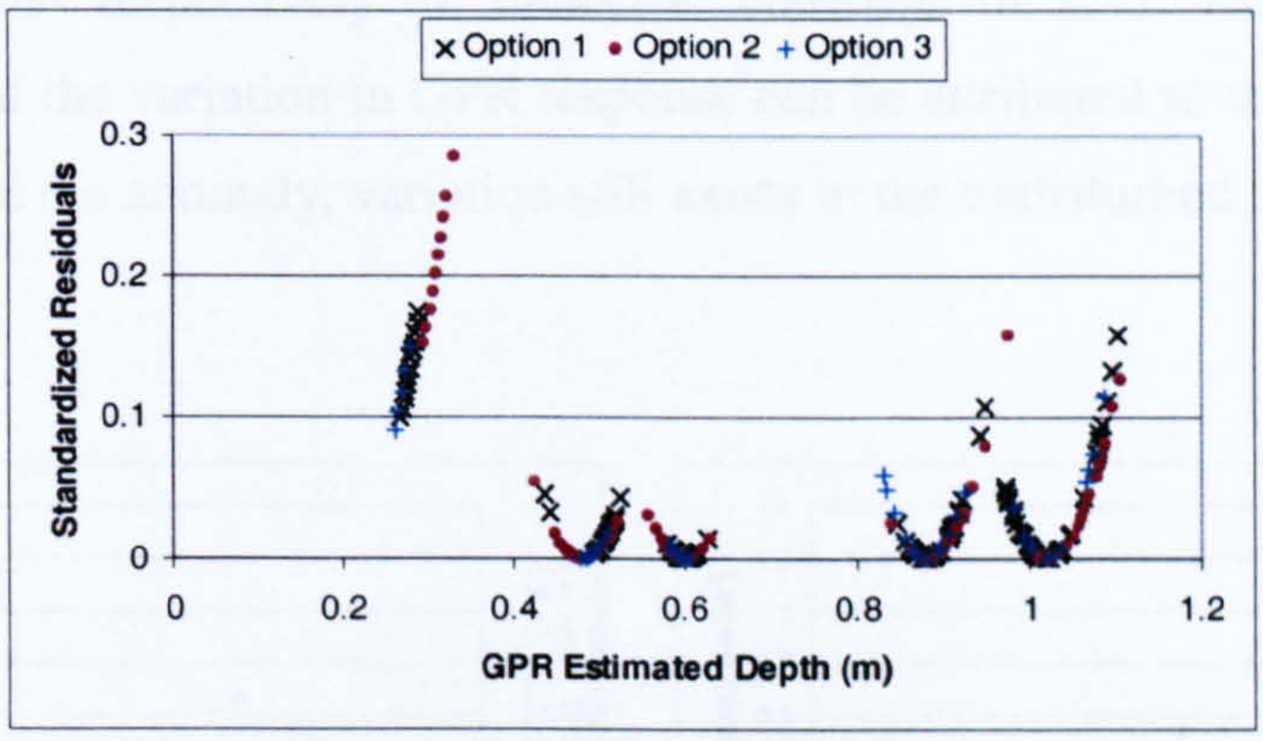

Figure 6.14: Standard residuals for all three depth analysis options (see Table 6.10) for comparing each option.

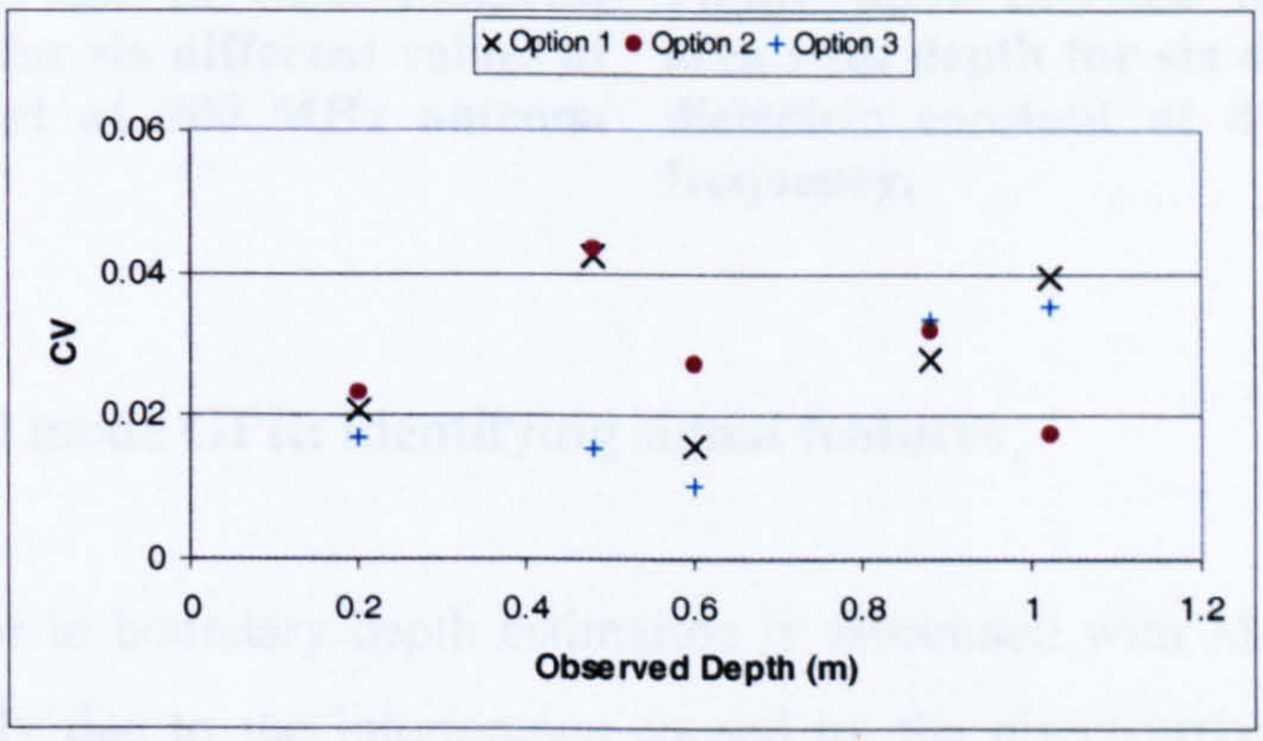

Figure 6.15: Changes in depth estimation variation with depth for all three options.

6.3.2.3 Summary

In summary it can be seen that variability in the depth estimation is primarily a function of errors associated with the direct arrivals, which produce large near-surface estimation error, and the presence of an anomaly, which increases estimation error with depth. The anomaly increases variation with depth due to its interaction with the GPR footprint. The anomalous object is therefore imaged whilst the GPR is not directly over it producing events that arrive later in time. The increase of subsurface area imaged with depth due to the footprint means that smaller-scale variation as a result of minor layer fluctuations is reduced. Figures 6.16 and 6.17 show the theoretical increase in footprint area (assuming an ellipse and calculated using equations 3.10 and 3.11) with depth for 900 and 450 MHz antenna frequencies respectively for dielectric constants of 1, 5, 10, 15, 20, and 25. Although much of the variation in GPR response can be attributed to the influence of the GPR footprint and the anomaly, variation still exists in the undisturbed data.

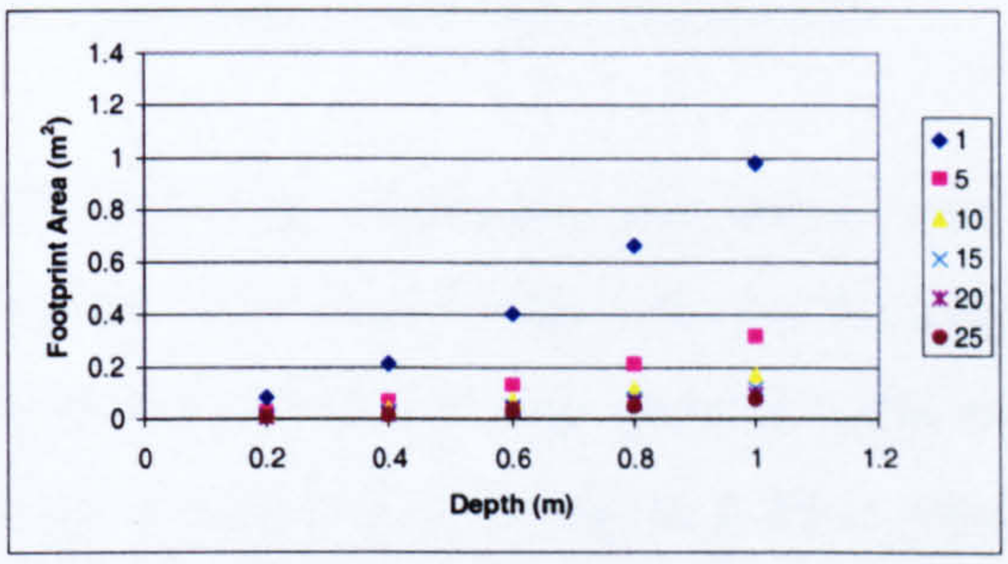

Figure 6.16: Increase in GPR footprint area with depth for six different values of dielectric constant at 900 MHz antenna frequency.

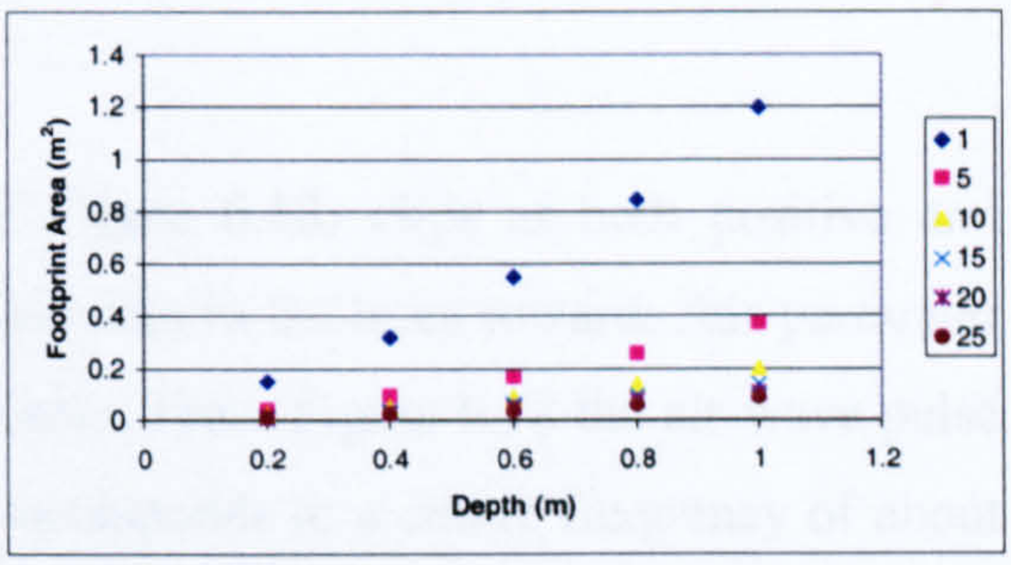

Figure 6.17: Increase in GPR footprint area with depth for six different values of dielectric constant at 450 MHz antenna frequency.

6.3.3 Suspended mode GPR: identifying signal features

The greatest error in boundary depth estimation is associated with M1 / M2 boundary. This is principally due to the interference caused by the direct arrivals. An important characteristic of GPR antennas is the coupling between Tx- and Rx- antennae, which can obscure reflections from shallow buried targets and can substantially limit the dynamic range of the whole GPR system (Yarovoy and Ligthart, 2000). The strong antenna-ground interaction can significantly change the antenna's characteristics and produces noticeable antenna clutter (Chen *et al.*, 2000) and it is this clutter that appears to dominate the first

7ns of the ground-coupled traces. The surface coupling and antenna ringing present problems which make it difficult to obtain any quantitative information from the near surface without signal processing (Saarenketo and Scullion, 2000). With the radar in direct contact with the ground (the usual mode of operation) the isolation of the first (surface) reflection from the ground-wave is difficult. The high amplitude and ringing noise of the direct arrivals has a large impact on the observability of amplitudes further down in the profile. One potential means of overcoming the problem associated with near surface identification of events is to lift the GPR antennae off the surface. This technique has the advantage of enabling the characteristics of the direct arrivals to be investigated in more detail.

Figure 6.18 shows the average time domain trace using 900 MHz antennas suspended 0.95 m above the centre of the LTF. The air-wave and air-ground interface response wavelets are clearly identifiable (**a** and **b** respectively). Whilst 0.95 m is sufficient to isolate the air-ground interface from the air-wave and improve near-field clarity compared to ground-mode (Figure 6.19), a suspension height of 0.4m produces interference between the two events as shown in Figure 6.20.

The high-magnitude air-wave arrival ((a) on Figure 6.18) clips at both positive and negative amplitudes. This will bias the amplitude data in the trace towards this particular waveform, producing non-stationary characteristics. From Figure 6.18 the air-wave pulse duration can be determined as 2.05 ns which corresponds to a centre frequency of about 732 MHz. The finite extent of the GPR antenna as well as its metal shielding have significant effects on the pulse shape and the nature of the radiation pattern (Lampe and Holliger, 2000). This confounds the fact that, despite a 1.5-cycle pulse being transmitted, an actual receiver response is never concentrated into a single pulse of well defined width and there is always some low-level response, either in the form of minor lobes or a slowly decaying tail, preceding and succeeding the main peak (Rihaczek, 1996). The final characteristic of the transmitted pulse is the noise that occurs after 3 ns on Figure 6.18. This noise may propagate through the subsurface. Such noise may occur because the source pulse consists of more than one wavelength and may have a complex waveshape (Reynolds, 1997). This is often a consequence of the fact that the antenna may radiate a non-exact derivative of the generator pulse (Yarovoy and Ligthart, 2000). The reflection at the air-ground interface ((**b**) on Figure 6.18) is not an exact replica of the transmitted pulse, with reduced magnitude and duration (1.54 ns) which corresponds to a higher

frequency of 974 MHz and suggests reflection of higher frequencies and propagation of lower frequencies. The noise and ringing present in the transmitted pulse is not identifiable due to interference with other subsurface signals.

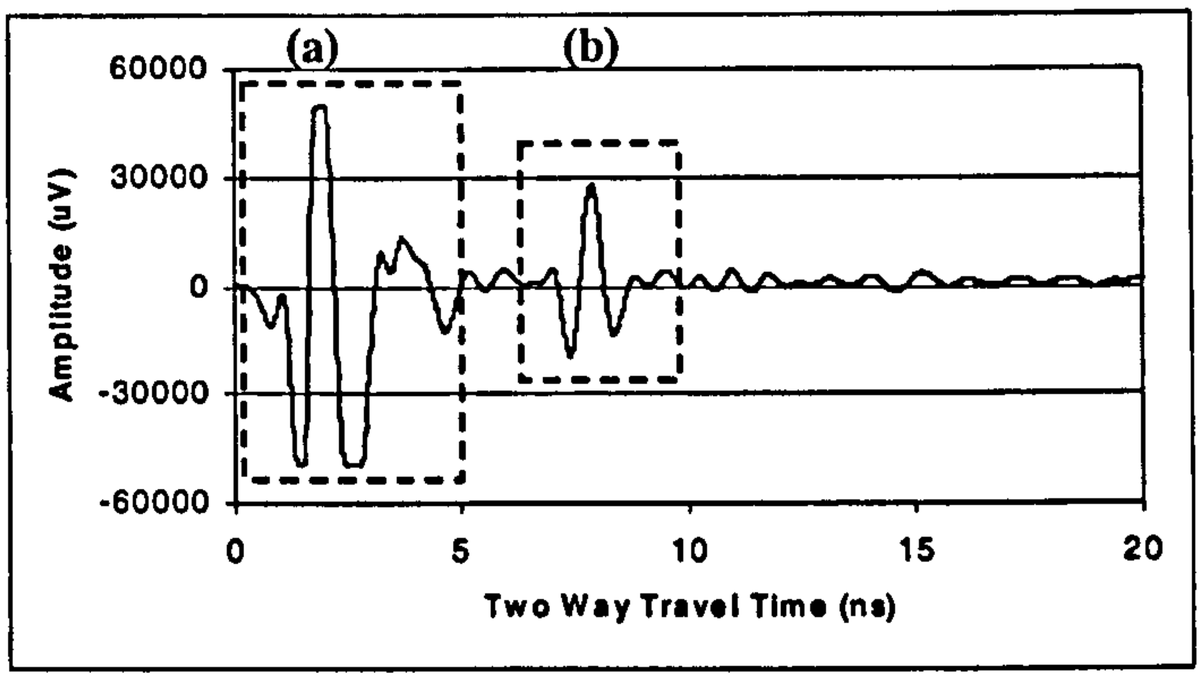

Figure 6.18: Identification of main trace components using GPR suspended 0.95m above LTF centre. Wavelet (a) is the transmitted pulse. Wavelet (b) is the reflection at the air-ground interface.

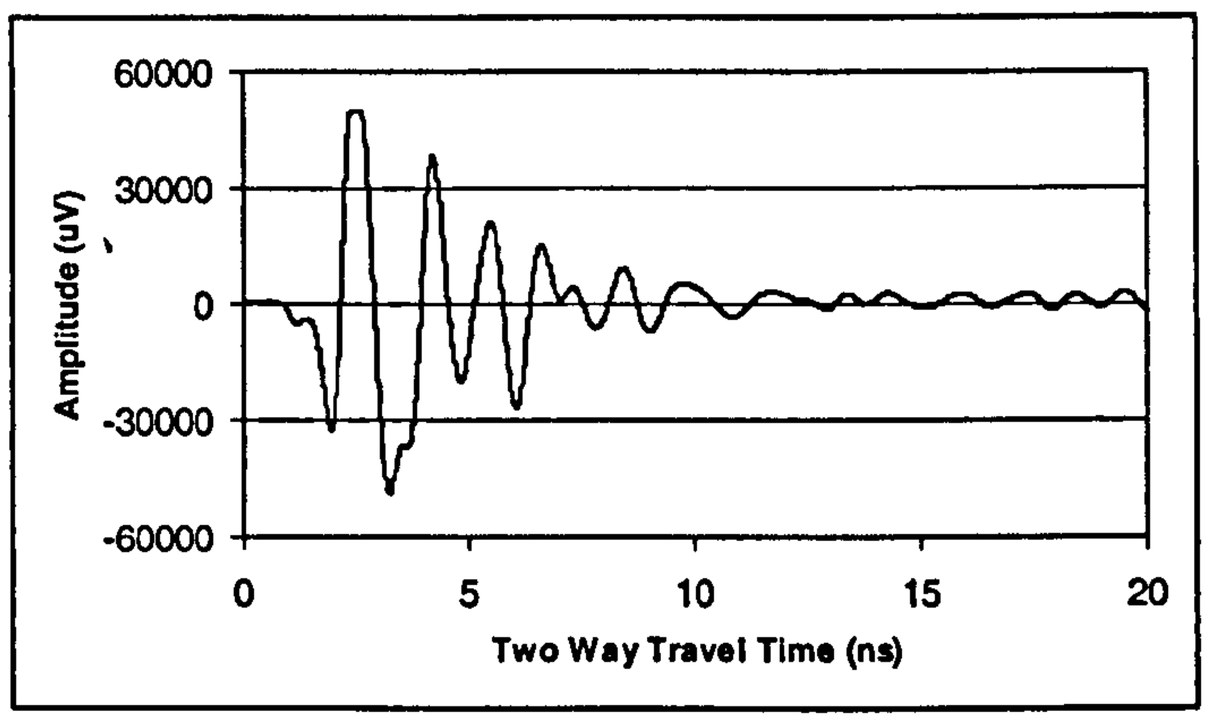

Figure 6.19: Associated trace to that shown in Figure 6.18 but with antennae on ground surface.

Despite facilitating greater clarity in the near-surface zone, much of the transmitted energy is radiated into the air in suspended mode and reaches the ground over a much broader area, producing a reduction in subsurface amplitude values and a measurement that is averaged over a far greater area (Figure 6.16 indicates an area of 0.47 m^2 at 0.95 m antenna suspension). Because less energy propagates into the subsurface in suspended-mode, penetration depth will decrease. The weak subsurface reflections become more difficult to identify. The impacts of the small dielectric anomaly at the centre of the LTF cannot be detected in the suspended mode signal response. Comparison of two suspended

mode responses, at the centre of the LTF (Figure 6.20) and 0.5 m off-centre (where there is no anomaly) (Figure 6.21), produces no discernible difference in the early-time waveform. Conversely, in ground-mode additional events occur in the centre trace indicating the presence of something in the near-subsurface. In the current research the preservation of propagation energy is critical because the signal may be severely attenuated by the presence of moisture. Therefore, the rest of this research will use ground-mode only. A GPR which could be used in suspended mode with antennae designed to focus the transmitted energy straight into the ground would be one way of improving the near-surface resolution, depth of penetration, and reflection amplitudes, although surface roughness may scatter transmitted energy away from the receiving antenna.

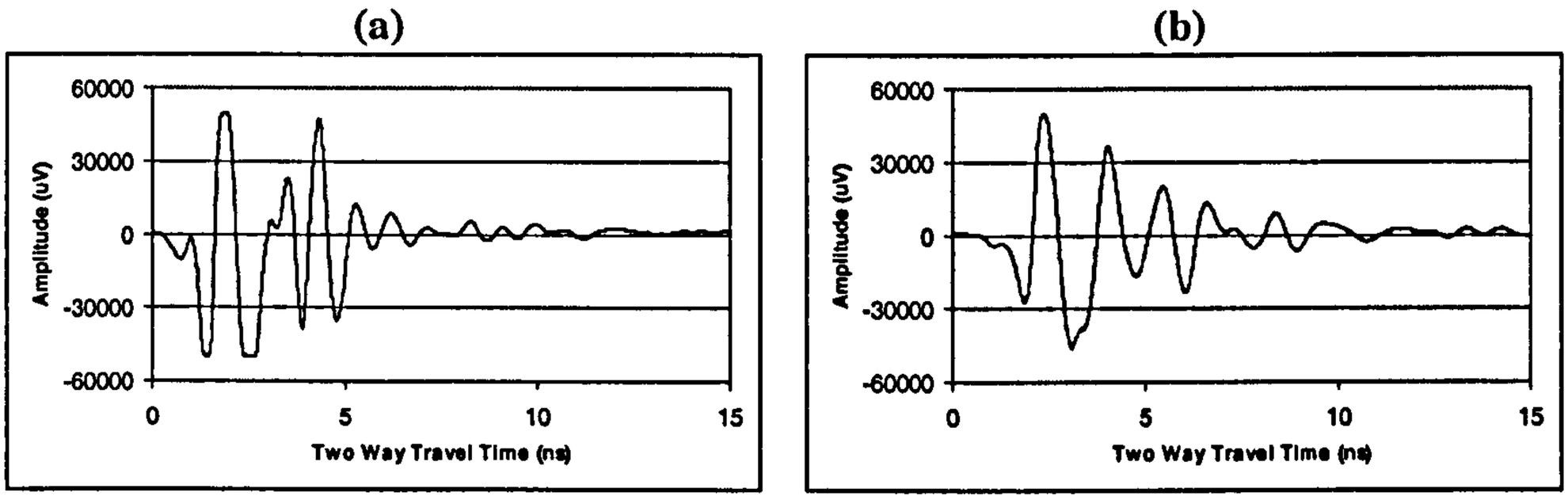

Figure 6.20: Identification of main trace components at 900 MHz. **(a)** Antennae suspended at 0.4 m above the ground at the centre of the LTF. **(b)** Antennae on ground surface at centre of the LTF.

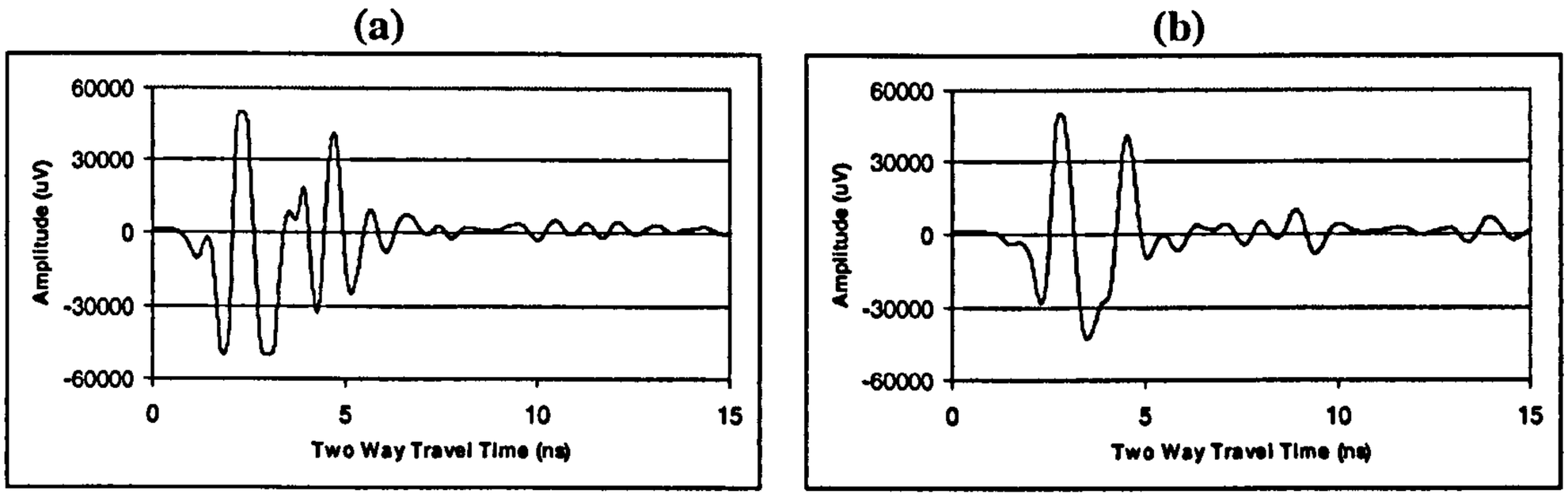

Figure 6.21: Identification of main trace components at 900 MHz. **(a)** Antennae suspended at 0.4 m above the ground at 0.5 m left of centre of the LTF. **(b)** Antennae on ground surface at 0.5 m left of centre of the LTF.

6.3.4 Amplitude depth slices

Many users of GPR interpret the records using only a superficial examination of the images to specify that an object has been detected or that a reflector exists (Tillard and Dubois, 1995). Reflector identification and anomaly analysis are the basic interpretations of radar time sections (Gao, 2000). Whilst reflections are often picked up according to the continuity and similarity characteristic of the events, anomalies are usually analysed based on the amplitudes, waveform, and pattern of the events (Gao, 2000). An analysis of the spatial distribution of the amplitudes of reflected waves is important because these changes are the direct result of changes in the makeup of subsurface units (Conyers and Goodman, 1997). The aim in this aspect of the research is to relate spatial variability in GPR response to spatial variability in the dielectric properties of dry layered materials. To characterise the variability in horizontal and vertical GPR response, amplitude depth slices can be used. In this approach maps of dielectric anomaly can be generated for user-determined depths. Amplitude slices are usually made in equal time intervals, with each slice representing an approximate thickness of buried material if velocity analyses are performed in advance and time depth corrections are made (Conyers and Goodman, 1997). Digital amplitude reflection data can be averaged in the vertical window to reduce noise or reduce the chance of creating artificial amplitude anomalies at the intersection of slices and subsurface beds (Conyers and Goodman, 1997). The variation within these depth slices can be characterised by the mean and CV of the amplitudes.

6.3.4.1 Depth slice maps

After performing a time-depth correction using the layer-specific *ThetaProbe* estimations of SPV (see Table 6.9), maps were constructed for the raw amplitude values every 0.2 m down through the subsurface, starting from the surface. Figure 6.22 shows the resulting depth slices for both antenna frequencies. Due to the presence of the direct arrivals there is little variation in the slices at 0 and 0.2 m although for the latter mean amplitude is of a high negative magnitude for 900 MHz and a high positive magnitude for 450 MHz. This discrepancy occurs because the direct arrivals are broader at 450 MHz and occupy more of the depth profile as demonstrated in Figure 6.23 which compares the direct arrivals for the mean 900 and 450 MHz traces. From 0.4 m beneath the surface an extended semi-circular anomaly is imaged from the centre of the grid (y = 1 m) to the back of the grid (y

= 1.5 m). The object is exaggerated in the y-direction with disturbance between x = 0.65-1.15 m. For 450 MHz the object appears narrower in the x-plane and of higher magnitude than the 900 MHz results. This occurs because the second positive cycle of the 450 MHz direct arrivals still affects data at this depth. With increasing depth the GPR response spreads and weakens such that there is an homogenisation of amplitude values with depth. Amplitude variability appears to be greater in the 450 MHz images and the area of the affected signals is greater at the lower frequency. This is due to its greater footprint area. At 450 MHz, additional horizontal anomalies are visible in the y-plane either side of the anomaly at 1.0 m depth and at x = 0.6 m at 1.2 m depth. It is unclear what causes these features but they may have something to do with error in vertical discretization.

The amplitude slices suggest an anomaly that is approximately 0.5 m by 0.5 m in size. The disturbance caused by the detected anomaly corresponds to the hyperbolae present in the vertical profile domain, which occur as a consequence of the GPR footprint. This produces changing patterns of amplitude down through depth resulting in the semi-circular repetitions of positive and negative amplitudes. Depth slices at an arbitrary depth will sample a waveform at an arbitrary point producing potentially false amplitude values. At 0.4 m depth a high positive amplitude centre is surrounded by high negative amplitudes. At greater depth, additional positive and negative amplitudes occur. This implies a negative leading edge to the reflection wavelet (confirmed by the vertical profile images, especially Figure 6.9) at a depth nearer to the surface than 0.4 m. A negative reflection implies an object with a higher dielectric constant than the material above it. The size will be over-estimated by the GPR footprint, which covers a long-axis distance of 0.25 m and 0.3 m at 900 and 450 MHz antenna frequencies respectively. It is known that the object is a *ThetaProbe* centred at x=1.0 m, y=1.0 m, and z=0.2 m (beneath the surface), and because it contains metal components represents a source of higher dielectric constant in the subsurface. Due to the sampling resolution and the effect of the GPR footprint, the *ThetaProbe* (dimensions: 4 cm diameter and about 17 cm long (Delta-T Devices Ltd., 1998)) appears much larger than it actually is.

The GPR can therefore be used for anomaly detection even with minimal processing. More important for this research is the impact of the presence of the anomaly on the GPR measurement of subsurface variability. It is probable that the disturbance caused by the anomaly will prevent GPR estimation of the limited variation previously identified in the

material properties. This issue is now addressed by looking at the 3-D variability of the amplitudes.

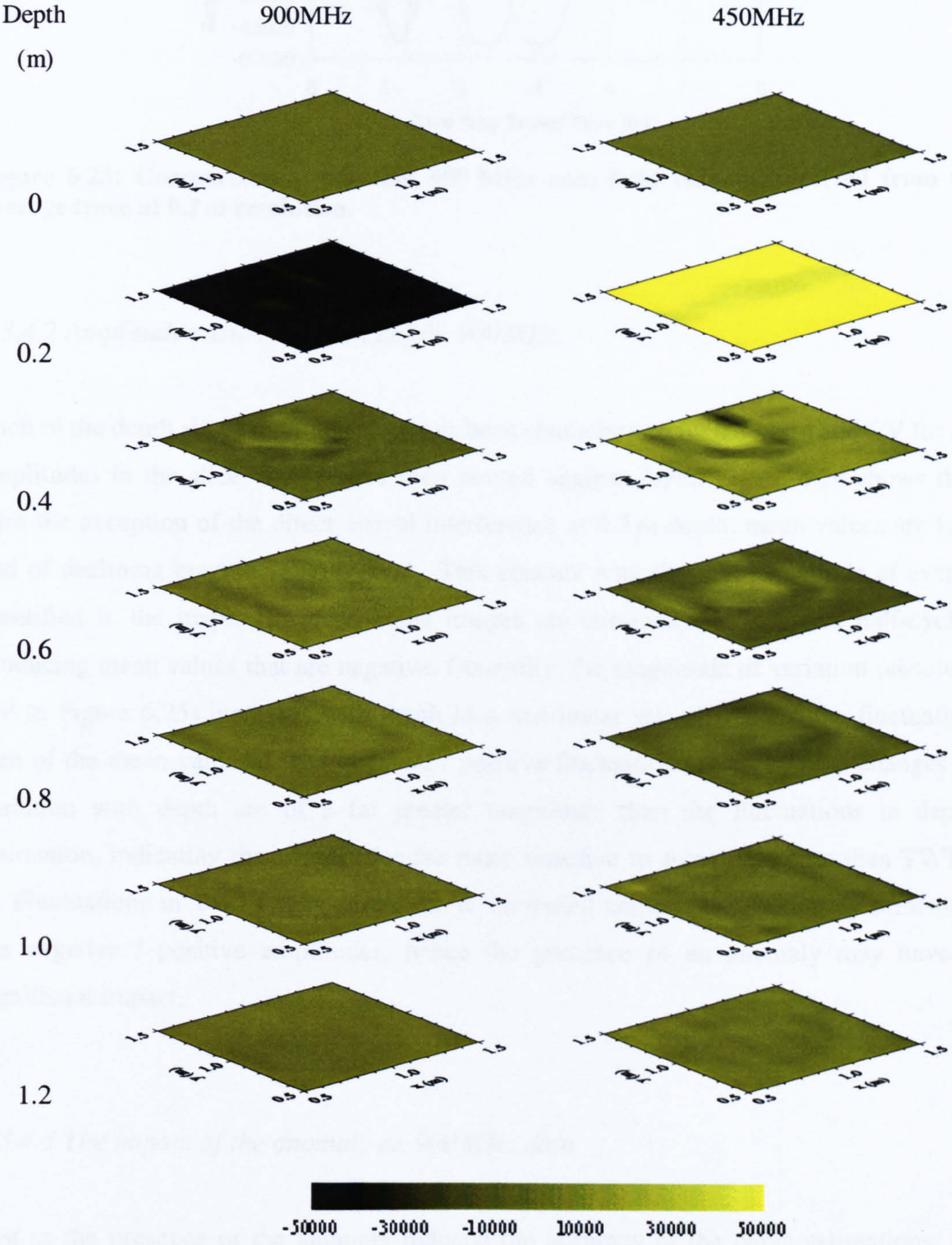

Figure 6.22: Amplitude (uV) depth slices for dry material configuration at 900 MHz and 450 MHz antenna frequencies.

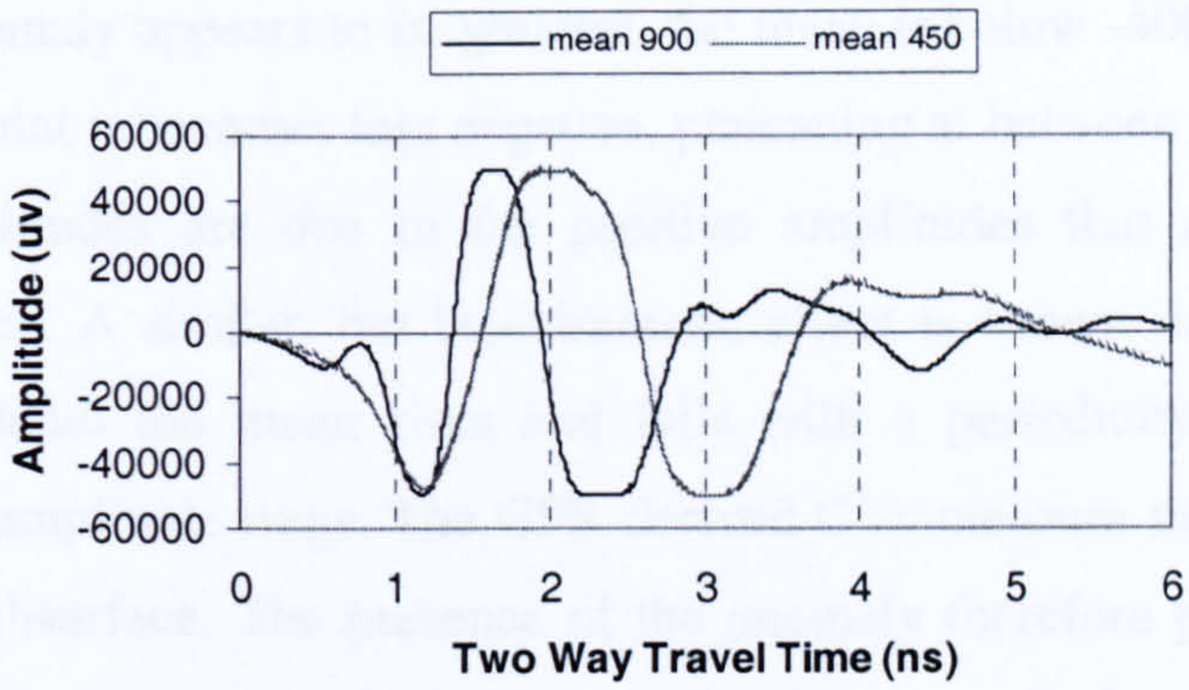

Figure 6.23: Comparison of 450 and 900 MHz near-field response derived from an average trace at 0.2 m resolution.

6.3.4.2 Amplitude variability with depth: 900 MHz

Each of the depth slice amplitude maps has been characterised by the mean and CV for all amplitudes in the slice. These were then plotted against depth. Figure 6.24 shows that with the exception of the direct arrival interference at 0.2 m depth, mean values are low and of declining magnitude with depth. This concurs with the low magnitude of events identified in the maps. However, some images are dominated by negative half-cycles producing mean values that are negative. Generally, the magnitude of variation (absolute CV in Figure 6.25) increases with depth in a non-linear way. However, the fluctuating sign of the mean values causes negative / positive fluctuations in CV. These changes in variation with depth are of a far greater magnitude than the fluctuations in depth estimation, indicating that amplitudes are more sensitive to signal variation than TWTT is. Fluctuations in TWTT may contribute to increased amplitude variation by offsetting the negative / positive amplitudes; hence the presence of an anomaly may have a significant impact.

6.3.4.3 The impact of the anomaly on 900 MHz data

Just as the presence of the anomaly reduced the accuracy of the depth estimations, its presence is a major factor preventing accurate GPR estimation of the variation in subsurface materials. This effect is shown by differences in profiles (Figures 6.26 (mean) and 6.27 (CV)). Most profiles (taken from x = 1.5 m to x = 0.5 m) have mean amplitudes which fluctuate between ±2000 uV depending on their depth. At 0.4 m depth, where the

presence of the anomaly appears to be greatest, the mean is below -4000 uV until about y = 0.9 m at which point it becomes less negative, plateauing at between -2000 to -4000 uV. These higher amplitudes are due to the positive amplitudes that are caused by the anomaly disturbance. A similar, but less dramatic effect is shown in the data at 0.6 m depth. At 0.8 m depth the mean rises and falls with a periodicity that matches the dimensions of the amplitude rings. The GPR derived CVs measure the total variation in its image of the subsurface. The presence of the anomaly therefore produces very high CVs where it affects the image and much smaller CVs where it does not. At all depths between 0-0.6 m CVs are relatively constant between profiles with values between ±2. It is noticeable that the spread in CV values after y = 0.9 m increases for these depths confirming greater CV in profiles affected by the anomaly. Below 0.8 m variation appears to be significantly increased in profiles that appear unaffected at shallower depths. Both 0.8 and 1.0 m depths have high magnitude CVs between y = 0.5 and 0.9 m which exhibit a rise and fall pattern. At y = 1.0 m, 0.8 m depth has returned to ±2. At 1.0 m depth, CV is high at y = 0.7 m. The cause of these variations is twofold. Because the mean values are of low magnitude, any signal disturbance may produce significant effects on the statistical value. Along the profiles this disturbance exhibits variably periodic patterns due to the semi-circular nature of horizontal response. Thus over some profiles, amplitudes can fluctuate between positive and negative values regularly, whilst on others they do not. Such spatial patterns occur due to the GPR footprint (and are therefore more evident in the 450 MHz response) and could be analysed using semivariograms. They may potentially be used to characterise the nature of the subsurface anomaly.

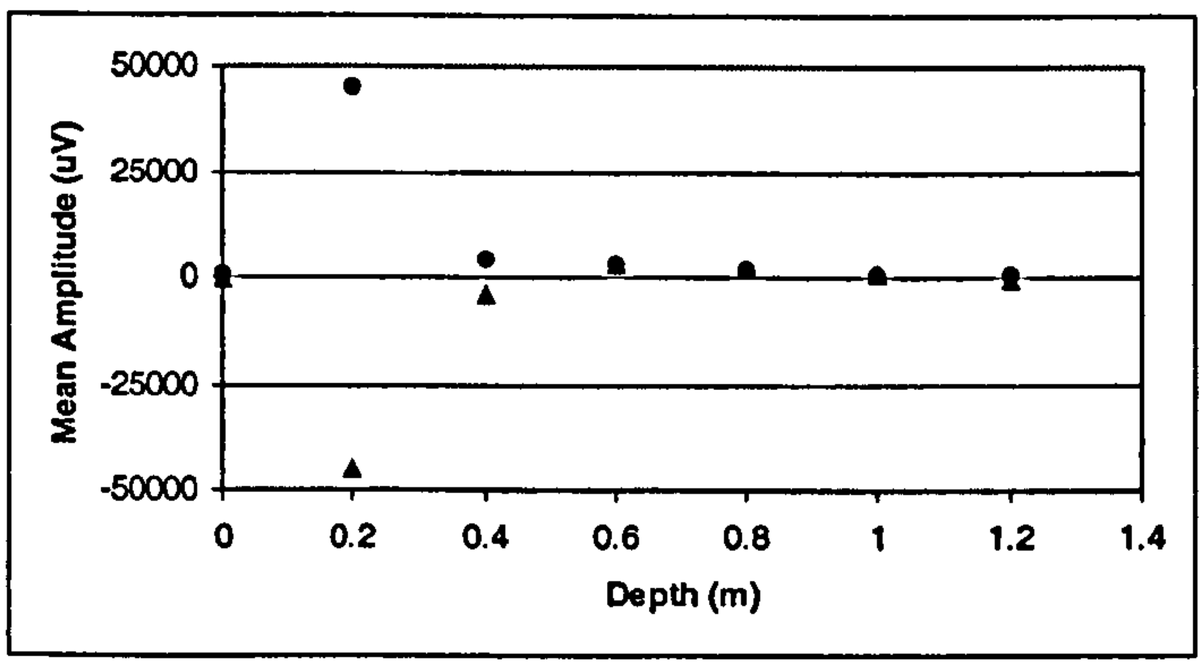

Figure 6.24: Mean amplitude for each depth slice at 900 MHz. Circles are absolute values; triangles are real values.

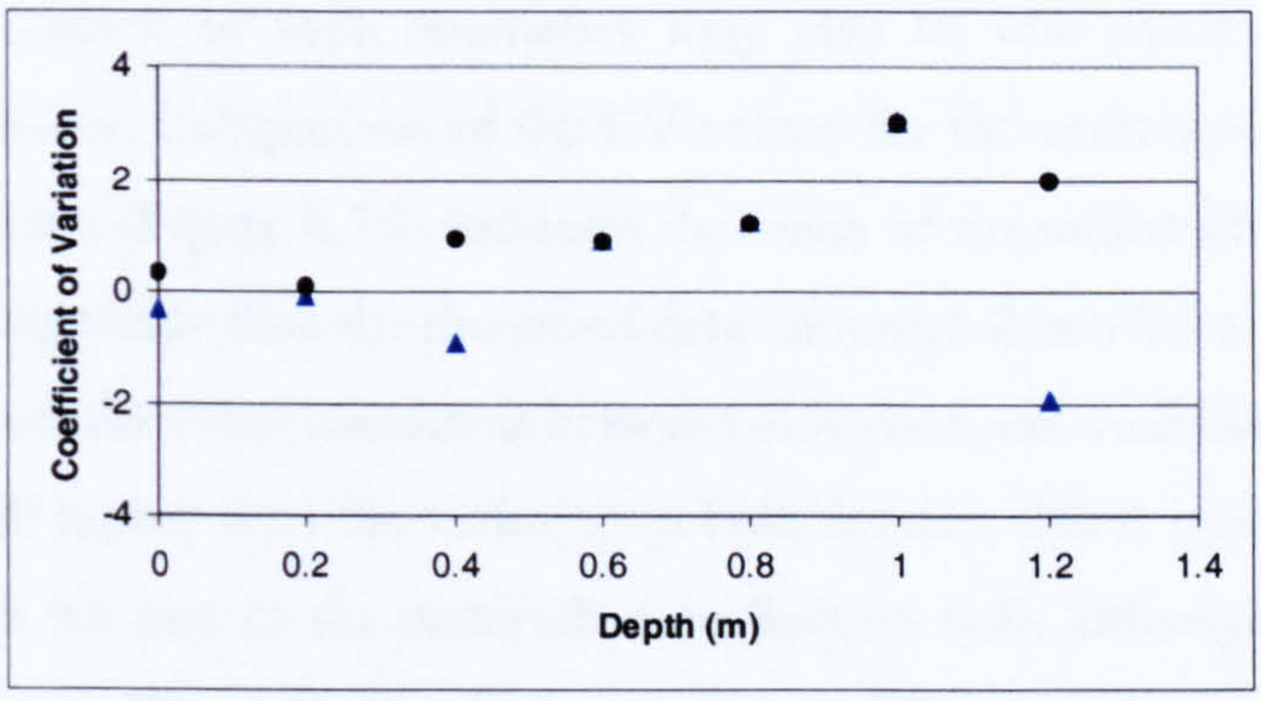

Figure 6.25: Mean CV for each depth slice at 900 MHz. Circles are absolute values; triangles are real values.

CV is exaggerated by the occurrence of negative and positive values, which suggests that using absolute values may improve the results. This reduces the magnitude of the deeper CVs but maintains the magnitude of the shallower CVs because amplitude magnitudes are similar at depth irrespective of sign so that when the sign is removed, the values are much closer producing less variability. Shallower amplitude extremes are greater irrespective of sign such that variation remains high. However, even after this correction, GPR signal CVs remain too high compared to those for the material properties. This indicates that the anomaly is the primary source of variability in the GPR response.

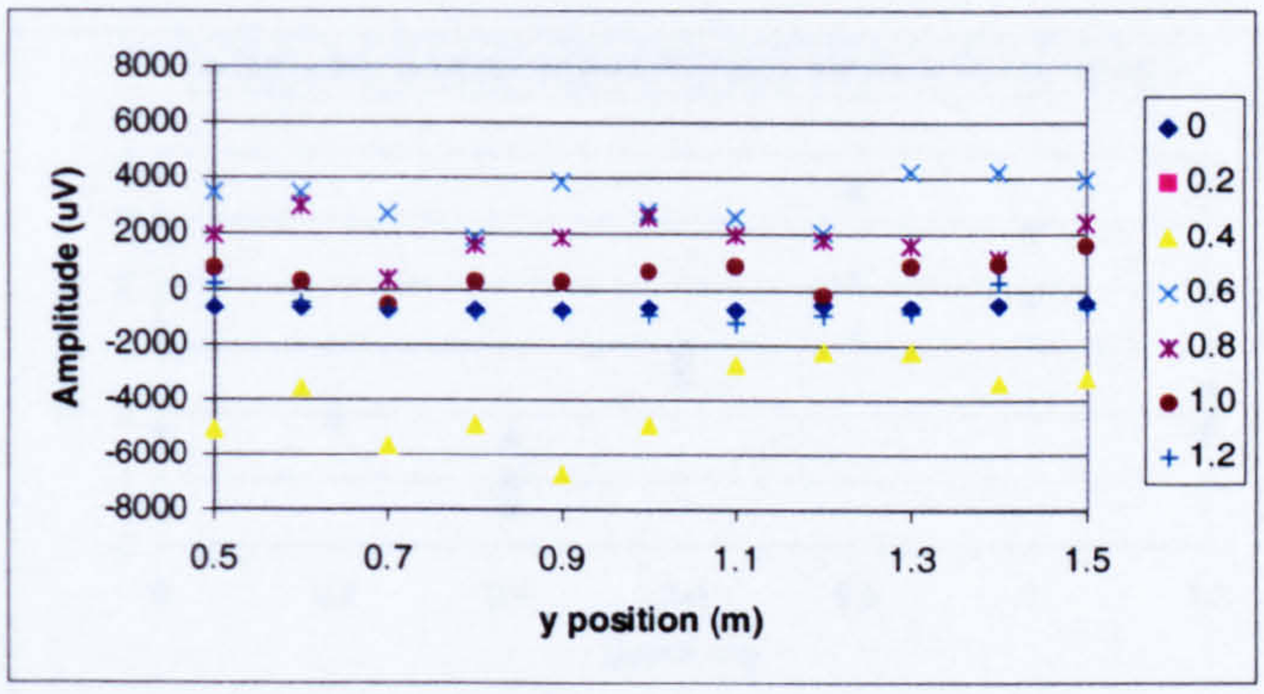

Figure 6.26: Variation of mean amplitude at different depths and along transects at 900 MHz.

To approximate the variability in material, undisturbed traces should be used. Due to the spreading of the hyperbolae the number of disturbed traces increases with depth so that by 1 m all profiles are disturbed to some extent. At 0.4 m the disturbed profiles are numbers 1-7, whilst the undisturbed profiles are numbers 8-11. This is also valid for 0.6 m, but not

for 0.8-1.2 m. Removal of such anomalies may also be one means of assessing the background variability. Comparison of the CV values for the undisturbed, disturbed, and total trace amplitudes (Figure 6.28) indicates that each of the undisturbed CVs (for 0-0.6 m) are of lower magnitude than the disturbed data, although 0 and 0.2 m are unaffected by the anomaly and are therefore consistent between disturbed and undisturbed data. Each of these values is still higher than the variation in bulk density, initial moisture content, and dielectric constant for any of the materials (see Section 6.2), although the initial VMC matches most closely. This indicates that variation in GPR response even in the absence of disturbed profiles, is still greater than in the subsurface material properties.

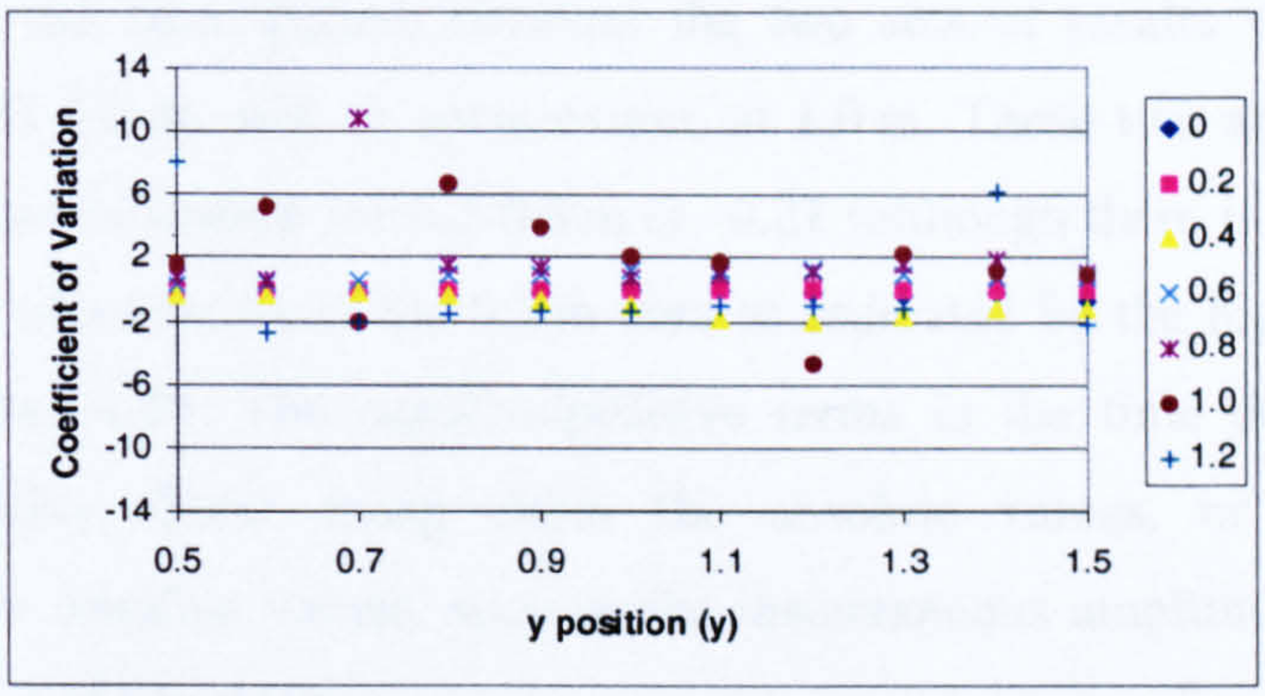

Figure 6.27: Variation of CV at different depths and along transects at 900 MHz.

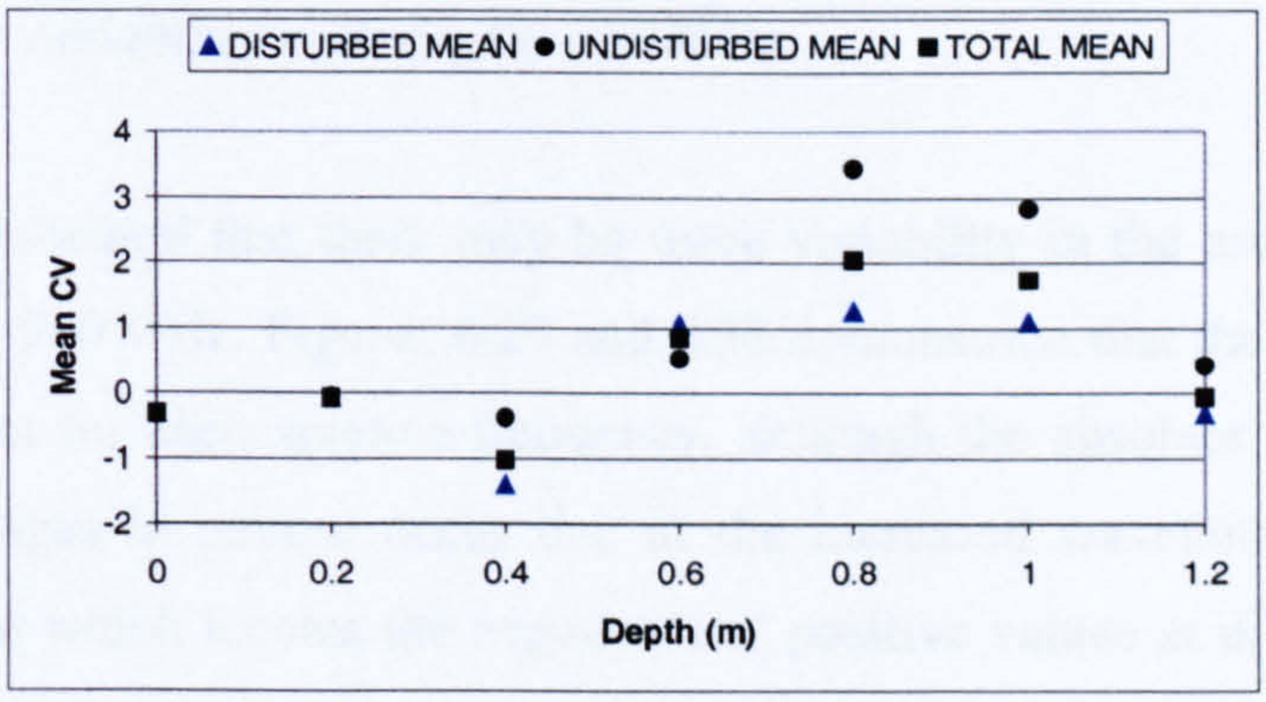

Figure 6.28: Comparison of variation (mean CV) in GPR response with depth for disturbed (by anomaly), undisturbed and all traces.

6.3.4.4 Sampling resolution

Differences in variation between GPR response and material properties can be expected to change with the horizontal resolution of the GPR survey. A higher resolution may

increase variation by introducing more variable data or may decrease variation by increasing certainty in the recorded data. As a preliminary investigation variation at 0.2m resolution 900 MHz is compared with 0.1 m resolution 900 MHz response. Data were collected independently rather than by sub-sampling the higher resolution data in order to assess potential repeatability in GPR response. There is limited statistical difference between 0.2 m and 0.1 m resolution and therefore resolution is less important to the quantitative analysis of signal characteristics than it is to visual interpretations, although this will most likely depend on the nature of the subsurface variability itself (i.e. with finer resolution more small-scale variation may be detected). Mean amplitude is very similar between the different resolutions; differences between the two are never greater than 2000 uV (2% error). Variability is constant between different sampling resolutions. CVs behave with the same pattern between the two sets of results with two notable exceptions at 0 and 1.2 m, and, to some extent, at 1.0 m. These two are different by 6, whilst the maximum difference for 0.2-0.8 m is –0.21 (although there is a tendency for a greater magnitude of variation in the 0.2 m data as indicated by the higher CV values), and for 1.0 m it is –1.94. The negative/positive terms in the time domain data may exaggerate variability. Thus, using either the absolute values, or something that approximates those absolute values, such as the instantaneous amplitude, may be more useful in an analysis of variability.

6.3.4.5 Amplitude variability with depth: 450MHz

The depth maps indicated that there may be more variability in the amplitudes for 450 MHz compared to 900 MHz. Figures 6.29 and 6.30 demonstrate that the pattern of mean and CV is different for each antenna frequency, although the absolute mean values are very similar. Changes in pattern occur due to the increased wavelength of the lower frequency response which locates the negative and positive values at different depths to the 900 MHz data. Absolute mean for 900 MHz, and summed over all depths, is about 15000 uV higher than for 450 MHz. This can be expected to produce lower CV values. Whilst this is generally true for shallow depths, the depths which demonstrated the greatest variation at 900 MHz show even greater variation for 450 MHz. Table 6.11 demonstrates that with the exception of 0.2, 0.4 and 1.2 m depths variation in amplitude values (using absolute CV as an indication of magnitude of variation), are greater for 450

MHz than for 900 MHz. This occurs because of increased standard deviation at 450 MHz (28455 uV compared to 15888 uV for 900 MHz) at these depths.

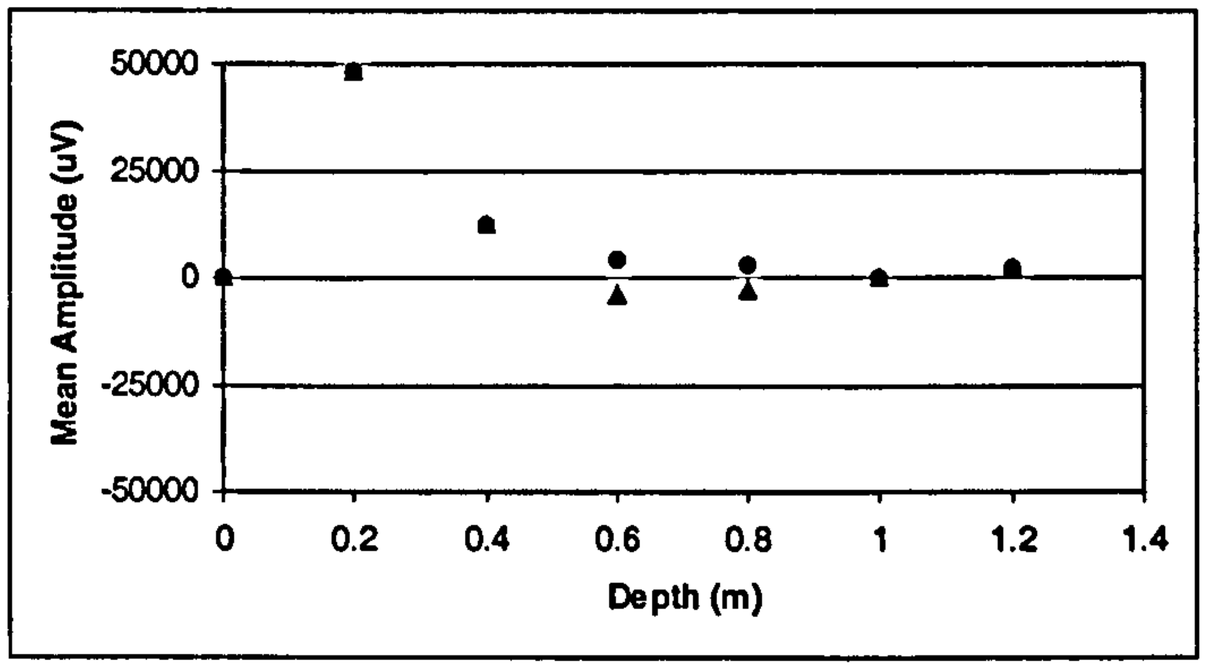

Figure 6.29: Mean amplitude for each depth slice at 450 MHz. Circles are absolute values; triangles are real values.

The primary cause of this increased variation for 450 MHz is due to the increased wavelength at this frequency. This not only reduces resolution and increases uncertainty in the part of the waveform analysed using arbitrary depth slices, but also results in higher magnitude amplitudes. It is these higher magnitudes of 450 MHz responses which increase CV by increasing the discrepancy between values that are negative and positive when disturbance is introduced. This could be improved by using absolute amplitude values but generally 450 MHz is more susceptible to subsurface disturbance than 900 MHz and, therefore, the latter frequency is more appropriate for background variability investigations.

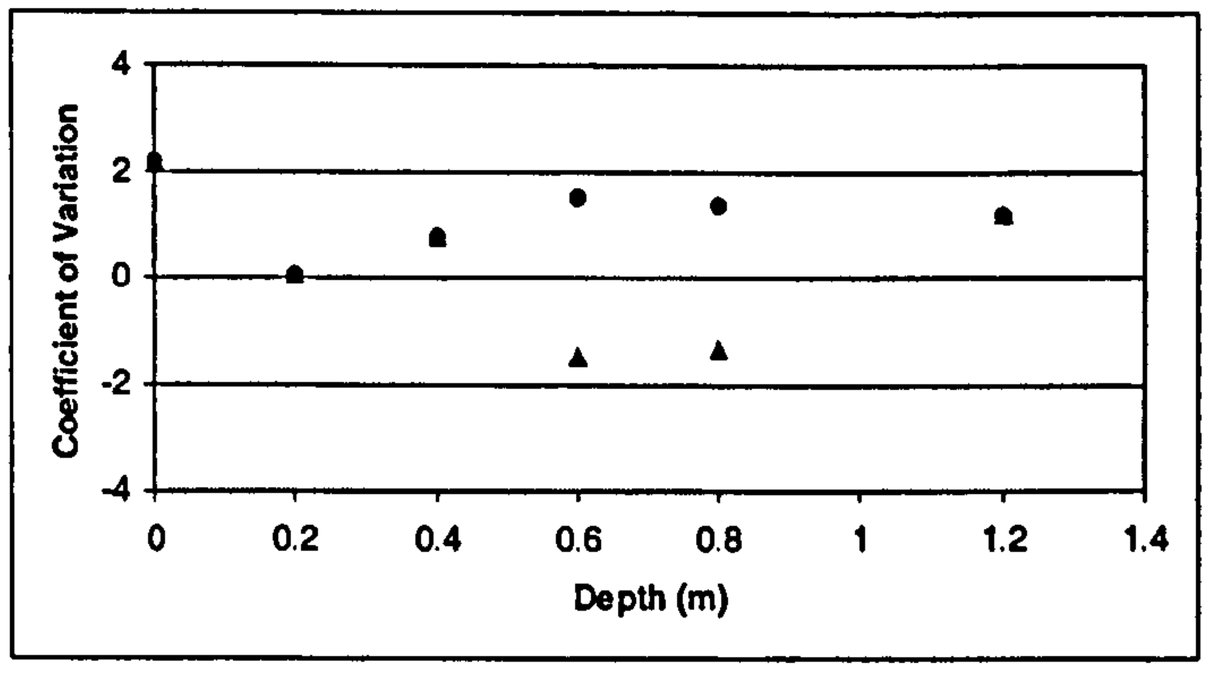

Figure 6.30: Mean CV for each depth slice at 450 MHz. Circles are absolute values; triangles are real values.

Depth Beneath Surface (m)	Frequency with higher signal variation (MHz)	Increase in CV
0	450	1.809
0.2	900	0.028
0.4	900	0.208
0.6	450	0.653
0.8	450	0.131
1.0	450	12.194
1.2	900	0.834

Table 6.11: Magnitude of variation comparison for 900 and 450 MHz.

6.3.4.6 Assessing material properties using GPR depth slices

Using the arbitrary amplitude depth slice maps, the data are selected at the precise depth increment with no subjective consideration of what is being selected. There is no control over which part of the waveform has been detected such that events, unrelated in space, may be selected which may indicate an anomaly where there is in fact not one. This will be exaggerated by error in the time-depth correction. This uncertainty is increased in the presence of noise. For assessing variation in material properties the implications of this discretization are more serious: the arbitrary nature of the depth results in the capture of data that does not correspond to the layer of interest. To overcome the potential error associated with a depth-scale point-specific amplitude value, and to investigate the potential GPR response to individual subsurface layers the data were divided into the six layers based on the estimations of boundary depth derived in Section 6.3.2. Using this technique it is not possible to derive a unique amplitude value so a statistic that represents the signal characteristics in the subsurface needs to be selected. The mean, CV, maximum, minimum, and range were used because any variation in signal will affect these values. These statistics are then categorised based on their mean and CV. There are no significant relationships between depth and either the material properties or the GPR statistics, or between the GPR statistics and the material properties. This indicates that any variation in GPR response is not the result of material property variation.

6.3.4.7 Summary

The above analysis shows that the variability in GPR response is due to vertical amplitude variations associated with contrasts between layers and variations induced by the presence of a small anomaly rather than horizontal variations in response induced by material property variation. GPR is extremely sensitive to unexpected subsurface targets.

Interpretation of subsurface variability using GPR data should be very carefully considered to ensure that the variability is not distorted by the presence of objects. Assessment of material property variation is not possible owing to the arbitrary nature of the depth slices. This can be overcome by using the GPR data that corresponds to the actual material layers. The GPR results are very sensitive to the nature of the vertical discretization such that the polarity and magnitude of an event may deviate from the expected. There is no effect of horizontal sampling resolution on the derived data, other than less ability to interpret individual events at lower resolutions. Variability is greater for 450 MHz than 900 MHz, suggesting that the latter is more appropriate for subsurface variability studies in the materials and conditions investigated here.

6.4 SUMMARY: IMPLICATIONS FOR GPR-VMC RELATIONSHIPS

An analysis of the variation of GPR response in the absence of moisture has been presented. The radar has been shown to effectively and reliably identify material boundaries. The variation in GPR response is largely due to layering, with the limited variation in material properties being largely undetectable in the horizontal plane. In the dry situation the material property variation is itself minimal, whilst GPR assessment of this variability is apparently not possible. Material characteristics of individual layers are almost impossible to assess using GPR when material variability is low and especially in the presence of an anomaly, or when there is moderate variation in layer thickness. The presence of an anomaly will distort depth estimations and statistical characterisations in a way that interacts with antenna frequency (higher variation with lower frequency), depth of investigation and footprint area (anomaly increases variation as its effect spreads with depth), and horizontal resolution (too coarse a resolution will leave the effect of an anomaly undetected).

The images of horizontal GPR response are dominated by the anomaly that is present. The fact that the radar has been shown to be effective in delineating subsurface amplitude variations in simple materials, suggests that the radar has the potential for water body detection and spatial VMC estimation. However, in order to assess the spatial variation of subsurface moisture, a means of deriving an estimate of that VMC needs to be developed. Without high-resolution transects and visual interpretation it would not be possible to determine to what extent a trace is affected by an anomaly. Furthermore, developing a

relationship in a spatial context is prohibited by the susceptibility of GPR to anomaly presence, which may mask the impacts of moisture on the GPR signal; especially when the subsurface is relatively dry.

The implications of these analyses in the absence of moisture for the development of GPR-VMC relationships are that:

- static GPR should be used to eliminate error associated with changing subsurface conditions in space,
- using an increased number of stacks and averaging more than one static trace should minimise any other sources of variation, and
- 900 MHz antennae should be used because they have higher resolution, less variability and the control of the measurement volume is better than using lower frequencies.

Although only time domain data have been investigated, it has been noted that the dependence of the results on the sign of the amplitude can hinder attempts at statistical signal characterisation. This could be accommodated for by using absolute values or by an approximation, such as the envelope amplitude. Despite, the fact that differences within individual materials are low, differences between materials in terms of porosity and hydraulic conductivity are, in fact, substantial. Between materials these differences mean that the GPR is likely to respond not only to changing volumetric conditions but also changes in moisture distribution. Moisture distribution may vary between materials, producing differences in GPR response by generating variable reflection patterns. This can be expected to obscure the GPR estimation of moisture content. The measurement volume should therefore be constrained to control moisture distribution as much as possible. Using this information, the remaining sections of this thesis address the development of a GPR-VMC relationship, and its subsequent testing and application.

CHAPTER SEVEN: DEVELOPING GPR PARAMETERS FOR VOLUMETRIC MOISTURE CONTENT MEASUREMENT

7.1 INTRODUCTION

In the previous chapter the characteristics of the GPR response in the absence of moisture were discussed in detail. This work provides a background to the main aim of this research which is to characterise and understand GPR response to changes in subsurface moisture and to develop, test and apply a quantitative means of estimating VMC using GPR signal parameters derived in reflection profiling mode. Chapter Four discussed a large number of potential means of deriving moisture content from GPR data. Due to the requirements of simplicity and efficiency, the emphasis of this research is on direct statistical methods for characterisation of GPR signal response using minimal processing. The design of the experiments (Section 5.2.4) facilitates an analysis of the GPR signal response and its relationship to independent estimates of changing VMC (provided by *ThetaProbes*) using these methods. Chapter Six showed that although there is limited variation in material properties within materials, significant differences exist between materials. Of particular importance are the variations in porosity and hydraulic conductivity which may produce variable moisture distributions. To reduce the effect of such variability on GPR response, GPR data must be acquired from a constant location. To ensure hydrological control, and decrease potential moisture variation, the measurement volume must be small. Only 900 MHz antennae are used owing to their reduced separation, higher vertical resolution, and smaller footprint size (as discussed in Chapter Six).

This Chapter begins with an analysis of the GPR data using traditional methods because visual analysis is important for all subsequent statistical analyses. Whilst these techniques cannot provide a direct quantitative assessment of VMC, they enable an analysis of signal propagation velocities. Statistical characterisation and understanding of GPR response using the five basic visualisations then aims to develop a relationship to estimate VMC using a single GPR parameter. A full range of statistics will be investigated to establish which produce the most consistently significant results between materials. After selecting an appropriate relationship and relating the results to physical processes, implications for further analysis, interpretation and application are highlighted. The method is then tested prior to its application for spatial VMC estimation in subsequent chapters.

7.2 TRADITIONAL DATA ANALYSES

7.2.1 Visual interpretation

Visual Interpretation of GPR data will provide a basis for subsequent quantitative analysis of the GPR data, by allowing identification of start and end times, signal features (character of direct arrivals, internal reflection events, noise, etc.), and velocity analysis. Figure 7.1 shows a sequence of average time domain traces derived from 20 static traces for each water increment in each experiment arranged as a B-scan. These data were imported from Microsoft EXCEL into SURFER to create an image. The x-axis represents the number of each experimental run after each successive water increment (of 51 each). The associated average calibrated *ThetaProbe* VMC for each material and each experimental run is shown in Figure 7.2, which demonstrates a linear increase in VMC with each water increment. At higher VMCs there is increased scatter in the data, due to differences in porosity between materials and errors in the *ThetaProbe* estimations (discussed in Section 6.2.4). Figure 7.2 demonstrates the average VMC throughout the STF profile; this VMC is the target of the quantitative analyses. The y-axis in Figure 7.1 represents the two-way travel time (TWTT). All traces were aligned at G_0.

These time domain images demonstrate that upon addition of increasing volumes of water, the number, magnitude and timing of identifiable signal features is not consistent between materials or within material experiments. These signal features take five basic forms:

- Changes occur in the direct arrivals when water is added. An apparent polarity reversal occurs in which the sign of the first half-cycle changes from negative to positive for saturated responses in all materials and for some non-saturated materials (especially for M3-M6). The magnitude of this positive peak is very variable and indicates signal interference. This may increase uncertainty in near-surface interpretation.
- An additional band of reflections occurs after the direct arrivals. This is most clear on M3-M5 and may be related to a decrease in the velocity of the ground-wave inducing a delay in this direct arrival travel time. It could also be caused by a reflection generated at a wetting front, but this would involve it occurring later in time each time more moisture was added.

- Changes in internal reflections are very variable. A reflection arrives earlier in time, approaching the surface for some materials (e.g. M1 and M2). This could be caused by a rising water table in these materials with high hydraulic conductivity. Very broad, high magnitude events occur throughout the entire time window on some traces. These are most evident on low VMC responses in M3-M5, and tend to obscure later events.
- Generally there is a retreating (arrives later in time) and weakening reflector visible for each experiment, which might represent the lower limit of the STF. It is not visible on some images, especially at higher VMCs or where there are more early-time events. There seems to be a complete absence of this event from the M6 results.
- The data demonstrate that as the material gets wetter, the later reflections decrease in magnitude and become fewer in number. This occurs at high moistures and on all M6 traces.

All of these effects are related in some way to the addition of the moisture to the different materials, indicating a potential interaction of VMC and its distribution. There is clearly some kind of variable behaviour influencing GPR response, which may impact upon VMC estimations. The interference manifested on the visual radargrams will alter the amplitude results and therefore influence the development of quantitative relationships. They therefore need to be explained and understood in terms of their cause and impact on signal characterisation. Whilst offering no quantitative means of estimating VMC, this brief visual interpretation indicates response-features, which may effect subsequent statistical characterisation and interpretation. Visual interpretation of amplitude spectra is much less useful in identifying GPR response to changing moisture conditions than using the raw trace data, whilst using the instantaneous amplitude provides a very similar interpretation. Both instantaneous phase and instantaneous frequency provide images that are largely un-interpretable, suggesting that these would be of limited use for developing a GPR parameter VMC relationship.

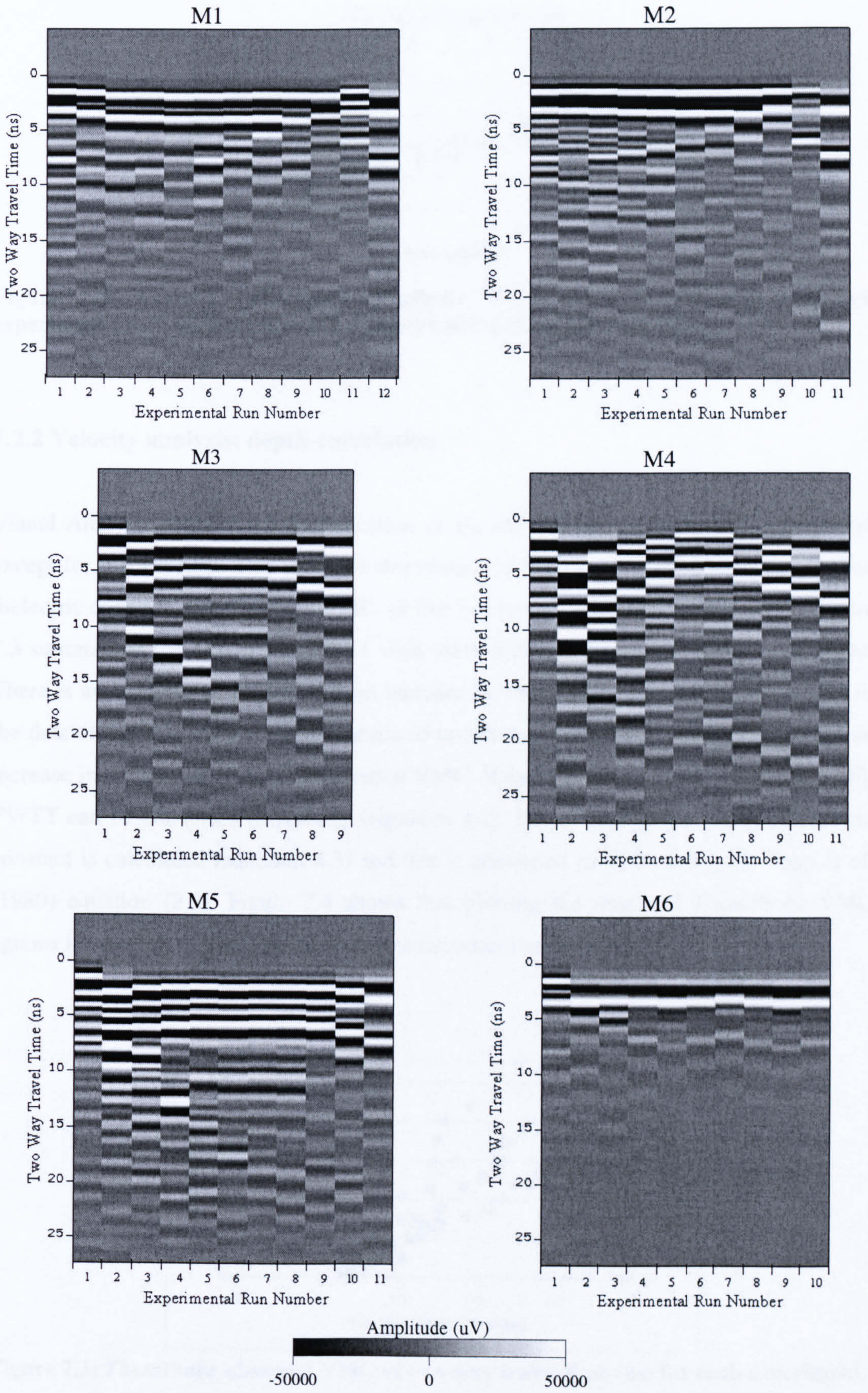

Figure 7.1: Mean time domain traces for each experimental run arranged as radargrams (B-Scans) for each material M1-M6.

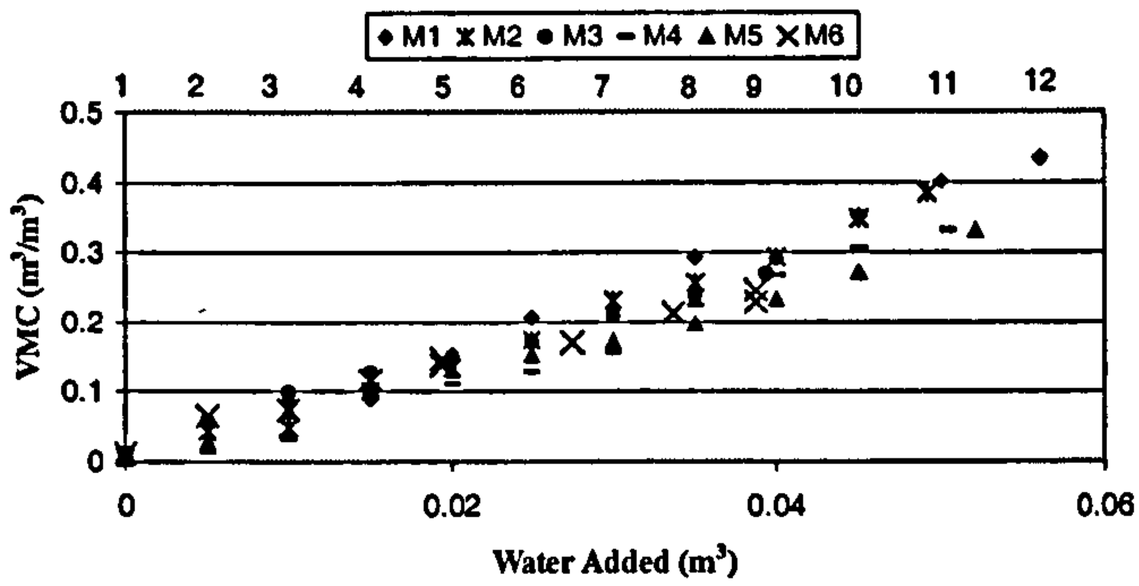

Figure 7.2: Average calibrated *ThetaProbe* VMC for each material and each experimental run (indicated by the numbers above the groups of data).

7.2.2 Velocity analysis: depth-correlation

Visual Analysis enabled the identification of G_0 and the end time for each experiment except for the M6 runs. This provides an estimate of TWTT that can be used to calculate dielectric constant, and therefore VMC, or that can be related directly to the VMC. Figure 7.3 summarises the changes in TWTT with water addition for each material experiment. There is an increase of TWTT with an increase in VMC. Increased spread and scatter in the data at higher VMCs is due to increased uncertainty in reflector identification and an increase in the spread of the experimental VMC. If depth is known (0.58 m for the STF), TWTT can be converted to velocity (equation 4.2). From velocity the relative dielectric constant is calculated (equation 4.3) and this is converted to VMC using the Topp *et al.* (1980) equation (2.9). Figure 7.4 shows that plotting the observed *ThetaProbe* VMC against the predicted VMC produces the same pattern as for TWTT.

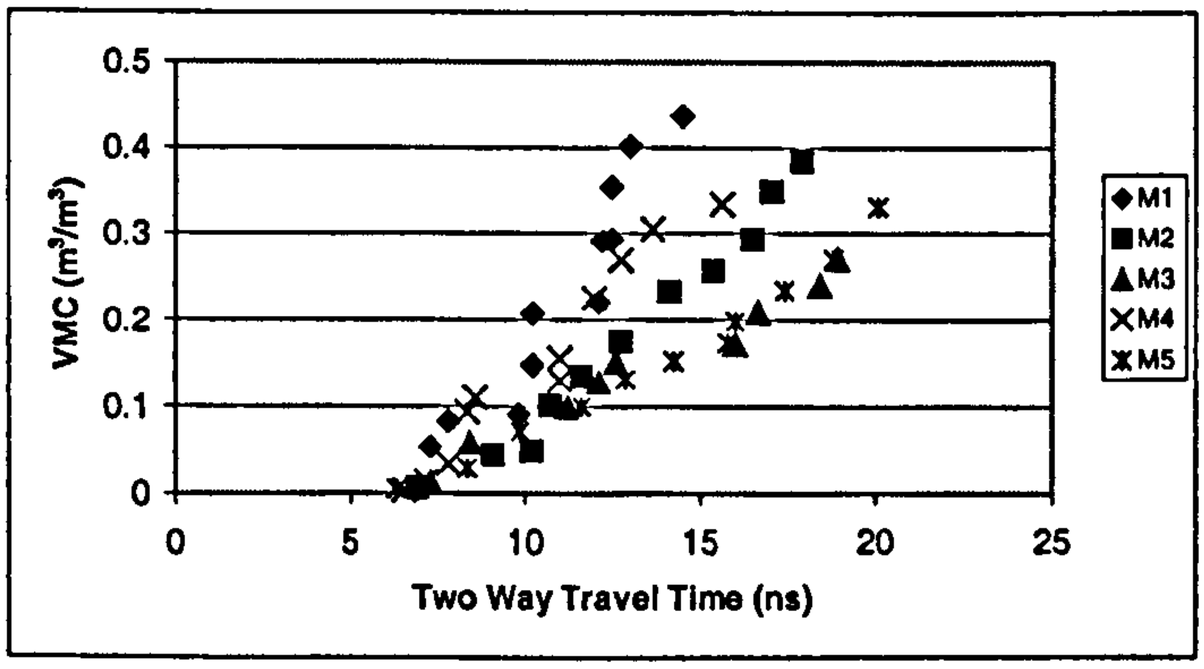

Figure 7.3: *ThetaProbe* observed VMC vs two-way travel time (ns) for each experiment.

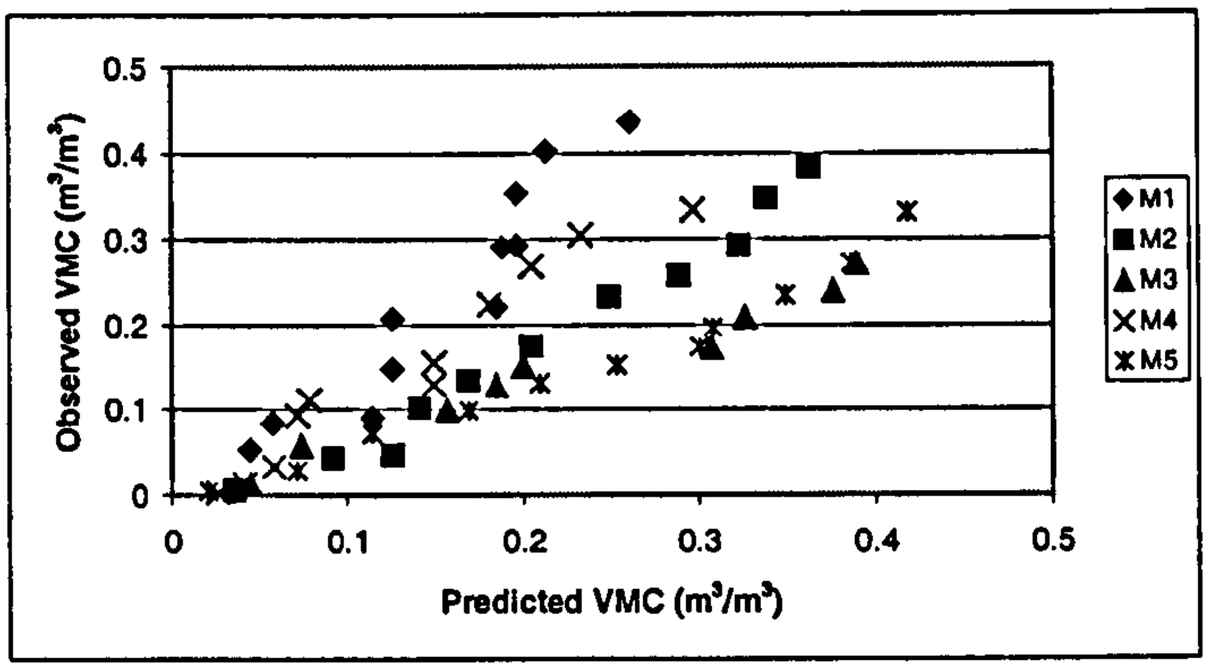

Figure 7.4: *ThetaProbe* observed vs predicted (Topp *et al.* (1980) conversion) VMCs for each experiment.

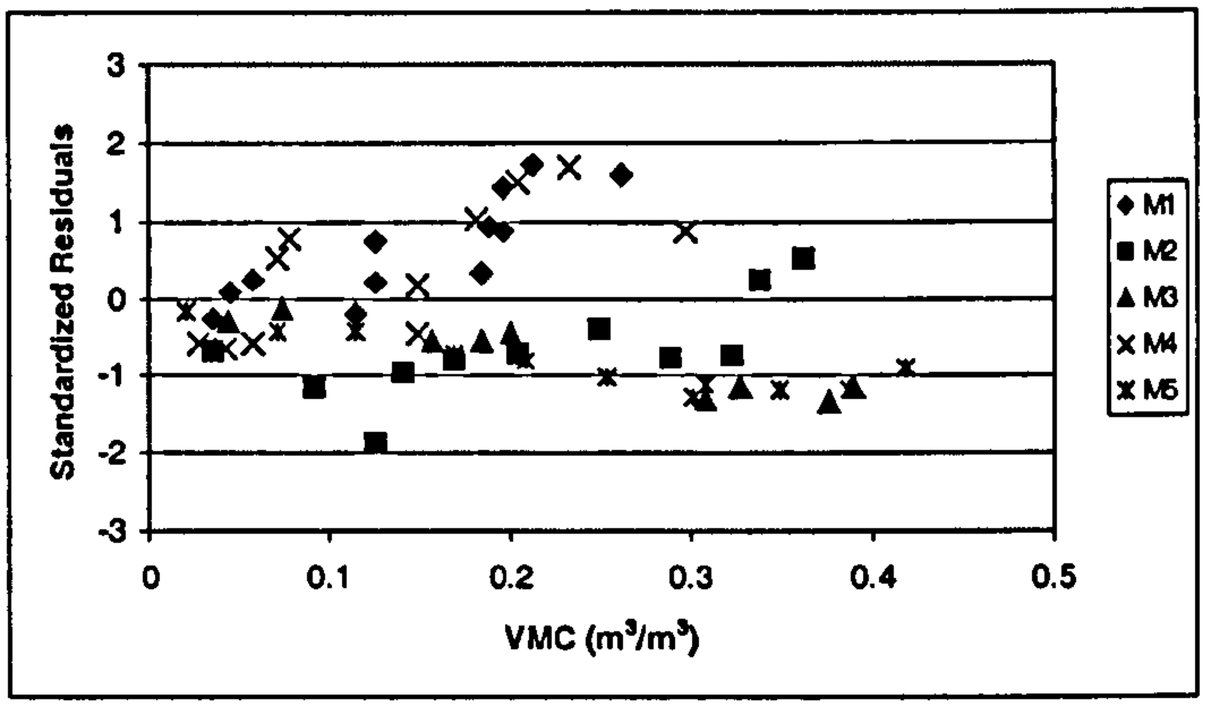

Figure 7.5: Standard residuals for each experiment associated with Figure 7.4.

Figure 7.4, and the standard residuals in Figure 7.5, indicate that error in VMC estimation is variably under- or over-estimated. The results are especially poor at greater than 0.2 m^3/m^3. Although the standard residuals never exceed 1.96, there are very definite patterns to the values, suggesting estimation error. There is a tendency for all materials to be overestimated slightly at very low VMCs. For M1, M2, and M4 there is a tendency towards underestimation with increasing predicted VMC. For M2 this tendency is manifested as an increasingly accurate estimation. For M3 and M5 there is a tendency towards increased overestimation with increased predicted VMC. This is confirmed by the linear significance results in Table 7.1, which demonstrate slope values over one for M1, M2 and M4 and under one for M3 and M5. The similarity between Figure 7.4 and Figure 7.3 demonstrates that the error in the VMC estimation is controlled primarily in the accuracy of the TWTT estimate. Although it has a tendency to overestimate at lower VMCs the experiment that had the greatest clarity in reflector identification, M2, provides the best match between predicted and observed data. This suggests that reduced clarity leads to increased TWTT estimation error and this produces very poor results using the

Topp *et al.* (1980) conversion. The absolute deviations of the GPR VMC estimates from the observed *ThetaProbe* VMC estimates are shown in Table 7.2. Maximum absolute error is poor, especially for M1. Mean error (between 0.0332 and 0.0825 m^3/m^3) is high given that it is relative to a ThetaProbe measurement, which has its own error. Error is greater than the error in the *ThetaProbe* calibrations (see Section 6.2.4) showing the error associated with the TWTT estimations.

Material	Constant	Slope	r^2	t	P	N
M1	-0.0558	1.8678	0.9179	10.5721	9.52E-07	12
M2	-0.0631	1.1687	0.9777	19.8683	9.62E-09	11
M3	-0.0002	0.6521	0.9651	13.9088	2.35E-06	9
M4	-0.0237	1.2981	0.9520	13.3638	3.06E-07	11
M5	-0.0255	0.7589	0.9710	17.3574	3.16E-08	11

Table 7.1: Linear regression significance results for *ThetaProbe* VMC (y) vs Topp *et al.* (1980) VMC estimate (x).

Material	Absolute Deviation from expected (m^3/m^3)			
	Mean	standard deviation	Maximum	minimum
M1	0.0791	0.0648	0.1893	0.0093
M2	0.0332	0.0178	0.0773	0.0103
M3	0.0798	0.0470	0.1368	0.0162
M4	0.0340	0.0193	0.0718	0.0068
M5	0.0825	0.0360	0.1272	0.0168

Table 7.2: Mean, maximum, and minimum absolute deviation from observed *ThetaProbe* VMC when using the Topp *et al.* (1980) VMC estimate (x)

Thus depth-correlation approaches provide a direct means of estimating the average VMC above a reflector, although these results are variable between materials. Depth-correlation analyses are fundamentally limited by a number of aspects evident from the variation in the B-scan images:

- Direct arrivals make estimation of TWTT over their depth of influence impossible. This was estimated to be about 0.3 m in Chapter Seven. Therefore it is of limited use for near surface analysis.
- The subsurface reflector must be strong. If not, attenuation may reduce its magnitude so that it is lost entirely (as in M1 and M6) or obscured by noise (as in M4 and M5).
- Multiple reflection events may occur. These may give the impression of a continuous event and may result in misidentification. This will obscure the target reflection and produce false TWTT estimations. In later experiments the emerging ground-wave can be seen to separate fully from the air-wave arrival. At later times, in the same traces,

events occur that appear to suggest a retreating reflector. In fact these retreat at the same rate as the ground-wave indicating that this is a multiple of the ground-wave. Consequently, the velocity measurement does not correctly measure STF VMC. However, the velocity change of the ground-wave can be used to approximate the VMC in this zone.

This method is further limited by:

- The identification of the relevant reflector is highly subjective; the more complex the GPR response, the less confidence there is in reflector identification.
- The requirement for a constant depth reflector is not a problem for these controlled laboratory investigations (in which the depth to STF base is constant). If reflector depth is not constant (e.g. variable bedrock boundary) it is not known whether or not this is due to natural depth changes or changes in VMC (or anything else) above it.
- When applied to only one known subsurface reflection the method only gives an average VMC above that point. For application to other depths, other reflection events need to be identified. This is a complicated process where signal disturbance is high.
- In the absence of any information on the subsurface it would not be possible to ascertain whether or not the reflection should be positive or negative. Misidentifying a negative response as a positive one, or vice versa, can produce further TWTT estimation error.
- This estimation error will depend on the frequency character and resolution of the reflector and near-by events. Lower frequency response will produce longer duration wavelets that increase estimation error.

In summary, in a simple and controlled situation depth-correlation can provide accurate VMC estimation. However, accuracy cannot be guaranteed due to combinations of interference (noise and multiples) and attenuation. Consequently, mean estimation error can be up to 0.0825 m^3/m^3 relative to *ThetaProbe* estimates. Thus there is a clear need for other means of assessing VMC changes in the subsurface using GPR data.

7.3 RELATIONSHIPS BETWEEN STATISTICAL SIGNAL CHARACTERISTICS AND VMC

7.3.1 Introduction

Limitations in visual (no quantitative estimation) and velocity (time consuming, event ambiguity and identification) methods mean that more direct techniques need to be developed. Thus, the main purpose of this research is to establish relationships that use a derivable GPR parameter to estimate quantitatively VMC in a spatial context. The aim is to identify statistics that produce significant relationships with VMC and to eliminate those that are statistically insignificant. To maximise measuring the effect of VMC on the GPR signal, the STW analysis scale, discussed in Chapters Four and Five is used because this ensures a constant measurement depth. Visual analysis has demonstrated that it is not always possible, even in a controlled laboratory environment, to identify the lower limit of the STF. This prevents adequate control of the measurement depth. Therefore, knowledge of the dielectric constant (from *ThetaProbes*) can be used to determine the theoretical TWTTs and from this the nearest event (in time) of appropriate sign can be selected. Although the measurement depth can be controlled for, despite additional error associated with the non-linear depth-scale, the dynamic nature of the GPR footprint is impossible to control and means that the horizontal component of the measurement volume will change when the VMC changes.

This section begins with an initial analysis in which the statistical results are collated, correlated and tested for linear significance (using STATISTICA), and then those relationships that are significant for all six materials are selected for further analysis after a discussion of the causes of the statistical signal characterisations. This will identify limitations and discuss exclusions and, if necessary, re-analysis of the data can be performed. Following this, a method will be selected based on the consistency of its coefficient of determination for each material and the nature of the relationship will be explained with recourse to the visual analysis and hydrology. The section finishes with a look at some of the potential limitations of the method in its current state of development.

7.3.2 Statistical signal characterization

7.3.2.1 Initial analysis

A total of 378 statistical characterisations (five visualisations, 12 statistics, and six materials) were investigated. Only fourteen statistics provide significant linear relationships with VMC for all materials. Figures 7.6-7.19 demonstrate the experimental data for these parameters. Table 7.3 summarises the acronyms for all significant relationships referred to throughout the text. The table includes methods that are significant for later analyses and others that are relevant to the subsequent discussion. Table 7.4 summarises all significant linear relationships for the initial data analysis. Only three of the basic visualisations provide significant results: time domain, amplitude spectra, and instantaneous amplitude. The lack of interpretability in the instantaneous phase and frequency images for M2 is carried through to their statistical characterisation for all materials. Of the 14 results, eight are from the frequency domain data suggesting that moisture response is most clearly manifested in this domain. The significant responses from each of these domains are now discussed.

Domain	Statistic	Acronym	Figure Number
Time Domain	Mean	TAM	N/A
	Standard Deviation	TAS	7.6
	Variance	TAV	7.7
	Kurtosis	TAK	7.8
Amplitude Spectra	Mean	ASM	7.9
	Median	ASMED	7.10
	Mode	ASMOD	7.11
	Standard Deviation	ASS	7.12
	Variance	ASV	7.13
	Minimum	ASMIN	7.14
	Maximum	ASMAX	7.15
	Range	ASR	7.16
Instantaneous Amplitude	Mean	MIA	7.17
	Median	MEIA	7.18
	Skewness	SKIA	7.26
	Coefficient of Variation	CVIA	7.19
Instantaneous Frequency	Sum	IFS	7.27

Table 7.3: Acronyms for the statistics referred to in the text. Also indicated is the Figure number for each relationship.

Signal Parameter	M1			M2			M3		
	R^2	t	p	R^2	t	p	R^2	t	p
TAS	0.826	-6.887	4.3E-05	0.875	-7.929	2.4E-05	0.824	-5.718	7.2E-04
TAV	0.830	-6.976	3.8E-05	0.906	-9.323	6.4E-06	0.812	-5.503	9.0E-04
TAK	0.690	4.714	8.2E-04	0.636	3.967	3.3E-03	0.759	4.689	2.2E-03
ASM	0.740	-5.335	3.3E-04	0.735	-5.000	7.4E-04	0.723	-4.277	3.7E-03
ASMED	0.546	-3.468	6.0E-03	0.740	-5.058	6.8E-04	0.833	-5.902	6.0E-04
ASMOD	0.641	-4.223	1.8E-03	0.449	-2.706	2.4E-02	0.768	-4.814	1.9E-03
ASS	0.740	-5.336	3.3E-04	0.683	-4.399	1.7E-03	0.614	-3.337	1.2E-02
ASV	0.740	-5.332	3.3E-04	0.521	-3.127	1.2E-02	0.596	-3.217	1.5E-02
ASMIN	0.499	-3.157	1.0E-02	0.687	-4.444	1.6E-03	0.733	-4.380	3.2E-03
ASMAX	0.613	-3.982	2.6E-03	0.601	-3.679	5.1E-03	0.559	-2.977	2.1E-02
ASR	0.613	-3.979	2.6E-03	0.600	-3.677	5.1E-03	0.558	-2.974	2.1E-02
MIA	0.824	-6.833	4.6E-05	0.879	-8.104	2.0E-05	0.810	-5.455	9.5E-04
MEIA	0.795	-6.223	9.8E-05	0.859	-7.411	4.1E-05	0.638	-3.509	9.9E-03
CVIA	0.721	5.080	4.8E-04	0.814	6.278	1.4E-04	0.709	4.128	4.4E-03

Table 7.4a: Summary of significant relationships between GPR signal statistic and VMC for M1-M3 for the initial analysis.

Signal Parameter	M4			M5			M6		
	R^2	t	p	R^2	t	p	R^2	t	p
TAS	0.772	-5.528	3.7E-04	0.964	-15.423	8.9E-08	0.843	-6.550	1.8E-04
TAV	0.735	-4.996	7.4E-04	0.975	-18.581	1.7E-08	0.831	-6.273	2.4E-04
TAK	0.937	11.55	1.1E-06	0.863	7.544	3.5E-05	0.860	7.023	1.1E-04
ASM	0.759	-5.330	4.7E-04	0.795	-5.902	2.3E-04	0.851	-6.759	1.4E-04
ASMED	0.674	-4.315	1.9E-03	0.570	-3.453	7.2E-03	0.796	-5.583	5.2E-04
ASMOD	0.564	-3.410	7.8E-03	0.559	-3.381	8.1E-03	0.732	-4.677	1.6E-03
ASS	0.745	-5.126	6.2E-04	0.809	-6.172	1.6E-04	0.715	-4.483	2.0E-03
ASV	0.564	-3.411	7.7E-03	0.713	-4.729	1.1E-03	0.741	-4.786	1.4E-03
ASMIN	0.415	-2.528	3.2E-02	0.770	-5.493	3.8E-04	0.767	-5.130	9.0E-04
ASMAX	0.691	-4.490	1.5E-03	0.737	-5.020	7.2E-04	0.506	-2.865	2.1E-02
ASR	0.691	-4.490	1.5E-03	0.736	-5.012	7.3E-04	0.504	-2.854	2.1E-02
MIA	0.848	-7.086	5.8E-05	0.946	-12.615	5.0E-07	0.930	-10.30	6.8E-06
MEIA	0.810	-6.190	1.6E-04	0.875	-7.926	2.4E-05	0.874	-7.455	7.2E-05
CVIA	0.948	12.83	4.4E-07	0.806	6.106	1.8E-04	0.966	15.139	3.6E-07

Table 7.4b: Summary of significant relationships between GPR signal statistic and VMC for M4-M6 for the initial analysis.

The significant relationships for the time domain data indicate that increasing subsurface VMC reduces variation about the mean (though the magnitudes of variance result in stronger relationships for coarser materials (M1 and M2)). This implies that either fewer peaks occur or that the peaks that do occur generally are of reduced magnitude. Visual interpretation showed that, in fact, both of these options occur, although the latter one dominates. With the increased time window necessary to maintain the measurement depth, the decreased magnitude of the peaks produces a further decline in overall magnitudes. The significant relationship for TAK (Figure 7.8) indicates increased peakedness in the time domain data. However, the decreased number and magnitude of

peaks appears to contradict this result. Increased TAK indicates bias generated by the high magnitude direct arrivals relative to the low magnitude events that occur later in time. With the increased time window this effect is maximised. The occurrence of reflections that may be associated with a water table or a wetting front generate values which further increase the kurtosis value; fluctuations in these subsurface features, produce significant variation in the kurtosis values with moisture.

Differences between M1-M6 appear to be more obvious on TAK (Figure 7.8) than TAS (Figure 7.6) and TAV (Figure 7.7). It is clear that the dry values for M6 TAS and TAV are lower than the other materials. Using TAK, M6 is more isolated with a higher value than the other materials: it is more peaky. Comparison of the dry traces in Figures 7.20 and 7.21 shows that this is the case. For M1-M5, the direct arrivals are followed by additional, relatively high magnitude peaks within the time window of interest (0-7 ns). For M6, the direct arrivals are followed by low magnitude events. The presence of the later high magnitude events has another fundamental effect on the responses: the rate of amplitude (TAS and TAV) decline or TAK increase is greater for M6. This occurs because as the time window increases only low magnitude data are added to the statistical calculation. For M6 the relative proportion of low magnitude data increases more rapidly due to the absence of high magnitude events. Thus the anomalous behaviour of M6 can be explained by its absence of high magnitude response after the direct arrivals. A physical explanation of this behaviour is required.

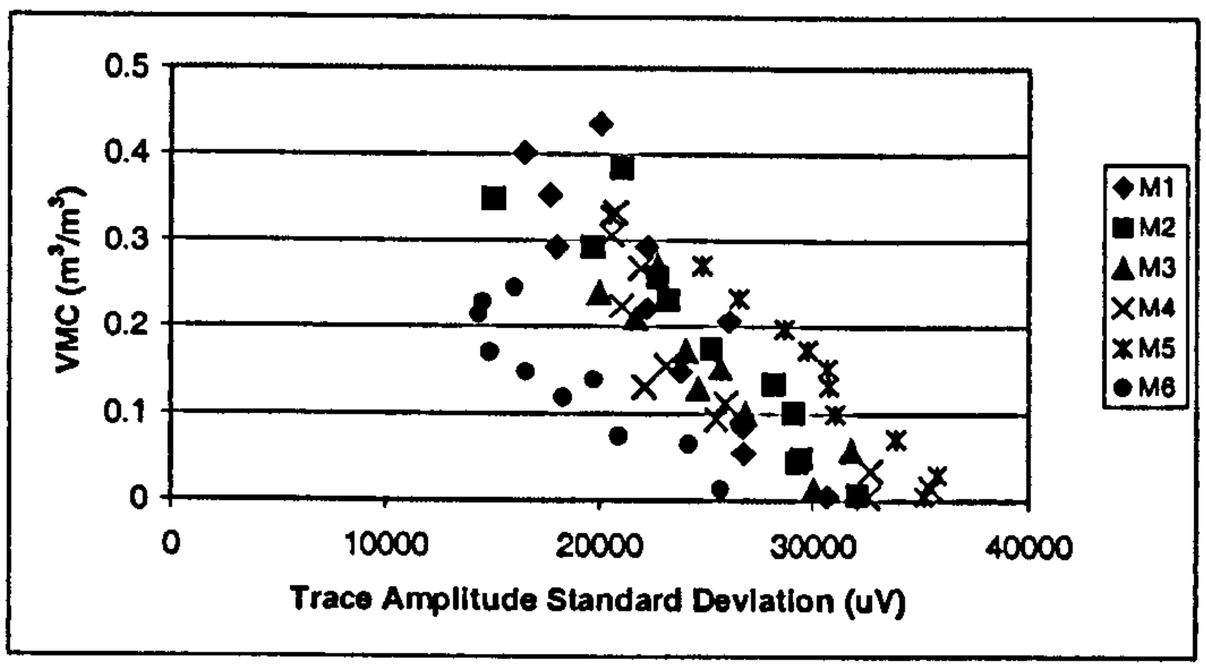

Figure 7.6: Calculated GPR trace amplitude standard deviation (TAS) and observed average STF VMC for each material.

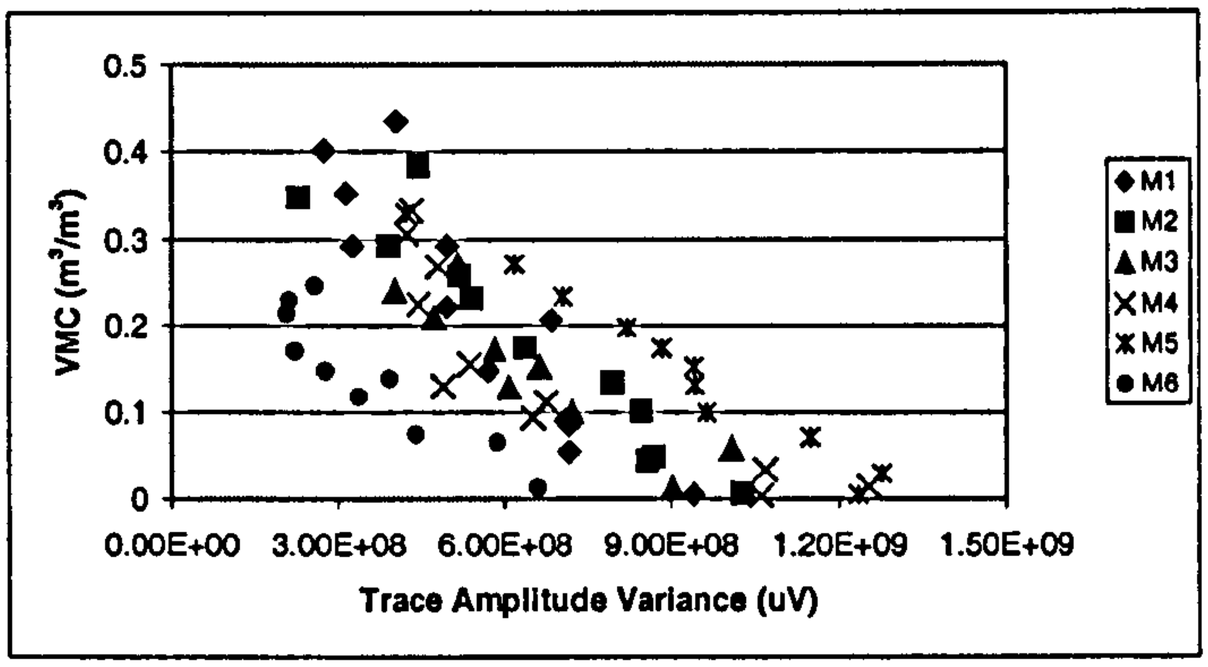

Figure 7.7: Calculated GPR trace amplitude variance (TAV) and observed average STF VMC for each material.

Using the time domain data, three GPR response aspects can be identified:

1) Amplitude variation about the mean generally decreases with increased VMC due to the reduced magnitude of signal events. This, in turn, impacts on the data by increasing the kurtosis through promoting amplitude discrepancy between the direct arrivals and the rest of the trace (i.e. the relative peakedness increases as later-time events reduce in magnitude whilst the magnitude of the direct arrivals remains constant). Declining magnitudes indicate the dominant process is signal attenuation.
2) Two tentative and broad groups of textural dependence can be identified: those with high magnitude events after the direct arrivals (M1-M5) and those without (M6). Study of the dry traces indicates that this too may be an attenuation phenomenon. However, in this case moisture is not the only factor.
3) Anomalous dry and saturated values act to increase scatter in the experimental data, indicating potential differences between dry, wet, and saturated conditions.

If these aspects of response occur, other time domain statistics would be expected to produce significant relationships. The mean (TAM) produces significant relationships for all materials except M4 and M6. For M4 a non-linear relationship exists which is distorted by a single positive mean value (run number three) that occurs due to the ringing apparent in Figure 7.1 (M4), and scatter at higher VMCs. M6 also exhibits scatter at higher VMCs. Thus the relationship fails because of its dependence on negative and positive means (these tend to cancel each other, especially when the magnitude tends towards zero) and its sensitivity to extremes. These extremes also affect the time domain minimum, maximum, and range data. In Chapter Six, high magnitude events in the near field (direct arrivals) prevented reliable depth estimation, anomaly detection, and variability assessment due to the fact that the transmitted pulse saturates and clips at ±50k

uV. This means that in the time domain maximum, minimum, and range are always the same (+50kuV, -50kuV, and 100kuV respectively).

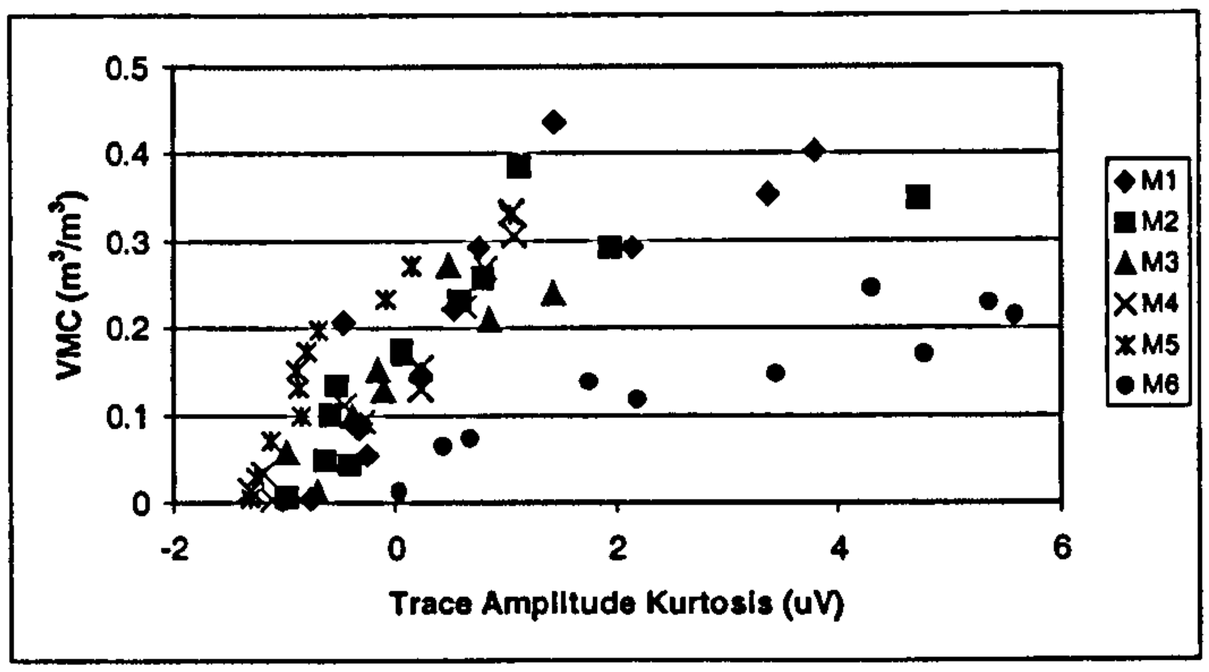

Figure 7.8: Calculated GPR trace amplitude kurtosis (TAK) and observed average STF VMC for each material.

The results from the amplitude spectra demonstrate five characteristics:

1. Declining values with increased VMC. This means that amplitude response at all frequencies involved in the response may decline, but it is more likely that it is dominated by declines at specific, more dominant frequencies. However, this is not associated with a consistent change in centre frequency (as indicated by insignificant relationships for this parameter), and so may be more to do with spectra complexity rather than a specific moisture related response.
2. Susceptibility to anomalies. This is consistent for all significant statistics. The anomalies occur with drier materials; in particular without any added water. This indicates a fundamental change in GPR signal frequency upon the addition of water.
3. The data also indicate a dichotomy in the data (especially in mean (ASM; Figure 7.9), standard deviation (ASS; Figure 7.12) and variance (ASV; Figure 7.13)), which effectively produces groups of response with high GPR values until about 0.15m^3/m^3, a transitional zone between 0.15-0.2 m^3/m^3 over which values spread over a large range, then a zone after 0.2 m^3/m^3 in which GPR decreases rapidly with increased VMC. This pattern is evident on maximum (ASMAX; Figure 7.15) and range (ASR; Figure 7.16) too but not on minimum (ASMIN; Figure 7.14) in which scatter occurs because of the tendency towards 0 uV at the high-frequency extreme of the GPR bandwidth. Range is therefore similar to the maximum. This dichotomy suggests that amplitude spectra methods can distinguish between high and low moisture conditions but will be unable to resolve smaller VMC variations.

4. There is greater spread in the amplitude spectra data compared to the other data which would reduce accuracy in VMC estimation.
5. M6 does not appear to be so isolated from the other materials. Whilst this may indicate textural-independence using amplitude spectra methods, it is more likely a function of the increased scatter, the dichotomy and the susceptibility to anomalous results.

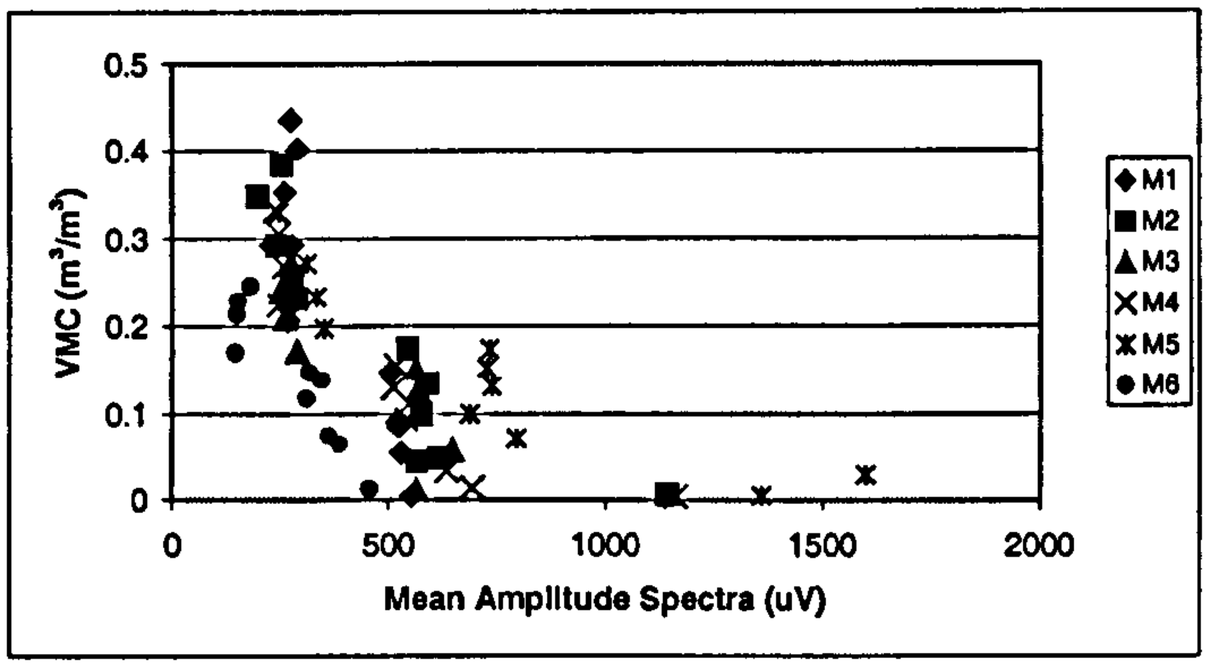

Figure 7.9: Calculated GPR mean amplitude spectra (ASM) and observed average STF VMC for each material.

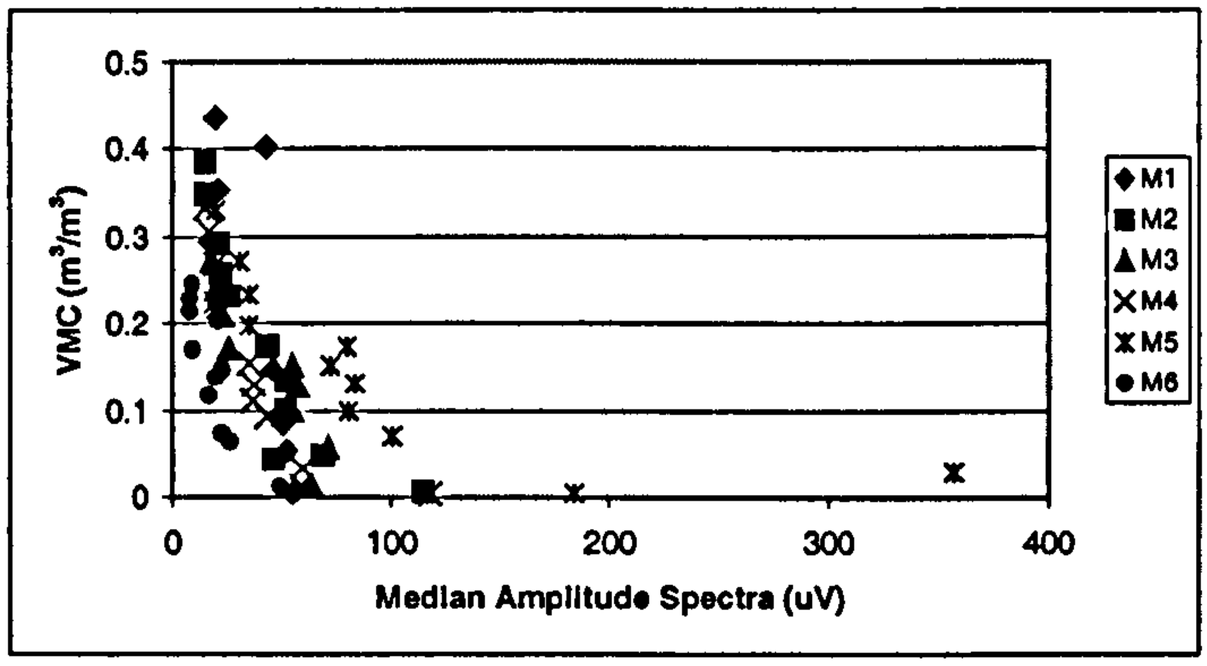

Figure 7.10: Calculated GPR median amplitude spectra (ASMED) and observed average STF VMC for each material.

The three significant results for the instantaneous amplitude data are different from the time domain data but demonstrate the same basic processes of attenuation reducing amplitudes. MIA (Figure 7.17) shows that M6 again has much lower initial values, although the rate of amplitude is consistent between materials. To some extent there is a divergence of M1-M5 values at the near-saturation moisture extreme. Compared to TAM, MIA works because, unlike the time domain data, it is not affected by negative or positive

values cancelling each other. The scatter and spread of data using the median (MEIA; Figure 7.18) suggest that this parameter only weakly represents the GPR's response to VMC. CVIA (Figure 7.19) trends in the opposite direction with increasing CV as VMC increases. For CVIA this is due to a greater and significant decrease in mean compared to a lesser and insignificant decline in the standard deviation. There is a clear separation between the two groups of materials (M1-M5 and M6), which is effected by the same processes as for the time domain data. Whilst in instantaneous amplitude data the combination of the real and imaginary traces introduces variability in the maximum, the results are still dominated by the clipped values and so fluctuate below 50k uV. The minimum tends towards zero but fluctuates depending upon noise. Consequently, random fluctuations in range occur.

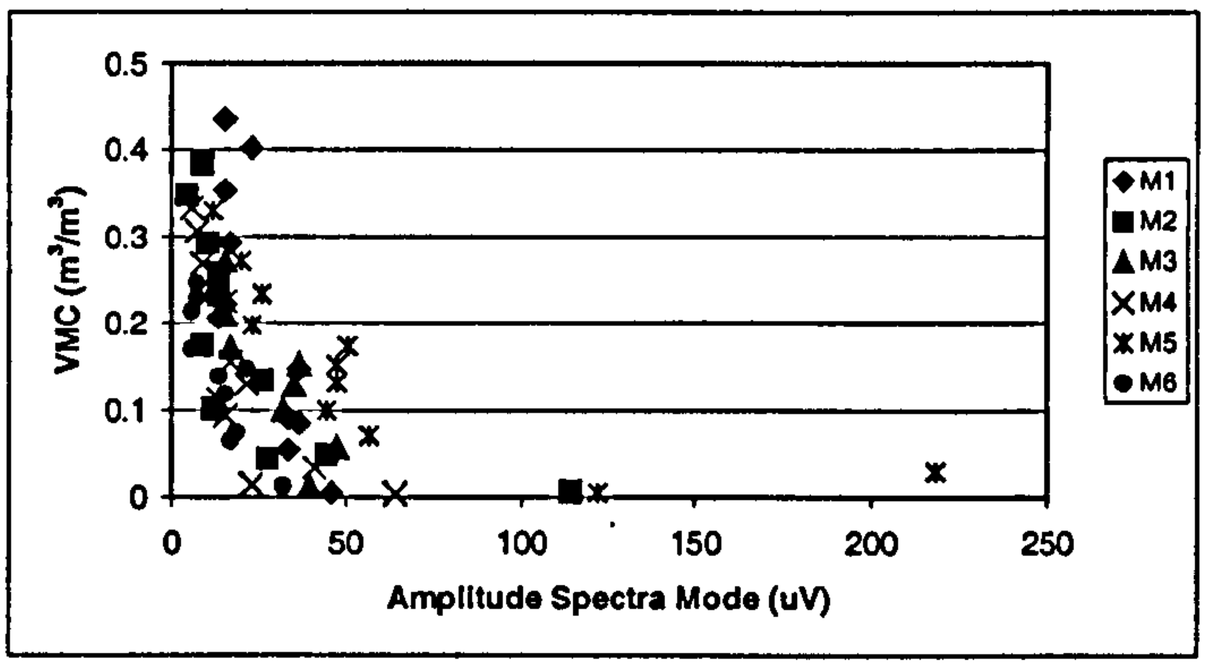

Figure 7.11: Calculated GPR amplitude spectra mode (ASMOD) and observed average STF VMC for each material.

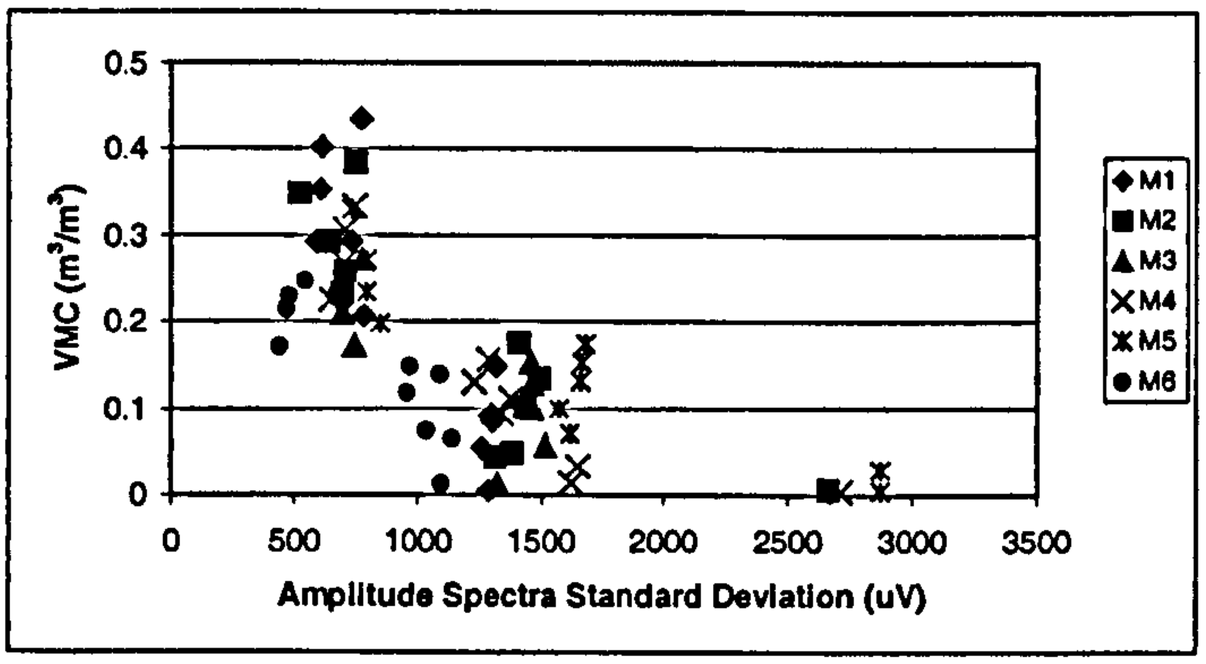

Figure 7.12: Calculated GPR amplitude spectra standard deviation (ASS) and observed average STF VMC for each material.

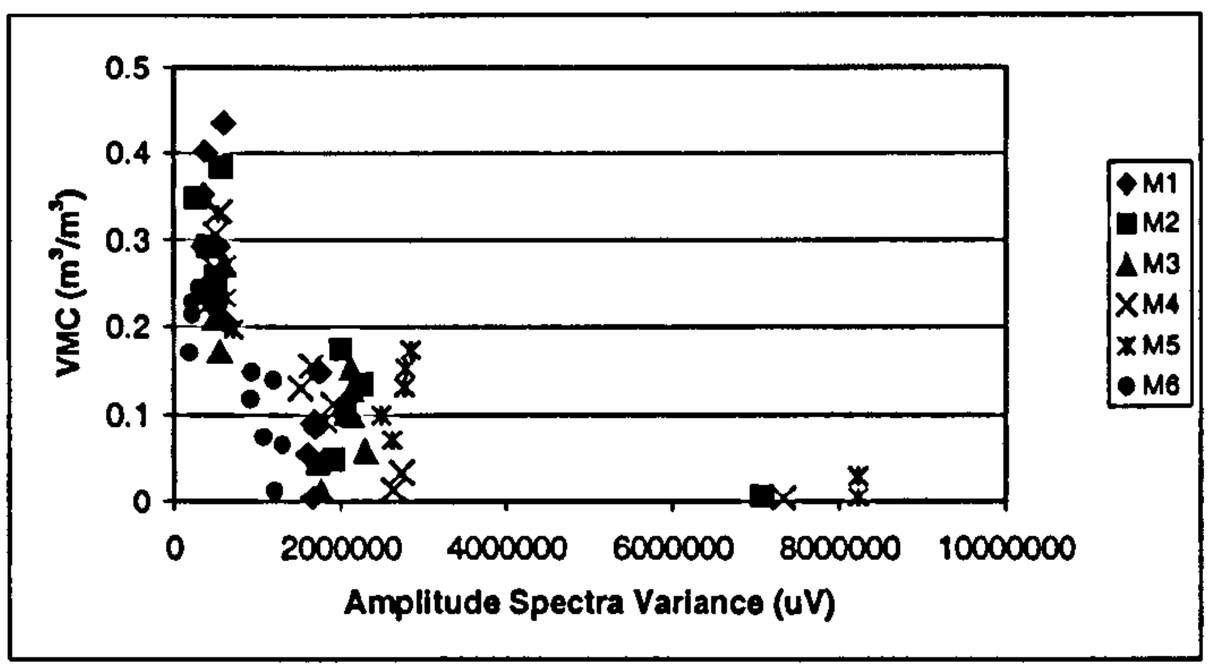

Figure 7.13: Calculated GPR amplitude spectra variance (ASV) and observed average STF VMC for each material.

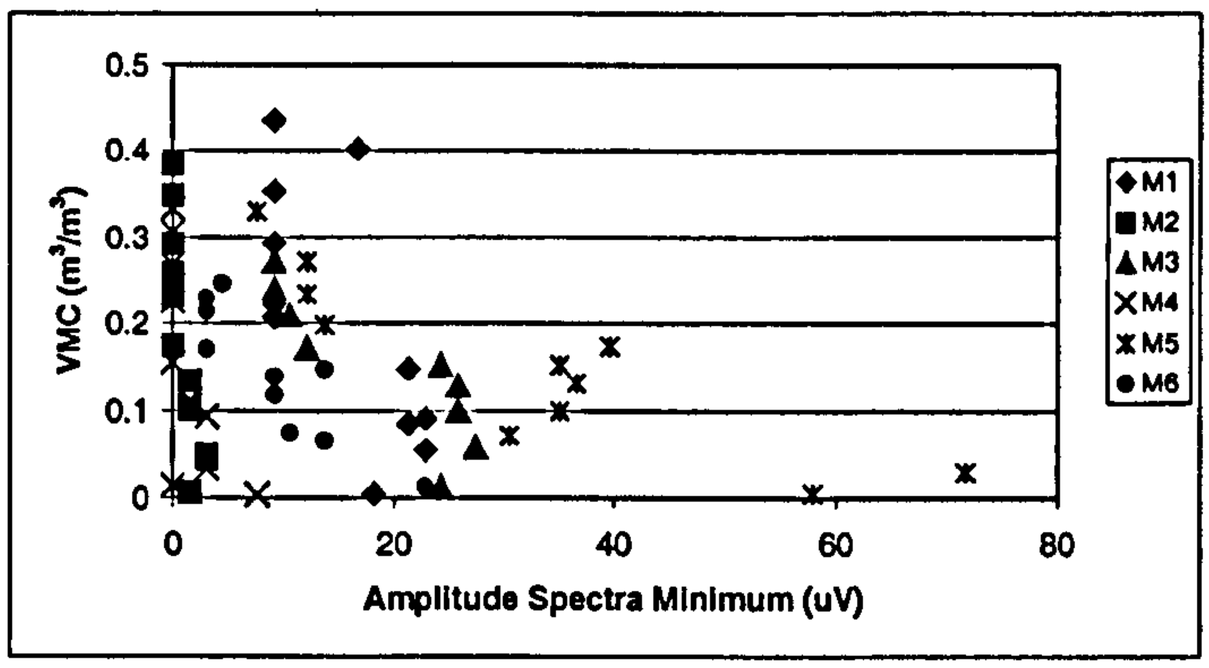

Figure 7.14: Calculated GPR amplitude spectra minimum (ASMIN) and observed average STF VMC for each material.

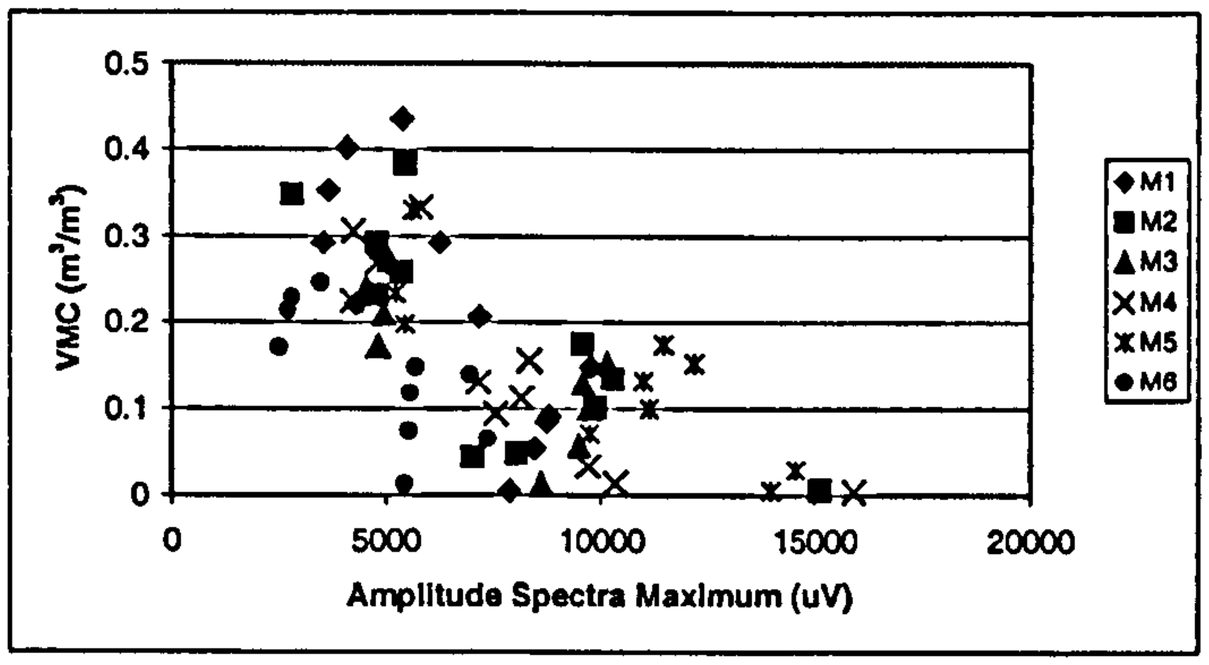

Figure 7.15: Calculated GPR amplitude spectra maximum (ASMAX) and observed average STF VMC for each material.

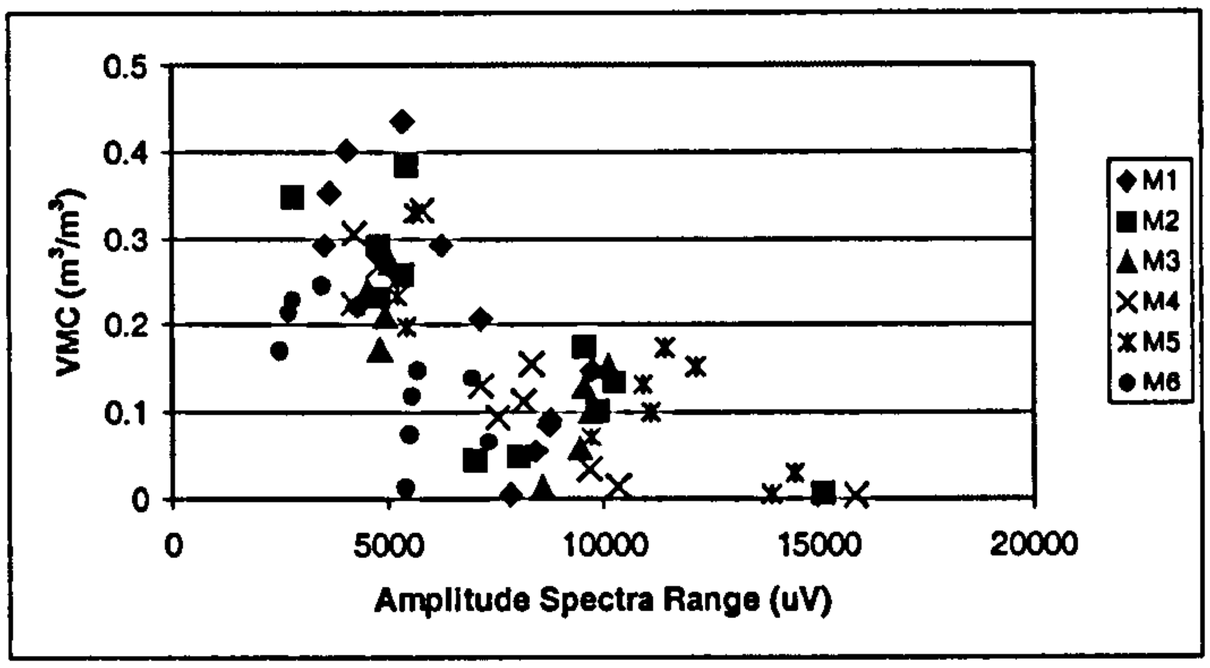

Figure 7.16: Calculated GPR amplitude spectra range (ASR) and observed average STF VMC for each material.

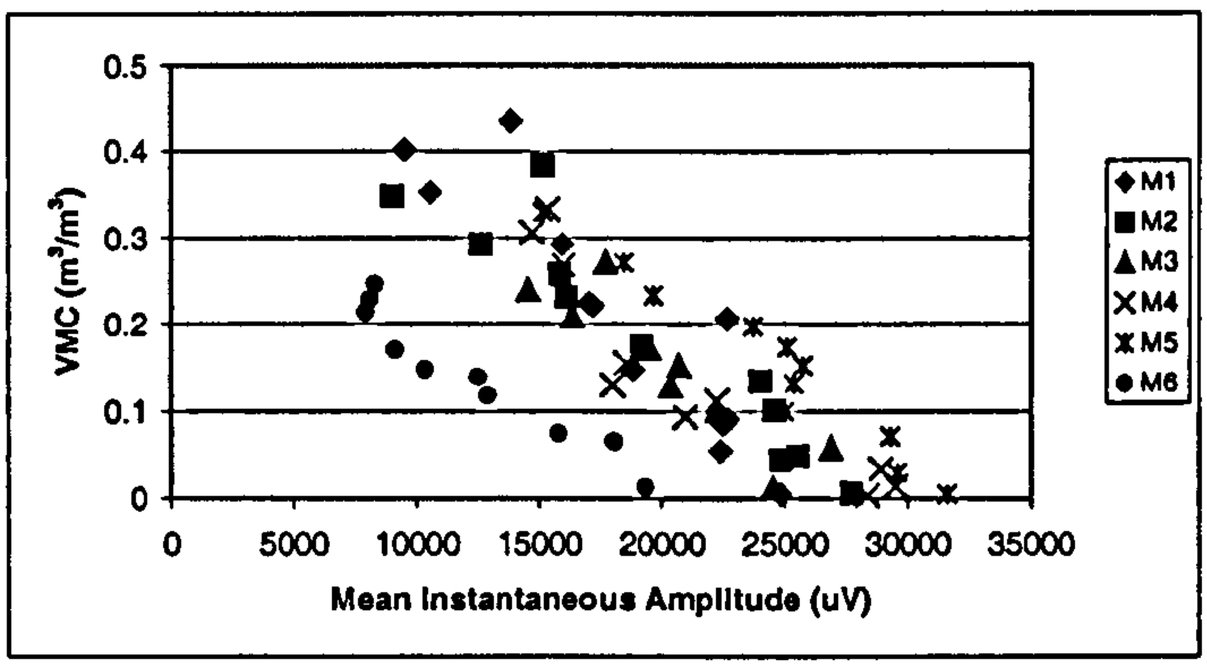

Figure 7.17: Calculated GPR mean instantaneous amplitude (MIA) and observed average STF VMC for each material.

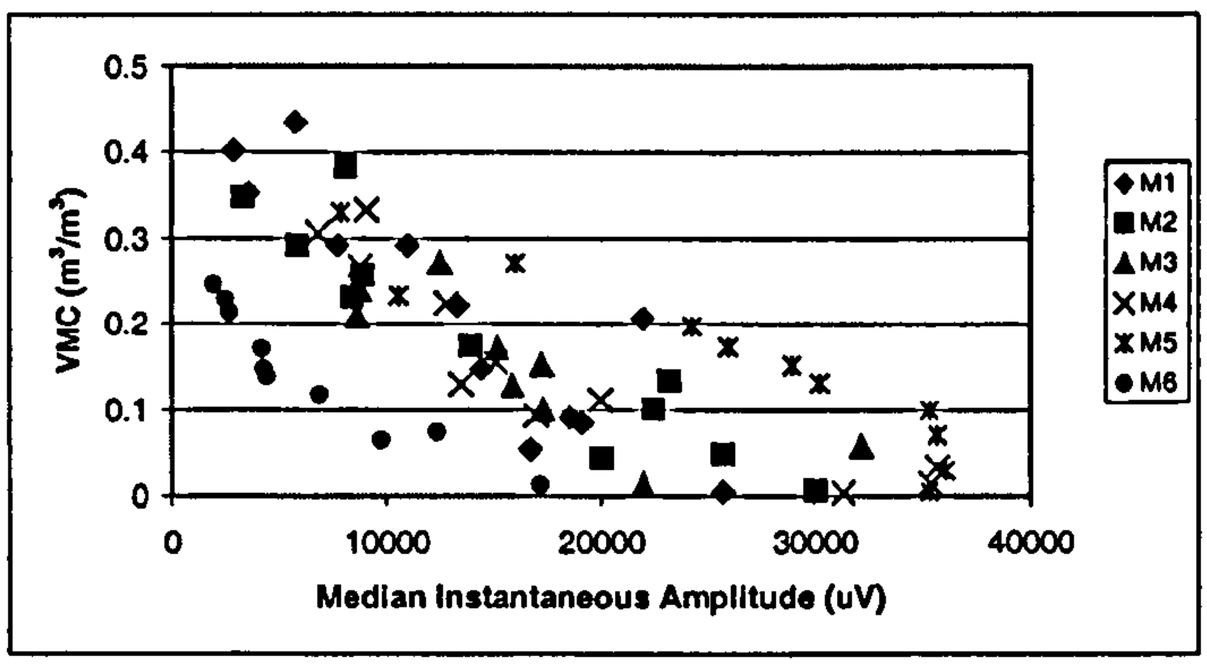

Figure 7.18: Calculated GPR median instantaneous amplitude (MEIA) and observed average STF VMC for each material.

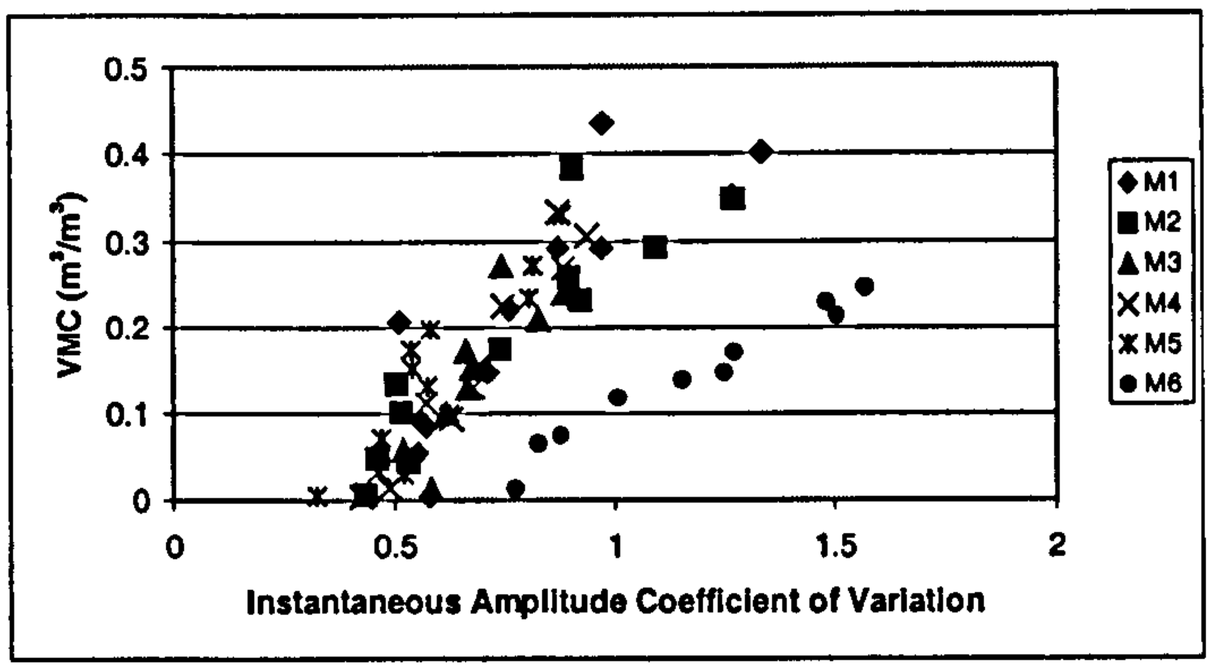

Figure 7.19: Calculated GPR instantaneous amplitude coefficient of variation (CVIA) and observed average STF VMC for each material.

7.3.2.2 The direct arrivals

The direct arrivals present three problems for data analysis: they bias statistics, they obscure near-surface data, and they tend to be very variable after the addition of water. To overcome the statistical bias imposed by the direct arrivals, common GPR processing often removes them. The statistical structure is fundamentally changed owing to the removal of the primary cause of the non-stationary behaviour. Generally, removal is achieved through subtraction, muting (e.g. Sénéchal *et al*,. 2000), or windowing in which only data not affected by the direct arrivals are analysed (e.g. Knight *et al*. (1997) and Rea and Knight (1998)). The two latter options prevent analysis of near-surface data. The first option would suffice provided the direct arrivals are constant for every GPR trace collected. As has been shown in Chapter Six, the ground-wave will vary depending on subsurface dielectric conditions, and this can potentially interfere with the transmitted signal. The visual data (Figure 7.1) confirm fluctuations in the direct arrivals for some materials after the addition of water. In these situations, subtraction can only work on a trace-specific basis producing an increase in analysis time. Changes in the direct arrivals indicate changes in some aspect of the subsurface or the GPR coupling with it. Removing the direct arrivals on a trace-specific basis may therefore remove important data associated with the moisture behaviour. Thus an understanding of these events is required prior to any time consuming processing attempt. As an alternative to removal, it may be possible to use signal-modelling techniques to 'rebuild' the clipped signals and thus obtain information on the actual amplitudes; in particular maximum, minimum, and range. The GPR Interpretation Software 'GRADIX' uses a spline interpolation function to do this but it does not maintain absolute information on the amplitudes and the resulting

data do not have anything to do with the subsurface conditions (Slee (Interpex Ltd.), pers. comm). This reduces the potential for comparing results between experiments.

7.3.2.3 Dry and saturated data

In addition to the affect of the direct arrivals, initial results tend to be poor due to the inclusion of the dry and saturated data, which present anomalous results and increase scatter. The anomalous data are often of a much higher value for the GPR data. This can be expected to bias the form of relationship towards non-linear. The scatter at saturation occurs as a function of different saturation moisture contents (porosity) although this principally causes increased divergence of results between different materials as VMC increases.

Mean traces for each dry experiment are illustrated in Figure 7.20 for M1-M3 and Figure 7.21 for M4-M6. The traces appear very similar between G_0 and the STF base event (0-7 ns). Small differences in timing exist which reflect differences in dielectric constant between materials (see Table 6.9). The similarities between traces mean that the GPR consistently images the subsurface structure and that any differences between traces in subsequent experimental data can be attributed solely to some moisture-induced response. M6 provides an exception demonstrating reduced late-time event magnitudes compared to the other materials due to signal attenuation, which produces lower magnitude response. At saturation (Figures 7.22 and 7.23), the traces again align well for M1-M5, although the STF base is more difficult to identify. Again M6 is an exception, being severely attenuated. Differences in porosity mean that VMC and Dielectric Constant values are different for each material and this affects travel times and attenuation. At moisture saturation, signals are severely attenuated for all materials, especially for M6. Saturated data are also affected by the high-magnitude ground-wave, which, due to decreased SPV, arrives later. Whilst all other data are severely attenuated, the ground-wave increases the response magnitude and therefore the value of the statistic. The timing of saturation of the near-surface layer determines the effect the ground-wave has on the signal statistics. A rising water table means that the ground-wave will be delayed in time later in the experimental runs (e.g. M1 and M2). Therefore, the ground-wave will only affect the later data. In finer-grained materials, the near-surface layer remains wet after the first moisture

addition so that the ground-wave move-out occurs throughout the later runs. Consequently, the impact is less obvious for these materials (M3-M6).

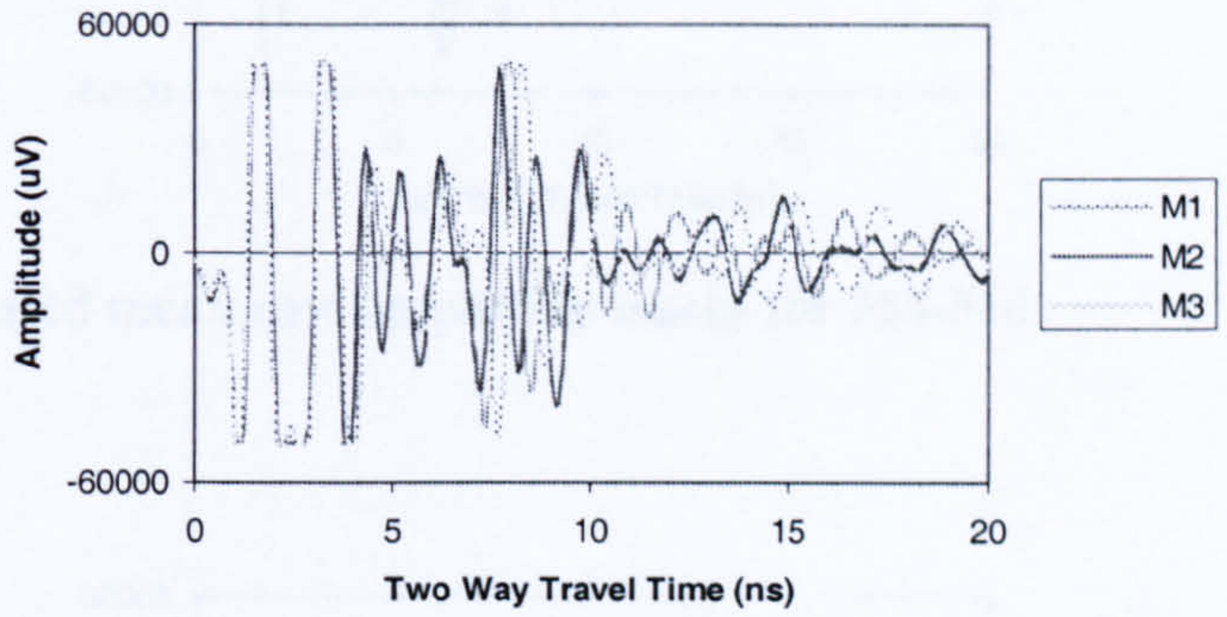

Figure 7.20: Dry mean raw amplitude traces for M1-M3

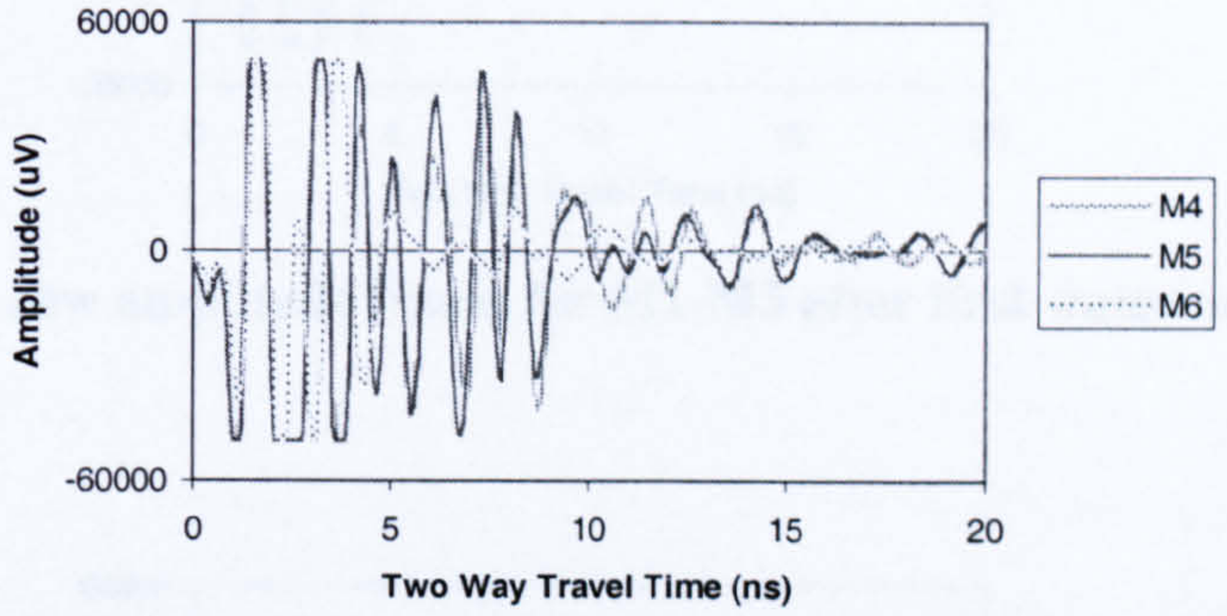

Figure 7.21: Dry mean raw amplitude traces for M4-M6

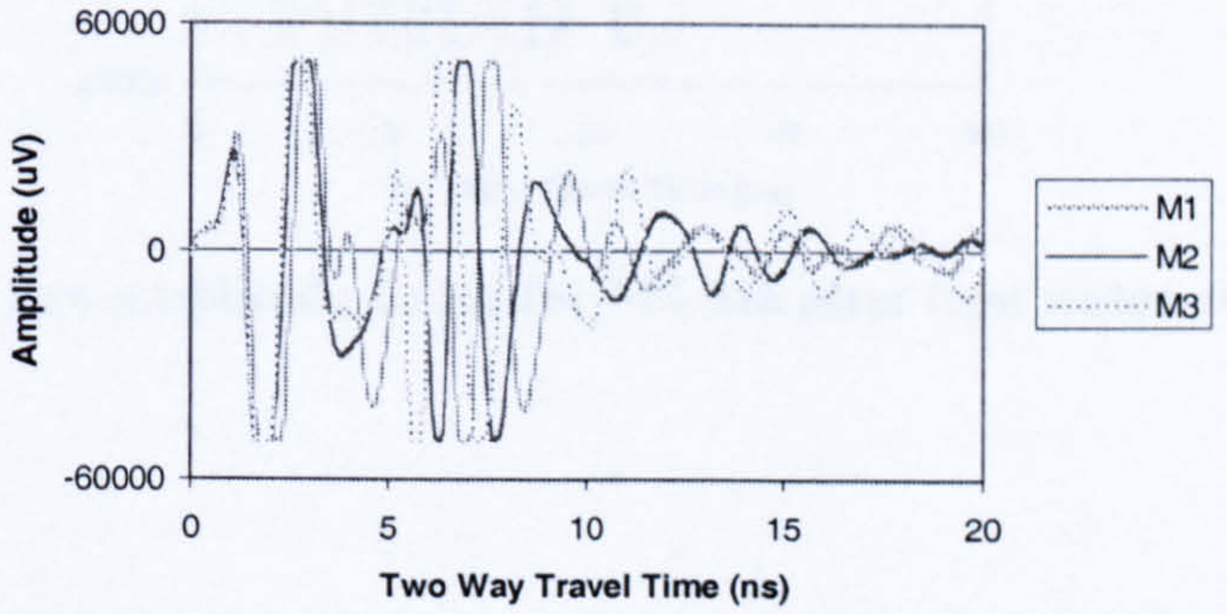

Figure 7.22: Saturated mean raw amplitude traces for M1-M3

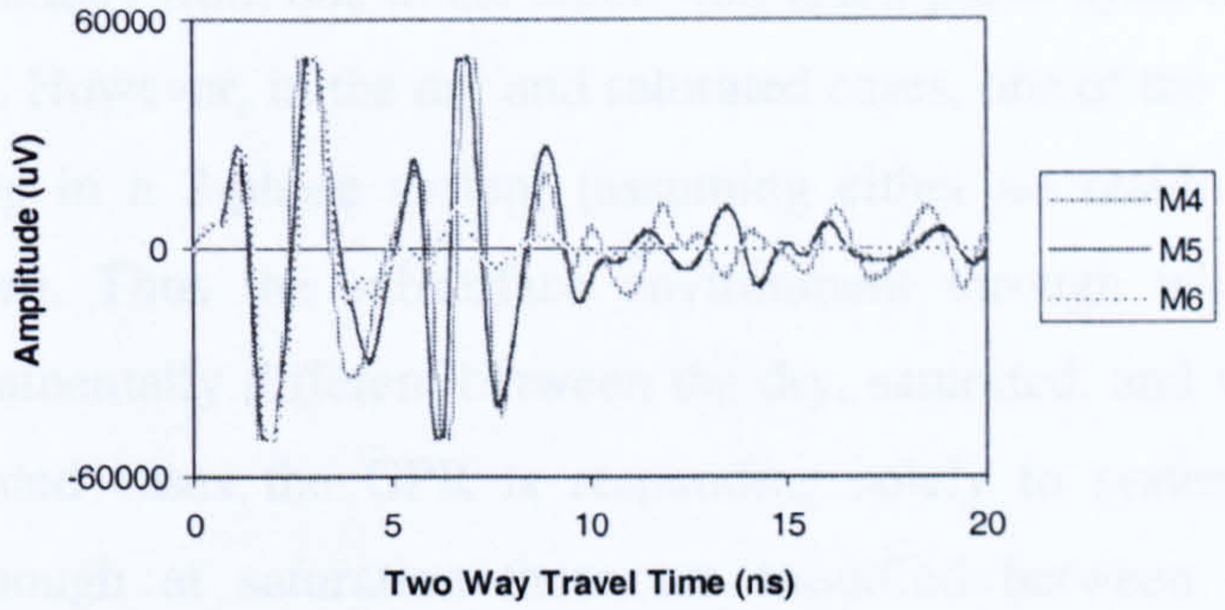

Figure 7.23: Saturated mean raw amplitude traces for M4-M6

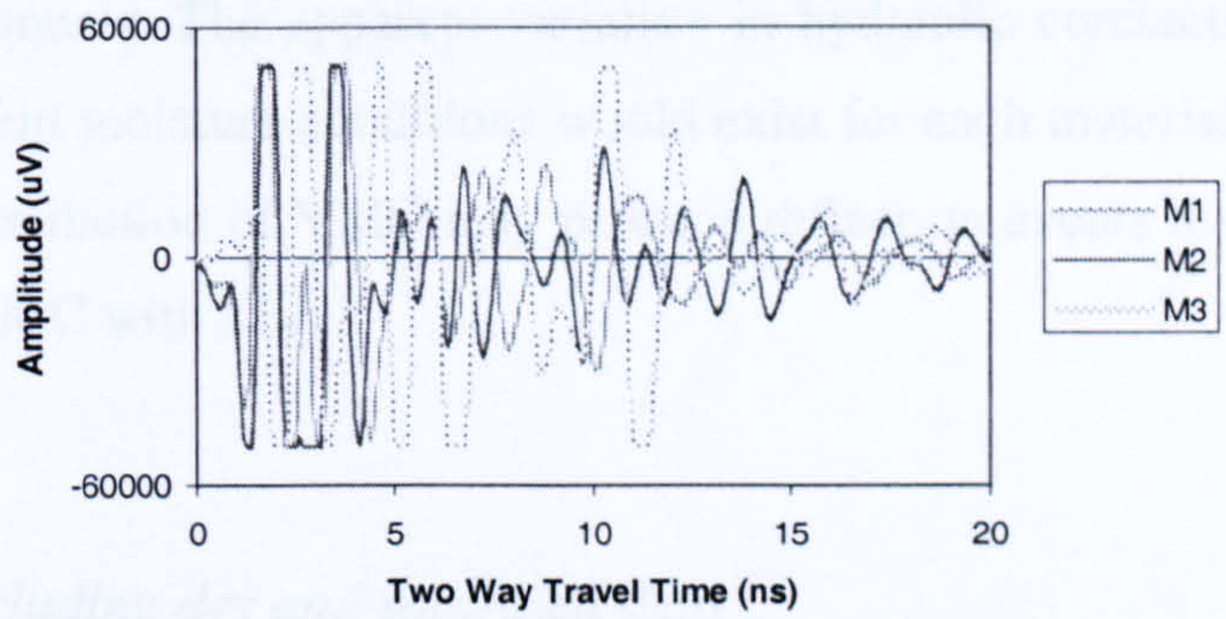

Figure 7.24: Mean raw amplitude traces for M1-M3 after first water addition.

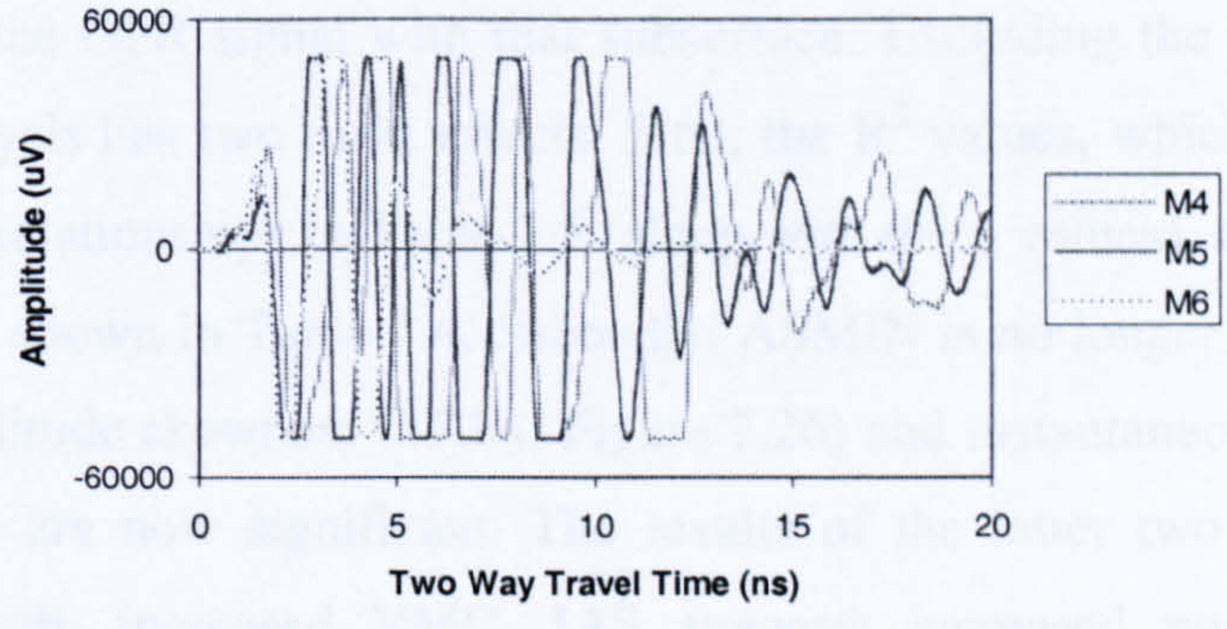

Figure 7.25: Mean raw amplitude traces for M4-M6 after first water addition.

Between these two moisture extremes, traces should continue to match solely as a function of the changing VMC. Figures 7.24 to 7.25 demonstrate that while dry and saturated traces are almost identical between materials, after the first moisture addition the GPR traces become very different within, and between different materials. This is confirmed by the original time domain B-scans (Figure 7.1) which show that all wet

traces differ considerably from one to the other. Soil is a 3-phase system consisting of air, water and particles. However, in the dry and saturated cases, one of the three components is missing resulting in a 2-phase system (assuming either no residual water (dry) or complete saturation). Thus the subsurface environment through which the signal is propagated is fundamentally different between the dry, saturated, and wet conditions. In the dry and saturated cases the GPR is responding solely to system and subsurface characteristics although at saturation these are modified between materials by the saturation moisture content, and its associated attenuation of the signal, more than the material dielectric constant. The two-phase systems produce an homogeneous environment whilst the three-phase system can potentially consist of variable distributions of the three components. The apparent variation in hydraulic conductivity and porosity indicate that different moisture conditions would exist for each material. In particular, an inhomogeneous distribution of VMC may produce reflection events that are inconsistent with the trend of VMC with MIA.

7.3.2.4 Results excluding dry and saturated data

The dry and saturated data act to obscure the moisture relationships because the subsurface environment is fundamentally different, both hydrologically and in terms of the interaction of the GPR signal with that subsurface. Excluding the dry and saturated data from the analysis has two main effects. First, the R^2 values, which are summarised for the significant relationships in Table 7.5 (along with the p values), are improved over the original values shown in Table 7.4. Secondly, ASMIN is no longer significant, while instantaneous amplitude skewness (SKIA; Figure 7.26) and instantaneous frequency sum (IFS; Figure 7.27) are now significant. The results of the latter two both indicate an increased value with increased VMC. IAS suggests increased positive skew with increased VMC which may be a result of decreasing later-time magnitudes relative to the more constant higher magnitudes associated with the direct arrivals. IFS indicates that the frequency at which an amplitude maxima occurs increases with VMC.

Signal Parameter	M1			M2			M3		
	R^2	t	p	R^2	t	p	R^2	T	p
TAS	0.854	-6.831	1.3E-04	0.930	-9.607	2.8E-05	0.924	-7.812	5.5E-04
TAV	0.858	-6.943	1.2E-04	0.959	-12.75	4.2E-06	0.895	-6.537	1.3E-03
TAK	0.784	5.382	6.6E-04	0.745	4.522	2.7E-03	0.935	8.465	3.8E-04
ASM	0.728	-4.629	1.7E-03	0.869	-6.825	2.5E-04	0.824	-4.831	4.8E-03
ASMED	0.404	-2.330	4.8E-02	0.858	-6.506	3.3E-04	0.864	-5.636	2.4E-03
ASMOD	0.531	-3.012	1.7E-02	0.593	-3.195	1.5E-02	0.835	-5.030	4.0E-03
ASS	0.815	-5.944	3.4E-04	0.771	-4.858	1.8E-03	0.751	-3.880	1.2E-02
ASV	0.791	-5.499	5.7E-04	0.729	-4.334	3.4E-03	0.753	-3.907	1.1E-02
ASMAX	0.723	-4.572	1.8E-03	0.558	-2.973	2.1E-02	0.661	-3.123	2.6E-02
ASR	0.723	-4.570	1.8E-03	0.558	-2.971	2.1E-02	0.661	-3.120	2.6E-02
MIA	0.852	-6.797	1.4E-04	0.956	-12.27	5.5E-06	0.952	-10.01	1.7E-04
MEIA	0.724	-4.577	1.8E-03	0.890	-7.530	1.3E-04	0.811	-4.629	5.7E-03
SKIA	0.759	5.013	1.0E-03	0.895	7.704	1.2E-04	0.948	9.521	2.2E-04
CVIA	0.819	6.011	3.2E-04	0.927	9.454	3.1E-05	0.920	7.573	6.4E-04
IFS	0.803	5.702	4.5E-04	0.831	5.864	6.2E-04	0.719	3.580	1.6E-02

Table 7.5a: Summary of significant relationships between GPR signal statistic and VMC for M1-M3 with dry and saturated results excluded.

Signal Parameter	M4			M5			M6		
	R^2	t	p	R^2	T	p	R^2	t	p
TAS	0.745	-4.519	2.7E-03	0.968	-14.535	1.7E-06	0.758	-4.685	2.2E-03
TAV	0.705	-4.092	4.6E-03	0.962	-13.327	3.1E-06	0.739	-4.446	3.0E-03
TAK	0.931	9.751	2.5E-05	0.858	6.508	3.3E-04	0.834	5.929	5.8E-04
ASM	0.934	-9.980	2.2E-05	0.744	-4.513	2.8E-03	0.788	-5.094	1.4E-03
ASMED	0.943	-10.75	1.3E-05	0.574	-3.069	1.8E-02	0.791	-5.144	1.3E-03
ASMOD	0.558	-2.972	2.1E-02	0.528	-2.798	2.7E-02	0.592	-3.189	1.5E-02
ASS	0.916	-8.746	5.1E-05	0.758	-4.687	2.2E-03	0.738	-4.440	3.0E-03
ASV	0.927	-9.418	3.2E-05	0.656	-3.652	8.2E-03	0.761	-4.715	2.2E-03
ASMAX	0.888	-7.442	1.4E-04	0.688	-3.929	5.7E-03	0.638	-3.516	9.8E-03
ASR	0.888	-7.435	1.5E-04	0.687	-3.924	5.7E-03	0.638	-3.514	9.8E-03
MIA	0.837	-5.989	5.5E-04	0.890	-7.529	1.3E-04	0.893	-7.645	1.2E-04
MEIA	0.804	-5.354	1.1E-03	0.849	-6.275	4.1E-04	0.839	-6.044	5.2E-04
SKIA	0.748	4.554	2.6E-03	0.901	7.990	9.2E-05	0.872	6.918	2.3E-04
CVIA	0.956	12.36	5.2E-06	0.613	3.330	1.3E-02	0.981	19.206	2.6E-07
IFS	0.645	3.568	9.1E-03	0.770	4.837	1.9E-03	0.542	2.877	2.4E-02

Table 7.5b: Summary of significant relationships between GPR signal statistic and VMC for M4-M6 with dry and saturated results excluded.

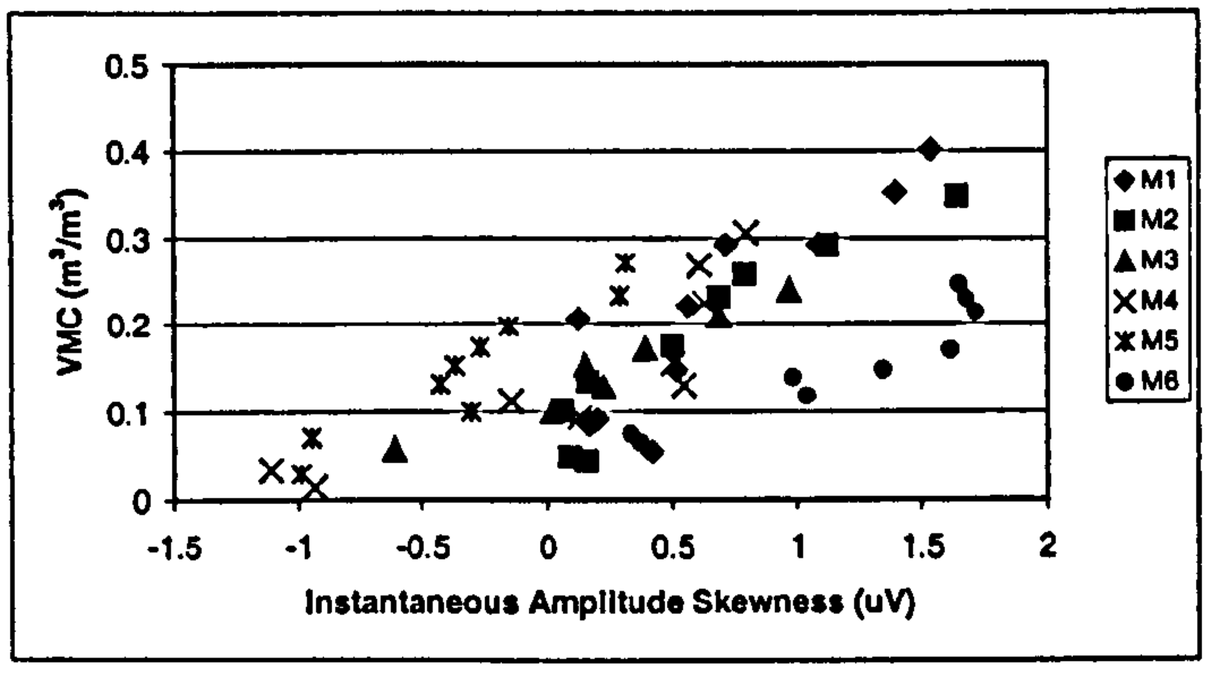

Figure 7.26: Calculated GPR instantaneous amplitude skewness (SKIA) and observed average STF VMC for each material.

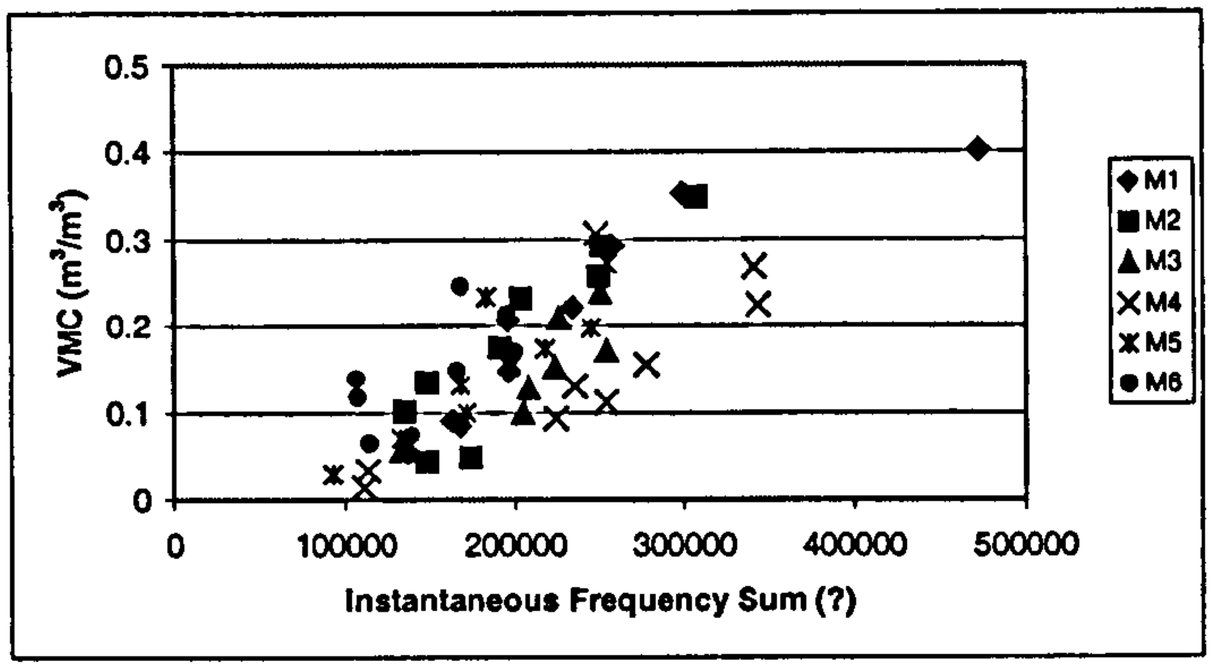

Figure 7.27: Calculated GPR instantaneous frequency sum (IFS) and observed average STF VMC for each material.

7.3.2.5 Non-linearity

Investigation of Figures 7.6 to 7.19 showing the full data results indicates that another source of error may be due to the non-linear nature of the relationship between GPR parameters and VMC. Thus the analysis was repeated for the significant linear relationships to assess any improvement if a non-linear best fit exists. Table 7.6 indicates the R^2 of the best-fit relationships for each of the significant relationships shown in Table 7.5. Non-linear functional forms are highlighted. Whilst many results maintained a linear best-fit, there were improvements. There is a tendency for TD and TF methods to be non-linear for the finer-grained, more complex materials (M3-M6) whilst for AS approaches the non-linear results appear to occur for the coarser materials. This is confirmed by Table 7.6 which shows the resulting R^2 and p values.

7.3.2.6 Method selection

A number of statistics have been identified which provide significant relationships with VMC for every material. Although the combination of a variety of statistics may aid interpretation, for estimation of VMC, a single relationship should be established. To do this the R^2 value of each material-specific relationship are added together for each significant relationship excluding the dry and saturated data. The resulting R^2 values are then ranked according to greatest sum as indicated on Table 7.7. Although this could have been approached by lumping all material results together for each statistic and deriving a single coefficient of determination, the non-linear forms for some relationships, and the apparent material-specific behaviour, makes this method inappropriate. Table 7.7

summarises the ranking for each statistic using the linear relationships only and the best-fit relationships; many of which include non-linear data. Although the statistics are ranked in a different order for the best-fit relationships compared to the original linear relationships, the most important feature is that MIA is ranked first in both cases. It is also important to note that often the improvement is not that large. This suggests that linear forms would suffice and that non-linearity is caused by data that biases the form as a consequence of some minor variation in response. This may be due to scatter or may be related to the changes in the radargram, perhaps as a consequence of the moisture distribution. Although MIA does not have the highest R^2 for every material, its summed R^2 indicates relative consistency between different materials. This presents the opportunity for texture-independent application. Furthermore, this method provides a signal characteristic that describes changes in magnitude, timing, and waveform, and is insensitive to sign because it uses positive values. Most importantly, it characterises signal attenuation with increased VMC.

7.3.2.7 Mean instantaneous amplitude: MIA

The first-place ranking for MIA is deceptive because it implies that MIA provides a consistent relationship for each material compared to the other methods and therefore there is no material-dependence in the relationship. However, like all methods MIA exhibits distinct differences between M1-M5 and M6. Furthermore, different functional forms of relationship appear to occur for each material with a tendency towards a non-linear form for finer-grained, more complex materials. These are summarised in Table 7.8 and are indicated on Figure 7.28, which shows the experimental data excluding the dry and saturated points. This would suggest that a broad two-group classification is inappropriate because M3 and M4 have functional forms that more closely match M6. The nature of signal response is clearly related to material characteristics and their effect on moisture distributions. If this were not the case then all traces would demonstrate similarity after moisture addition. It is also possible that the effect of moisture distribution can produce a greater impact on the GPR response than the VMC itself through determining the generation of reflections. MIA is less sensitive to reflection generation than time domain methods because it only considers absolute values and the envelope of the waveform rather than the specifics of dielectric gradients but it is still very sensitive to additional reflections. Thus it is necessary to explain GPR signal response within the

context of material-induced moisture distributions to try and establish whether the VMC or its distribution have the most dominant affect on the GPR signal statistics.

Signal Parameter	Coefficient of Determination (R^2)					
	M1	M2	M3	M4	M5	M6
TAS	0.854	0.930	**0.948**	**0.955**	0.968	**0.841**
TAV	0.858	0.959	**0.953**	**0.954**	**0.966**	**0.836**
TAK	0.784	0.745	0.935	0.931	0.858	**0.911**
ASM	**0.802**	**0.879**	0.824	0.934	**0.877**	0.788
ASMED	**0.556**	**0.900**	0.864	**0.972**	**0.904**	0.791
ASMOD	**0.615**	**0.676**	**0.841**	**0.718**	**0.876**	**0.619**
ASS	**0.837**	**0.809**	**0.752**	0.916	**0.817**	0.738
ASV	**0.837**	**0.809**	0.753	0.927	**0.829**	0.761
ASMAX	0.723	**0.636**	**0.682**	0.888	**0.694**	0.638
ASR	0.723	**0.636**	**0.681**	0.888	**0.694**	0.638
MIA	0.852	0.956	**0.958**	**0.940**	0.890	**0.959**
MEIA	**0.748**	**0.907**	**0.899**	**0.923**	0.849	**0.958**
SKIA	0.759	0.895	0.948	**0.873**	0.901	**0.937**
CVIA	0.819	**0.930**	**0.932**	0.956	**0.615**	0.981
IFS	**0.916**	0.831	**0.854**	**0.860**	**0.886**	0.542

Table 7.6: Summary of significant best-fit relationships between GPR signal statistic and VMC for M1-M6 with dry and saturated results excluded. Non-linear relationships are in bold.

Method	Linear relationships		Best-fit relationships	
	Summed R^2	Rank	Summed R^2	Rank
TAS	5.1783	3	5.4953	3
TAV	5.1174	5	5.5244	2
TAK	5.0868	6	5.1642	7
ASM	4.8872	8	5.1044	8
ASMED	4.4337	11	4.9867	9
ASMOD	3.6378	15	4.3452	13
ASS	4.7499	9	4.8681	12
ASV	4.6158	10	4.9150	10
ASMAX	4.1568	13	4.2614	14
ASR	4.1546	14	4.2596	15
MIA	5.3802	1	5.5550	1
MEIA	4.9166	7	5.2839	5
SKIA	5.1219	4	5.3120	4
CVIA	5.2165	2	5.2333	6
IFS	4.3095	12	4.8876	11

Table 7.7: Summed coefficient of determination, and resulting rank, for each statistical relationship using the linear relationships and the best-fit relationships.

Material	Best-Fit Relationship				Linear Significance Results		
	Form	Parameter 1	Parameter 2	R^2	R^2	t	p
M1	Linear	0.5873	-2.13E-05	0.8524	0.8524	-6.7972	0.0001
M2	Linear	0.5171	-1.76E-05	0.9556	0.9556	-12.2682	5.48E-06
M3	Logarithmic	-0.3073	3.1909	0.9576	0.9525	-10.0083	0.0002
M4	Exponential	4.4802	-0.0002	0.9401	0.8367	-5.9885	0.0005
M5	Linear	0.6354	-1.96E-05	0.8901	0.8901	-7.5293	0.0001
M6	Exponential	0.6177	-0.0001	0.9592	0.8930	-7.6448	0.0001
Overall	Exponential	0.6535	-0.0001	0.5124	0.5082	-7.2593	2.12E-09

Table 7.8: Summary of best-fit relationships for MIA for each material. Significance results are for the linear relationships at $p < 0.05$. Parameter 1 is the intercept for linear relationships and a constant for non-linear ones. Parameter 2 is the slope for linear relationships and the logarithm or exponent for non-linear ones.

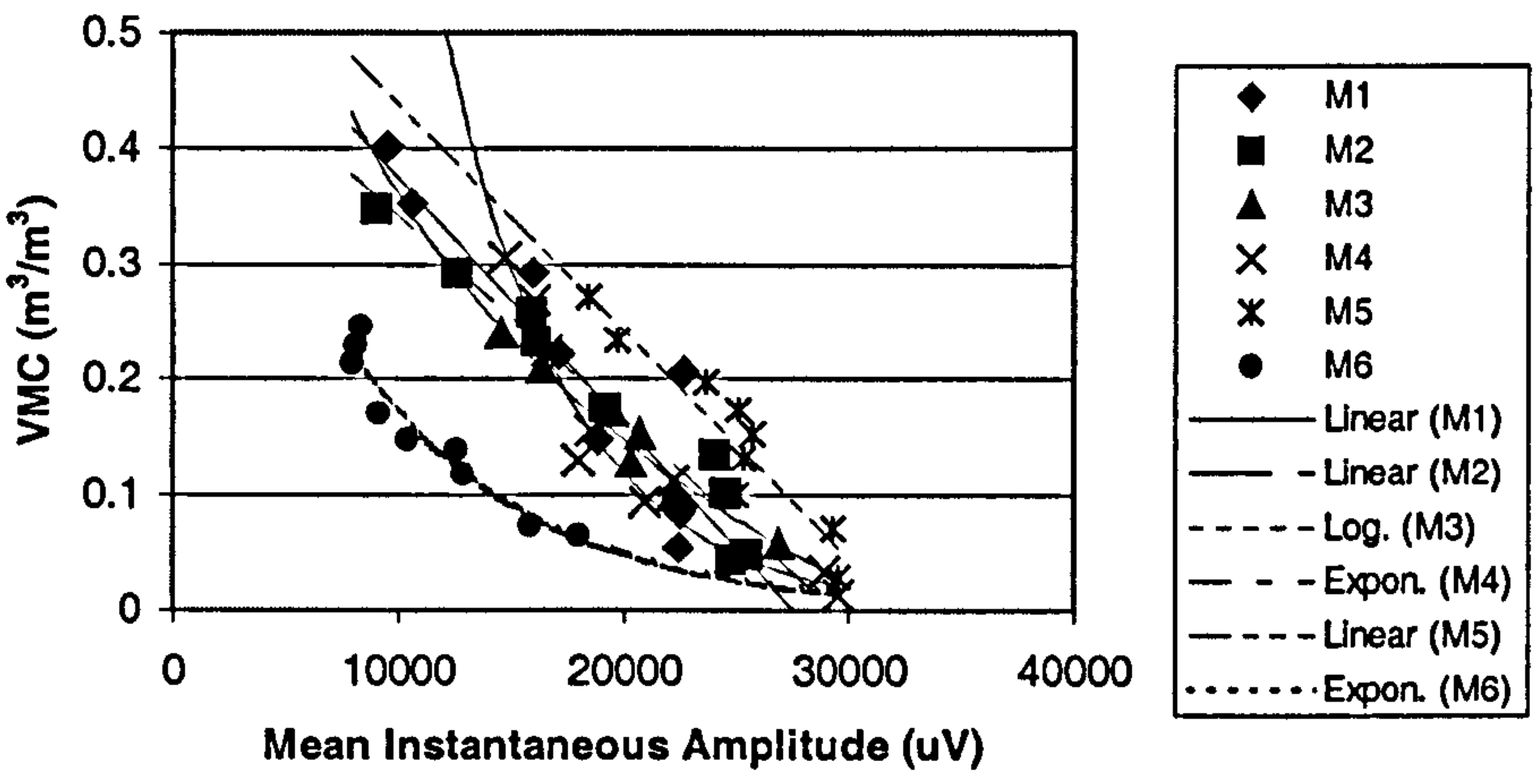

Figure 7.28: Fitted relationships between mean instantaneous amplitude (uV) and VMC (m^3/m^3) for each of the six experimental materials.

7.3.3 Explaining GPR signal response

7.3.3.1 Introduction

Visual analysis identified some very variable signal behaviour between different materials upon the addition of water. Material differences are also expressed in the developed MIA-VMC relationship. Because the statistics are derived from the signal, it can be expected that the variable behaviour is responsible for differences in the relationship between materials. It is the aim, here, to identify potential causes for these variable responses with a view to understanding more fully this response and the developed relationships, and with a view to improving further the applicability of the developed method of VMC estimation. The following sections seek to explain the observed characteristics of GPR

response within the context of these variable moisture distributions, address the impact that they may have on signal characteristics, and determine whether the VMC or its distribution affects the response the most. It certainly appears that the variation in distribution between materials is greater than the variation in average VMC [distribution means that some zones have above average VMC and some have below average VMC]. In Chapter Six it was demonstrated how sensitive the GPR was to a single anomaly. Clearly, therefore, changes in the generation of reflections would be expected to dominate response.

7.3.3.2 Variable moisture distributions

Figures 7.29 to 7.34 confirm that differences exist between moisture distribution for each experimental run. At each depth (see Section 5.2.3.2) the VMC was recorded by only one *ThetaProbe* (with more *ThetaProbes* there would be too much interference with the GPR signal). *ThetaProbe* estimations were assumed horizontally constant and a 0.6 m by 0.6 m image of distribution was constructed in SURFER. This is equivalent to viewing the STF from its side. The images were created as a contour map using only the sampled data points (this limits interpolation error). Three distinct groups of variable moisture distribution can be identified:

- A rising water table, which produces a distinct wet and dry zonation, occurs as a consequence of the high hydraulic conductivities of M1 and M2.
- A wetting front which progresses slowly down through the STF profile. This only occurs for M6 and produces three moisture zones: high-moisture near the surface, moderate moisture beneath the first zone, and low moisture at the base of the facility. The low hydraulic conductivity of M6 ensured saturation of the near-surface zone and prevented infiltration of much of the added water producing a longer duration experiment.
- A combination of wetting front and water table behaviour is evident for M3-M5. This occurs for intermediate textures and is of variable complexity. The complexity of this behaviour appears to be dependent on both the hydraulic conductivity and porosity, which affect the rate of vertical movement and the VMC of the front and the complexity of moisture gradients, and the exploitation of preferential flow-paths (these may be associated with the *ThetaProbe* wiring). Of these, M4 exhibits a

wetting front and water table concordantly, while M3 and M5 exhibit a water table rise only after the wetting front reaches the STF base. Water tables appear to advance with VMC values approaching saturation. Conversely, the wetting fronts descend with a nearly saturated front and a less wet zone of moisture above it. In M5 this is further complicated by a nearly stationary zone of higher moisture at about 0.2m below the surface with declining VMCs above and below it.

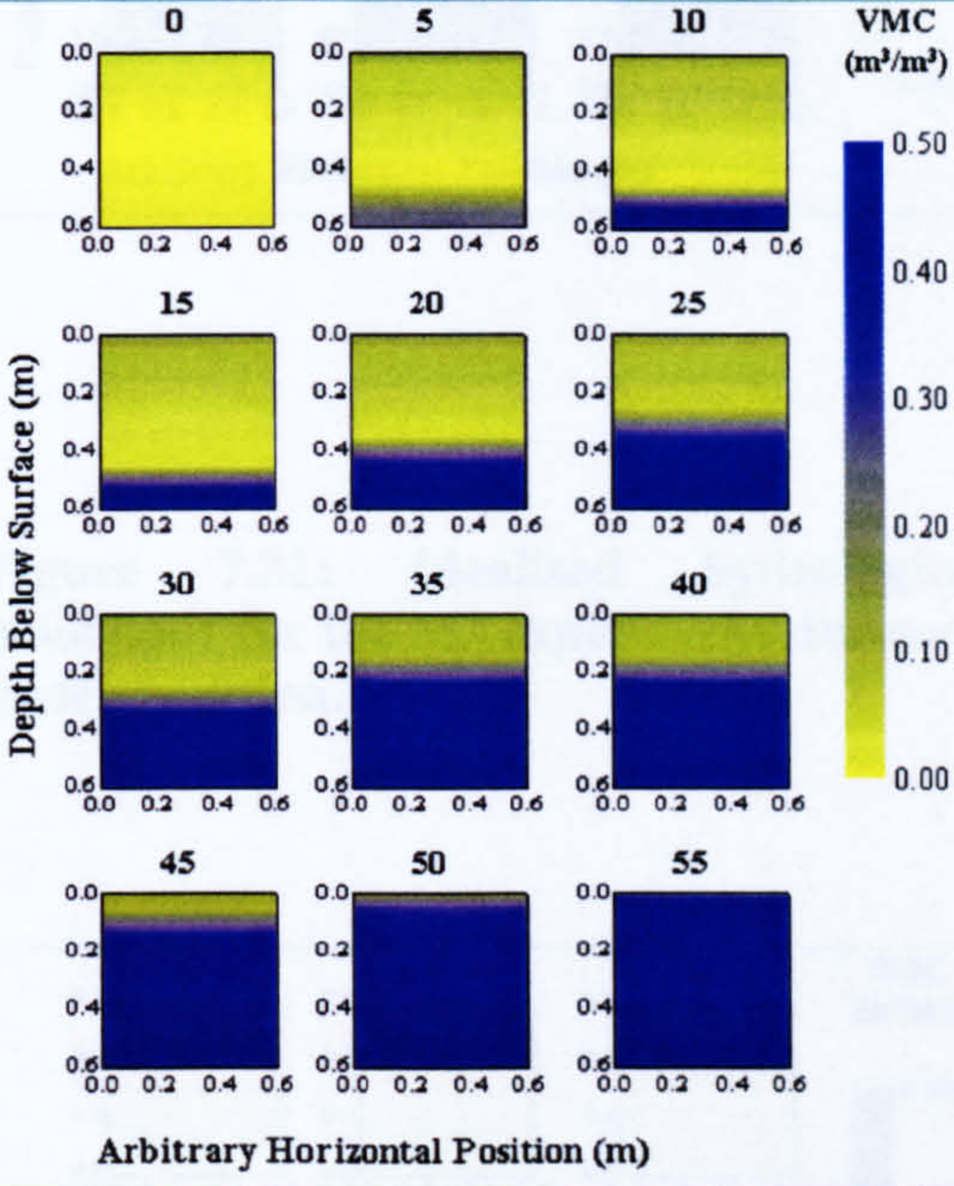

Figure 7.29: Idealised hydrological behaviour for the M1 experiments for each water addition.

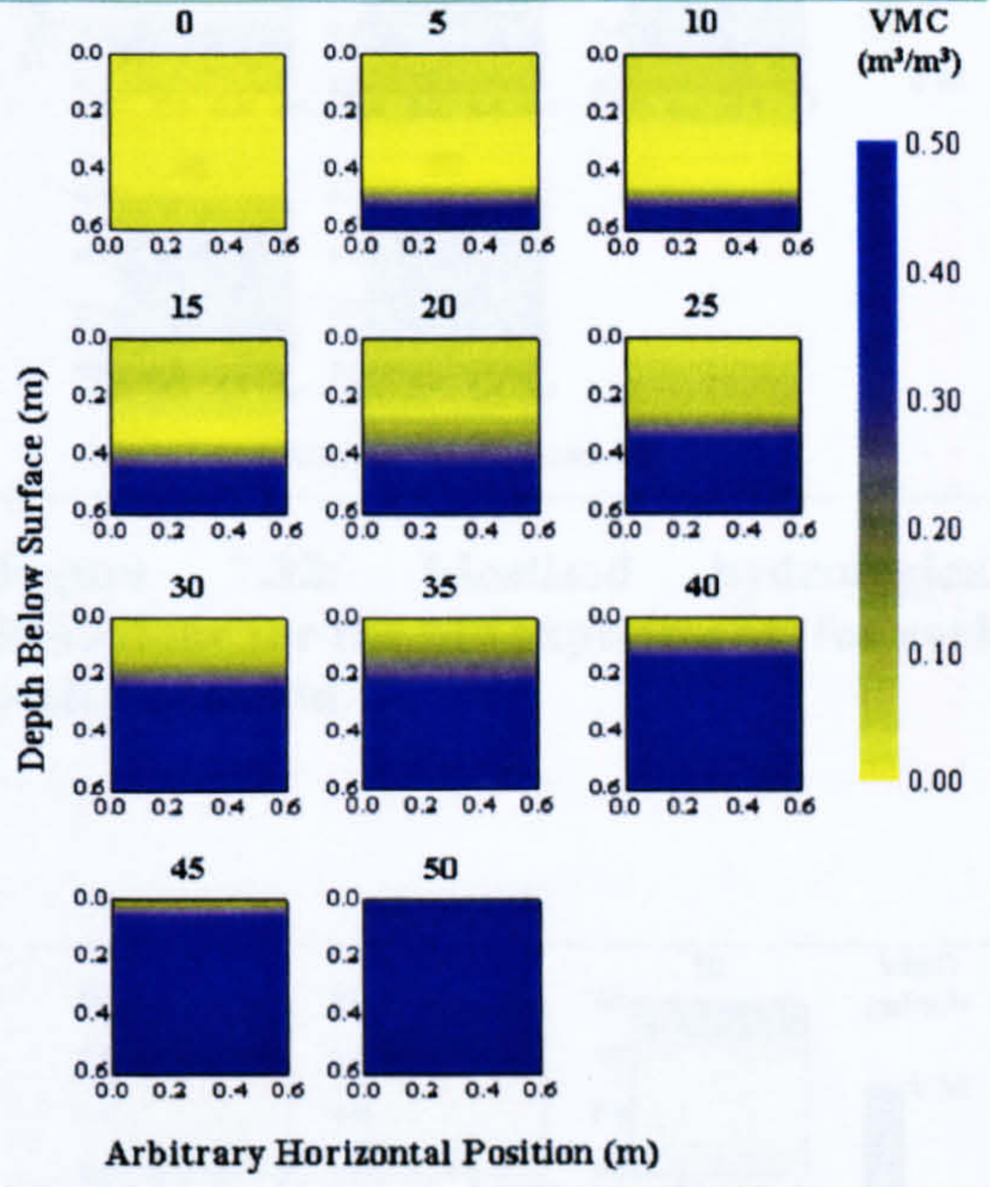

Figure 7.30: Idealised hydrological behaviour for the M2 experiments for each water addition.

Figures 7.29 to 7.34 give the impression of spatially invariant vertical moisture movement. Experimental observations indicate that in a small volume of apparently homogeneous material, there is significant spatial variation in the distribution of moisture. This is probably related to the relatively high variation in the hydraulic conductivities of the experimental materials. Recording static GPR data minimises the impact of the internal spatial variability of these small-scale moisture distributions and produces a result that should be more dependent upon the dominant moisture layering. However, the existence of fingers of moisture movement may promote scattering of the GPR signal promoting additional complexity in the GPR response and producing moisture distributions that are even less controlled or similar between materials.

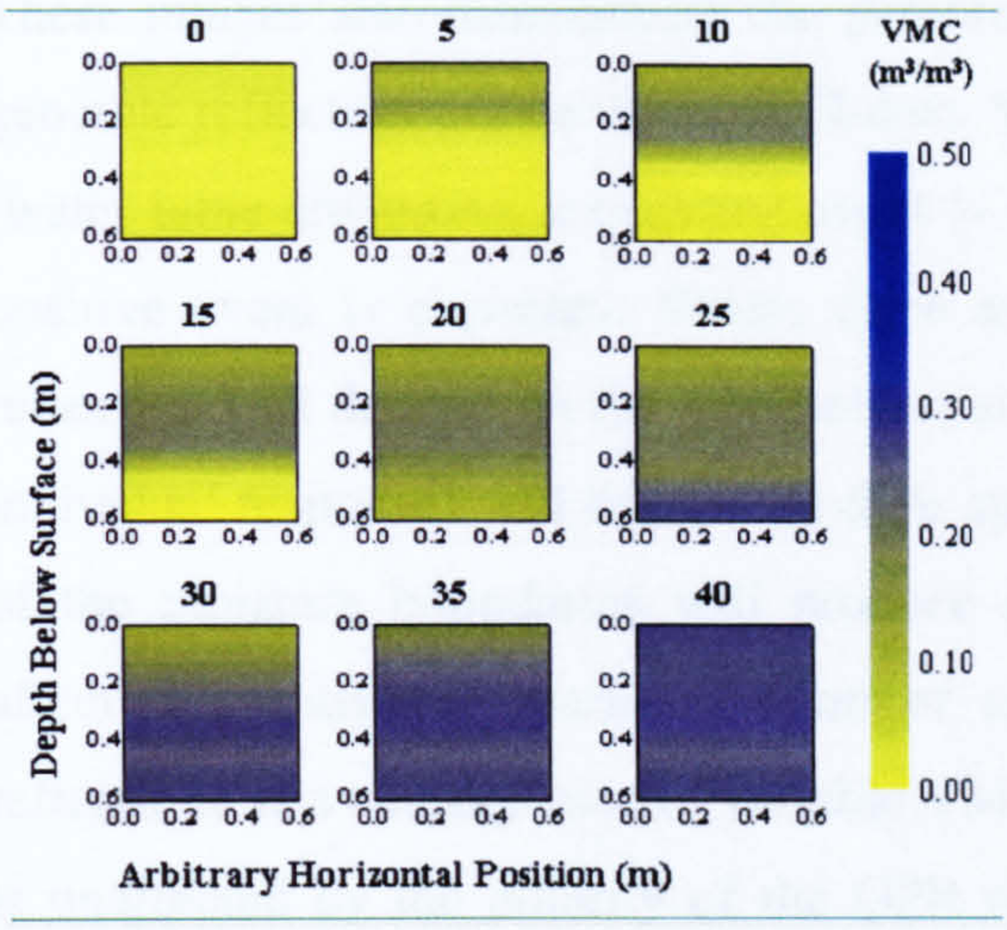

Figure 7.31: Idealised hydrological behaviour for the M3 experiments for each water addition.

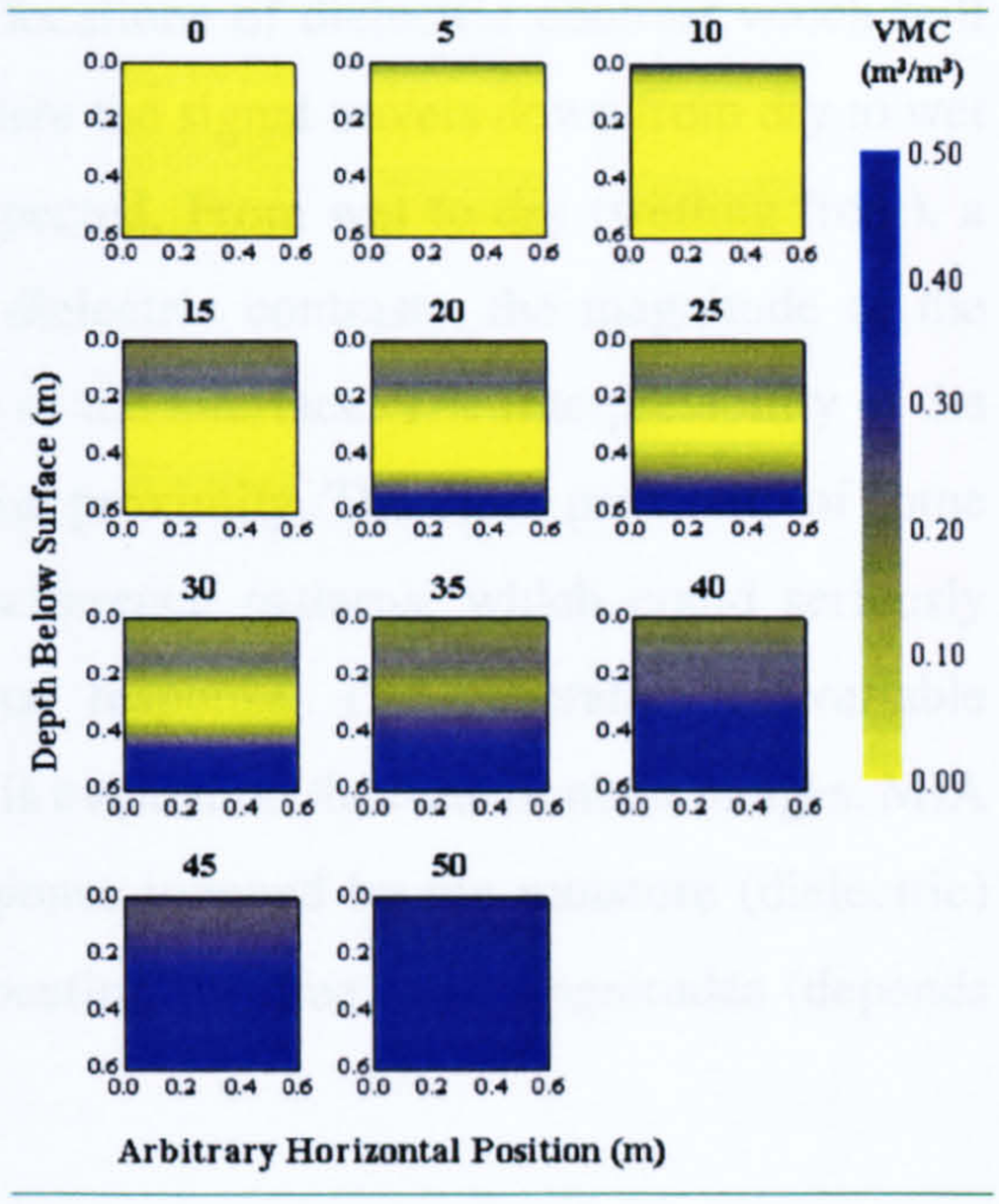

Figure 7.32: Idealised hydrological behaviour for the M4 experiments for each water addition.

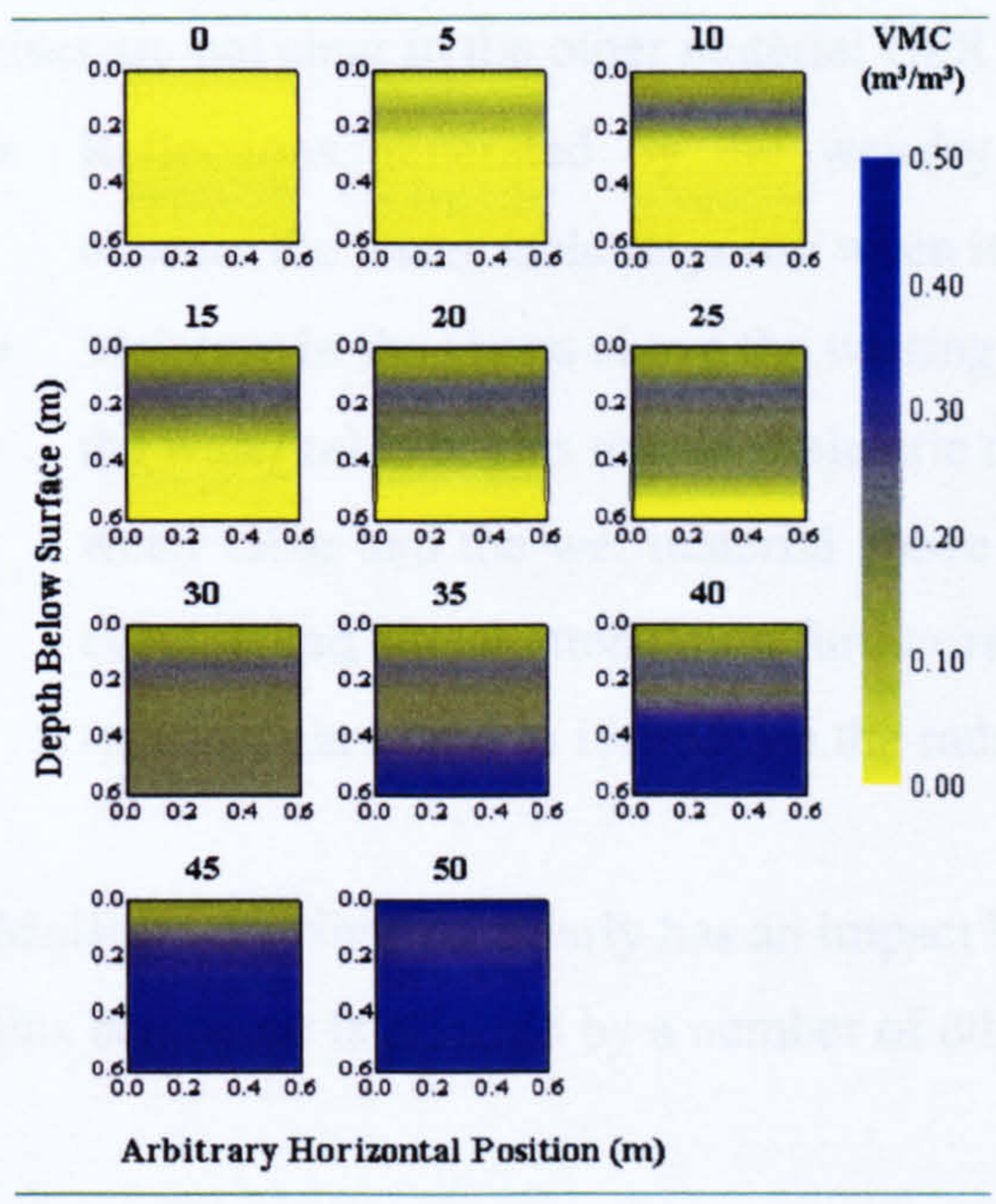

Figure 7.33: Idealised hydrological behaviour for the M5 experiments for each water addition.

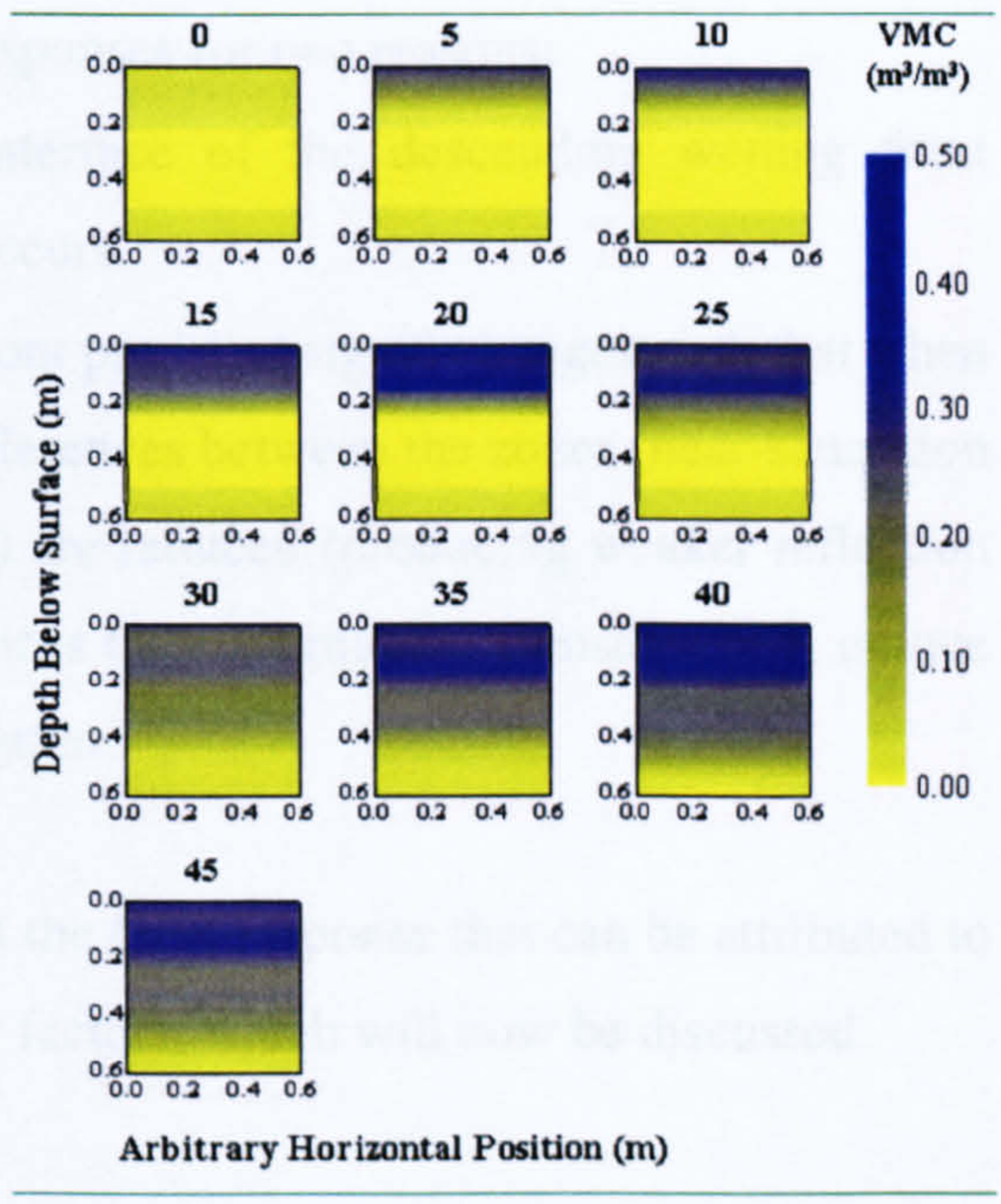

Figure 7.34: Idealised hydrological behaviour for the M6 experiments for each water addition.

These images also demonstrate the potential locations of dielectric contrast which will generate reflection events in the GPR data. Where the signal travels down from dry to wet (water table situation), a negative event is expected. From wet to dry (wetting front), a positive event is expected. Where there are dielectric contrasts, the magnitude of the reflection will depend on the VMC either side of the interface. The interpretability of the individual responses will depend on their spatial proximity. The close proximity of some of the moisture boundaries will produce interference patterns, which could seriously affect the statistical characterisation of signal response. The generation of variable reflections as a consequence of variable VMC is evident on the time domain images. MIA is unaffected by the polarity of the GPR response induced by the moisture (dielectric) gradient. MIA is simply a function of their location (in time) and magnitudes (depends upon dielectric contrast and attenuation).

The effect of moisture distribution is most apparent in the rising and retreating of events in the radargrams. The rise is evident of the M1 and M2 results. These have the highest hydraulic conductivities and allow moisture to rise as a water table from the outset. Thus a high-magnitude negative reflection is generated at the dry-wet interface. Water table rises are not clear in the other material GPR responses for two reasons:

- Reflections generated by the wet-dry interface of the descending wetting front obscure the water table response when it occurs.
- Moisture in the layers above the wetting front produces signal changes such that when the water table begins to rise, dielectric differences between the zones (near-saturation water table and the wet material above it) are reduced (producing weaker reflection events), and signal attenuation further reduces their magnitude. Consequently, unique responses are hard to identify on the radargram.

Moisture distribution clearly has an impact but the GPR response that can be attributed to this behaviour is affected by a number of other factors, which will now be discussed.

7.3.3.3 Attenuation: weakening and loss of events

The main factor influencing the signal response is the attenuating effect of the increased VMC. It is this which dominates the decline in amplitude values evident in the majority of the statistical relationships; particularly the MIA-VMC relationship. Attenuation has a

limited effect on the transmitted pulse (because it travels through the air) but will affect the ground-wave. It also severely reduces the magnitudes of later-time events. Attenuation interacts with moisture distribution such that:

- Changes in water distribution produces changes in reflection pattern and this affects trace data.
- In a water table (WT) movement the major reflection event will have a negative polarity, which will dominate the analysis.
- In a wetting front (WF) movement the major reflection event will have a positive polarity, which will dominate the analysis.
- This will be confounded by the fact that in WT the event occurs before the attenuating water, whilst in WF the event occurs after the attenuating water and is thus likely to be significantly changed. A non-linear decrease in response may be expected as more VMC occurs above the reflection event in WF.
- In complex distributions, both effects are seen producing complex responses. This means that relationships become very weak due to the variability in reflection response.
- If there are highly variable reflection events, the amplitude content is likely to be significantly different than if there is a homogeneous subsurface in which only VMC varies. In addition to VMC distribution, this may be due to other subsurface anomalies such as stones.

The principal effect of these changes is to alter the rate of amplitude decline and it is this that may produce a non-linear functional form. However, scatter in the experimental data has a far more important effect on the relationship than the distribution of moisture; although the causes of this scatter are, to some extent, dependent on this distribution.

7.3.3.4 Move-out of the ground-wave

As the near-surface VMC increases, the ground-wave will move out relative to the air-wave because it will take longer to travel the same distance due to a reduction in propagation velocity. In M1 and M2 the ground-wave only appears separate from the air-wave near saturation due to water table rise. This produces higher MIA values near to saturation. For M6, attenuation dominates and the ground-wave occurs in association with interference between itself and the air-wave. For M3-M5, the wetting front creates a variable distribution of moisture. This initially delays the ground-wave. As the much

wetter front descends through the profile and is replaced by lower VMC in the near surface zone, the ground-wave velocity increases and occurs earlier in time. It retreats again when the water table saturates the material. Consequently, the fluctuating band of events is caused by fluctuations in the timing of the ground-wave as the VMC changes in the near-surface zone in response to changes in moisture movement and distribution. This produces pseudo-hyperbolae on M3-M5 data. This is shown in Figure 7.35 in which the approximate time of ground-wave arrival (derived from Figure 7.1) is plotted against the VMC in the top 0.155 m of the STF for each experiment. This shows that:

- M1 and M2 cluster at 2-3 ns until near saturation when TWTT increases to about 7 ns.
- M3 demonstrates a low rate of TWTT increase (between 4.5-6 ns) after first addition as VMC rises.
- M4 and M5 cluster and scatter between 4-6 ns until near-saturation when they exceed 6 ns.
- M6 produces constant values at around 4 ns with the exception of the dry condition.

These data have to be interpreted with caution because, although they demonstrate the expected behaviour, they are subject to the usual problems of event identification. They are especially affected by the near-surface disturbance (ringing, direct arrival changes) and, in the case of M6, attenuation of all data.

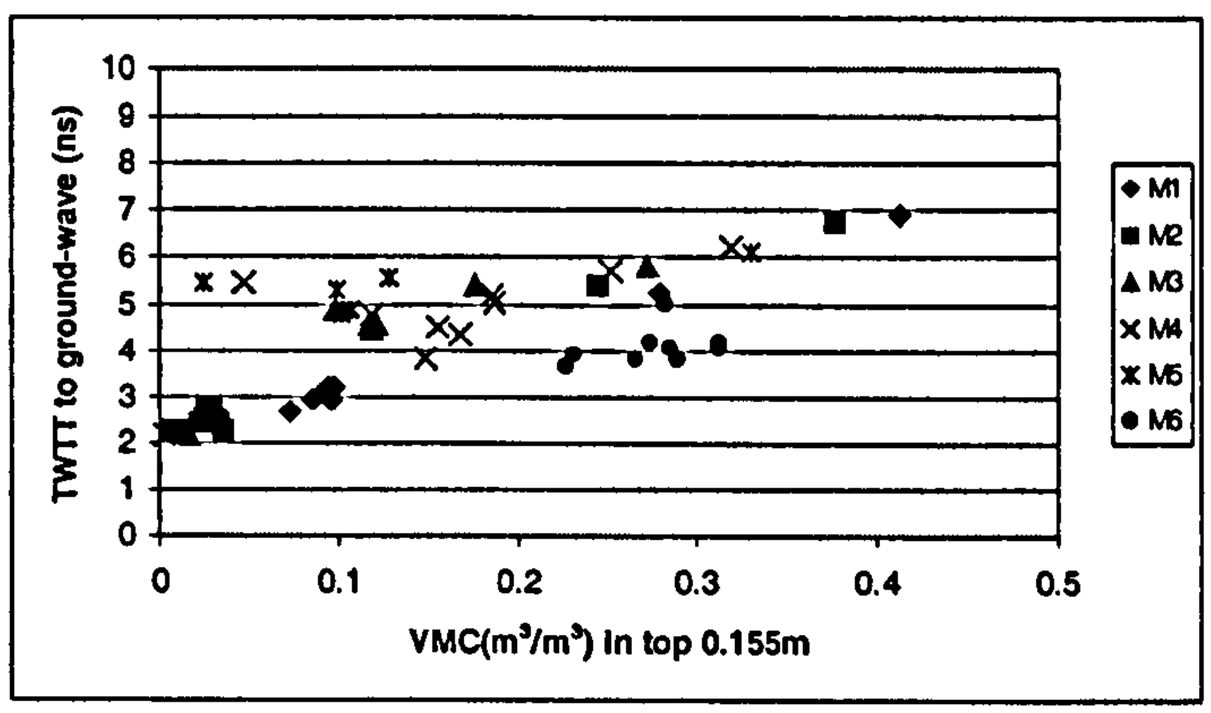

Figure 7.35: Ground-wave arrival time (ns) plotted against observed VMC (*ThetaProbe*) in the top 0.155 m of the STF profile.

The ground-wave has a higher magnitude than most of the other signal events (except for the air-wave, and some unattenuated dry/wet interfaces) and is less severely attenuated by the water in the surface. For MIA the higher magnitude of this event produces an increase in MIA relative to what it would have been had the ground-wave remained with the air-wave. Consequently, MIA remains more or less constant with an increased VMC until

after a certain volume of water has been added. A slight decline in value is observed due to the attenuation of later-time events. This effect is most clearly manifested in the low VMC data of M5. The implications of this are significant:

- MIA measures signal attenuation and can therefore indicate VMC.
- Distribution of moisture can affect the travel times of various signal components (especially the ground-wave) and this will mask the attenuation affect.
- The attenuation effect will re-appear after the addition of a variable volume of water.
- Therefore, although VMC is measured, the technique is also sensitive to the actual volume of water added.
- This means that the depth of investigation will also become important and the distribution of moisture will have a more subtle influence.

7.3.3.5 Polarity reversals and ringing

Two other sources of interference occur which further produce scatter in the data. The apparent polarity reversal of the expected negative peak at the start of the direct arrivals, which becomes a positive peak, is not a phenomenon associated with saturation otherwise it would only occur in the last trace of each experiment. Nor is it associated with local near surface saturation because full saturation is never achieved until after the last addition when no further water can enter the facility. Furthermore, it is not associated with water that is in contact with the radar antennae otherwise all wet experiments would demonstrate this behaviour.

A near surface dielectric discontinuity in which a lower dielectric constant occurs below a thin layer of higher dielectric constant at the surface will produce a positive reflection. If this reflection is of sufficient magnitude and near enough to the surface it can be expected to combine with the air-wave and ground-wave wavelets producing interference in the signal at early TWTTs. The proximity of the reflection to the surface determines the magnitude of the positive event at the start of the total waveform with the magnitude declining and a tendency towards an undisturbed transmitted pulse as the wetting front moves deeper into the profile. The other consequence of this narrow band of trapped moisture near the surface is high magnitude ringing. This interferes with all reflections that may occur below this event preventing identification and producing artificially high MIA values. For the coarser materials such interference does not occur and interference is

largely confined to the base reflection caused by the dry-wet interface response. Frequency response also demonstrated that a change in coupling was effected through the change from dry to wet conditions. Consequently, signal events will occur with varying duration such that the combination of wavelets becomes less predictable. This both enhances the positive responses and produces significant changes at saturation.

7.3.3.6 Summary

Only by considering the specific hydrological behaviour and associated dielectric behaviour can the GPR response be understood, interpreted and, ultimately analysed. Because the moisture, and therefore dielectric, behaviour is known the potential response can be investigated theoretically using the reflection coefficient at each of the layer boundaries. Whilst instantaneous amplitude may provide better moisture predictions because it effectively uses absolute values, if the hypothesis that much of the variability in wet response is due to differences in moisture distribution, then using time domain, real amplitude values is vital, at least for interpretation purposes, because the sign of the reflection will indicate the direction of the dielectric contrast and therefore of the moisture gradient, should one exist.

7.3.4 Re-assessing the MIA-VMC relationship

7.3.4.1 What does MIA measure?

Through a combination of the theoretical knowledge outlined in Chapter Three and the experimental observations outlined above and in Chapter Six, the physical meaning of the MIA value can be understood. The MIA value represents the relative change in trace instantaneous amplitude over a selected time window. Across this time window (TW), the received signal is a function of the direct arrivals (DA), the total of the observed dielectric contrasts (TDC), and all sources of signal weakening (attenuation) (L). This can be expressed:

$$MIA = f(DA, TDC, L, TW) \tag{7.1}$$

In conjunction with DA, TDC is the main source of MIA increase. Reflections increase MIA in a way that depends on the magnitude of dielectric contrast. However, with each reflection less energy is propagated further into the subsurface producing a relative loss of signal energy. This will be enhanced by scattering losses associated with small objects, although this did not affect the STF experiments. The effect of signal loss is a singular reduction in MIA through decreasing the instantaneous amplitudes. The direct arrivals result in a very high magnitude response at the start of the trace, the air-wave component of which is more or less constant unless disturbed by the sources of interference discussed. In these experimental data, the instantaneous amplitude is less sensitive to interference in the direct arrivals than the time domain results. This formulation ignores the power output of the GPR system, which would determine the actual MIA values, suggesting that different GPR systems would produce different MIA values. However, the actual relationship between MIA and VMC should be unaffected other than requiring a slight adjustment to the intercept. In future it may be possible to reduce such system-specificity by using normalised values (i.e. a ratio of output to input) but this is not explored here.

In essence, equation 7.1 suggests that with fewer or weaker reflections or greater signal attenuation the signal response becomes weaker and MIA is reduced. The attenuation of a signal is caused by absorption, due to the conductivity losses in the ground and the spreading out of energy over a larger surface area with increasing depth (Conyers and Goodman, 1997). Attenuation is defined by equation 3.4 and depends on electric, magnetic, and dielectric properties. Xu and McMechan (1997) show that the combined effect of all three attenuation mechanisms is higher than that by any one separately. However, it is not possible to separate by measurement at a single frequency these components of loss (Daniels *et al.*, 1988). If the ground is conductive, GPR waves will be absorbed (Xiong and Tripp, 1997) because conductivity along the propagation path increases signal decay exponentially (Du and Rummel, 1994). This is expressed by (McCann *et al.*, 1988):

$$E_x = E_0 e^{-\alpha x} \tag{7.2}$$

where E_x is the electric field strength at the propagation distance, x, α is the attenuation coefficient, and E_0 is the peak electric field strength. Spreading losses for a spherical

wave occur at a rate $1/x$ (Du and Rummel, 1994). These two aspects of attenuation produce signal decline with propagation distance. Because, increased TW is usually taken to mean increased depth, it would appear that the decline in MIA is a function of the increased time window used to calculate the MIA value for each successive water increment.

Figure 7.45 demonstrates that increasing the time window (by increments of 2.5 ns) for the dry traces for each material experiment, increases the relative proportion of low magnitude IA values that contribute to the average value, thereby reducing it. These relationships (summarised in Table 7.9) produce very significant linear results, although they are, in fact, non-linear. The strength of the non-linear relationships appears to suggest that, in fact, all that is being measured is the decrease in MIA with increasing TW. However, in this part of the research, the increase in TW represents a constant, and controlled depth of 0.58 m, rather than a relative increase in depth. The increased TW is a physical consequence of the water content, which decreases the signal propagation velocity. Therefore, to maintain a constant measurement depth, the time window must expand. Thus the spreading losses are constant and exponential loss becomes solely dependent on the attenuation coefficient.

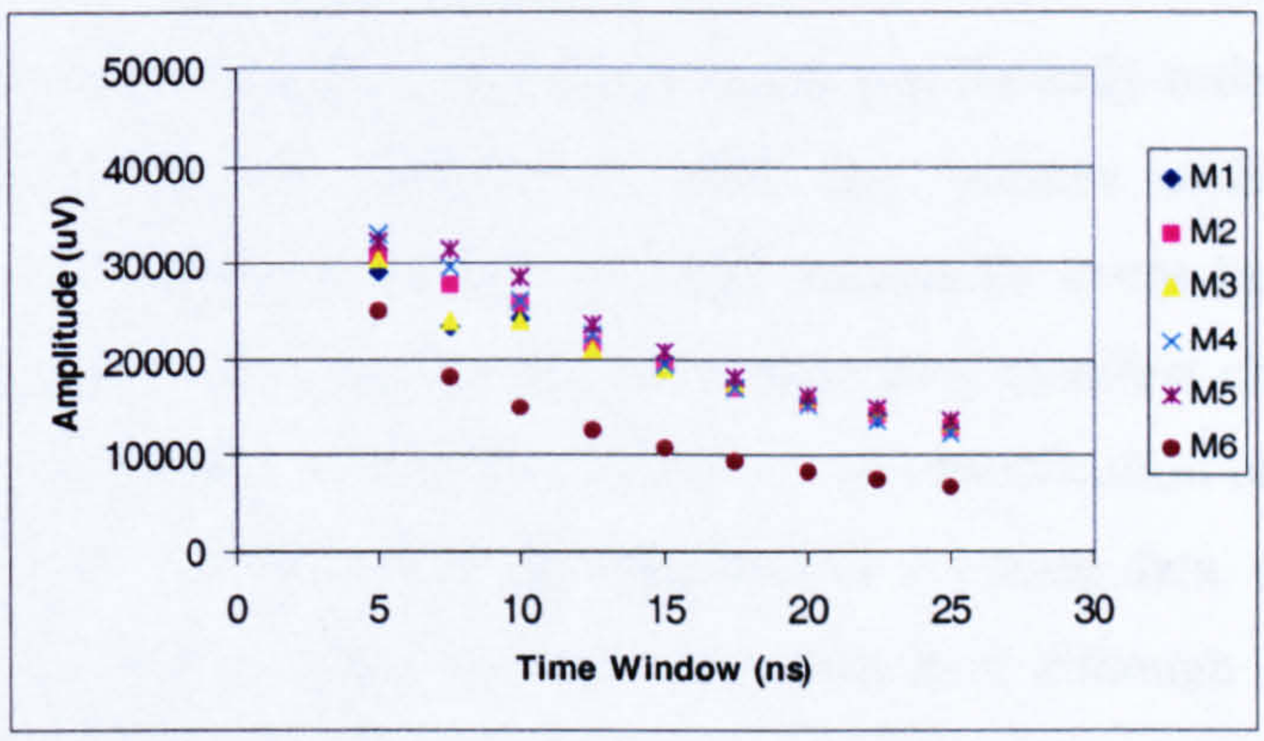

Figure 7.36: Decline in MIA with increasing time window sizes (2.5 ns increments) for dry traces in the M1-M6 experiments.

Material	R^2	t	p
M1	0.883	-7.761	5.4E-05
M2	0.978	-18.975	6.2E-08
M3	0.937	-10.930	4.4E-06
M4	0.963	-14.480	5.1E-07
M5	0.918	-9.487	1.3E-05
M6	0.888	-7.965	4.5E-05

Table 7.9: Linear significance results for the data presented in Figure 7.36.

The principal loss mechanism in rocks and soils, certainly at frequencies greater than 500 MHz, is the absorption of energy by the water present in the material pore space (Daniels *et al.*, 1988). Thus, because the MIA value is shown to decline with increased water content, it can be concluded that this is dominated by the signal loss associated with increased water content. The term $\sigma/\omega\varepsilon$ in equation 3.4 represents the loss factor, P, which is directly proportional to conductivity and inversely proportional to the relative dielectric constant and signal frequency (see Chapter Three for more detail on these components) (Reynolds, 1997). Over a constant depth of material an increase in VMC will increase both the conductivity and the relative dielectric constant.

This analysis has shown that the MIA value represents a combination of the total dielectric contrast and the collective signal loss processes. Of these loss processes, the attenuation of the signal by the increase in effective conductivity throughout a constant depth of material as its VMC increases appears to dominate the MIA-VMC relationship. There are two issues that require caution in the interpretation of the developed relationship. The direct arrivals have already been discussed as producing a source of bias in the relationship results because the attenuation effect is measured relative to the apparent constancy of the direct arrivals. The developed relationships take into consideration the relatively small differences in the direct arrivals observed in the experimental data and these are identified as increasing scatter in the results. However, where there is interference in the direct arrivals that significantly reduces the envelope magnitude of this feature, the estimate of MIA may become under-estimated (and therefore VMC over-estimated) because the high magnitude event has been removed. Removing the direct arrivals is not an option because they manifest changes associated with the subsurface moisture (see Section 7.3.2.2) so an identification of the potential for this affect is necessary through visual interpretation of the trace data. Another potential problem associated with the direct arrivals is the fact that, although the measurement depth is constant, and therefore so are all processes of signal loss with depth, the direct arrivals (especially the transmitted pulse component of them), retain the same duration while the rest of the time window expands. Thus the measurement of attenuation is enhanced and possibly exaggerated by the direct arrivals. Therefore relative attenuation is measured. This has implications for the further application of the method in a way that is related to the time window.

To control for depth, the time window was changed for each experimental run. However, this method is inappropriate for application in the absence of detailed a priori knowledge concerning two-way travel times. The use of an arbitrary time window, identifiable on a radargram, enables the limit of investigation to be approximated. However, using a constant time window across variable VMC can be expected to reduce the accuracy of the MIA-VMC relationship and may even render the method inapplicable. When applying the method to a constant time window, the depth of measurement is likely to be more variable, and therefore spreading and exponential losses will also be more variable. The relationship is likely to become less reliable, because the accuracy of the actual VMC estimations will be reduced, and the relative magnitudes will be smoothing the estimated VMC distribution. This may give the impression of less variability in the subsurface moisture than there actually is.

7.3.4.2 Influence of time window

The impact of using a constant time window on the developed relationships was investigated by calculating the MIA value at each VMC over a time window from G_0 to 25 ns for all experiments using time window increments of 2.5 ns. Observed VMC (*ThetaProbe*) was plotted against calculated MIA. The experimental data for M2 are presented as an example in Figure 7.37. The relationships, and their significance, are showing in Table 7.10.

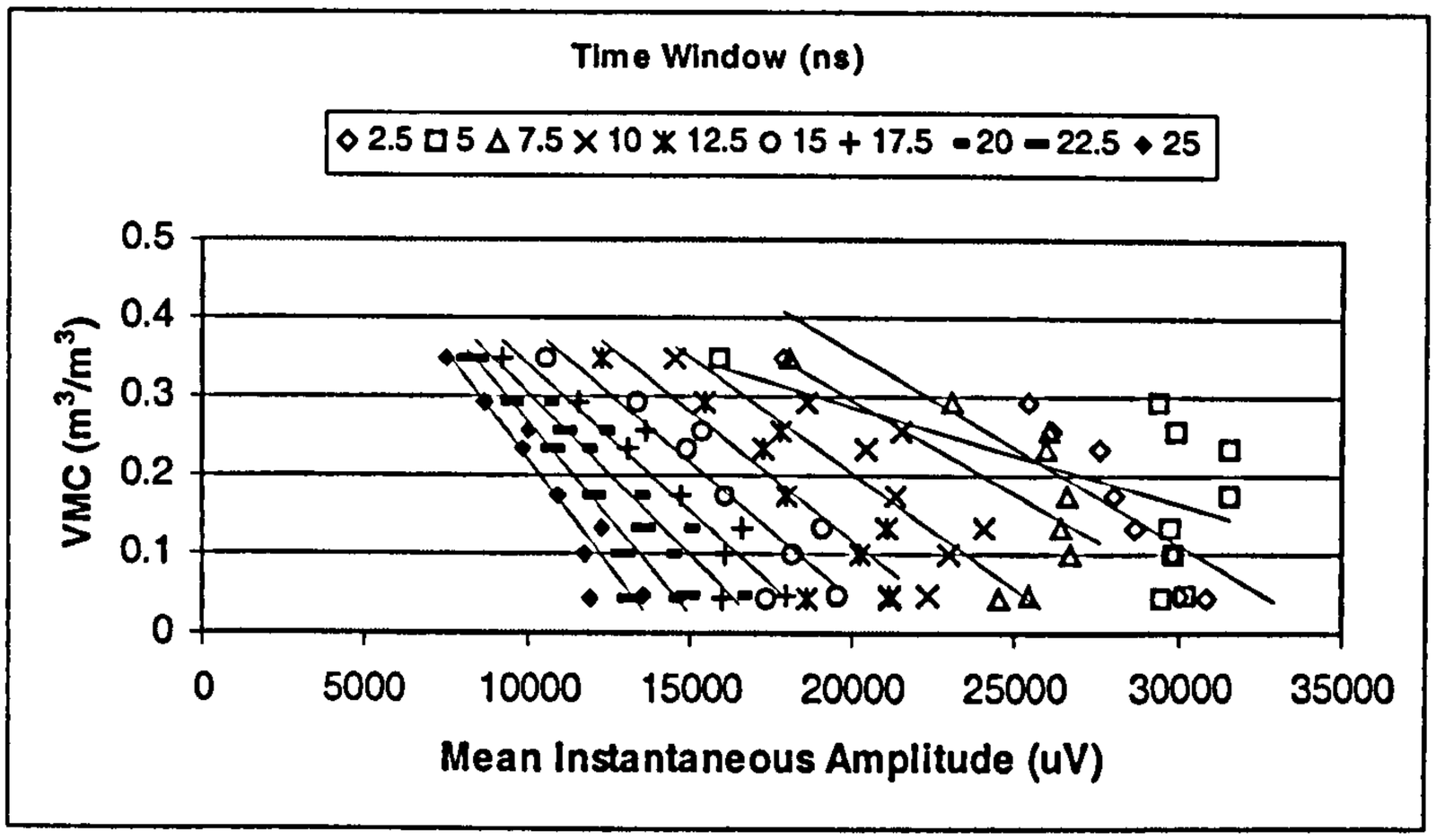

Figure 7.37: Relationship between MIA and VMC for M2 at ten constant time window sizes.

Time Window (ns)	R^2	t	P	N	Intercept	Slope
2.5	0.7712	-4.8580	0.0018	9	0.8441	-2.4E-05
5	0.2965	-1.7176	0.1296	9	0.5302	-1.2E-05
7.5	0.3662	-2.0111	0.0842	9	0.7675	-2.4E-05
10	0.5735	-3.0681	0.0181	9	0.7944	-3E-05
12.5	0.7423	-4.4904	0.0028	9	0.7707	-3.3E-05
15	0.8341	-5.9323	0.0006	9	0.7317	-3.4E-05
17.5	0.8836	-7.2902	0.0002	9	0.7152	-3.7E-05
20	0.8899	-7.5229	0.0001	9	0.7179	-4.1E-05
22.5	0.8973	-7.8202	0.0001	9	0.7498	-4.8E-05
25	0.8979	-7.8481	0.0001	9	0.7607	-5.4E-05

Table 7.10: Linear siginificance tests for the relationship between MIA (x) and VMC (y) for ten constant time window sizes.

A number of aspects are apparent:

- At short time windows the MIA-VMC relationship becomes insignificant (at 5 and 7.5 ns) or very weakly significant (2.5 and 10 ns). This occurs due to the proximity of the direct arrivals, which increase the magnitude of MIA and scatter in the results.
- The relationships become stronger with increased time window.
- It is also clear that with each increase in time window, the base MIA value (i.e. the MIA value under the driest conditions), is reduced. This effect is less clear in the intercept values because of the increasing steepness of the relationship with increasing time window.

It can be concluded that an analysis conducted at a constant time window still measures the attenuation effect discussed previously. Due to the decreased VMC range for the same VMC range (steeper relationship), increased MIA estimation error may have a greater adverse effect on the estimations of VMC. More significantly, though, is the fact that the attenuation measurement is still valid and can therefore be applied to estimate VMC distributions in the subsurface; although the absolute amplitude values may not always be accurate.

7.3.4.3 Models for VMC estimation.

MIA measures VMC primarily through the effect of the latter on signal attenuation, relative to the constancy of the direct arrivals. Variable moisture distributions have a dramatic impact on the visual imagery but tend to promote scatter (which acts to obscure the relationship) and a tendency towards a non-linear form in the MIA-VMC relationship. A distinction can be made between those materials that attenuate the signal in the absence

of moisture and those that do not, although it was also suggested that the different functional forms of the relationships negate this simplification. Table 7.8 shows that with the exception of M4, there is little improvement between linear and non-linear relationships. In particular, M1, M2, and M5 remain as linear functions, whilst the R^2 improvement for M3 is only 0.0051. Thus in four of the five materials in the first group, linear relationships apply. For M4, the exponential form is principally the result of a change in gradient (MIA values decline less rapidly) effected by increased attenuation and to some extent the reduction of near-surface disturbance (especially ringing). Thus it can be shown that there is an inherent tendency towards linear MIA decline with increased VMC.

Conversely, the non-linear form for M6 does not appear to fit this pattern. However, material attenuation and moisture attenuation of the GPR signal reaches a certain point in which the MIA can decline no further although average VMC continues to rise. This promotes ideal data conditions for a power function to fit the data. The GPR has actually met its limit of application in this material and can no longer record changes in amplitude and so amplitude tends to fluctuate randomly. Thus after 0.2 m^3/m^3 a linear relationship breaks down and using a power function would produce inaccurate VMC estimations. This implies that the GPR is incapable of estimating VMCs greater than 0.2 m^3/m^3 in materials that attenuate the signal. This is in fact deceptive because the average full STF VMC is lower than the VMC in the upper half where the moisture has distributed. Thus the limit of the GPR estimate is actually about 0.3 m^3/m^3 across a soil volume of 0.3 m depth.

With this information it is possible to treat the two groups of data in a way that facilitates a single linear function applied to the two sets of data. All data for M1-M5 were lumped together after dry and saturated data were excluded and a linear function fitted. The result is shown of Figure 7.38. Also shown on this figure is the linear function for M6. This second function excludes the dry and saturated data, and all data at its limit of application. Table 7.11 summarises the two linear VMC estimation models, GI (for M1-M5) and GII (for M6), which estimates VMC using MIA as its input.

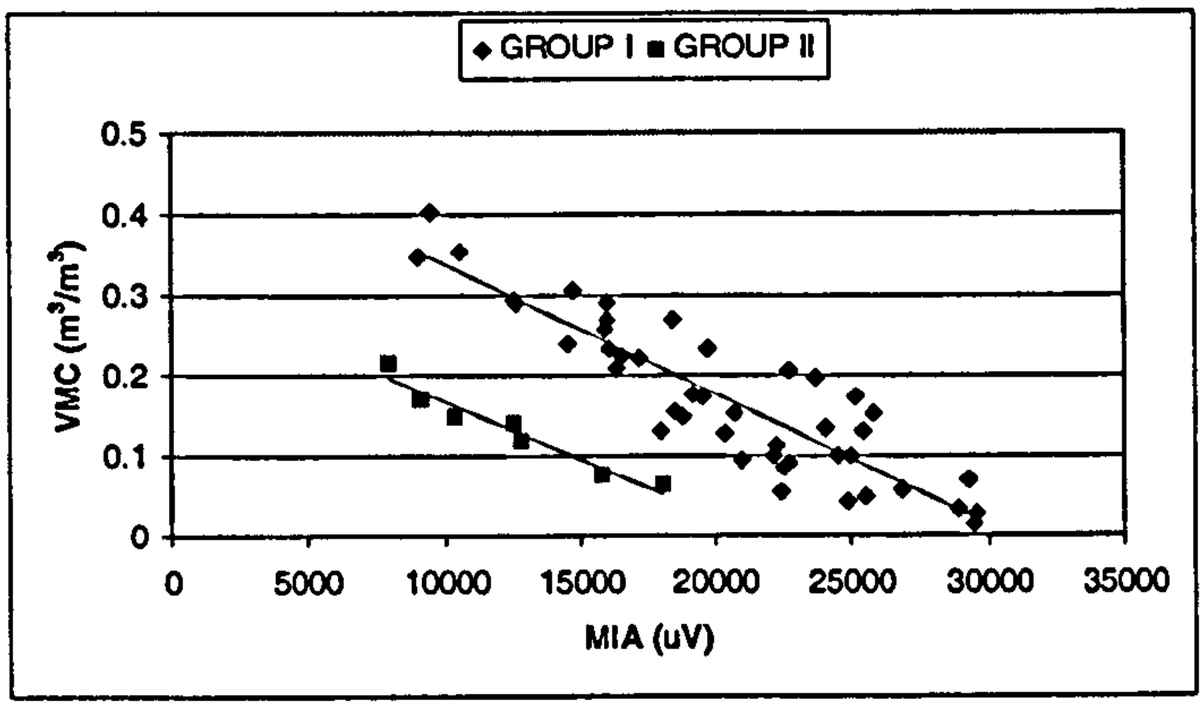

Figure 7.38: Linear GI and GII relationships fitted to the MIA VMC data.

Group	R^2	t	p	N	Constant	Slope
One (GI)	0.799339	-12.9348	3.06E-16	44	0.500845	-1.6E-05
Two (GII)	0.940541	-8.89337	0.000299	7	0.307562	-1.4E-05

Table 7.11: Summary of significance results for GI and GII linear VMC estimation models.

Both produce significant linear relationships, although the R^2 is much larger for GII. This is due to the fewer data points that reduces the scatter in the data; hence, the much lower p value for GI. The lower slope value for GII is indicative of the greater rate of MIA decline with increased VMC (although it actually shows a reduced rate of VMC decline as the MIA value increases). The intercept value (constant) corresponds very closely to the maximum VMC in the two groups. The distinguishing feature between these two groups of results is the clay content. M1-M5 have no clay content, whilst M6 has a clay fraction of about 45%. It is feasible that GPR results can be converted to VMC using two types of equation: one for clay materials and one for non-clay materials. However, it is more appropriate to think in terms of an equation for materials that attenuate the signal when dry, and an equation for materials that do not. This interpretation is justified on the basis that a simple empirical model is incapable of distinguishing between clay content and other sources of potential signal attenuation. Although a physically-based model of the signal attenuation process would be preferable to such an empirical model, all of the sources of variability in GPR response identified in the research so far, are approximated.

Although two groups can be identified it is possible that these are in fact part of a continuum in which the parameters of the linear model are dependent on soil texture, particularly clay content, and other response characteristics. Both model parameters differ between the two groups, although the constant for GI is far larger than for GII, while the

difference in slope is relatively small. The slope distinguishes the small difference in the rate of MIA decline with increased VMC in combination with the material attenuation effect. Conversely, the constant fundamentally conveys the degree of attenuation between the attenuating and non-attenuating materials. An important future development of this work would be to identify the values of the model parameters using materials that have a known attenuation factor in order to assess the potential physical meaning of these parameters. Having established that, for the purposes of this research, two potentially distinct groups of GPR-VMC response exist, it is necessary to test the original relationships on a material-specific basis and test the linear relationships on a group basis to assess to what extent this approach is justified.

7.4 TESTING THE MIA-VMC RELATIONSHIP

7.4.1 Testing material-specific relationships

7.4.1.1 Non-linear relationships

The developed MIA-VMC relationships were tested using the same experimental configuration but as water drained from the base of the STF. Figure 7.39 indicates that for the coarse materials (M1 and M2) drainage is very rapid due to their high hydraulic conductivities and almost all of the added water drains. For the materials with lower hydraulic conductivities drainage takes much longer and a large amount of added water is retained in the material. Furthermore, the finer grained materials retain more moisture throughout the STF profile. No drainage occurred for M6 and therefore average VMC remained constant although it did redistribute. Figures 7.40 and 7.41 present the plots of observed VMC against predicted VMC and their corresponding standard residuals for each material. The results demonstrate an overall logarithmic relationship between predicted and observed VMC with a great deal of scatter. The magnitude of some of the deviations suggest that the method developed only works for the laboratory experiments with which the relationship was created. However, this logarithmic form considers the results for all materials together, whilst the data for individual material tests reveals that for most materials the model predictions are reasonably accurate. Further analysis reveals that the logarithmic form is principally controlled by the large VMC estimations associated with M4. This is confirmed by the strong linear relationship that occurs if

saturated data and the M4 data are excluded. GPR responses for saturated materials produced anomalous results for model development and should therefore also be excluded for model testing. The M4 estimations can be up to 0.7 m^3/m^3 producing values that, at a maximum, can be out by 0.443 m^3/m^3. The plot of standard residuals (Figure 7.41) allows differences between observed and predicted data to be compared between materials and shows that the wrong functional form may have been used for the systematic component of the relationship (Burt and Barber, 1996). In particular the model appears to overpredict at higher moistures. With recourse to the original relationship (Figure 7.28, Table 7.8) it is clear that at higher VMCs, the exponential rise is so steep that a small change in MIA may result in a large change in VMC.

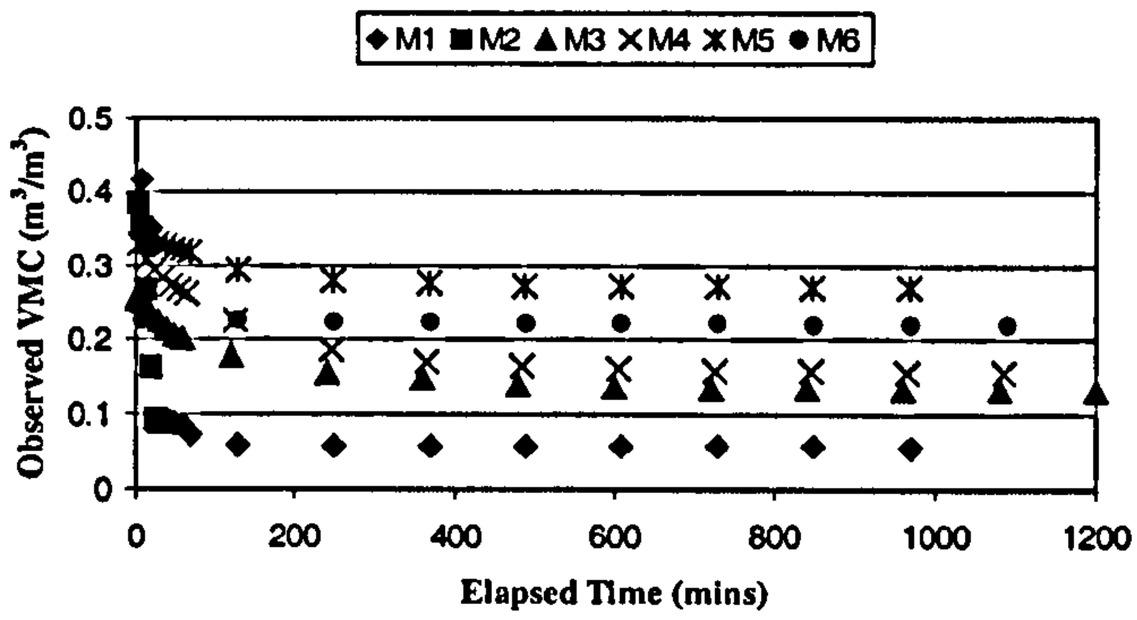

Figure 7.39: Average *ThetaProbe* VMC for STF drainage experiments.

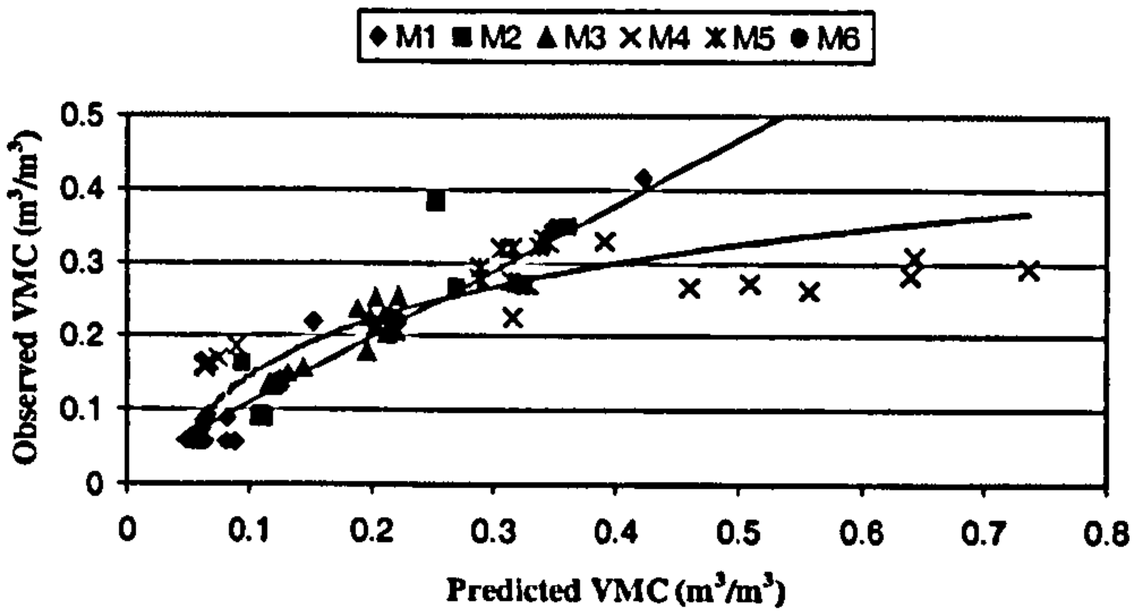

Figure 7.40: Observed (*ThetaProbe*) VMC plotted against predicted (GPR) VMC for each material experiment estimated using the material specific equations. Fitted logarithmic line shows the overall trend in all data. Fitted linear line shows overall trend after removing saturated data and M4 results.

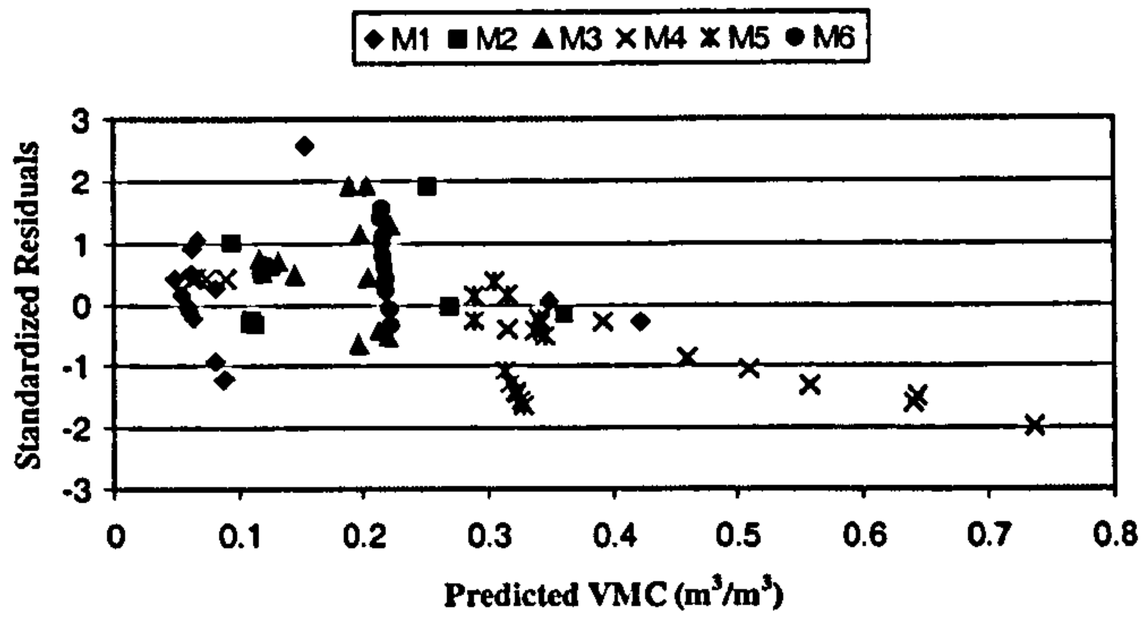

Figure 7.41: Plot of standard residuals for each material experiment based on material specific equations.

7.4.1.2 Linear model for M4

The problem with the M4 model can be accommodated by using the next best-fit linear relationship ($R^2 = 0.8367$):

$$VMC = -1.702E\text{-}05MIA + 0.4993 \quad (7.3)$$

Using this improves predictions and residuals (Figures 7.42 and 7.43). Now maximum error is only 0.062 m^3/m^3 which is a significant improvement. This lends further support to the idea that each relationship tends towards a linear form despite having a non-linear best-fit. Further error is introduced by variation in the recorded MIA values. This is related to the hydraulic conductivity and its effect on the rate of drainage, and the texture of the material that determines the retention of water. In combination these affect the distribution of the moisture that then affects the nature of reflection events and the ground-wave.

For the coarse materials (M1 and M2) the high hydraulic conductivities allow rapid drainage and the coarse texture minimises particle surface retention such that for any given average VMC, the distribution will be the same for wetting and draining materials. The GPR reflection pattern remains consistent and therefore VMC estimation produces a maximum error (relative to *ThetaProbe* VMC) similar to that achieved using depth correlation approaches with values of 0.065 m^3/m^3 for M1 and 0.070 m^3/m^3 for M2. For M6 the estimations cluster because no drainage occurs. Moisture redistribution moves water down through the profile so that a weaker, highly attenuated event occurs slightly later in time. This generates increased variability in the MIA estimate producing small

changes in estimated VMC (maximum absolute error is 0.013 m^3/m^3) resulting in a high spread of the residuals. For the intermediate particle sizes (M3-M5), the results demonstrate clustering at higher observed VMCs and a decrease in predicted VMC with a decrease in observed VMC. This does not occur for M5 because drainage ceases after a small decline in VMC (Figure 7.39). In the decreasing section of the M3-M5 results, the maximum absolute error is 0.062 m^3/m^3 for M4 and 0.018 m^3/m^3 for M3 whilst in the clustering section this error is 0.059 m^3/m^3 for M4, 0.048 m^3/m^3 for M3, and 0.058 m^3/m^3 for M5. Whilst this error appears acceptable, there is a possibility that the error is greater in the clustering section. This suggests that problems will arise in application of the models to areas of high VMC. The clustering effect occurs because movement down through the profile of the moisture generates a low amplitude reflection, which occurs later in time along with a ground-wave which moves earlier in time. The interaction of these two events produces amplitude fluctuations, which continue while the dry-wet interface is still very close to the surface. The response is further complicated by the tendency for near-saturated MIA values to be higher than at slightly lower VMCs, and as a result, the relationship, near saturation, is reversed. It is therefore possible to obtain two VMC estimates for the same MIA value.

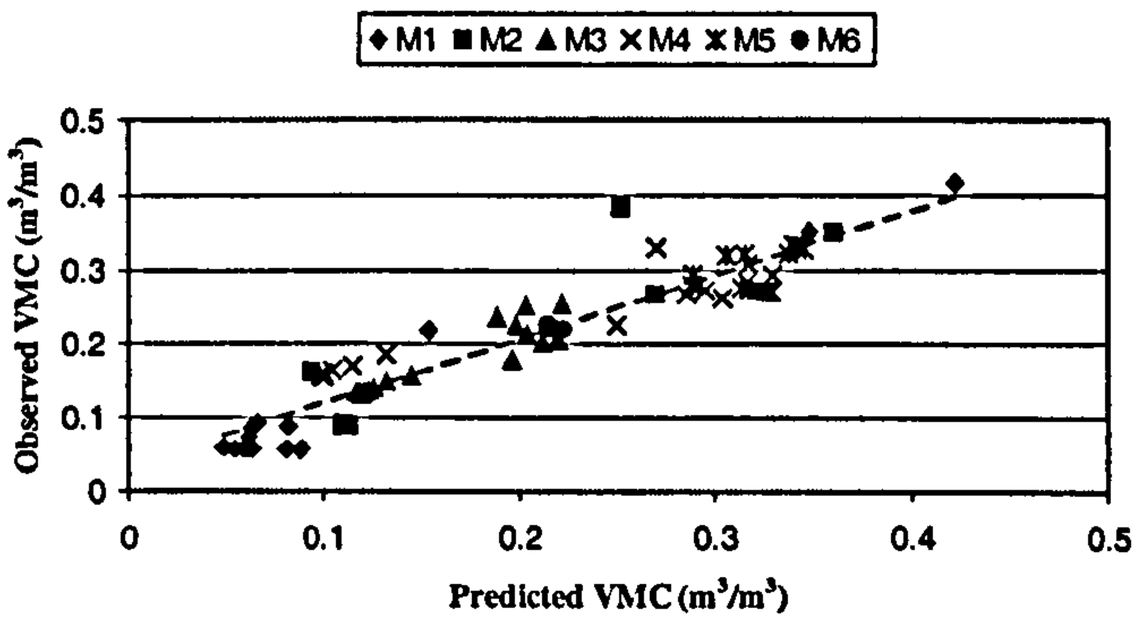

Figure 7.42: Observed (*ThetaProbe*) VMC plotted against predicted (GPR) VMC for each material experiment estimated using the material specific equations except for M4 in which the next best-fit linear equation is used to estimate VMC.

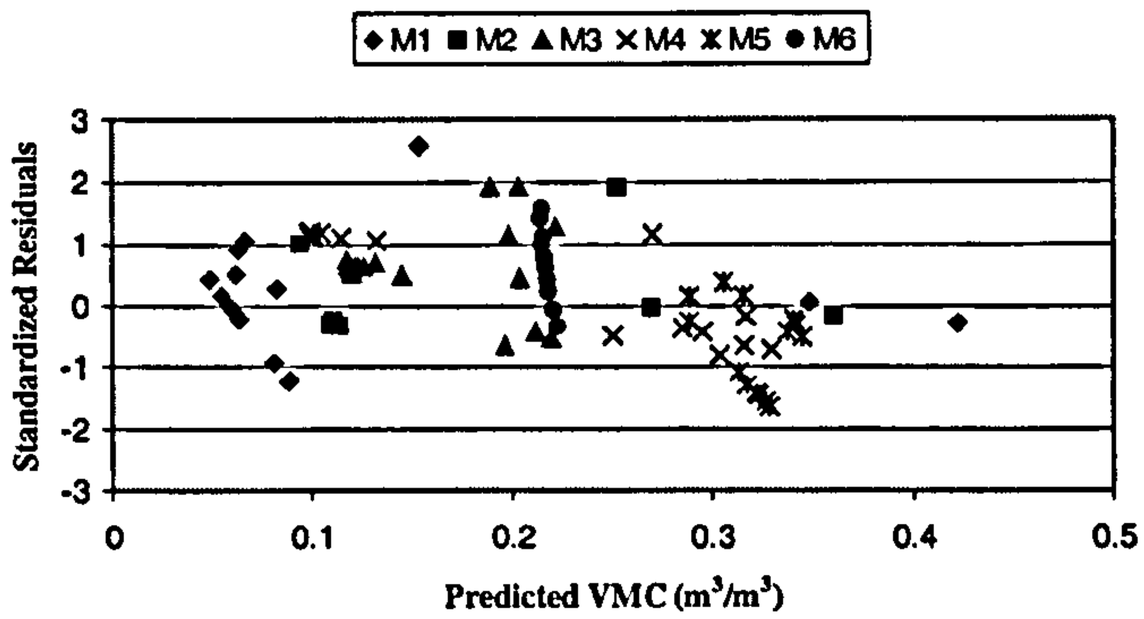

Figure 7.43: Plot of standard residuals for each material experiment based on material specific equations except for M4 in which the next best-fit linear equation was used to estimate VMC.

7.4.2 Testing group one and two relationships

Having established the expected error using material specific relationships, it is necessary to test the accuracy of the equations for each identified group. If predictions have more error for the group equations it suggests that material-specific relationships would be more reliable. The data were also tested on the drying runs and show very good RMS Error values, peaking at 0.0617 m^3/m^3 for M5 (Table 7.12). Thus under controlled laboratory conditions in which *a priori* subsurface information is available, the error in VMC estimations is low. This means that the method developed has the potential for VMC estimation and, therefore, assessment of subsurface moisture distributions.

Material	RMSE (m^3/m^3) based on testing of material-specific and group equations	
	Material Specific	Group Equations
M1	0.0235	0.0416
M2	0.0581	0.0572
M3	0.0231	0.0204
M4	0.2094 (0.0476)*	0.0389
M5	0.0325	0.0617
M6	0.0073	0.0305

Table 7.12: RMSE estimation error using material-specific and group equations for the drying experiments. *Figures in brackets show value if the linear equation is used.

In theory, if the GI and GII responses are part of a continuum based on the clay content of a material it should be possible to calibrate the model parameters according to the clay content. This would require a far greater range of material experiments and identification of the physical meaning of the slope and constant. It may also become necessary to

develop compound linear relationships, which are able to account for the change in rates of amplitude decline as VMC increases.

7.5 SUMMARY AND CONCLUSIONS

A method of accurately and reliably deriving estimates has been developed and successfully tested (maximum RMS Error is 0.0617 m^3/m^3) based on the mean instantaneous amplitude, which declines in a linear fashion with increasing VMC. The dominant physical process behind this relationship is signal attenuation by moisture, although there are a number of factors that act to increase scatter in the experimental data, such as moisture distribution, interference of the direct arrivals and down through the subsurface profile, and the interactions between these factors and the GPR signal response. To facilitate complete understanding of the nature of the quantitative GPR response to changing conditions of VMC, it is recommended that individual traces are interpreted to identify potential sources of error in the estimation. Within the context of this research, two classes of model exist. These are applicable to materials that attenuate the GPR signal and those that do not. Further work is required to clarify this issue. Through accurately estimating VMC, the method presented offers the potential to assess subsurface moisture distributions and their variability. This is the focus of the next Chapter, which will extend the investigations to more complex subsurface environments consisting of more than one material at greater depths, increased subsurface variability, and moisture distributions that vary through space, and investigate the effect of using a lower antenna frequency, because attenuation increases with frequency.

CHAPTER EIGHT: GPR ESTIMATION OF SUBSURFACE MOISTURE VARIABILITY

In Chapter Seven a method was outlined by which GPR could be used to estimate VMC in the near subsurface using reflection profiling mode data with minimal processing. Whilst the technique provides no direct physical parameter, it is based on a proxy estimation of attenuation; the mean instantaneous amplitude (MIA). The current method is applicable to homogeneous materials and the estimation of an average subsurface VMC in a controlled volume of material. Depth was constrained to a maximum of 0.6m and antennae measured data from precisely the same horizontal location. In addition to the limitations of depth of application and homogeneity of materials, the initial model development was limited in terms of the variability of subsurface moisture and the frequency of the antenna system used (900 MHz). Using this method, maximum RMS error is 0.0617 m^3/m^3 when testing the two equations developed. Ideal laboratory conditions and *a priori* information on the subsurface environment will be rare in the majority of applications, requiring the use of a constant time window. Applying the developed GI and GII equations, which reflect the degree of signal attenuation caused by a material, to a constant time window can be expected to increase estimation error and smooth patterns of estimation. The main focus of this chapter is to extend the use of GPR to the analysis of spatial soil moisture variation and to greater depth with the aim of classifying the degree of variation in the wet and dry response and to identify the further limitations of the method prior to field application to two situations of varying subsurface moisture conditions.

8.1 COMPARING DRY AND WET GPR RESPONSE

To facilitate the analysis of VMC distributions before and after wetting through space and at greater depths in more complex material configurations, five experiments were conducted as outlined in Chapter Five. Idealised hydrological responses (Figure 8.1) for the dry and wet conditions for each experiment were estimated using *ThetaProbes* calibrated for each material. The distribution of *ThetaProbes* was concentrated around each pipe outlet for each experimental run. Therefore, the most detailed subsurface moisture data is available in these zones. The moisture response from the previous experimental run serves as the main dry response where *ThetaProbes* have been moved.

Where *ThetaProbes* are not moved, the new VMC value is used. To provide the basic background data in those areas of the LTF not covered by *ThetaProbes*, dry VMC values from the STF experiments were used. Although these only provide approximations to the moisture distributions, they do indicate the development of subsurface moisture patterns to which the GPR should respond. For E1 the GPR was placed on the surface at 0.6 m depth below the final surface (at 0 m) before it was added for the later runs. Similarly, for E2 the GPR was placed at 0.4 m depth before material was added for the remaining runs. For E5 a 0.05 m thick brick layer was placed on the material surface. Moisture response is very weak in E2 and E5 due to the high hydraulic conductivity of the materials involved (M1 and M2). For E1 the same problem exists but moisture clearly gets trapped at the M2/M3 interface (at 0.8 m) and moves slowly down through M3 and M5. The increased volume of water added in E3 and E4 (see Table 5.6) produces higher magnitude response (up to 0.1515 m^3/m^3 in E3). The concentration of moisture is aided by the low hydraulic conductivity of the M6 material. Consequently, there is limited drainage from the M6 layer after these wet runs.

The GPR transects associated with each of these moisture conditions are shown in Figures 8.2-8.6. These Figures represent unprocessed GPR data acquired at 900 MHz. To assist in identification of deeper events a constant gain of 5 is applied to each image. The horizontal position represents traces collected at 0.01 m spacing between the start and end points indicated on the images. For each of the experiments performed the quality of the visual data and the ability to discriminate a given water body were variable even with substantial testing of a variety of gains and filters. These figures show clearly that in some instances the effects of water presence can be detected while in other situations there is no evidence of water interference. Figures 8.2-8.6 highlight a number of observable changes in the radar returns that can be characteristic of the presence of a body of water *i.e.*

- the loss and weakening of lower reflections,
- the presence of water obfuscates noisy reflections from within the water body (this may decrease subsurface variation in GPR response),
- the water is not discernible from any other reflector, but certain reflections may exhibit increased magnitude.

More detailed aspects of the GPR response for each experiment can be identified and these can be used to interpret the GPR VMC estimations in subsequent sections of this chapter:

- Limited differences exist between E1 wet and dry and E2 wet and dry, although the centre of the images is dominated by *ThetaProbe* reflection events.
- For E1 and E2 there is an additional horizontal event at depth which occurs on the wet images. This is associated with the added water moving rapidly down through the high hydraulic conductivity materials (M1 and M2) and becoming trapped at the M2/M3 interface due to the lower hydraulic conductivity of M3. Such trapped moisture (a perched water table) produces a negative reflection event in the radargram as expected.
- For E3-E5 the addition of the M6 layer produces severe signal attenuation but the GPR still manages to image lower layers.
- After the addition of water in E3 and E4 there is severe signal attenuation that produces loss of reflectors at depth and under the moisture. An area is clearly imaged demonstrating the detection of pools of water by its attenuating affect on the signal.
- E5 shows very little difference between the dry and wet conditions because the water was added to a high hydraulic conductivity layer, allowing rapid movement to depth. This was undetectable due to the attenuated signal which had to travel through a wet M6 layer.
- Another important aspect of the images is the direct arrival disturbance in E1-E4 but not in E5. This can be expected to have an impact on MIA-VMC estimation.

The loss and weakening of reflectors is characteristic of all the materials studied as long as the water is able to build up *in situ* and does not drain away rapidly. E3 and E4 show the greatest impact of the water on the signal due to the relatively low hydraulic conductivity of M6, which allows water to concentrate. Conversely, where the material has a high hydraulic conductivity (e.g. E2) the water is able to dissipate rapidly resulting in two problems for visual techniques. First, water does not create such a high dielectric contrast when dispersed so that the magnitude of reflections is reduced. Secondly, the water may only be detected at a material boundary where hydrologically conductive material overlies less conductive material forcing accumulation and dispersion along the boundary. This means that depth estimation may be inaccurate or that a water body may move out of the GPR's feasible detection range. The weakening and loss of later time events and other sources of disturbance render the depth-correlation approach almost impossible due to the problems associated with identifying a reflector for the task; especially for the wet conditions.

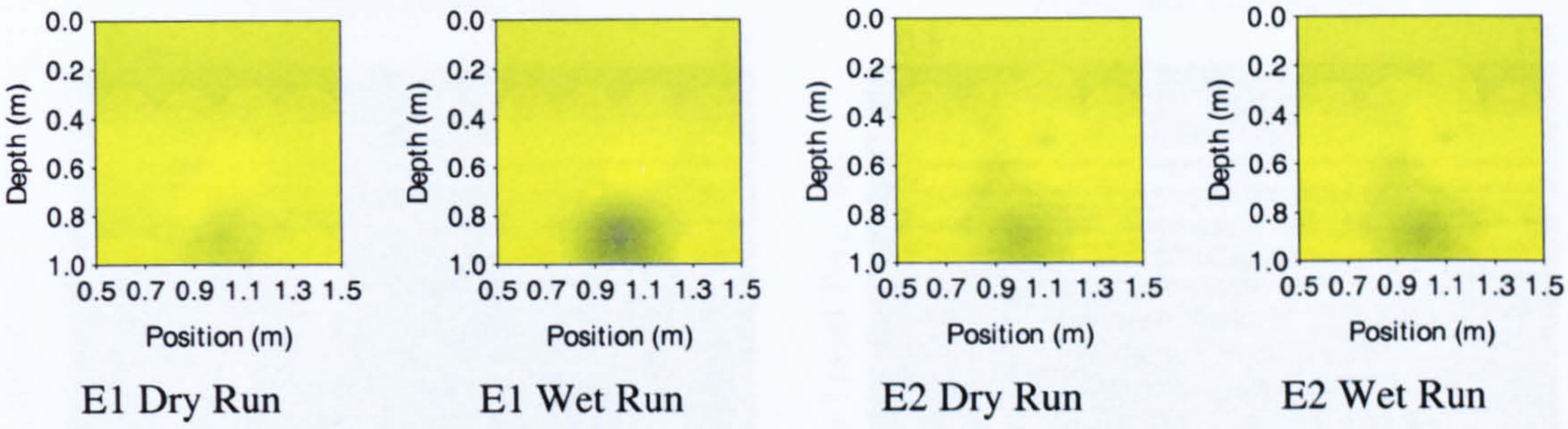

Figure 8.1: Idealised experimental hydrology for each experimental run (E1-E5, dry and wet).

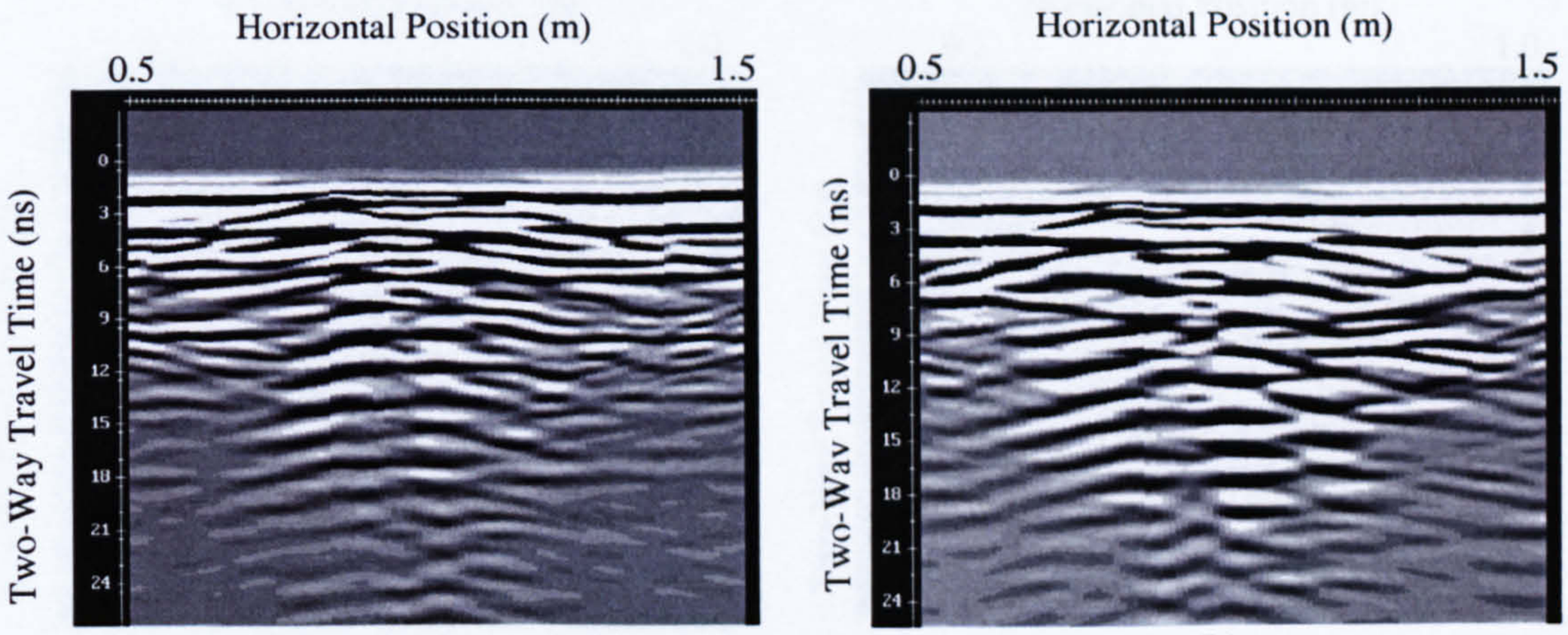

Figure 8.2: GPR transects for (a) before and (b) after water addition for E1. Acquired at 900 MHz. Constant gain of 5 applied.

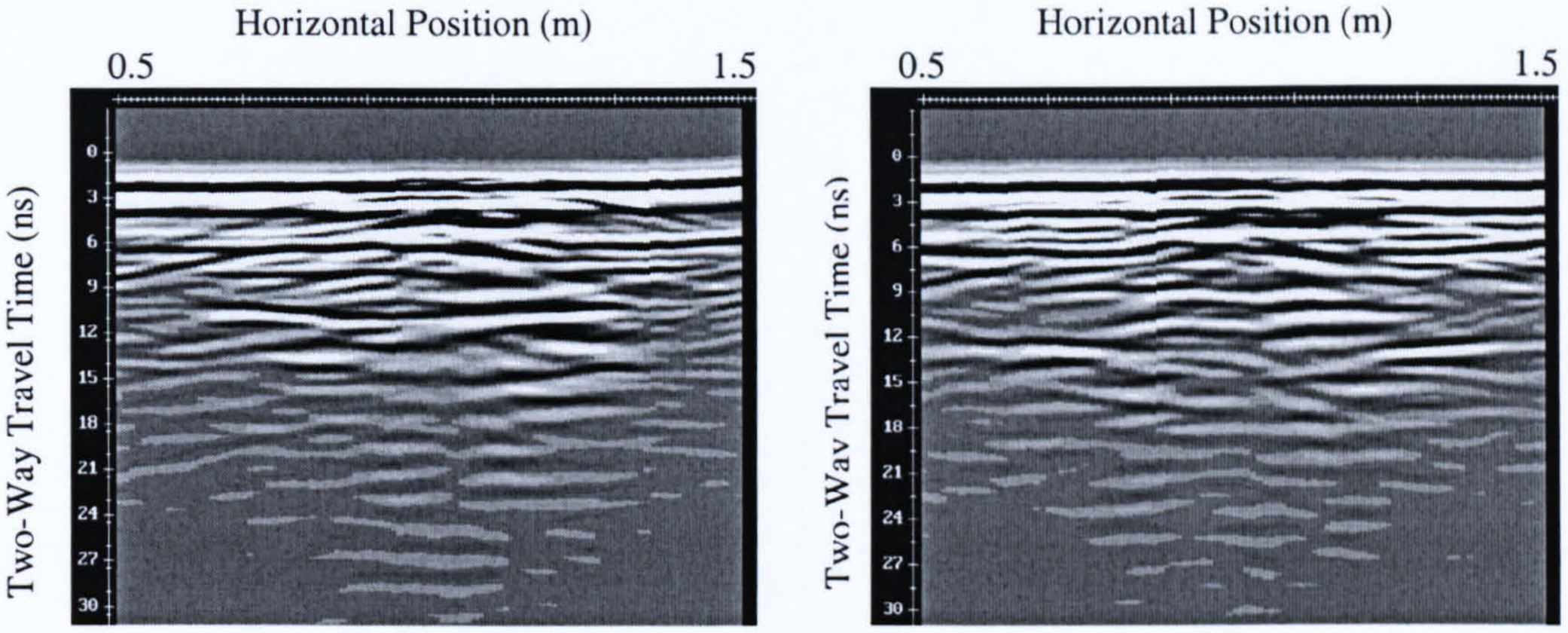

Figure 8.3: GPR transects for (a) before and (b) after water addition for E2. Acquired at 900 MHz. Constant gain of 5 applied.

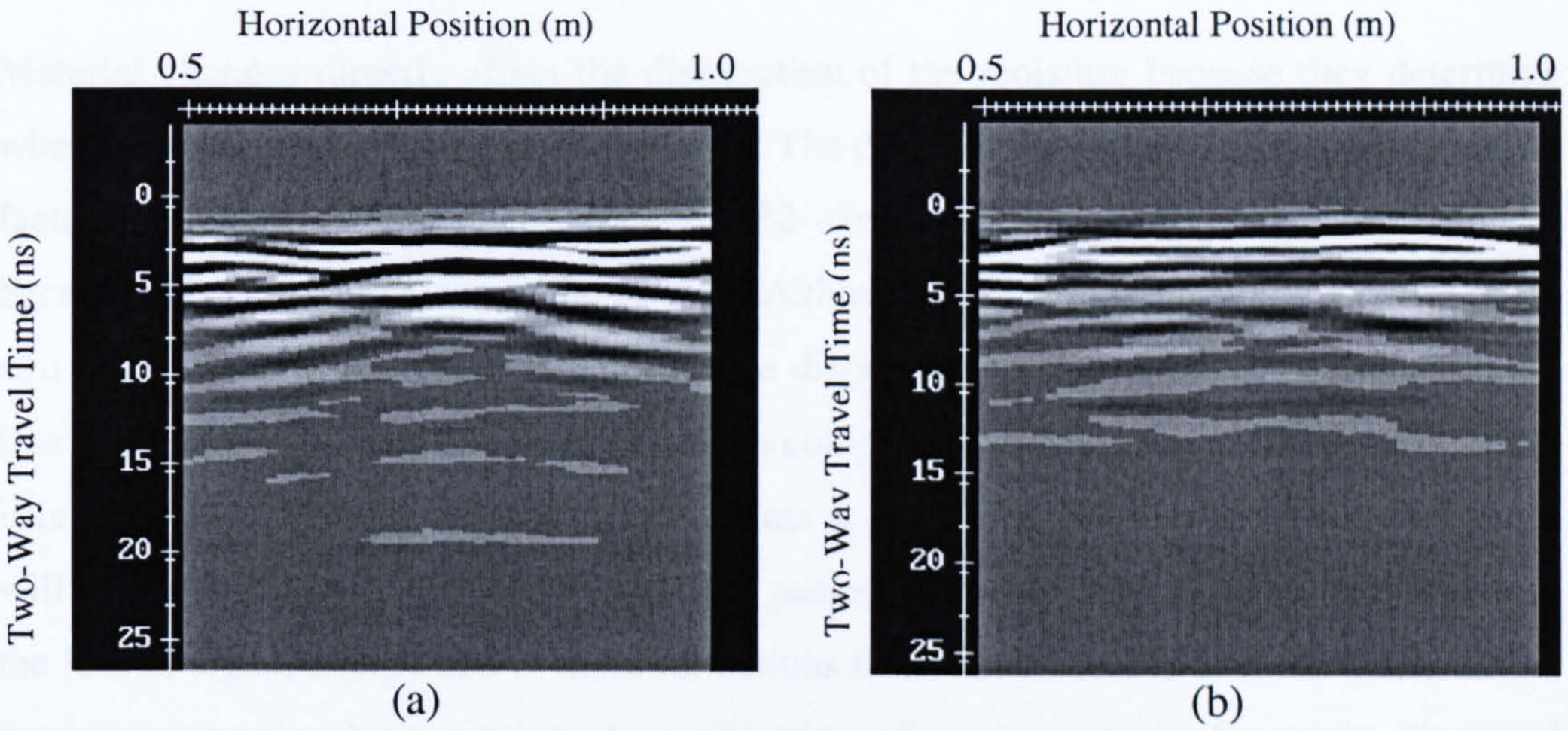

Figure 8.4: GPR transects for (a) before and (b) after water addition for E3. Acquired at 900 MHz. Constant gain of 5 applied.

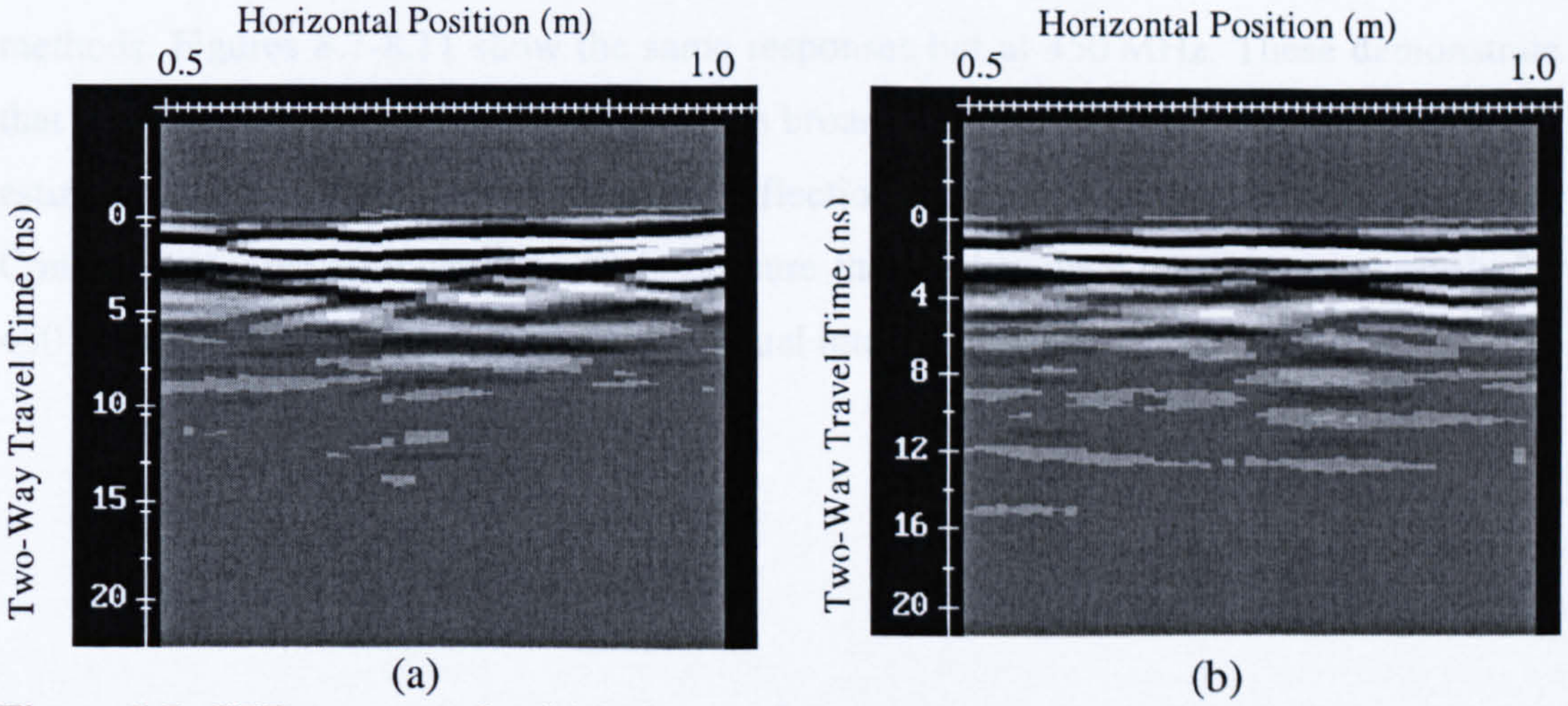

Figure 8.5: GPR transects for (a) before and (b) after water addition for E4. Acquired at 900 MHz. Constant gain of 5 applied.

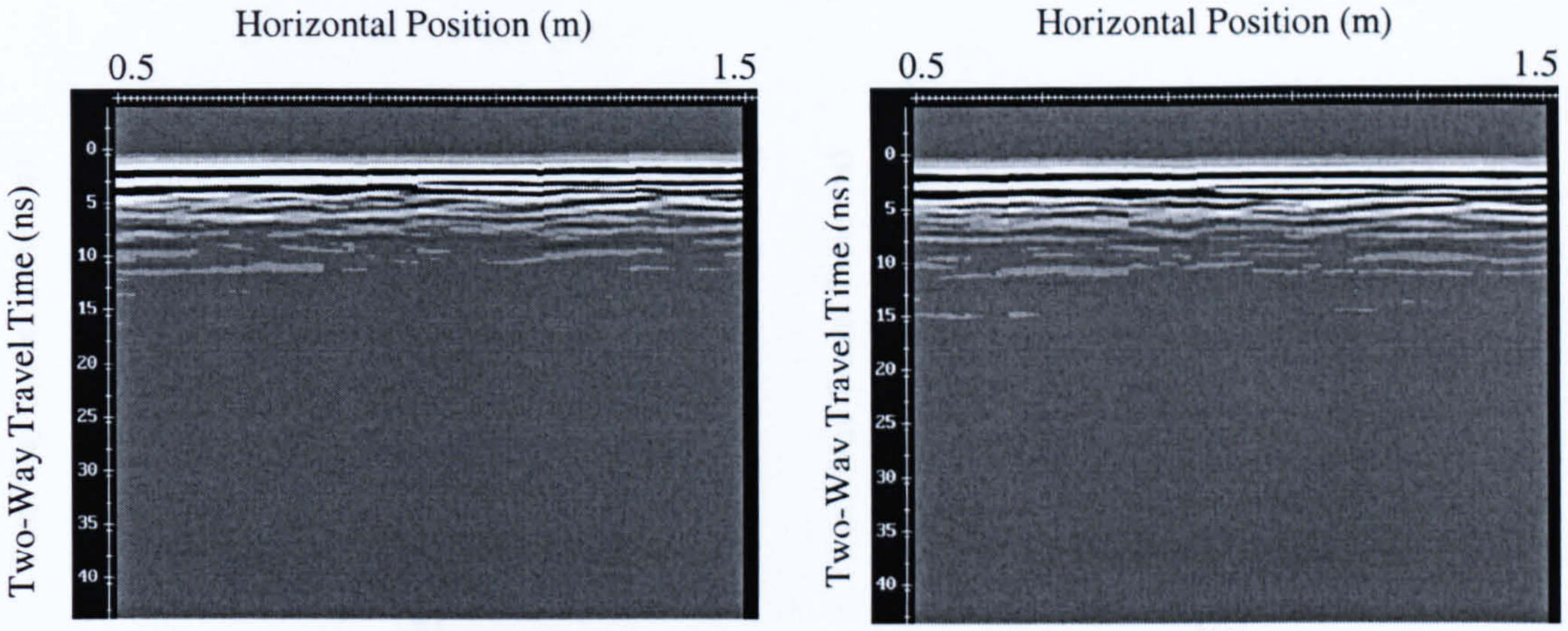

Figure 8.6: GPR transects for (a) before and (b) after water addition for E5. Acquired at 900 MHz. Constant gain of 5 applied.

Material changes directly affect the distribution of the moisture because they determine whether or not it will diffuse or concentrate. The depth of the water can be a complicating factor. Although dispersed, the water in E2 can be seen to have some visual impact because it is relatively close to the surface. Although in the clay, the shallow outlet in E4 still has a visual impact. However, in E5 the dispersed water is covered by clay although it is in the same material as E2. The result is complete non-detection of the water because it is difficult to identify any subsurface events at all. For a shallow water body the radar will respond strongly. For deeper water the passage through the subsurface may increase the loss of signal energy due to more reflections from other sources or more material that contributes to signal attenuation. A combination of weak response due to the dispersed nature of the water and signal degradation caused by overlying material and depth diminishes the response so as to be undetectable in the signal; particularly using visual methods. Figures 8.7-8.11 show the same responses but at 450 MHz. These demonstrate that the 450 MHz responses consist of much broader reflection bands, less accurate depth estimation and no loss of the later water reflections compared to the 900 MHz response. Consequently, the stronger reflections obscure the weaker ones much more severely for 450 MHz making it much less useful for visual interpretation.

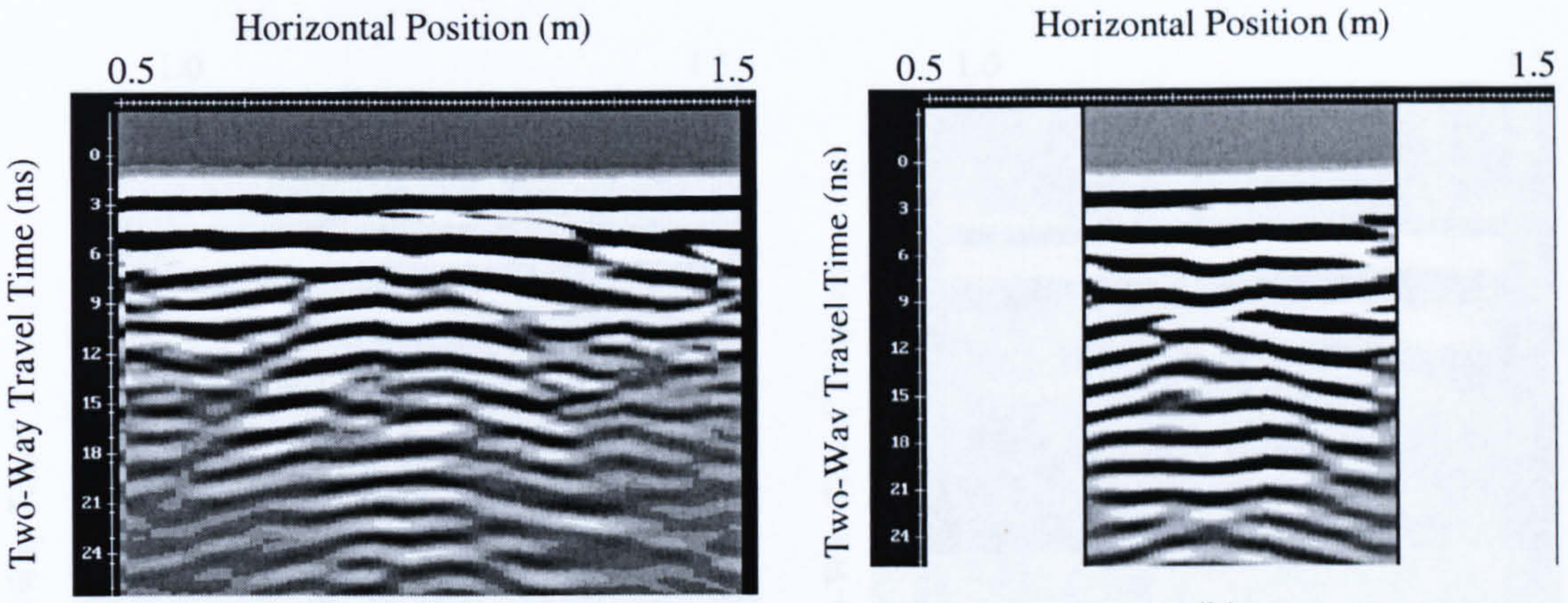

Figure 8.7: GPR transects for (a) before and (b) after water addition for E1. Acquired at 450 MHz. Constant gain of 5 applied. Data acquired only over x = 0.75-1.25 m for (b).

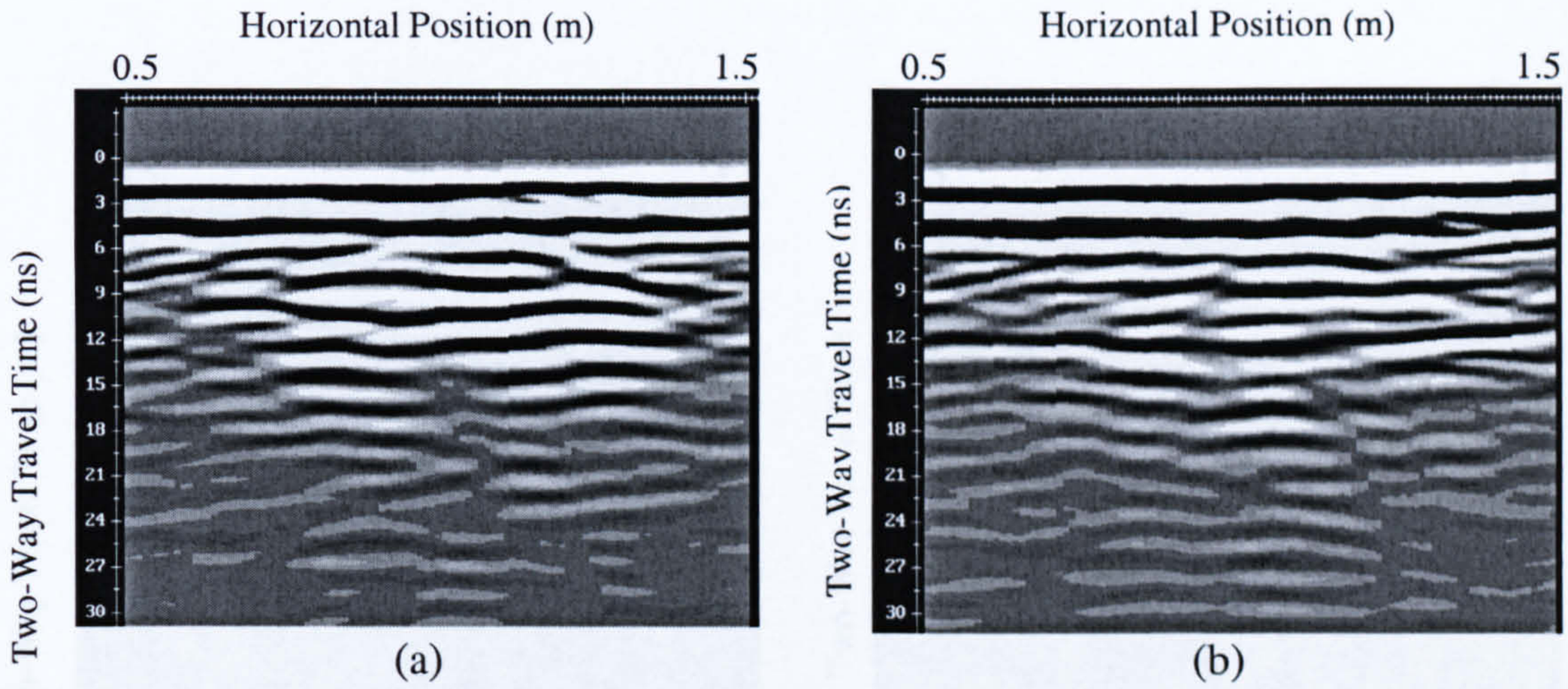

Figure 8.8: GPR transects for (a) before and (b) after water addition for E2. Acquired at 450 MHz. Constant gain of 5 applied.

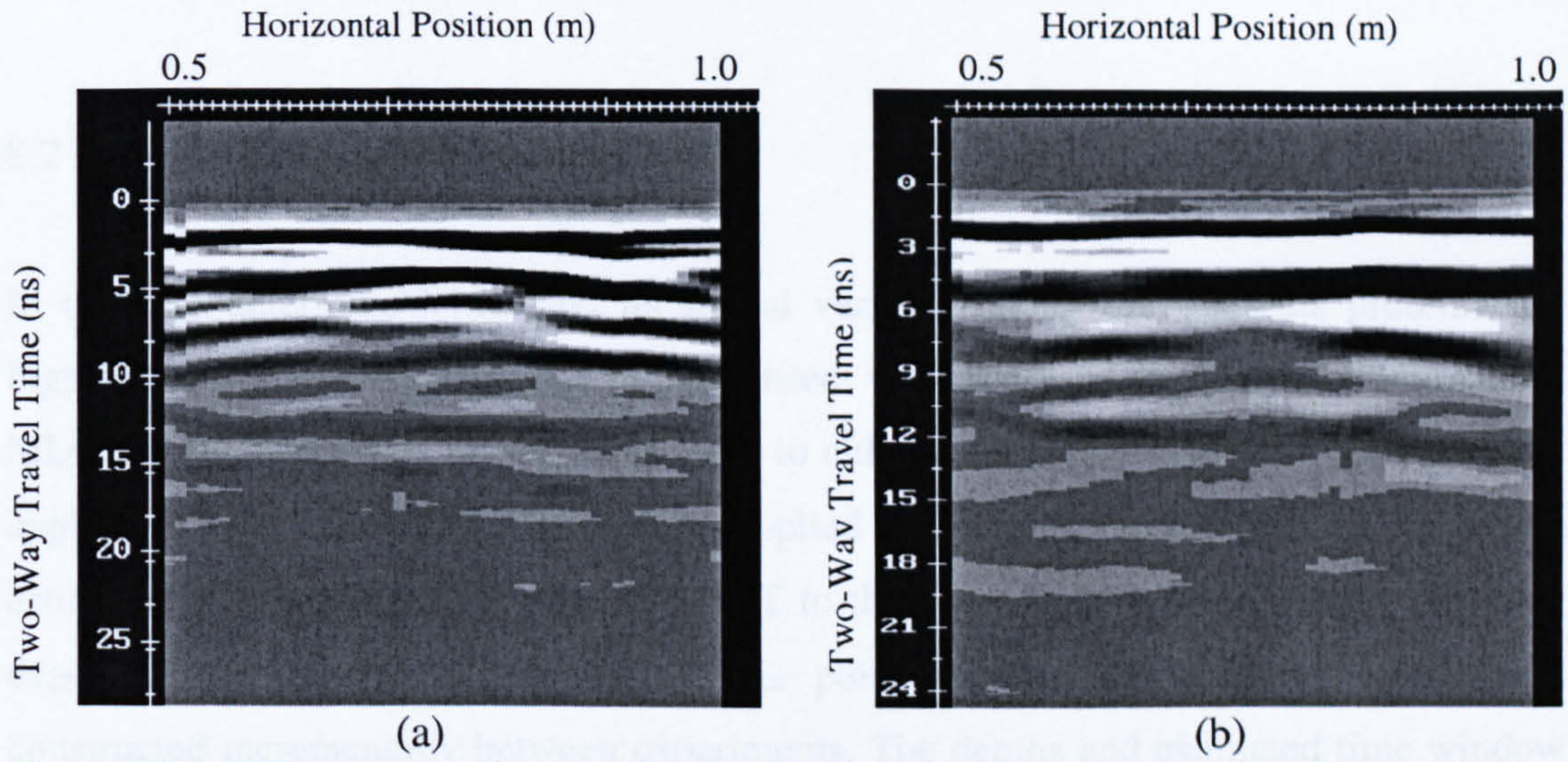

Figure 8.9: GPR transects for (a) before and (b) after water addition for E3. Acquired at 450 MHz. Constant gain of 5 applied.

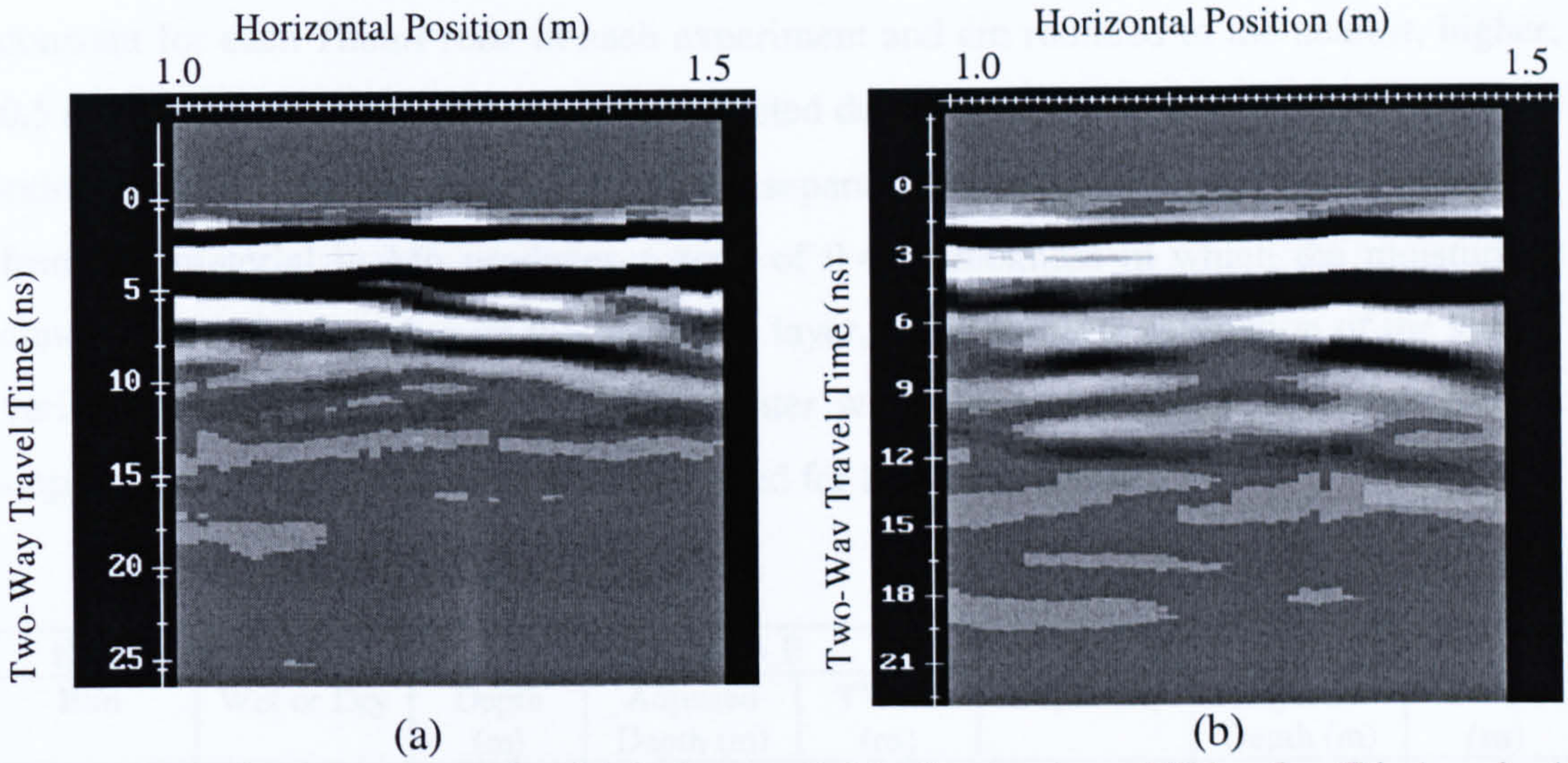

Figure 8.10: GPR transects for (a) before and (b) after water addition for E4. Acquired at 450 MHz. Constant gain of 5 applied.

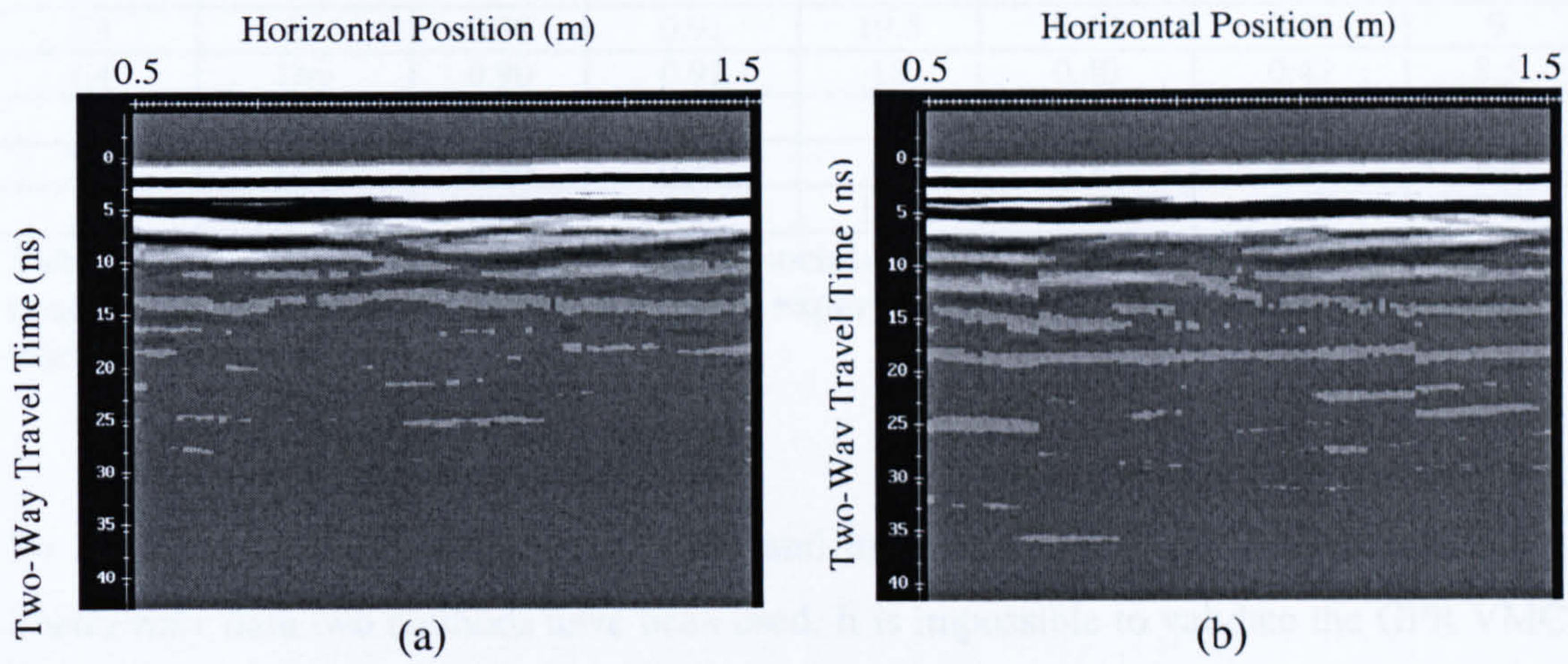

Figure 8.11: GPR transects for (a) before and (b) after water addition for E5. Acquired at 450 MHz. Constant gain of 5 applied.

8.2 ESTIMATING VMC VARIATION

In order to determine VMC and its spatial variation along the transects presented in Figures 8.2-8.11, each radar trace in the transect was processed to provide an estimate of MIA. This estimate was then used as input to either a GI or GII model. These data were applied to two scales of LTF wetting. Applied to the Full Profile (FULL), MIA was estimated from G_0 to an estimate of TWTT to the base of the LTF M5 layer. Different experiments had different depths to this point because the material profile was constructed incrementally between experiments. The depths and estimated time window are shown in Table 8.1. These time windows are based on the highest derived dielectric

constant for each *ThetaProbe* in each experiment and are rounded to the nearest, higher, 0.5 ns. They were calculated using the adjusted depth values, which take into account the extra distance travelled due to the antenna separation. For E3 to E5 the lack of drainage from the material in M6 produces a zone of 0.4 m thickness in which the moisture is concentrated. By focusing on this ACTIVE layer, more accurate estimation of the spatial variation of VMC is expected. For E5 water was added in a deeper layer but has no impact. Therefore, both scales are considered for this experiment.

Experiment Details		FULL SCALE			ACTIVE SCALE		
Run	Wet or Dry	Depth (m)	Adjusted Depth (m)	TWTT (ns)	Depth (m)	Adjusted Depth (m)	TWTT (ns)
E1	Dry	0.40	0.42	6	0.40	0.42	6
E1	Wet	0.40	0.42	7	0.40	0.42	7
E2	Dry	0.60	0.61	9	0.60	0.61	9
E2	Wet	0.60	0.61	9	0.60	0.61	9
E3	Dry	0.90	0.91	13.5	0.40	0.42	6.5
E3	Wet	0.90	0.91	19.5	0.40	0.42	9
E4	Dry	0.90	0.91	18	0.40	0.42	8.5
E4	Wet	0.90	0.91	19	0.40	0.42	9
E5	Dry	0.90	0.91	18	0.40	0.42	8.5
E5	Wet	0.90	0.91	18.5	0.40	0.42	8.5

Table 8.1: Depth of investigation and associated time window for the two scales of analysis (FULL and ACTIVE) for each experimental run. Adjusted depth considers antenna separation.

To compare the GPR estimates of VMC and its variation with the limited subsurface *ThetaProbe* data two methods have been used. It is impossible to validate the GPR VMC estimation at each trace location in the laboratory experiments because the *ThetaProbes* are larger than the sample spacing (0.04 m compared to 0.01 m) and it would require more *ThetaProbes* than could feasibly be used without substantially interfering with the hydrological conditions. For this reason *ThetaProbes* were concentrated around each leak site and at the centre of each material layer. For the VMC estimates, the accuracy of the GPR estimation is determined by comparing the average estimation of all traces at both scales with the average *ThetaProbe* estimations at these scales. Through this approach the ability of the GPR to estimate a spatial VMC average can be assessed. This approach has the advantage of compensating for differences in measurement volume between *ThetaProbe* (0.3 m^3) and GPR (unknown and variable). However, this approach makes no consideration of the actual spatial variation along a transect and therefore while the average value may be accurate, the actual point estimations may be wrong. The main focus of this research is to assess moisture distributions. To satisfy this aim, the actual

accuracy of the VMC estimation is less important than both the repeatability of the estimation and the relative variation in VMC estimates. To this end the variation is more important than the absolute VMC values, although consideration of the potential error in the distribution as a consequence of poor estimates of the VMC must always be made. To assess moisture distribution and variation the CV of GPR response is compared with the CV of the *ThetaProbe* moisture estimation.

8.2.1 GPR VMC estimation for E1 to E5.

Table 8.2 compares the predicted and observed VMC data for E1 to E5 at both scales and both frequencies using the time window data in Table 8.1. The GI equation was used for E1 and E2 and the GII equation was used for E3-E5, based on the materials involved (Table 5.6). The results show that all predictions are overestimated compared to the observed data. This overestimation, which at its greatest is 0.26 m^3/m^3 for FULL and 0.17 m^3/m^3 for ACTIVE, is greater than in the model testing. FULL predictions are clearly greater than ACTIVE predictions for E3-E5; being on average 0.087 m^3/m^3 greater for 900 MHz and 0.085 m^3/m^3 for 450 MHz. This is due to the increased amount of low magnitude instantaneous amplitude data involved in the calculation at this scale. The equality in over estimation at FULL compared to ACTIVE for both wet and dry indicates a consistent improvement in estimation using ACTIVE for both frequencies. It also demonstrates the benefit of correctly targeting the volume in which the moisture occurs. The improved estimation for the ACTIVE layer may be because the water was added in this layer. This demonstrates that applying the relationship to the correct depth of investigation is critical to VMC estimation because applying the model to too great a depth, or too long a time window causes over-prediction. This occurs because amplitude values decrease with signal propagation time. If the relationship is to be applied at greater depths, then some way of accounting for this effect needs to be introduced.

Estimation error is generally greater for dry conditions compared to wet conditions. This can be explained by the fact that the original relationships developed in Chapter Seven excluded dry and saturated data. Comparing the dry and wet estimation error in Table 8.2, it is apparent that the mean error for E1-E5 dry is 0.0236 m^3/m^3 greater than wet for 900 MHz Full (dry mean = 0.1905 m^3/m^3; wet mean = 0.1682 m^3/m^3); 0.0334 m^3/m^3 greater than wet for 900 MHz Active (dry mean = 0.1425 m^3/m^3; wet mean = 0.1113 m^3/m^3);

0.0193 m^3/m^3 greater than wet for 450 MHz Full (dry mean = 0.1317 m^3/m^3; wet mean = 0.1136 m^3/m^3); and 0.0323 m^3/m^3 greater than wet for 450 MHz Active (dry mean = 0.0868 m^3/m^3; wet mean = 0.0559 m^3/m^3). This error is relatively small compared to the actual error for the predictions and other sources of error clearly exist.

Error in 450 MHz estimation (Full = 0.1226 m^3/m^3; Active 0.0714 m^3/m^3) is generally less than error in 900 MHz estimation (Full = 0.1793 m^3/m^3; Active 0.1269 m^3/m^3) at both scales. For E3 and E4 the estimations of VMC are better if 450 MHz antennae are used but the estimations are still too large. It is likely that the broader wavelets for the lower frequency result in a greater MIA due to a broader envelope of higher magnitude. The increased value of MIA produces lower VMC estimations. For E5 the 900 MHz results are better than the 450 MHz results for the ACTIVE layer. For 450 MHz, ACTIVE VMCs are underestimated by a maximum of 0.059 m^3/m^3. This indicates the need for accommodating frequency differences in a more complex model.

Generally, the error for E5 is the smallest of all the experiments. At the ACTIVE scale VMC estimation is especially accurate, being well within the range of the Chapter Seven model test errors. The fact that the prediction is accurate for E5 implies that there is something different between this experiment and E1-E4. The magnitude of error suggests that the developed models are very situation specific and will therefore only be applicable for similar experimental conditions to those used in the STF experiments. If this is so then the technique is inappropriate for moisture estimation and should be abandoned in favour of a more reliable technique. However, it is possible that there are reasons for the prediction error. These may be related to the equations themselves, or the experiments, or other specific issues that were not detectable using the small-scale STF investigations. Errors in the average VMC estimation may reflect errors in spatial variation estimation. Therefore, before investigating the potential causes of this error, the spatial patterns and estimation of variation will be presented.

EXPERIMENT DETAILS			FULL PROFILE VMC (m^3/m^3)			ACTIVE LAYER VMC (m^3/m^3)		
Run	Wet or Dry	Frequency (MHz)	Observed	Predicted	Difference	Observed	Predicted	Difference
E1	Dry	900	0.0092	0.1240	-0.1148	0.0092	0.1240	-0.1148
	Wet	900	0.0294	0.1184	-0.0890	0.0294	0.1184	-0.0890
E2	Dry	900	0.0136	0.2754	-0.2618	0.0136	0.2754	-0.2618
	Wet	900	0.0136	0.2385	-0.2249	0.0136	0.2385	-0.2249
E3	Dry	900	0.0268	0.2316	-0.2048	0.0317	0.1748	-0.1431
	Wet	900	0.0852	0.2719	-0.1867	0.1392	0.2379	-0.0987
E4	Dry	900	0.0389	0.2590	-0.2201	0.0429	0.2100	-0.1671
	Wet	900	0.0812	0.2672	-0.1860	0.1159	0.2284	-0.1125
E5	Dry	900	0.0709	0.2218	-0.1509	0.1071	0.1328	-0.0257
	Wet	900	0.0718	0.2260	-0.1542	0.1066	0.1378	-0.0312
E1	Dry	450	0.0092	0.0804	-0.0712	0.0092	0.0804	-0.0712
	Wet	450	0.0244	0.0542	-0.0298	0.0244	0.0542	-0.0298
E2	Dry	450	0.0135	0.1721	-0.1585	0.0135	0.1721	-0.1585
	Wet	450	0.0138	0.1573	-0.1435	0.0138	0.1573	-0.1435
E3	Dry	450	0.0300	0.1834	-0.1534	0.0319	0.1022	-0.0703
	Wet	450	0.0817	0.2360	-0.1543	0.1361	0.1712	-0.0351
E4	Dry	450	0.0390	0.2099	-0.1710	0.0437	0.1184	-0.0747
	Wet	450	0.0786	0.2123	-0.1337	0.1116	0.1202	-0.0085
E5	Dry	450	0.0708	0.1751	-0.1043	0.1070	0.0478	0.0592
	Wet	450	0.0710	0.1774	-0.1064	0.1065	0.0437	0.0628

Table 8.2: Comparison of observed (*ThetaProbe*) and predicted (GPR) average VMCs for each experiment (E1-E5) at both antenna frequencies.

8.2.2 Spatial distribution and variation of moisture

Having established the degree of error in average profile VMC estimation using the GPR it is necessary to investigate the ability to assess spatial variability along the transects and how this relates to the hydrological data. This is vital for the final parts of this research in which spatial estimations will be used to establish subsurface moisture conditions for the detection of water leaks and hillslope hydrology. Figures 8.12 to 8.23 show the before and after leak VMC estimations for E1-E5 for the FULL profile and ACTIVE layer at two antenna frequencies, 900 MHz and 450 MHz. For E5 the results include a brick pavement, which was added to simulate conditions more representative of an urban water leak. The continuous line on each figure illustrates the difference between wet and dry VMC estimates and can be used to identify regions of maximum change. These are most likely to be the result of water leaked into the subsurface. The variation in Figures 8.12 to 8.23 is quantified using the CV, which is outlined along with the mean and standard deviation for each run at both scales and frequencies in Table 8.3.

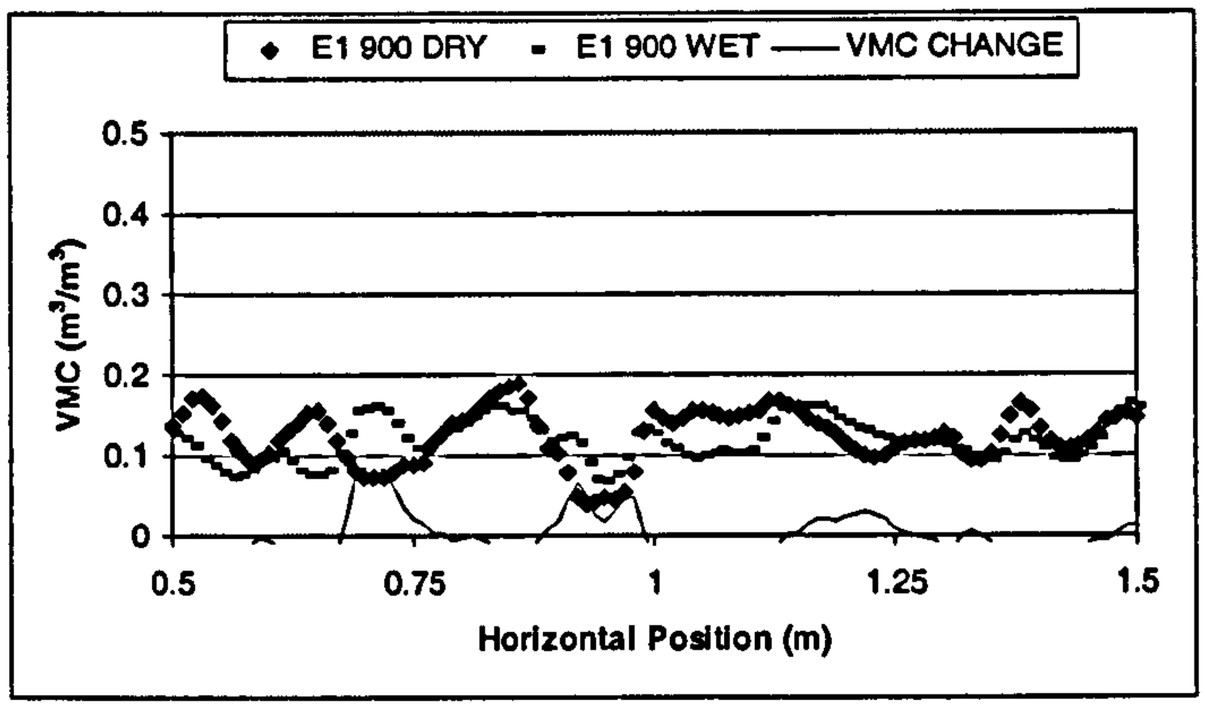

Figure 8.12: Predicted VMC at 900 MHz for the FULL profile for E1 before (dry) and after (wet) addition of water (at x = 1.0 m). Continuous line shows the difference in estimated VMC between the before and after conditions.

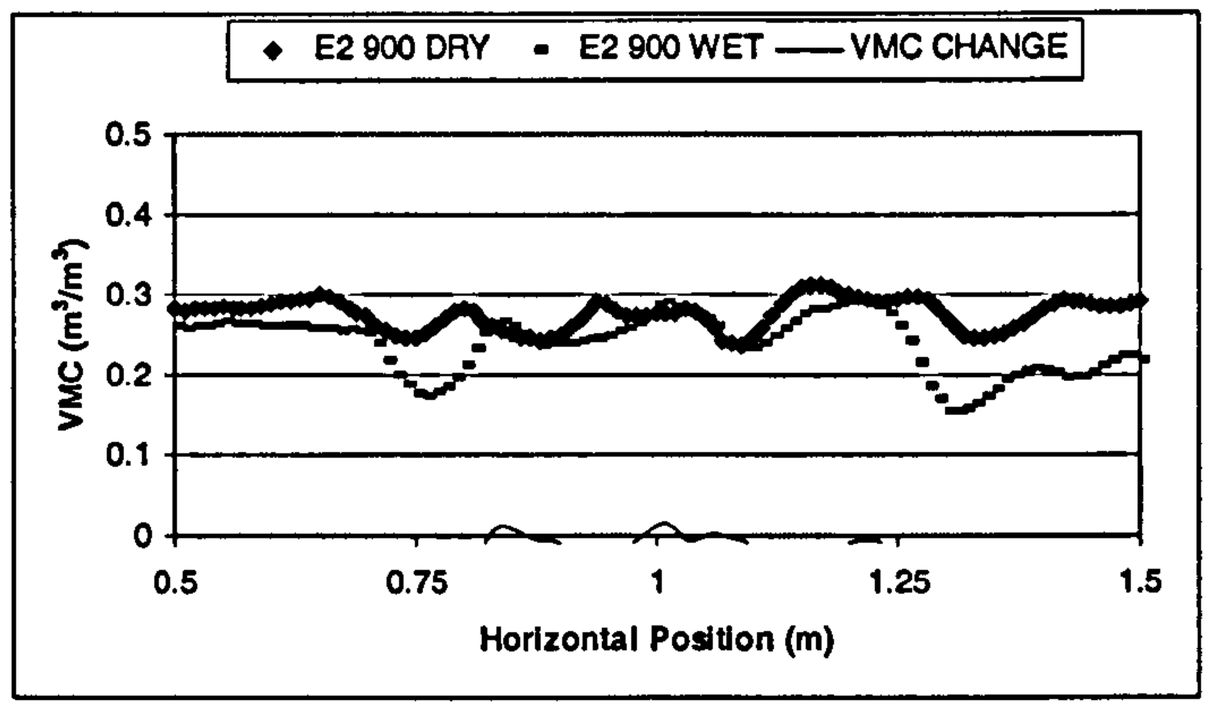

Figure 8.13: Predicted VMC at 900 MHz for the FULL profile for E2 before (dry) and after (wet) addition of water (at x = 1.0 m). Continuous line shows the difference in estimated VMC between the before and after conditions.

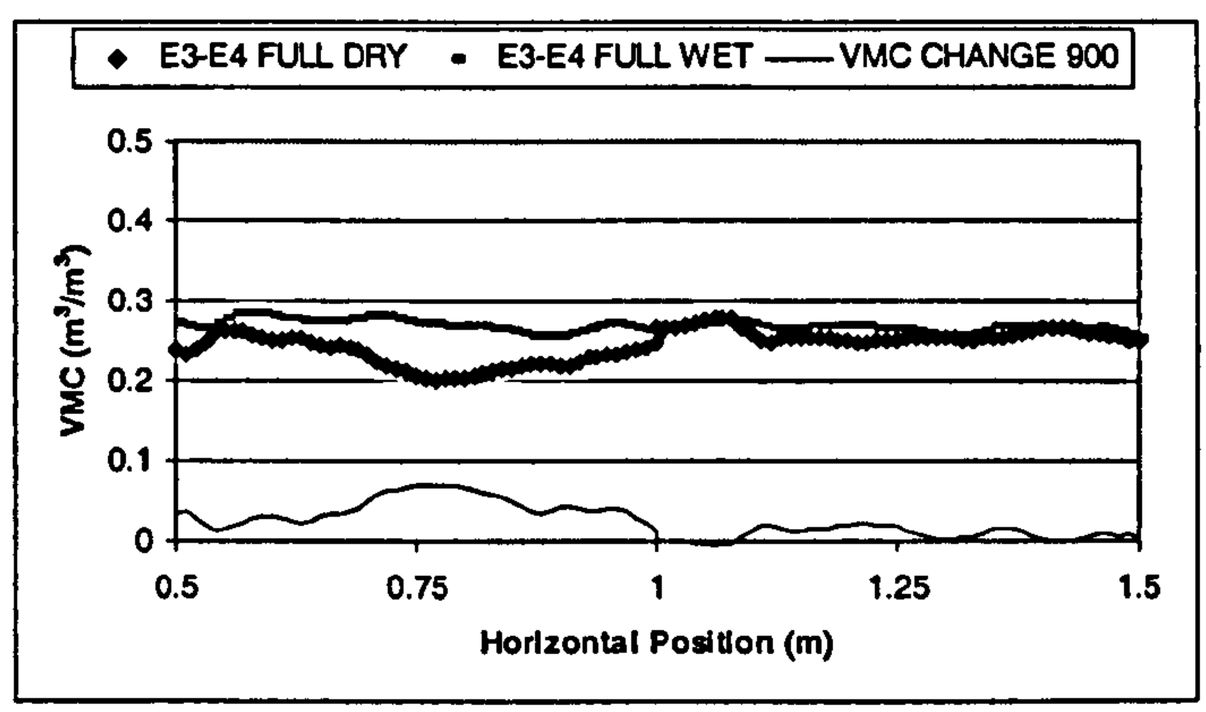

Figure 8.14: Predicted VMC at 900 MHz for the FULL (M6) profile for E3 (0.5-1.0 m) and E4 (1.0-1.5 m) before (dry) and after (wet) water addition (E3 at x = 0.75, E4 at x = 1.25, both at z = 0.2). Continuous line shows the difference in estimated VMC between the before and after conditions.

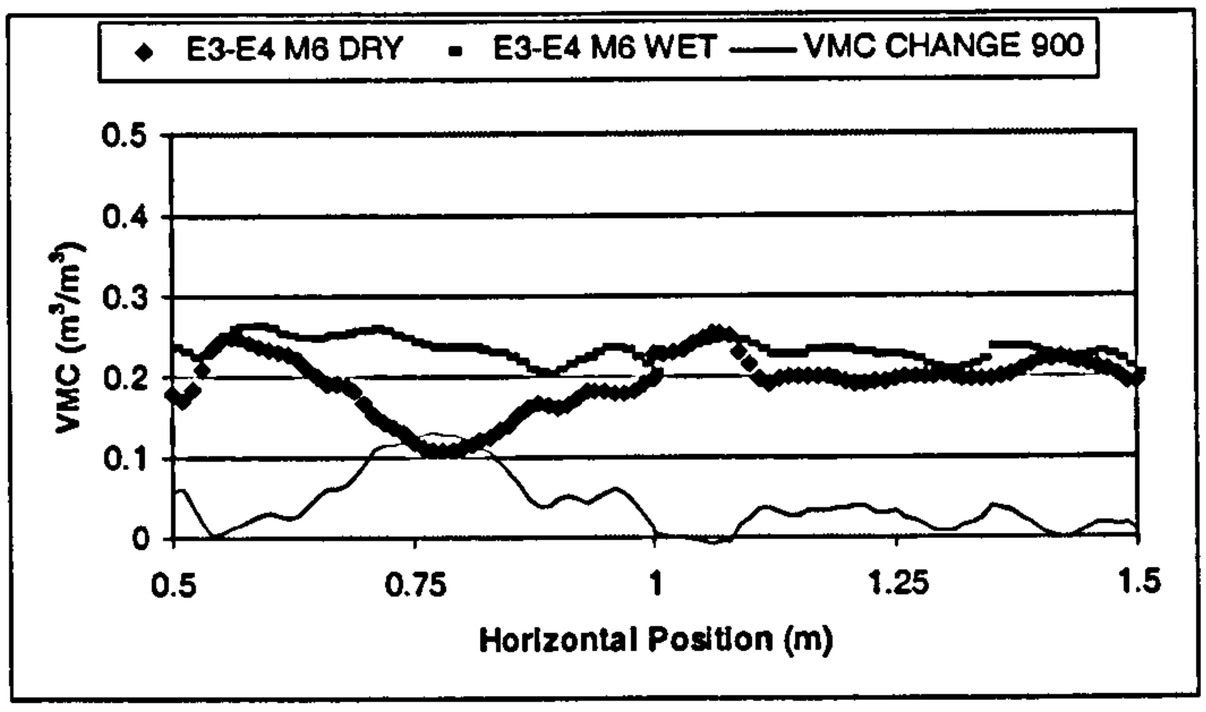

Figure 8.15: Predicted VMC at 900 MHz for the ACTIVE (M6) profile for E3 (0.5-1.0 m) and E4 (1.0-1.5 m) before (dry) and after (wet) water addition (E3 at x = 0.75, E4 at x = 1.25, both at z = 0.2). Continuous line shows the difference in estimated VMC between the before and after conditions.

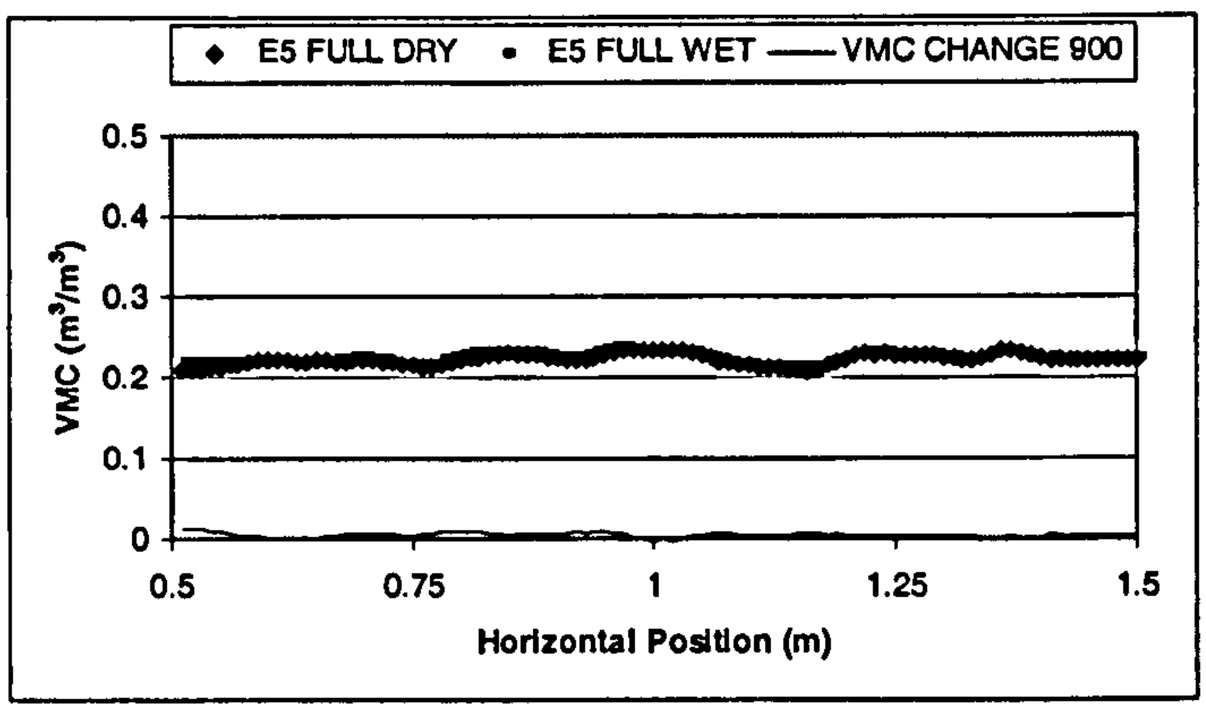

Figure 8.16: Predicted VMC at 900 MHz for the FULL (M6) profile for E5 before (dry) and after (wet) addition of water (at x = 1.0 m). Continuous line shows the difference in estimated VMC between the before and after conditions.

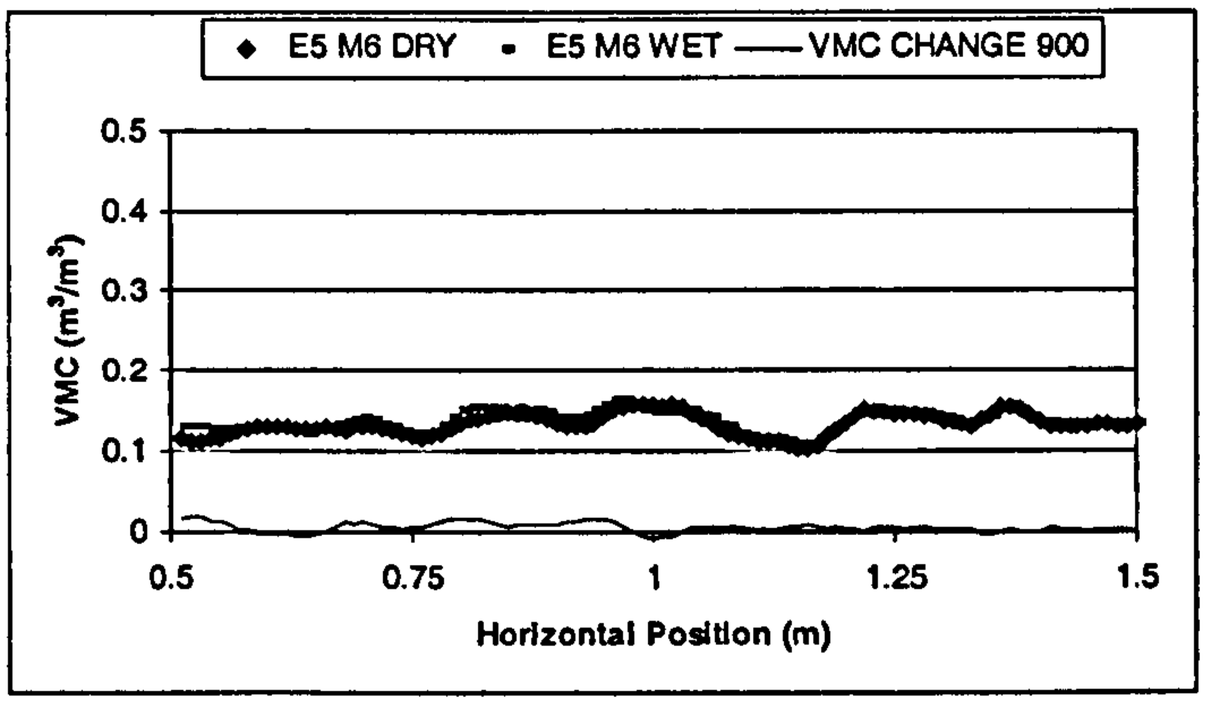

Figure 8.17: Predicted VMC at 900 MHz for the ACTIVE (M6) profile for E5 before (dry) and after (wet) addition of water (at x = 1.0 m). Continuous line shows the difference in estimated VMC between the before and after conditions.

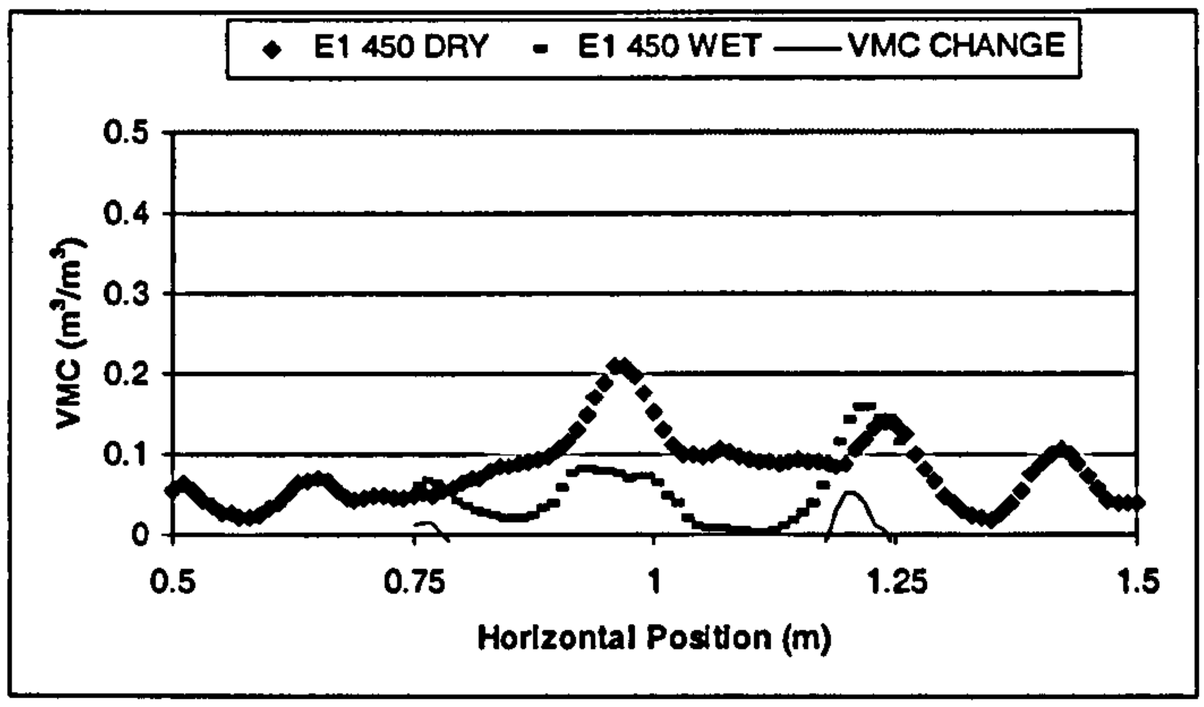

Figure 8.18: Predicted VMC at 450 MHz for the FULL profile for E1 before (dry) and after (wet) addition of water. Continuous line shows the difference in estimated VMC between the before and after conditions.

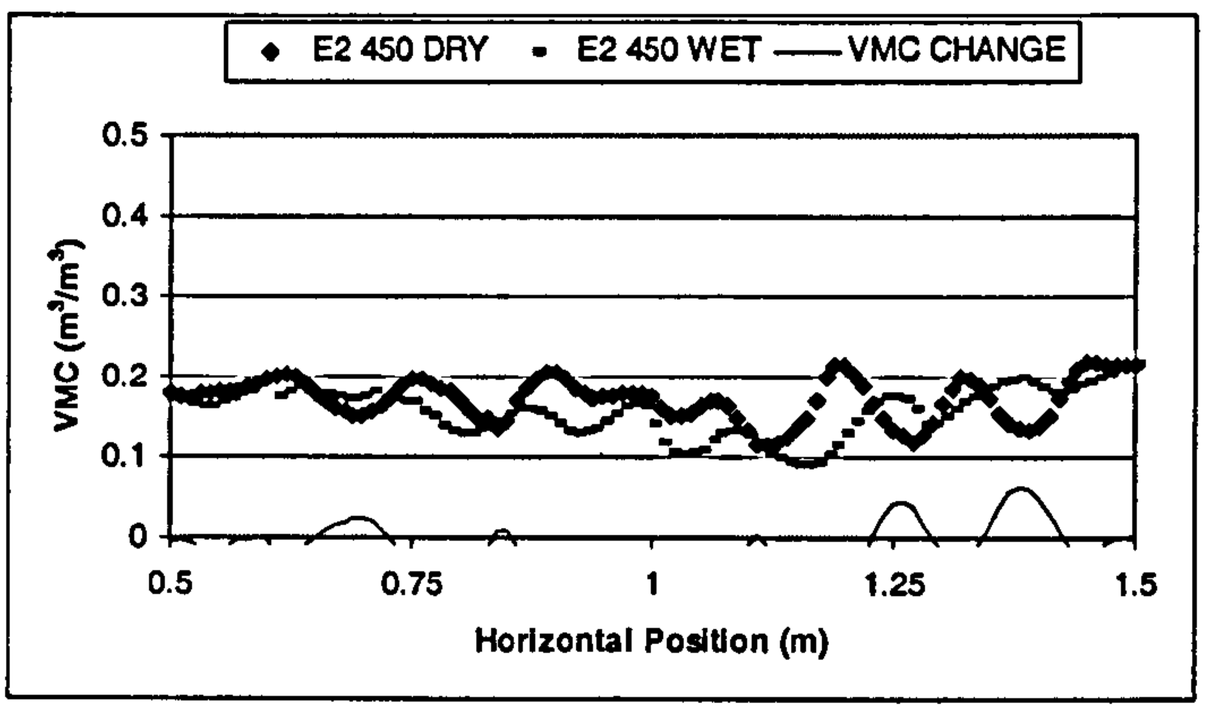

Figure 8.19: Predicted VMC at 450 MHz for the FULL profile for E2 before (dry) and after (wet) addition of water (at x = 1.0 m). Continuous line shows the difference in estimated VMC between the before and after conditions.

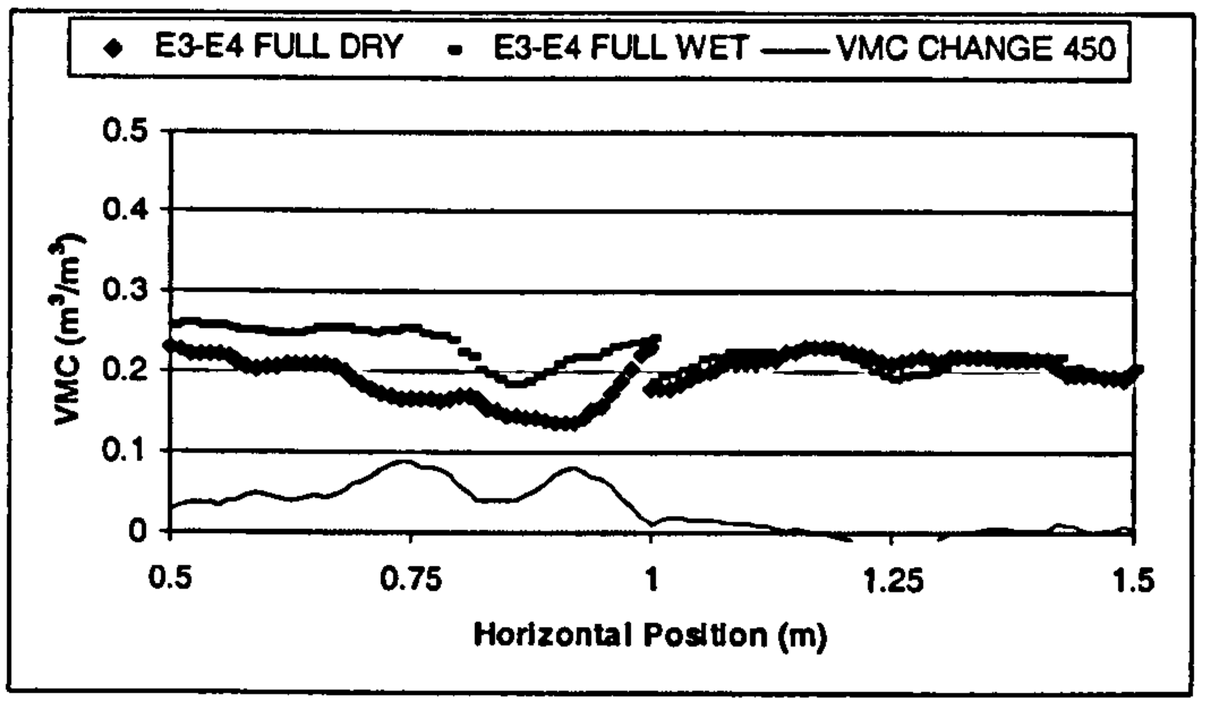

Figure 8.20: Predicted VMC at 450 MHz for the FULL profile for E3 (0.5-1.0 m) and E4 (1.0-1.5 m) before (dry) and after (wet) water addition (E3 at x = 0.75, E4 at x = 1.25, both at z = 0.2). Continuous line shows the difference in estimated VMC between the before and after conditions.

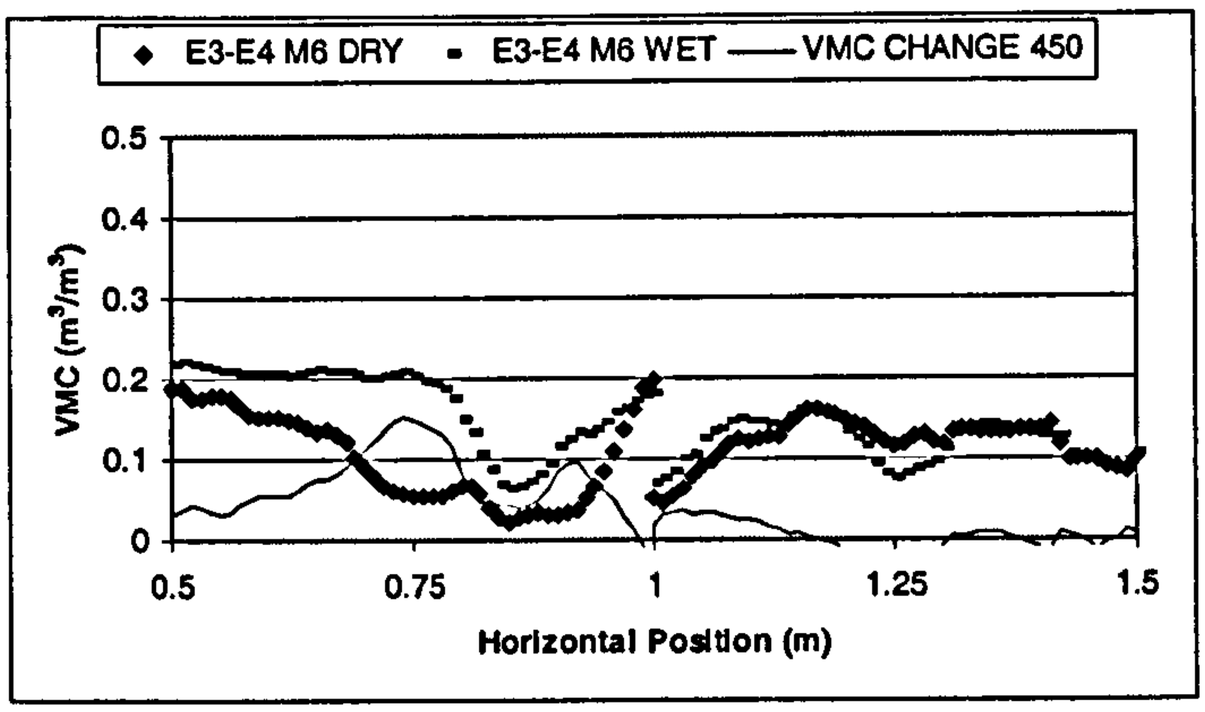

Figure 8.21: Predicted VMC at 450 MHz for the ACTIVE (M6) profile for E3 (0.5-1.0 m) and E4 (1.0-1.5 m) before (dry) and after (wet) water addition (E3 at x = 0.75, E4 at x = 1.25, both at z = 0.2). Continuous line shows the difference in estimated VMC between the before and after conditions.

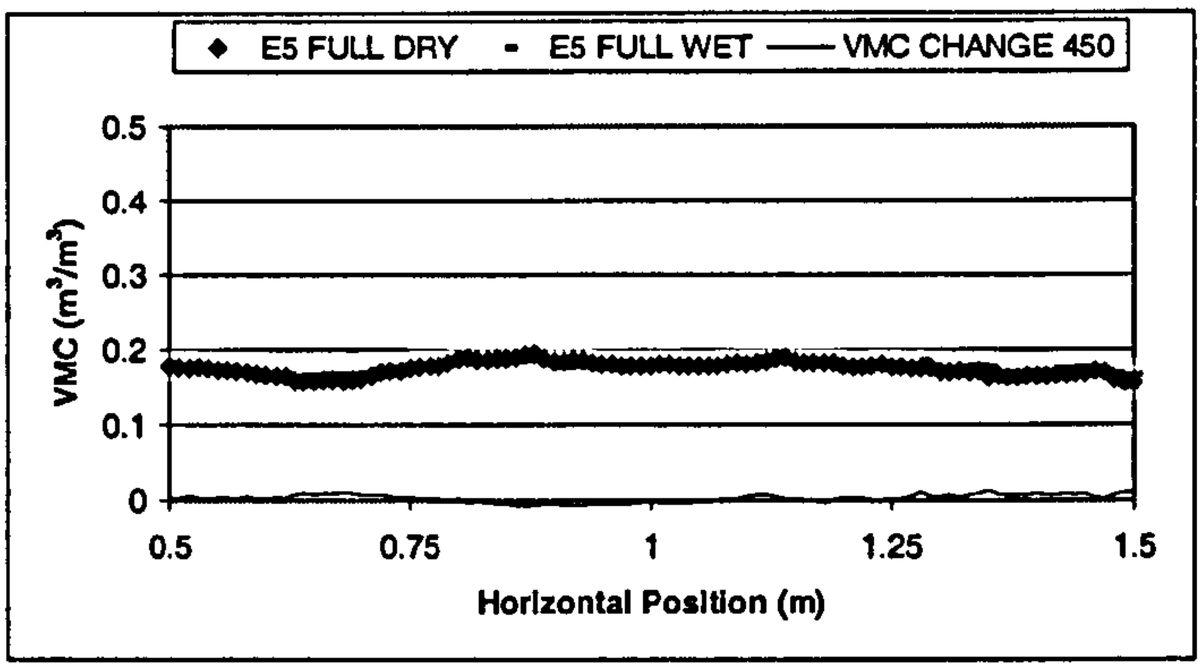

Figure 8.22: Predicted VMC at 450 MHz for the FULL profile for E5 before (dry) and after (wet) addition of water (at x = 1.0 m). Continuous line shows the difference in estimated VMC between the before and after conditions.

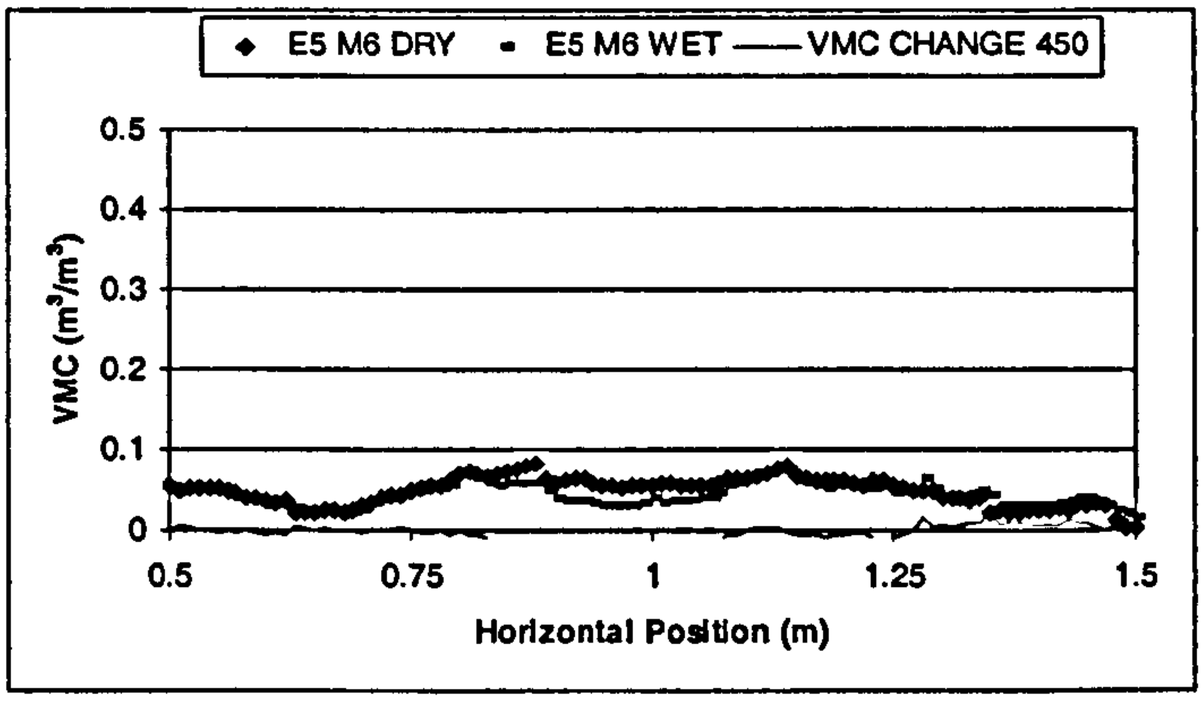

Figure 8.23: Predicted VMC at 450 MHz for the ACTIVE (M6) profile for E5 before (dry) and after (wet) addition of water (at x = 1.0 m). Continuous line shows the difference in estimated VMC between the before and after conditions.

There are a number of important characteristics of these figures. There is a great deal of variation in wet and dry responses along the transects for E1 and E2. Furthermore, there is no consistent pattern of increased VMC in the wet runs compared to the dry runs. Whilst for E1, the wet run seems less varied than the dry run, the opposite is true for E2. In E2 there appears to be a general decrease in estimated VMC. There is a suggestion of increased VMC at the centre of the profile that corresponds to a slight local rise in VMC at this location after moisture was added. There is great similarity between wet and dry results for E4, although VMC does rise in the M6 layer. This increase in VMC appears to be less than in the moisture distributions (Figure 8.1). Conversely, in E3 there is a significant rise in VMC over the zone of added water, although the VMC values at the edge are consistent between wet and dry runs. This result suggests that a high moisture content existed in these areas before any moisture was added. The added water acts to flatten the predicted moisture distribution rather than increase VMC above the background. The addition of moisture appears to reduce subsurface variation; an observation supported by the GPR imagery. This suggests that there is some source of disturbance identifiable on the dry GPR data, which produces interference in the GPR signal, especially on E3. This may result in the patterns of VMC being falsely represented by the GPR.

Moisture distributions appear much smoother at the FULL scale compared to the ACTIVE scale. This can be explained by the greater amount of lower magnitude instantaneous amplitude values used to estimate MIA as a consequence of greater signal attenuation with depth. Thus it is clearly important to define the measurement depth because there is a large impact on the moisture distribution. If only the ACTIVE layer is used the moisture distribution is maintained for all experiments but the estimated VMCs are reduced. Furthermore, the relative magnitudes become more extreme. This has the effect of increasing the coefficient of variation compared to the full profile. It suggests that for the detection of moisture variability, the depth of investigation is less important for moisture distribution than it is for quantitative VMC estimation. The E5 data also demonstrate the smoothing of moisture distributions that occurs as a result of using a larger time window for the analysis. At the FULL scale no observable differences between the wet and dry transects occur. At the ACTIVE scale, which uses a shorter time window, there appears to be greater fluctuation in VMC along the transects compared with the FULL scale. In addition, there are small increases in VMC identifiable at the ACTIVE scale. For E5, there is little difference in the estimates, which produces similar

wet and dry coefficients of variation. Effectively, therefore, using the FULL data smoothes out the moisture variation, whilst focusing in on the zone in which the moisture body occurs identifies moisture differences more reliably. This confirms the suggestion made in Chapter Seven that using a constant time window will smooth the moisture distribution; especially if the constant time window is too long.

EXPERIMENT DETAILS			FULL PROFILE VMC (m^3/m^3)			ACTIVE LAYER VMC (m^3/m^3)		
Run	Wet or Dry	Frequency (MHz)	Mean	Standard Deviation	CV	Mean	Standard Deviation	CV
E1	Dry	900	0.1240	0.0337	0.2722	0.1240	0.0337	0.2722
	Wet	900	0.1184	0.0255	0.2155	0.1184	0.0255	0.2155
E2	Dry	900	0.2754	0.0190	0.0690	0.2754	0.0190	0.0690
	Wet	900	0.2385	0.0359	0.1504	0.2385	0.0359	0.1504
E3	Dry	900	0.2316	0.0188	0.0813	0.1748	0.0413	0.2365
	Wet	900	0.2719	0.0076	0.0281	0.2379	0.0169	0.0711
E4	Dry	900	0.2590	0.0085	0.0329	0.2100	0.0177	0.0845
	Wet	900	0.2672	0.0049	0.0182	0.2284	0.0099	0.0433
E5	Dry	900	0.2218	0.0066	0.0299	0.1328	0.0134	0.1007
	Wet	900	0.2260	0.0059	0.0260	0.1378	0.0126	0.0915
E1	Dry	450	0.0804	0.0424	0.5280	0.0804	0.0424	0.5280
	Wet	450	0.0542	0.0430	0.7936	0.0542	0.0430	0.7936
E2	Dry	450	0.1721	0.0262	0.1523	0.1721	0.0262	0.1523
	Wet	450	0.1573	0.0304	0.1932	0.1573	0.0304	0.1932
E3	Dry	450	0.1834	0.0301	0.1639	0.1022	0.0568	0.5554
	Wet	450	0.2360	0.0230	0.0974	0.1712	0.0486	0.2838
E4	Dry	450	0.2099	0.0135	0.0642	0.1184	0.0276	0.2331
	Wet	450	0.2123	0.0125	0.0591	0.1202	0.0264	0.2195
E5	Dry	450	0.1751	0.0092	0.0524	0.0478	0.0176	0.3682
	Wet	450	0.1774	0.0060	0.0340	0.0437	0.0134	0.3076

Table 8.3: Variability in GPR VMC estimations (mean, standard deviation, CV) for all experiments (E1-E5), at both scales (FULL and ACTIVE), and both frequencies (900 and 450 MHz).

Not only does using 450 MHz produce lower VMC estimates than 900 MHz, but it produces fundamentally different moisture distributions. These distributions appear to consist of greater fluctuation than the 900 MHz data, a feature confirmed by the greater CVs for each experiment when focusing on the ACTIVE layer. It is possible that reduced signal attenuation at lower frequencies results in the preservation of signal variability at 450 MHz. With the exceptions of E1 and E2, wet variation is reduced compared to dry variation. This suggests that there is a consistent effect of moisture on signal attenuation at different frequencies. The differences in variation are particularly large for E3 but are relatively small for E4 and E5. This occurs because the actual VMC differences are less (Figures 8.18 to 8.23).

To summarise, the addition of moisture acts to reduce the apparent variation in the subsurface. Focusing in on the zone of moisture increases the variation compared to using the FULL zone. This occurs because the variation associated with the VMC changes is considered more accurately. However, Figure 8.24 shows that the CVs for the GPR data are lower than for the *ThetaProbe* data. For the *ThetaProbe* data, the data are consistent between experimental runs. However, the GPR results only approximately follow the pattern results for 450 MHz being particularly poor. This suggests that there are a number of sources of error in the VMC estimations using the technique developed and that these inaccuracies feed back into the spatial pattern. These issues will now be discussed.

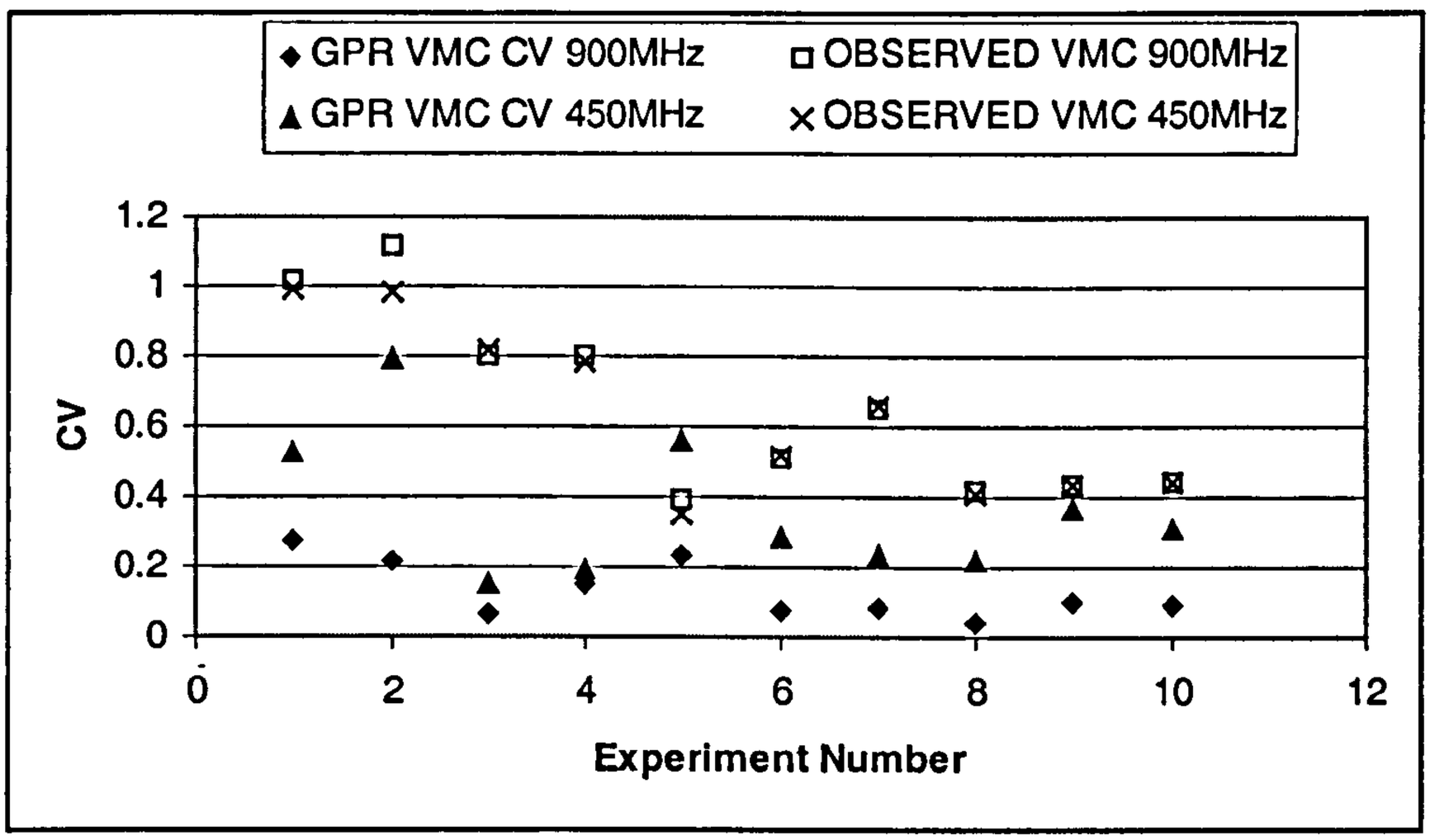

Figure 8.24: Comparison of GPR estimations of moisture variation with observed *ThetaProbe* estimates of variation for all experiments at both antenna frequencies. Experiment numbers refer to (1) E1 dry, (2) E1 wet, (3) E2 dry, (4) E2 wet, (5) E3 dry, (6) E3 wet, (7) E4 dry, (8) E4 wet, (9) E5 dry, (10) E5 wet.

8.3 ERROR IN SPATIAL VMC ESTIMATION

The sources of error, and the approaches to accommodating them, may potentially impact upon the nature of the spatial distributions derived using the GPR. There is significant variation in VMC estimation between experiments. Particularly implausible are VMC estimates of greater than 0.25 m^3/m^3 for dry experiments and the significantly drier estimates for E5 and 450MHz experiments. Uncertainty also exists in the patterns of moisture distribution derived using GPR. In the following sections, potential causes of this error are identified and considered. Through this approach it may be possible to accommodate these limitations in the future application of the models and thereby expand

the potential range of application of the model. Having established the potential effects on model accuracy, and attempting to account for these effects, the spatial variation of the subsurface moisture will then be reconsidered.

8.3.1 The form of relationship

Results of the analysis of VMC estimation using the original non-linear functional forms (Table 7.8) for E3-E5 were presented previously in Charlton and Mulligan (2001) and are summarised here in Table 8.4. For the full material profile the E3 and E4 900 MHz GPR VMC estimates exceed the observed *ThetaProbe* VMC by up to 0.322m^3/m^3, while this overestimation is significantly less for E5 (maximum 0.173 m^3/m^3). Prediction of VMC is improved if only the ACTIVE layer is considered, although estimations are still overpredicted by a maximum of 0.178 m^3/m^3 for E3 and E4. For E5 this over-prediction is reduced to only 0.011 m^3/m^3. The fact that the relationship is a non-linear function means that errors in MIA estimation may have substantial impacts on the resulting estimates. In particular this may produce extreme over- or underestimation and at the same time may produce distortions in the spatial estimates. This is shown in Figures 8.25 and 8.26, which indicate greater variation in VMC estimations using the ACTIVE scale for both E3 and E4 at 900MHz. This is confirmed by increases in the CV. The application of a particular model to a given area may produce poor results that go undetected if a model of different function is required due to differences in material properties and subsurface moisture behaviour. Thus for accurate VMC estimation using GPR there is a need for site-specific calibration until more is known about the relationship between MIA and VMC.

The functional form of the predictive relationship should not affect VMC estimations because the GI and GII equations are linear. However, the model parameters are different. Changing the constant changes only the absolute VMC value and therefore the pattern of VMC is preserved, although this will be sensitive to the actual returned MIA values. In contrast, the slope may change the distribution pattern. To investigate this effect, the GI equation was applied to the E3 ACTIVE MIA results (Table 8.2 and Figure 8.15). By subtracting the GII VMC estimations derived using the correct equation from the GI estimations, the magnitude of pattern disturbance can be determined for both wet and dry conditions. Both lines (Figure 8.27) are very flat demonstrating that there is limited difference in pattern when using either of the equations. The maximum VMC difference

is 0.021 m^3/m^3 for dry and 0.009 m^3/m^3 when wet. This indicates that although the differences are small and the GPR patterns are reliable, the drier the moisture condition the more sensitive the GPR pattern is to the increased variation in distributions at lower VMCs.

EXPERIMENT DETAILS			FULL PROFILE VMC (m^3/m^3)			ACTIVE LAYER VMC (m^3/m^3)		
Run	Wet or Dry	Frequency (MHz)	Observed	Predicted	Difference	Observed	Predicted	Difference
E3	Dry	900	0.027	0.267	-0.24	0.032	0.158	-0.126
	Wet	900	0.085	0.407	-0.322	0.139	0.317	-0.178
E4	Dry	900	0.039	0.322	-0.283	0.043	0.19	-0.147
	Wet	900	0.081	0.384	-0.303	0.116	0.268	-0.152
E5	Dry	900	0.071	0.237	-0.166	0.107	0.113	-0.006
	Wet	900	0.071	0.244	-0.173	0.107	0.118	-0.011
E3	Dry	450	0.03	0.161	-0.131	0.032	0.07	-0.038
	Wet	450	0.082	0.274	-0.192	0.136	0.178	-0.042
E4	Dry	450	0.039	0.171	-0.132	0.044	0.074	-0.03
	Wet	450	0.079	0.202	-0.123	0.112	0.086	0.026
E5	Dry	450	0.071	0.14	-0.069	0.107	0.051	0.056
	Wet	450	0.072	0.138	-0.066	0.107	0.048	0.059

Table 8.4: Comparison of observed (*ThetaProbe*) and predicted (GPR) average VMCs for each experiment (E1-E5) at 900 MHz, using original non-linear relationships (see Table 7.8).

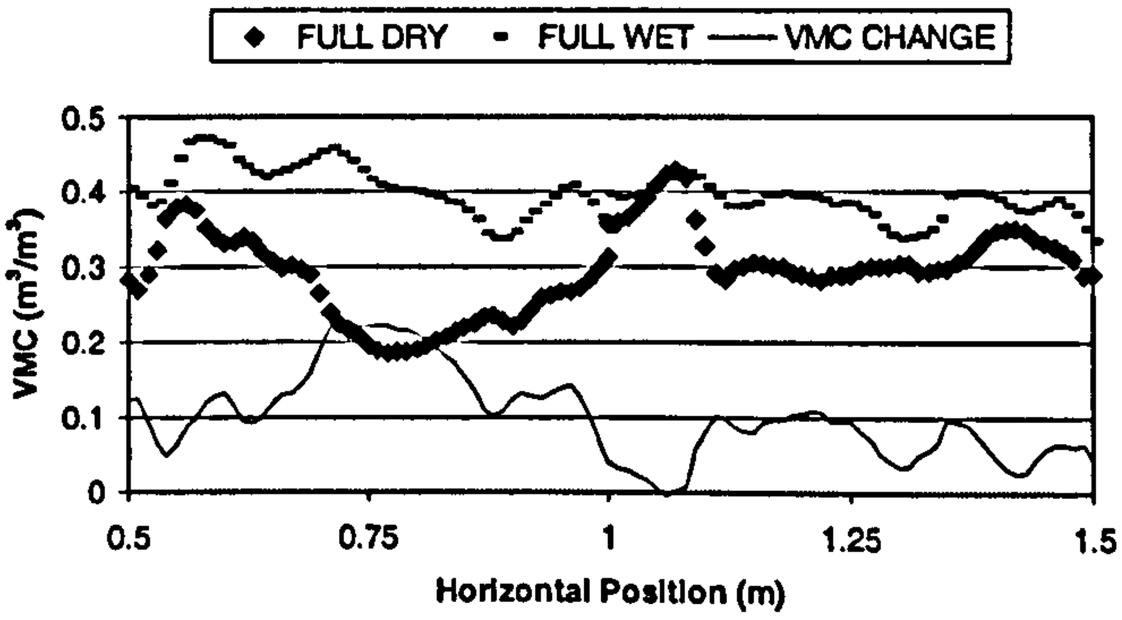

Figure 8.25: Predicted VMC at 900 MHz for the FULL profile for E3 (0.5-1.0 m) and E4 (1.0-1.5 m) before (dry) and after (wet) water addition (E3 at x = 0.75, E4 at x = 1.25, both at z = 0.2) using the original non-linear relationships. Continuous line shows the difference in estimated VMC between the before and after conditions.

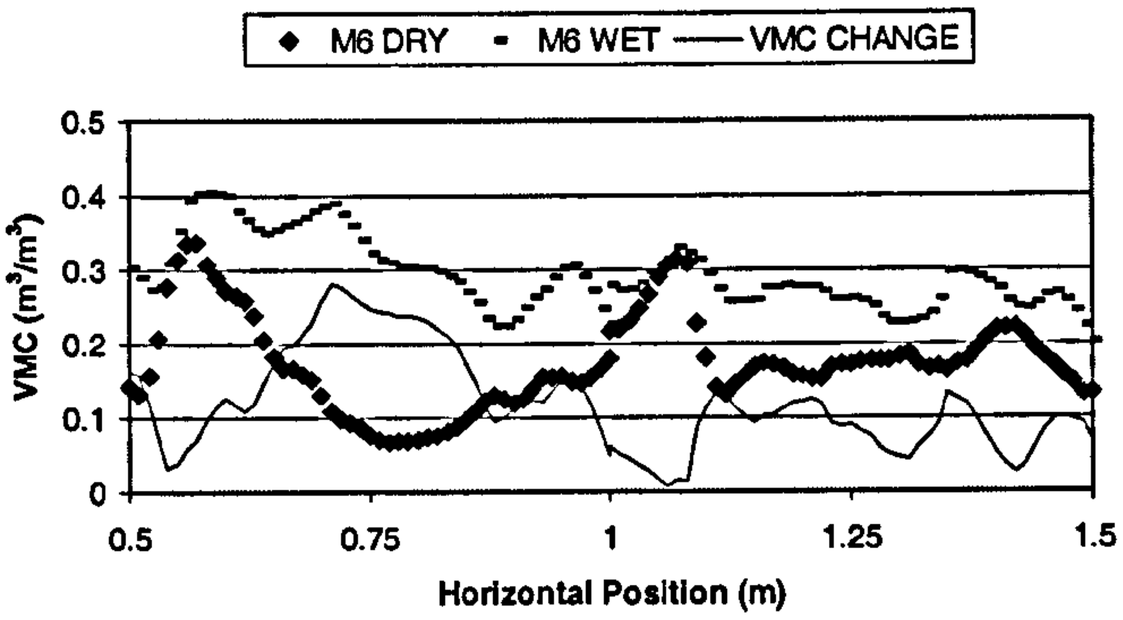

Figure 8.26: Predicted VMC at 900 MHz for the ACTIVE (M6) profile for E3 (0.5-1.0 m) and E4 (1.0-1.5 m) before (dry) and after (wet) water addition (E3 at x = 0.75, E4 at x = 1.25, both at z = 0.2) using the original non-linear relationships. Continuous line shows the difference in estimated VMC between the before and after conditions.

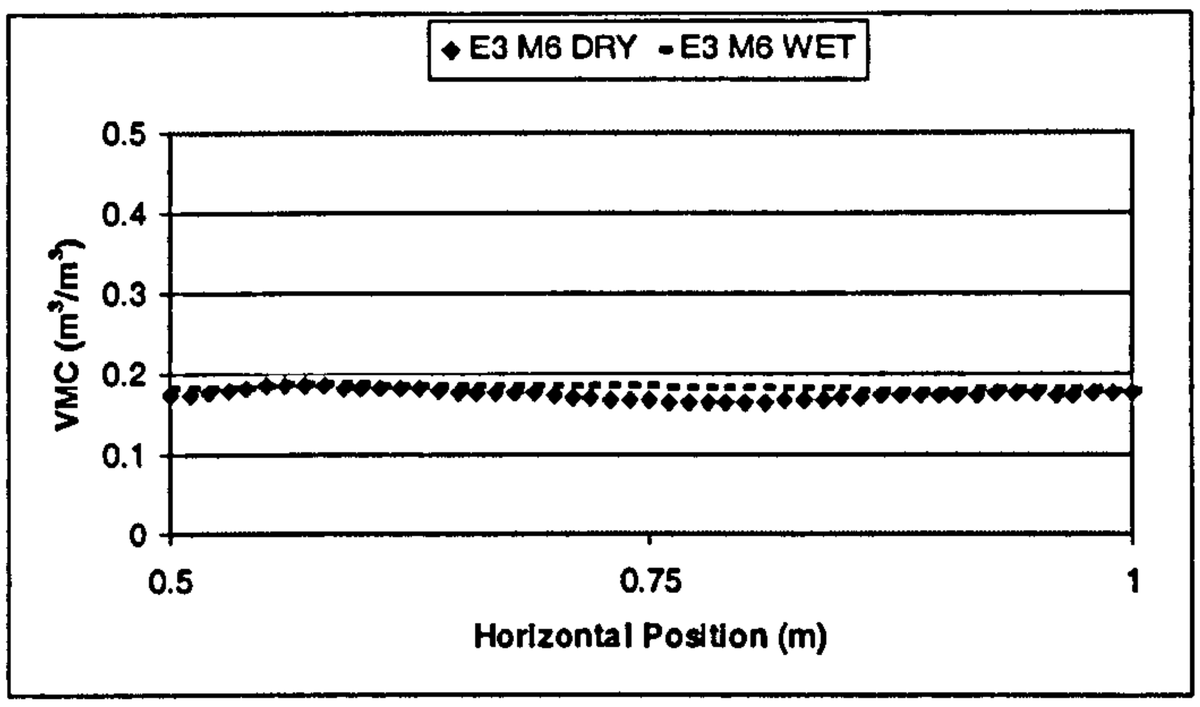

Figure 8.27: Error associated with estimation of VMC pattern for E3 wet and dry calculated by subtracting the GII results from the GI results.

8.3.2 Time windows and investigation depth

In addition to the equations being different, the time windows used to estimate MIA in Charlton and Mulligan (2001) were different from those used in this research. The GII equation was applied to the 900 MHz MIA data for E3-E5 derived in Charlton and Mulligan (2001). The results of the predictions are presented in Table 8.5. These results are improved over using the non-linear material-specific equations and are slightly improved compared to the data presented in Table 8.2. These time windows were derived using more detail of the spatial variation of TWTTs (using *ThetaProbe* data) and the improvement indicates the advantage of using as much detailed *a priori* subsurface information as possible when trying to estimate VMC, because it removes the relatively small error introduced by using an average and constant time window. A far greater

source of error is introduced when the time window over which the MIA is calculated is fundamentally different from that which defines the measurement depth.

EXPERIMENT DETAILS			FULL PROFILE VMC (m^3/m^3)			M6 LAYER VMC (m^3/m^3)		
Run	Wet or Dry	Frequency (MHz)	Observed	Predicted	Difference	Observed	Predicted	Difference
E3	Dry	900	0.0270	0.2128	-0.1858	0.0320	0.1449	-0.1129
	Wet	900	0.0850	0.2612	-0.1762	0.1390	0.2323	-0.0933
E4	Dry	900	0.0390	0.2351	-0.1961	0.0430	0.1748	-0.1318
	Wet	900	0.0810	0.2549	-0.1739	0.1160	0.2150	-0.0990
E5	Dry	900	0.0710	0.2017	-0.1307	0.1070	0.1194	-0.0124
	Wet	900	0.0710	0.2049	-0.1339	0.1070	0.1239	-0.0169

Table 8.5: Comparison of observed (*ThetaProbe*) and predicted (GPR) average VMCs (calculated by applying GII equation to the MIA values derived by Charlton and Mulligan (2001)) for each experiment.

If, as has been shown, the water concentrated in the ACTIVE layer, then extending the analysis to greater depths (using the full soil profile rather than just the M6 layer) where it is drier should reduce the VMC further. Instead the estimated VMCs for the full profile increase. Any process that decreases MIA estimates will result in overestimations of VMC. It has been demonstrated in Chapter Seven that the use of a larger time window than necessary can produce lower MIA values as a result of increased attenuation and spreading losses. With these increased losses, the moisture distribution is smoothed because there is greater variability in the depth that the estimate is calculated from due to the variation of moisture patterns.

8.3.3 The direct arrivals and subsurface interference

The MIA-VMC relationship clearly estimates the VMCs accurately for E5 but not E1-E4 and this calls into question its general applicability, even in situations in which the host material into which the water leaks remains the same. Comparison of Figures 8.28 to 8.30 demonstrate that the direct arrivals are very different between the E3, E4 and E5 mean traces and the E3 and E4 direct arrivals do not match the transmitted pulse in the M6 experiments (Chapter Seven). Figures 8.14 and 8.15 demonstrate that the VMC estimations for E3 and E4 are improved over the zone of *ThetaProbes*. Conversely, in E1 and E2 (Figures 8.12 and 8.13) the *ThetaProbes* promote increased interference. The E5 direct arrivals (Figure 8.30) are very similar to a transmitted pulse (T_x) derived by suspending the GPR antennae at 0.95 m above the material surface (see Chapter Six). For

the initial development the relationship was dependent on a strong direct arrival (T_x and ground-wave) presence, while this is absent from the E3 and E4 profiles (e.g. Figure 8.31). The minimisation of the direct arrivals in the zone away from the *ThetaProbes* in these experiments means that the weak hyperbola as a result of the *ThetaProbe* has more impact on the resulting MIA for these experiments. This increases values of MIA in the *ThetaProbe* zone, decreasing VMC estimations, making them appear more accurate (0.05 m^3/m^3 compared to >0.25 m^3/m^3). The *ThetaProbe* reflections therefore effectively compensate for the weakening of the direct arrivals. Thus in the absence of strong and coherent direct arrivals, the predictive model becomes unreliable and is very sensitive to subsurface variability. Consequently, the VMC estimation becomes affected more by subsurface features thereby distorting the derived moisture distribution. This may, in practice, become a limiting factor for application of the technique to more complex field investigations.

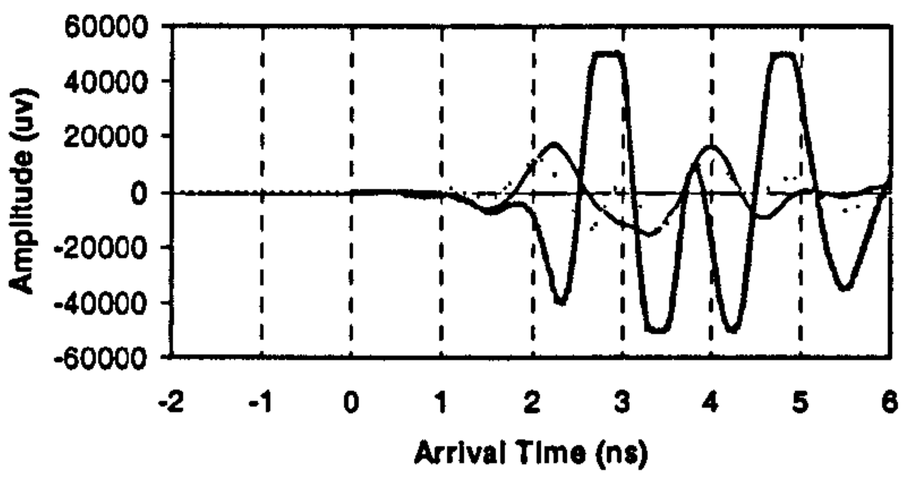

Figure 8.28: Comparison of mean dry (thin full line) and wet (broken line) direct arrival response at 900 MHz for E3 with dry trace from original M6 experiments (thick full line).

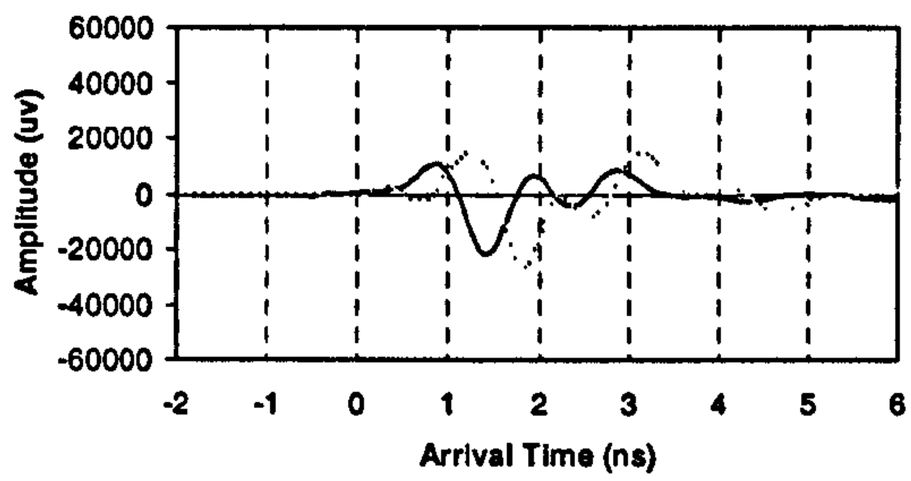

Figure 8.29: Comparison of mean dry (full line) and wet (broken line) direct arrival response at 900 MHz for E4.

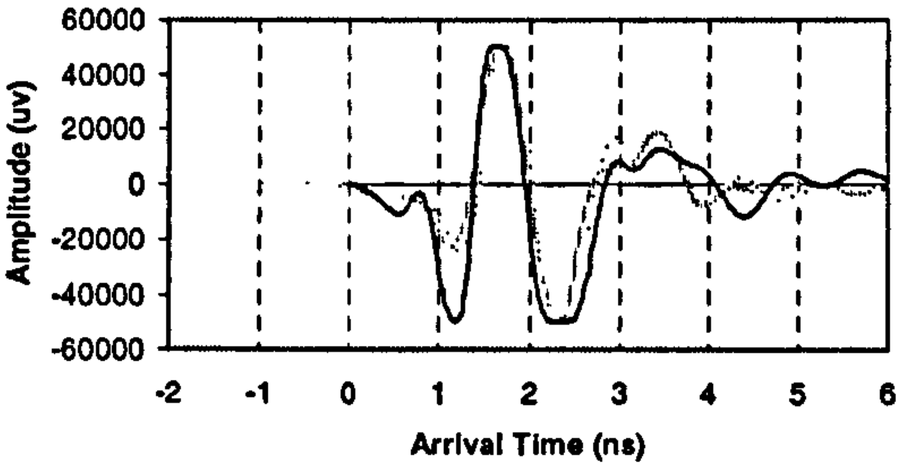

Figure 8.30: Experimentally derived transmitted pulse (full line) at 900 MHz acquired by suspending the antennae at 0.95 m above a dry surface. Compared with dry (faint line) and wet (faint dashed line) direct arrival response for E5. Traces aligned to match in time.

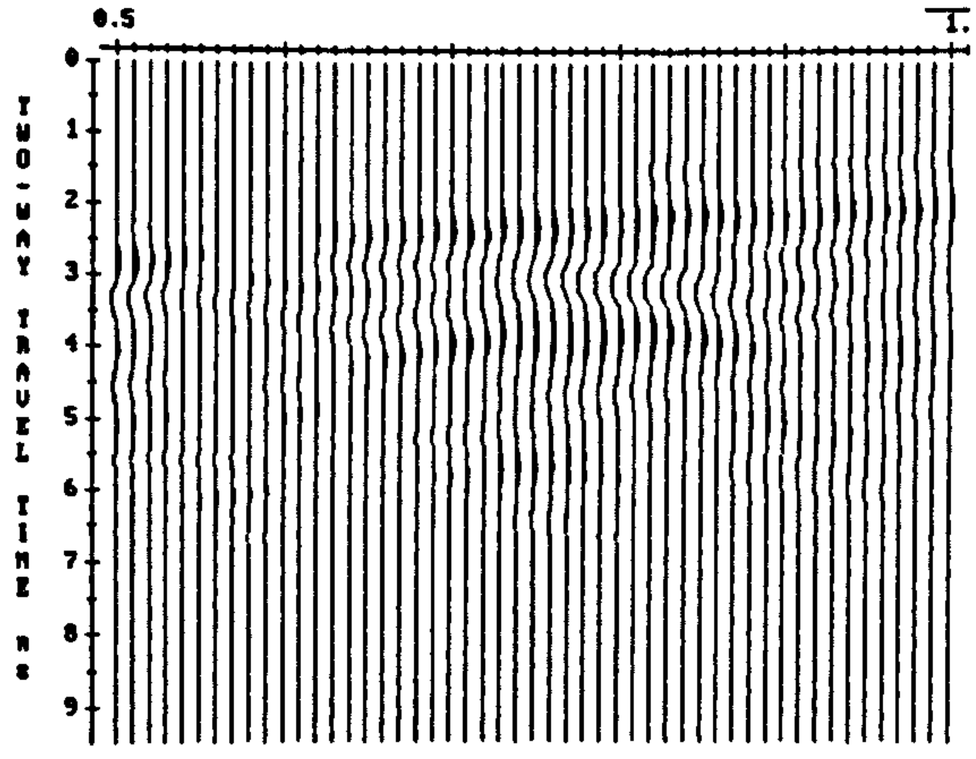

Figure 8.31: GPR profile of E3 dry at 900 MHz. Horizontal axis is position (m) and vertical axis is TWTT (ns)

Other possible causes for the poor estimations include swelling of the clay material upon wetting, which may have resulted in the observed *ThetaProbe* VMC estimations being recorded lower than their real values. However, this would not affect the dry E3 and E4 results. During the addition of water in E3 the material subsided just above the water outlet. However, this would not affect the E4 results. Another possibility could be the re-laying of the layer in E5 after this subsidence but this is unlikely to produce such extreme differences. The brick layer that was added as a pavement would be drier and may result in improved estimations. However, it is suggested that the brick layer does not improve results by reducing the effective VMC but by increasing the coupling of the antennae with the ground.

8.3.4 Antenna coupling

The presence of the T_x pulse is critical to the success of the model and ground coupling affects the shape and duration of the downward wavelet (Reynolds, 1997) because the close proximity of the surface affects the radiated fields from the dipole and the source wavelet is sensitive to the dielectric properties of the medium (Roberts, 2000). Tests, carried out in Plynlimon (see Chapter Nine) and summarised in Figure 8.32, show that the nature of the signal response depends on both the elevation of one antenna off the ground and which antenna has become decoupled. Coupling will also be affected by the degree of antenna contact with the ground and will therefore be sensitive to surface roughness. The decoupling can be expected to increase transmission into the air resulting in signal loss. Signals may also bounce back and forth between the antennae and the ground surface. This may increase the superposition of time-delayed negative wavelets such that negative and positive amplitudes may combine producing no apparent amplitude response, or a very reduced one. If this occurs, then the direct arrivals will also be effectively removed from the instantaneous amplitude traces.

In E1 and E2, the direct arrivals remain relatively intact due to the relatively flat surface, although there is poorer coupling with the gravel in E2. In E5 the brick surface means that the GPR is well coupled with the surface producing similar conditions to the relationship development experiments. The direct arrivals in E5 are the most coherent of all five experiments. Furthermore, the moisture that exists in the M6 layer of the dry run acts to minimise differences caused by the presence of *ThetaProbes*. In E3 and E4 the coupling

is affected by two aspects. First the larger rock fragments in E4 increase surface roughness for this experiment. This roughness contrasts with the smoother surface of E3 producing coupling problems at around 1.0 m and beyond 1.5 m for E4. Because the 900 MHz antennae have a separation of 0.17 m it can be expected that results will be poorer at 0.17 m either side of 1.0 m and 0.17 m before 1.5 m. This appears to occur on Figures 8.14 and 8.15. At 0.5 m the smoother E3 surface changes into material with more rock fragments and an increase in elevation so that coupling becomes increasingly worse. The coupling of the GPR antennae with the surface is clearly very important to the overall applicability of the model used for estimating VMC from MIA. Thus use of the GPR on uneven surfaces will result in large VMC estimation errors. One way to resolve this may be to use the GPR in suspended mode. In addition to the coupling, two other factors affect the ability of the model to estimate VMCs accurately. Estimated VMC values are reduced if a lower antenna frequency is used and become less accurate for drier conditions.

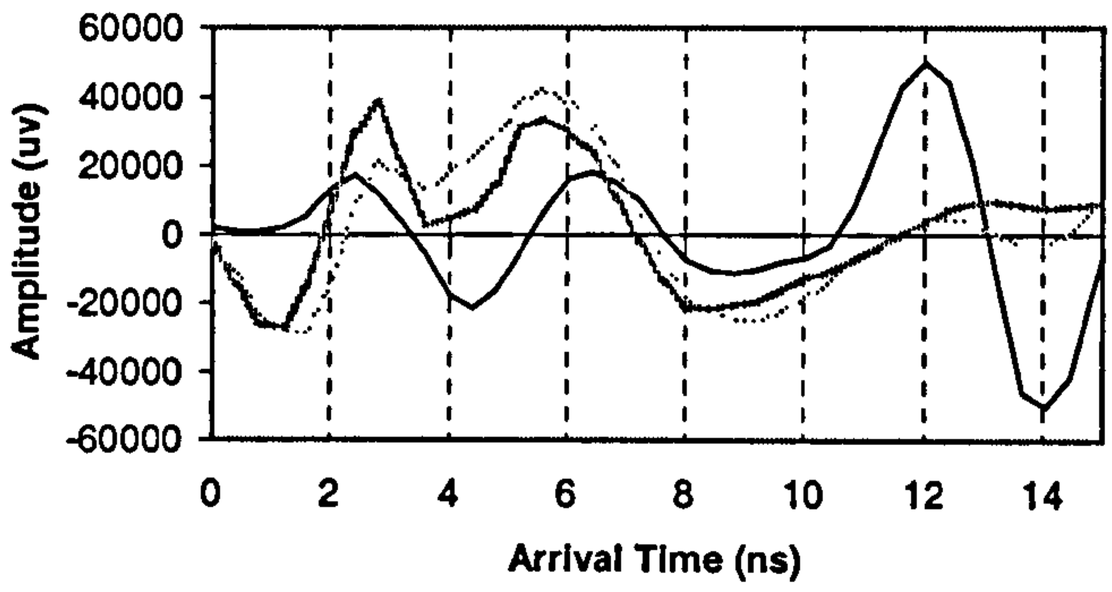

Figure 8.32: Variation of response with antenna ground coupling. Transmitter lifted 0m (full line), 0.15 m (thick dashed), and 0.25 m (thin dashed) off the ground whilst receiver remains in contact. Uses 900 MHz antennae.

8.3.5 Relative subsurface wetness

The relative wetness of the subsurface at the time of profiling affects the estimation of VMC because the developed equations were limited in their range of application to intermediate VMCs (see Chapter Seven). Consequently, increased error is expected in subsurface zones which are very dry or very wet. This explains the poor estimations for E1 and E2 and at the edges of E3 and E4 for the dry runs. E5 estimations are accurate because much of the subsurface environment is already wet. The relative wetness also acts to alter subsurface variation and its interaction with direct arrival interference. When

dry, there is considerable variation when high dielectric targets (such as *ThetaProbes*) are present (see Chapter Six). With the addition of water, variability is reduced due to changes in dielectric constant distribution. In particular, pore space filled with air becomes filled with water. This slowly homogenises the dielectric constant through a material volume. As the pore space becomes increasingly filled with water, variability will increase again because the solid material has the lower dielectric constant. However, the signal attenuation of the water acts to maintain this relatively low variability. The implication of this is that the drier the conditions, the less reliable the spatial distribution of moisture measured by the GPR becomes because the GPR becomes increasingly responsive to subsurface targets that obscure the VMC effect.

8.3.6 The effects of antenna frequency

In addition to the problems identified above, there is clearly a difference between the 450 MHz and 900 MHz predictions. The basic process has been outlined as increased MIA due to the broader wavelets (especially the direct arrivals) at lower frequencies. This produces a higher MIA resulting in lower VMC estimations. The effect of this is apparent in the improved VMC estimations at 450 MHz when using the original GII relationship. However, clearly this would provide false estimations and therefore a means of correcting for different frequencies is required. In this instance the 450 MHz needs to be corrected to the 900 MHz response. The higher MIA values at 450 MHz compared to 900 MHz are clearly demonstrated in Figure 33 for E5 dry.

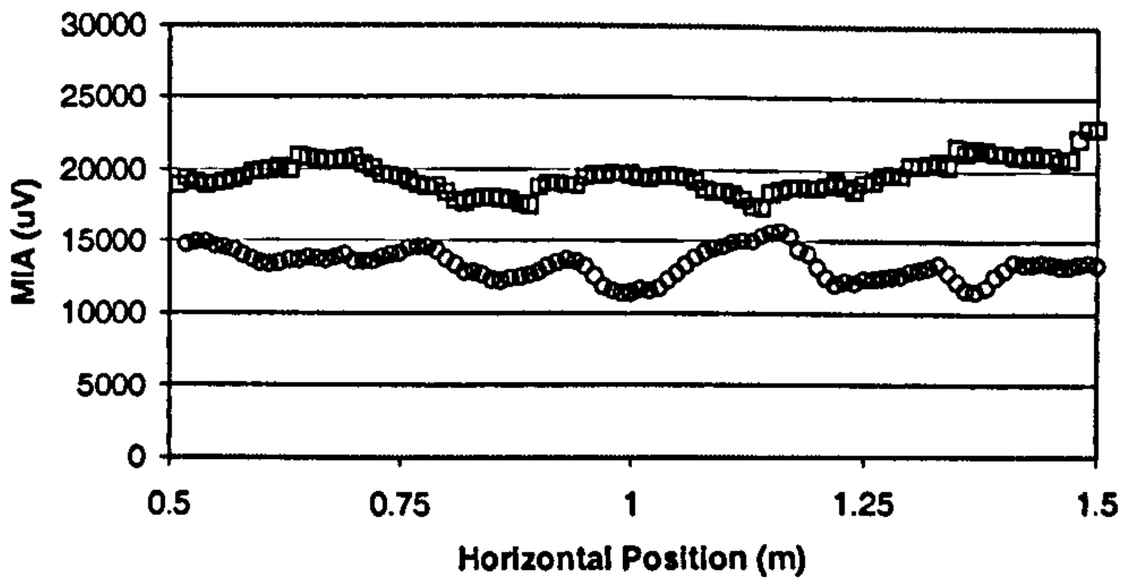

Figure 8.33: Correcting for frequency differences in returned MIA values. Original MIA at 450 MHz (squares), original MIA at 900 MHz (circles), and corrected MIA (dashes).

A more fundamental problem with the lower frequency is the different moisture distribution derived. This tends to be characterised by greater fluctuation and sensitivity to subsurface objects. The reasons for these differences in spatial pattern relate to the increased measurement volume of the 450 MHz antennae (increased antenna offset and footprint), greater uncertainty in depth (Chapter Six), and increased antenna wavelength. This latter feature means that a different image of the subsurface is generated. Clearly, the GPR is not simply recording VMC distributions when spatial data are acquired. Thus an extension of the method to include a more comprehensive consideration of antenna frequency, and even multi-frequency imaging, may provide more certainty in subsurface moisture distributions. Olhoeft and Smith (2000) recommend the use of two antennae, the higher frequency (at or above 1 GHz) to acquire thickness information and the lower frequency (at or below 500 MHz) to acquire accurate moisture content measurements.

The relaxation of the water molecule produces an increase in attenuation with frequency (Carcione, 1996). The presence of water means that the imaginary part of ε tends to increase above ~100 MHz with the result that there is a steady rise of attenuation with frequency (McCann *et al.*, 1988). Because attenuation by water is the primary factor determining the MIA value used to estimate the VMC, the decreased attenuation at 450 MHz compared to 900 MHz causes the higher MIA values at this lower frequency. Because the attenuation coefficient is a linear function of frequency (McCann *et al.*, 1988), this effect can be corrected for by decreasing the intercept value of the GI and GII equations. Because the lower frequency records different patterns, the aim is to produce predictions similar to those for 900 MHz in terms of average VMC and error, using the 450 MHz data. Using the E5 dry data because this correctly estimates VMC using 900 MHz antennae, the target values are an average VMC of 0.1328 m^3/m^3 and an error of -0.0258 m^3/m^3. Making the slope more positive (-0.9497×10^{-5}) improves both the average estimation and the error. However, it changes the relative magnitudes and therefore moisture distribution. Thus areas will appear much wetter or drier. In order to preserve the relative magnitudes of the estimation just the constant was changed. By increasing the constant from 0.3076 to 0.3926 the pattern is preserved and the average estimation (0.1328 m^3/m^3) and error (-0.0258 m^3/m^3) equal that for 900 MHz. Although a physically based means of correction is ultimately preferred, this would require further understanding and more detailed modelling of the contributing factors to the MIA value outlined in Section 7.3.3.4. The correction applied is adequate for the current research because estimation and error are equal at both frequencies.

8.3.7 Summary: implications for VMC distribution estimation

Disturbance of the direct arrivals, especially through coupling or near-surface objects, introduces lower MIA estimations and therefore higher VMC. If this were spatially invariable then adjusting the model constant would accommodate this feature. However, changes in surface topography reduce contact with the surface and introduce disturbances. The magnitude of this disturbance depends on the magnitude of the decoupling and this clearly varies in space. To accommodate this variable effect, which may produce distorted estimation patterns, it is necessary to ensure perfect coupling (which is clearly not possible in the presence of micro-topography or plants), only sample where coupling is possible (this would render high-resolution surveys impossible), identify through further experimentation an acceptable error in direct arrival coupling, or use GPR in suspended mode (although this introduces the problems of surface roughness, weaker propagated signal, and increased measurement area due to the footprint). These two latter options are worthy of further investigation in order to improve reliability in GPR estimations. It is important to remember that disturbance in the direct arrivals is not simply due to coupling problems. Objects, such as a thin layer of moisture, stones, or *ThetaProbes*, generate reflections that are able to distort these first signal events. The direct arrivals are directly affected by the subsurface to which the antennae are coupled (as discussed in Chapter Six), and changes in surface moisture will affect the ground-wave. Thus, some of the disturbance identified in the direct arrivals is a direct consequence of the moisture that is being measured.

Success in estimation is also highly dependent on the relationship between the weakening of the direct arrivals (which is variable in space) and the complexity of the subsurface. If the direct arrivals are weak then VMC will be over estimated. However, if the direct arrivals are weak but a near-surface target produces a reflection, then this compensates for the weakening of the direct arrivals to some extent, producing less overestimated values. This effect is clear on E3. Consequently, the success of the GPR estimation becomes less dependent upon the VMC but more dependent upon the distribution of disturbance throughout the subsurface, which may compensate for the loss of the direct arrivals. However, if the direct arrivals are intact then this would lead to underestimation. Clearly there is a trade-off between the different effects of potential sources of error. Therefore, an interpretation of the GPR data, and complete understanding of the survey conditions

(site, data acquisition, etc.) becomes vital for determining the actual accuracy of GPR estimation.

With perfect coupling this source of error in moisture pattern should be minimised as long as the effect of subsurface anomalies can be isolated and removed. However, with variable disturbance in the direct arrivals and increased disturbance in the subsurface, relative estimations of VMC may become increased or decreased compared to what they should be. This could produce smoothing of the moisture pattern or increased differences between different areas. This limitation has the potential to prevent confident leak detection and may potentially limit analyses of subsurface moisture variability.

8.4 WATER LEAK DETECTION USING GPR-DERIVED MOISTURE DISTRIBUTIONS

8.4.1 Detection of laboratory water leaks

The way in which water was leaked into the subsurface and the materials in E1-E5 allows an analysis of the spatial distribution of VMC to be used to detect the bodies of water associated with water leaks. The potential for leak detection is greatly enhanced by the ability to compare before and after leak moisture distributions. In conjunction with a knowledge of the principal limitations of the technique for spatial estimation as outlined above, the potential for leak detection can be assessed.

The difference between wet and dry is very clear for E3 and E4, peaking at 0.13 m^3/m^3 for E3 (Figure 8.15). This allows a leak to be identified at 0.6-1.0 m. An increased difference between wet and dry runs also occurs at 1.1-1.3 m. These locations correspond to the approximate locations of the water leak centres. Using this method, the leaks in E1, E2, and E5 (Figures 8.12, 8.13, and 8.17) are not detectable. For E1 and E2 there is a hint of wetter conditions at 1 m where the leak was centred but the variation in response (wet conditions often appear much drier) and the detection of 'leaks' in E1 at 0.95 and 1.25 m suggests that the GPR is assessing some other source of variation. For E5 the lack of detection in the visual GPR imagery is confirmed by the close match between wet and dry VMC estimates; both in terms of value and spatial distribution. This is potentially due to the greater depth of the leak and the attenuating effect of the initial moisture content in

the clay layer near the surface but could also be due to high hydraulic conductivity of the material into which this leak takes place allowing the water to diffuse and drain more rapidly. The observed VMC data for E1, E2 and E5 show that these leaks were not detected because they did not concentrate; they drained away. Thus there was no leak to detect at the time of the GPR profiles. Therefore, a subsurface environment with high hydraulic conductivities may prevent the successful application of GPR to water leak detection.

At 450 MHz the leak detected at 900 MHz is less obvious for E3 and almost not detectable for E4 despite the higher volume of added water for this leak (Table 5.6). This too may result from the increased footprint at this lower antenna frequency further suggesting that the 450 MHz antennae are less effective at leak detection than the 900 MHz ones, but also has an explanation due to the material properties. For E4, the rock fragments in M6 present pathways for increased and more rapid drainage than in the more closely packed material in E3 in which the drainage rate is dramatically reduced. The 450 MHz transects were taken about 40minutes after the leak events compared to only about 5mins for the 900 MHz transects. This enabled the VMC to return to near its initial value by the time the 450 MHz data were collected. For E5 the material was re-laid (due to some subsidence in E3 which may have had some effect on the wet transect results) and this, in combination with natural redistribution (three days separated the runs), accounts for the more even moisture distribution exhibited by this material. Because the material was still wet, the impact of the sources of interference is still minimised.

The results show that successful detection of a water leak depends on the timing of the GPR transect, the interaction of the moisture with the host material, the depth of the leak, and the antenna frequency. In addition to limitations with the range of application much of the problem is due to error in the spatial estimation of VMC. The success of the technique for leak detection relies on three features.

First, the nature of the leak and the subsurface environment in terms of the substrate and hydrology clearly affects the moisture distribution. The surface material may also attenuate the signal (as does M6) or increase signal loss through scattering. Secondly, the ability of the sources of error to be avoided (in particular large objects or coupling). Thirdly, the ability to compare before and after leak conditions. This will clearly not be possible in routine leak detection. Reduced variability at leak sites within the zone of the

leak can manifest itself as a more consistent VMC value. However, without the ability to compare before and after leak profiles (or grids), it would not be possible to determine the cause of the high VMC value. For example, in E3 the leak is identifiable because of the difference in VMC estimations between the wet and dry runs. This difference actually occurs due to the effect of the moisture on a subsurface feature that fundamentally disturbs the VMC estimation and the poor coupling that occurs. Thus if just the leak run was performed, a relatively invariable subsurface VMC distribution would be estimated and not a leak. The requirement to compare wet and dry data can be approximated through the comparison of a leak site with a non-leak site in the same area. However, this would be a very poor approximation because, if the GPR is responding primarily to subsurface features and other sources of error, then this same effect on the estimated moisture distribution will be observed.

The complexity of the subsurface environment means that the technique developed so far may fail in terms of leak detection in the urban subsurface. The presence of pipes, boulders and other material is likely to produce disturbance in the GPR response, which may obscure any moisture signal in the ways identified in the laboratory. To investigate the potential effects of this uncertainty the method of estimating the spatial distribution of moisture was applied to two mains water leaks in London, UK.

8.4.2 Thames Water leak detection

This investigation aims specifically to detect the patterns of subsurface moisture associated with two mains water leaks of different sizes. Compared to the small-scale laboratory leaks, these field leaks are much larger (size, magnitude and rate), occur in a far more cluttered and noisy subsurface environment (pipes, rocks, road, pavement, cars etc.), and do not benefit from an ability to compare before and after leak images. Successful detection would pave the way for further testing of the method for this application.

Details of the surveys were discussed in Chapter Five. In the absence of any data for moisture validation, or any CMP or dielectric data to assist definition of the necessary time window over which to calculate MIA, profiles were processed with gain and displayed. Examples are given in Figure 8.34. These indicate very little signal response

after about 20 ns. MIA was calculated between G_0 and this time limit for each selected trace and both the GI and GII equations were applied to estimate VMC. No data were available on the material properties or complexity but the M6 material from the laboratory was extracted from an excavation prior to leak pipe repair at another site. This would suggest that the GII equation is more appropriate. Two additional features will contribute to the inaccurate estimation of the VMC values: the lower frequency used (450 MHz) and the greater depth of investigation, which may lower MIA through increased attenuation. This latter problem may produce smoothing of the moisture distributions making leak detection more difficult. Using the estimated VMC values, grids were constructed from 13 profiles spaced at approximately 0.2 m across the suspected leak. Each profile was acquired using a step size of 0.02 m resolution. This was sub-sampled to 0.1 m resolution for quantitative analysis. This sub-sampling has no effect on returned MIA values (e.g. the mean MIA for an Adam's Square (Table 5.8) profile at x = 1.2 m is 8004.622 using 0.02 m and 8006.77 using 0.1 m).

Figure 8.34 shows the Adam's Square leak site using the GII equation to estimate the VMC in the subsurface. This equation produces a very similar moisture distribution to the GI equation (not shown) although the magnitudes of the VMC estimation are lower using GII. Also prominent in the images are interpolation artefacts that are derived from using the default linear kriging routine in SURFER and are a consequence of the higher spatial resolution in the y-plane compared to the x-plane. To aid in interpretation of these moisture results, time domain radargrams are presented for every 0.8 m. These use a constant gain of 5 to enhance reflector definition.

There is no clear evidence of a subsurface leak although three distinct moisture zones can be identified:

- Zone One, at approximately y = 0-1 m, consists of very dry moisture values. Apparent low moisture values in this zone occur as a consequence of transects that are shorter than their neighbours producing interpolation lows.
- Zone Two, between y = 1-2.3 m, consists of much wetter conditions although towards x = 2.4 m this zone narrows. This is a consequence of an apparent moisture gradient between y = 1-2.3m which becomes steeper at this end of the grid. Within this zone, there is a region of very high moisture which stretches between x = 1.0 m to 2.4 m.
- Zone Three occurs at y > 2.3 m although the transition from Zone Two has a tendency to start closer to y=1.2 m the larger the x distance. This zone is characterised by

moderate moisture estimates and has considerable variability in pattern, although some of this is again an interpolation artefact.

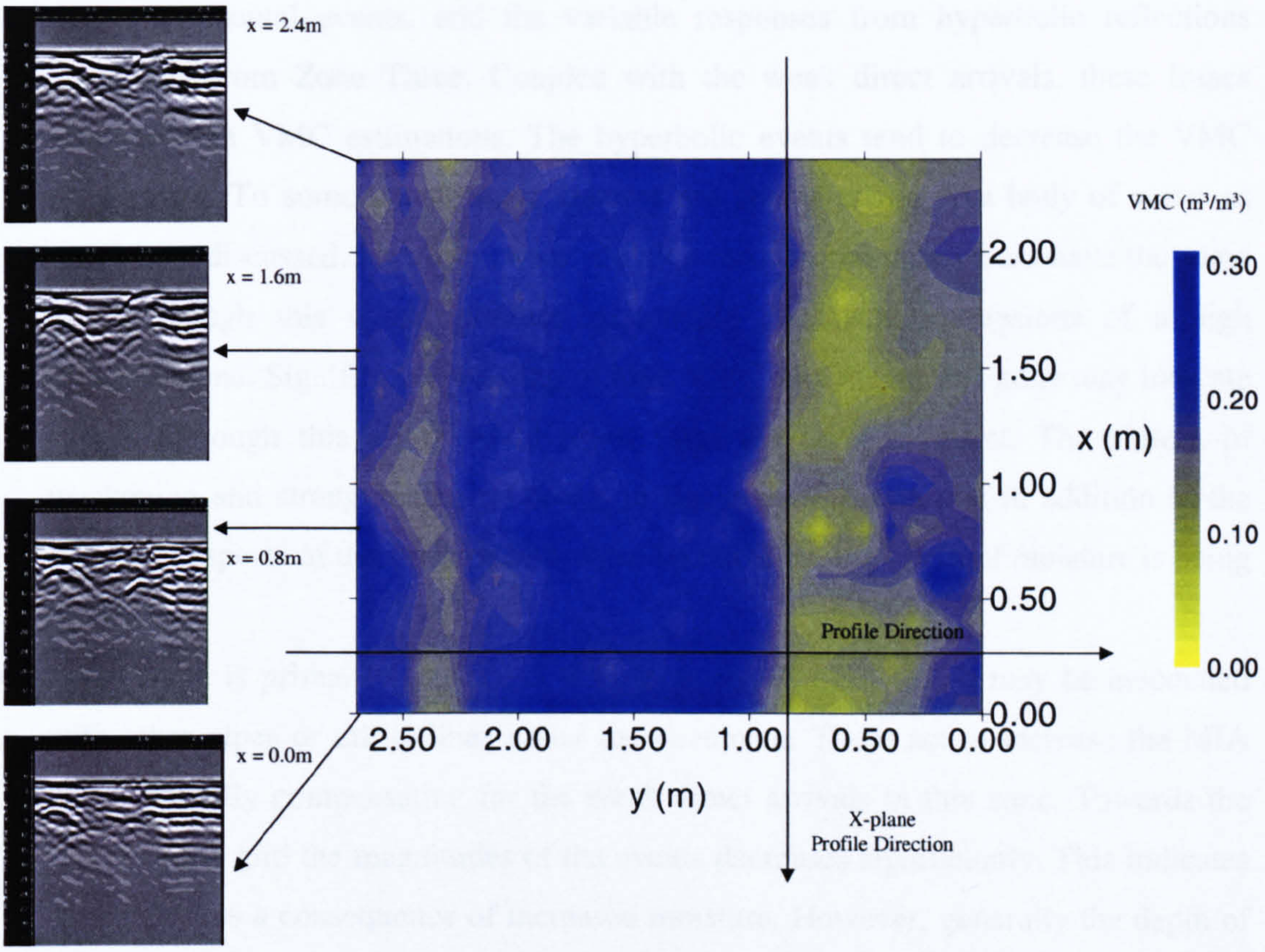

Figure 8.34: Grid of derived VMC estimates over the Adams' Square leak site at 450 MHz. Associated time domain radargrams every 0.8 m. x-plane profile extends approximately 5 m either side of x = 1.2 m.

This information does not conclusively indicate the presence of a water leak although the gradients that exist in Zone Two in both the x- and y-planes may indicate some response associated with a subsurface water body. However, the radargrams indicate that there are very specific causes of these apparent moisture responses. These are:

- Zone One is particularly affected by high magnitude horizontal reflectors which come to an abrupt stop at the start of Zone Two. These high magnitude events are characteristic of road surfaces, which are constructed with a number of layers, and compensate for the weakening of the direct arrivals, which is characteristic of all zones. The transect in the x-plane (Figure 8.35) confirms this coupling effect with the road surface and demonstrates the effect of subsurface re-bars used to strengthen the road. These produce regular patterns of sharp hyperbolic events. At about 8 m, a

drainage cover is traversed producing high magnitude ringing. The consequence of all of these high magnitude events is to produce an effective dry zone. This is misleading.

- Zone Two is affected by the weakening of subsurface reflectors, the sudden cessation of the horizontal events, and the variable responses from hyperbolic reflections emanating from Zone Three. Coupled with the weak direct arrivals, these losses produce high VMC estimations. The hyperbolic events tend to decrease the VMC estimations. To some extent these features are characteristic of a body of water as previously discussed. However, water flowing through the pipe would have the same effect, though this would produce reasonably consistent dimensions of a high moisture zone. Significant spreading of high VMC away from this zone may indicate a leak although this effect could result from the GPR footprint. The pattern of weakening and strengthening reflectors in this zone suggests that in addition to the structural aspects of the subsurface imaged by the GPR, the effect of moisture is being detected.
- Zone Three is primarily associated with large hyperbolas, which may be associated with other pipes or utility lines under the pavement. These act to increase the MIA value, partially compensating for the weak direct arrivals in this zone. Towards the centre of the grid the magnitudes of the events decreases significantly. This indicates attenuation as a consequence of increased moisture. However, generally the depth of penetration throughout the three zones is reasonably consistent indicating that there is no significant signal attenuation occurring as a result of changing moisture distributions.

In summary, there is potentially a water leak located at about x = 1.2 m and y = 1.2 m on Figure 8.34. However, the GPR is to a large extent measuring subsurface structure much more than it is measuring VMC patterns. Fortunately, moisture attenuation of the GPR signal manifests itself as the weakening of fairly continuous structural reflection events. The tendency appears to be for moisture to accumulate next to the pipe and spread away from the pipe with decreasing VMC under the path. Unfortunately, the Thames Water GPR Team collected no information concerning site conditions other than the surface is path at y > 1 m and road at y < 1 m and that the leak is expected, based upon correlator analyses, to be located in the centre of the grid. Whilst the difference between path and road may explain differences in coupling and horizontal layering, the lack of further data prevents the definitive location of a moisture leak. On-site validation would have been

required in order to achieve this. Another feature of the GPR survey that prevents confident assessment of whether or not the derived moisture patterns are in fact moisture or some combination of other complex responses, is the relatively high spacing of the GPR profiles. This prevents identification of potential continuous events (other than in the x-plane profile) and smaller-scale disturbances, which may indicate further detail with regards to the moisture distribution.

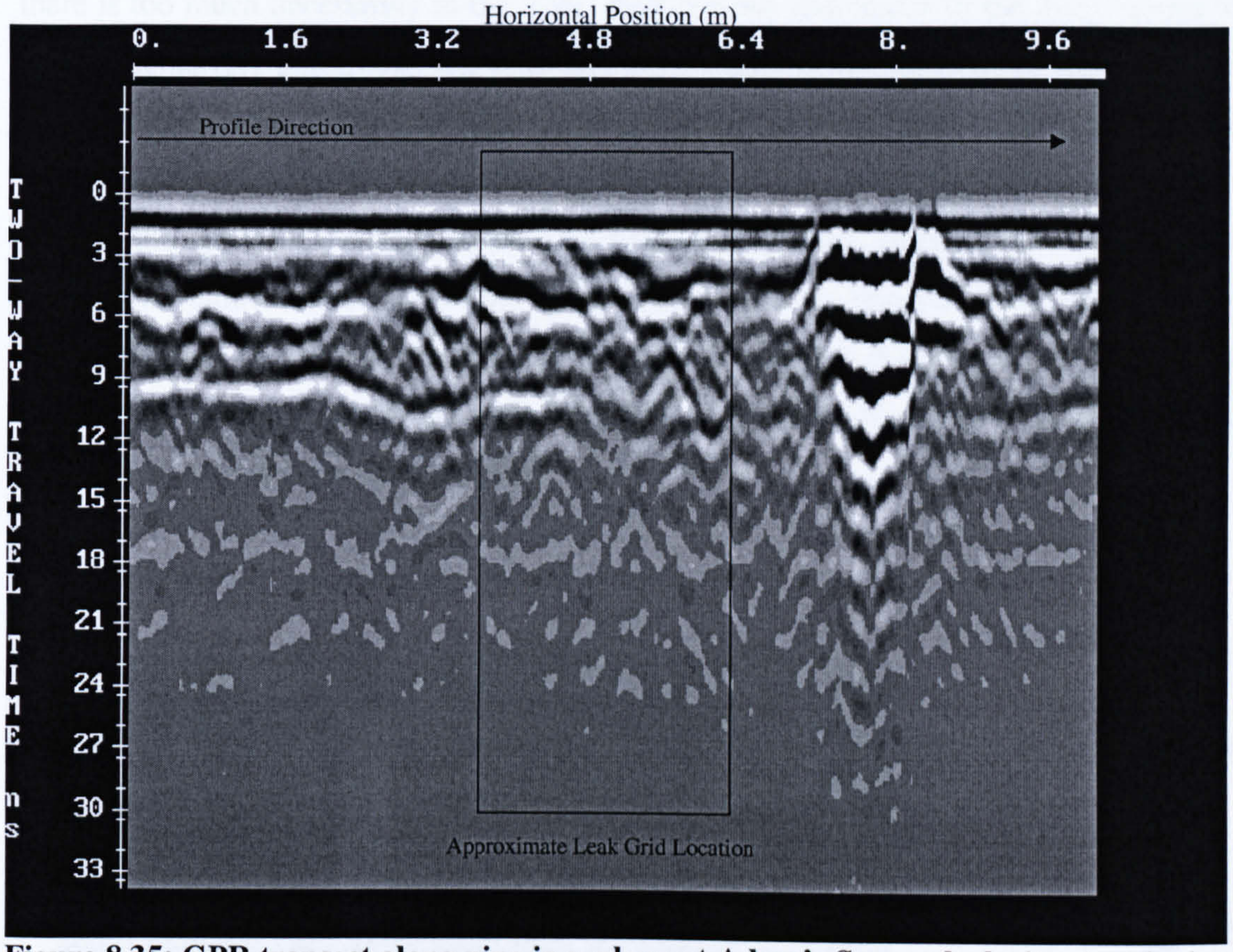

Figure 8.35: GPR transect along pipe in x-plane at Adam's Square leak site. Acquired at 450 MHz by Thames Water Utilities GPR Team. Constant gain of 10 applied.

The sensitivity of the GPR to coupling problems and subsurface structural features is demonstrated clearly by the Cromwell Road leak. Moisture distribution (Figure 8.36) is subject to substantial variation across the grid, partially due to interpolation errors but largely due to changes in coupling as shown in the accompanying radargrams. These radargrams demonstrate a large hyperbola, which is associated with the much larger mains pipe (0.9 m compared to 0.1 m for the Adam's Square pipe). Above this event there are a number of smaller hyperbolae, which act to disrupt the continuity of the horizontal events. These produce spatially variable interference in the GPR response and usually

have a lower reflection magnitude. Across the grid the direct arrivals are much stronger than at Adam's Square producing drier VMC estimates. It is when there is interference in these signal features that the GPR produces patches of high VMC. It is also possible that subsurface features have a greater impact on the GPR image. Certainly a number of large objects are detected which act to reduce estimated VMC.

It is clear from these brief analyses that the principal problem with leak detection is that there is too much uncertainty in the VMC distributions and causes of the distributions to state conclusively that a leak has been detected. Not only does this mean that detection still becomes overly dependent upon subjective interpretation, but it is likely that for the method to be effective, a large amount of time consuming processing will be required to remove the apparent over-dependence on structural features. In particular, migration of the data to remove the effects of the hyperbolas may be an important first step. Without site excavation to validate the complexity of the subsurface environment, it will not be possible to detect a mains water leak. Therefore, a considerable amount of further work, or an alternative approach, is required.

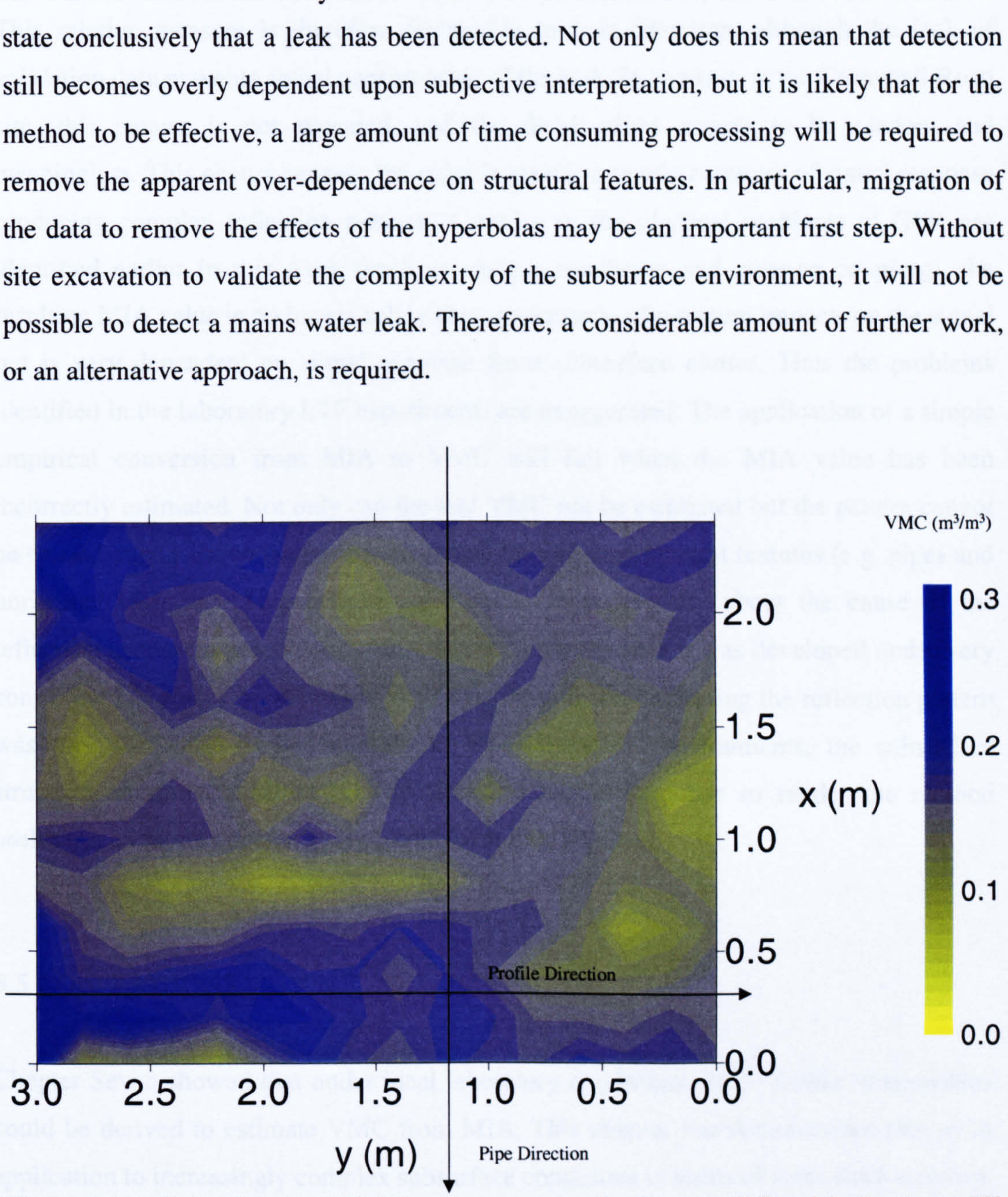

Figure 8.36: Grid of derived VMC estimates over the Cromwell Road leak site at 450 MHz.

The application of the method to a poorly controlled, complex subsurface in order to detect mains water leaks was not successful. Limitations in the MIA method and the GPR technique itself produce too much uncertainty. The absence of calibration data means that the estimation of VMC becomes a relative measure. This is clearly demonstrated by the fact that the GI and GII equations give the same distribution of VMC but very different absolute VMC values. Given that water leaks are assumed to be a zone of higher moisture, this relative measure of pattern should successfully identify a leak. At the Adam's Road site, the highest VMC is along the pipe and in a zone near the pipe location. This relative measure is therefore favourable to leak detection, although the lack of validation data prevents actual confirmation of the leak. In contrast, at the Cromwell Road site, this pattern is not repeated, and the distributions appear to be random and meaningless. This occurs because the radar is sensitive to other sources of signal response producing complex reflection patterns. Coupled to the physical problems of GPR use identified earlier in this work (such as surface roughness and antenna coupling), the resulting MIA value is no longer solely the consequence of moisture impacts on the signal but is very dependent on signal response from subsurface clutter. Thus the problems identified in the laboratory LTF experiments are exaggerated. The application of a simple empirical conversion from MIA to VMC will fail when the MIA value has been incorrectly estimated. Not only can the real VMC not be estimated but the pattern cannot be trusted due to dependence on a variety of subsurface structural features (e.g. pipes and horizontal layering). This reflects an increase in uncertainty about the cause of the reflection events. In practice, the MIA method fails because it was developed under very controlled laboratory conditions in which the only feature affecting the reflection pattern was the VMC and its distribution. In more complex environments, the subsurface structure interferes sufficiently with the GPR signal response to render the method useless. A different approach is required for leak detection.

8.5 CONCLUSIONS

Chapter Seven showed that under ideal laboratory conditions, very reliable relationships could be derived to estimate VMC from MIA. This chapter has demonstrated that upon application to increasingly complex subsurface conditions in terms of subsurface structure and materials, greater depth, and variable moisture distributions, certainty in the estimation becomes less reliable. This is demonstrated by the variable success in detecting

five laboratory subsurface moisture conditions using the LTF and the failure of the technique to detect two urban water leaks. Where there is little signal disturbance (e.g. E5), the VMC estimation technique works well to estimate the average VMC of a moisture distribution. The greater the error in the VMC estimation, the less reliable becomes the estimation of moisture distribution, making the study of spatial variability and moisture patterns difficult. Furthermore, an accurate estimation of the average VMC does not mean that the distribution of moisture has been determined correctly. These problems are related to subsurface material conditions and to the GPR technique itself. However, limitations in the MIA-VMC method and flaws in some aspects of the experimental design and methodology, are the primary causes of the failure of the technique.

Estimation of moisture variation and leak detection is constrained by the material characteristics of the subsurface environment, which also determine the moisture distribution. Under drier conditions, the GPR becomes very sensitive to subsurface features. The immediate consequence of this is the generation of variable reflection events, which act to increase MIA and therefore decrease estimated VMC and produce increased variation in GPR response. Where the general site-specific conditions are more amenable to either accumulation of water (as in most natural soils) or propagation of the GPR signal (sandy soils, dry clay soils, shallow investigations) the GPR technique is more successful. Both the visual imagery and the VMC estimates demonstrate less variation in the wet conditions, primarily through a reduction in subsurface scatter and increased attenuation. This can be used for the identification of subsurface water bodies and water leaks; though in practical application this fails due to the ambiguity of complex subsurface response. Effects specific to the developed GPR technique, including frequency (wavelength, footprint, relative amount of attenuation), time window and depth, and form of the relationship (the values of the intercept and slope), also produce further error in the estimation of VMC. Alone, or in combination, these errors can result in VMC estimations that are to some extent arbitrary, random (assuming random subsurface variation), and often meaningless (because the MIA depends as much upon factors that are unrelated to the VMC as it does on the VMC itself).

The fundamental cause of VMC estimation error using the MIA-VMC method appears to be errors associated with the derived MIA values. Any process or reflection event that results in MIA values that are too high or too low for the empirical conversion will

produce inaccurate estimations of VMC that are either too low or too high, respectively. There are many sources of variability that act to produce values of MIA that do not result in accurate predictions. Such impacts include the interrelated effects of antenna coupling, topography, and near surface objects on the character of the direct arrivals. An uneven surface may produce poor antenna coupling with the ground, resulting in a reduction in the magnitude of the direct arrivals. This would produce a reduced MIA value and therefore over-estimate VMC. Near-surface objects may act to counter this reduction in MIA by generating a strong reflection. However, if the direct arrivals are unaffected, a strong near-surface reflection may increase the MIA value, giving the impression of much drier conditions. It is possible that because the direct arrivals are not always the strongest signal event (as shown in Figure 8.32), the developed model between MIA and VMC becomes invalidated. This is likely because the model is very dependent on the high magnitude direct arrivals, which, as demonstrated in Chapter Seven, minimise the impact of changes in reflection pattern on the value of MIA. It is for these reasons that E5, in which the flat surface produces good antenna coupling and intact direct arrivals, is successful. It is clear that these processes can operate to increase or decrease the MIA value. Any means of overcoming this limitation, such as using suspended mode GPR to ensure coherent direct arrivals, would improve the general applicability of the developed technique.

In addition to the problems with the direct arrivals and near-surface reflectors, the other fundamental flaw with the MIA-VMC method is its over-sensitivity to other objects in the subsurface. This further reduces certainty in the estimation by increasing reflection magnitudes and therefore distorting the MIA and VMC estimates. This was clearly demonstrated by the attempts at urban water leak detection. These two sets of data demonstrated that with increasing complexity the technique becomes less reliable. The application to the detection of urban water leaks failed due to the ambiguity of signal response in such situations. Thus the method is over-dependent on subsurface structure and if this changes, at least extensively, then it is not only VMC that is being measured. It is possible that for leak detection, the estimation of some other hydrological variable, such as total moisture, may be more appropriate, although this may still be subject to the same limitations. Furthermore, for field applications in hillslope hydrology, VMC is a critical parameter as discussed in Chapter Two. However, it would appear that for such an application a more robust means of deriving VMC is required; one that is less sensitive to highly variable reflection patterns.

It seems that the less similar the subsurface is to the experimental conditions under which the method was developed, the worse the estimation. The method is likely to produce very loose approximations of a moisture distribution that are distorted beyond recognition by strong reflectors in the subsurface that were not present in the initial development of the model. The method is therefore impractical and inapplicable to the majority of potential situations. This might therefore be a fundamental limitation of any simple empirical technique that uses a characteristic of the GPR signal rather than attempts to fully understand the physical processes involved in the GPR response. This suggests a need to model GPR response using physically-based models. Whilst the original development of the method appears to have resulted in applicability only to very similar subsurface structural environments, some of the uncertainty in the results in this chapter could have been avoided if the experiments had been performed differently. Improvements in the design and a simplification of the overall methodology may well have produced results in this section which, while still highlighting the fundamental flaws with the method, may have reduced some of the uncertainty in the causes of particular results. Such improvements will be discussed in more detail in Chapter Ten.

Despite all of the problems identified with the method, this Chapter has demonstrated that GPR, using the method developed in this research, offers the potential for estimation of relative VMC distributions. However, the effects of the potential spatial variability in the estimation error must be understood in order to interpret correctly a GPR estimation of the moisture pattern. Only through detailed interpretation can the uncertainty in both VMC estimations and the resulting distributions, as well as the causes of additional events, be accounted for when assessing resulting distribution estimations. While not allowing accurate estimations of distributions, this would enable zones of potentially accurate VMC to be identified. Thus, to a limited extent, spatial distributions of moisture can be assessed using GPR, which enables the identification of a variety of subsurface moisture conditions in the laboratory and, therefore, potentially in field applications where there is increasing complexity in subsurface, and other environmental conditions.

For application to a more complex field situation, site-specific validation is required until more is known about the specifics of the different sources of variation in the GPR VMC estimation. Explanations for why the GPR method to estimate VMC and its distribution succeeds or fails are very situation specific; such is the complexity of GPR measurement. An ability to identify the sources of variation in response would greatly improve the

interpretation of the resulting estimated VMC distributions. This is the focus of the next chapter.

CHAPTER NINE: ASSESSMENT OF SOIL MOISTURE DISTRIBUTION USING GPR IN THE CYFF CATCHMENT, PLYNLIMON, WALES

9.1 INTRODUCTION

The relationships between MIA and VMC developed and tested in Chapter Seven have been investigated in detail in Chapter Eight. It has been shown that with increasing subsurface complexity and conditions less controlled than in the STF experiments, the methods become increasingly prone to error, which acts to obscure a measurement of GPR signal attenuation by subsurface moisture. This is expressed particularly through estimation of the VMC value but also through uncertainty in moisture distribution. Fundamental limitations relate to the range of application of GPR, the effect of antenna coupling, subsurface complexity and the depth of investigation on returned data, and factors that relate to the data acquisition of the GPR such as frequency and measurement volume. These limitations are increased as subsurface complexity and ambiguity in subsurface response increases. An understanding of these factors is vital to interpret GPR estimations of VMC.

It is the aim of this Chapter to assess the potential of GPR in studying the distribution of hillslope soil moisture at high spatial resolution with a view to understanding the relationship between hydrological inputs, subsurface moisture patterns, and hydrological outputs as a soil wets and dries seasonally. The emphasis is on assessing the potential of the technology and of identifying further sources of error and limitation rather than providing a detailed discussion of hillslope hydrological response. Recommendations are made concerning whether the approach is worthy of more thorough investigation within the hydrological sciences.

A field campaign was conducted at an existing field site in the Cyff Catchment, Plynlimon, Wales (see Chapter Five) between July 1999 and October 1999. An additional visit in April 2000 was used to collect data from a specially developed 2m by 2m plot constructed above the existing plot on a single hillslope. The following sections present an analysis of GPR data collected across the new plot in order to assess the potential offered by GPR in hydrological investigations. After the selection and initial validation of an appropriate laboratory model, the relationship between the GPR-estimated soil moisture distribution, the site characteristics, and the hydrological inputs and outputs, and

its hydrological implications are discussed. To assess its potential it is equally important to identify further limitations and potential improvements to the method to facilitate its future application.

9.2 VALIDATING VMC ESTIMATIONS

9.2.1 Validating laboratory relationships.

9.2.1.1 Selecting a relationship

Figure 9.1 shows that the soil material, collected from 24 samples from the seven *ThetaProbe* test pits, clearly varies with depth. Near the surface there is a relatively low clay content and relatively high sand content in the fine earth fraction. In this zone there is an increase in silt content with depth. There is a peak in clay content at 0.2 m depth with values up to 93% (by mass). High clay contents also occur deeper in the profile. The mean fine earth fractions are shown in Table 9.1, which shows that, as an average over the entire soil volume, each component has equal representation. Table 9.1 also demonstrates that variation in clay content throughout the plot is greater than for the other fractions. Thus, generally the soil volume has moderate signal attenuation potential although this may be highly variable from space to space. Its vertical zonation is particularly significant with regards to the changes in clay content with depth. This means that the application of either the GI or GII equations may succeed in accurate estimation of VMC. Of particular concern, is the potential rate of signal attenuation with changing water content as a result of the attenuation of the signal by the variable clay content. This effect may be offset against the increasing stone content with depth, which effectively reduces the total pore volume of the soil profile (Van Wesemael *et al.*, 1999). This may reduce the effective VMC measured by the GPR, thereby decreasing the signal attenuation affect.

The estimation of absolute VMC is less important in the current research because the patterns of moisture are the prime concern of the investigation. However, the changing rate of material-induced signal attenuation may result in distortions of the spatial pattern as a consequence of clay content. To reduce this uncertainty, the two GPR-VMC relationships were applied to data from seven test pits to assess model accuracy. The more

accurate the VMC estimation across these seven pits, the more reliable the assessed VMC distribution. For the initial testing, both laboratory equations will be used with the aim of determining which provides the most accurate GPR estimations of VMC and to assess whether or not it is necessary specifically to calibrate the model.

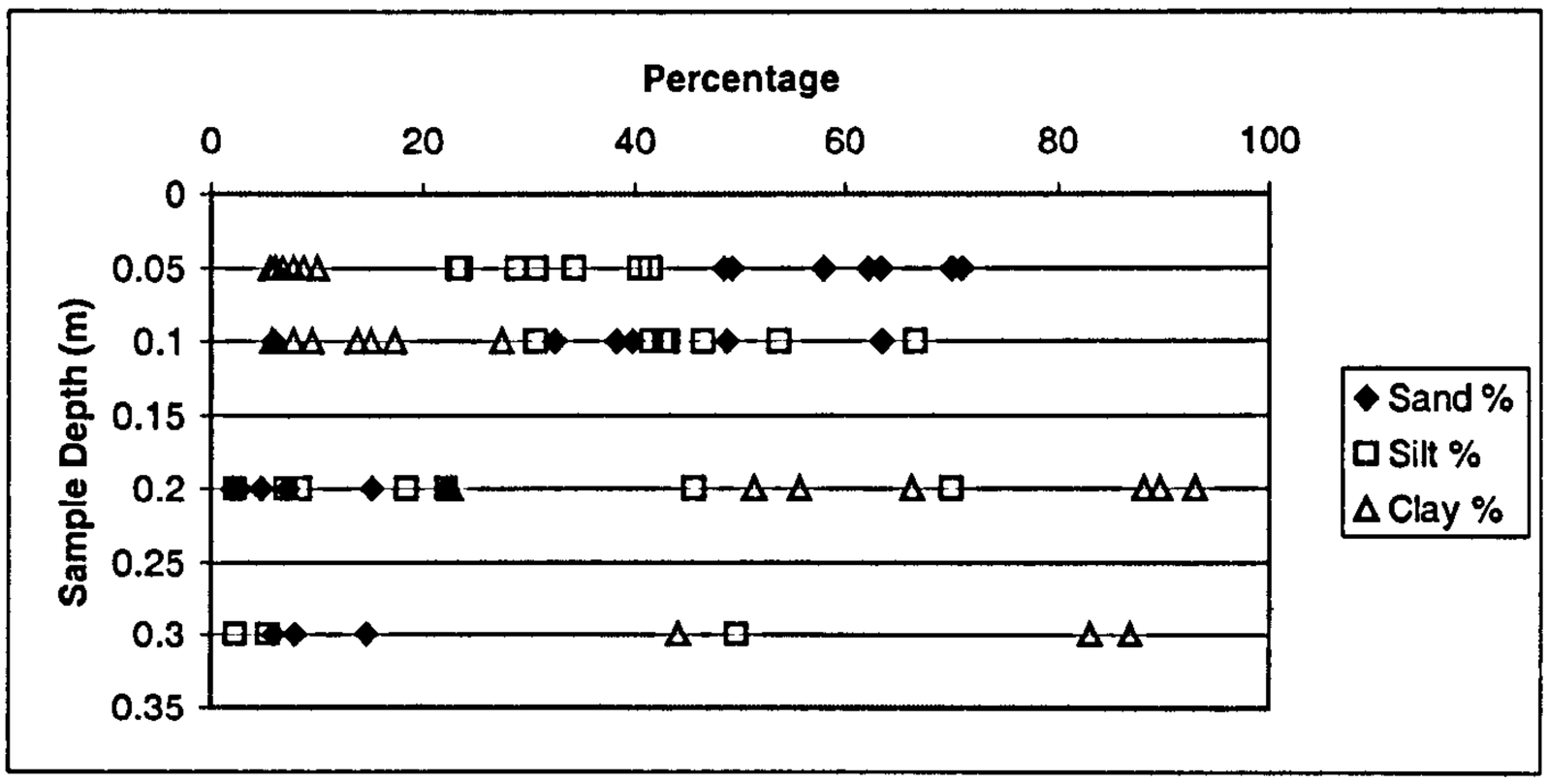

Figure 9.1: Percentage fraction of fine earth components (sand, silt, clay) for 24 samples collected at different depths from small-plot *ThetaProbe* test pits.

Fraction	Mean Percentage	CV
Sand	32.82	0.76
Silt	32.49	0.59
Clay	34.69	0.95

Table 9.1: Mean fine earth fractions for the experimental plot soil and its variation.

9.2.1.2 Validation methodology

The preparation of the data for the validation and the validation procedure are outlined in Figure 9.2. First the *ThetaProbe* data were prepared. Over the six data collection periods, the seven *ThetaProbe* test pits provided 42 average profile VMC samples. To provide an average VMC for the profile, three surface *ThetaProbe* readings at 0.1 m spacing over the pits were averaged to one value for surface VMC. An average of the surface VMC and the *ThetaProbe* estimates of VMC at 0.1 and 0.3 m depth were then used to calculate an average through the profile. The *ThetaProbe* readings at each depth for each pit for each visit were converted to VMC using the calibration values shown in Table 9.2. These were derived from samples collected and presented in Howe (2000) and averaged to the depths of the probes in the new plot. The *ThetaProbe* VMC data in Figure 9.3 demonstrate that subsurface moisture is substantially lower than surface moisture, although surface

moisture is subject to greater drying and wetting throughout the summer and autumn periods. The larger magnitude of these surface VMC estimates produces a drying and wetting trend in the average profile VMC.

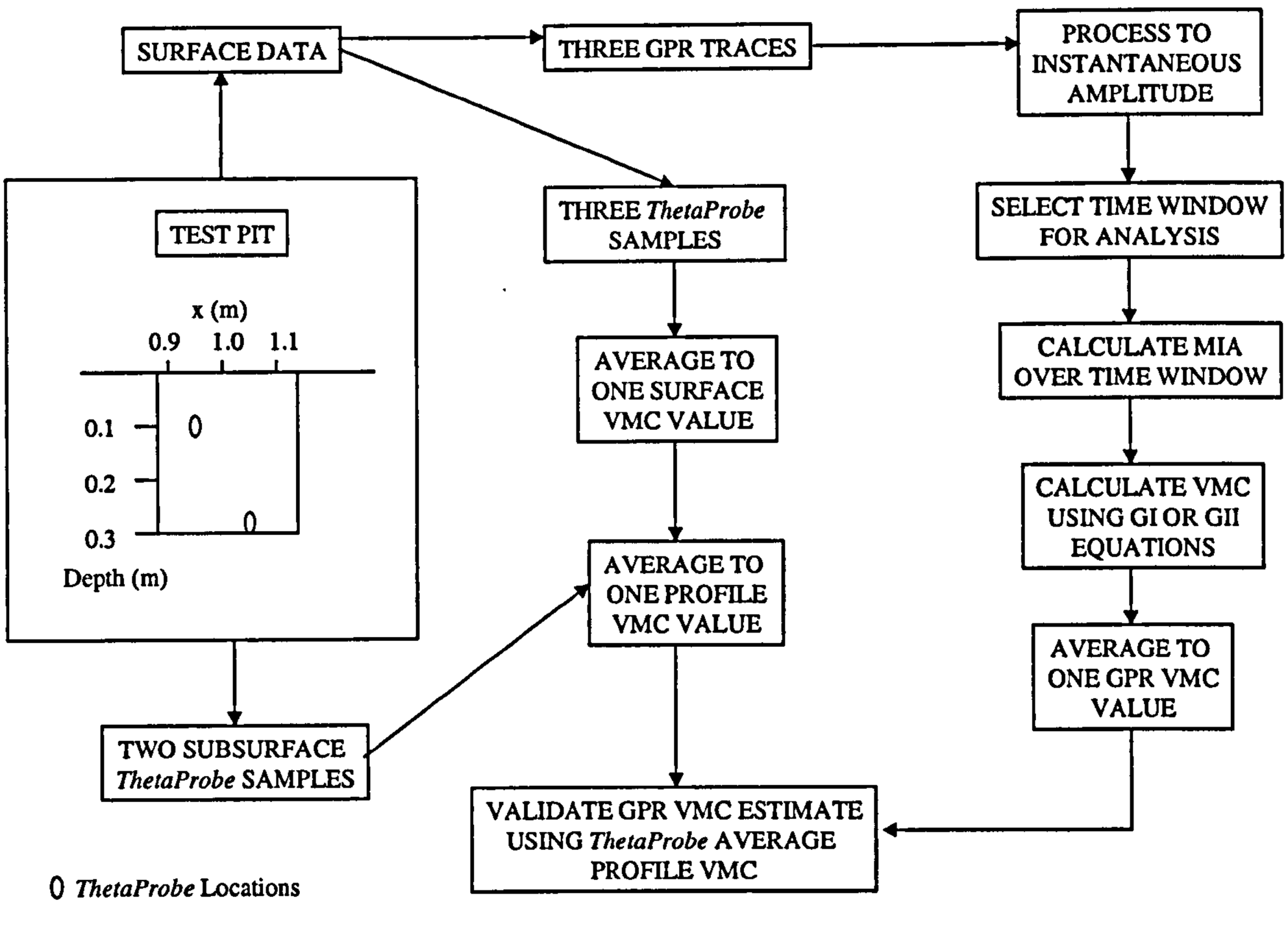

Figure 9.2: Validation methodology: collection, preparation and analysis of GPR and *ThetaProbe* data from test pit for validation of GPR VMC estimates.

An estimate of VMC for each of the 42 samples using GPR was derived from three GPR traces collected at 0.1 m spacing across each soil pit for each visit. These traces were sampled from the 900 MHz grid data. 900 MHz data are used because this frequency requires no further modification of the equation prior to application (as would the 450 MHz data). The MIA value for each trace was calculated using a time window of 25 ns from G_0. This value was derived using an approximate limit identifiable on a GPR transect acquired across the centre of the grid for each visit. These three MIA estimates are then averaged to provide one value for each test pit. Each of these 42 MIA values was used to estimate VMC using the two laboratory equations.

ThetaProbe Depth (m)	a_0	a_1
0	1.320	8.590
0.1	1.345	8.860
0.3	1.440	7.665

Table 9.2: *ThetaProbe* calibration parameters. Derived from data presented in Howe (2000).

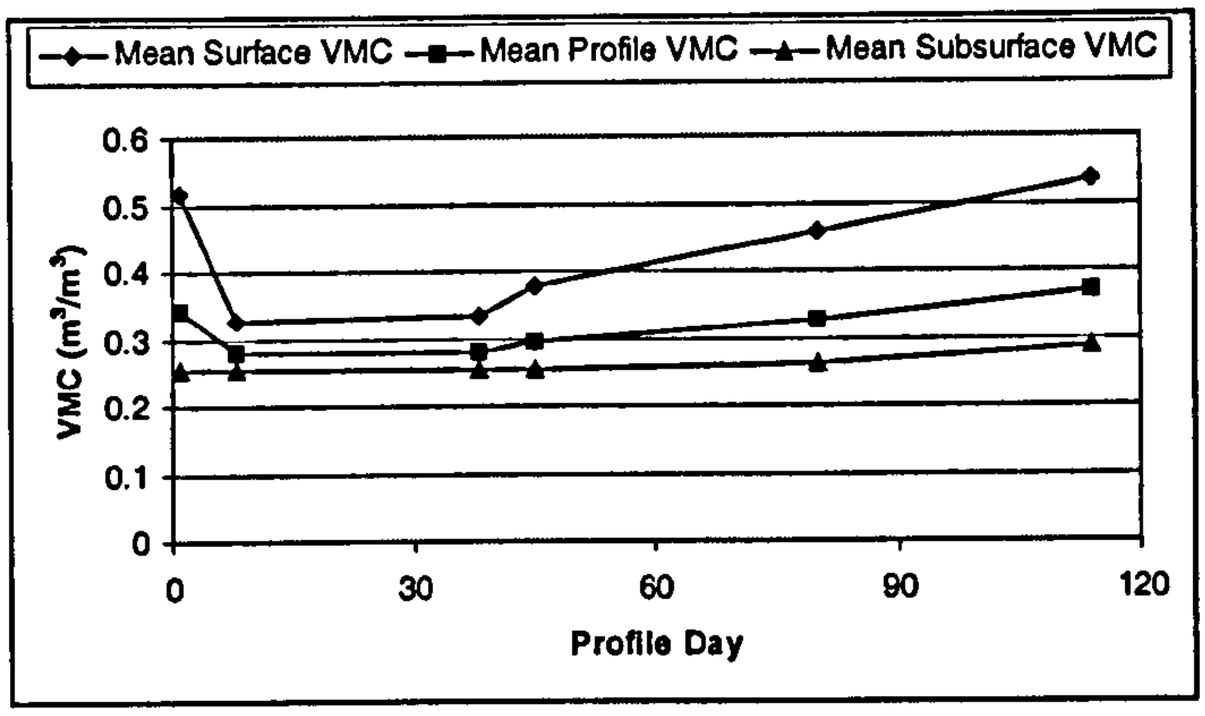

Figure 9.3: Mean observed *ThetaProbe* moisture: comparison of mean profile, mean surface, and mean subsurface VMC.

9.2.1.3 Validation results

The results of plotting the observed VMC against the predicted VMC for GI and GII are shown in Figure 9.4. This figure demonstrates higher estimated VMC for GI compared with GII, a constant pattern of estimations, and a greater range of VMC in the observed VMCs. The GI equation overestimates the VMC with an RMS error of 0.11 m^3/m^3, whilst the GII equation underestimates the VMC with an RMS error of 0.09 m^3/m^3. Table 9.3 summarises the mean, standard deviation and CV for the observed VMC and the GI and GII predictions, showing that variation in the GPR estimates is less than the variation in the *ThetaProbe* data. An RMS error of about 0.10 m^3/m^3 is too high to estimate VMC across a space in which the range of average observed VMC is only 0.15 m^3/m^3. This demonstrates the need to calibrate the GPR equations.

9.2.1.4 ThetaProbe error

The discrepancy between the surface and subsurface values indicates that there is a problem with the observed *ThetaProbe* VMC estimates. Independent VMC estimates derived using a bulk density ring and shown in Figure 9.5, demonstrate that, although

there is substantial scatter in the data, VMC is higher at the surface than in the subsurface. The magnitude of difference between surface and subsurface data is much smaller than that shown in the *ThetaProbe* data. These high VMC estimations are a consequence of the low bulk density observed in the plot (Figure 9.6). Bulk density increases with depth producing a corresponding decline of VMC with depth. These independent estimates were derived in April 2000 after a wet winter period and the surface was visibly saturated. This suggests that the drier subsurface moisture during the period between July to October, and the increased bulk density with depth, explain these differences. However, a set of data acquired just prior to extracting the 14 *ThetaProbes* from the plot in April 2000 show that the *ThetaProbe* data still underestimate subsurface VMC (mean *ThetaProbe* estimation is 0.2940 m^3/m^3 (CV = 0.0434) for all 14 *ThetaProbe* samples compared to 0.5879 m^3/m^3 (CV = 0.1477) for all data on Figure 9.5), indicating that the error is in the estimate and not the time of year.

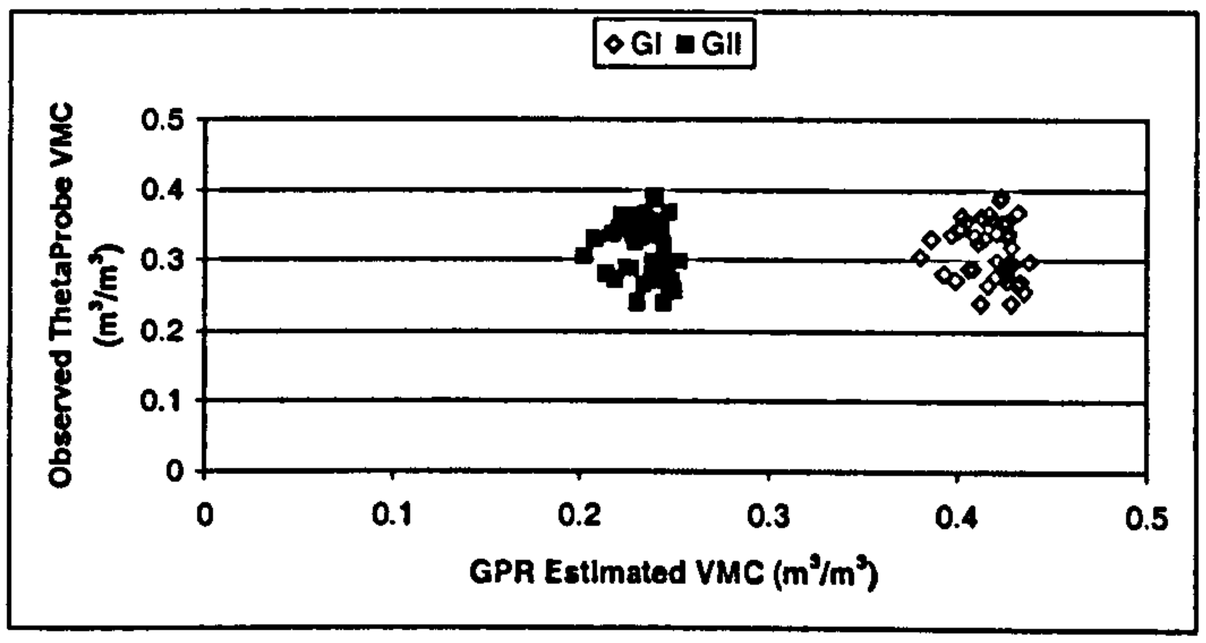

Figure 9.4: Observed *ThetaProbe* profile VMC for 42 samples plotted against GPR estimated VMC calculated using both the GI and GII equations.

Statistic	Observed *ThetaProbe* VMC (m^3/m^3)	GI Estimated VMC (m^3/m^3)	GII Estimated VMC (m^3/m^3)	Adjusted Observed *ThetaProbe* VMC (m^3/m^3)
Mean	0.3165	0.4169	0.2345	0.4310
Standard Deviation	0.0404	0.0136	0.0119	0.0447
CV	0.1276	0.0327	0.0506	0.1037
RMS Error		0.1096 (0.0500)	0.0928 (0.2022)	

Table 9.3: Summary statistics for the observed *ThetaProbe* mean profile VMC and the GPR VMC estimations using the GI and GII equations (values in brackets indicate RMSE using adjusted observed VMC data).

Rather than being a feature of lower VMC, the underestimation of subsurface VMC using *ThetaProbe* occurs because the Data-logger, powered by a single 6 V battery and a solar

panel, is unable to provide an excitation voltage to each of the probes when 14 are connected to the logger. *ThetaProbe* is designed to work with an input voltage of between 5-15 V (Delta-T Devices, 1998). The surface data were acquired using one probe connected to a 6V battery and read using a multimeter. Its estimates therefore correspond closely to the bulk density VMC data. With only three probes connected to the logger in the field on July 7th recorded voltages (data provided by Howe) were ~300 mV higher than on July 8th when eleven probes were added to the logger when the new plot was constructed. This equates to a VMC drop of 0.21 m^3/m^3 in a 31 hour period. Some of this drop may be attributed to changes in *ThetaProbe* location but this was minimised by calculating the average VMC difference using all depths together. The rate of drying for the three probes over a period of 31 hours prior to the *ThetaProbe* additions indicates a decrease in voltage of only 6 mV; clearly not enough to contribute significantly to the 300 mV drop.

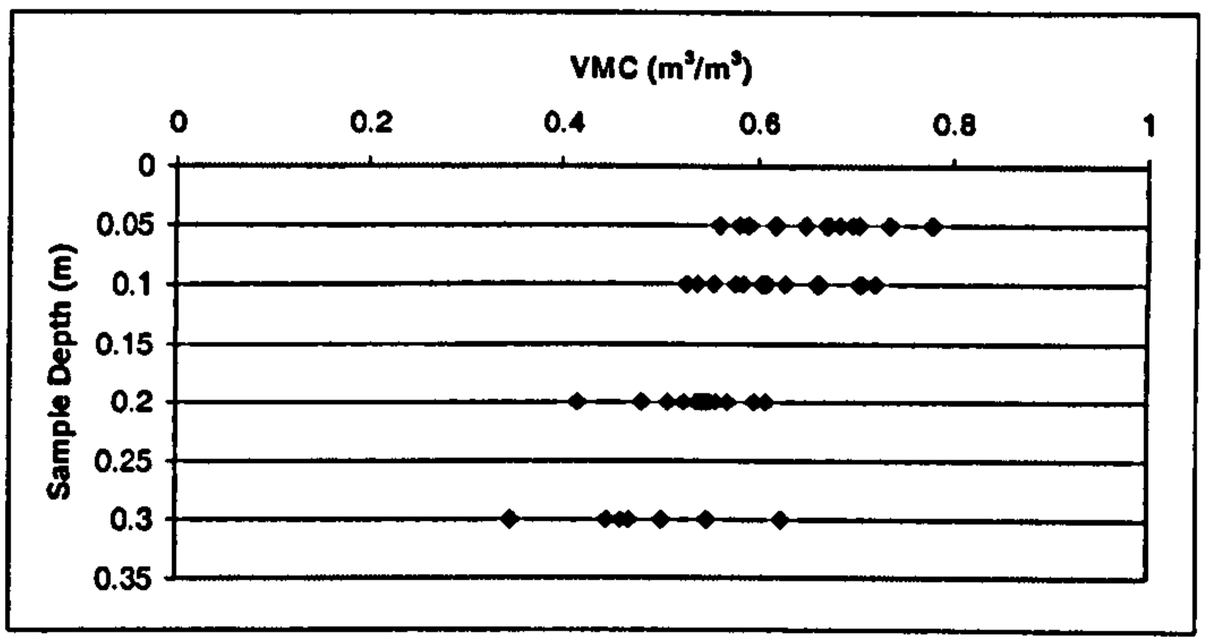

Figure 9.5: Observed VMC with depth derived using a bulk density ring (42 samples).

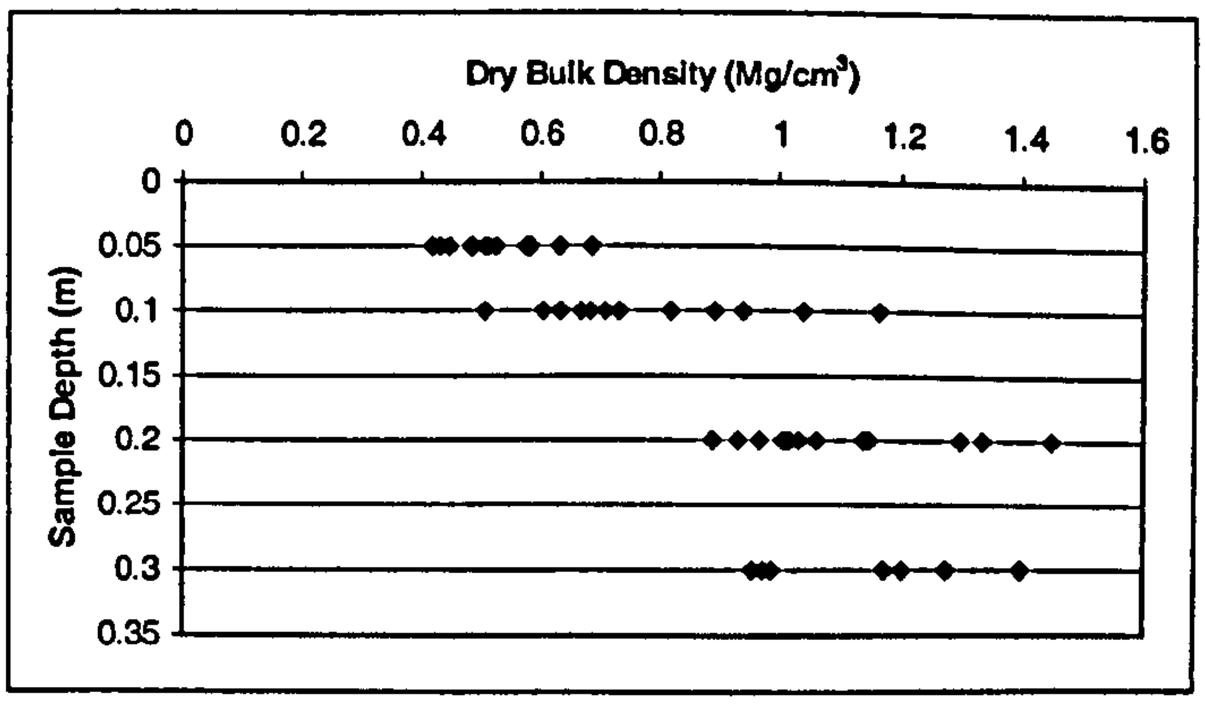

Figure 9.6: Measured dry bulk density with sample depth (42 samples)

For the three *ThetaProbe* configuration the probes were wired to allow sequential excitation. Due to the increased numbers of probes for more detail of subsurface moisture, it is not possible to wire in the probes for sequential excitation and therefore excitation is simultaneous for all probes. The drop in output voltage with increasing numbers of *ThetaProbes* connected to the logger was determined in the laboratory. All probes were suspended in water to provide a constant and maximum voltage response and the results are shown in Figure 9.7. After the addition of a 10th probe there is a sudden drop of about 185 mV, prior to which returned voltages are constant. Thus with more than nine *ThetaProbes* connected to the logger, the excitation voltage is diminished to such an extent that it is detrimental to the output voltage. Extrapolating a linear relationship fitted to the data in Figure 9.7 suggests that for 14 probes the decline in voltage should be about 300 mV. It is therefore proposed that a value of 300 mV is added to the subsurface voltage values in order to correct for the power problem assuming a linear relationship between power and output voltage after a threshold number of sensors is connected to the logger.

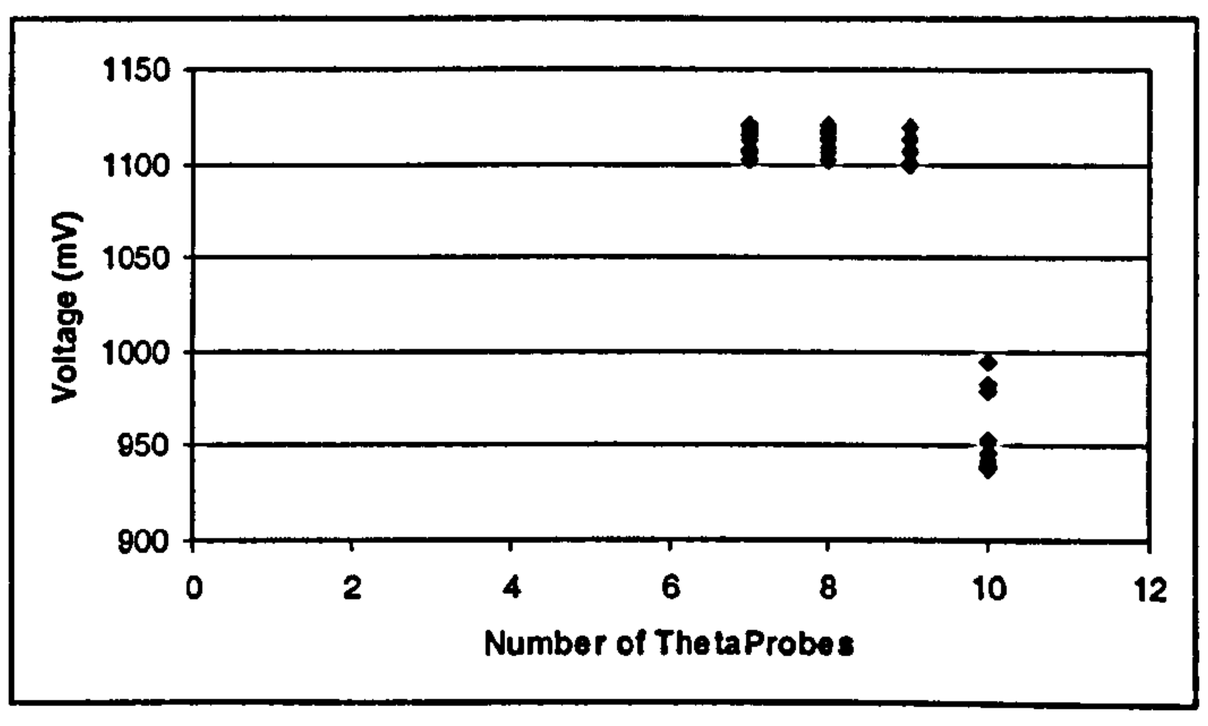

Figure 9.7: Decline in output voltage when more than nine *ThetaProbes* are connected to the DataTaker Datalogger.

9.2.1.5 Re-assessing VMC accuracy

Using the adjusted subsurface *ThetaProbe* data improves the GI estimation but worsens the GII estimation although the relative distributions remain the same as in Figure 9.4. Both equations underestimate the mean VMC for all data (Table 9.3) but GI only underestimates by 0.01 m^3/m^3. RMS error for GI is only 0.05 m^3/m^3 compared to 0.20 m^3/m^3 for GII. Whilst the GII results consistently underestimate the average VMC, the GI data are characterised by the under- and over-estimation of the data as indicated by comparing the non-standard residuals, which are plotted against the predicted VMC for

both equations in Figure 9.8. However, the patterns of over- and under-estimation are consistent between equations used as demonstrated by subtracting the GII estimations from the GI estimations in Figure 9.9. The results, shown for each sample point in Figure 9.10, show a maximum range of error of 0.017 m^3/m^3 between the estimates. This means that although distributions may be smoothed or exaggerated by the relative magnitudes of over- or under-estimation, this effect is due to the actual GPR MIA values and not the independent *ThetaProbe* values or the conversion equations.

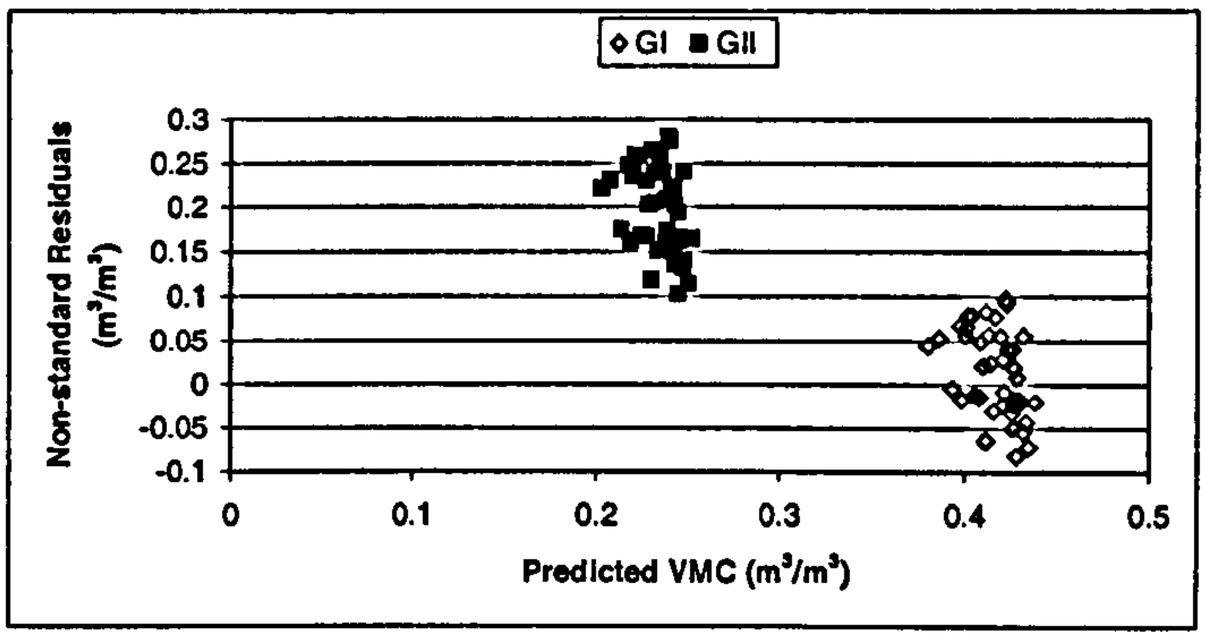

Figure 9.8: Non-standard residuals for GPR estimated VMC using GI and GII equations compared to observed *ThetaProbe* VMC plotted against the GPR estimations.

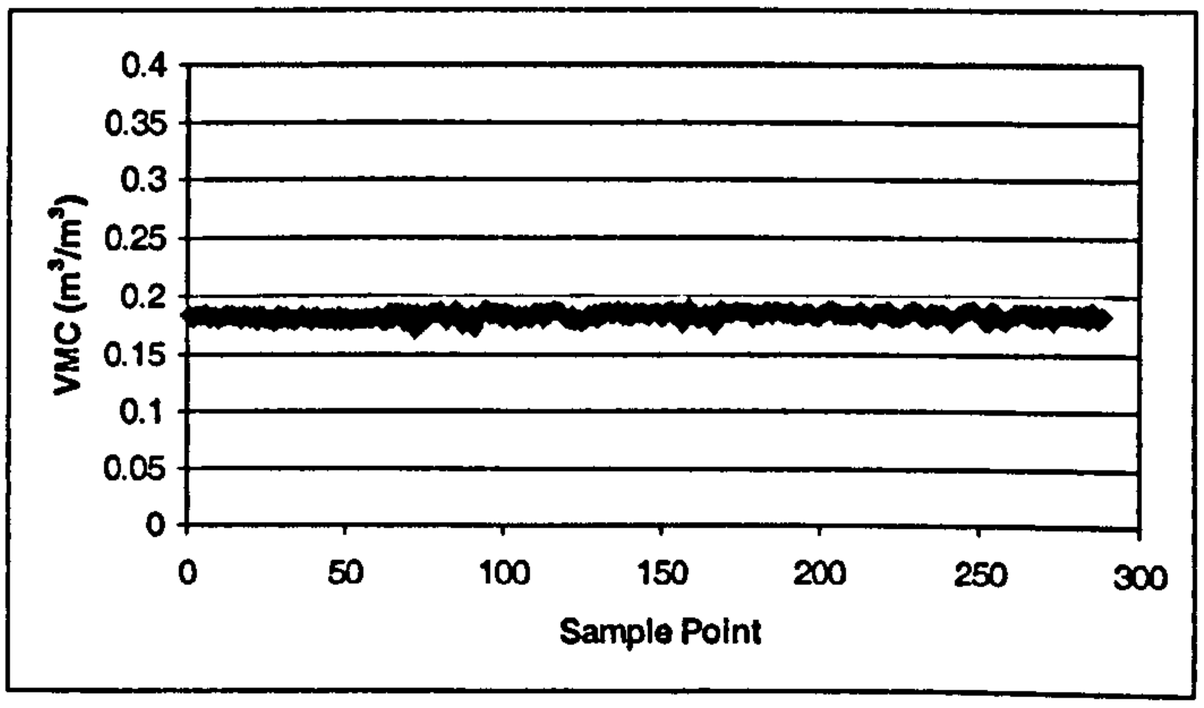

Figure 9.9: Difference between GI and GII VMC estimations for each sample point.

9.2.1.6 Balancing the sources of estimation error

Having corrected the observed VMC data the error in VMC estimation using GI is reduced to only 0.05 m^3/m^3 for all pit data. This enables subsurface moisture to be estimated with sufficient precision to assess moisture patterns. It is currently unclear whether the use of the GI equation implies that clay content determines the choice of equation or whether other sources of error dominate, such that application of the equation

is possible provided it is calibrated. To some extent the accuracy is surprising considering the potential sources of error associated with field GPR data acquisition. Chapter Eight indicates that perhaps the greatest of these relates to interference of the direct arrivals, primarily through coupling problems, and the value of the time window used to derive the MIA value. Variability in the direct arrivals occurs throughout the GPR data collected in the Plynlimon GPR datasets, although no consistent pattern was found between visits, or between test pits. Where there is a tendency towards increased direct arrival disturbance there is a tendency to bias estimations to higher VMCs due to the weakening of the MIA values. Because this lowering of magnitudes results in higher VMC estimations than might otherwise be expected, it has the effect of increasing the accuracy of the estimation of high observed VMC. This effect is compounded by the large time window used in these analyses (25 ns) compared to in the STF experiments in Chapter Seven (<20 ns). The use of a 25 ns TW implies lower returned MIAs producing further increases in estimated values of the VMC and may also smooth the moisture distribution as outlined in Chapters Seven and Eight. It appears that increased error in estimation value can act to improve VMC estimations.

9.2.2 Re-assessing the spatio-temporal evolution of soil moisture

Figure 9.10 shows the mean soil profile VMC compared with the corrected mean surface and subsurface VMC *ThetaProbe* estimates derived from all soil test pits. The temporal evolution for these data remains the same as for Figure 9.3. However, the subsurface and mean estimates are relatively higher (wetter) than in the original data presented in Figure 9.3. Furthermore, it is now clear that the mean profile VMC is moderated by the wetter subsurface values, producing a relatively consistent average profile VMC through the dry period (Profile Days 1-60) and a gradual rise in the wetter period (Profile Days 60-120). Problems with the Data-logger mean that confirmation of the smaller-scale (diurnal) fluctuations of the average moisture response of the plot is not possible. The different moisture response at different depths (subsurface and surface) indicates a divergence in the drying rates between the surface (higher) and subsurface (lower and relatively invariable). This is 'decoupling' and suggests that a measurement of surface soil water content no longer constitutes a measurement of the integrated soil water content in the profile (Capehart and Carlson, 1997). The current data only show the mean VMC estimated at each depth for all seven *ThetaProbe* test pits and therefore do not consider

the potential spatial variability of this process. The data from these pits indicate that associated with the drying of the surface relative to the subsurface layers (as indicated by Figure 9.10), the variation in results (Figure 9.11) is considerably greater at the surface, demonstrating an increase in CV over the dry period and a decrease over the wet period. Moisture variation through the entire soil profile is maintained at constant level by the relatively low variability in the subsurface moisture.

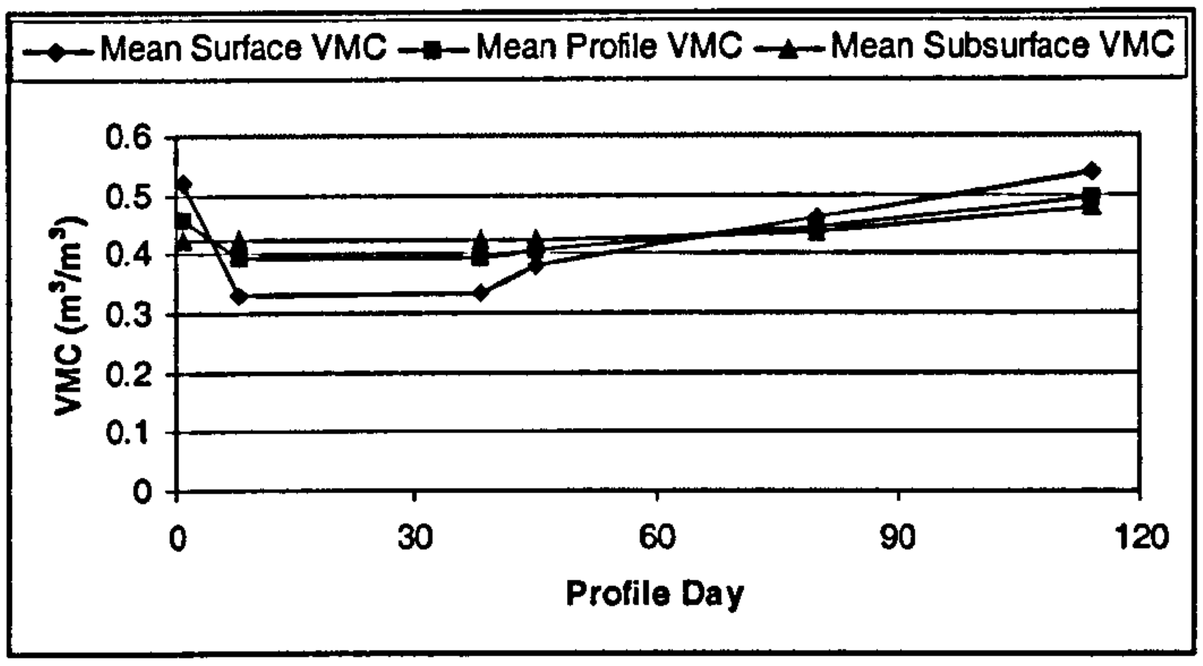

Figure 9.10: Mean observed corrected *ThetaProbe* moisture: comparison of mean profile, mean surface, and mean subsurface VMC.

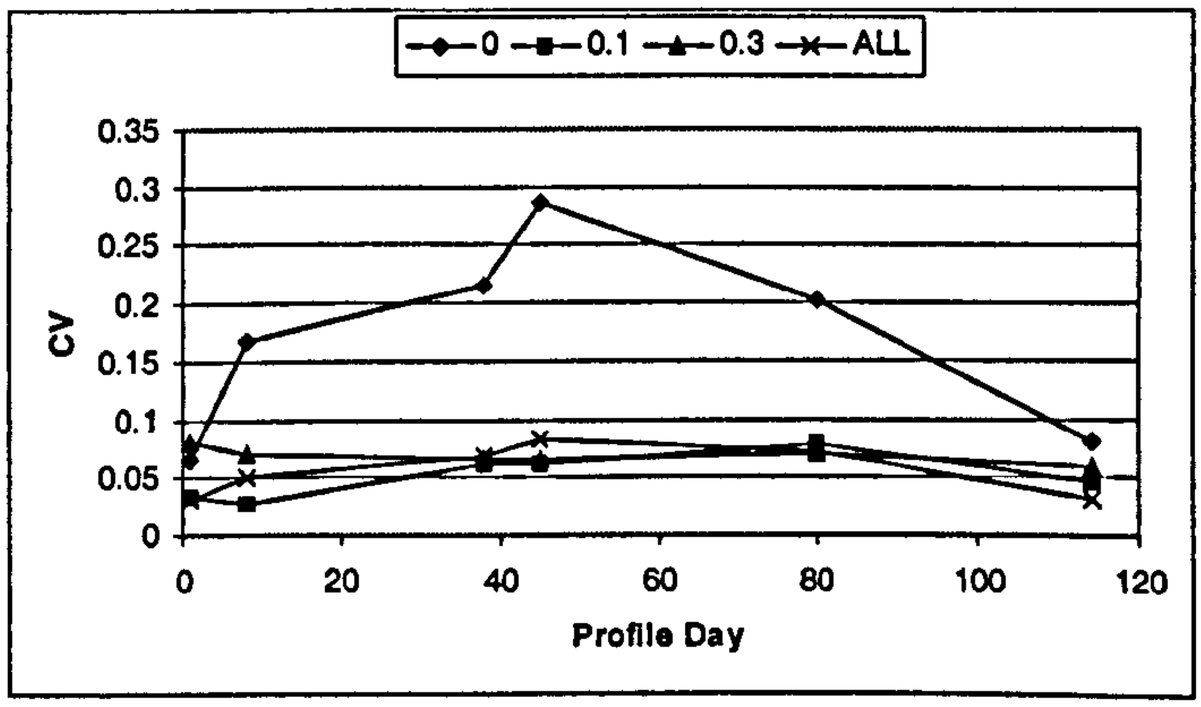

Figure 9.11: Observed corrected *ThetaProbe* moisture variability: comparison of mean profile CV, mean surface CV, and mean subsurface CV.

There are three implications for this research. First, the increased spatial variation suggested by the soil pits at the surface needs confirming as does the apparent stability of moisture in the subsurface. Secondly, the increased variation in the surface may adversely affect surface runoff by reducing connectivity, whilst the stability in moisture in the subsurface should produce relatively stable throughflow. Thirdly, GPR, which offers the only way to assess this potential variation across the plot, should record the average profile distribution and therefore should appear relatively stable. These issues are now

investigated using GPR estimations of VMC applied to 0.1 m horizontal resolution grids over the experimental plot.

9.3 GPR ASSESSMENT OF SPATIO-TEMPORAL MOISTURE VARIATION

The GPR MIA estimate of VMC produces an average VMC with an RMS error (relative to the *ThetaProbe* estimates) of 0.05 m^3/m^3, although individual point error can still be up to 0.10 m^3/m^3. Thus the GPR is capable of imaging a combination of surface and subsurface moisture patterns. The GPR has been used to estimate VMC in order to investigate the spatial patterns of VMC that develop as a plot dries and wets over a 4-month period. The following sections seek to present the GPR moisture distributions and explain the apparent moisture response within the context of subsurface behaviour. The principal aim is to identify the patterns of GPR estimated VMC, and to understand the cause of these patterns. Using this information it should be possible to discuss the implications for hillslope response and therefore to assess the potential of the GPR in hillslope hydrological applications.

9.3.1 GPR estimated moisture distributions

9.3.1.1 GPR moisture distributions

Figure 9.12 shows the GPR VMC estimates for each profile day. These Figures exaggerate the observed variation in the spatial patterns because there is only a maximum range of VMC of only 0.15 m^3/m^3 between grids. Set in the context of this limited range of variation, there appears to be limited change in spatial moisture patterns as the soil dries and wets through time in response to changes in moisture input from rainfall. However, the results do show some characteristics:

- In the absence of significant rainfall, drying is initially concentrated around the *ThetaProbe* test pits.
- This is followed by greater drying around the edges of the plot and patchy patterns in the centre of the plot. The areas that dry appear to have lower initial moisture values on Profile Day One.

- The results suggest continuous drying until after Profile Day 38, although day 80 shows an increase in relative dryness.
- An area of consistently higher VMC exists in a small topographic hollow at x = 0.2-0.8 m and y = 0.5-1.4 m.

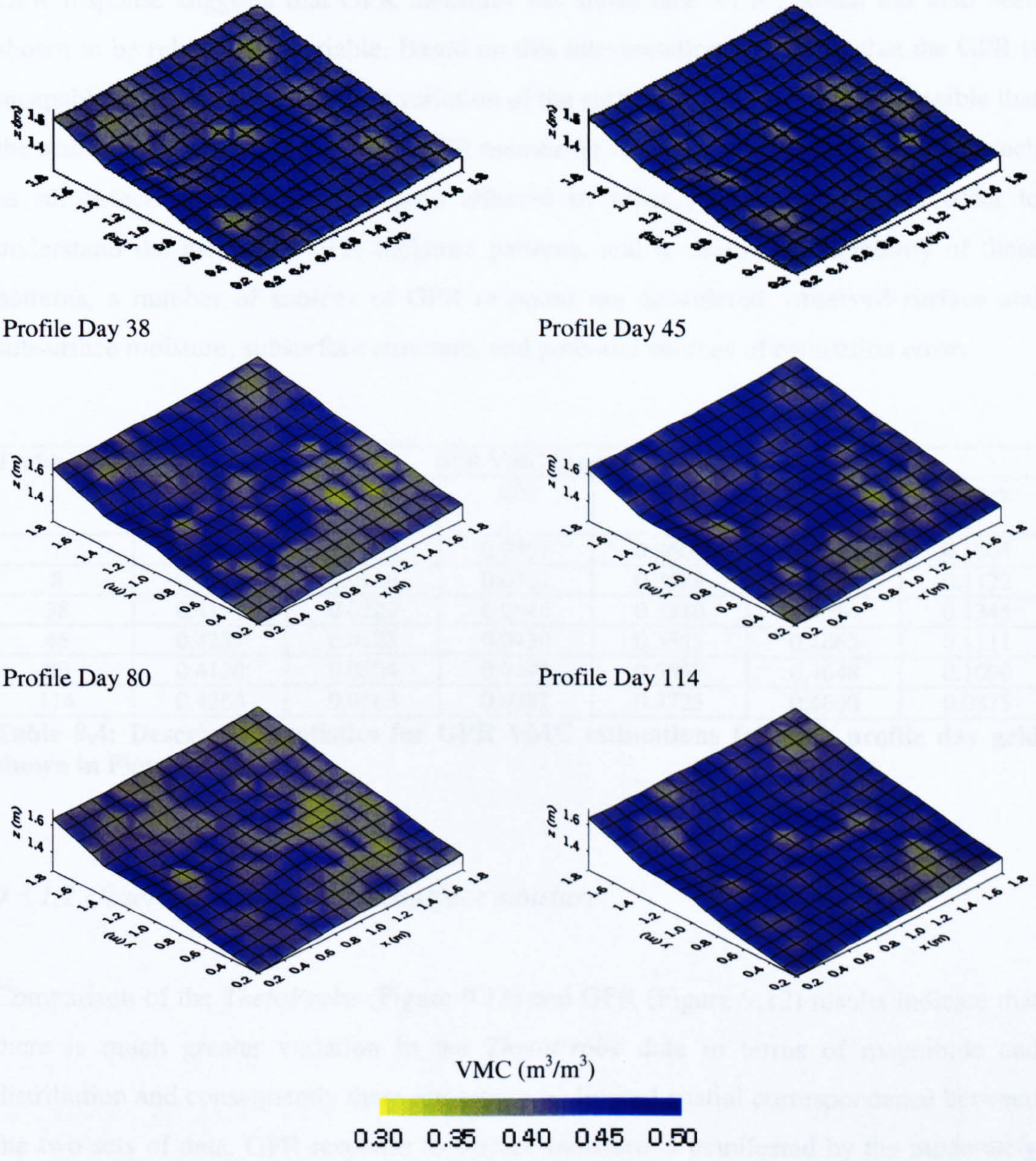

Figure 9.12: Grids of GPR estimated VMC using the GII equation applied to MIA values calculated over a time window of 25 ns for each profile day.

The results imply stability in GPR estimations of moisture distribution through time. This can be quantified by comparing the mean estimated VMC for the plot for each grid. These

values are shown in Table 9.4 and show a maximum range of mean estimated VMC of 0.019 m^3/m^3. The temporal stability of the estimations is confirmed by the relatively small changes in the range of VMC estimations, although this does tend to increase in the dry period and decrease in the wetter period. The range in estimation within grids is as large as between grids (0.135 m^3/m^3). The limited variation in the GPR estimations is further confirmed by the constant CV values for each profile day (Table 9.4). The stability of the GPR response suggests that GPR measures the subsurface VMC, which has also been shown to be relatively invariable. Based on this interpretation it is likely that the GPR is incapable of estimating the higher variation of the surface moisture. It is also possible that the stability is a consequence of the GPR measuring something other than the VMC (such as subsurface structure) or has been affected by other sources of error. In order to understand the estimated GPR moisture patterns, and to assess the reliability of these patterns, a number of sources of GPR response are considered: observed surface and subsurface moisture, subsurface structure, and potential sources of estimation error.

Profile Day	GPR VMC Estimations (m^3/m^3)					
	Mean	Standard Deviation	CV	Minimum	Maximum	Range
1	0.4245	0.0169	0.0397	0.3609	0.4615	0.1005
8	0.4318	0.0156	0.0361	0.3528	0.4649	0.1122
38	0.4190	0.0229	0.0546	0.3310	0.4654	0.1345
45	0.4257	0.0183	0.0430	0.3552	0.4663	0.1111
80	0.4130	0.0204	0.0495	0.3557	0.4648	0.1090
114	0.4263	0.0163	0.0382	0.3725	0.4600	0.0875

Table 9.4: Descriptive statistics for GPR VMC estimations for each profile day grid shown in Figure 9.12.

9.3.1.2 Observed surface and subsurface moisture

Comparison of the *ThetaProbe* (Figure 9.13) and GPR (Figure 9.12) results indicate that there is much greater variation in the *ThetaProbe* data in terms of magnitude and distribution and consequently there appears to be limited spatial correspondence between the two sets of data. GPR response to surface moisture is manifested by the moderately changing patterns of drying shown in the GPR plot data; especially across the top of the plot. With increased rainfall from the second August visit onwards (Profile Day 45) the surface appears to wet up- and across-slope away from the hollow. This pattern is less clear on the GPR data.

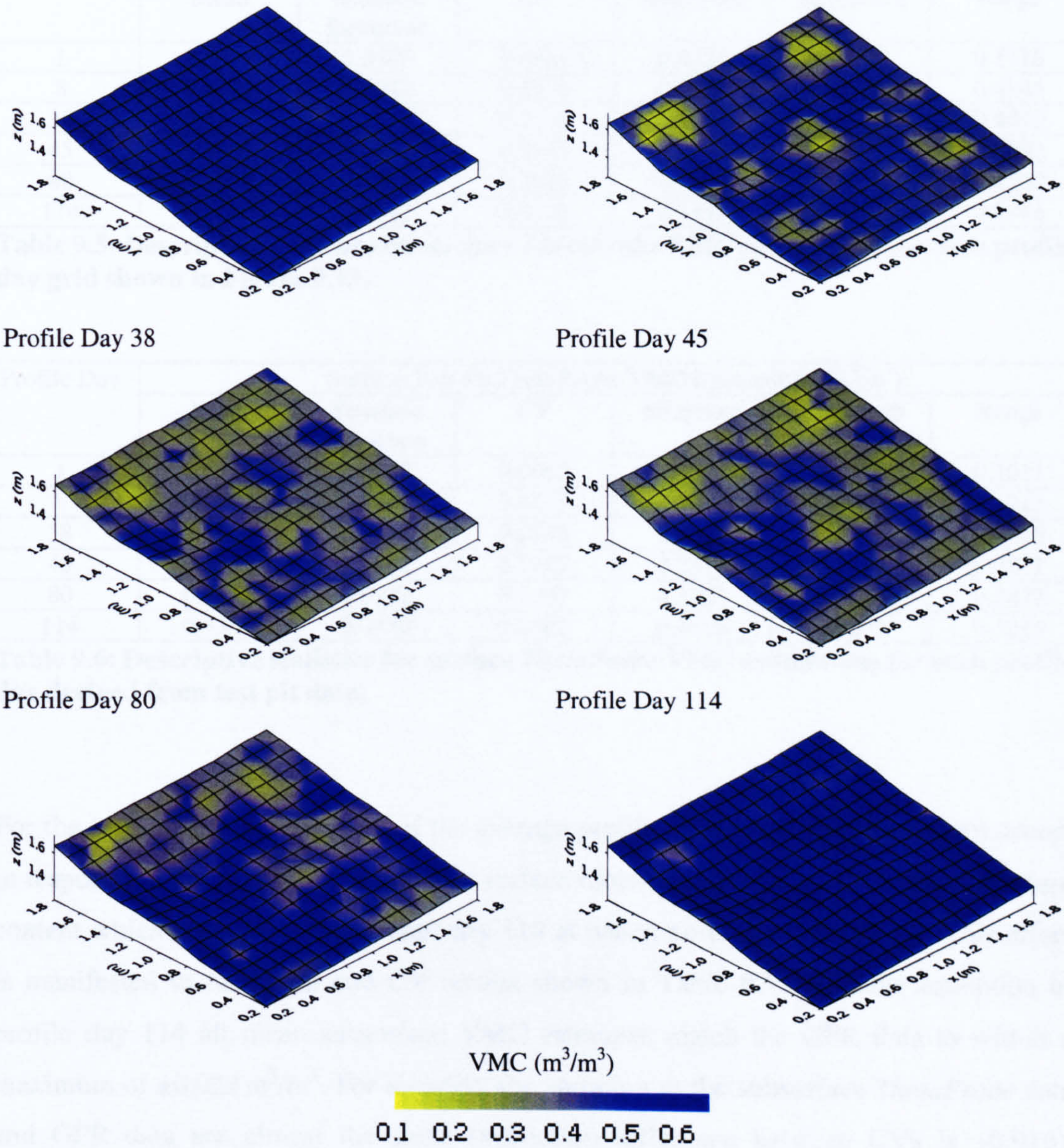

Figure 9.13: Grids of GPR *ThetaProbe* VMC for each profile day.

Comparison of Tables 9.5 and 9.6 shows that differences exist between the surface grid data and the surface pit data; with the latter drying more rapidly and generally demonstrating higher variation, although the range of moisture values is less. This indicates that strong spatial differences occur in the surface VMC and also that the pits, upon construction, provided zones of preferential surface drying. Compared to the GPR data the range of VMC estimations is far greater using the *ThetaProbe* surface data and there is also greater spatial variation. In addition, the surface *ThetaProbe* data demonstrate strong seasonal patterns in mean and CV in much the same way as shown in Figures 9.10 and 9.11.

Profile Day	Surface Grid *ThetaProbe* VMC Estimations (m^3/m^3)					
	Mean	Standard Deviation	CV	Minimum	Maximum	Range
1	0.5559	0.0306	0.0551	0.4324	0.6042	0.1718
8	0.4359	0.0842	0.1930	0.1124	0.5968	0.4844
38	0.3848	0.0814	0.2115	0.1921	0.6000	0.4079
45	0.3951	0.0858	0.2172	0.2056	0.5947	0.3892
80	0.4608	0.0933	0.2025	0.1962	0.6172	0.4210
114	0.5690	0.0417	0.0732	0.3459	0.6205	0.2746

Table 9.5: Descriptive statistics for surface *ThetaProbe* VMC estimations for each profile day grid shown in Figure 9.13.

Profile Day	Surface Test Pit *ThetaProbe* VMC Estimations (m^3/m^3)					
	Mean	Standard Deviation	CV	Minimum	Maximum	Range
1	0.5176	0.0343	0.0662	0.4724	0.5735	0.1011
8	0.3280	0.0548	0.1671	0.2667	0.3979	0.1313
38	0.3344	0.0718	0.2146	0.2349	0.4175	0.1826
45	0.3782	0.1084	0.2867	0.2317	0.5188	0.2871
80	0.4592	0.0922	0.2007	0.3203	0.5676	0.2473
114	0.5359	0.0430	0.0802	0.4866	0.6082	0.1216

Table 9.6: Descriptive statistics for surface *ThetaProbe* VMC estimations for each profile day derived from test pit data.

For the test pit data the majority of the average profile drying and wetting pattern occurs in response to the drying and wetting in surface moisture rather than subsurface moisture content which remains constant until day 114 at which point it begins to rise. This effect is manifested in the mean and CV results shown in Table 9.7. With the exception of profile day 114 all mean subsurface VMC estimates match the GPR data to within a maximum of $\pm 0.023\ m^3/m^3$. For all grids, the variation in the subsurface *ThetaProbe* data and GPR data are almost the same (maximum difference between CVs is +0.016), although variation in the *ThetaProbe* data is marginally larger. Based on the accuracy of the GPR validation (Section 9.2), it seems that the lack of variation in the subsurface moisture is estimated by the GPR. However, the range of moisture estimations in the GPR data is consistently larger than in the subsurface *ThetaProbe* data. Whilst some of this may be due to the greater number of GPR samples (249) compared to pit data (14), in the same way as for the surface *ThetaProbe* grid and pit data, it would appear that some other factor contributes. Before considering problems associated with the measurement of moisture, it is first necessary to consider the characteristics of the subsurface.

Profile Day	Subsurface Test Pit *ThetaProbe* VMC Estimations (m^3/m^3)					
	Mean	Standard Deviation	CV	Minimum	Maximum	Range
1	0.4234	0.0235	0.0556	0.4000	0.4633	0.0633
8	0.4233	0.0194	0.0459	0.3995	0.4507	0.0512
38	0.4221	0.0233	0.0551	0.4010	0.4593	0.0583
45	0.4221	0.0233	0.0551	0.4010	0.4593	0.0583
80	0.4355	0.0264	0.0607	0.4114	0.4791	0.0677
114	0.4762	0.0220	0.0461	0.4454	0.5052	0.0598

Table 9.7: Descriptive statistics for subsurface *ThetaProbe* VMC estimations for each profile day derived from test pit data.

9.3.1.3 The role of subsurface structure

Because subsurface structure does not change with time, this may explain the apparent consistency in GPR results. Howe (2000) demonstrated that soil horizons and bedrock boundaries could be identified using GPR in the Cyff Catchment. Soil augering and excavation of a trench and soil test pits (Figure 5.8) during plot construction, confirm these events. One principal subsurface structural feature in the current plot is a high concentration of unconsolidated shale at variable depths across the plot. Figure 9.14a gives an indication of the depth to this zone across the experimental plot at 0.4 m resolution although this figure exaggerates the dimensions of the deep and shallow zones. Although a high stone content occurs consistently across the plot at variable depths below 0.3 m, the figure indicates a significant proportion of the plot having only 0.15-0.2 m of fine earth soil. Augering is unable to penetrate through rock fragments that occur in the subsurface and give the impression of very shallow soils. An example of such a rock fragment is shown in Figure 5.8b. These very shallow depths are taken as anomalies and the soil thickness across the plot re-plotted in Figure 9.14b with these points set at 0.3m. This figure shows deeper soils towards the top of the plot and towards the topographic hollow. Comparison of Figure 9.14b with the GPR moisture distributions indicates strong association between dry zones and shallow depths along the lower edge of the plot and diagonally from about x = 0.2, y = 1.8 to about x = 1.0 to y = 1.0. Both of these features on the GPR responses are consistent between profile days, although their relative magnitude changes.

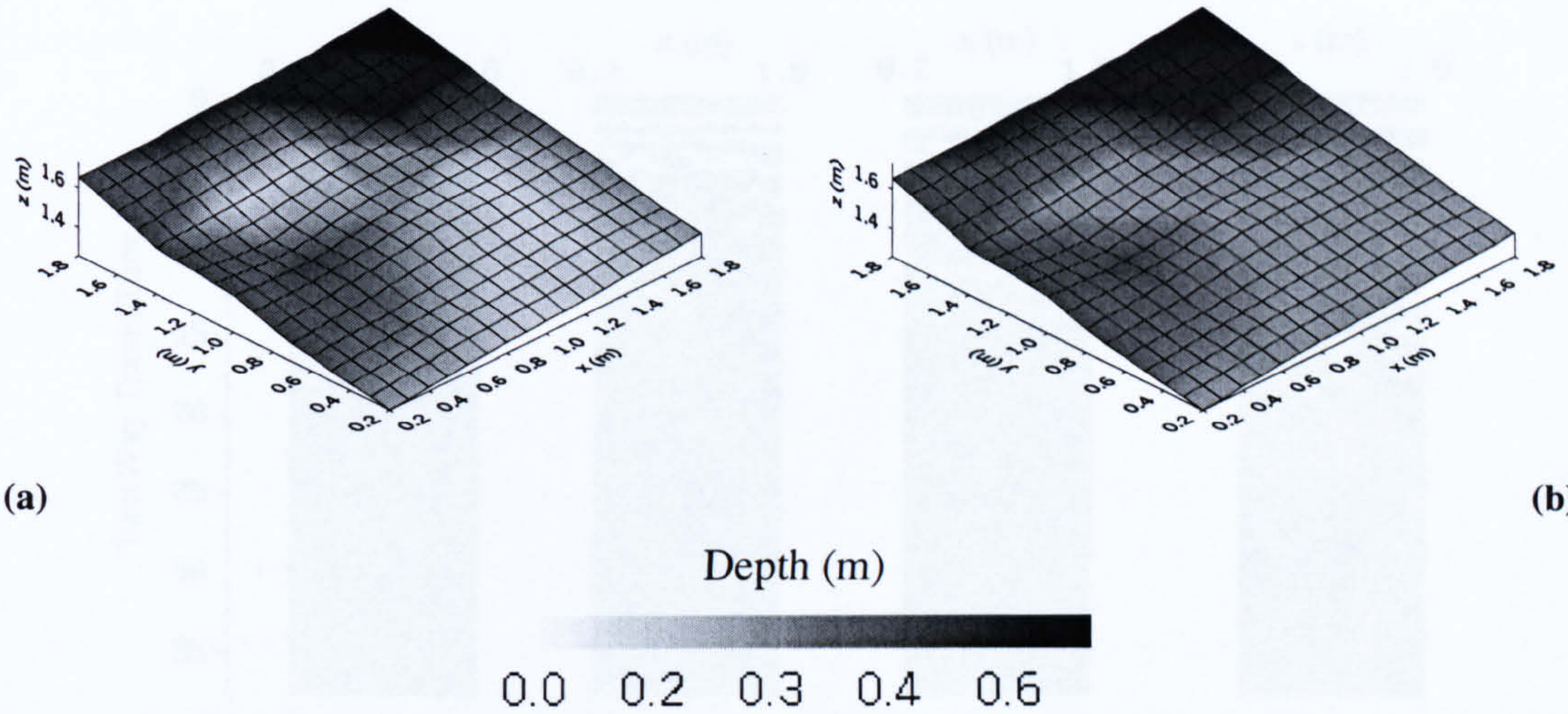

Figure 9.14: Depth to stone layer (a) with anomalous rock fragments, (b) without anomalous rock fragments.

If there were no moisture effect, all GPR reflections would be constant through time (profile days) and GPR moisture patterns would be identical. Using profiles at y=1.6 m (where there is limited test pit disturbance, relatively even topography, and potential for identifiable subsurface structures) a number of differences between GPR data can be seen as time evolves (Figure 9.15). Figure 9.15 shows variation in both timing and magnitude of subsurface events across one transect. There is sufficient variation in the responses to indicate changes in moisture conditions, either at the surface or in the subsurface. The changes in GPR responses are as follows:

- Changes in the direct arrivals that get increasingly disturbed and appear to get broader (indicating changes in coupling with the surface as a consequence of changes in VMC).
- The test pits containing the *ThetaProbes* are visible when dry on day eight. By day 45 these disturbances are obscured by changes in the direct arrivals.
- Generally there is a retreat and weakening in reflections. These changes are small but indicate an increase in VMC.
- There is a suggestion of a near-horizontal reflector at x=0.8-1.8 evident from day 45 although the coherency of this event is variable. On day 80 it is truncated and by day 114 it is less linear.
- The interpreted stone boundary is not clear on the figures due to disturbance from *ThetaProbes* and the sample spacing of 0.1 m. There is a suggestion of a shallowing event from x=0.2-0.4, which then dips away in time. It is possible that the subsurface stone boundary is not as consistent as it appears in the crudely interpolated image.

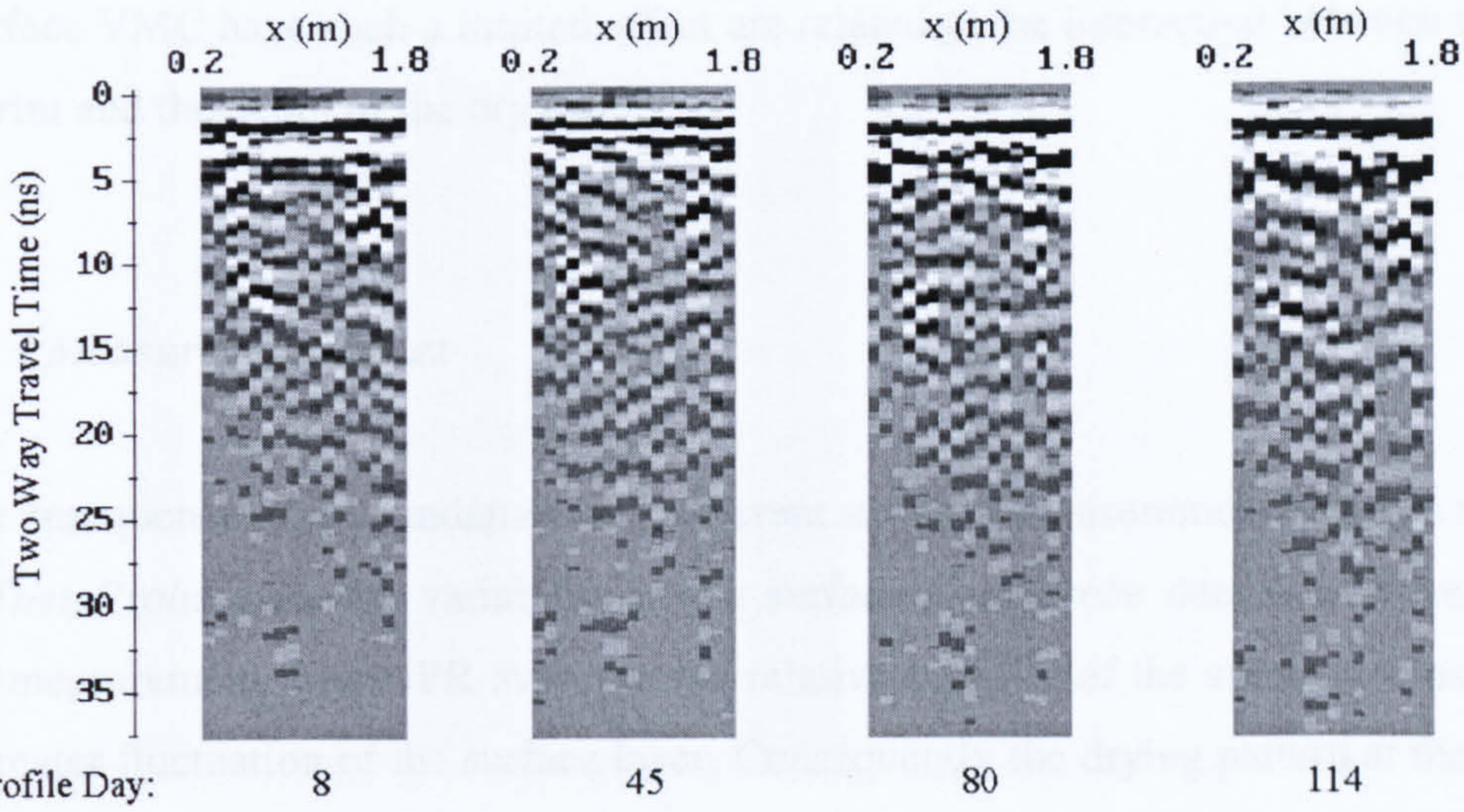

Figure 9.15: Changes in GPR response with profile day.

The subsurface structure is principally manifested as a layer of very high stone content. This effectively reduces the total pore volume of the soil profile (Van Wesemael *et al.*, 1999) and reduces the effective VMC throughout the soil profile. The GPR measures an integrated VMC estimate through a depth determined by the time window. The depth of investigation, and the calculation of the MIA value, included much of the stone layer. When the stone layer is closer to the surface of the soil, the GPR measures a reduced effective volume of moisture, because much of that volume is occupied by stones. Therefore, this effective drying in space manifests itself on the GPR image as zones of relatively drier soil, which are relatively constant throughout the field campaign. There are two further effects. First, compared to the subsurface *ThetaProbe* data, this shallow soil produces a greater range of VMC estimate because the GPR measures total volume whereas the *ThetaProbe* measures only the VMC in the fine earth material. Furthermore, the *ThetaProbes* only measure VMC in the relatively stable subsurface zones; not deeper where it is possibly drier. Secondly, the shallower zones appear to be more affected by surface drying than other zones across the plot. This occurs because if the thin surface layer of soil dries, it proportionally has greater effect on the GPR response, because a greater amount of the vertical profile is effectively dry. After reconsidering the response, it is argued that the surface *ThetaProbe* VMC estimation manifests itself in those parts of the plot where the GPR measurement of the subsurface is already dry (i.e. shallow soil) or where the magnitude of surface drying is greatest (i.e. at the top of the plot). The surface moisture has a weak influence on the GPR estimation. The reasons why the high variation

in surface VMC have such a limited effect are related to the interaction between the GPR footprint and the depth of the dry layer.

9.3.1.4 Measurement scales

As a consequence of the fundamentally different scales of measurement between the GPR and *ThetaProbe* data, the variability in the surface *ThetaProbe* data is averaged in the GPR measurement. The GPR averages the relative stability of the subsurface as well as the greater fluctuation of the surface layer. Consequently the drying pattern at the surface appears as a lower magnitude pattern whose areal influence is less broad. It is possible that the domination of the subsurface values in the GPR moisture patterns is a consequence of the greater sample volume at depth. This is a consequence of two aspects. The drying surface layer is relatively thin, being at most less than 0.1 m (the depth from surface to first subsurface *ThetaProbe*). If the soil profile is a maximum of 0.6 m then this equates to only 17% of the depth contributing significant moisture variation. The GPR footprint means that the moisture estimate is derived from an area rather than a point, and this area increases with depth. The usual GPR response in low dielectric constant media is not maximised directly below the antenna (Arcone, 1995) and the spread of the signal depends upon the characteristics of the surface; as the dielectric constant increases, the directionality (increased focusing) of the antenna increases (Annan. 1997). The measurement area at 0.1 m depth is 0.0096 m^2, and this corresponds to about 8% of the area at 0.6 m depth (0.1251 m^2). Thus, it is clear that the thin drying layer at the surface will have very little dielectric and attenuative contribution to the actual signal response. Furthermore, the area that the antennae occupy on the ground surface is approximately 0.08 m^2; this gives some indication of the area over which a surface response may occur. An important way of developing greater certainty in the causes of the GPR spatial pattern would be to compare GPR results with surface *ThetaProbe* estimations averaged over a larger area. This may allow an assessment of the extent to which the surface moisture patterns measured by *ThetaProbe* are, in fact superimposed over the top of the subsurface GPR results, but distorted by differences in sampling volume.

9.3.1.5 Summary

The characteristics of the GPR moisture patterns has been decomposed into the potential causes of the response. Three main characteristics occur:

- The variation is limited through space and time principally as a consequence of the limited variation in subsurface moisture, which the integrated measurement of profile moisture records effectively.
- Two consistently drier zones occur in association with shallower depths as a consequence of a layer containing a very high concentration of stones. This layer acts to decrease VMC by adding a reflection event to the GPR data (producing higher MIA values) and also reduces the total pore volume over the measurement depth and thereby reducing the effective VMC measured by the GPR. This effect could be stronger if it were not for the fact that there is high moisture in the soil above the stone layer, which attenuates the signal. This suggests that the GPR responds to the total moisture in a soil profile as well as the VMC.
- The impact of high variation in surface moisture is only weakly manifested in the GPR estimation, except in areas where there is significant drying or where drier conditions existed previously. The effect of the high variation in surface moisture in the GPR moisture patterns is minimised because the GPR and *ThetaProbe* estimates are acquired over the different surface areas and the GPR measures the variation in the total soil profile of which the thin drying layer is only a small part.

9.3.2 Implications of GPR estimated moisture distributions

The VMC patterns indicate changes in the connectivity at the surface as a consequence of increased variation with drying, but less so deeper in the profile where moisture patterns are stable. The hillslope environment was wet all throughout the field campaign and the surface variations in moisture and connectivity are not transmitted much deeper in the soil profile. Thus, at least for this part of the hillslope, subsurface moisture movement is likely to be consistent throughout the year, whilst overland flow patterns may be more variable. This suggestion can be investigated by comparing the observed variation, with the GPR variation and with the output of moisture from the plot as either throughflow or overland flow. It is expected that with increased drying, connectivity decreases (variation increases) and outflow at the surface or in the subsurface will decrease. The moisture

estimates have indicated increased variation in the very near-surface zone, but limited changes in the subsurface. Thus overland flow is expected to decrease with drying whilst throughflow should remain more constant. Unfortunately, problems with the Datalogger in the field prevented a comprehensive record of any continuous data of rainfall, overland flow or throughflow. Thus it is not possible, using the current data, to confirm these potential implications.

9.4 CONCLUSIONS

The GPR technique for estimating soil moisture patterns throughout this research was successfully applied to the mapping of moisture at the field plot-scale in the Cyff Catchment, Plynlimon, Wales. The average VMC profile estimated using GPR corresponds closely (RMS Error of 0.05 m^3/m^3) with the observed *ThetaProbe* data. Again it must be noted that this accurate estimation of average plot VMC does not guarantee an accurate estimation of the moisture distribution throughout the plot. A number of technique-specific errors appear to interact with the plot hydrology to produce moisture patterns that are reasonably stable throughout the year. Whilst surface VMC varies considerably over the four-month observation period, the GPR is more sensitive to the relative invariability of the subsurface moisture, although the estimations are affected by a subsurface stone layer, which acts to reduce the effective VMC measured by the GPR. Where the stone layer is nearer to the surface, the drying at the surface has a greater impact on the GPR estimation of VMC. Compared to the urban leak data, the reduced subsurface and surface disturbance (no pipes, no change between path and road) produces more reliable results. The results also appear improved over the LTF WET experiments, although the complete moisture pattern cannot be validated because of incomplete coverage across the plot.

Although apparently successful this chapter confirms the problems identified with the method in Chapter Eight. Although less affected by subsurface objects generating random zones of high MIA than the results in Chapter Eight, this work has illustrated very clearly that the MIA measurement is dependent on several properties of soils that are not related to the VMC. The many sources of error identified in Chapter Eight offer the potential for variable interrelationships between these sources. Consequently, these interactions may occur in a complex manner producing unaccountable changes in MIA values. Whilst

some of these factors have a direct impact on the GPR response, some also affect the VMC. Furthermore, the interrelationships between some of these factors mean that it is impossible to isolate only VMC response in the GPR signal. Therefore, the technique fails to give a convincing impression of moisture pattern whilst at the same time indicating a number of aspects of the subsurface related to moisture behaviour that can clearly be identified using GPR

Again the complexity of the subsurface environment produced uncertainty in the GPR MIA value. It is possible that had the soil been deeper and less complex (fewer layers and no stones) the potential impact of the subsurface on the GPR response, directly, and indirectly, through the impact on moisture distribution, may have been reduced and the results may have been more easily interpretable in terms of moisture. The soil layering produces different reflection patterns than occurred in the chapter seven data. As discussed in chapter eight significant divergence from the original subsurface structure may invalidate the developed method. Reflections from layers produce differences in MIA that will be particularly noticeable where the direct arrivals are interfered with. Although, variations in topography were minimised by site selection, the presence of a hollow and the occasional plant did produce problems with antenna coupling resulting in dramatic reductions in MIA. The spatial variation of these coupling patterns has a strong influence on the resulting moisture distribution. The presence of subsurface objects, such as the *ThetaProbes* and stones, can produce strong reflections that can either increase the MIA in a random fashion or can counter the reduction in MIA caused by the loss of the direct arrivals. Consequently, the GPR VMC measurement becomes less likely to actually represent the variation in subsurface moisture. The GPR, through its sensitivity to subsurface objects, may on many occasions not be measuring VMC, although it is very likely to be measuring something of hydrological significance. In this context the changes in material properties that occur with the horizontal layering across the plot (especially the very stony layer) are particularly important through their influence on the potential distribution of moisture.

One notable problem with the field investigations is due to the fact that conditions appeared not only stable throughout the field campaign, but also very wet. Whilst this may have improved VMC estimations by reducing the impact of the sources of variability that affected the laboratory runs, it was noted in chapters seven and eight that the method may be inappropriate for either very dry or very wet conditions as a consequence of the

range of VMC used for the development of the model. It is possible that the near-saturated conditions resulted in moisture homogeneity such that only subsurface 'structure' was being imaged.

It is also possible that the limited spatial variability observed in the GPR VMC estimations is related to the small size of the study area used in the research. It is likely that over an area of only 4 m^2, the actual moisture variation would have been very small, thus preventing assessment using a tool which is very sensitive to subsurface structure. A larger study area had initially been tested (10 m by 30 m) but it proved impossible to cover the area at sufficient resolution at both frequencies and with supporting surface *ThetaProbe* data in one session. Separating grids across too much time during the same trip would have produced problems with changing moisture conditions (given the propensity to rain) and would have reduced the completion rate of GPR surveys. Furthermore, such a large area would have prevented as much control on the inputs and outputs of the system and would have required a far greater number of subsurface instruments that were not available. With the resulting uncertainty in GPR VMC estimates it was impossible to discern whether or not the apparent lack of variation in subsurface moisture throughout the period of investigation was due to GPR problems or an actual stability in the moisture as implied by the network of *ThetaProbes*. The *ThetaProbes* which were themselves subject to error and do not cover the plot area sufficiently to confirm moisture distribution. Furthermore, had there been no problems with the support data, more could have been understood in terms of the subsurface moisture.

Clearly a great deal more work is required to overcome great limitations in the application of such a basic equation, but the method displays great potential to be used directly for mapping of subsurface moisture patterns, even at such a small-scale of investigation. More importantly, combination of the technique with existing techniques may indicate the degree to which the surface variation is influencing subsurface estimation. Thus, combination of techniques may greatly enhance understanding of moisture patterns.

CHAPTER TEN: SUMMARY, CONCLUSIONS AND FUTURE RESEARCH

In Chapter One the primary objective of this research was to develop and apply GPR to the estimation of VMC and its spatial distribution. The following chapters outlined current knowledge concerning subsurface moisture and GPR, and aimed to integrate the two through an understanding of existing and potential methods of estimating VMC using GPR. For high resolution mapping of moisture distribution, limitations of existing techniques mean that there is a clear requirement for a non-invasive tool for the estimation of moisture patterns and content for a variety of environmental applications. This has been attempted using GPR in reflection profiling mode. GPR does not provide a direct measure of VMC and therefore some aspect of the GPR signal needs to be selected in order to derive its value. A methodology was developed that integrated a variety of controlled laboratory experiments (controlled subsurface structure, materials, GPR system, hydrology) and field investigations (uncontrolled leak detection and controlled hillslope plot), to understand GPR response to incrementally more complex subsurface situations and to develop GPR-VMC relationships in four stages. From this work a number of conclusions can be drawn.

The first stage of the research (Chapter Six) involved an assessment of GPR signal response in the absence of moisture in order to understand the basic features of, and controls on, GPR response, to establish the ability of GPR to estimate subsurface material and structural properties (layering, anomalous targets), and to make recommendations, based upon operational limitations, for the design of subsequent experiments. It was found that:

- GPR provided accurate information on vertical variation within the subsurface, in the absence of subsurface structural anomalies (a *ThetaProbe*). The higher resolution of the 900 MHz antennae proved to be more suited to this analysis.
- The limited variation in material properties in the horizontal plane is undetectable using GPR; especially in dry conditions when GPR is more sensitive to subsurface objects. The presence of an anomaly means that, under dry conditions, detailed profiling of material properties will not be possible.
- Vertical and horizontal variation in GPR response increases with depth as a consequence of the anomaly.
- Variation in GPR response is increased by using a lower antenna frequency as a consequence of increased signal wavelength and footprint dimensions.

- For interpretation of quantitative assessment of GPR responses it is necessary to collect high resolution profile data; otherwise the anomaly may not be detected and the moisture response may become obscured.

The second stage of the research (Chapter Seven) aimed to develop models for estimating VMC using a variety of signal parameters, and to assess their accuracy and repeatability within the context of application to subsequent analyses of moisture patterns. It can be concluded that:

- Under controlled laboratory conditions, a method of characterising GPR response to changing VMC in a variety of earth materials was successfully developed after the initial investigation of a number of potential signal characteristics.
- The mean instantaneous amplitude (MIA) provides a combined estimate of subsurface dielectric contrasts, signal attenuation, and other effects on the waveform, and declines in value with increasing VMC.
- Anomalous behaviour identified in the dry and saturated moisture conditions suggests that this technique is only applicable to intermediate moisture contents (three-phase subsurface conditions).
- The effects of variations in moisture distribution act to increase scatter in the experimental results rather than preventing estimation of the VMC.
- Disturbance of the direct arrivals, to which the method is very sensitive, may limit application to more complex environments. GPR traces should always be interpreted to identify the problem.
- The developed relationships are dependent on *a priori* knowledge of subsurface conditions, which allow the measurement volume to be controlled. In the absence of this control, the use of a constant time window, produces weaker relationships, and may potentially smooth moisture distributions estimated using the method. It will still provide accurate estimations of VMC.
- The experimental materials could be placed into two groups of linear relationship; the differences between these models being a function of the material's propensity to attenuate the signal when dry. This is seen primarily as a function of the clay content.
- Subsequent testing of both models under identical laboratory conditions indicated a maximum RMS Error of 0.06 m^3/m^3, which although not directly comparable to the *ThetaProbe* values due to fundamental differences in measurement volume, demonstrates that the method was able to provide consistent and repeatable estimations of VMC.

Application of the method, in the third stage of the research (Chapter Eight), demonstrated that under more complex experimental and subsurface conditions, the accuracy of the GPR estimations of VMC were reduced. Specific findings include:

- Average VMC is overestimated as a consequence of the weakening of direct arrivals due to uneven surfaces, which affects the coupling of the antennae to the ground, whilst using a time window that is too long enhances this overestimation. If there is a consistent disturbance, then the method is still applicable, and moisture patterns will be estimated properly, but the actual VMC estimations will become relative values.
- By reducing the depth of investigation, moisture distributions may be more accurately assessed. This implies that in conjunction with varying moisture distributions, the measurement of VMC is dependent upon the total moisture integrated over the measurement volume.
- Lower antenna frequency measures a different spatial distribution of moisture, is more sensitive to subsurface variability that is not a result of VMC changes, and produces drier VMC estimates as a consequence of a combination of less sensitivity to attenuation effects and broader wavelets, which produce increased high magnitude amplitude content. It is recommended that for moisture analysis in the near-subsurface using GPR in reflection profiling mode, a higher antenna frequency should be used.
- As suggested in Chapter Six, the GPR is very sensitive to subsurface structural anomalies. This distorts VMC estimations in both pattern and magnitude especially when subsurface conditions are very dry. Dry conditions act to increase variability in GPR signal response and this enables wet conditions to be identified as areas of relative invariability.
- This technique, combined with high-resolution visual data, allows GPR to be used in the comparison of wet and dry moisture conditions in the lab, provided the subsurface material conditions are conducive to the accumulation of water (e.g. low hydraulic conductivity, interface between materials of different hydraulic conductivity) or to the penetration of the GPR signal (i.e. not wet clays).

Although laboratory investigations of moisture distribution can be successful, the application of the technique to the detection of the moisture patterns associated with two mains water leaks was inconclusive and subject to interpretation. The reasons for this are that:

- The complexity of the subsurface, coupled with the inability to compare the before and after wetting conditions renders the technique inappropriate in the absence of validation data.
- The absence of any validation data, or detailed site information, prevented detailed interpretation of the specific causes of a signal response and, therefore, the accuracy of the estimated moisture patterns could not be assessed.

The laboratory experiments demonstrate that GPR has the potential to detect mains water leaks through the assessment of subsurface moisture patterns. However, improvements in the understanding of the GPR response to the complex urban subsurface environment are required before it can be reliably applied under field conditions.

The benefits of an approach employing detailed knowledge of environmental conditions are illustrated through an additional field study of moisture distributions at the plot scale in the Cyff Catchment, Plynlimon, Wales, in the fourth stage of this research (Chapter Nine). In comparison to the limited success of the method to detect laboratory and field moisture leaks, the relatively wet conditions of the field plot provided a successful demonstration of the GPR technique for assessing limited variation in hillslope moisture patterns. Unfortunately, problems with other sources of data prevent any conclusive discussion of the relationship between moisture inputs, VMC patterns and moisture outputs. The conclusions of the field investigation are:

- The sources of error present in GPR signal response can combine to reduce or increase estimation accuracy. In the Cyff Catchment application, such problems appear to enhance the moisture estimation accuracy ($0.05\,m^3/m^3$). However, complex interrelationships exist between many sources of error in the MIA estimate, so that this accuracy does not necessarily provide increased certainty in the spatial pattern derived using the technique. Furthermore, the accuracy is relative to an estimate of VMC that is derived from *ThetaProbes*, which are subject to their own error.
- GPR measures an integrated value of VMC throughout the soil profile, confirming that it is sensitive to the total volume of water in the volume measured, and as a consequence returns an average VMC that relates to all components of the subsurface environment.
- However, the GPR measurement is more sensitive to the subsurface moisture conditions than the surface moisture conditions because the estimation is acquired from an increased volume of material due to the greater footprint with increased depth.

- In this context it is suggested that the GPR measurement of VMC is not taken from a three-phase soil system consisting of fine earth soil material, air and water but a four component system consisting of fine earth, air, water, and gravel / rock fragment content, which is traditionally considered not part of the soil texture. The integrated measurement of subsurface VMC is therefore dependent on the subsurface structure, and provides greater information on the total profile moisture than a measurement at the surface would.
- However, the technique still does not enable estimation of VMC at different depths beneath the surface. Furthermore, the GPR measurement is sensitive to the depth of the dry surface layer, which acts to decrease the GPR VMC estimate, especially in conjunction with a shallow stone-free soil layer.

Despite the apparent success of the technique in its initial development and subsequent application, there are clearly many limitations to the method. Many of these have been discussed above and may prevent the successful application of the technique in the majority of circumstances. Once the GPR is removed from the same experimental setting as that in which the method was developed, the estimates become subject to too much uncertainty caused by any number of the factors discussed above. The general applicability of the MIA-VMC method is fundamentally limited by its over-sensitivity to surface roughness and the presence of strong and variable reflectors in the subsurface.

Surface roughness affects antenna coupling such that the usually stable direct arrivals become of variable, usually reduced, magnitude. This invalidates the model as developed in the laboratory. Subsurface scattering of the signal by subsurface objects generates reflections. Objects may scatter energy away or towards the receiver producing weaker or stronger returns respectively. If there is sufficient subsurface complexity, or a substantial reflection occurs, the resulting MIA value will be distorted. Estimated VMC will therefore be inaccurate and the spatial pattern will not be truly represented. Where the direct arrivals have been reduced, a strong near-surface reflector may compensate producing an apparently accurate VMC estimation. This has important repercussions because it means that it is not only VMC that is being measured. The effectiveness of the technique becomes a trade off between subsurface moisture content, its spatial variation, and the variation that exists in the absence of water.

Although sensitive to surface roughness in other ways, suspended mode GPR would ensure coherent direct arrivals overcoming the first of the major limitations discussed above. The data presented in this research suggest that if this limitation is overcome then the sensitivity to subsurface objects would be reduced because the method is very dependent on the direct arrivals. However, the use of suspended mode GPR would have involved modifying the selected signal characteristic and redesigning the STF experiments. By suspending the antennae sufficiently off the ground it is possible to separate the air and ground-waves (see Chapter Six) so that the air-wave could be ignored. The selected characteristic would probably estimate surface moisture more accurately because a direct measurement of the ground-wave and its change with moisture would be made. However, the decreased depth of penetration would render this approach applicable to surface moisture investigations only, whilst the increased GPR footprint at the surface would reduce the utility of the technique for small scale investigations.

The other sources of error in MIA estimation identified in this research present further limitations in the actual applicability of the method, which cannot be overcome by simply suspending the antennae. The length of the time window used in the analysis is a fundamental limitation of the method because it affects the MIA value. Thus the method is unlikely to work in complex sites where there is considerable variability in moisture or other subsurface characteristics. It is very important to correctly target the volume of interest, otherwise estimations will be wrong. Therefore, to be effective more *a priori* detail on time window is required for reliable estimation of VMC.

It can be seen therefore that the developed MIA-VMC models are very situation specific; being suitable only for similar experimental conditions and therefore difficult to generalise. This is a flaw with the empirical method and therefore proper physical modelling should be attempted. The empirical approach employed in this research means that more than just the physical response to moisture is being measured. A theoretical approach is necessary in order to understand quantitatively the relationships between radar measurements and the soil geophysical parameters (Le Toan *et al.*, 1999). Existing synthetic modelling approaches allow this to be put into practice but are generally too simplistic to address the complexities outlined in this research. An alternative is to derive an actual physical parameter. Using CMP approaches the dielectric constant is determined. From RPM data it should be possible to derive the signal attenuation. The

system is too complex to model in a fully defined physical sense. Whilst the physical interactions can be modelled some of the technical limitations cannot. Empirical methods tend to work more effectively in situations where there is a significant amount of unknown complexity.

As discussed in chapter eight many of the limitations with the method and its subsequent application relate to a number of potential flaws in the experimental design and methodology, which if properly addressed may have reduced a large proportion of the uncertainty in the results presented in the latter parts of this research. The research suffered as a result of experimental complexity and some blatant omissions from the experiments and analysis performed. The research attempted to investigate too many different aspects (development, testing, laboratory, field water leaks, field moisture variation). Considering the amount of effort involved in deriving simple empirical relationships that are still fraught with difficulties in application, the research should have concentrated on the development of the technique as a priority and less on the applications. Such an approach may well have resulted in a more robust method of using direct GPR techniques to estimate VMC and to investigate, in future, its spatial variation.

In reality the differences between the development of a technique for water leak detection and a technique for the analysis of the spatial variation of soil moisture prevented the success of the method. This occurred primarily as a result of the experimental constraints that were placed upon the research to achieve both aims. To achieve both, VMC had to be estimated. If only the water leak application had been considered, a different approach to leak detection could have been developed based more on the changes in GPR response under leak conditions. The trade off between leak detection and VMC estimation informed a tendency to increase the importance of moisture pattern over moisture value. For leak applications the relative differences of moisture were more important than the absolute values. However, this is not necessarily the case for hillslope hydrology applications, in which patterns may remain very similar but may effect hillslope response very differently depending on the actual volume of moisture. Furthermore, the sensitivity of GPR to subsurface objects renders the GPR return pattern unreliable in terms of its representation of subsurface moisture; even for water leak detection.

The LTF experiments demonstrate a number of problems related to the aim to detect leaks and assess spatial patterns of moisture. Water was run into the facility for each

experiment but was stopped before any GPR data were collected. This was done to ensure that the water distribution could be measured without its content and distribution changing significantly through the addition of any further water. However, this meant that there was no leak in progress while the GPR was in use, whilst for mains water leaks the water would continue to flow. Thus, scaled leak conditions were not adequately reproduced in the laboratory. Although this is justified through the attempt to identify leaks through the detection of the water bodies associated with them this represents a conflict of interests between moisture distribution and water leaks. Furthermore, stopping the water prevented any useful 450 MHz data being collected. Related to this is a flaw in the methodology, which relates to the comparison of before and after leak GPR data. Such an approach would work in principle if pre- and post-wetting conditions can be compared. In reality, this is not possible.

The detection of moisture variability was hindered by the complexity of the developed subsurface structure. Variation in GPR response was caused by the layering of materials and the presence of anomalies, such as the *ThetaProbe*. In future investigations only a single material should be used in the LTF to overcome the uncertainty with having layers by simplifying the subsurface environment, therefore making the results more easily interpretable. The subsurface should also have been simplified by excluding subsurface anomalies. This would have enabled a more general, more physical method to be developed. However, without the *ThetaProbe* anomalies there would have been no means of validating GPR estimations of VMC and its distribution. There are also a number of issues related to the use of *ThetaProbes* to validate moisture:

- In the LTF and Plynlimon experiments there was insufficient *ThetaProbe* coverage to verify distributions. Increased numbers of *ThetaProbes* would have interfered with both GPR response and moisture distribution.
- The accuracy of the GPR method cannot be assessed adequately because the estimates of VMC are relative to those of the *ThetaProbes*, which themselves have considerable error.
- If the *ThetaProbes* have error associated with their estimates of VMC, and the MIA-VMC model is based upon these *ThetaProbe* estimates, then the developed GPR model will have some inherent unaccountable error that may produce problems in its subsequent application.

An alternative to the use of *ThetaProbes* was not feasible given that most of the other means of deriving moisture have their own error and, with the exception of the gravimetric method, would interfere with GPR response. However, use of the gravimetric method would have required excavation of the subsurface. This would have made the existing repeatable STF runs impossible to implement. It would also limit the number of investigations and the range of materials and VMCs investigated.

An alternative approach to assessing the reliability and accuracy of the developed method would have been to compare it against the standard GPR method for deriving moisture estimates. The omission of any CMP analyses against which to ground the MIA-VMC method is a serious limitation of the research. Originally, CMP analysis featured strongly in the research methodology although emphasis was given to RPM data. CMP data that were collected were of very poor quality, preventing the derivation of signal propagation velocities and, therefore, VMC. Any future work should attempt to compare the MIA-VMC method against CMP data.

In addition to the practical reasons for the design choices made in this research, a number of other problems influenced the design and outcome of this research. The first relates to the limitations of learning a new technique. With greater knowledge and experience of the use of GPR, the design of the experiments would have been better informed and a number of the recommendations outlined above could have been implemented. Some problems relate to a series of technological problems (such as the GPR breaking down, problems with data loggers, laptops and batteries in the field and laboratory, and the construction of the LTF) and some relate to the commitment to the CASE partner. The latter issue affected both laboratory work (in particular, the LTF experiments were rushed and were performed before the STF ones) and the urban leak detection field work (exclusion from field work design and implementation resulted in only 450MHz data being collected, grids of insufficient resolution, and no validation data). A higher level of integration with the Thames team in both the laboratory and the field would have benefited the research considerably.

Implications for future research:

The GPR has shown itself to be a technique that enables the moisture patterns of the subsurface to be investigated. In retrospect, a number of aspects of this research could have been done very differently. If the research were to be re-done it should incorporate many of the recommendations above. These improvements should be implemented in any further research. In addition to improving the experimental methodology, there are many unresolved issues that come out of this research. To apply the developed technique successfully with increasing confidence a considerable amount of further research is required in order to:

- **Clarify issues relating to the GPR VMC estimation.** The physical basis of the method needs to be assessed in much more detail, and ultimately a physical model that integrates many of the different aspects of the moisture response should be developed. It is important to determine the true role of texture and especially clay content on the VMC relationship, address the uncertainty in the issue of measurement volume, and to determine precisely what the GPR responds to (VMC, integrated VMC, total water). It is currently necessary to calibrate and validate the relationships on a site-specific basis.
- **Clarify issues of GPR use and analysis.** It is possible that through improving the understanding of ground-mode response and combining it with suspended mode assessments (to determine surface moisture more precisely using the reflection at the air-ground interface), coupled with improvements in system design (such as increased focusing of energy), that the information available for estimating spatial distributions of VMC can be maximised. Another area of improvement would be in the pre-processing of the raw GPR data. In addition to a significant dependence of the results on the direct arrivals, no processing was employed to correct for problems such as drift, wow, and DC shift. This means that a variety of system-specific errors may be introduced in the data presented. An assessment of the potential of using different GPR systems is also recommended; at least from the point of view of assessing the repeatability of the method.
- **Extend the research** to drier, more complex environments covering larger areas. Assessment of the method in drier environments and at larger scales would increase the potential range of application of the method and assess the true potential of the method for spatial variability studies; perhaps incorporating geostatistics and investigation of scale issues. The potential for combined studies using techniques at

different scales (*ThetaProbe*, GPR, SAR), is very strong, offering comprehensive information on soil moisture. Using a combination of these techniques (GPR and *ThetaProbe*) enabled the investigation of different scales of analysis and different depths.

In conclusion, a method has been developed that successfully estimates VMC, accurately and efficiently, under controlled conditions in the laboratory. Application to more complex environments and to estimation of subsurface moisture distributions has been attempted with varying degrees of success as a consequence of a significant number of inter-related factors which influence the GPR response. Many of these are worthy of further research and development to ensure the routine application of the method to a variety of situations.

APPENDIX ONE: METHOD FOR HYDRAULIC CONDUCTIVITY DERIVATION

Zhang (1997) proposed a two-term numerical solution to describe the infiltration process under the disk infiltrometer for any infiltration time as follows:

$$I = (C_1 t^{1/2} + C_2 t) \qquad \text{(A1.1)}$$

where C_1 ($ms^{-1/2}$) and C_2 (ms^{-1}) are parameters which can be related to soil sorptivity and hydraulic conductivity by

$$C_1(h_0) = A_1 S(h_0) \qquad \text{(A1.2)}$$

$$C_2(h_0) = A_2 S(h_0) \qquad \text{(A1.3)}$$

where A_1 and A_2 are non-dimensional coefficients and h_0 (≤ 0) is the tension value of the infiltrometer (2cm for the minidisk infiltrometer (Decagon, 1998)). C_1 and C_2 are obtained by fitting the data vs. time with equation (5.1) using a maximum neighbourhood method (see Decagon (1998) and Zhang (1997) for details). The soil sorptivity and hydraulic conductivity can be determined by

$$S(h_0) = C_1 / A_1 \qquad \text{(A1.4)}$$

$$K(h_0) = C_2 / A_2 \qquad \text{(A1.5)}$$

Because only hydraulic conductivity is of interest here A_2 can be defined as follows:

$$A_2 = \frac{11.65(n^{0.1} - 1)\exp[2.92(n - 1.9)\alpha h_0]}{(\alpha r_0)^{0.91}} \qquad n \geq 1.9 \qquad \text{(A1.6)}$$

$$A_2 = \frac{11.65(n^{0.1} - 1)\exp[7.5(n - 1.9)\alpha h_0]}{(\alpha r_0)^{0.91}} \qquad n < 1.9 \qquad \text{(A1.7)}$$

where n and α are the van Genuchten parameters for the soil and r_0 is the disk radius (1.59cm for the minidisk infiltrometer). Values of A_2 were derived from a look up table in the application.

REFERENCES

Annan, A.P. *(1996)* Transmission dispersion and GPR, *Journal of Exploration Geophysics* 0, 2, 125-136.

Annan, A.P. (1997) *Ground Penetrating Radar Workshop Notes*. Sensors and Software Inc., Ontario.

Annan, A.P., Bauman, P., Greenhouse, J.P., Redman, J.D. (1991) *Geophysics and DNAPLs*, **PEMD#69**, Sensors and Software Incorporated, Ontario.

Annan, A.P., Davis, J.L., Vaughan, C.J. (1984) Radar mapping of buried pipes and cables, *Sensors and Software Inc., Technical Note 1.*

Arcone, S.A. (1995) Numerical studies of the radiation patterns of resistively loaded dipoles, *Journal of Applied Geophysics* 33, 39-52.

Arcone, S.A. and Delaney, A.J. (1982) *Measurement of ground dielectric properties using wide-angle reflection and refraction.* CRREL Report 82-6.

Barnes, A.E. (1998) The complex seismic trace made simple, *The Leading Edge*.

Benallegue, M., Normand, M., Galle., S., Dechambre, M., Taconet, O., Vidal-Madjar, D., Prevot, L. (1994) Soil moisture assessment at a basin scale using active microwave remote sensing: the Agriscatt '88 Airborne Campaign on the Orgeval watershed, *International Journal of Remote Sensing* 15 (3), 645-656.

Berndtsson, R. and Larson, M. (1987) Spatial Variability of infiltration in a semi-arid environment, *Journal of Hydrology* 90, 117-133.

Beven, K. (1981) Kinematic Subsurface Stormflow, *Water Resources Research* 17 (5), 1419-1424.

Beven, K. (1997) Process, heterogeneity and scale in modelling soil moisture fluxes. In: Sorooshian, S., Gupta, H.V., Rodda, S.C. (1997) (Eds.) *Land Surface Processes in Hydrology: Trials and Tribulations of Modeling and Measuring*, NATO ASI Series, Vol I, 46, Springer-Verlag Berlin, 191-213.

Beven, K.J. and O'Connell, P.E. (1985) General report on water balance computation techniques. In: *New Approaches in Water Balance Computations*, 41-46.

Blöschl, G. and Sivapalan, M. (1995) Scale issues in hydrological modelling: a review. In: Kalma, J.D. and Sivapalan, M. (Eds.) (1995) *Scale Issues in Hydrological Modelling*, Wiley, Chichester, 9-48.

Boll, J., Kung, K-J., S., Ritter, W.F., Hendrickx, J.M.H., Herbert, S.J., Daliparthy, J., Tomer, M.D., Steenhuis, T.S. (1993) Detection of textural interfaces using ground-penetrating radar, *Sensors and Software Inc., Proceedings of the Thirteenth Annual AGU "Hydrology Days", March 30 - April 2, 1993*. Colorado State University, Fort Collins, CO.

Bonham-Carter, G.F. (1994) *Geographic Informations Systems for Geoscientists: Modelling with GIS*, Pergamon, Kidlington.

Boryssenko, A., Boryssenko, O., Lishchenko, A., Prokherenko, V. (2000) Inspection of internal structure of walls by subsurface radar. In: *Proceedings of the Eighth International Conference on Ground Penetrating Radar*, 23-26 May 2000, Gold Coast, Australia, D.A. Noon, G.F. Stickley, and D. Longstaff, Editors, SPIE Vol. 4084, 32-35, SPIE, 2000.

Braun, S. and Feldman, M. (1997) Time-frequency characteristics of non-linear systems, *Mechanical Systems and Signal Processing 11* (4), 611-620.

Burt, J.E. and Barber, G.M. (1996) *Elementary Statistics for Geographers*, 2nd Edition, The Guildford Press, New York.

Burt, T.P., Butcher, D.P. (1985) Topographic controls of soil moisture distributions, *Journal of Soil Science* 36 (3), 469-486.

Buttle, J.M. and House, D.A. (1997) Spatial variability of saturated hydraulic conductivity in shallow macroporous soils in a forested basin, *Journal of Hydrology* 203, 127-142.

Caldecott, R., Poirier, M., Scofea, D., Svoboda, D.E., Terzuoli, A.J. (1988) Underground mapping of utility lines using impulse radar, *IEE Proceedings* 135, F4, 343-353.

Calder, I.R. (1997) Approaches for measuring and modelling soil moisture. In: Sorooshian, S., Gupta, H.V., Rodda, S.C. (1997) (Eds.) *Land Surface Processes in Hydrology: Trials and Tribulations of Modeling and Measuring*, NATO ASI Series, Vol I 46, Springer-Verlag Berlin, 215-237.

Capehart, W.J. and Carlson, T.N. (1997) Decoupling of surface and near-surface soil water content: a remote sensing perspective, *Water Resources Research* 33 (6), 1383-1395.

Carcione, J.M. (1996) Ground-penetrating radar: Wave theory and numerical simulation in lossy anisotropic media, *Geophysics* 61, 6, 1664-1677.

Carlsten, S., Johansson, S., Worman, A. (1995) Radar techniques for indicating internal erosion in embankment dams, *Journal of Applied Geophysics* 33, 143-156.

Chanzy, A., Tarussov, A., Judge. A., Bonn, F. (1996) Soil water content determination using a digital ground-penetrating radar, *Soil Science Society of America Journal* 60, 1318-1326.

Charlton, M.B. and Mulligan, M. (2001) Efficient detection of mains water leaks using ground-penetrating radar, Proceedings of Subsurface *and Sensing Technologies and Applications III, San Diego, CA, SPIE Vol. 4491.*

Chatfield, C. (1996) *The Analysis of Time Series: An Introduction*, 5th Edition, Chapman and Hall, London.

Chen, C.H. (1986) Seismic and underwater acoustic waveform analysis. In: *Handbook of Pattern Recognition and Image Processing*, T.Y. Young and K-S. Fu, Editors, 527-544, Academic Press, San Diego, 1986.

Chen, C-C., Rao, K.R., Lee, R. (2000) A Modified Ultra-Wide Bandwidth Dielectric Rod Antenna for GPR Applications. In: *Proceedings of the Eighth International Conference on Ground Penetrating Radar*, 23-26 May 2000, Gold Coast, Australia, D.A. Noon, G.F. Stickley, and D. Longstaff, Editors, SPIE Vol. 4084, 2-6, SPIE, 2000.

Chen, K.S., Yen, S.K., Huang, W.P. (1995) A simple model for retrieving bare soil moisture from radar-scattering coefficients, *Remote Sensing and Environment* 54, 121-126.

Collins, M.E. and Doolittle, J.A. (1987) Using ground penetrating radar to study soil microvariability, *Soil Science Society of America Journal* 50, 491-493.

Collins, M.E., Doolittle, J.A., Rourke, R.V. (1989) Mapping depth to bedrock on a glaciated landscape with ground-penetrating radar, *Soil Science Society of America Journal* 53, 1806-1812.

Connor, F.R. (1982) *Signals*, Second Edition (Introductory Topics in Electronics and Telecommunication). Edward Arnold, London.

Conyers, L.B. and Goodman, D. (1997) *Ground Penetrating Radar, An Introduction for Archaeologists*, Altamira Press, London.

Cracknell, A.P. and Hayes, L.W.B. (1991) *Introduction to Remote Sensing*, Taylor and Francis, London.

Daniels, D.J., Gunton, D.J., Scott, H.F. (1988) Introduction to subsurface radar, *IEE Proceedings* 135, F4, 278-316.

Davidson, D.A. and Watson, A.I. (1995) Spatial variability in soil moisture as predicted from Airborne Thematic Mapper (ATM) data, *Earth Surface Processes and Landforms* 20, 219-230.

Davis, J.L. and Annan, A.P. (1989) Ground-penetrating radar for high-resolution mapping of soil and rock stratigraphy, *Geophysical Prospecting* 37, 531-551.

Delta-T Devices Ltd. (1998) *Theta Probe Soil Moisture sensor Type ML2 User Manual ML2-UM-1.*

Dingman, S.L. (1994) *Physical Hydrology*. Prentice Hall, New Jersey.

Dobson, M.C., Ulaby, F.T., Hallikainen, M.T., El-Rayes, M. (1985) Microwave dielectric behavior of wet soil – Part II: Dielectric mixing models, *IEEE Transactions on Geoscience and Remote Sensing* GE-23 (1), 35-46.

Doolittle, J.A. and Collins. M.E. (1995) Use of soil information to determine application of ground penetrating radar, *Journal of Applied Geophysics* 33, 101-108.

Downing, R.A. and Wilkinson, W.B. (Eds,) (1991) *Applied Groundwater Hydrology*, Clarendon Press, Oxford.

Du, S. and Rummel, P. (1994) Reconnaissance studies of moisture in the subsurface with GPR. In: *Proceedings of the Fifth International Conference on Ground Penetrating Radar, Kitchener, Ontario, 12-16 June 1994*, 1241-1248.

Dunkerley, D.L. (1995) Surface stone cover on desert hillslopes; parameterizing characteristics relevant to infiltration and surface runoff, *Earth Surface Processes and Landforms* 20, 207-218.

Dyck, S. (1985) Overview on the present status of the concepts of water balance models. In: *New Approaches in Water Balance Computations*, 3-19.

Engman, E.T. and Chauhan, N. (1995) Status of microwave soil moisture measurements with remote sensing, *Remote Sensing of the Environment* 51, 189-198.

Feldman, M. (1997) Non-linear free vibration identification via the Hilbert Transform, *Journal of Sound and Vibration* 208 (3), 475-489.

Fisher, E., McMechan, G.A., Annan, P.A. (1992) Acquisition and processing of wide-aperture ground-penetrating radar data, *Geophysics* 57 (3), 495-504.

Fitzjohn, C., Ternan, J.L., Williams, A.G. (1998) Soil moisture variability in a semi-arid gully catchment: implications for runoff and erosion control, *Catena* 32, 55-70.

Foody, G.M. (1991) Soil moisture content ground data for remote sensing investigations of agricultural regions, *International Journal of Remote Sensing* 12 (7), 1461-1469.

Gao, L. (2000) GPR Survey of Different Archaeological Sites in China. In: *Proceedings of the Eighth International Conference on Ground Penetrating Radar*, 23-26 May 2000, Gold Coast, Australia, D.A. Noon, G.F. Stickley, and D. Longstaff, Editors, SPIE Vol. 4084, 356-361, SPIE, 2000.

Gilson, E.W., Redman, J.D., Pilon, J., Annan, A.P. (1996) *Near Surface Applications of Borehole Radar*, **PEMD #126**, Sensors and Software Inc., Ontario.

Goodchild, M.F., Parks, B.O., Steyaert, L.T. (1993) (Eds.) *Environmental Modeling with GIS*, OUP, Oxford.

Grant, E.H., Sheppard, R.J., South, G.P. (1978) *Dielectric Behaviour of Biological Molecules in Solution*, Clarendon Press, Oxford.

Greaves, R.J., Lesmes, D.P., Lee, J.M., Toksöz. M.N. (1996) Velocity variations and water content estimated from multi-offset, ground-penetrating radar, *Geophysics* 61 (3), 683-695.

Gregory, P.G. (1994) Resource capture by root networks. In *Resource Capture by Crops*, 77-97.

Hallikainen, M.T., Ulaby, F.T., Dobson, M.C., El-Rayes, M., Wu, L-K. (1985) Microwave dielectric behavior of wet soil – Part I: Empirical models and experimental observations, *IEEE Transactions on Geoscience and Remote Sensing* GE-23 (1), 25-34.

Hammond, J.K. and White, P.R. (1996) The analysis of non-stationary signals using time-frequency methods, *Journal of Sound and Vibration* 190 (3), 419-447.

Hasted, J.B. (1973) *Aqueous Dielectrics*, Chapman and Hall, London.

Heuvelman, W.J. and McInnes, K.J. (1997) Spatial variability of water fluxes in soil: a field study, *Soil Science Society of America Journal* 61, 1037-1041.

Hillel, D. (1980) *Fundamentals of Soil Physics*. Academic Press, New York.

Hoogmoed, W.B., Klaij, M.C., Brouwer, J. (1991) Infiltration, runoff and drainage in the Sudano-Sahelian zone. In: *Soil Water Balance In The Sudano-Sahelian Zone* (Proceedings of the Niamey Workshop, February 1991). IAHS Publ. No. 199, 85-98.

Hook, W.R. and Livingston, N.J. (1995) Errors in converting time domain reflectometry measurements of propagation velocity to estimates of soil water content, *Soil Science Society of America Journal* 59, 35-41.

Howe, A. (2000) *Ground Penetrating Radar for the parameterisation of subsurface hydrological properties*, Unpublished PhD Thesis, King's College London, University of London.

Hromadka, T.V., Guymon, G.L., Pardoen, G.C. (1981) Nodal Domain Integration Model of Unsaturated Two-Dimensional Soil-Water Flow: Development, *Water Resources Research* 17 (5), 1425-1430.

Ibáñez Garduño, D., Lorenzo Cimadevila, H., Álvarez Béjar, R., Garduño Monroy, V.H. (2000) Prospecting with ground radar in an active creep-fault zone. In: *Proceedings of the Eighth International Conference on Ground Penetrating Radar*, 23-26 May 2000, Gold Coast, Australia, D.A. Noon, G.F. Stickley, and D. Longstaff, Editors, SPIE Vol. 4084, 602-606, SPIE, 2000.

Ifeachor, E.C. and Jervis, B.W. (1993) *Digital Signal Processing: A Practical Approach*, Addison-Wesley, Wokingham, England.

Inagaki, M. (2000) More informative interpretation of GPR records by theoretical speculation based on dielectric phenomena. In: *Proceedings of the Eighth International Conference on Ground Penetrating Radar*, 23-26 May 2000, Gold Coast, Australia, D.A. Noon, G.F. Stickley, and D. Longstaff, Editors, SPIE Vol. 4084, 200-205, SPIE, 2000.

Iskander, D.R., Zoubir, A.M., Chant, I. (2000) Time-varying spectrum based detection of landmines using ground penetrating radar. In: *Proceedings of the Eighth International Conference on Ground Penetrating Radar*, 23-26 May 2000, Gold Coast, Australia, D.A. Noon, G.F. Stickley, and D. Longstaff, Editors, SPIE Vol. 4084, 65-68, SPIE, 2000.

Jackson, T.J., Le Vine, D.M., Swift, C.T., Schmugge, J., Schiebe, F.R. (1995) Large area mapping of soil moisture using the ESTAR Passive Microwave Radiometer in Washita '92, *Remote Sensing and Environment* 53, 27-37.

Jackson, T.J., Schmugge, J., Engman, E.T. (1996) Remote sensing applications to hydrology: soil moisture, *Hydrological Sciences Journal* 41 (4), 517-530.

Jakeman, A.J., Beck, M.B., McAleer, M.J. (Eds.) (1993) *Modelling Change in Environmental Systems*, Wiley, Chichester.

John, B. (1992) Soil moisture detection with airborne passive and active microwave sensors, *International Journal of Remote Sensing* 13 (3), 481-491.

Jones, J.A.A. (1986) Some limitations to the a/s index for predicting basin-wide patterns of soil water drainage. *Zeitschrift Fur Geomorphologie* NF60, 7-20.

Jones, J.A.A. (1997) Pipeflow contributing areas and runoff response, *Hydrological Processes* 11, 35-41.

Kachanoski, R.G., Gregorich, E.G., van Wesenbeeck, I.J. (1988) Estimating spatial variations of soil water content using noncontacting electromagnetic inductive methods, *Canadian Journal of Soil Science* 68, 715-722.

Kalma, J.D. and Sivapalan, M. (Eds.) (1995) *Scale Issues in Hydrological Modelling*, Wiley, Chichester.

King, M.L (2000) Locating a subsurface oil leak using ground penetrating radar. In: *Proceedings of the Eighth International Conference on Ground Penetrating Radar*, 23-26 May 2000, Gold Coast, Australia, D.A. Noon, G.F. Stickley, and D. Longstaff, Editors, SPIE Vol. 4084, 346-350, SPIE, 2000.

Kirkby, M.J. (1978) *Hillslope Hydrology*. Wiley, Chichester.

Knight, R.J. and Nur, A. (1987) The dielectric constant of sandstones, 60 kHz to 4 MHz, *Geophysics* 52, 5, 644-654.

Knight, R., Tercier, P., Jol, H. (1997) The role of ground penetrating radar and geostatistics in reservoir description, *The Leading Edge*, November 1997.

Knoll, M.D. and Knight, R. (1994) Relationships between dielectric and hydrogeologic properties of sand-clay mixtures, *Proceedings of the Fifth International Conference on Ground Penetrating Radar, Kitchener, Ontario, 12-16 June 1994*, 45-61.

Kung, K.-J. S. and Lu, Z.-B. (1993) Using ground-penetrating radar to detect layers of discontinuous dielectric constant, *Soil Science Society of America Journal* 57, 335-340.

Lampe, B. and Holliger, K. (2000) Finite-Difference Modelling of Ground-Penetrating Radar Antenna Radiation. In: *Proceedings of the Eighth International Conference on Ground Penetrating Radar*, 23-26 May 2000, Gold Coast, Australia, D.A. Noon, G.F. Stickley, and D. Longstaff, Editors, SPIE Vol. 4084, 556-560, SPIE, 2000.

Le Thoan, T., Davidson, M., Mattia, F., Borderies, P., Chenerie, I., Manninen, T., Borgeaud, M. (1999) Improved Observation and Modelling of Bare Soil Surfaces for Soil Moisture Retrieval, *Earth Observation Quarterly* 62, 20-24.

Lorrain, P. and Corson, D.R. (1979) *Electromagnetism: Principles and Applications*, Freeman and Company, San Francisco.

Malicki, M.A., Plagge, R., Roth, C.H. (1996) Improving the calibration of dielectric TDR soil moisture determination taking into account the solid soil, *European Journal of Soil Science* 47, 357-366.

Manley, R.G. (1945) *Waveform Analysis: A Guide to the Interpretation of Periodic waves, Including Vibration Records*, Chapman and Hall Ltd, London.

Marshall, T.J., Holmes, J.W., Rose, C.W. (1996) *Soil Physics* (3rd Edition), Cambridge University Press.

McBratney, A.B. and Webster, R. (1986) Choosing functions for semi-variograms of soil properties and fitting them to sampling estimates, *Journal of Soil Science* 37, 617-639.

McCann, D.M., Jackson, P.D., Fenning, P.J. (1988) Comparison of the seismis and ground probing radar methods in geological surveying, *IEE Proceedings, Vol. 135, Pt. F, No. 4*, 380-390.

McCormack, M.D., Zaucha, D.E., Dushek, D.W. (1993) First-break refraction event picking and seismic data trace editing using neural networks, *Geophysics* 58 (1), 67-78.

McLaughlin, D., Kinzelbach, W., Ghassemi, F. (1993) Modelling Subsurface Flow and Transport. In: Jakeman, A.J., Beck, M.B., McAleer, M.J. (Eds.) (1993) *Modelling Change in Environmental Systems*, Wiley, Chichester, 133-161.

McManus, J. (1988) Grain size determination and interpretation. In: Tucker, J. (Ed.) (1988) *Techniques in Sedimentology*, Blackwell.

Monteith, J.L., Scott, R.K., Unsworth, M.H. (1994) *Resource Capture by Crops*. NUP, Nottingham.

Moore, I.D., O'Loughlin, E.M., Burch, G.J. (1988) A contour based topographic model for hydrological and ecological applications, *Earth Surface Processes and Landforms* 13, 305-320.

Moore, I.D., Turner, A.K., Wilson, J.P., Jenson, S.K., Band, L.E. (1993) GIS and Land-Surface-Subsurface Process Modeling. In: Goodchild, M.F., Parks, B.O., Steyaert, L.T. (1993) (Eds.) *Environmental Modeling with GIS*, OUP, Oxford, 196-230.

Mulligan, M. (1996) *Modelling hydrology and vegetation change in a degraded semi-arid enironment*, Unpublished PhD Thesis, King's College London, University of London.

Mulligan, M. and Charlton, M.B. (1999) *GPR for the rapid and efficient detection of mains water leaks* – Final Report to Thames Water Utilities.

Newson, M.D. and Harrison, J.G. (1978) Channel studies in the Plynlimon experimental catchments, *Institute of Hydrology Report No. 47*, Wallingford.

Nissen, H.H., Moldrup, P., Henriksen, K. (1998) High-Resolution Time Domain Reflectometry Coil Probe for Measuring Soil Water Content, *Soil Science Society of America Journal* 62, 1203-1211.

Nussbaum, A. (1966) *Electromagnetic and Quantum Properties of Materials*, Prentice-Hall, London.

OFWAT *1994-1995 Report on the cost of water delivered and sewage collected*, Office of Water Services, 1995.

Olhoeft, G.R. (2000) Maximising the information return from ground penetrating radar, *Journal of Applied Geophysics* 43, 175-187.

Olhoeft, G.R. and Smith, S.S. (2000) Automatic processing and modeling of GPR data for pavement thickness and properties, In: *Proceedings of the Eighth International Conference on Ground Penetrating Radar*, 23-26 May 2000, Gold Coast, Australia, D.A. Noon, G.F. Stickley, and D. Longstaff, Editors, SPIE Vol. 4084, 188-193, SPIE, 2000.

Oonincx, P.J. (1997) *On Time-Frequency Analysis and Time Limitedness*, Centrum voor Wiskunde en Informatica Rapport, PNA-R9720.

Or, D. and Wraith, J. M. (2000) Comment on "On water vapor transport in field soils" by Anthony T. Cahill and Marc B. Parlange, *Water Resources Research*, 36 (10), 3103-3107.

Olver, A.D. and Cuthbert, L.G. (1988) FMCW radar for hidden object detection, *IEE Proceedings* 135, F4, 354-361.

Paloscia, S., Pampaloni, P., Chiarantini, L., Coppo, P., Gagliani, S., Luzi, G. (1993) Multifrequency passive microwave remote sensing of soil moisture and roughness, *International Journal of Remote Sensing* 14 (3), 467-483.

Paltineanu, I.C. and Starr, J.L. (1997) Real-time soil water dynamics using multisensor capacitance probes: Laboratory calibration, *Soil Science Society of America Journal* 61, 1576-1585.

Peplinski, N.R., Ulaby, F.T., Dobson, M.C. (1995) Dielectric properties of soils in the 0.3-1.3GHz Range, *IEEE Transactions on Geoscience and Remote Sensing* 33, 3, 803-807.

Perdok, U.D., Kroesbergen, B., Hilhorst, M.A. (1996) Influence of Gravimetric water content and bulk density on the dielectric properties of soil, *European Journal of Soil Science* 47, 367-371.

Persson, M. (1997) Soil solution electrical conductivity measurements under transient conditions using time domain reflectometry, *Soil Science Society of America Journal* 61, 997-1003.

Prasfika, D.W. (1994) *Water Supply Planning*, Krieger Publishing Company, Florida.

Radin, J.W. (1993) Water relations in controlled environments and the field. In: *Interacting Stresses on Plants in a Changing climate*, 467-483.

Rea, J. and Knight, R. (1998) Geostatistical analysis of ground-penetrating radar data: a means of describing spatial variation in the subsurface, *Water Resources Research*, 34 (3), 329-339.

Redman, D., Parkin, G., Annan, P. (2000) Borehole GPR measurement of soil water content during an infiltration experiment. In: *Proceedings of the Eighth International Conference on Ground Penetrating Radar*, D.A. Noon, G.F. Stickley, and D. Longstaff, Editors, SPIE Vol. 4084, 501-505, SPIE, 2000.

Reppert, P.M., Morgan, F.D., Toksöz, M.N. (2000) Dielectric Constant Determination Using Ground-Penetrating Radar Reflections Coefficients, *Journal of Applied Geophysics* 43, 189-197.

Reynolds, J.M. (1997) *An Introduction to Applied and Environmental Geophysics*, Wiley, Chichester.

Rihaczek, A.W. (1996) *Principles of High-Resolution Radar*, Artech House, London.

Roberts, R. (2000) Examination of the effect of antenna-surface distance on the radiation of a GPR antenna. In: *Proceedings of the Eighth International Conference on Ground*

Penetrating Radar, 23-26 May 2000, Gold Coast, Australia, D.A. Noon, G.F. Stickley, and D. Longstaff, Editors, SPIE Vol. 4084, 702-703, SPIE, 2000.

Robinson, J.S. and Sivapalan, M. (1995) Catchment-scale runoff generation by model aggregation and similarity analyses. In: Kalma, J.D. and Sivapalan, M. (Eds.) (1995) *Scale Issues in Hydrological Modelling*, Wiley, Chichester, 311-330.

Roth, C.H., Malicki, M.A., Plagge, R. (1992) Empirical evaluation of the relationship between soil dielectric constant and volumetric water content as the basis for calibrating soil moisture measurements by TDR, *Journal of Soil Science* 43, 1-13.

Rutter, A.J. (1969) *Plant-Water Relationships In Outdoor Environments*. Inaugural Lecture Imperial College of Science and Technology, London.

Saarenketo, T. (1998) Electrical Properties of water in clay and silty soils, *Journal of Applied Geophysics* 40, 73-88.

Saarenketo, T. and Scullion, T. (2000) Road evaluation with ground penetrating radar, *Journal of Applied Geophysics*, 43, 119-138.

Sabburg, J., Ball, J.A.R., Hancock, N.H. (1997) Dielectric behavior of moist swelling clay soils at microwave frequencies, IEEE *Transactions on Geoscience and Remote Sensing* 35 (3), 784-787.

Sai, B. and Lighthart, L.P. (2000) Improved GPR data preprocessing for detection of various landmines, In: *Proceedings of the Eighth International Conference on Ground Penetrating Radar*, 23-26 May 2000, Gold Coast, Australia, D.A. Noon, G.F. Stickley, and D. Longstaff, Editors, SPIE Vol. 4084, 80-84, SPIE, 2000.

Schmugge, T. and Jackson, T. (1997) Passive microwave remote sensing of soil moisture. In: Sorooshian, S., Gupta, H.V., Rodda, S.C. (1997) (Eds.) *Land Surface Processes in Hydrology: Trials and Tribulations of Modeling and Measuring*, NATO ASI Series, Vol I 46, Springer-Verlag Berlin, 239-261.

Selby, M.J. (1993) *Hillslope Materials and Processes* (2nd Edition). Oxford University Press, Oxford.

Sénéchal, P., Perroud, H., Garambois, S. (2000) Geometrical and Physical Parameters Comparison Between GPR Data and Other Geophysical Data. In: *Proceedings of the Eighth International Conference on Ground Penetrating Radar*, 23-26 May 2000, Gold Coast, Australia, D.A. Noon, G.F. Stickley, and D. Longstaff, Editors, SPIE Vol. 4084, 618-623, SPIE, 2000.

Sensors & Software Inc. (2001) *Tips – Using Signal Polarity*. EKKO Update January 2001, 2-3.

Sensors and Software Inc. (1996) *PulseEkko 1000 Run Manual*, Ontario.

Shen, L.C., Savre, W.C., Price, J.M., Athavale, K. (1985) Dielectric properties of reservoir rocks at ultra-high frequencies, *Geophysics* 50 (4), 692-704.

Shiavi, R.G. and Bourne, J.R. (1986) Methods of Biological Signal Processing. In:Young, T.Y. and Fu, K-S. (1986) (Eds.) *Handbook of Pattern Recognition and Image Processing*, Academic Press, San Diego, 545-568.

Shih, S.F. and Doolittle, J.A. (1984) Using radar to investigate organic soil thickness in the Florida Everglades, *Soil Science Society of America Journal* 48, 651-656.

Sivakumar, M.V.K., Wallace, J.S., Renard, C., Giroux, C. (1991) *Soil Water Balance In The Sudano-Sahelian Zone* (Proceedings of the Niamey Workshop, February 1991). IAHS Publ. No. 199. IAHS Press, Institute of Hydrology, Wallingford, UK.

Sorooshian, S., Gupta, H.V., Rodda, S.C. (1997) (Eds.) *Land Surface Processes in Hydrology: Trials and Tribulations of Modeling and Measuring*, NATO ASI Series, Vol I, 46, Springer-Verlag Berlin.

Speight, J.G. (1980) The role of topography in controlling throughflow generation: a discussion, *Earth Surface Processes and Landforms* 5, 187-191.

Summerfield, M.A. (1991) *Global Geomorphology*. Longman.

Tarussov, A. and Bonn, F. (1994) Soil survey from light research aircraft using a ground-penetrating radar, *First International Airborne Remote Sensing Conference and Exhibition,* 11-15 September *1994,* Strasbourg, France.

Tillard, S. and Dubois, J-C. (1995) Analysis of GPR data: wave propagation velocity determination, *Journal of Applied Geophysics* 33, 77-91.

Timlin, D.J., Ahuja, L.R., Ankeny, M.D. (1994) Comparison of three field methods to characterize apparent macropore conductivity, *Soil Science Society of America Journal* 58, 278-284.

Timlin, D.J. and Pachepsky, Y.A. (1996) Comparison of three methods to obtain the apparent dielectric constant from time domain reflectometry wave traces, *Soil Science Society of America Journal* 60, 970-977.

Topp, G.C., Davis, J.L., Annan, A.P. (1980) Electromagnetic Determination of Soil Water Content: Measurements in Coaxial Transmission Lines, *Water Resources Research* 16 (3), 574-582.

Topp, G.C., Davis, J.L., Annan, A.P. (1982) Electromagnetic determination of soil water content using TDR: I. Applications to wetting fronts and steep gradients, *Soil Science Society of America Journal* 46, 672-678.

Torrence, C. and Compo, G.P. (1998) A Practical Guide to Wavelet Analysis, *Bulletin of the American Meteorological Society* 79 (1), 61-78.

Van Der Beken, A., Herrmann, A. (1985) *New Approaches In Water Balance Computations.* IAHS Publ. No. 148. IAHS Press, Institute of Hydrology, Wallingford, UK.

van Oevelen, P.J. (1998) Soil Moisture Variability: a comparison between detailed field measurements and remote sensing measurement techniques, *Hydrological Sciences Journal* 43 (4), 511-520.

Van Overmeeren, R.A. (1993) Georadar for Hydrogeology, *Sensors and Software Inc.*.

Van Overmeeren, R.A., Sariowan, S.V., Gehrels, J.C. (1997) Ground penetrating radar for determining volumetric water content; results of comparative measurements at two test sites, *Journal of Hydrology* 197, 316-338.

Van Trees, H.L. (1968) *Detection, Estimation, and Modulation Theory Part 1*, Wiley, London.

van Wesemael, B., Poesen, J., Figueiredo, T. (1995) Effects of rock fragments on physical degradation of cultivated soils by rainfall, *Soil & Tillage research*, 33, 229-250.

van Wesemael, B., Mulligan, M., Poesen, J. (1999) Spatial patterns of soil water balance on intensively cultivated hillslopes in a semiarid environment: the impact of rock fragments and soil thickness, submitted to *Hydrological Processes.*

Walley, W.B. (1990) *Properties of materials and geomorphological explanation.* Oxford University Press, London.

Ward, R.C. and Robinson, M. (1990) *Principles of Hydrology* (3rd Edition), McGraw-Hill, London.

Weiler, K.W., Steenhuis, T.S., Boll, J., Kung, K-J.S. (1998) Comparison of Ground Penetrating radar and TDR as soil water sensors, *Soil Science Society of America Journal* 62, 1237-1239.

Weimann, A., Von Schönermark, Schumann, A., Jörn, P., Günther, R. (1998) Soil moisture estimation with ERS-1 SAR data in the East-German loess soil area, *International Journal of Remote Sensing* 19 (2), 237-243.

Wensink, W.A. (1993) Dielectric properties of wet soils in the frequency range 1 - 3000 MHz, *Geophysical Prospecting* 41, 671-696.

Western, A.W., Blöschl, G., Grayson, R.B. (1998) Geostatistical characterisation of soil moisture patterns in the Tarrawarra catchment, *Journal of Hydrology* 205, 20-37.

Western, A.W., Grayson, R.B., Blöschl, G., Willgoose, G.R., McMahon, T.A. (1999) Observed spatial organization of soil moisture and its relation to terrain indices, *Water Resources Research* 35 (3), 797-810.

Wilkinson, W.B. and Brassington, F.C. (1991) Rising Groundwater Levels – an international problem. In: Downing, R.A., Wilkinson, W.B. (Eds,) (1991) *Applied Groundwater Hydrology*, Clarendon Press, Oxford, 35-53.

Wishart, T. (1996) *On Sonic Art – New and Revised Edition*, Contemporary Music Studies, Volume 12 (Emmerson, S. (Ed.)), Harwood Academic Publishers, Amsterdam.

Xiong, Z. and Tripp, A.C. (1997) Ground-penetrating radar responses of dispersive models, *Geophysics* 62 (4), 1127-1131.

Xu, T. and McMechan, G.A. (1997) GPR attenuation and its numerical simulation in 2.5 dimensions, *Geophysics* 62 (1), 403-414.

Yarovoy, A.G. and Ligthart, L.P. (2000) Ultra-wideband antennas for ground penetrating radar. In: *International Symposium on Antennas for Radar Earth Observation,*

Symposium Proceedings, 8-9 June 2000, Delft University of Technology, The Netherlands, 1-5.

Young, D.R. and Nobel, P.S. (1986) Predictions of soil-water potentilas in the North-western Sonoran Desert, *Journal of Ecology* 74, 143-154.

Young, R.A., Deng, Z., Sun, J. (1995) Interactive processing of GPR data, *The Leading Edge*, April 1995, 275-280.

Zeng, X. and McMechan, G.A. (1997) GPR characterization of buried tanks and pipes, *Geophysics* 62 (3), 797-806.

Zhang, R. (1997) Determination of Soil Sorptivity and Hydraulic Conductivity from the Disk Infiltrometer, *Soil Sci. Soc. Am. J.* 61, 1024-1030.

Ziemer, R.E., Tranter, W.H., Fannin, D.R. (1998) *Signals and Systems: Continuous and Discrete*. 4th Edition. Prentice Hall.